Sediment concentrations

and

Sediment transport

in case of

Irregular breaking waves

"Experimental results series A and B"

Part H: Text

August 1995

Bart Grasmeijer
Rico Sies

Preface

In 1986 an experimental programme to investigate sediment transport rates has been started as a joint effort of the Delft University of Technology and DELFT HYDRAULICS. The objective was to improve experiments for investigation and to get experimental data. Since then, two series of experiments were executed in a flume of the Laboratory of Fluid Mechanics. In the first study sand bed material of 200 μm was used. In the second study a similar programme was carried out using sand bed material of 100 μm. A third experimental programme was carried out in a basin of DELFT HYDRAULICS. In this programme the influence of varying wave angle was studied.

Last year, we participated in a fourth experimental programme. The experiments were carried out in a flume of the Laboratory of Fluid Mechanics (Delft University of Technology). In this programme the sediment transport rates in case of breaking waves were investigated. The results of the experiments were compared with the second - ("the earlier 100-μm-flume-study, 1988") and the third programme ("the earlier 100-μm-basin-study, 1992").

For convenience the present report is divided in two parts. Part H contains all text and illustrative figures, part I contains all tables and figures of the experimental data.

We would like to thank the employees of the Laboratory of Fluid Mechanics for their assistance during execution of the experiments and of course Prof Dr L.C. van Rijn for his guidance during these experiments, and his advice for interpretation of the experimental results.

B.T. Grasmeijer

E.M. Sies

August 1995

Contents

4 Experimental results series A

List of symbols

α	:	correction factor returnflow formulae	[-]
γ	:	apparent roughness increase coefficient	[-]
δ	:	mean bed level	[m]
Δ	:	relative sediment density	[-]
δ_b	:	mixing layer	[m]
ϵ	:	porosity	[-]
η	:	water surface elevation	[m]
κ	:	constant of Von Karman	[-]
λ	:	ripple length	[m]
μ	:	mean value	[-]
ν	:	kinematic viscosity	[m^2/s]
ρ	:	correlation coefficient	[-]
ρ_s	:	density of sediment	[kg/m^3]
ρ_w	:	density of fluid	[kg/m^3]
ϕ	:	current wave angle	[°]
ω	:	wave frequency ($2\pi/T_p$)	[s^{-1}]
ω'	:	wave frequency in case of waves and current ($2\pi/T_p$']	[s^{-1}]
A_{asym}	:	asymmetry factor	[-]
$A_{b,on,tot}$	:	horizontal orbital displacement amplitude in onshore direction ($\hat{U}_{b,on,tot}/\omega$')	[m]
b	:	flume width	[m]
B	:	coefficient in the Kalinske-Frijlink-Bijker formula	[-]
c	:	concentration	[kg/m^3]
$\underline{c}$	:	time- and bed-averaged concentration	[kg/m^3]
$\underline{\underline{c}}$	:	time- and bed averaged concentration	[kg/m^3]
c'	:	concentration fluctuation	[kg/m^3]
c_a	:	absolute wave celerity	[m/s]
c_r	:	relative wave celerity	[m/s]
D_s	:	grain diameter suspended sediment	[m]
D_x	:	grain diameter exceeded by x% by weight	[m]
E_{xx}	:	wave energy	[m^2/Hz]
f	:	wave frequency	[s^{-1}]
F_d	:	distribution coefficient	[-]
f_{high}	:	wave frequency (f > 0.7 Hz)	[s^{-1}]
F_i	:	bottom concentration increase factor	[-]
f_{low}	:	wave frequency (f < 0.7 Hz)	[s^{-1}]

f_p	:	peak frequency	[s^{-1}]
g	:	acceleration of gravity	[m/s^2]
h	:	water depth	[m]
H	:	wave height	[m]
H_{rms}	:	root mean square wave height	[m]
H_s	:	significant wave height	[m]
k	:	wave number ($2\pi/L$)	[m^{-1}]
$K_{s,app}$	:	apparent bedroughness parameters	[m]
$K_{s,phys}$	:	physical bedroughness parameters	[m]
L	:	wave length	[m]
L'	:	wave length relative to current	[m]
L_b	:	bed load	[kg/m^2]
L_s	:	suspended load	[kg/m^2]
L_t	:	total load	[kg/m^2]
m_0	:	0-order moment wave spectrum	[m^2]
m_2	:	2-order moment wave spectrum	[m^2.Hz]
p	:	porosity	[-]
q	:	power coefficient	[-]
Q_b	:	fraction of breaking waves	[-]
r	:	mean ripple height	[m]
ß	:	ratio of sediment and fluid mixing coefficient	[-]
S_b	:	bed load transport	[kg/sm]
S_s	:	suspended load transport	[kg/sm]
S_{tot}	:	total load transport	[kg/sm]
S_x	:	sediment transport in cross-shore direction	[kg/sm]
S_y	:	sediment transport in long-shore direction	[kg/sm]
t	:	coordinate of time	[s]
$T_{0,2}$	:	average zero-crossing period	[s]
T_p	:	wave spectrum peak period	[s]
T_p'	:	wave spectrum peak period relative to current	[s]
T_z	:	zero-crossing period	[s]
U	:	fluid velocity	[m/s]
$\underline{U}$	:	time- and bed-averaged fluid velocity	[m/s]
$\overline{\underline{U}}$	:	time- and bed-averaged fluid velocity	[m/s]
U'	:	fluid velocity fluctuation	[m/s]
U_*	:	shear velocity	[m/s]
U_{*c}	:	shear velocity by current	[m/s]
U_{*cw}	:	shear velocity by current and waves	[m/s]

$\hat{U}_{b,on/off,tot}$	:	horizontal orbital velocity amplitude of the *total velocity signal* in on- respectively offshore direction just outside the boundary layer	[m/s]
$\hat{U}_{b,on/off,low}$	:	horizontal orbital velocity amplitude of the *low frequency signal* (T>5s) in on- respectively offshore direction	[m/s]
$\hat{U}_{b,on/off,high}$	:	horizontal orbital velocity amplitude of the *high frequency signal* (T<5s) in on- respectively offshore direction	[m/s]
U_m	:	depth-averaged fluid velocity	[m/s]
V	:	sediment volume	[m^3]
w_{ss}	:	fall velocity suspended sediment	[m/s]
x,y,z	:	length coordinates	[m]
y	:	power coefficient	[-]
z_+	:	reference level relative to mean bed level	[m]
z_0	:	zero velocity level	[m]
z_1	:	adapted zero velocity level	[m]

1 Introduction

Coastal changes occur mostly as a result of changes in sediment transport along the coast. If at cross-section A (Figure 1.1), the sediment transport is for any reason larger (or smaller) than at cross-section B, accretion (or erosion) will take place in between the two cross-sections. For prediction of coast-lines in the future, the prediction of the net sediment transport is therefore essential. Various models, such as that of Bijker, Van Rijn, Nielsen, Engelund & Hansen and Ackers & White are available to predict the sediment transport by knowledge of wave height and current strength. The reliability of these models is unknown because data under field conditions are scarce. Only few relations between sediment transport, current velocity and wave height are known.

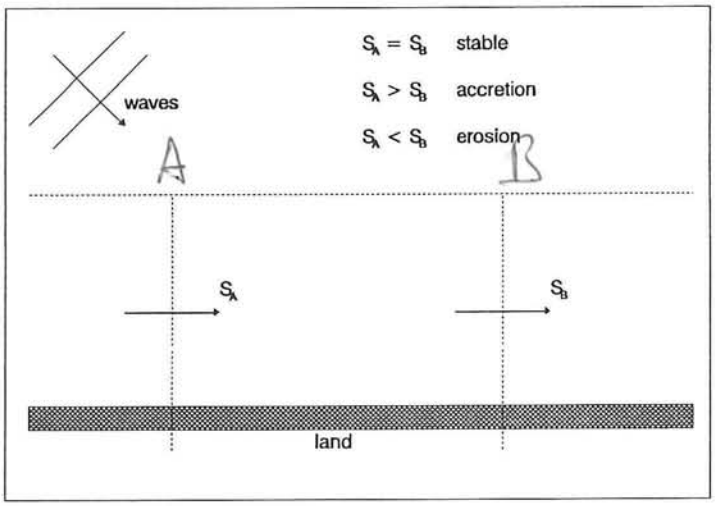

Figure 1.1 Transport mass balance.

For these reasons a laboratory study was carried out to extend the knowledge of the basic phenomena in morphological processes. The study contains experiments in which sediment concentrations and fluid velocities have been measured in case of irregular breaking waves alone and in combination with a current.

Some of the present results will be compared with the results of the three earlier studies done by Van der Kaaij & Nieuwjaar (1987), Van Kampen & Nap (1988) and Havinga (1992). These studies will herein be referred to as *the earlier 200-μm-flume-study (1987)*, *the earlier 100-μm-flume-study (1988)* and *the earlier 100-μm-basin-study (1992)*.

Chapter 2 deals with the sediment transport basics. Two types of sediment transport, the longshore and the cross-shore sediment transport are discussed and the objectives of the present experiments are presented.

In Chapter 3 the experimental set up is described. The measured parameters, methods and instruments are discussed. The experimental programme of the series A and the series B1 and B2 are presented.

Chapter 4 covers the experimental results from test series A. The wave characteristics, fluid velocities and the influence of these parameters on the sediment concentration, sediment load and sediment transport are studied.

Chapter 5 deals with the experimental results from test series B1 and B2. The distribution of the sediment concentrations, fluid velocities, sediment loads and sediment transport rates over a sand bar are studied.

In Chapter 6 a comparison is made between the measurements and the sediment transport models by Van Rijn and Bijker. Transport rates, concentration profiles and velocity profiles are compared.

In Chapter 7 a list of conclusions and recommendations is presented.

2 Sediment transport computation

2.1 Sediment transport basics

The computation of the sediment transport rate can be done by multiplying the sediment concentration with the sediment velocity and integrating this product over the water depth. The sediment concentration over the depth is caused by stirring up of sediment particles from the sand bed. The stirring up process is induced by wave and current movement in the near bed zone.

Assuming that the sediment velocity is equal to the fluid velocity, the sediment transports can be computed from:

$$S_y(x,y,t) = \int_0^{h(x,y)+\eta(x,y,t)} c(x,y,z,t) * U_y(x,y,z,t)\, dz \qquad (2.1)$$

$$S_x(x,y,t) = \int_0^{h(x,y)+\eta(x,y,t)} c(x,y,z,t) * U_x(x,y,z,t)\, dz \qquad (2.2)$$

where

S_y (x,y,t)	:	Local instantaneous sediment transport rate per unit width in longshore direction	(kg/sm)
S_x (x,y,t)	:	Local instantaneous sediment transport rate per unit width in cross-shore direction	(kg/sm)
c(x,y,z,t)	:	Local instantaneous sediment concentration	(kg/m^3)
U_y (x,y,z,t)	:	Local instantaneous y-component of the fluid velocity	(m/s)
U_x (x,y,z,t)	:	Local instantaneous x-component of the fluid velocity	(m/s)
x	:	Horizontal coordinate, cross-shore	(m)
y	:	Horizontal coordinate, longshore	(m)
z	:	Height above mean bed level	(m)
t	:	Time	(s)
η	:	Water surface elevation	(m)
h(x,y)	:	Water depth	(m)

Measuring instantaneous fluid velocity (see Figure 2.1) and sediment concentration is quite difficult. Bosman (1985) investigated the concentration as a function of time. The concentration c(z,t) was measured within a wave period, at a fixed point about 3 cm above mean bed level. Figure 2.2 shows ensemble mean concentrations based on averaging over 99 periods and standard deviations. Based on random scatter of the concentrations, it is obvious that Bosman concluded that it is not practical to relate the instantaneous concentrations to the instantaneous fluid velocities.

In the present study both instantaneous and averaged values of concentrations and velocities have been measured. The analysis of the results is herein focussed on the time-averaged values.
This implies that a part of the total sediment transport is neglected as is shown below.
Defining:

$$c(x,y,z,t) = \overline{\overline{c}}(y,z) + c'(x,y,z,t) \tag{2.3}$$

$$U_y(x,y,z,t) = \overline{\overline{U_y}}(y,z) + U_y'(x,y,z,t) \tag{2.4}$$

$$U_x(x,y,z,t) = \overline{\overline{U_x}}(y,z) + U_x'(x,y,z,t) \tag{2.5}$$

where

$\overline{\overline{c}}$	:	Time- and bed-averaged component of the local instantaneous concentration	(kg/m³)
c´(x,y,z,t)	:	Fluctuating component of the local instantaneous concentration	(kg/m³)
$\overline{\overline{u_y}}$	:	Time- and bed-averaged component of the local instantaneous fluid velocity in y-direction	(m/s)
$\overline{\overline{u_x}}$	:	Time- and bed-averaged component of the local instantaneous fluid velocity in x-direction	(m/s)
U_y´(x,y,z,t)	:	Fluctuating component of the local instantaneous fluid velocity in y-direction	(m/s)
U_x´(x,y,z,t)	:	Fluctuating component of the local instantaneous fluid velocity in x-direction	(m/s)

The fluctuating components are caused by:

- orbital fluid movements, induced by the waves
- fluctuations in the main flow

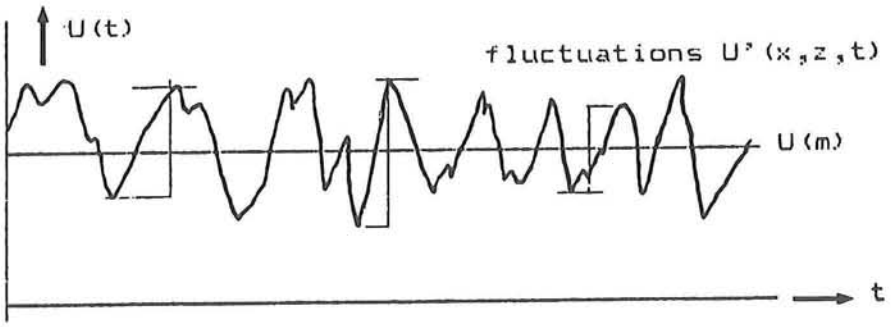

Figure 2.1 Velocity signal

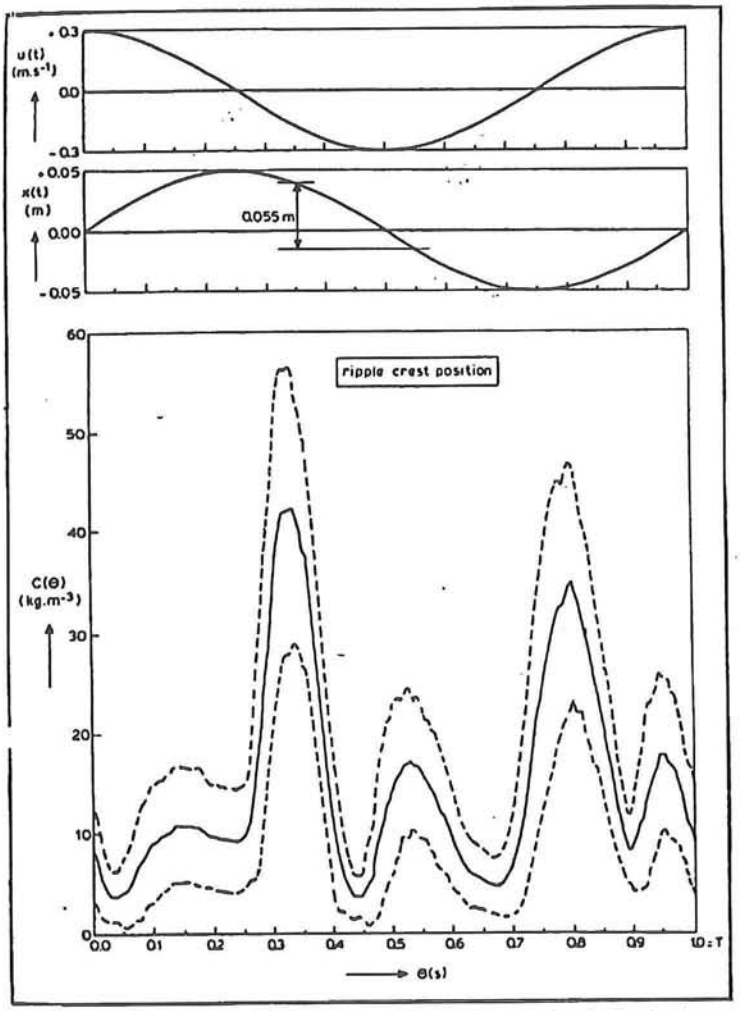

Figure 2.2 Ensemble mean and total standard deviation of concentration in single period T, T = 1 s; U0 = 0.30 m/s

Turbulence and the irregularity of waves will increase this effect.

Substituting Eq.2.3 and Eq.2.4 into Eq.2.1 leads to:

$$S_y(x,y,z,t) = \int_0^{h(x,y)+\eta(x,y,t)} c(x,y,z,t) * U_y(x,y,z,t)\,dz =$$

$$\int_0^{h(x,y)+\eta(x,y,t)} \overline{\overline{c}}(y,z) * \overline{\overline{U_y}}(y,z)\,dz + \int_0^{h(x,y)+\eta(x,y,t)} c'(x,y,z,t) * \overline{\overline{U_y}}(y,z)\,dz +$$

$$\int_0^{h(y)+\eta(y,t)} \overline{\overline{c}}(y,z) * U_y'(x,y,z,t)\,dz + \int_0^{h(x,y)+\eta(x,y,t)} c'(x,y,z,t) * U_y'(x,y,z,t)\,dz \qquad (2.6)$$

Comparable relations are found for $S_x(x,y,z,t)$.

Averaging over time and bed (in x-direction), the total sand transport, is defined as:

$$S_y(y) = \overline{\overline{S_y}}(x,y,t) \qquad (2.7)$$

$$S_x(y) = \overline{\overline{S_x}}(x,y,t) \qquad (2.8)$$

And substitution of Eq.2.6 into Eq.2.7 yields:

$$S_y(y) = \overline{\overline{\int_0^{h(y)} \overline{\overline{c}}(y,z) * \overline{\overline{U_y}}(y,z)\,dz}} + \overline{\overline{\int_0^{h(y)} c'(x,y,z,t) * \overline{\overline{U_y}}(y,z)\,dz}} +$$

$$\overline{\overline{\int_0^{h(y)} \overline{\overline{c}}(y,z) * U_y'(x,y,z,t)\,dz}} + \overline{\overline{\int_0^{h(y)} c'(x,y,z,t) * U_y'(x,y,z,t)\,dz}}$$

$$S_y(y) = \int_0^{h(y)} \overline{\overline{c}}(y,z) * \overline{\overline{U_y}}(y,z)\,dz + \overline{\overline{\int_0^{h(y)} c'(x,y,z,t) * U_y'(x,y,z,t)\,dz}} \qquad (2.9)$$

and for x-direction:

$$S_x(y) = \int_0^{h(y)} \overline{\overline{c}}(y,z) * \overline{\overline{U_x}}(y,z)\,dz + \overline{\int_0^{h(y)} c'(x,y,z,t) * U_x'(x,y,z,t)\,dz} \qquad (2.10)$$

Eq.2.9 and Eq.2.10 show that the total sediment transport is divided into two parts:
The first part is determined by time- and bed-averaging. It represents the transport of sediment by U(z), as if there is a steady current. Therefore this part of the sediment transport is defined as the *current-related sediment transport.*
The second part of the sediment transport is mainly caused by the orbital movements, U(x,y,z,t), effected by the irregular waves. So this part is called *the wave-related sediment transport.* Sometimes one uses the terms of respectively convective and diffusive transport.

Eq.2.9 is a useful approximation of Eq.2.1. For the current-related sediment transport it is sufficient to measure time- and bed-averaged velocities and concentrations.
In the present study and the earlier studies this resulted in an estimation of the current-related sediment transport. To investigate the relative importance of the wave-related sediment transport, the instantaneous values of concentration and fluid velocity were measured with the Acoustical Sediment Transport Meter (ASTM) and the Electro Magnetic Fluid velocity meter (EMS). Further information can be found in Chapter 3.

2.2 Longshore and cross-shore sediment transport

Waves approaching a coast, will reach the coast under a small angle, caused by refraction. The radiation stress, generated by the breaking waves under a small angle, and bottom friction stresses, result in a longshore current. Figure 2.3 shows two cross-sections, in which two different sediment transport processes are present.

The sediment transport in cross-section A represents a longshore sediment transport. This means stirring up of sediment, by waves and current, transported by a rather steady longshore current, which is wave- and/or tide-induced.
Through cross-section B, a cross-shore sediment transport is present. In this case, the velocity oscillations U´(x,y,z,t), introduced by orbital movements, do strongly influence the transport of sediment, during a wave period.

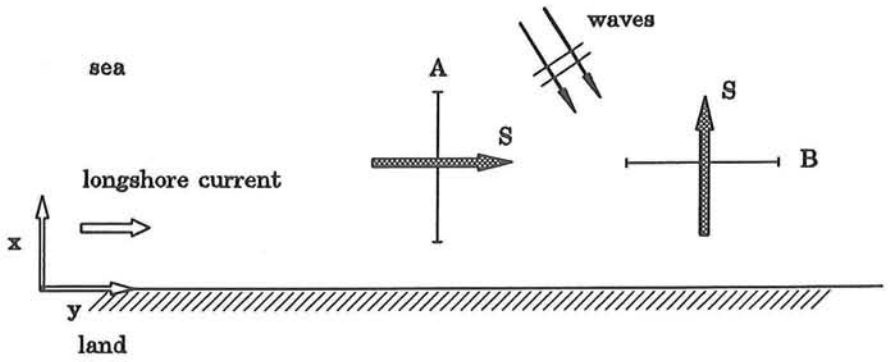

Figure 2.3 Longshore and cross-shore sediment transport

The longshore sediment transport is assumed to be represented by the current-related part of the total sediment transport (see Eq.2.9):

$$S_y(y) = \int_0^{h(y)} \bar{\bar{c}}(y,z) * \bar{\bar{U}}_y(y,z)\,dz \qquad (2.11)$$

This is because of the fact that the fluid velocity does not depend on time (the longshore current is rather constant at each point above the mean bed level), and because the time- and bed-averaged concentration c(z) can be measured with reasonable accuracy.

For cross-shore sediment transport, this simplification (Eq.2.11) is not a very accurate one. The parameter $U_x(y,z,t)$ and the parameter $c(y,z,t)$ do strongly depend on time. In this case, the wave-related sediment transport plays a much more important role than in the longshore transport process.

In the earlier studies the relation between current and waves, in following or opposing direction and under an angle, and the sediment transport by non-breaking waves was investigated. In the present study the influence of the breaking of waves is investigated.
In all experiments time- and bed-averaged velocities were measured and also the instantaneous values of the sediment concentration and the fluid velocity, to investigate the importance of the wave-related sediment transport. An estimation of the cross-shore sediment transport can be made now.

2.3 Objective of the present experiments

1. Identification of the relationship between current-related sediment transport, wave height and current velocity, and comparison with the earlier 100-μm-basin-study (1992).
2. Investigation of the influence of breaking waves on the current-related sediment transport parameters.
3. Verification of the Bijker model and the Van Rijn model for the current-related suspended sediment transport.
4. Investigation of effective bed-roughness of wave- and current-induced ripples.
5. Investigation of the distribution of the cross-shore suspended sediment transport over a sand bar.
6. Investigation of the influence of the wave height on the distribution of the cross-shore suspended sediment transport over a bar.
7. Investigation of the wave-related part of the sediment transport rate and the cross-shore sediment transport. (Not presented in this report.)

3 Experimental set up

3.1 The 'Grote Speurwerk'-flume

3.1.1 Description of the physical model

All experiments were conducted in the 'Grote Speurwerk'-flume, a flume of the Laboratory of Fluid Mechanics of the Faculty of Civil Engineering of the Delft University of Technology. Figure 3.1 shows a sketch of the flume.
The total length of the flume is 45 m, the width 0.8 m and the flume has a depth of 1.0 m. This makes it possible to perform experiments with a 30 m bed length.

The flume consists of various sections (see Figure 3.1):

A - Wave-generator section
B/E - In- and out-flow section
C - Test section
D - Section with wave damping slope structure

3.1.2 Wave generation

The irregular waves are generated by the irregular movements of the wave paddle. The desired wave spectrum is created by a computer file. The spectrum is single topped, with a peak frequency of 0.4 Hz and a JONSWAP-shape. The wave height is also a variable in the computer-file, and can be adapted for more accuracy by an amplifier.

3.1.3 Current generation

The current enters the flume through the inflow section B. Current in the wave direction, which is investigated only in this experiment, is generated by opening gate valves 1 (see Figure 3.1), while gate valves 2 are closed. By manipulating gate valve 1 for inflow and measuring the Rehbock weir and the fluid velocity at $z = 0.4 * h$ ($\approx$ mean velocity profile), the desired discharge can be obtained. A permanent weir, situated just in front of section E is used to achieve the desired water depth of 0.70 m, by adjusting the height of this weir.

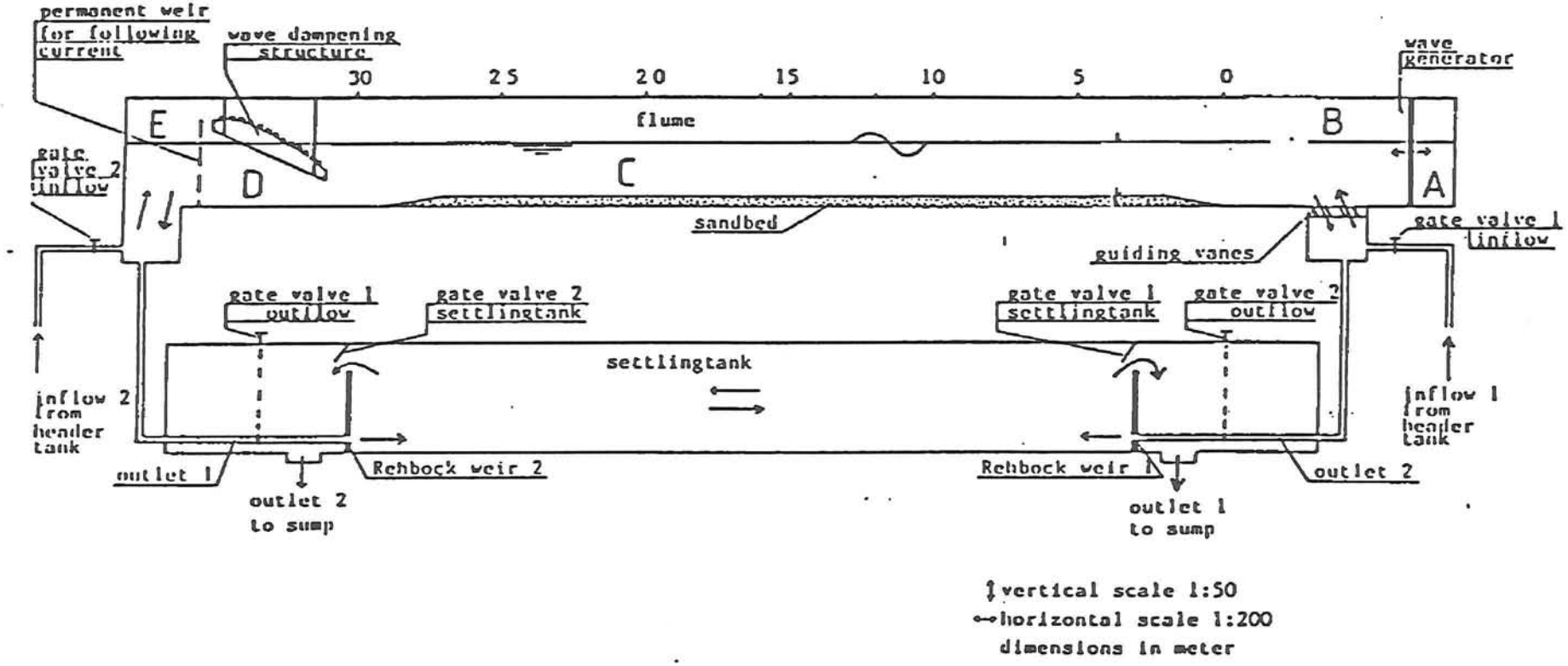

Figure 3.1 Sketch of the flume

3.1.4 Test section

For test series A at the front of the sand bed a fixed-bed slope of 1:20 was situated to create a water depth of approximately h=0.30 m at the test section (18 m from beginning sand bed). The sand bed had a slope of 1:100 to provide enough length in which the wave height and percentage breaking waves remained constant (See Figure 3.2).
In series B the sediment transport processes over a sand bar are studied. The sand bar is a representation of the sand bar at Egmond, the Netherlands. The seaward upsloping part of the sand bar has a slope of 1:20. The water depth on top of the bar is 0.30 m. The downsloping part of the sand bar has a slope of 1:25, and the landward upsloping part in the profile has a slope of 1:63 (See Figure 3.3).

3.1.5 Wave damping structure

To reduce wave reflections as much as possible, the effect of the wave damper was examined in the earlier 200-μm-flume-study (1987) and the 100-μm-flume study (1988). Based on the results of these studies, the wave damper was placed in the flume. The reflection coefficient, defined as the ratio of the reflected wave height H_r and the incident wave height H_i, was found to be less than about 0.1 in these studies. In this study about the same magnitude of the reflection coefficient is assumed.

3.2 Sediment

As in the earlier studies, the sediment used in the present study was 'Asser sand'. Because the sediments originated from nature, it had to be washed out, before it was brought in the flume. A layer of about 0.25 m sand was brought in a reservoir with an area of 1 m^2. Water was added from the bottom of the reservoir, and by stirring the sand and water mixture, the silt and pollutions were washed out. After that, the sand was brought in the flume and leveled in the desired bottom profile.
Twice during the experimental period, a bed material sample was taken. The characteristics of the bed material were determined in the VAT, the Visual Accumulation Tube at DELFT HYDRAULICS. Table 3.1 shows the results of the average values of the two experiments.

D_x	D_{10} [μm]	D_{50} [μm]	D_{90} [μm]
mean sediment size	76	95	131

Table 3.1 Mean D_x-values of the bed material

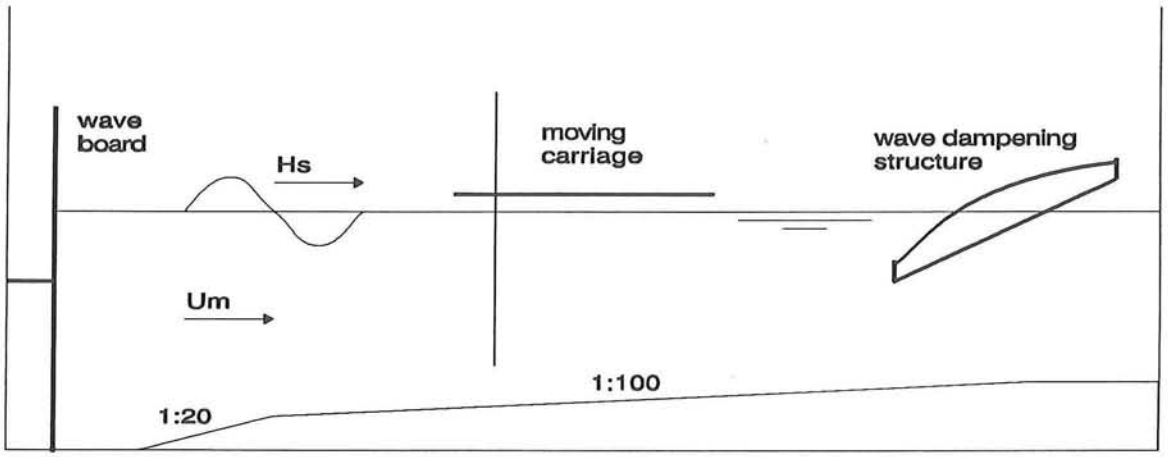

Figure 3.2 Physical model with measuring section, series A

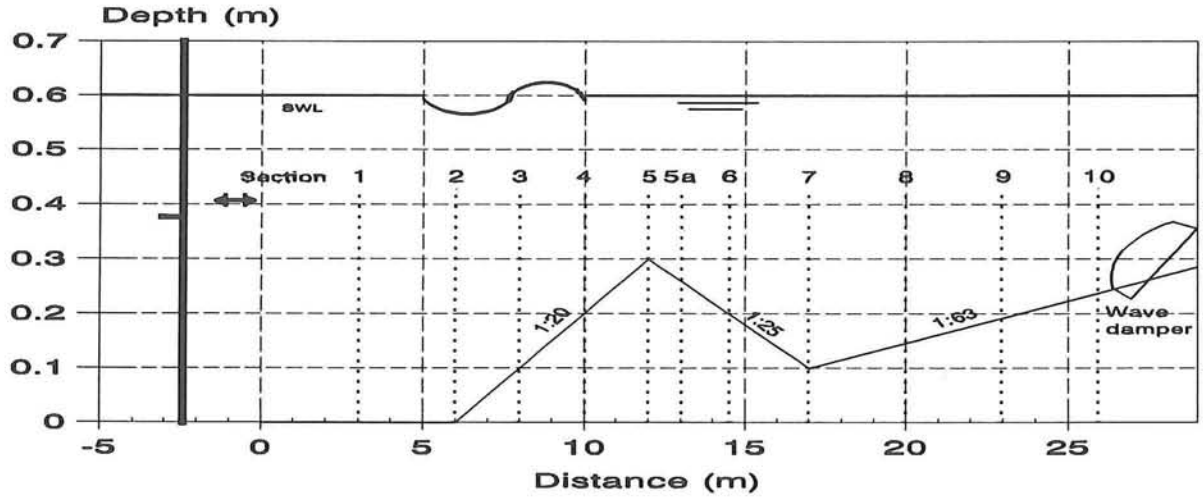

Figure 3.3 Physical model with measuring sections, series B

Because of the fact that the sediment was brought into suspension by wave movement and transported along the flume, there was a loss of mostly fine material. At regular times the sand bed was resupplied and mixed.

3.3 Measured parameters, methods and instruments

3.3.1 Introduction

The following measuring methods will be discussed:

- Time- and bed-averaging

The following parameters, and the instruments used to measure these parameters during the experiments, will be discussed:

- Mean bed level
- Discharge
- Water level
- Wave parameters and spectrum
- Sediment concentration
- Fluid velocity
- Ripple parameters
- Particle diameters of bed material
- Particle diameters of suspended material and fall velocity

Also the measuring principle of the ASTM will be discussed in this paragraph.

3.3.2 Time- and bed-averaging

Local and instantaneous concentration measurements show random variations of 50 to 100% (Bosman, 1982, 1985), because of their sensitivity for local conditions, especially in the near bed zone. A time- and bed-averaging method can be used to reduce variations in the concentration measurements. The bed-averaging was performed as in former studies: the measuring instruments were mounted on a moving carriage (See Figure 3.4 and Photo 3.1). In series A the carriage moved over 0.70 m and vice versa, with a speed of 0.02 m/s. In series B the carriage moved over only 15 cm, because of the presence of the steep bar slopes.

3.3.3 Mean bed level

To determine the mean bed level δ in the measuring section, a Profile Follower (PROFO) was used (See Photo 3.2). This instrument was mounted on the moving carriage. The

PROFO-signal was simultaneously stored in the computer and averaged by a Mean Value Meter (MVM). The computer program and the MVM both gave the mean value of δ, the distance between the mean bed level and a chosen reference level ('zero-level'), in this case the bottom level at the beginning of the flume. The mean bed level was determined before and after each experiment. The mean value of δ was used to determined the final height of the measuring instruments above mean bed level.

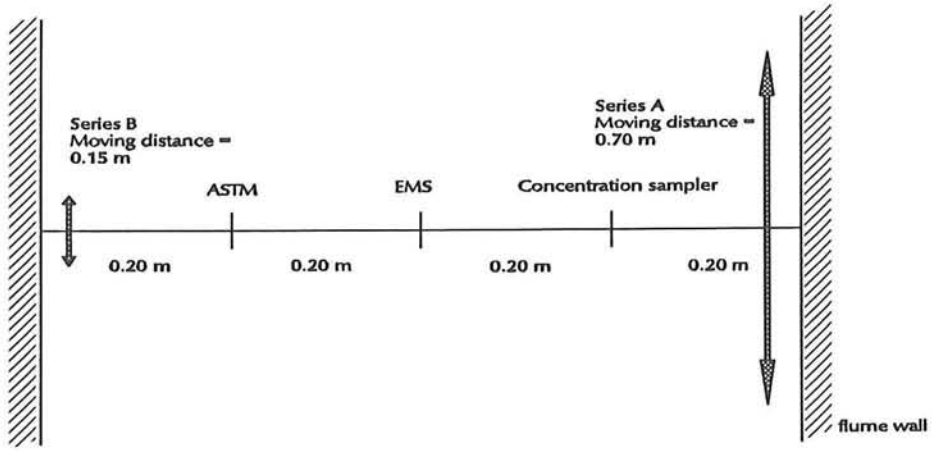

Figure 3.4 Carriage, moving distances and probes

3.3.4 Discharge

To get an estimation of the desired current velocity U_m, the discharge Q was measured using a Rehbock weir. The accuracy of the Rehbock weir from the 'Grote Speurwerk' flume in case of a small discharge is approximately 10 %. Also the fluid velocity was measured at a height of 0.4*h, as an indication of the mean velocity.

3.3.5 Water level

The water level in the flume was measured at one point. Near the wave board the water level was determined using an point gauge. During each test the water level could decrease with 2 to 4 mm, as a result of the pumping system and the splashing of the breaking waves.

This water level was also related to the zero-level, so the water depth relative to the mean bed level, h, can be determined as:

$$h = h_0 - \delta$$

3.3.6 Wave parameters and spectrum

Series A: In each experiment, the wave spectrum was determined at two locations in the flume. One wave height meter (WHM) was placed on the carriage and the second was placed 0.70 m behind the carriage, to check the first.
Series B: In each experiment, the wave spectrum was determined at two locations in the flume. One wave height meter (WHM) was placed on the carriage and one on top of the sand bar. The output of the WHM placed on the carriage was used to represent the wave conditions at the measuring section, while the other wave height meter was used to check the uniformity of the wave conditions in the flume.
The data of the WHM's are stored in the computer (See Photo 3.3 and 3.4). These files have been analysed using the software package AUKE-PC, developped by DELFT HYDRAULICS. The output of the programs are several wave and spectrum parameters. The output given by AUKE-PC were a.o.:

- significant wave height ($H_{1/3}$)
- peak frequency (f_p)
- peak period ($T_p = 1/f_p$)
- moments (m_0, m_2, m_4)
- zero crossing period ($T_z = \sqrt{(m_0/m_2)}$)
- wave height ($H_{m0} = 4*\sqrt{m_0}$)
- narrowness spectrum ($\epsilon 2$)
- broadness factor spectrum ($\epsilon 4$)

With the software package it was possible to create an exceedance curve and an energy density spectrum. The wave height distribution can be described by a Rayleigh distribution, because the spectrum is single topped (Battjes, 1982).

3.3.7 Sediment concentration measurements

The sediment concentrations measurements were carried out using an array of 10 brass intake tubes of 3 mm internal diameter (See Figure 3.5 and Photo 3.5). This concentration sampling instrument was attached to the moving carriage; the openings of the intake tubes were placed perpendicular to the current direction. Each tube was connected to a pump, bringing the sediment and water mixture with a 1.5 m/s intake velocity in a 10 l bucket. The intake tubes were used to determine the concentration distribution over the water depth.

In the earlier 100-μm-flume-study (1988) a test was carried out to study the influence of the measuring equipment on the measured concentrations. A comparison was made between the array of 10 intake tubes and a single intake tube. The conclusion was, that the differences in concentration between the array of 10 intake tubes and the single tube are within the standard deviation of the concentration.

The sediment concentrations were measured by the following procedure, which is almost the same as in the earlier studies. First, with the use of the PROFO, the mean bed level δ was determined. The concentration sampler was then adjusted just above the highest ripple top. This was 2.0 or 2.5 cm above mean bed level, depending on the height of the ripples. For adjusting, the water level was used, which was related to the reference level. Before starting the test, the carriage was moved along the measuring section. This was done to check whether the sediment concentration sampler was moving freely over the ripples.

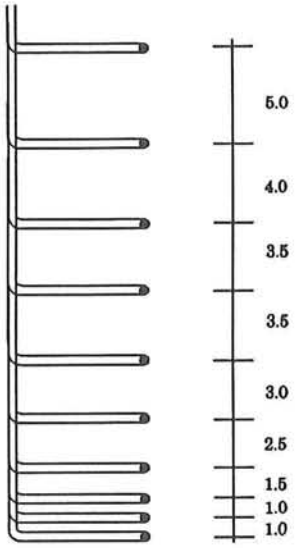

Figure 3.5 Concentration sampler with distance between intake tubes (measures in cm)

The test was now ready to start, the carriage moving to perform bed-averaging, and the pumps running for 10 minutes. In this time the ten buckets were filled (See Photo 3.6). After filling, the water in the buckets was poured off and the remaining sediment was washed out in a volume meter (See Photo 3.7). The volume meter consists of 10 small calibrated glass cylinders with decreasing diameters (See Photo 3.8). By reading the height of the sediment in the cylinder, the wet sediment volume was measured. Using a calibration table for each cylinder, the dry mass was determined for every bucket. In the calibration table a correction factor, the so-called trapping factor, was used to determine the concentration properly. This trapping factor is necessary to eliminate errors in the

measured concentration, because of the fact that the sediment particles can not completely follow the curved water particles trajectories to the intake tubes placed perpendicular to the wave direction (Bosman, Van der Velden and Hulsbergen, 1987).
In all, two series of concentration measurements were carried out during each test. After the two series again the mean bed level was measured. Based on these two concentration measurements, a mean, minimum and maximum of the concentrations was determined.
All sediment samples were collected in one sample bottle for analysis of the fall velocities (w_{10}, w_{50}, w_{90}) and the particle diameters (D_{10}, D_{50}, D_{90}) of the suspended sediment for each test. These parameters were determined by the Visual Accumulation Tube of DELFT HYDRAULICS.
In all experiments instantaneous sediment concentrations were measured by means of the ASTM (see Section 3.3.12).

3.3.8 Fluid velocity measurements

The fluid velocities were measured using an Electro Magnetic Velocity meter (EMS), see Photo 3.1. This instrument generates an electro magnetic field; the degree of disturbance of this field is a measure for the fluid velocity at the position of the measuring volume of the probe, which is 3 mm below the probe. The time-averaged fluid velocity was determined using a mean value meter (MVM). The MVM averages the electronical input signal over a chosen time period. A period of 300 seconds appeared to give reproducible results.
The EMS was also attached to the moving carriage. The fluid velocities were measured at the same height positions above mean bed level as the intake tubes of the concentration sampler. The measuring height of the EMS was adjusted using the reading scale of the attached to the EMS and the ASTM.
In all tests, instantaneous fluid velocities were also measured by means of the ASTM (see Section 3.3.12).

3.3.9 Ripple parameters

In each experiment ripple registrations were made using the PROFO (See Photo 3.2) and a penrecorder. These registrations were done before and after each test.
From these registrations the following ripple parameters were determined:

- mean ripple height r
- mean ripple length λ
- mean ripple steepness r/λ

The observed ripples are shown in Photo 3.9 and 3.10.

3.3.10 Particle diameters of bed material

Two bed material samples were taken during all tests. These two samples were analysed in the Visual Accumulation Tube of DELFT HYDRAULICS. The particle diameters D_{10}, D_{50} and D_{90} were computed from the measured fall velocity values. See also Section 3.2, Table 3.1.

3.3.11 Particle diameters of suspended material and fall velocity

Also the suspended sediment samples of each experiment, were analysed in the Visual Accumulation Tube of DELFT HYDRAULICS. Based on these results the particle diameters D_{10}, D_{50} and D_{90}, and the fall velocity parameters w_{10}, w_{50} and w_{90} can be determined. The magnitude of the suspended sediment size is presented in Tables 3.2 and 3.3.

D_x	D_{10} [μm]	D_{50} [μm]	D_{90} [μm]
Mean	74	94	130
Minimum	64	82	112
Maximum	85	114	149

Table 3.2 Sediment size suspended material, series A

D_x	D_{10} [μm]	D_{50} [μm]	D_{90} [μm]
Mean	64	85	121
Minimum	50	69	97
Maximum	77	96	134

Table 3.3 Sediment size suspended material, series B

A detailed description of the VAT is given in the 200-μm-flume-study (1987).

3.3.12 ASTM-measurements

In morphological studies the transport of suspended sediment is important. In some of these studies the sediment transport is computed from separate velocity- and concentration measurements. This method is very laborious and the time-averaged sediment transport is only measured in a restricted number of measuring points.

For sediment transport measurements DELFT HYDRAULICS developed an Acoustical Sediment Transport Meter (ASTM), see Photo 3.1. The instantaneous concentrations and velocities are determined simultaneously by measuring scattered ultrasonic energy. This energy is transmitted by a probe containing piezo-electric crystals. A transducer receives the scattered signal from the transmitter. Sediment particles in the measuring volume reflect the ultrasonic energy. The reflected energy is detected by the transducer. By determining the Doppler-shift between the received - and the transmitted signal, the velocity of the sediment particles can be measured. The intensity of the received signal is related to the number of sediment particles in the measuring volume and can be used as a measure for the sediment concentration. For large sediment concentrations, the received signal is too weak for accurate measurements. The scattered signal can be corrected with the help of a second transducer. This transducer directly receives part of the transmitted signal (see Figure 3.6). The relation between the output signal of the ASTM and the concentration and velocity is approximately linear.

During each experiment the ASTM measurements were done simultaneously with the EMS measurements. At 10 different heights above the bed the instantaneous concentrations and velocities were measured during 5 minutes. A calibration factor for the ASTM output signal (voltage) was computed using the concentrations from the pump measurements of series A. For the present study the calibration was found to be:

$$c(t) = 2.55 * V \qquad (3.1)$$

where	c(t)	:	bed-averaged concentration	(kg/m^3)
	V	:	output signal ASTM	(Volt)

The time-averaged concentrations and velocities measured with the ASTM, obtained from mean value meters, are presented in the Experimental Data Tables (Part I). The instantaneous concentrations and velocities will be used to estimate the wave related part of the sediment transport. The results of these computations will be presented in a later report.

3.3.13 Measuring procedure

1. Calibration of the EMS at still water.

2. Generation of the desired discharge by starting the pump system, opening the valves and measuring the mean velocity at approximately 0.4 h above the bed (experiments with current).

3. Generation of the desired water depth by adjusting the overflow weir.

4. Calibration of the wave height meters.

5. Switching on wave generator.

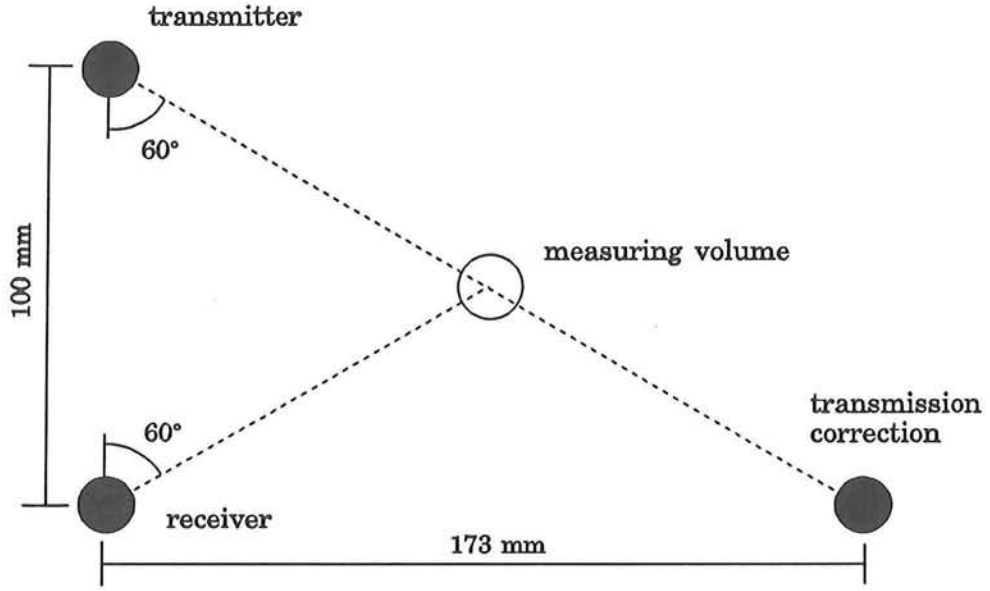

Figure 3.6 Acoustical Sediment Transport Meter

6. Waiting period of 15 minutes for generation of the characteristic ripple pattern and checking of the significant wave height and water depth.

7. Determination of the water temperature.

8. Turning off wave generator.

9. Registration of the ripple pattern with the PROFO and determination of the mean bed level.

10. Installation of the concentration sampler, the velocity meter and the ASTM just above the highest ripple top.

11. Switching on wave generator.

12. Starting computer program for data processing of wave height meters, EMS and ASTM.

13. Starting pump measurements simultaneously at 10 heights above mean bed level (15 minutes).

14. Measuring concentrations and velocities with ASTM and velocities with EMS at 10 heights above mean bed level (5 minutes per height above the bed).

15. Determination of sediment concentrations with the volume meter and putting the samples in the sample bottles.

16. Determination of the ripple migration. Drawing 6 ripples on the flume window and determination ripple migration after approximately 5 minutes. (Only experiments with current.)

17. Turning off wave generator.

18. Determination of the water depth with a point gauge and the mean bed level with the PROFO after the measurement.

19. Measuring of fluid velocities at 10 heights above mean bed level (5 minutes per height above mean bed). Only experiments with current.

20. Turning off flow by closing the valves and turning off the pump system (experiments with current).

21. Calibration of the EMS at still water (for determination of the drift, see 1.).

3.3.14 Experimental programme

Experimental programme Series A

In series A of the present study 23 experiments were carried out in the 'Grote Speurwerk' flume of the Laboratory of Fluid Mechanics (Delft University of Technology). In a water depth of h=0.30 m, experiments were done with three different wave heights and three different current velocities. The experiments are identified by a test number:

T xx yy zz

where	xx	:	significant wave height H_s	(m)
	yy	:	depth-averaged fluid velocity U_m	(m/s)
	zz	:	ordernumber	

In Table 3.4 the experimental programme of series A of the present study is presented. In this table the approximate H_s and U_m values are given; in the Experimental Data Tables and Table 4.2.1 (Part I) the precise values for the wave height and the current velocities

are presented.

	H_s = 0.10 m	H_s = 0.14 m	H_s = 0.16 m
U_m = 0.00 m/s	T 10 00 1 T 10 00 2	T 14 00 1 T 14 00 2 T 14 00 3	T 16 00 1 T 16 00 2 T 16 00 3
U_m = 0.10 m/s	T 10 10 1 T 10 10 2 T 10 10 3	T 14 10 1 T 14 10 2 T 14 10 3 T 14 10 4	T 16 10 1 T 16 10 2
U_m = 0.20 m/s	T 10 20 1 T 10 20 2	T 14 20 1	T 16 20 1 T 16 20 2
U_m = 0.30 m/s		T 14 30 1	

Table 3.4 Experimental programme series A

Experimental programme Series B

In series B measurements have been made in 10 cross-sections. In series B1 a relatively small wave height was present. The wave height on top of the bar was 0.177 m. The incoming wave height was 0.160 m.
In series B2 the wave height was slightly larger. On top of the sand bar a wave height of 0.201 m was measured. The incoming wave height was 0.189 m.
In series B1 measurements were made in cross-sections: 1, 2, 3, 4, 5, 6, 7, 8, 9, 10. In series B2 measurements of the wave height, sediment concentration and fluid velocity were made in cross-sections 1, 2, 3, 4, 5, 5a, 6, 7, 8, 9 (see Figure 3.3).

In Chapter 4 and Chapter 5 the experimental results of series A and series B will be presented.

Photo 3.1 The measuring instruments: ASTM, EMS and concentration sampler

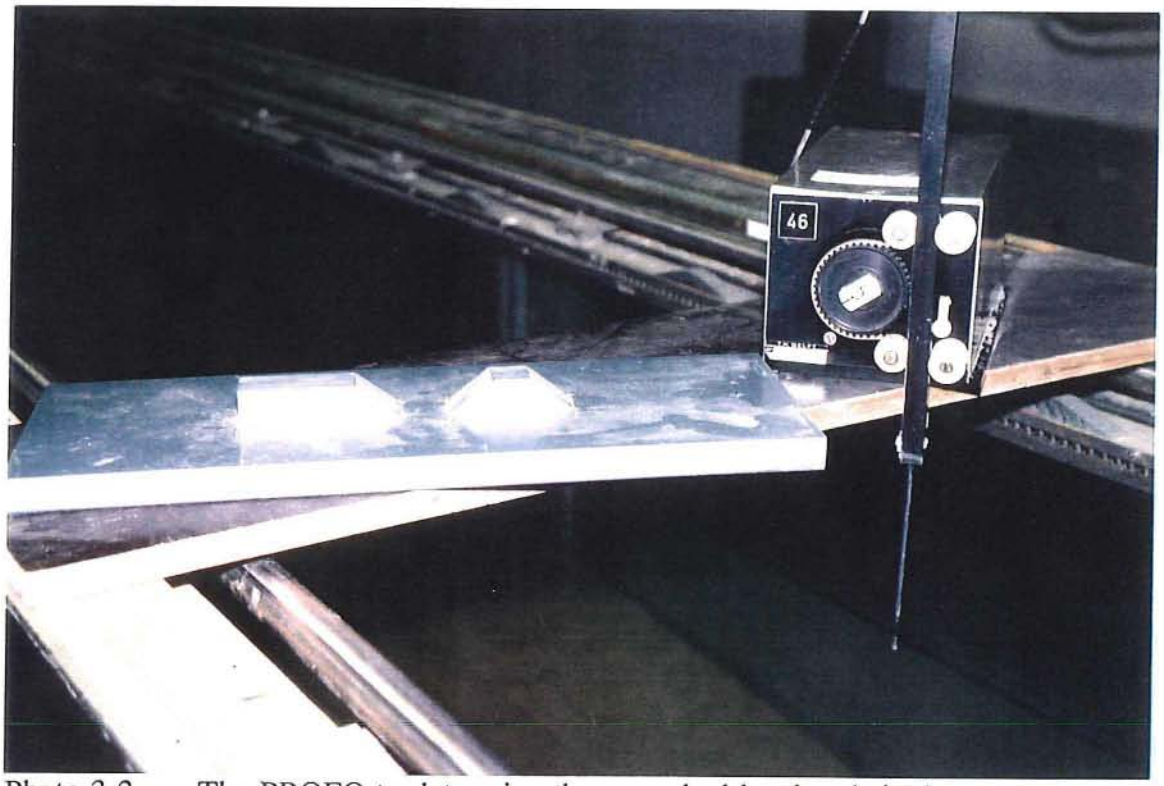

Photo 3.2 The PROFO to determine the mean bed level and ripple parameters

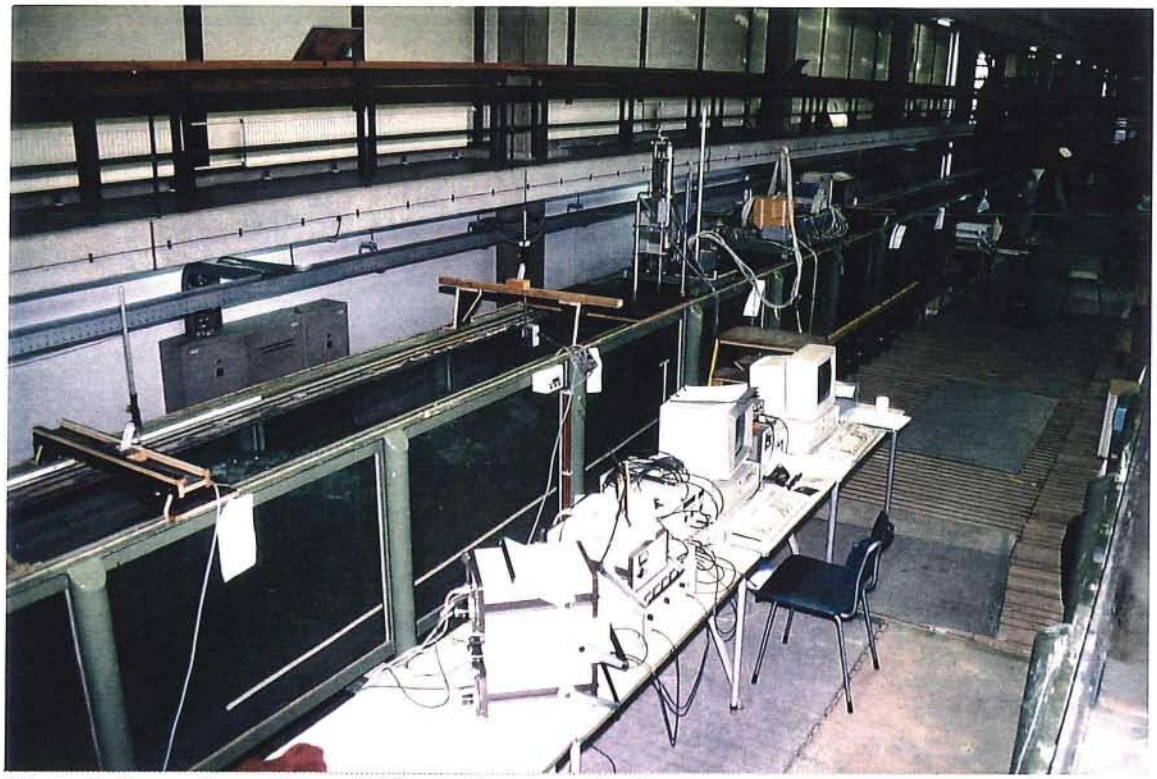

Photo 3.3 Overview of 'Grote Speurwerk' flume

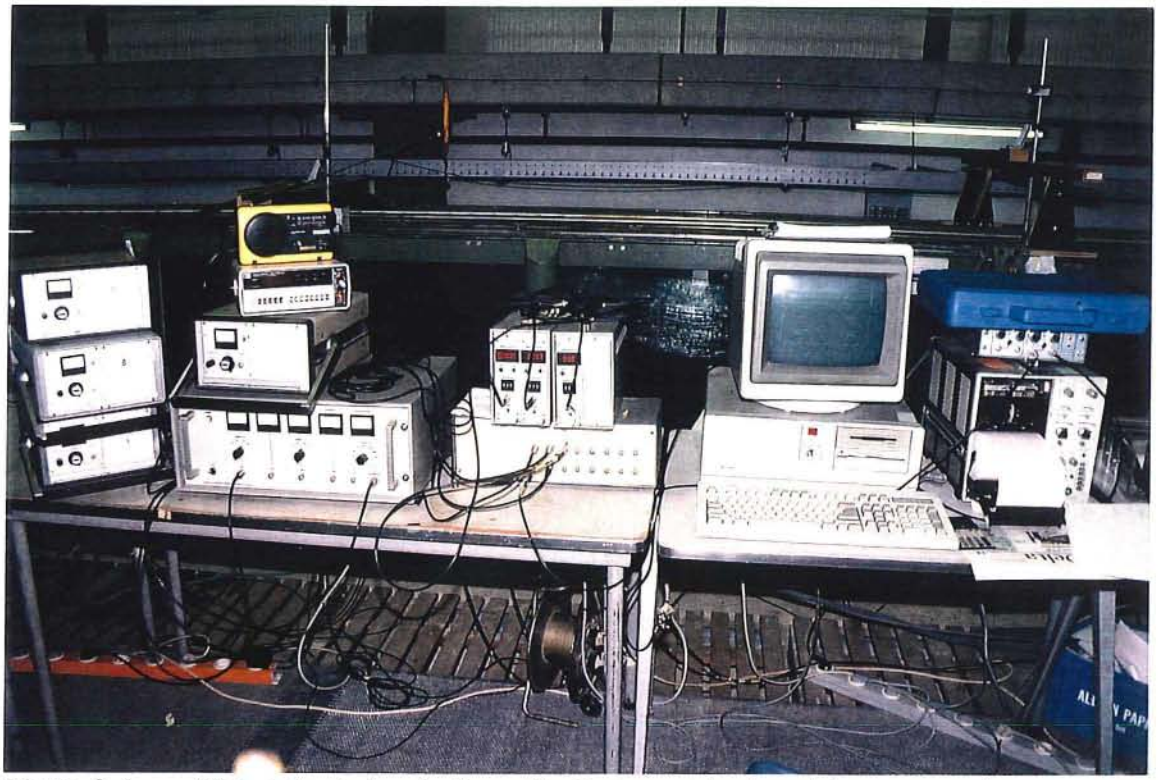

Photo 3.4 The output signals from the instruments stored in a computer

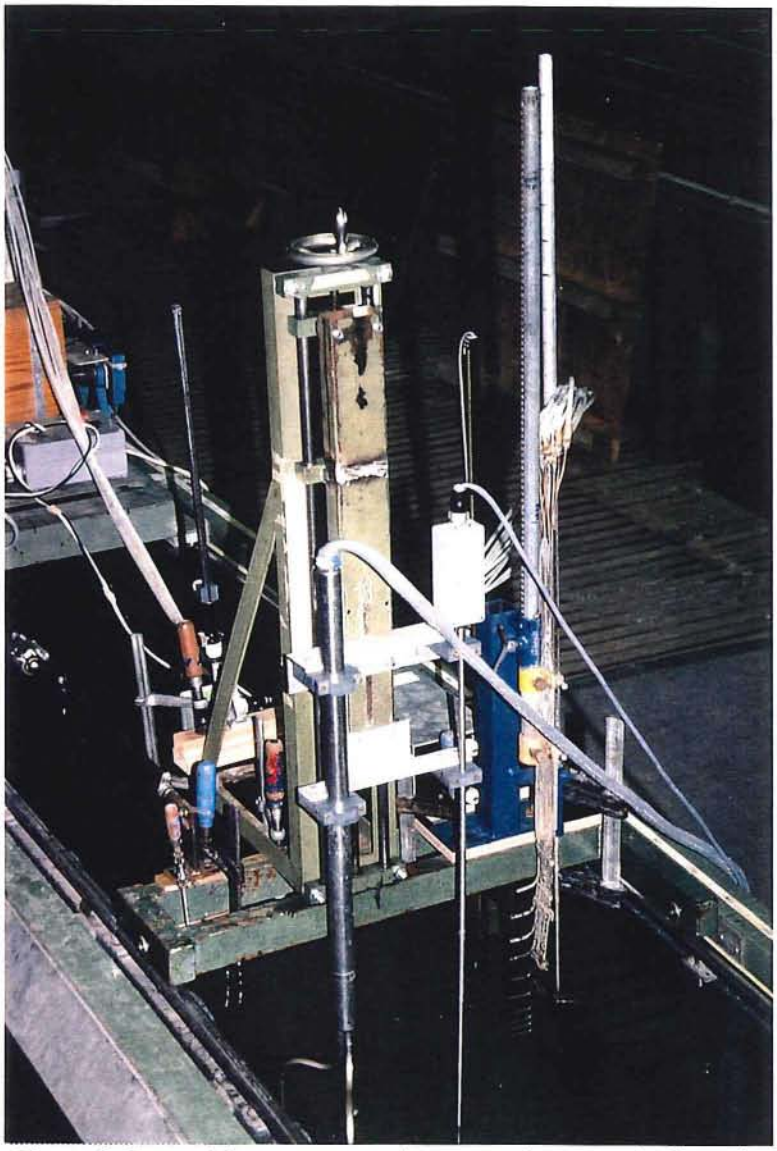

Photo 3.5 The concentration sampler attached to the moving carriage

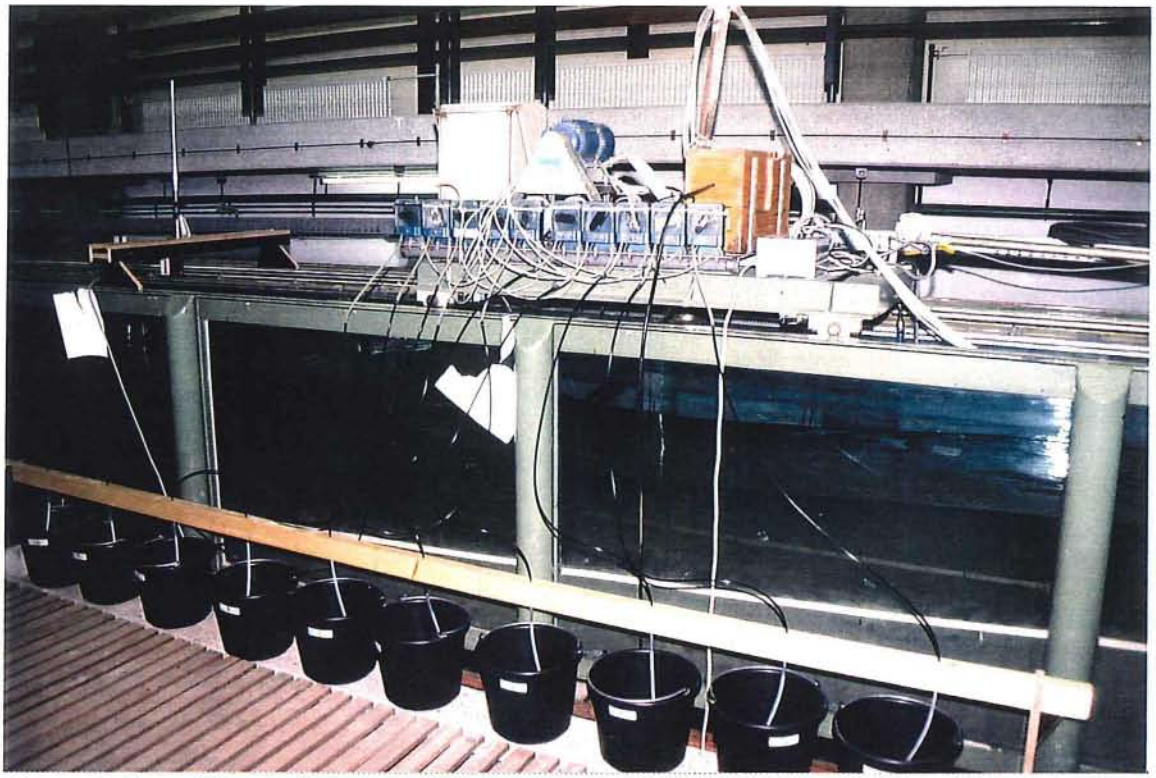

Photo 3.6 The sediment and water mixture brought into a 10 l bucket

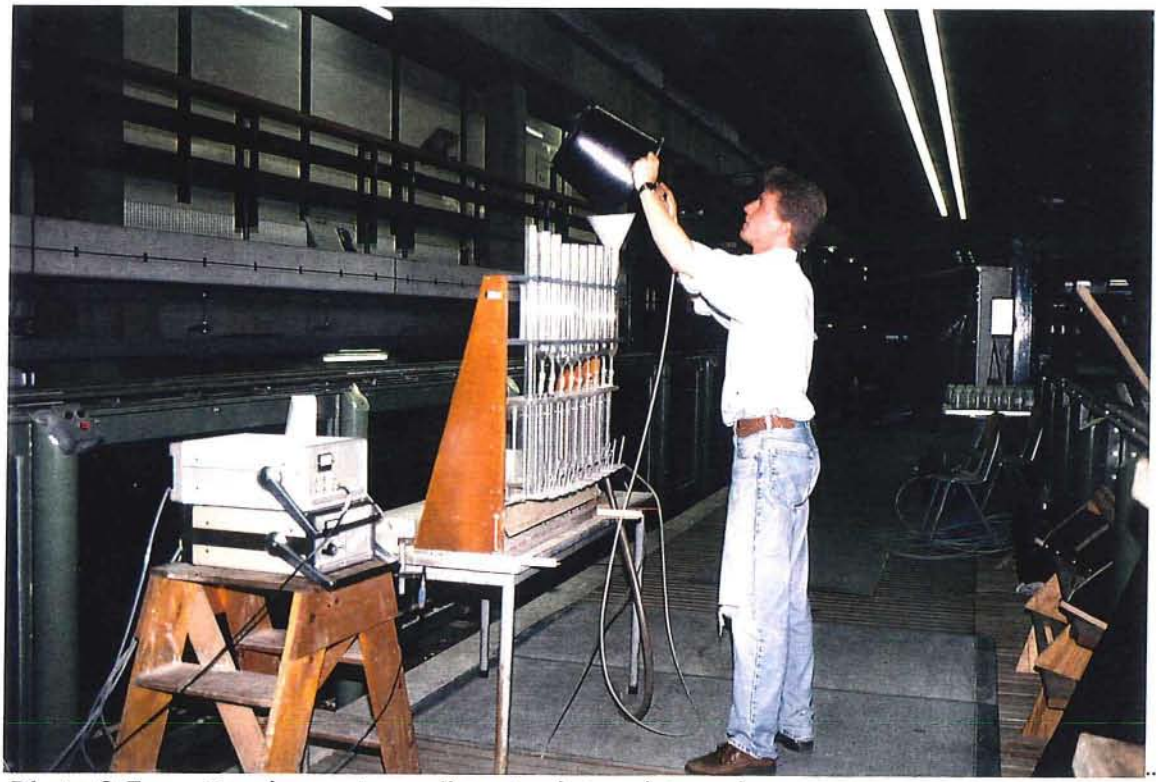

Photo 3.7 Pouring water-sediment mixture into volume meter

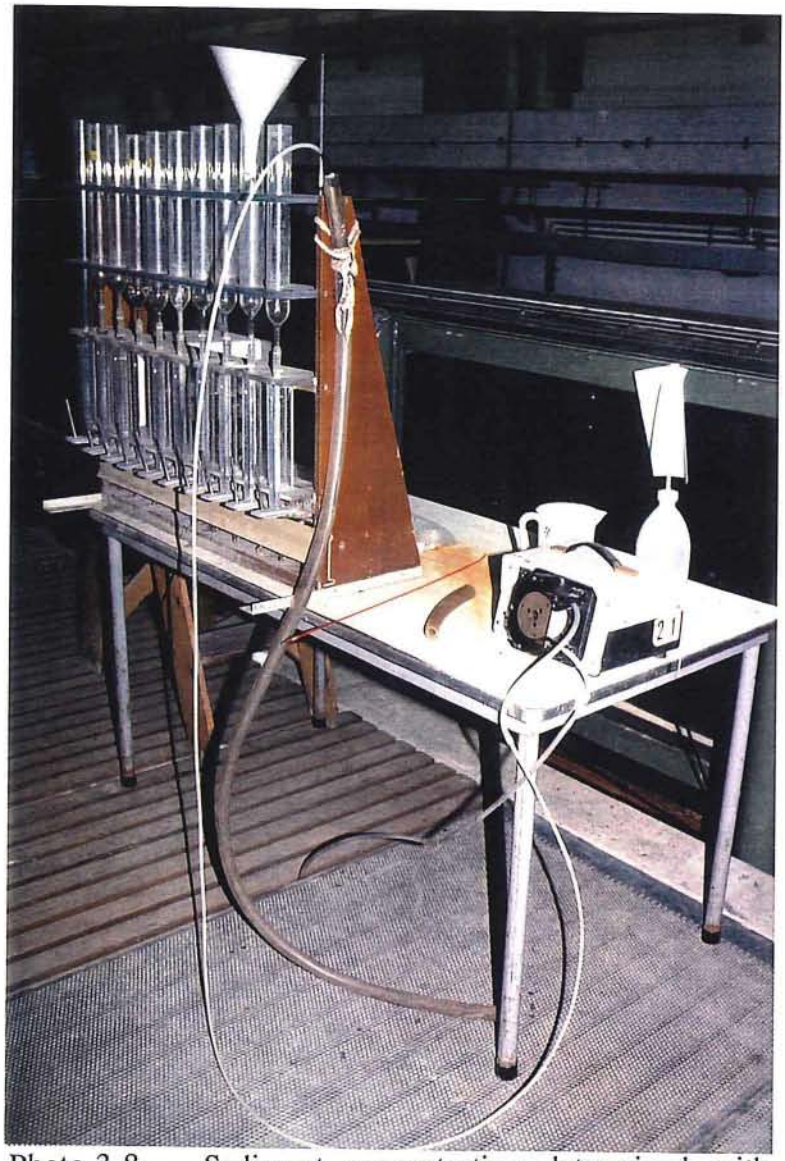

Photo 3.8 Sediment concentration determined with the volume meter

Photo 3.9 Ripples formed by wave and current movements

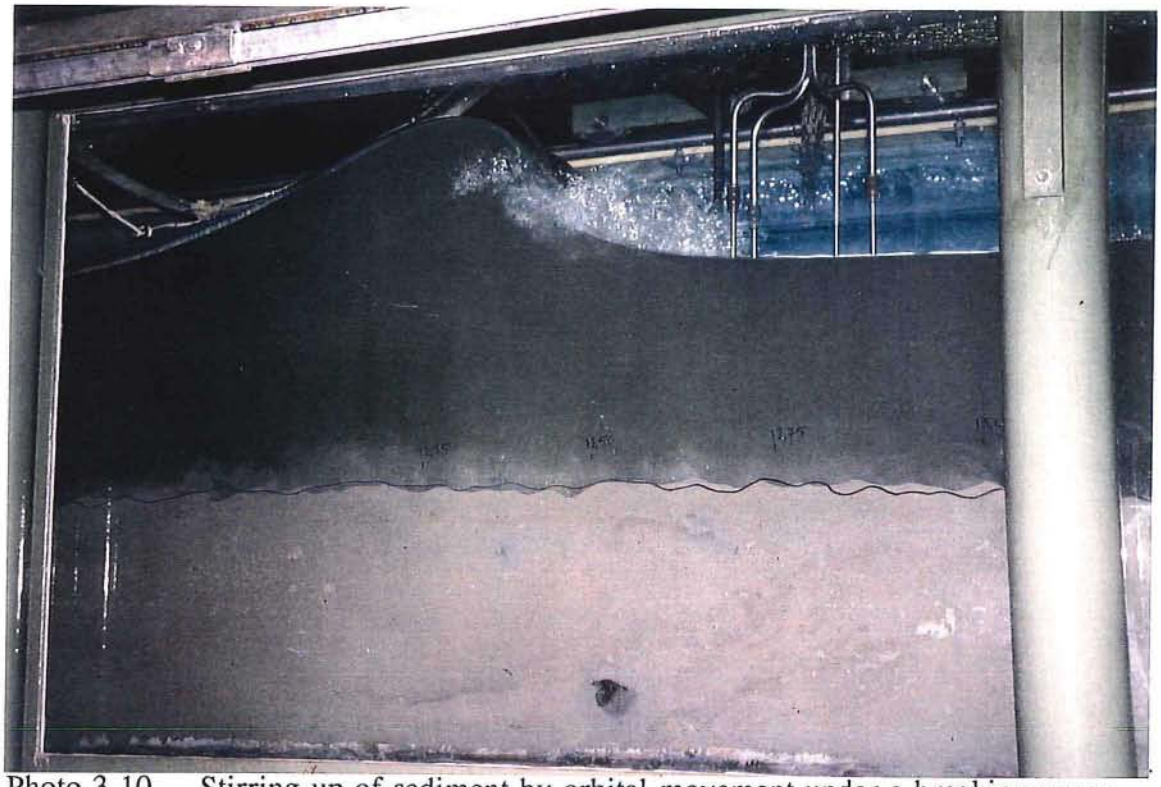

Photo 3.10 Stirring up of sediment by orbital movement under a breaking wave

4 Experimental results A-series

4.1 General

As indicated in Chapter 3 the experiments are divided into two series. In this chapter the results of the first series A are analysed and presented. Series B1 and B2 will be dealt with in Chapter 5.

The objectives of the experiments done in testseries A are:

1 Identification of the relationship between current related sediment transport, wave height and current velocity, and comparison with earlier studies.
2 Investigation of the influence of the breaking of waves on the current related sediment transport parameters.
3 Investigation of effective bed roughness of wave and current induced ripples.

In Figure 4.1 a sketch of the flume is presented.

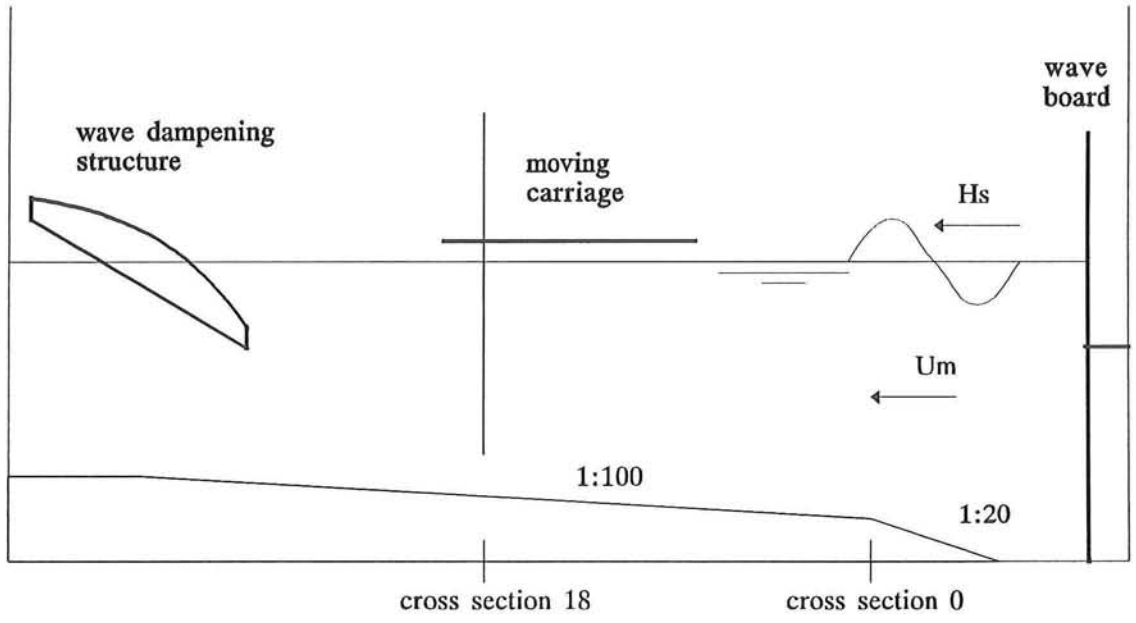

Figure 4.1 Sketch of the flume with measuring section

Water entering the flume had no initial sediment load. The concentrations profiles had to be build up completely in the section with the sand bed. To provide enough length to reach equilibrium concentrations over the depth, the measuring section was situated at a distance of 18 m from the beginning of the sand bed.

Some of the present results are compared with the results of the three earlier studies done by Van der Kaaij and Nieuwjaar (1987), Van Kampen and Nap (1988) and Havinga (1992). These studies will herein be referred to as "the earlier 200-μm-flume-study (1987)", "the earlier 100-μm-flume-study (1988) and "the earlier 100-μm-basin-study (1992)".

In this study mean, maximum and minimum values of the measurements are presented. In Part I of this report the basic data of all 23 experiments done in series A are given in tables. From these, the following parameters have been computed.

- Depth averaged fluid velocity
- Mean sediment loads L_s (three methods)
- Mean sediment transport rates S_s (three methods)

In the next sections, the following parameters will be described and discussed successively:

-	Wave characteristics	(4.2)
-	Fluid velocities	(4.3)
-	High- and low-frequency effects	(4.4)
-	Sediment concentration	(4.5)
-	Sediment loads	(4.6)
-	Sediment transport rates	(4.7)
-	Ripple parameters	(4.8)
-	Size and fall velocity of suspended sediment	(4.9)
-	Bed roughness	(4.10)

4.2 Wave characteristics

4.2.1 Wave spectra

The computed wave spectra are influenced by the presence of a current. Spectra, measured when waves travel with a following current, are less narrow then those measured without a current. In the present study the broadness factor ϵ_4 varied just slightly. The averaged values of ϵ_4 for different current strengths are given below. From this one can see that the variations in broadness are less than 3%.

U_m = 0.00 m/s $\quad\quad$ ϵ_4 = 0.728
U_m = 0.10 m/s $\quad\quad$ ϵ_4 = 0.745
U_m = 0.20 m/s $\quad\quad$ ϵ_4 = 0.750

In Figure 4.2 an example is shown of the spectral density function measured for H_s=0.14m and U_m=0.20 m/s.

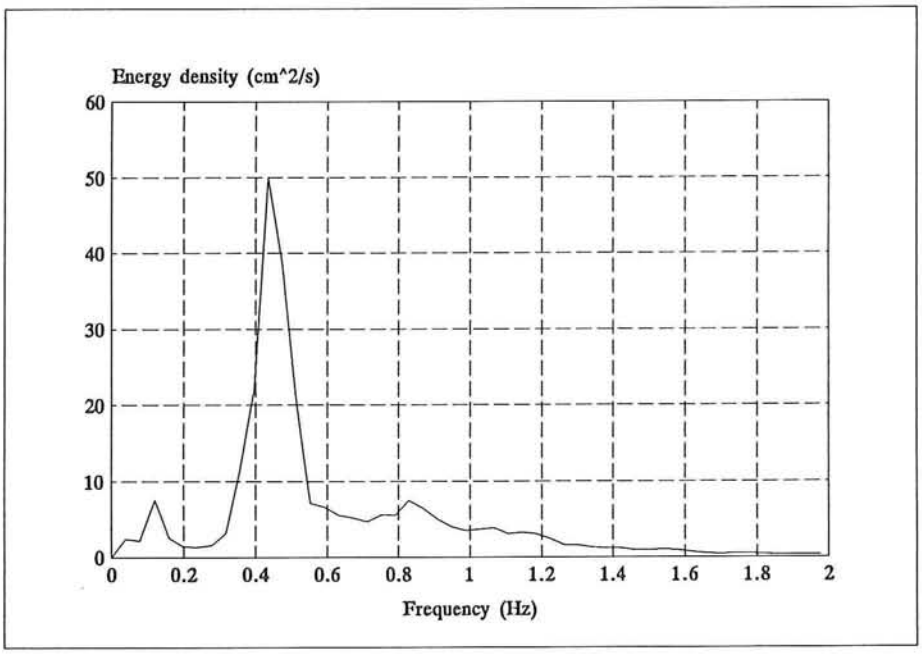

Figure 4.2 Energy density spectra, H_s=0.14 m, U_m=0.20 m/s

4.2.2 Wave length and peak period

When a current is combined with the waves, the length of the waves will be influenced. If a current is in the same direction as the wave propagation direction, the wave length will increase. This can be understood from the characteristic wave parameters.

$$k = \frac{2\pi}{L} = \frac{\omega}{c} = \frac{\omega'}{c'} \qquad (4.1)$$

where				
	c	:	wave celerity	(m/s)
	c'	:	wave celerity in case of waves and current	(m/s)
	ω	:	wave frequency, $2\pi/T_p$	(1/s)
	T_p	:	wave spectrum peak period	(s)
	ω'	:	wave frequency in case of waves and current, $2\pi/T_p'$	(1/s)
	T_p'	:	wave spectrum peak period relative to the current	(s)
	k	:	wave number, 2π/L	(1/m)

$$c' = c + U_m \qquad (4.2)$$

where				
	U_m	:	depth averaged fluid velocity	(m/s)

Substitution of Eq.4.2 in Eq.4.1 gives:

$$\omega' = c'.k = (c + U_m).k = \omega + k.U_m \qquad (4.3)$$

where			
	kU_m	:	Doppler-shift

For dispersive waves holds:

$$\omega = \sqrt{gk \tanh kh} \qquad (4.4)$$

where				
	g	:	acceleration of gravity	(m/s^2)
	h	:	waterdepth	(m)

Substitution of Eq.4.4 in Eq.4.3:

$$\omega'\sqrt{\frac{h}{g}} = \sqrt{kh \tanh kh} + \frac{U_m}{\sqrt{gh}}kh \qquad (4.5)$$

The peak period relative to the current T_p' and the wave length L can be computed numerically from the waterdepth h and the absolute peak period T_p which are known parameters. The results of the above computations are given in Table 4.2.1 (Part I). Comparing the experiments with and without a current it can be observed that the relative period T_p' and wave length L in the presence of a current are at maximum 12% larger than the absolute wave period and wave length without a current.

4.2.3 Orbital movement parameters

Two parameters, which characterize the wave action just above the bed, are introduced here:

- $\hat{U}_{b,on,tot}$: a characteristic orbital horizontal *onshore* velocity amplitude just outside the wave boundary layer (m/s)
- $\hat{U}_{b,off,tot}$: a characteristic orbital horizontal *offshore* velocity amplitude just outside the wave boundary layer (m/s)
- $\hat{A}_{b,on,tot}$: a characteristic orbital horizontal displacement amplitude just outside the wave boundary layer (m)

The characteristic orbital velocities $\hat{U}_{b,on,tot}$ and $\hat{U}_{b,off,tot}$ were computed for each experiment as the significant on- and offshore peak velocity, defined as the average of the one-third largest velocity amplitudes (see Section 4.4).

The characteristic orbital displacement $\hat{A}_{b,on,tot}$ was computed using the significant onshore peak velocity $\hat{U}_{b,on,tot}$ and the relative wave spectrum peak period T_p' to account for the presence of the current:

$$\hat{A}_{b,on,tot} = \frac{T_p'}{2\pi} * \hat{U}_{b,on,tot} \tag{4.6}$$

The results of the above computations are given in Table 4.2.1 (Part I).

4.2.4 Breaking waves

The maximum height of a wave is limited by a maximum wave steepness for which the wave form can remain stable. Waves reaching the limiting steepness will begin to break and consequently will dissipate a part of their energy. From theoretical considerations the limiting steepness is found to be:

$$\frac{H}{L} = \frac{1}{7} \tanh\left(\frac{2\pi h}{L}\right) \tag{4.7}$$

In deep water Eq.4.7 reduces to:

$$\frac{H}{L} = \frac{1}{7} \approx 0.142 \tag{4.8}$$

In shallow water Eq.4.7 becomes:

$$\frac{H}{L} = \frac{1}{7} \frac{2\pi h}{L} \approx 0.9 \frac{h}{L} \tag{4.9}$$

As can be seen the breaking of a wave occurs due to:

- maximum wave steepness, H_s/L
- maximum wave height-water depth ratio, H_s/h

In Figure 4.2 (Part I) the relation between the ratio H_s/h and the fraction of breaking waves Q_b is presented for different values of the wave steepness H_s/L.

The computed relation between the wave height-water depth ratio H_s/h, the wave steepness H_s/L and the fraction of breaking waves Q_b using a least square method is found to be:

$$Q_b = 9.9 * 10^{-6} * \left(\frac{H_s}{h}\right)^{14.5} * \left(\frac{H_s}{L}\right)^{-5.9} \tag{4.10}$$

where				
	Q_b	:	fraction of breaking waves	(-)
	H_s	:	significant wave height	(m)
	h	:	mean water depth	(m)
	L	:	wave length	(m)

The correlation between this formula and the measured Q_b has a value of ρ=0.978. The correlation factor gives an estimation of the reliability of the formula, which is maximum for $\rho = 1.00$.

4.3 Fluid velocities

4.3.1 General

The time- and bed-averaged velocities were measured as is described in Section 3.3.8. For each experiment the velocities were only measured once. In the Figures 4.3.A.1 - 4.3.A.23 (Part I) the velocity profiles of all experiments are presented. The experiments are identified by a test number:

T xx yy zz

where	xx	:	significant wave height H_s	(cm)
	yy	:	depth averaged fluid velocity U_m	(cm/s)
	zz	:	ordernumber	

For example: T 10 10 2 stands for an experiment with an approximate significant wave height of 10 cm, and an approximate mean current of 10 cm/s. This is the second test done with this wave height and current velocity.

In case of waves without a current, the absolute velocities are given. These velocity profiles are presented in the Figures 4.3.A.1 - 4.3.A.8 (Part I). Negative velocities were measured in seaward direction. The mean heights above the mean bed level z are divided by the mean water depth h.

In the Figures 4.3.A.1 - 4.3.A.8 (Part I) also the velocities measured with the Acoustical Sediment Transport Meter (ASTM) are presented. This instrument determines the velocity of the sand particles by measuring scattered ultrasonic energy. From the figures it can be seen that the velocity of the sand particles measured with the ASTM is systematically smaller than the fluid velocity measured with the EMS. This may be explained by the inertia of the sediment particles.

When a current is superimposed on the waves, the time- and bed-averaged velocities U(z) are divided by the depth-averaged velocity U_m measured in the current alone situation. The mean heights above the mean bed level z are divided by the mean water depth h. This is shown in Figures 4.3.A.9 - 4.3.A.23 (Part I). By making U(z) and z dimensionless, the velocity profiles, measured in different experiments can be compared.

To determine the depth-averaged velocity U_m from the measured velocities, two assumptions have been made.

First assumption: The velocity between the mean bed level and the lowest measuring point are represented by a function, corresponding with a logarithmic velocity distribution in case of a rough bed (Van Rijn 1986):

$$U(z) = U_1 \left(\frac{z}{z_1}\right)^{0.25} \qquad for\ 0 < z < z_1 \tag{4.11}$$

where	U_1	:	fluid velocity in first measuring point above the bed	(m/s)
	z_1	:	height above bed of first measuring point	(m)
	z	:	height above mean bed level	(m)

Second assumption: The mean velocity between the highest measuring z_{10} and the water surface are assumed to be equal to the measured velocity in the highest measuring point (U_{10}).

Now the depth averaged fluid velocity is determined as:

$$U_m = \frac{1}{h} \sum_{i=1}^{N} \frac{(U_i + U_{i-1}) * (z_i - z_{i-1})}{2} \tag{4.12}$$

where	U_m	:	depth averaged fluid velocity	(m/s)
	U_i	:	mean time- and bed-averaged velocity at height z_i above mean bed level	(m/s)
	N	:	total number of points (including extrapolated points)	(-)
	h	:	water depth	(m)

4.3.2 Current alone

In each experiment current velocities were also measured in absence of waves. This was done to determine the bed roughness, caused by the bed forms, generated by waves and a current.

In this section the velocity profile, in case of current alone will be analysed. This was done by comparison of the measured velocity profile, with a theoretical logarithmic distribution, presented as:

$$U(z) = \frac{U^*}{\kappa} \ln\left(\frac{z}{z_0}\right) \tag{4.13}$$

where	U(z)	:	current velocity at level z	(m/s)
	U^*	:	bed-shear velocity	(m/s)
	z	:	height above mean bed level	(m)
	z_0	:	roughness length scale (zero velocity level)	(m)

κ : the Von Karman constant (=0.4) (-)

The bed roughness length of Nikuradse K_s is computed as:

$$K_s = 33 * z_0 \qquad (4.14)$$

In the earlier 100-μm-flume-study (1988) the Vanoni-Brooks method (1957) was used to eliminate the influence of the flume walls in the estimation of the bed roughness. This method was not used in the present study because the water surface slope was not measured. In the present study it was assumed that for $z/h < 0.75$ the influence of the sidewall-roughness is negligible and the velocity profile is completely determined by the bed roughness. Therefore, to reduce sidewall effects of the flume, the lowest nine measuring points ($z/h < 0.75$) were used in the fitting procedure.

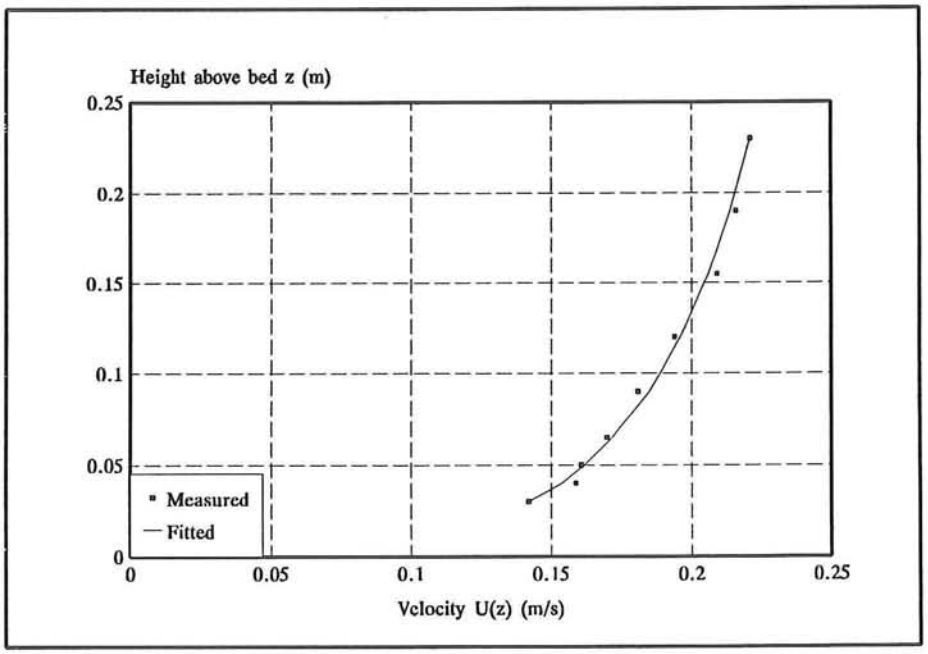

Figure 4.3 Measured and fitted velocity profile

In Figure 4.3 an example is shown of the fitted velocity profile compared to the measured profile. The correlation between the measured velocities and the fitted profile was always higher than $\rho = 0.97$. The examination of the bed roughness related to ripple parameters will be discussed in Section 4.10.

4.3.3 Wave influence

As can be observed in Figures 4.3.A.1 - 4.3.A.23 (Part I), the velocity profiles measured in case of current and waves differ from the profiles measured in case of a current alone.

Compared with the current-alone situation, the velocities measured when current and waves are present are:

- Relatively small in the near bed zone ($z/h < 0.3$)
- Still small but the difference is less in the middle layer ($0.3 < z/h < 0.6$)
- Relatively small in the upper layer ($0.6 < z/h < 0.8$)

The influence of the wave height and current strength on the observed differences is summarized as follows:

- Increasing the current strength U_m with a constant wave height leads to a decrease of the differences.

- Increasing the significant wave height H_s with a constant current velocity leads to an increase of the differences (see Figures 4.3.B - 4.3.D, Part I).

- The differences are largest in case of large wave height in combination with a weak current.

Although the wave-induced reduction of the velocities is larger in the present study, as a result of a shallower waterdepth, the change in shape of the velocity profile caused by wave action was also found in the earlier studies (100-μm-flume-study, 200-μm-flume-study) for waves propagating with a current ($\phi = 0°$).

In the earlier 100-μm-basin-study (1992) it was found that the velocities measured in case of current and waves were relatively large in the upper layers ($0.5 < z/h < 0.8$) compared to the current alone situation. This increase in velocity was more pronounced with an increasing current-wave-angle from $\phi = 60°$ to $\phi = 120°$.

In the earlier 100-μm-flume-study (1988) and 200-μm-flume-study (1987) it was also found that, for waves propagating against the current ($\phi = 180°$), the velocities in the upper layers were relatively large compared to the current alone situation.

In the present study the velocities in the upper layers ($0.5 < z/h < 0.8$) are found to be relatively small compared to the current alone situation. In this case waves are propagating with the current ($\phi = 0°$). This was also found in the earlier 100-μm-flume-study (1988) and 200-μm-flume-study (1987) for waves following the current.

The following conclusions can be drawn from the above:

- At a current-wave-angle of $\phi = 0°$ waves superimposed on a current lead to a decrease in velocities in the upper layer ($0.5 < z/h < 0.8$) compared to the current alone situation.

- At a current-wave-angle of $\phi = 60°$ waves superimposed on a current lead to an increase in velocities in the upper layer ($0.5 < z/h < 0.8$) compared to the current alone situation.

- From $\phi = 60°$ to $\phi = 180°$, the increase in velocities in the upper layer ($0.5 < z/h < 0.8$) compared to the current alone situation becomes more pronounced with increasing current-wave-angle.

In the earlier 100-μm-basin-study (1992) it was found that the velocities measured in the near bed zone ($z/h < 0.3$) in case of current and waves were relatively small compared to the current alone situation. The velocities in the near bed zone had the lowest values for $\phi = 90°$ compared to $\phi = 60°$ and $\phi = 120°$.

This decrease in velocity in the near bed zone ($z/h < 0.3$) caused by wave action was also found in the present study. In the earlier 100-μm-flume-study (1988) and 200-μm-flume-study (1987) it was found that this decrease is more pronounced for opposing waves ($\phi = 180°$) compared to following waves ($\phi = 0°$).

The following conclusion can be drawn:

- At every current-wave-angle, waves superimposed on a current lead to decreasing velocities in the near bed zone ($z/h < 0.3$) compared to the current alone situation. The extent of this decrease depends on the complicated interaction between the waves, the current and the generated ripple pattern.

4.3.4 Mass transport and return flow

Water particles are predicted to move in closed orbits by linear wave theory; i.e., each particle returns to its initial position after each wave cycle. Morison and Crooke (1953) compared laboratory measurements of particle orbits with wave theory and found, as had others, that particle orbits were not completely closed. This difference is due to the mass transport phenomenon, which is discussed in this section. The action of mass transport, extended over a long period, can be important in carrying sediment onshore or offshore, particularly seaward of the breaker position.

The massflux between wave-trough and wave-crest can be denoted by:

$$m = Q_b * m_b + (1-Q_b) * m_{nb} \tag{4.15}$$

where	m_x	:	mass flux contribution by breaking (b) and non-breaking (nb) waves	(kg/sm)
	Q_b	:	fraction of breaking waves	(-)

According to Svendsen (1984) the potential contribution of fully breaking waves to the total mass flux is given by:

$$m_b = (1 + 7 * \frac{h}{L}) * \frac{E}{c} \tag{4.16}$$

where	c	:	wave celerity	(m/s)
	E	:	$\frac{1}{8}\rho g(H_{rms})^2$, wave energy per unit surface area	(kg/s^2)
	h	:	water depth	(m)
	L	:	wave length	(m)

The contribution of non-breaking waves to the total mass flux is given by:

$$m_{nb} = \frac{E}{c} \tag{4.17}$$

Substitution of Eq.4.16 and Eq.4.17 in Eq.4.15 gives:

$$m = (1 + 7 * \frac{h}{L} * Q_b) * \frac{E}{c} \tag{4.18}$$

To balance the mass transported in the direction of the wave travel, the return flow $U_{mean,return}$ is found to be:

$$U_{mean\ return} = \frac{m}{\rho * h} \tag{4.19}$$

$$U_{mean,return} = (1 + 7 * \frac{h}{L} * Q_b) * \frac{\frac{1}{8} * \rho * g * H_{rms}^2}{\rho * h * c} \tag{4.20}$$

$$U_{mean,return} = \frac{1}{8} * (1 + 7 * \frac{h}{L} * Q_b) * \frac{g * H_{rms}^2}{h * c} \tag{4.21}$$

For relatively shallow water Eq.4.21 becomes Eq.4.22. Besides this formula of Svendsen two other expressions for the return flow are given below. A comparison of the three formulae is given in Table 4.3.1 (Part I).

Svendsen (1984):

$$U_{mean,return} = \frac{1}{8} * (1 + 7 * \frac{h}{L} * Q_b) * (\frac{H_{rms}}{h})^2 * c \tag{4.22}$$

Stive and Wind (1986):

$$U_{mean,return} = 0.1 * (\frac{g}{h})^{0.5} * H_{rms} \tag{4.23}$$

Van Rijn (1990):

$$U_{mean,return} = 0.125 * (\frac{g}{h})^{0.5} * \frac{H_s^2}{h_t} \tag{4.24}$$

where				
	g	:	acceleration of gravity	(m/s^2)
	h	:	water depth	(m)
	h_t	:	water depth below wave trough	(m)
	H_{rms}	:	root mean square wave height	(m)
	H_s	:	significant wave height	(m)
	L	:	wave length	(m)
	Q_b	:	fraction of breaking waves	(-)

4.4 Asymmetry effects in velocities

4.4.1 General

In this section the asymmetry in the velocity signal caused by wave asymmetry will be discussed. In the Tables 4.4.1 and 4.4.2 (Part I) the asymmetry of the velocity signal is presented. For the lowest three measuring points of an experiment, the on- and offshore orbital peak velocity (average of the one third largest velocity amplitudes) is computed. The signals are separated into the frequency domains of long waves ($T > 5$ s) and short waves ($T < 5$ s).

The asymmetry in the velocity signal is computed by subtraction of the average velocity from the measured signal, filtering of the new signal and calculation of the orbital peak velocities from the filtered signal. An example of the measured velocity signal, the high frequency signal ($T < 5$ s) and the low frequency signal ($T > 5$ s) is presented in Figure 4.4.A (Part I). The following parameters are presented in the tables 4.4.1 and 4.4.2:

$\hat{U}_{b,on/off,high}$	:	horizontal orbital velocity amplitude of the *high frequency signal* ($T<5$s) in on- respectively offshore direction	(m/s)
$\hat{U}_{b,on/off,low}$	:	horizontal orbital velocity amplitude of the *low frequency signal* ($T>5$s) in on- respectively offshore direction	(m/s)
$\hat{U}_{b,on/off,tot}$	:	horizontal orbital velocity amplitude of the *total velocity signal* with substraction of the average velocity, in on- respectively offshore direction	(m/s)

4.4.2 Wave asymmetry

From the Tables 4.4.1 and 4.4.2 (Part I) it can be seen that for each experiment the onshore velocity is much higher than the offshore value (average onshore 42% larger than offshore). This difference is caused by the wave asymmetry (the wave crests are relatively higher than the wave troughs are low).

Also for the high-frequency signal the onshore component is found to be larger than the offshore component (average onshore 64% larger than average offshore, so even more asymmetry).

For the low frequency signal the asymmetry is less pronounced and this time the peak offshore values are larger (average 5%) than the peak onshore orbital velocities.

From the Tables 4.4.1 and 4.4.2 (Part I) it appears that the orbital peak velocity components for low-frequency are quite large. The wave height of the standing long wave observed in the flume after turning off the waveboard was never larger than 0.5 cm, which will not lead to the relatively large peak velocities for the low frequency signal found in the experiments. The driving mechanism for this slow variation of the velocity may be found in the groupiness of the short waves. The groupiness has two effects:

- The variations in short wave energy and associated radiation stresses drive so-called bound long waves, which travel at the group velocity of the short waves.
- In groups of high short waves, more sediment is stirred up due to the greater orbital velocities than in groups of small short waves. A variation in short wave energy thus leads to a variation in concentration.

The covariance between short wave energy and long wave velocity is negative if bound long waves are the dominant long wave phenomenon. A simple way to detect bound long waves is to look at the covariance function of short wave energy and long wave elevation. The results of these computations will be presented in a later report in which the instantaneous velocities and concentrations will be analyzed.

In the present study orbital peak onshore velocities of the low frequency signal of 5.7 cm/s (H_s = 0.10 m) to 14.7 cm/s (H_s = 0.16 m) are measured. It is plausible that for H_s = 0.14 m and H_s = 0.16 m, the low frequency velocity will contribute to the stirring up of sediment.

Figure 4.4.B (Part I) shows the influence of the wave steepness H_s/L on the velocity asymmetry factor A_{asymm} defined as:

$$A_{asymm} = \frac{\hat{U}_{b,on,high}}{\hat{U}_{b,on,high} + \hat{U}_{b,off,high}} \qquad (4.25)$$

From this figure it can be seen that, although not pronounced:

- An increasing wave steepness H_s/L leads to an increasing wave asymmetry.

In Figure 4.4.C (Part I) the influence of the wave height-water depth ratio H_s/h on the velocity asymmtery factor A_{asymm} is presented. From this figure it can be seen that, although not pronounced:

- An increasing H_s/h ratio leads to an increasing wave asymmetry.

Further analysis is needed to get more insight in the effect of the wave asymmetry on the sediment transport.

4.5 Sediment concentrations

4.5.1 General

The measured time- and bed averaged concentration profiles for all experiments are presented in Figures 4.5.A.1 - 4.5.A.23 (Part I), in which the mean, maximum and minimum concentration values at different heights above the bed have been plotted. The concentration values are also given in the experimental Data Tables (Part I). In the present study the time- and bed averaged concentration profile was determined as follows:

- For each experiment the heights above mean bed were determined by averaging the heights measured before and after the experiment, so before and after two pump-measurements.
- The measured concentrations for each experiment were determined by averaging two pump-measurements.

This method differs from the method used in the earlier 100-μm-basin-study (1992) where different experiments with approximately the same wave height and aproximately the same height above the bed were averaged.

In the present study a different method is used to prevent that errors made in one measurement will influence the others. Being able to compare different measurements with approximately the same wave height is another benefit of using this method.

In all experiments the instantaneous concentrations and velocities were measured by means of the Acoustical Sediment Transport Meter (ASTM). The output signal of the ASTM (in Volts) is linear with the sediment concentration. Calibration of the signal is needed to take into account the influence of the sediment particle size. Using linear regression on the output signal of the ASTM and the concentrations measured simultaneously with the pump sampler, a calibration factor was computed. This factor had a value of 2.55 for these experiments. In the Figures 4.5.A.1 - 4.5.A.23 (Part I) the time- and bed averaged concentrations measured with the ASTM are presented together with the pump measurements.

The ASTM determines the concentrations and velocities by measuring scattered ultrasonic energy. In case of breaking waves not only sediment but also airbubbles cause a scattering of the transmitted signal. For the ASTM signal therefore only the lowest nine measuring points are taken into account. For some measurements the sediment concentrations in the upper layers were too small to be measured by the ASTM, in that case only the lowest 5 or 6 measuring points were taken into account.

The instantaneous concentrations and velocities will be used to estimate the wave related part of the suspended sediment transport. The results of these computations will be presented in a later report.

4.5.2 Wave height influence

The significant wave height H_s, influences the concentration profile, as the Figures 4.5.B - 4.5.D (Part I) show:

- Increasing the significant wave height, H_s, leads to an increase in concentrations. The increasing orbital velocities lead to the stirring up of more sediment.

- Increasing the significant wave height, H_s, leads to a slightly more uniform concentration profile. The turbulence caused by increasing orbital velocities and breaking of waves leads to a more uniform concentration profile. This can easily be seen from the mass balance described by Eq.4.26. An increasing diffusion coefficient implies a decreasing concentration gradiënt. This effect may however be small because an increasing wave height also causes a decrease of the ripple height and additional less vortices.

$$w * c(z) + \epsilon_s(z) \frac{dc(z)}{dz} = 0 \qquad (4.26)$$

where				
	w	:	fall velocity of the sediment particles	(m/s)
	c(z)	:	average concentration at level z above the bed	(kg/m^3)
	ϵ_s	:	diffusion coefficient for sediment	(m^2/s)
	z	:	height above the bed	(m)

The more uniform profile with increasing wave height was also noted in the earlier 200-μm-flume-study (1987). It was not found in the earlier 100-μm-flume-study (1988) and 100-μm-basin-study (1992).

In Figure 4.3 three concentration profiles with different wave heights are presented. From this figure it can be seen that a *'more uniform profile'* does not mean a *'uniform profile'*. In case of *'a uniform profile'* the factor between the highest and the lowest measuring point would have a value of $c_{highest}/c_{lowest}=1$. From Figure 4.4 it can be seen that this is not the case. A *'more uniform profile'* therefore means an increasing factor between the concentrations measured in the highest - and the lowest measuring point, which can still mean that this factor has a value of for example 0.01.

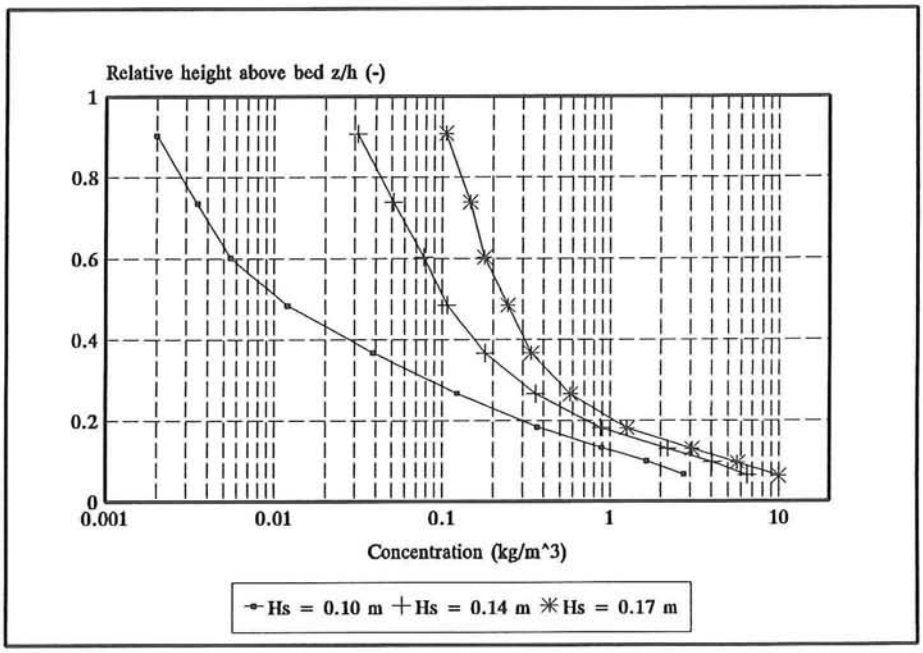

Figure 4.4 More uniform concentration profile with increasing wave height

4.5.3 Current velocity influence

The current strength influences the concentrations as follows (see Figures 4.5.E - 4.5.G, Part I):

With a significant wave height of $H_s = 0.100$ m

- An increasing current strength leads to smaller concentration magnitudes in the near bed zone and increasing concentrations in the upper layers. The current induced mixing becomes apparently more important with increasing current velocities, resulting in an increasing vertical transport of sediment particles to the upper layers.

With a significant wave height of H_s = 0.140 m

- An increase in current strength from U_m = 0 m/s to U_m = 0.10 m/s leads to a less uniform profile and decreasing concentrations, especially in the upper part of the profile (z/h > 0.3). This may be caused by a decreasing wave steepness and thus less breaking waves.

- An increase in current strength from U_m = 0.10 m/s to U_m = 0.20 m/s leads to increasing concentrations and a somewhat more uniform profile in spite of a decrease in the number of breaking waves, probably because current related mixing becomes more important.

- An increase in current strength from U_m = 0.20 m/s to U_m = 0.30 m/s leads to increasing concentrations, because current related mixing becomes more important.

With a significant wave height of H_s = 0.156 m

- A stronger current causes a slight increase in concentrations in the upper part of the profile, smaller concentrations magnitudes in the near bed zone and a slightly more uniform profile caused by current induced mixing.

4.5.4 Influence of fraction of breaking waves Q_b

As can be seen from Figure 4.5.F (Part I) the number of breaking waves does influence the concentration profile, especially for a weak current ($U_m \leq 0.1$ m/s). As indicated in Section 4.2.2 a current in the same direction as the wave propagation causes an increasing wave length and thus a decreasing wave steepness which will lead to less breaking waves.

Although not only the number of breaking waves, but also the current strength is a variable, one could carefully say from the experiments done with a wave height of H_s = 0.14 m (Figure 4.5.F, Part I) that more breaking waves lead to a more uniform concentration profile, especially in the upper part of the profile. The value for the wave height-water depth ratio in these experiments: H_s/h = 0.47.

Considering the experiments done with a wave height of H_s = 0.156 m (Figure 4.5.G, Part I), it can be seen that this phenomenon is less pronounced and the influence of the current strength becomes more decisive. The wave height-water depth ratio with this significant wave height: H_s/h = 0.52.

In the present study the waves break in a way that is often referred to as a 'spilling breaker'. The influence of 'spilling breakers' on the velocity - and the concentration profile is strongest in the upper part of the profile. The influence of the breaking of waves on sediment transport computations will be discussed in Section 4.7.4.

4.6 Sediment loads

4.6.1 General

The sediment load is defined as the total amount of moving sediment per unit bed surface area:

$$L_t = \int_{z=0}^{h} c(z)\, dz \tag{4.27}$$

where	L_t	:	total load	(kg/m^2)
	c(z)	:	time- and bed-averaged concentration at height z	(kg/m^3)
	h	:	water depth	(m)

Here, the total load consists of two parts, the load in the bed load layer and the suspended load:

$$L_b = \int_{z=0}^{\frac{r}{2}} c(z)\, dz \tag{4.28}$$

$$L_s = \int_{z=\frac{r}{2}}^{h} c(z)\, dz \tag{4.29}$$

$$L_t = L_b + L_s \tag{4.30}$$

where	L_b	:	load in bed load layer	(kg/m^2)
	L_s	:	suspended load	(kg/m^2)
	r	:	mean ripple height	(m)

As in the earlier 100-μm-basin-study (1992) in the present study only the suspended load L_s was computed.

To compute the suspended load, the sediment concentrations in the zones below the lowest and above the highest measuring point must be known. This was done by extrapolation. Three extrapolation methods were used (Figure 4.5). These three methods are described in Appendix 2, here only the results and the applied method for further computation are discussed.

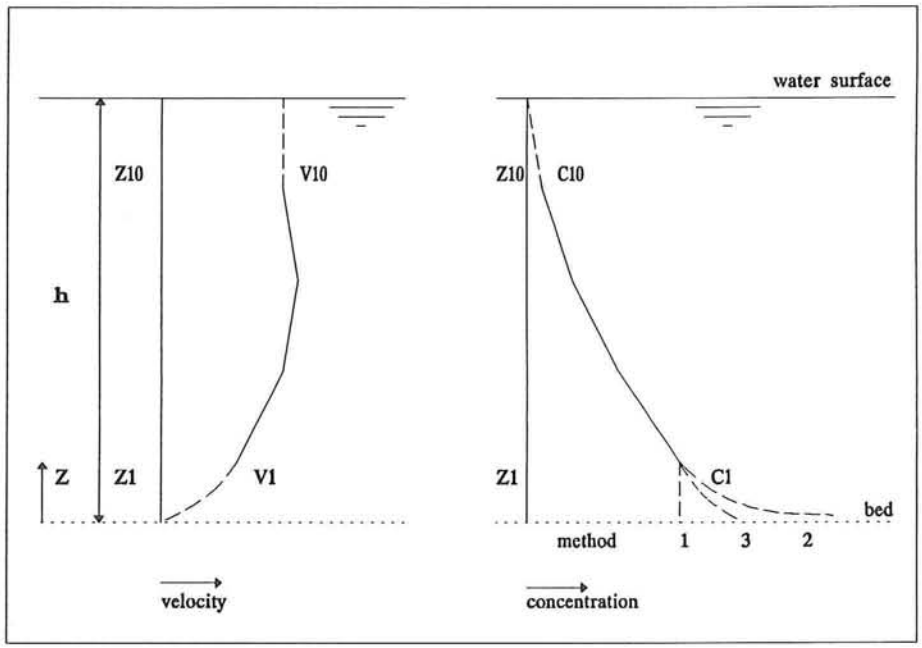

Figure 4.5 Extrapolation of profiles

The values found for c_{bed} (defined as the concentration at $z = 2 * D_{50}$ above the bed and determined by extrapolation) are presented in the Data Tables in Part I. The results using the second method, are quite different when compared to method 1 and method 3. The second method is supposed to give an upper limit. In most of the experiments this method gives the maximum concentration for c_{bed}, and therefore significant higher values for the suspended loads and transport rates. Because of these facts it was decided that method 2 was not applicable for further computation.

For the earlier 100-μm-basin-study (1992) method 1 and 3 gave comparable results (mean difference less than 1%). In the present study the mean difference between method 1 and method 3, considering the sediment loads is 33%. Therefore, contrary to the earlier 100-μm-basin-study (1992), in series A of the present study it was decided not to average the values of method 1 and 3.

Method 1 is supposed to give a lower limit while method 2 gives an upper limit for the sediment concentrations in the unmeasured zone near the bed. Method 3 was assumed to give the most accurate results for L_s and S_s. These values are presented in Table 4.6.1 (Part I).

4.6.2 Wave height influence

Increasing the wave height H_s, leads to a larger suspended load L_s. Table 4.1 shows the wave height influence. For example, an increase of the wave height from H_s = 0.10 m to 0.14 m, at a current velocity U_m = 0.10 m/s, leads to an increase of the suspended load by a factor 1.8. The relation between the wave height and the sediment load is also presented in Figure 4.6.A (Part I).

Increase H_s:	Increase factors suspended load		
	U_m = 0.00 m/s	U_m = 0.10 m/s	U_m = 0.20 m/s
0.10 to 0.14 m	2.3	1.8	2.9
0.14 to 0.16 m	1.3	1.9	1.6
0.10 to 0.16 m	3.0	3.3	4.5

Table 4.1 Increase factors suspended load

Considering the largest wave height difference, from H_s = 0.10 to 0.16 m, one can draw the conclusion that the increase of the suspended load becomes more pronounced with increasing current strength. This is contrary to the results of the earlier studies (200-μm-flume-study 1987, 100-μm-flume-study 1988, 100-μm-basin-study 1992) where the increase factors became smaller with increasing current strength.

Comparing measurements of the earlier 100-μm-flume-study (1988) with approximately the same wave height, the suspended loads found for waves alone in the present study are larger, while the increase factors are significantly smaller. This difference may be explained by the large wave height-water depth ratio H_s/h in the present study compared to the earlier study. In Section 4.6.4 the influence of the wave height-water depth ratio

H_s/h on the suspended load L_s will be studied.

4.6.3 Current strength influence

In Table 4.2 the influence of the current strength on the suspended load is presented. A same tendency as for the wave height influence is found. Considering the largest difference in current velocity, from 0.00 to 0.20 m/s, the increase factors become larger with increasing wave height. This is again in contradiction with the earlier 100-μm-basin-study (1992). The influence of the current strength on the sediment load can also be seen in Figure 4.6.B (Part I).

Increase U_m:	Increase factors suspended load		
	H_s = 0.10 m	H_s = 0.14 m	H_s = 0.16 m
0.00 to 0.10 m/s	0.9	0.7	1.0
0.10 to 0.20 m/s	0.7	1.2	1.0
0.00 to 0.20 m/s	0.7	0.8	1.0

Table 4.2 Increase factors suspended load

In the following conclusions on the influence of the current strength U_m on the suspended load L_s will be drawn. Parameters such as the relative ripple height r/h, the orbital velocities $\hat{U}_{b,on,tot}$ and $\hat{U}_{b,off,tot}$ and the fraction of breaking waves Q_b will also be taken into account. In the Tables 4.3, 4.4 and 4.5, averaged values for L_s and the different parameters are presented.

With a significant wave height of $H_s = 0.10$ m (see Table 4.3):

- The decrease of the loads with increasing current velocity is caused by a decrease of the concentrations in the near bed zone (see Section 4.5.3 and Figure 4.5.E, Part I). The decrease of the loads is related to the wave-induced changes of the velocity distribution in the near bed zone. The interaction between waves and current results in an increasing turbulence which leads to an increasing shear stress, higher ripples and a decrease of the velocities in the near bed zone, especially in the onshore direction (see Table 4.3 where the average values are given).

- In the earlier 100-μm-flume-study (1988) and the 100-μm-basin-study (1992) it was also found that a weak current ($U_m \approx 0.1$ m/s) superimposed on the waves leads to a decrease of the loads. This phenomenon is related with the velocity decrease in the near bed zone ($z/h < 0.3$) caused by waves superimposed on a current (see Section 4.3.3). In the earlier 200-μm-flume-study (1987) a weak current hardly changed the loads.

U_m (m/s)	L_s (kg/m^2)	r/h (-)	$\hat{U}_{b,on,tot}$ (m/s)	$\hat{U}_{b,off,tot}$ (m/s)
0.00	0.156	0.029	0.283	0.197
0.10	0.144	0.030	0.264	0.202
0.20	0.106	0.039	0.256	0.194

Table 4.3 Sediment loads L_s with increasing U_m for $H_s = 0.10$ m

With a significant wave height of H_s = 0.14 m (see Table 4.4):

- The decrease of the loads with increasing depth averaged velocity from U_m=0.00 to 0.10 m/s is caused by a less uniform concentration profile and decreasing concentrations, especially in the upper part of the profile (see Section 4.5.3 and Figure 4.5.F, Part I). Less breaking waves and a decrease of the velocity in the near bed zone, especially in the offshore direction might be a reason (Table 4.4).

- The increase of the loads with increasing depth averaged velocity from U_m = 0.10 to 0.30 m/s is caused by increasing concentrations and a more uniform concentration profile (see Section 4.5.3 and Figure 4.5.F, Part I). An increase of the velocity in the near bed zone both in the on- and offshore direction might be a reason (Table 4.4).

U_m (m/s)	L_s (kg/m^2)	r/h (-)	$\hat{U}_{b,on,tot}$ (m/s)	$\hat{U}_{b,off,tot}$ (m/s)	Q_b (%)
0.00	0.362	0.021	0.353	0.265	5.6
0.10	0.253	0.023	0.342	0.246	4.1
0.20	0.303	0.040	0.377	0.256	3.5
0.30	0.389	0.066	0.390	0.284	3.1

Table 4.4 Sediment load L_s with increasing U_m for H_s = 0.14 m

With a significant wave height of H_s = 0.16 m (see Table 4.5):

- A stronger current causes a slight increase in concentrations in the upper part of the profile, smaller concentrations magnitudes in the near bed zone and a slightly more uniform profile caused by current induced mixing. These effects hardly influence the sediment load. (see Section 4.5.3 and Figure 4.5.G, Part I). The relatively large velocities in the near bed zone are not influenced by the depth-averaged velocity U_m (Table 4.5).

- In the earlier 200-μm-flume-study (1987) and the 100-μm-flume-study (1988) it was also found that a large significant wave height causes a less pronounced increase of the suspended load L_s with increasing current strength.

U_m (m/s)	L_s (kg/m^2)	r/h (-)	$\hat{U}_{b,on,tot}$ (m/s)	$\hat{U}_{b,off,tot}$ (m/s)	Q_b (%)
0.00	0.473	0.021	0.392	0.272	10.2
0.10	0.471	0.027	0.409	0.272	19.8
0.20	0.481	0.028	0.397	0.346	21.2

Table 4.5 Changing sediment load L_s with increasing U_m for H_s = 0.16 m

It is striking to see that in contradiction with the earlier studies, the sediment load in the present study does not change or even decreases for stronger currents. The increase factors for the suspended load were found to be much larger in the earlier studies, this because the ratio H_s/h in the present study is large compared to the earlier studies. The influence of H_s/h on the suspended sediment load L_s will be studied in Section 4.6.4.

4.6.4 Influence ratio H_s/h

In the Figures 4.6.C - 4.6.E (Part I) the relation between the wave height-water depth ratio H_s/h and the suspended sediment load is presented. A comparison has been made with the earlier 200-μm-flume-study (1987), the earlier 100-μm-flume-study (1988) and the earlier 100-μm-basin-study (1992). From these figures it can be seen that:

- An increasing H_s/h leads to increasing sediment loads.

- When no current is present (U_m = 0.0 m/s) the influence of the water depth h on the sediment load L_s is more pronounced compared to the current and waves situation.

4.7 Sediment transport rates

4.7.1 General

As is pointed out in Chapter 2, the sediment transport rates are computed from the time- and bed-averaged concentrations and velocities. In this section only the time- and bed-averaged sediment transport will be discussed, so, the wave related part of the total sediment transport will be neglected here. The definition for the current related suspended sediment transport is:

$$S_s = \int_{\frac{1}{2}r}^{h} c(z) * u(z)\, dz \qquad (4.31)$$

where	S_s	:	suspended sediment transport	(kg/sm)
	r	:	mean ripple height	(m)
	c(z)	:	time- and bed-averaged concentration at height z above the bed	(kg/m^3)
	u(z)	:	time- and bed-averaged fluid velocity at height z above the bed	(m/s)

4.7.2 Suspended sediment transport

Numerical computations of the depth-integrated suspended sediment transport S_s requires the specification of velocities and concentrations at equal elevations above the bed (equal z values). The depth-integrated suspended sediment transport S_s is computed as:

$$S_s = \sum_{i-1}^{n} \frac{1}{2} (U_i * c_i + U_{i-1} * c_{i-1}) * (z_i - z_{i-1}) \qquad (4.32)$$

where	U_i	:	fluid velocity at height z_i above the bed	(m/s)
	c_i	:	sediment concentration at height z_i above the bed	(kg/m^3)
	n	:	total number of points (including extrapolated values)	(-)

Three different methods (see Appendix 2) are applied to represent the sediment concentrations in the unmeasured zone near the bed, so three different values for the suspended sediment transport are obtained and implemented in the data base (S_{s1}, S_{s2}, S_{s3}). The results are given in the Data Tables of Part I. For further computation the value for S_{s3} is used as suspended load transport.

As in the earlier 100-μm-basin-study (1992), in the present study only the suspended sediment transport S_s was computed. Comparison with the earlier 200-μm-flume-study (1987) and 100-μm-flume-study (1988) is possible because, as was concluded in those studies, the influence of the bed load transport on the total transport is small (S_b/S_t * 100% < 7%).

4.7.3 Relationship between S_s, H_s and U_m

In Section 4.7.2 the computation has been explained. Now it is possible to study the relationship between the suspended sediment transport S_s and the parameters H_s and U_m. The parameters are presented in Part I, Table 4.2.1. The relationship between H_s, U_m and the suspended sediment transport S_s is presented in the Figures 4.7.A and 4.7.B (Part I).

4.7.3.1 Influence wave height

The relation between S_s and H_s will be investigated. This relation (for constant U_m) can be described by:

$$S_s = \alpha * H_s^q \tag{4.33}$$

In which α and q still depend on the depth-averaged fluid velocity U_m. The parameters are computed for constant U_m by a least square method using varying significant wave heights. The results and the correlation ρ between the formulae and the measurements are presented in Table 4.6 (see also Figure 4.7.A, Part I).

U_m (m/s)	present study			100-μm-basin-study
	α	q	ρ	q
0.00	-200.0	5.2	0.99	
0.10	1.0	2.4	0.79	2.5
0.20	7.7	2.8	0.99	2.0

Table 4.6 Dependence of S_s on H_s

For the earlier 100-μm-basin-study (1992) the values for α and q were interpolated and are only valid for $0.16 < H_s/h < 0.35$ with h=0.40 m. In that study it appeared that $\alpha \approx 1$. The values for α and q found in the present study are valid for $0.33 < H_s/h < 0.55$ with h=0.30 m. In Section 4.7.3.3 a comparison between the two studies will be made.

4.7.3.2 Influence velocity

The relationship between the suspended sediment transport and the depth-averaged velocity will be investigated. This relationship can be described by:

$$S_s = \beta * U_m^y \qquad (4.34)$$

In which the parameters ß and y still depend on the significant wave height. The parameters are computed for constant H_s by a least square method using varying depth-averaged velocities. The results and the correlation ρ between the formulae and the measurements are presented in Table 4.7 (see also Figure 4.7.B, Part I).

H_s (cm)	present study			100-μm-basin-study
	ß	y	ρ	y
10.1	0.08	1.2	0.94	2.8
14.1	0.91	2.0	1.00	2.3
15.7	0.92	1.8	1.00	2.1

Table 4.7 Dependence of S_s on U_m

For the earlier 100-μm-basin-study (1992) the values for ß and y were inter- and extrapolated and are only valid for $0.16 < H_s/h < 0.35$ with $h = 0.40$ m. In that study it appeared that $\beta \approx 1$. The values for ß and y found in the present study are valid for $0.33 < H_s/h < 0.55$ with $h = 0.30$ m. In the next section a comparison between the two studies will be made.

4.7.3.3 Comparison with earlier study

From the analysis under 4.7.3.1 and 4.7.3.2 the following conclusions can be drawn:

- In case of a strong current ($U_m = 0.20$ m/s) the value for q found in the present study ($q = 2.8$) is relatively large compared to the earlier 100-μm-basin-study (1992) ($q = 2.0$). This means a more pronounced influence of the wave height on the sediment transport.

- The values for y found in the present study are relatively small compared to the earlier 100-μm-basin-study, especially in case of a small wave height. This means a less pronounced influence of the current strength on the suspended sediment transport.

- The difference between the two studies may be related to the difference in wave-induced changes of the velocity distribution in the near bed zone. In the earlier 100-μm-basin-study the wave height to water depth ratio varied from $H_s/h = 0.16$ to 0.35, while in the present study this parameter varies from $H_s/h = 0.33$ to 0.55. This will have its effect on the velocities in the near bed zone, especially on the asymmetry (onshore velocity larger than offshore, see Section 4.4.2).

4.7.4 Empirical sediment transport formula

It is possible to represent the S_s-values by an empirical transport formula, wherein S_s depends on U_m, H_s/h, Q_b and the asymmetry effects in the velocities. Although the formula will not be correct, one can get a better insight in the relationship between S_s and U_m and the importance of the several parameters such as the onshore peak velocity $\hat{U}_{b,on,tot}$, the offshore peak velocity $U_{b,off,tot}$, the wave height-water depth ratio H_s/h and the fraction of breaking waves Q_b. A first formula is chosen in the form:

$$S_s \approx a * U_m^b * \hat{U}_{b,on,tot}^c * \hat{U}_{b,off,tot}^d * (\frac{H_s}{h})^e * (1-Q_b)^f \qquad (4.35)$$

where	S_s	:	suspended load transport	(kg/sm)
	U_m	:	depth-averaged fluid velocity	(m/s)
	$\hat{U}_{b,on,tot}$	:	onshore orbital peak velocity	(m/s)
	$U_{b,off,tot}$	:	offshore orbital peak velocity	(m/s)
	H_s/h	:	wave height-water depth ratio	(-)
	Q_b	:	fraction of breaking waves	(-)
	a,b,c,d,e,f	:	experimental coefficients	

This formula was fitted to data from the earlier 100-μm-basin-study ($0.16 < H_s/h < 0.35$) and from the present study ($0.33 < H_s/h < 0.55$).

Simple approach neglecting the influence of H_s/h and Q_b

In this case the influence of frequency effects in the velocity, the ratio H_s/h and the fraction of breaking waves Q_b on S_s are neglected. Using a least square method the following formulae were found:

In Section 4.4.2 it was found that an increasing H_s/h ratio leads to an increasing wave asymmetry (onshore velocity larger than offshore value). This may be an explanation for the more pronounced influence of the onshore velocity and the less pronounced influence of the offshore velocity in the present study compared to the earlier 100-μm-basin-study (1992). In the present study the H_s/h ratio varied from $H_s/h=0.33$ to 0.55 while in the earlier 100-μm-basin-study (1992) this parameter varied from $H_s/h=0.16$ to 0.35. It can be concluded that:

- An increasing H_s/h ratio leads to an increasing influence of the onshore orbital peak velocity $\hat{U}_{b,on,tot}$ and a decreasing influence of the offshore orbital peak velocity $\hat{U}_{b,off,tot}$ on the suspended sediment transport S_s.

In the next paragraph the influence of the wave height-water depth ratio H_s/h and the fraction of breaking waves Q_b on the empirical formula will be studied.

Influence H_s/h and Q_b on empirical formula

In Section 4.7.3.3 it was concluded that the more pronounced influence of the wave height H_s and the less pronounced influence of the current strength U_m in the present study, compared to the earlier 100-μm-basin-study (1992), is related with the difference in wave height-water depth ratio H_s/h between the two studies. In the earlier study this ratio varied from $H_s/h = 0.16$ to 0.35, while in the present study this parameter varied from $H_s/h = 0.33$ to 0.55.

In this section the influence of the wave height-water depth ratio H_s/h and the fraction of breaking waves Q_b on the empirical sediment transport formula will be studied. The following formulae were found using a least square method.

using data from present study:

$$S_s \approx 4.8 * U_m^{2.0} * \hat{U}_{b,on,tot}^{1.4} * \hat{U}_{b,off,tot}^{-0.5} * \left(\frac{H_s}{h}\right)^{1.3} * (1-Q_b)^{-1.0} \qquad (4.39)$$

using data from earlier 100-μm-basin-study:

$$S_s \approx 53.5 * U_m^{2.4} * \hat{U}_{b,on,tot}^{1.0} * \hat{U}_{b,off,tot}^{1.3} * \left(\frac{H_s}{h}\right)^{0.7} \qquad (4.40)$$

The correlation between the empirical formula and the measurements increased to a value of respectively $\rho=0.997$ (Eq.4.39) and $\rho=0.999$ (Eq.4.40).

These formulae are valid within the limits for H_s/h mentioned above and a waterdepth of respectively $h=0.30$ m (Eq.4.39) and $h=0.40$ m (Eq.4.40).

From the empirical formulae it can be seen that the wave height-waterdepth ratio H_s/h is an important parameter in determining the suspended sediment transport S_s. While the on- and offshore peak velocity $\hat{U}_{b,on,tot}$ and $\hat{U}_{b,off,tot}$ are important for the stirring up of material from *the bed*, the depth averaged velocity U_m and the orbital velocities in the middle and upper layers are responsible for the stirring up of sediment to *higher regions*. The extent of this effect depends on the wave height-water depth ratio H_s/h. From the above it can be concluded that:

- The influence of H_s/h on the suspended sediment transport is important, especially for the stirring up of sediment to the middle and upper layers.

The breaking of waves results in an increasing turbulence. In Section 4.5.4 it was found that, with a wave height of $H_s=0.14$ and a water depth of $h=0.30$ m, more breaking waves lead to a more uniform concentration profile. It can be concluded that:

- The influence of the fraction of breaking waves Q_b on the suspended sediment transport is of some importance, especially for the stirring up of sediment to the middle and upper layers.

Increasing the fraction of breaking waves from $Q_b=3.5\%$ to 20% for example leads to an increase of the suspended sediment transport S_s by 21% neglecting the influence of the other parameters. Increasing the H_s/h ratio from 0.45 to 0.55 leads to an increase of the suspended sediment transport S_s by 30% neglecting the influence of the other parameters.

Conclusions on empirical transport formulae

From the analysis under the previous paragraphs the following conclusions can be drawn:

- The use of the measured onshore velocity $\hat{U}_{b,on,tot}$ and $\hat{U}_{b,off,tot}$ instead of a calculated U_b in the empirical transport formula results in a higher correlation between the measurements and the formula.

- The influence of the depth averaged velocity U_m on the suspended sediment transport is less pronounced with increasing H_s/h.

- The influence of the *onshore* orbital peak velocity $\hat{U}_{b,on,tot}$ on the suspended sediment transport S_s is more pronounced with increasing H_s/h.

- The influence of the *offshore* orbital peak velocity $\hat{U}_{b,off,tot}$ on the suspended sediment transport S_s is less pronounced with increasing H_s/h.

- The influence of H_s/h on the suspended transport is important, especially for the stirring up of sediment to the middle and upper layers.

- The influence of the fraction of breaking waves Q_b on the suspended sediment transport is important, especially for the stirring up of sediment to the middle and upper layers.

- With a wave height-water depth ratio varying from $H_s/h = 0.16$ to 0.35 and $h = 0.40$ m, the sediment transport can be represented by a reliable ($\rho = 0.999$) empirical formula wherein S_s depends on U_m, $\hat{U}_{b,on,tot}$, $\hat{U}_{b,off,tot}$ and H_s/h.

- With a wave height-water depth ratio varying from $H_s/h = 0.33$ to 0.55 and $h = 0.30$ m, the sediment transport can be represented by a reliable ($\rho = 0.997$) empirical formula wherein S_s depends on U_m and $\hat{U}_{b,on,tot}$, $\hat{U}_{b,off,tot}$, H_s/h and Q_b.

4.8 Ripple parameters

4.8.1 General

Ripples are formed by wave and current movements, yielding a bed form that is specific for the hydraulic conditions at that moment. On the other hand the bed form influences the water movement in the near bed zone, and therefore also the concentrations in the near bed zone. Here the ripple parameters and the bed forms will be discussed. For each experiment the ripple parameters were determined, in wave and current direction. During these experiments, with increasing intensity of water movement, the following bed forms occured, defined as:

- 2-dimensional ripples: regular ripple-shaped bed, with ripples in wave direction.
- 2.5-dimensional ripples: semi-regular ripple-shaped bed, with some ripples not in wave direction.

Other forms, like "dunes" or a "flat bed" were not observed in the present study. The bed form for each experiment is listed in the tables with experimental data under "BFT bedf type: ".

To describe these ripples, the following parameters are used:

- ripple height (r)
- ripple length (λ)
- ripple steepness (r/λ)

These parameters were determined in the direction of the current and in the direction of the waves. Also the mean values were estimated which are presented in Table 4.8.1 (Part I). These parameters will be described in the next section.

To study the influence of the water movement in the near bed zone on the ripple characteristics, the following dimensionless parameters are used:

$(U_{b,on,tot})^2/\Delta g D_{50}$	to describe the influence of the *onshore* orbital peak velocity
$(\hat{U}_{b,off,tot})^2/\Delta g D_{50}$	to describe the influence of the *offshore* orbital peak velocity
$(U_m)^2/\Delta g D_{50}$	to describe the influence of the current strength
$U_m/U_{b,on,tot}$	to indicate the importance of the current with regard to the waves

The ripple- and water movement parameters are presented in Table 4.8.1 (Part I)

4.8.2 Ripple height

The experiments in the present study showed mean ripple heights between 0.007 and 0.021 m (Table 4.8.1, Part I). This range is somewhat above the range that was found for the ripple heights in the earlier 100-μm-basin-study (1992).

The Figures 4.8.A.1 and 4.8.A.2 (Part I) show the relationship between the relative ripple height $r/A_{b,on,tot}$ and $r/A_{b,off,tot}$ and the water movement parameters $(\hat{U}_{b,on,tot})^2/\Delta g D_{50}$ and $\hat{U}_{b,off,tot}{}^2/\Delta g D_{50}$. From these figures it is clear that:

- Increase of the on- and offshore orbital peak velocities leads to a decrease of the relative ripple height due to erosion of the ripple crest.

Figure 4.8.B (Part I) shows the relationship between the relative ripple height r/h and the water movement parameter $(U_m)^2/\Delta g D_{50}$. From this figure it can be observed that:

- Increase of U_m leads to an increase of the relative ripple height. The ripples become higher and more three dimensional.

In Figure 4.8.C (Part I) the relationship between the relative ripple height $r/A_{b,on,tot}$ and the wave steepness H_s/L is shown. The following conclusion can be drawn from this figure:

- Increase of the wave steepness leads to a decrease of the relative ripple height.

4.8.3 Ripple length

In the present study mean ripple lengths ranging from 0.045 to 0.129 m were found (Table 4.8.1, Part I). In the earlier 100-μm-basin-study (1992) ripple lengths of 0.06 to 0.11 m were found and in the earlier 100-μm-flume-study (1988) ripple lengths of 0.06 to 0.145 m were measured.

The ripple lengths are depending on the velocities near the bottom. For increasing velocities the ripple lengths will decrease. Figure 4.8.D.1 and Figure 4.8.D.2 (Part I) show the relationship between the relative ripple lengths, $\lambda/A_{b,on,tot}$ and $\lambda/A_{b,off,tot}$, and the water movement parameters $(\hat{U}_{b,on,tot})^2/\Delta g D_{50}$ and $(U_{b,off,tot})^2/\Delta g D_{50}$. From these figures it can be concluded that:

- Increase of the on- and offshore orbital peak velocities leads to a decrease of the relative ripple length.

Figure 4.8.E shows the relationship between the relative ripple lengths λ/h and the water movement parameter $U_m{}^2/\Delta g D_{50}$. From this figure it can be concluded that:

- Increase of current strength leads to an increase of the ripple length. This in contradiction with the earlier 100-μm-basin-study (1992) where the opposite occured.

In Figure 4.8.F (Part I) the relationship between the relative ripple length $\lambda/A_{b,on,tot}$ and the wave steepness H_s/L is presented. From this figure it is clear that:

- Increase in wave steepness leads to a decrease of the relative ripple length.

4.8.4 Ripple steepness

The ripple steepness is defined as the ratio r/λ. An average steepness of $r/\lambda = 0.151$ was found in the present study. In the earlier 100-μm-basin-study (1992) and the 100-μm-flume-study (1988) values of $r/\lambda = 0.102$ and 0.134 were found.

In the Figures 4.8.G.1, 4.8.G.2 and 4.8.H (Part I) the influence of the parameters $(\hat{U}_{b,on,tot})^2/\Delta g D_{50}$, $(\hat{U}_{b,off,tot})^2/\Delta g D_{50}$ and $(U_m)^2/\Delta g D_{50}$ on the relative ripple steepness is presented. From these figures it can be observed that:

- An increasing orbital peak velocity ($\hat{U}_{b,on,tot}$ and $\hat{U}_{b,off,tot}$) leads to a decreasing ripple steepness r/λ, especially in case of a weak current.

- No clear relation between the ripple steepness r/λ and the current strength U_m can be found.

From Figure 4.8.I (Part I) it can be observed that the wave steepness very slightly influences the ripple steepness. Carefully one could draw the following conclusion:

- Increase in wave steepness leads to a slight decrease in ripple steepness.

4.9 Size and fall velocity of suspended sediment

In each experiment ten suspended sediment samples were obtained (ten measuring points over the depth). These samples were added together to make a bulk sample. Each bulk sample was analyzed in a settling tube to determine the fall velocity distribution. The Data Tables in Part I present the measured fall velocity of the suspended material w_{ss}. From this the suspended material size D_s can be computed.

In the Van Rijn transport model (see Chapter 6) this particle diameter is suggested as a representive diameter for the suspended sediment size. It should give the same value for the suspended load as that determined by the size-fraction method of Van de Graaff et al (1984).

Samples from the bed material were obtained to determine the particle diameters of the bed material presented in the Data Tables, D_{10}, D_{50} and D_{90}.

For well graded material, D_{50} will change with the height above the bed. Smaller particles are brought into suspension more easily and reach higher levels more easily. So at the top of the vertical there is relatively more of the finer material and D_{50} will be smaller than the D_{50} of the bottom material. In that case the D_{50} of the bed material can not be used as the representative diameter to calculate the fall velocity and determine the concentrations and loads. The D_s/D_{50} ratio gives an indication whether the bed material size can be used as a representative value for the suspended sediment size. In the present study an average of $D_s/D_{50}=0.99$ was found ranging from 0.86 to 1.20.

4.10.3 The ripple configuration

If the ripple configuration of the bed is 2-dimensional, the ripple geometry can be determined rather accurately. In the present study a 2.5-dimensional configuration was found meaning a less accurate determination of the ripple parameters than in case of a 2-dimensional bedform.

In case of a 3-dimensional configuration, the larger ripples may have a relatively larger contribution in the bed roughness than the smaller ones (100-μm-flume-study, Nap, Van Kampen 1988). To get a better accuracy, in the earlier 100-μm-flume-study the parameters H_{dom} and L_{dom} (dominating ripple height and length) were calculated. In these parameters the individual ripple heights and ripple lengths were weighted with the ripple lengths, so longer ripples gave a relatively larger contribution to H_{dom} and L_{dom}. The results of this computation was that the values H_{dom} and L_{dom} were about 10% larger than the mean values r and λ. As is suggested in the earlier 100-μm-study, the accuracy can also be increased by increasing the number of ripple measurements.

In the present study no 3-dimensional bedforms were found and more ripple measurements were done compared to the earlier 100-μm-flume-study (1988). Therefore, as in the earlier 100-μm-basin-study (1992), it is not necessary to compute the parameters H_{dom} and L_{dom} for the present study.

4.10.4 Determination of the bed roughness with current alone

As in the earlier studies, in each experiment the current velocity profile was also measured in absence of waves (see Chapter 3). These profiles have been investigated by fitting a logarithmic ditribution of the form:

$$U(z) = \frac{U^*}{\kappa} * \ln\left(\frac{z}{z_0}\right) \qquad \textit{for } z > z_0 \tag{4.41}$$

where	U(z)	:	mean current velocity at height z	(m/s)
	U^*	:	bed shear velocity	(m/s)
	z	:	height above reference level	(m)
	z_0	:	roughness length scale	(m)
	κ	:	Von Karman constant (= 0.4)	(-)

Here it is assumed that the reference level is equal to the mean bed level. In Section 4.10.8 it will be studied whether this assumption is correct.

The bed roughness can be computed form z_0 as:

$$K_{s,physical} = 33 * z_0 \qquad (4.42)$$

Using this method, the values of U^* and z_0 were estimated. To eliminate sidewall effects of the flume, the lowest nine measuring points ($z/h < 0.75$) were used in the fitting procedure. The correlation between the measured velocities and the fitted profile was always higher than $\rho = 0.97$. With Eq.4.42 $K_{s,physical}$ can be computed. These values are presented in Table 4.10.1 (Part I).

In the present study, a roughness range ($K_{s,physical}$) of 1.5 to 11.6 times the mean ripple height was found. The mean value for K_s:

$$K_{s,physical} \approx 6.6 * r \qquad (4.43)$$

The influence of the ripple height r and ripple length λ on the physical bed roughness $K_{s,physical}$ is presented in Figure 4.10.A and 4.10.B (Part I). In the earlier 100-μm-basin-study (1992), a roughness range of 0.1 to 1.5 times the mean ripple height was found. In the earlier 100-μm-flume-study (1988) this range was 3 to 10 times the mean ripple height.

In the earlier 100-μm-flume-study (1988) and the present study comparable roughness ranges were found. When compared to the earlier 100-μm-basin-study (1992), the difference in $K_{s,physical}$ between the studies is remarkable (approximately a factor 10). This difference may be caused by the influence of the flume walls in the present- and the earlier 100-μm-flume-study and by the fact that the ripples in the flume are more irregular than in the basin. Determination via the Vanoni-Brooks method gave in the earlier 100-μm-flume-study a roughness range of 2 to 6 times the mean ripple height. The Vanoni-Brooks method tries to eliminate the influence of the flume walls. The difference between the two earlier studies was reduced to a factor 6 by using the Vanoni-Brooks method.

The Vanoni-Brooks method was not used in the present study because the water surface slope was not measured. To reduce the influence of the flume walls the lowest nine measuring points ($z/h < 0.75$) were used in the fitting procedure.

4.10.5 The influence of the ripple steepness

For the ripple steepness, defined as mean ripple height devided by mean ripple length, in the earlier 100-μm-flume-study (1988) the following range was found:

$0.10 < r/\lambda < 0.17$

The ripple steepness range found in the earlier 100-μm-basin-study (1992):

$0.07 < r/\lambda < 0.13$

For the present study this steepness range is:

$0.12 < r/\lambda < 0.18$

The conclusion made in the earlier studies that when $r/\lambda > 0.1$ the influence of the ripple steepness on $K_{s,physical}$ becomes less clear, is also found here. In Figure 4.10.C (Part I) the relation between the physical bed roughness and the ripple steepness is presented. A comparison has been made between the different studies. From Figure 4.10.C (Part I) the following conclusions can be drawn:

- If the ripple steepness exceeds the value of 0.1, the roughness range varies from 0 to 14 times the ripple height. No significant trend can be observed.
- Within a steepness range of 0.1 to 0.2, a roughness range of 0 to 10 times the mean ripple height can be expected. For a steepness range of 0.05 to 0.1, the roughness range will be 0 to 3 times the mean ripple height.
- The difference between the flume studies (present-, 100-μm-flume- and 200-μm-flume-study) is remarkable compared to the basin study (100-μm-basin-study). In the flume studies a roughness range of $2 < K_s/r < 14$ is found, while in the basin studies a roughness range of $0 < K_s/r < 5$ is measured. This may be explained by the difference in current-wave-angle between the basin study and the flume studies and the influence of the side walls in the flume studies.

4.10.6 Roughness prediction for rippled bedforms

Many roughness predictors are available. Most of them are a function of the ripple and sediment characteristics:

$$K_{s,physical} = F(r,\lambda,r/\lambda,D_{50},D_{90})$$

As in the earlier studies, in the present study the roughness predictors of Van Rijn, Swart and Grant-Madsen have been used. The predictors are given by the following formulae:

Van Rijn:

$$K_{s,phys} = 20 * r * \frac{r}{\lambda} \tag{4.44}$$

Swart:

$$K_{s,phys} = 25 * r * \frac{r}{\lambda} \tag{4.45}$$

Grant-Madsen:

$$K_{s,phys} = 8 * r * \frac{r}{\lambda} + 190 * D_{50} * \sqrt{\theta' - 0.05} \tag{4.46}$$

where				
	r	:	ripple height	(m)
	λ	:	ripple length	(m)
	r/λ	:	ripple steepness	(-)
	D_{50}	:	grain diameter exceeded by 50% of the bed material by weight	(m)
	D_{90}	:	grain diameter exceeded by 10% of the bed material by weight	(m)
	θ'	:	Shields skin friction parameter	(-)

From Table 4.10.2 (Part I) it can be seen that the Van Rijn formula gives roughness predictions that are small compared to the fitted roughness. The measured $K_{s,physical}$ has an average of 6.6 * r_m. The roughness according to Swart agrees reasonably well with the fitted roughness, while the Grant-Madsen formula gives roughness predictions that are small compared to the fitted $K_{s,physical}$ values. In the next sections the bed roughness will be represented by an empirical formula based on ripple parameters and hydraulic conditions.

4.10.6.1 Empirical bed roughness formula based on ripple parameters

In this section the bed roughness will be represented by an empirical formula based on ripple parameters while the influence of the hydraulic conditions on K_s is neglected. The influence of the ripple parameters on the physical bed roughness is presented in the Figures 4.10.A - 4.10.C (Part I).

A first approximation is chosen in the same form as the Van Rijn (Eq.4.44) and the Swart (Eq.4.45) formulae. Using a least square method the following relation between the ripple parameters r, λ and K_s is found:

$$K_s = 42.7 * r * \frac{r}{\lambda} \tag{4.47}$$

There is no strong correlation between this formula and the measured bed roughness. In the next section the relation between the dimensionless hydraulic parameters and the physical bed roughness will be studied.

4.10.6.2 Empirical bed roughness formula based on hydraulic parameters

The bed roughness can be represented by an empirical formula based on the dimensionless hydraulic parameters, $(U_m)^2/\Delta g D_{50}$, $(\hat{U}_{b,on,tot})^2/\Delta g D_{50}$ and $(\hat{U}_{b,off,tot})^2/\Delta g D_{50}$. The influence of the hydraulic parameters on the physical bed roughness is presented in the Figures 4.10.D and 4.10.F (Part I). A formula is chosen in the form:

$$K_s = a * \left(\frac{U_m^2}{\Delta g D_{50}}\right)^b * \left(\frac{\hat{U}_{b,on,tot}^2}{\Delta g D_{50}}\right)^c * \left(\frac{\hat{U}_{b,off,tot}^2}{\Delta g D_{50}}\right)^d \tag{4.48}$$

where	r	:	ripple height	(m)
	U_m	:	depth-averaged fluid velocity	(m/s)
	$U_{b,on,tot}$	:	*onshore* orbital peak velocity	(m/s)
	$U_{b,off,tot}$	:	*offshore* orbital peak velocity	(m/s)
	Δ	:	relative sediment density	(-)
	g	:	acceleration of gravity	(m/s^2)
	D_{50}	:	grain diameter exceeded by 50% of the bed material by weight	(m)
	a,b,c,d	:	experimental coefficients	(-)

With a least square method the values of a, b, c and d can be computed:

$$K_s = 0.18 * \left(\frac{U_m^2}{\Delta g D_{50}}\right)^{0.21} * \left(\frac{\hat{U}_{b,on,tot}^2}{\Delta g D_{50}}\right)^{-0.24} * \left(\frac{\hat{U}_{b,off,tot}^2}{\Delta g D_{50}}\right)^{-0.17} \tag{4.49}$$

The correlation between the measured bed roughness and this computation has a value of $\rho = 0.723$.

4.10.7 Measured and predicted roughness range

In Table 4.10.2 (Part I) the measured and predicted K_s values are presented. In Table 4.8 a comparison is made between the measured roughness ranges of three different studies.

Study	Bed roughness K_s/r (-)		
	minimum	maximum	mean
Present study	1.5	11.6	6.5
100-μm-flume-study	2	6	3.8
100-μm-basin-study	0.1	1.5	0.8

Table 4.8 Measured bed roughness range (different studies)

When comparing the predicted roughness range between the different formulae the following results are found:

Formula	Bed roughness K_s/r (-)		
	minimum	maximum	mean
Van Rijn (Eq.4.44)	2.4	3.6	3.1
Swart (Eq.4.45)	3.0	4.4	3.8
Grant/Madsen (Eq.4.46)	1.8	2.7	2.2

Table 4.9 Predicted bed roughness range (present study)

4.10.8 The wave influence on the bed roughness

The bed roughness range from Section 4.10.7 has been obtained from measurements concerning currents in absence of waves. The waves will influence the current velocity profile by introducing extra roughness near the bed due to pressure forces. Because of this effect the current profile is shifted (see Figure 4.6). Figure 4.10.I (Part I) shows that

waves superimposed upon a current introduce an apparent roughness, expressed by the factor z_1/z_0. According to Lundgren (1972) outside a relative thin layer, the current velocity profile has the usual logarithmic form:

$$U(z) = \frac{U^*}{\kappa} * \ln\left(\frac{z}{z_1}\right) \qquad \textit{for } z > z_1 \tag{4.50}$$

where $U(z_1)=0$ and $K_{s,app}=33*z_1$

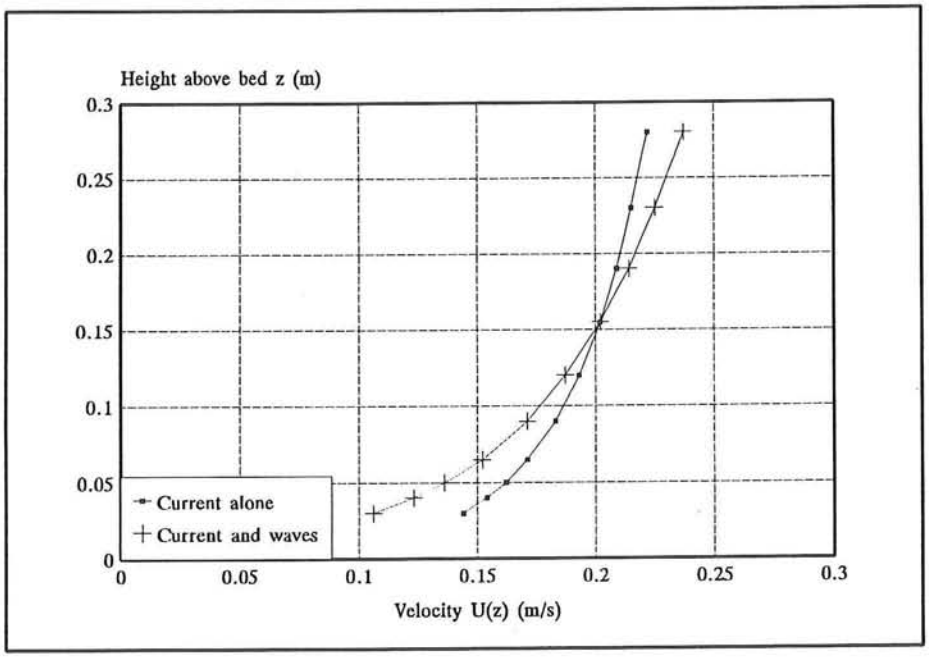

Figure 4.6 Velocity profile in case of current alone and current + waves

The apparent roughness increase is from $33*z_0$ to $33*z_1$. The logarithmic velocity profile was fitted to the seven lowest measuring points. The correlation between the fitted and the measured velocity profile was always higher than $\rho = 0.95$.

Based on the curve fitting method, the parameters U_* and z_1 were determined and $K_{s,app}=33*z_1$. In Table 4.10 a comparison is made between the measured apparent roughness ranges of three different studies.

Study	Apparent bed roughness $K_{s,app}/r$ (-)		
	minimum	maximum	mean
Present study	11.7	53.4	36.4
100-μm-flume-study	12.5	48.8	26.6
100-μm-basin-study	1.5	22.0	5.8

Table 4.10 Measured apparent bed roughness (different studies)

Furthermore the increase of the zero velocity level z_1/z_0 (= $K_{s,app}/K_{s,phys}$) and the increase in bed shear velocity U_{*cw}/U_{*c} have been determined. These parameters are presented in Table 4.10.3 (Part I) and in the Figures 4.10.I and 4.10.J (Part I) as a function of the relative orbital velocities $\hat{U}_{b,on,tot}/U_m$ and $\hat{U}_{b,off,tot}/U_m$. From these figures the following conclusions can be drawn:

- Waves superimposed on a current lead to an apparent increase in bed roughness. In the present study values for z_1/z_0 from 1.7 to 11.4 are found. The increase of the zero velocity level becomes less significant with increasing value of $\hat{U}_{b,on,tot}/U_m$ and $\hat{U}_{b,off,tot}/U_m$. A comparison with earlier studies is made in Table 4.11.

- The increase in bed shear velocity by wave influence is less pronounced than the increase in zero velocity level. Values for U_{*cw}/U_{*c} from 1 to 2 are found (see Figure 4.10.K and 4.10.L, Part I).

Study	Apparent roughness z_1/z_0		
	minimum	maximum	mean
Present study	2	11	6.1
100-μm-flume-study	1	10	4.3
100-μm-basin-study (depending on Φ)	1	30	13.7

Table 4.11 Apparent increase in bed roughness (different studies)

According to Van Rijn (1988) $K_{s,app}/K_{s,phys}$ can be described by:

$$\frac{K_{s,app}}{K_{s,phys}} = e^{(\gamma \frac{U_b}{U_m})} \tag{4.51}$$

where γ : coefficient dependent on the angle between the current and the waves, in case of following waves $\gamma = 0.75$.

For the experiments from the earlier 100-μm-flume-study (1988) in case of following waves a value of $\gamma = 0.72$ can be found. In the earlier 100-μm-basin-study (1992) values for γ ranging from 1.1 to 2.1 were found, depending on the current-wave-angle Φ, the maximum was found for Φ=90°.

Although fitting Eq.4.51 to data from the present study results in $\gamma = 0.54$, the correlation between the measured bed roughness and the computed values is not very high.

5 Experimental results B-series

5.1 General

This part of the report deals with series B of the tests. The objective of the experiments is to examine the distribution of the cross-shore suspended sediment transport over a bar. For computation of the suspended transport, fluid velocities and sediment concentrations have to be measured at different heights above the bed.

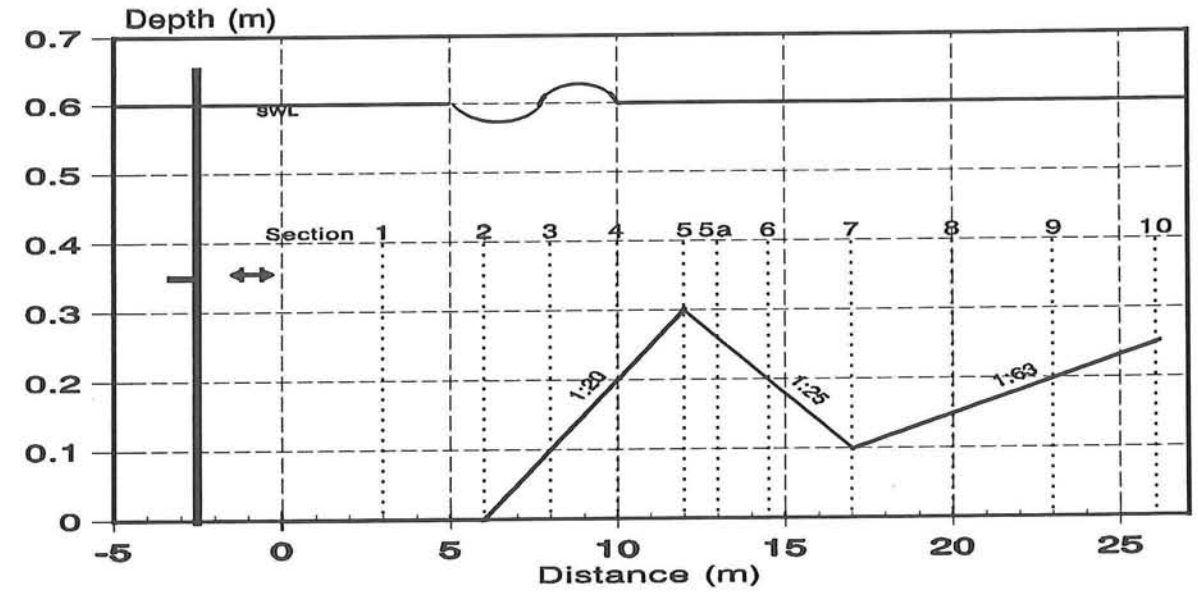

Figure 5.1 Physical model with measuring sections

The bottom profile that is used, is a representation of the bar that is present at the coast of Egmond, The Netherlands (see Figure 5.1). The moveable bed has a mean sediment size D_{50} of 100 μm.
The sediment concentrations and fluid velocities are measured in different measuring cross-sections, as is shown in Figure 5.1.
Two conditions are considered: series B1 with a relatively small wave height and series B2 with a slightly larger wave height. In both series no external current is present.
In every cross-section 10 measurements are made at different heights above the bed to determine the profile of the concentration and velocity.
The experiments are identified by a test number. The test number used in series B is slightly different from that used in series A:

T xx yy zz (5.1)

where	xx	:	Significant wave height	(cm)
	yy	:	Fluid velocity (always 00)	
	zz	:	cross-section number	

The basic data of every experiment is given in the Experimental Data Tables (Part I). Based on these data the following parameters have been computed:

- Depth-averaged fluid velocity
- Mean suspended sediment load L_s (three methods)
- Mean suspended sediment transport rate S_s (three methods)

This chapter will have the same structure as Chapter 4. The following parameters will be described and discussed:

- Wave characteristics (5.2)
- Sediment concentrations (5.3)
- Fluid velocities (5.4)
- Sediment loads (5.5)
- Sediment transport rates (5.6)
- Ripple parameters (5.7)
- Size and fall velocity of suspended sediment (5.8)

The operating procedure is always the same throughout this chapter. First the figures are analysed and then the conclusions are drawn. Then one by one these conclusions are tried to be explained physically.

5.2 Wave characteristics

5.2.1 Wave spectra

The wave spectra vary over the flume. The spectral evolution for both series is shown in Figures 5.2.A1 - 5.2.A20 (Part I).

It can be noticed that on the upsloping part of the bar energy is transferred to the higher frequencies. On this part of the bar bound harmonics, primarily second harmonics, (second peak appears at $f \approx 2*f_p$) are generated by interaction of waves. The breaking process in cross-section 6 has an overall dissipating effect, which is assumed to be proportional to the distribution of the energy over the frequencies (Beji, Battjes, 1992). The nearshore upsloping part in the flume shows another transfer of energy to the higher frequencies.

In Tables 5.2.1 and 5.2.2 (Part I) the values of m_0 and m_2 for every cross-section for both series B1 and B2 can be seen. These values represent the n-th moment of the spectrum:

$$m_n = \int_0^\infty f^n * E_{xx}(f)\, df \qquad (5.2)$$

where				
	m_n	:	n^{th}-order moment of spectrum	
	f	:	frequency	(Hz)
	E_{xx}	:	wave energy	(m^2/Hz)

The parameter m_0 represents the total energy in a cross-section. In *series B1* a gradual growth of energy can be noted up to cross-section 5 as a result of shoaling. In cross-section 6 dissipation of energy takes place due to the breaking of the waves, as can be noticed in the decreasing value of m_0. In cross-section 7 and 8 the spectral energy increases and a decrease in wave energy can be noticed in the last cross-sections, probably as a result of bottom dissipation (breaking did not occur).
In *series B2* no clear increase in m_0 can be noted in front of the top of the bar, probably because the dissipation by breaking waves and the bottom dissipation are in balance with the increase in energy as a result of the increase in wave height. Behind the sand bar the dissipation of energy by the breaking waves can be noticed. The spectral energy of the last cross-sections increases due to shoaling.

The parameter m_2 can be used to get information about the spectral distribution of the energy densities. m_2 is mostly used in combination with m_0:

$$T_{0,2} = \sqrt{\left(\frac{m_0}{m_2}\right)} \qquad (5.3)$$

where				
	$T_{0,2}$	:	Average zero-crossing period	(s)
	m_0	:	0-order moment spectrum	(m^2)
	m_2	:	2nd-order moment spectrum	($m^2.Hz^2$)

The transfer of wave energy to the higher frequencies can be noticed in the magnitude of $T_{0,2}$. More energy in the higher frequencies increases the mean frequency and thus decreases the average zero-crossing period.

In *series B1* (Table 5.2.1, Part I) an increase in the average zero-crossing period in cross-section 3 can be seen. Up to cross-section 5 a decrease in $T_{0,2}$ appears and then the period increases up to cross-section 8. $T_{0,2}$ decreases in cross-sections 9 and 10.

In *series B2* (Table 5.2.2, Part I) the average zero-crossing period decreases up to cross-section 5a. An increase can be noted up to cross-section 8 and $T_{0,2}$ increases in cross-section 9.

The increase in wave energy at the toe of the upsloping part of the bar, thus at the beginning of the shoaling-process, is mainly in the lower frequencies, around the peak frequency, as can be seen in the Figures 5.2.A1 - 5.2.A20 (Part I). An increase of the peak value can be noticed. This can be noted in cross-sections 3 (B1), 7 and 8 (both series). A transfer of wave energy to the higher frequencies is the result of the shoaling process up to cross-section 5(a).

The breaking process has been analysed in more detail. In the cross-sections 5 and 6 the distribution of the wave energy over the lower ($f < 1.5*f_p \approx 0.7$ Hz) and the higher frequencies ($f > 0.7$ Hz) has been determined. The breaking process in the cross-sections behind the top of the bar seems to have a different influence on the distribution of the spectral energy for series B1 and series B2.
In series B1 the spectral evolution during the breaking process is simular to the results of Battjes and Beji (1992). The wave energy dissipates proportional to the distribution of the energy over the frequencies (see Table 5.1). The increase factor between cross-section 5 and 6 is simular for the lower and the higher frequencies ($F_i(f_{low}) = F_i(f_{high})$).

F_i	:	increase factor for wave energy between two cross-sections	(-)
F_d	:	distribution factor: wave energy f_{high} / wave energy f_{low}	(-)
m_0	:	wave energy	(cm^2)
f	:	frequency	(Hz)
f_{low}	:	$f < 0.7$ Hz	
f_{high}	:	$f > 0.7$ Hz	

Cross-section	m_0 $f < 0.7$ Hz	F_i	m_0 $f > 0.7$ Hz	F_i	F_d
5	10.40	-	5.20	-	0.50
6	6.85	0.66	3.41	0.66	0.50

Table 5.1 Distribution of wave energy over the frequencies for series B1

In *series B2* the dissipation of the wave energy seems not to be proportional to the distribution of the energy over the frequencies (see Table 5.2).

Cross-section	m_0 $f < 0.7$ Hz	F_i	m_0 $f > 0.7$ Hz	F_i	F_d
5	12.01	-	5.24	-	0.44
6	8.04	0.67	4.71	0.90	0.59

Table 5.2 Distribution of wave energy over the frequencies for series B2

The dissipation of the wave energy in the lower frequencies seems larger compared to the dissipation of the wave energy in the higher frequencies ($F_i(f_{low}) < F_i(f_{high})$). These results are not according the results of Battjes and Beji (1992). Further analysis is needed to examine the difference between series B1 and series B2.

In cross-section 9 and 10 the shoaling-process is linked with the transfer of wave energy to the higher frequencies, and yields thus in a decrease in $T_{0,2}$.

5.2.2 Wave heights

In Tables 5.2.3 - 5.2.4 and Figures 5.2.B1 - 5.2.B2 (Part I) all wave height parameters are presented for the different cross-sections in series B1, respectively series B2. From these figures the classical shoaling and breaking process can be observed.
In cross-sections 2 and 3 the wave height decreases, while on the upsloping part of the sand bar the wave height increases. On top of the bar many of the waves break, and lose part of their energy, so the wave height decreases directly behind the top of the bar. The wave height decreases up to cross-section 8 and increases again in cross-section 9 for all wave parameters. From there on the shoaling process is dominant and the wave height grows. The decrease in cross-section 10 for series B1 may be a part of the shoaling process. The distribution over the flume of H_{mo}, calculated from the spectrum, differs somewhat from the other wave parameters.

The computer program *Durosta* is a computer program developed by DELFT HYDRAULICS. *Durosta* calculates the time-dependent cross-shore transport to predict the evaluation of the dune profile under storm surge conditions. Herein only the *Durosta*-prediction of the wave height distribution over the sand bar is compared with the measured magnitude of the wave height. This has been done for series B1 and B2.
The wave height distribution calculated by *Durosta* differs from the measured wave heights ($H_{1/3}$ and H_{rms}), as can be seen in Figures 5.2.B3 and 5.2.B4 (Part I). Up to cross-section 4 *Durosta* predicts wave heights that are too large. Between cross-section 4 and (just in front of) cross-section 6 the wave height predicted by *Durosta* is too small. From there on *Durosta* predicts too large wave heights.
This can be explained by fact that *Durosta* assumes a narrow wave spectrum, with a shape that does not change when passing the sand bar. In Section 5.2.1 it was found that this is incorrect. The program also assumes a constant wave height of all broken waves. The real wave height will vary and will, on average, be smaller than the wave height as assumed by *Durosta*.

5.2.3 Wave length, wave steepness and periods

For each cross-section the wave parameters L, H_s/L and H_s/h are presented in the Tables 5.2.5 and 5.2.6 (Part I). The value of H_s has been calculated as $H_{1/3}$.
The wave length has been calculated by using linear wave theory. This might not be

correct, because of the non-linear processes that take place in the flume (shoaling, breaking), but it is useful as an approximation.
It can be noticed in Figures 5.2.C1 - 5.2.C2 (Part I) that the wave length varies over the flume. Shallow water decreases the wave celerity and hence the wave length.

The wave steepness reaches its peak value on top of the bar, and decreases right behind it. This is the logical result of the increasing wave height (shoaling) and decreasing wave length (decreasing wave celerity) up to the top of the bar, and the decreasing wave height and increasing wave length behind the top of the bar.

Figures 5.2.C3 - 5.2.C4 and Tables 5.2.7 - 5.2.8 (Part I) show the distribution of the wave period over the flume. The wave periods react only slightly to the presence of the bar in the flume. T_p remains constant over the flume. $T_{1/3}$ and $T_{1/10}$ however, show a slightly increasing trend.

5.2.4 Percentage breaking waves: Q_b

Figure 5.2.D1 (Part I) shows the relationship between the percentage breaking waves Q_b and the wave height-water depth ratio.

The percentage breaking waves was determined as follows: a wave is defined to be broken, when, while passing the cross-section, there was foam on top of the wave. A restriction of this determination is that spilling waves break over a very long length, and so an individual wave will be counted in several cross-sections, and not only in the cross-section where it actually starts to break. Not taken into account in the determination of the percentage breaking waves is the 'history' of the broken wave. It is a fact, that a breaking wave that has broken a few meters back has not the same turbulence intensity and hence the same effect on the sediment concentrations as the breaking wave that actually breaks at the spot. The influence of the turbulence caused by the breaking wave decreases with the distance, because the energy of the breaking wave dissipates.

This means that by counting the foam on top of the waves the influence of the breaking waves on suspended load and transport is overestimated in cross-sections behind the top of the bar in this project. In the cross-sections behind the top of the bar still many waves pass with foam on top of the waves, but the turbulence intensity of these breaking waves may be small.

In Figure 5.2.D1 (Part I) two different processes can be observed. The waves in the upsloping zones start to break with a wave height-water depth ratio of about 0.5. The waves in the bar trough zone (downsloping) break while a smaller magnitude of H_s/h is present, because H_s is decreased by the breaking process, and the water depth is becoming larger.

Sometimes Q_b is used as the fraction breaking waves, i.e. in the formulas for the returnflow (see section 5.4.3).

5.3 Sediment concentrations

5.3.1 General

The figures used in this section show the mean values of the measured time- and bed-averaged sediment concentration for all tests. These are the values of the pump measurements. These values can also be found in the Experimental Data Tables (Part I). The sediment concentration profile was determined as follows:

- The height above mean bed was calculated by averaging the height before and after the measurements.
- The sediment concentration was determined by pumping water-sediment samples. The mean concentration of two pump-measurements was determined, at 10 different heights above the bed.

Also the instantaneous sediment concentrations were measured by means of the Acoustical Sand Transport Meter (ASTM). The time-and bed-averaged values of the ASTM are also included in the figures of Section 5.3.2.

5.3.2 Distribution of the concentration over the flume

Figures 5.3.A1 - 5.3.A20 (Part I) show the mean, minimum and maximum values of the measured time- and bed-averaged sediment concentration for all tests.
It can be seen that the two pump measurements do not differ that much from each other. The difference between the two pump measurements does on average not exceed 17 %.
There is one exception: cross-section 1 in series B1 shows a 30 % difference in concentration. This may be explained by the fact that the flume has not been flushed for a longer time before this measurement. This means that the smallest sediment particles, which are stirred up from the sand bed, are still in the flume and on top of the sand bed. This is due to the small fall velocity of these particles. During the time that the first pump measurements are taken, these particles are stirred up from the sand bed and directly pumped up by the sediment pumps. The second pump measurement gave much smaller values, which may be a result of a more uniform distribution over the whole depth of these very small particles, also above the measuring height. This is in contrast with the first one, when the particles were just stirred up and were mostly located in the lower regions.
After the first experiment the flume has been flushed periodically and so the smallest particles are removed from the system.

It has to be taken into account that a comparison is made between concentration profiles with quite different conditions. The parameters H_s/h, H_s/L and Q_b will vary along the flume. The distribution over the flume and values can be found in the tables and figures of the previous section (for example Figure 5.2.B1). This set of figures (Fig. 5.3.A1 - 5.3.A20) will, however, give a good insight in the way the sediment concentrations are varying over a bank.

The following conclusions can be drawn regarding the distribution of the sediment concentration over the flume:

- In front of the top of the bar and with the water depth becoming shallower an increase of the concentrations in general can be noticed.
- In front of the top of the bar and with the water depth becoming shallower a more uniform (See Section 4.5.2) concentration profile can be noted.
- Behind the top of the bar a decrease in concentration can be noticed.
- Behind the top of the bar the concentration profile becomes less uniform.
- On the landward upsloping part of the bottom profile, an increase in concentration can be noted.
- Also the concentration profile becomes more uniform on the landward upsloping part.
- The bottom sediment concentration (lowest measuring point) increases up to the top of the bar. Behind the top of the bar the bottom sediment concentration decreases up to cross-section 7, and reaches a smaller magnitude than in the first cross-sections. From there on the bottom concentration increases again.
- Compared to the pump measurements, the ASTM seems to give systematically smaller values for the sediment concentration.

The explanation for the increase in concentration in general are the increasing orbital velocities, when the waves pass the upsloping part of the sand bar. With the water depth becoming shallower, an increase in H_s can be noted, as a result of shoaling. But also H_s/h increases, and hence the fluid velocities at the bottom. The fluid velocity at the bottom is an important parameter for the stirring up of sediment particles.
Also the percentage of breaking waves increases. And breaking waves cause a high level of turbulence in the flume. This turbulence causes a larger exchange between fluid layers, ergo of sediment (see also Eq.4.26). This means a more uniform concentration profile on the upsloping part of the bar.
The opposite process takes place on the downsloping part of the bar, with decreasing H_s, a decreasing H_s/h ratio and a decreasing percentage breaking waves Q_b. This means a

decreasing concentration and less uniform profiles in this part of the flume.
On the nearshore upsloping part of the bottom profile the orbital velocities increase, with increasing magnitude of concentration and increasing uniformity of the concentration profile.

To get some insight in the process that determines the bottom sediment concentration, the influence of the peak orbital velocity in onshore direction, the percentage breaking waves and the ripple height on the bottom sediment concentration has been studied. The analysis of the bottom concentration has been performed in Section 5.3.6.

For the calibration of the ASTM use has been made of the sediment concentration measurements in series A. The circumstances in series A and series B are not identical. In series B the wave height, water depth, H_s/h and Q_b are larger than in series A. This may explain the difference in the results between the pump measurements and the ASTM. Another calibration for the ASTM should be carried out for series B.

5.3.3 Wave height influence

Herein the measured time- and bed-averaged sediment concentrations of series B1 are compared with the corresponding concentrations of series B2. This gives some insight in the influence of the wave height per cross-section.
The significant wave height influences the concentration profile in the cross-sections as follows (see Figures 5.3.B1 - 5.3.B9, Part I):

- An increase in wave height leads, in general, to an increase in concentrations in one cross-section.

- The influence of the wave height on the uniformity of the concentration profile depends on the location in the flume. In cross-section 1 and 2 the uniformity does not change for series B2 compared to B1. On the seaward upsloping part of the sand bar the influence of the increase in wave height is evident. The difference in uniformity between the profiles of the two series increases, when the waves propagate from cross-section 3 to cross-section 5. This means that the increase of the sediment concentration in the upper layers as a result of the increase in wave height increases with decreasing water depth. The difference in uniformity decreases behind the top of the bar (at cross-section 6), but becomes much larger on the nearshore upsloping part of the sand bed in the flume. The (small) concentrations in the upper layers increase in series B2 sometimes by a factor 4.5 (cross-section 7), while the bottom concentration only increases with about 50 %. The absolute increase is of course larger at the bottom.

- An increase in wave height leads to an increase in bottom concentration (lowest measuring point) that is almost constant (45 %) for the first three cross-sections (see Table 5.3). In cross-section 4 a smaller relative increase in bottom concentration for series B2 can be noted. In cross-section 5 the bottom concentration decreases with larger H_s. In cross-section 6 the bottom concentration doubles in series B2, and this increase decreases to 31 % in cross-section 8. In cross-section 9 the same relative increase in bottom concentration can be noticed in series B2 as the first three cross-sections in the flume have.

c_0 : Concentration in the lowest measuring point

Cross-section	c_0 series B1 [kg/m^3]	c_0 series B2 [kg/m^3]	Increase B1 -> B2 [kg/m^3]	Relative increase B1 -> B2 [%]
1	3.225	4.655	1.43	44.3
2	2.980	4.355	1.38	46.1
3	3.320	4.720	1.40	42.2
4	7.390	8.720	1.33	18.0
5	9.795	8.935	-0.86	-8.8
6	3.230	6.605	3.38	104.5
7	2.155	3.535	1.38	64.0
8	3.040	3.985	0.95	31.1
9	4.300	6.390	2.09	48.6

Table 5.3 Increase in 'bottom concentration' with increased wave height

The measurements of the 'bottom' concentration of series B1 and series B2 are comparable, because the mean difference in height of the measurement between both series is only 3 mm (maximum difference is 6 mm).

The increase of the concentration in series B2 can be explained by the increasing orbital velocities, as result of the larger H_s. An increase in orbital velocities leads to stirring up of more sediment from the sand bed.

The uniformity of the concentration profile is related to the turbulence in the flume. The more turbulence, the more equally the sediment is distributed over the vertical, because the exchange between fluid layers is larger. In series B2 more turbulence is generated on the upsloping part of the bar than in series B1. This explains the increasing difference in uniformity between the concentration profiles of series B1 and series B2 in the measuring cross-sections up to the top of the sand bar.
In cross-section 6 the increase in uniformity is somewhat smaller, because the percentage breaking waves is relatively large in both series.
The increasing uniformity of the concentration profiles in the last cross-sections with larger wave height may be explained by the higher level of turbulence in series B2, as a result of the increase of the orbital velocities. This means an increase of the vertical transport of sediment particles to the upper layers.

The increasing bottom concentration (lowest measuring height) with increasing wave height is the result of the increasing orbital velocity at the bed (see also Section 5.3.6). The smaller relative increase in bottom concentration in cross-section 4 may be explained as follows: the sand bed is plastered with relatively large sediment particles in cross-section 4, and forms a barrier for smaller sediment particles. This means less stirring up of sediment particles from the sand bed. The sediment present in the profile is re-distributed over the vertical due to the increase in turbulence. The redistribution of the sediment over the vertical means an increase of the sediment concentrations in the upper layers, and a decrease in the near bed zone in comparison with the first cross-sections. This process can also be present in cross-section 5. Another explanation is the measuring method. The analysis sofar is based on the assumption that the local sediment concentration distribution is caused by the local conditions (wave height, water depth, ripples, etc.) However, due to the return flow in fact the sediment concentration of a cross-section at a small onshore distance is measured, where the parameters have other values. This could be an explanation for cross-section 5, because this leads to a sediment concentration measurement of a cross-section with smaller orbital velocities (down-sloping). This means smaller magnitudes of the sediment concentrations.
In cross-section 6 in both series many waves break, but more vortices of the breaking waves reach the bottom and stir up the sediment in series B2. In cross-sections 7 and 8 this breaking process loses its influence on the bottom sediment concentration and the difference decreases. The increasing difference in cross-section 9 is again a result of the increasing fluid velocities at the bottom, because of increasing wave height and an increasing value of H_s/h.

5.3.4 Influence of H_s/h

The influence of the wave height-water depth ratio on the time- and bed-averaged concentration profile is discussed in this part of the report. The operating procedure is as follows: the concentration profiles are grouped in classes of H_s/h. First these classes and the averaged magnitude of the concentration profiles within the classes are compared. Then the sediment concentration profiles in these classes of H_s/h are mutually compared.

The percentage breaking waves Q_b is included in the figures, which can be used as an extra parameter for the analysis of the results in the next section. The parameter H_s/h influences the concentration profile, as follows (see Figures 5.3.C1 - 5.3.C7, Part I):

- Within each class of H_s/h the concentration profiles vary in uniformity and in magnitude of sediment concentration).

The following conclusions concern the averaged magnitude of the concentration of all concentration profiles within each class of H_s/h. The values for the sediment concentration have been averaged for all concentration profiles in each class. Because of the variation in uniformity and in magnitude of the sediment concentration, this can only be rough conclusions and they are mainly meant to show the trend of the influence of H_s/h (see Figure 5.3.C7).

- The averaged values of the concentration profiles within each class increase per class and hence with H_s/h.

- The averaged values of the bottom concentration of the profiles within each class increase with increasing H_s/h.

- The averaged values of the concentration of the upper layers increase with increasing H_s/h.

- The relative increase of the sediment concentration in the upper layers is larger than the relative increase in the near bed zone with increasing H_s/h. This means a more uniform profile with increasing H_s/h.

The explanation for the above-mentioned observations are the increasing orbital velocities and turbulence as a function of H_s/h. The increasing magnitude of (bottom) concentration is mainly influenced by the bottom velocity. The concentration in the upper layers and the uniformity of the concentration profile are mainly influenced by the turbulence that occurs in the flume.

A closer look at the concentration profiles within the classes shows the limitedness of the parameter H_s/h to fully describe the concentration profile. The variation in uniformity and in magnitude of sediment concentration is large. To get more insight into the process the percentage breaking waves Q_b is included as an extra parameter. This will be discussed in Section 5.3.5.

5.3.5 Influence of percentage breaking waves

Herein the influence of the percentage breaking waves Q_b on the time- and bed-averaged sediment concentration profiles is discussed. The concentration profiles are mutually compared per class of H_s/h.
In the Figures 5.3.C1 - 5.3.C6 (Part I) the influence of the percentage breaking waves on the concentration profile is presented. From these figures the following conclusions can be drawn:

- An increase in Q_b leads to an increase of the concentrations in the upper layers of the profile ($z/h > 0.2$), especially for larger values of Q_b.

- The relationship between Q_b and the sediment bottom concentration (lowest measuring point) is not very clear. An increase in Q_b may lead to an increase, but also to a decrease in bottom sediment concentration (lowest measuring point).

An increase in percentage breaking waves increases the turbulence in the flume, which will lead to more exchange between fluid layers and so the sediment concentration in the upper layers increases.
For small values of Q_b (smaller than 1 %) the influence of the breaking waves on the concentration profile is negligible. One or two collapsing breaking waves between the 500 waves that pass the cross-section do not have a strong influence on the time-averaged concentration profile.
The relationship between the percentage breaking waves and the bottom concentration (lowest measuring point) is not very clear (See also Section 5.3.6). But it is difficult to draw correct conclusions, because the magnitude of the concentration is only known in the measuring points, that are made dimensionless with the water depth. The lowest dimensionless measuring height differs from one sediment concentration profile to another. Interpolation of the concentration profile can be tricky, but extrapolation of the concentration profile is certainly not recommendable. This makes it somewhat difficult to compare the results of the measurements.
Often the concentration in the near bed zone decreases with increasing Q_b, but depending on the type of breaking waves and on the penetration depth of the vortices, the concentration in the near bed zone can also increase with increasing percentage breaking waves Q_b. If the vortices of the breaking waves reach the sand bed the concentration in the near bed zone will certainly increase.
The relationship between the sediment concentration in the lowest measuring point and the percentage breaking waves is not clear. A more detailed study of the bottom sediment concentration will be performed in Section 5.3.6.

5.3.6 Analysis of bottom sediment concentration

To get some insight in the process that affects the bottom sediment concentration, a small study has been performed. The bottom sediment concentration has been calculated by

extrapolation of the sediment concentration profile to the ripple top. The magnitude of the bottom concentration was calculated by averaging the values of method 1 and 3. (See Appendix 2.) The in/decreasing bottom sediment concentration is the result of the in/decreasing orbital velocity in the near bed zone as can be seen in Figure 5.3.D1 (Part I). The relation between the peak orbital velocity at the bottom and the bottom concentration seems to be a logarithmic one. This means that the influence of the peak orbital velocity on the bottom sediment concentration decreases with larger values of the peak orbital velocity. This may be related to the fact that with larger values of the peak orbital velocity, also other factors become important, such as the breaking of the waves.
The percentage breaking waves and the ripple height are also included in Figure 5.3.D1 (Part I). The influence of both parameters is not very clear. A very careful conclusion can be that an increase in Q_b leads to a decreasing bottom sediment concentration.
The bottom sediment concentration does not seem to be influenced by the height of the ripples in these experiments.
In Figure 5.3.D2 (Part I) the relation between Q_b and the bottom sediment concentration (extrapolation to ripple top) can be noticed. Again the process on the upsloping and the downsloping part of the sand bar can be noticed. The bottom concentration on *the upsloping part* of the bar increases significantly with a small percentage of breaking waves and reaches a peak value for Q_b = 1.8 %. An increase in breaking waves leads to a decrease in bottom concentration. The bottom concentration on *the downsloping part* increases with an increasing percentage of breaking waves.

5.3.7 Comparison A- and B-series

In Figures 5.3.E1 and 5.3.E2 (Part I) the sediment concentration profiles of series A (without current) have been compared with the sediment concentration profiles of series B. The concentration profiles of series A have been added in the H_s/h classes as used in Sections 5.3.4 and 5.3.5. The following conclusions can be drawn regarding the comparison between the A- and the B-series:

- For $0.325 < H_s/h < 0.375$ the difference between the concentration profiles of series A and series B is small. For every concentration profile of series A the magnitude of the concentration is in between the minimum and the maximum magnitude of the concentration as measured in series B.

- For $H_s/h > 0.425$ the sediment concentration profiles have the same magnitude of concentration for $z/h < 0.4$. In the upper layers it can be noticed that 2 concentration profiles in series A are less uniform compared to the concentration profiles as measured in series B. This means smaller magnitudes of the sediment concentration in the upper layers.

It looks like the two series do fit properly. The smaller uniformity of the 2 concentration profiles of series A may be explained by the relative small wave height compared to series B. This means also smaller orbital velocities at the bottom, stirring up of less

sediment particles from the sand bed and a smaller vertical transport of sediment particles to the upper layers.

5.4 Fluid velocities

5.4.1 General

The velocities presented in this part of the report are the time- and bed-averaged values. For each experiment the velocities were only measured once, but with two different probes: the Electro Magnetic Velocity-meter (EMS) and the Acoustical Sand Transport Meter (ASTM). More information about these probes can be found in the Sections 3.3.8 and 3.3.12. The values presented in this part of the report are derived from the EMS. The fluid velocity is measured at 10 different heights above the bed in every cross-section.

5.4.2 Distribution of the fluid velocity over the flume

In this section the distribution of the time- and bed-averaged velocity profile along the flume and the influence of the sand bar on the velocity profile will be discussed. The following conclusions can be made concerning the velocity profile (see Figures 5.4.A1 - 5.4.A20, Part I):

- The averaged fluid velocity is mainly seawards, especially in the upper layers of the profile.
- The fluid velocity is sometimes landwards, but only in the near bed zone. This occurs in series B1 in cross-section 1, 4, 7 and 8 and in series B2 the averaged velocity is landwards in cross-section 7 and 8 in the near bed zone.
- The fluid velocity increases in front of the top of the sand bar and with the water depth becoming shallower.
- The velocity profile becomes more uniform in front of the top of the sand bar and with the water depth becoming shallower.
- The fluid velocity decreases directly behind the top of the bar.
- Behind the top of the bar the velocity profile becomes less uniform.
- The velocity increases on the nearshore upsloping part of the sand bed.
- The averaged fluid velocity profile becomes chaotic in cross-section 4, 5, 5a and 6 in series B2. The values for the velocity show a large variation over the profile.

The net mass transport in the upper layers, between the wave trough and the wave top, is directed in the landward direction. To balance the onshore mass transport above the wave trough, the fluid velocity beneath the wave trough must be directed in the seaward direction. The seaward fluid velocity is the so-called return flow.
This explains the increase in velocity in front of the top of the sand bar and with the water depth becoming shallower. The wave height increases up to the top of the bar, and thus the net transport between the wave top and the wave trough. To balance this increase in landward fluid transport in the upper layers, the return flow increases.
The onshore drift near the bottom always occurs with non-breaking progressive waves. This is the Longuet-Higgins-effect (1953). It occurs because the horizontal and vertical velocities in a wave motion with a viscous bottom boundary layer are not exactly 90 degrees out of phase, as they would be in a perfectly inviscid wave motion. This gives rise to finite time-averaged shear stress terms, additional to the bottom shear stress. These additional shear stress terms grow from zero at the bed, towards an asymptotic value. These additional shear stress terms influence the ū-distribution over the vertical. The result is the onshore drift near the bottom, known as the Longuet-Higgins-effect (also known as streaming or boundary layer drift).

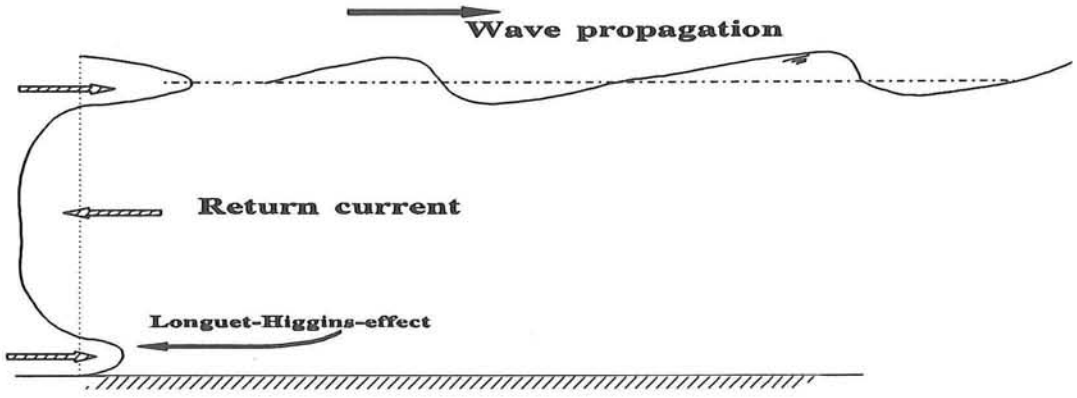

Figure 5.2 Time-averaged fluid velocity profile with the Longuet-Higgins effect

The increasing uniformity of the velocity profile in the first cross-sections of the flume is the result of the increase in turbulence, due to wave breaking and increasing orbital velocities. With this increase in turbulence the influence of the bottom friction decreases and a more uniform velocity profile is the result.
The decreasing velocity behind the top of the bar is the result of the decreasing wave height and thus the net mass transport above the wave trough. This decreases also the return flow in the cross-section.
The decreasing uniformity is related to the decreasing number of breaking waves. The

influence of the bottom friction increases and a less uniform velocity profile is the result. The landward upsloping part of the sand bed shows the same phenomena as the first one, this of course for the same reason.
The somewhat chaotic appearance of the time- and bed-averaged velocity profiles in cross-sections 4, 5, 5a and 6 must be the effect of the breaking waves. Important is the fact that breaking waves introduce a lot of air bubbles in the water. This may have its effect on the EMS velocity measurements.

5.4.3 Return flow and approximations

In this section the fluid velocity is averaged over the depth (See Appendix 2 and Section 4.3.1). The velocity distribution over the flume and the influence of the wave height will be discussed. Furthermore the accuracy of three approximations of the return flow will be checked.
The Figures 5.4.B1 - 5.4.B2 (Part I) show the depth-averaged fluid velocity for both series. The following conclusions can be drawn:

- The depth-averaged fluid velocity is in seaward direction in every cross-section; the return flow.
- A small decrease in velocity occurs in cross-section 3 for series B1 and cross-section 2 for series B2.
- From there on the velocity increases in both series till the top of the sand bar.
- Between cross-section 5 and 7 the depth-averaged velocity decreases.
- The velocity increases on the landward upsloping part of the sand bed.

A comparison between series B1 and series B2 shows the influence of the wave height:

- Increasing the wave height results in an increase in depth-averaged fluid velocity.

Most of the processes mentioned above can be explained by the distribution of the wave height over the flume. If the wave height increases, the return flow increases to counteract the increased net mass transport above the wave trough. The reversed process takes place with decreasing wave height.

Three approximations are used in this section. They were developed by

1. *Svendsen*
2. *Stive and Wind*
3. *Van Rijn*

Stive and Wind

$$U_{mean,return} = \alpha * (\frac{g}{h})^{0.5} * H_{rms} \qquad (5.6)$$

where α = 0.065, instead of 0.1 as proposed by Stive and Wind

g : acceleration of gravity (m/s^2)

No proposals are made to improve the formula developed by *Van Rijn*.

5.4.4 Wave height influence

In this section the time- and bed-averaged velocity profile of a cross-section in series B1 and the corresponding velocity profile of series B2 are compared. This will show the effect of an increased wave height on the velocity profile.
The velocity profile changes if the wave height increases (see Figures 5.4.C1 - 5.4.C9, Part I):

- The velocity increases with increasing wave height in series B2.
- The difference between the time- and bed-averaged fluid velocity of series B1 and B2 increases in front of the top of the sand bar on the upsloping part of the bed.
- Increasing the wave height in series B2 results in cross-section 4, 5 and 6 in a chaotic velocity profile.
- In cross-section 7 and 8 the difference between the magnitude of the velocity of both series decreases.
- In cross-section 9 this difference increases again as a result of the increased wave height in series B2.
- If the depth-averaged fluid velocity is small in series B1, then the increase in velocity mainly takes place in the upper layers of the water. At the bottom the influence of the increase in wave height is negligible.

The increase in velocity with increasing wave height is the result of the increased net mass transport above the wave trough.
The growing difference between the velocity profiles can be explained by the growing difference in wave height between the two series.
The chaotic velocity profiles, as result of the increasing wave height, that are observed in cross-section 4, 5 and 6 are probably the result of the air bubbles introduced by the breaking waves. The air bubbles harm the accuracy of the EMS-measurements.

The small difference between the two profiles in cross-section 7 and 8 is the result of the small increase in wave height in these cross-sections.
In cross-section 9 this increase in wave height grows and so does the difference in velocity.
The small velocity at the bottom seems to be determined by the location in the flume. An increase in velocity with increasing wave height has to take place in the upper layers, while the bottom velocity remains small in these cross-sections.

5.4.5 Influence of H_s/h

In this section the influence of H_s/h on the fluid velocity profile will be discussed. The time- and bed-averaged velocity profiles are divided in 6 classes of H_s/h. In these classes the velocity profiles are mutually compared.
From Figures 5.4.D1 - 5.4.D6 (Part I) the following observations are made:

- An increasing H_s/h ratio leads to increasing velocities.
- For $H_s/h < 0.375$ no large variation in uniformity and in magnitude of the velocity can be found. With larger values for H_s/h the variation in magnitude of the fluid velocity and in uniformity of the velocity profiles is larger.
- With large values of the H_s/h ratio the velocity profile has almost always a chaotic character.

The increase in velocity with increasing H_s/h is related to the increase in mass transport and return flow.

5.4.6 Influence of percentage breaking waves Q_b

The figures used in the previous section are also used here. The percentage breaking waves is included in the Figures 5.4.D1 - 5.4.D6 (Part I) to determine the influence of Q_b. The following conclusion can be made:

- An increase in Q_b introduces irregularities or leaps in the time- and bed-averaged velocity profile.

This can be explained by the introduction of air bubbles in the water with a larger number of breaking waves. This has a negative effect on the EMS.

5.4.7 Asymmetry in fluid velocity signal at the bottom

The asymmetry in the fluid velocity signal, as a result of wave asymmetry, will be discussed in this part of the report. The significant on- and offshore orbital velocities of the three lowest measurements in an experiment are computed for every test.
The procedure that has been executed will first be discussed. The procedure can be followed visually in Figure 5.4.E1 (Part I), which gives the EMS-signal throughout the procedure.
The first step was to determine the mean value of the velocity signal. This mean value was subtracted from the fluid velocity signal. The second step was to seperate the velocity signal into the frequency domains of long waves ($T > 2*T_p \approx 5$ s) and short waves ($T < 5$ s). The final step was to calculate the significant peak orbital velocity in on- and offshore direction. This value represents the average of the ⅓ largest velocity amplitudes. The magnitude of the peak orbital velocities in on- and offshore direction for all frequency domains are presented in Tables 5.4.1 and 5.4.2 (Part I).

The onshore peak orbital velocity in the velocity signal turned out to be larger compared to the offshore peak orbital velocity. In the high frequency domain this asymmetry is even more pronounced. In the low frequency domain the peak orbital velocity in offshore direction is larger than in onshore direction (see Table 5.4). This was also found in the earlier 100-μm-basin-study (1992).

Frequency Domain	Series B1		Series B2	
	$\hat{u}_{b,on} > \hat{u}_{b,off}$ (%)	range (%)	$\hat{u}_{b,on} > \hat{u}_{b,off}$ (%)	range (%)
total	15	-5 % to +40 %	19	- 7 % to 54 %
high	29	+3 % to +67 %	37	+ 5 % to 79 %
low	-9	-28 % to +10 %	-14	- 195 % to + 10 %

Table 5.4 Asymmetry in velocity signal

In Figures 5.4.E2 - 5.4.E7 (Part I) the on- and offshore fluid velocity for the lowest measurements for both series are presented. Also an asymmetry-factor is presented, defined as:

$$A_{asym} = \frac{\hat{u}_{b,on}}{\hat{u}_{b,on} + \hat{u}_{b,off}} \qquad (5.7)$$

where
A_{asym} : Asymmetry-factor (-)
$\hat{u}_{b,on}$: $u_{1/3}$ at the bottom in onshore direction (m/s)
$\hat{u}_{b,off}$: $u_{1/3}$ at the bottom in offshore direction (m/s)

- A strong increase in sediment loads in front of the top of the bar and with the water depth becoming shallower can be noticed. The magnitude of the sediment load increases with a factor 3. The sediment load reaches its largest value on top of the bar (series B1) or directly behind the top of the bar (series B2). The sediment load behind this point decreases.

- In cross-section 7 the smallest sediment load in the flume for series B1 can be found and a relative minimum in series B2.

- From cross-section 7 the sediment load increases. This increase is less pronounced compared to the seaward upsloping part of the sand bar.

The sediment load is related to the orbital velocities and thus linked with the wave height, the wave height-water depth ratio and the percentage breaking waves Q_b. So if these parameters, increase/decrease the load increases/decreases as can be concluded from Section 5.3.

5.5.2 Wave height influence

Comparing Figure 5.5.A1 (series B1) with Figure 5.5.A2 (series B2) in Part I shows the influence of the wave height on the suspended sediment load. The results of an increase in wave height are:

- An increasing wave height leads to increasing suspended sediment loads.

- The absolute increase in suspended load increases up to cross-section 3 with the higher waves in series B2.

- In cross-section 4 the increase in suspended load with higher waves is much smaller. The difference increases in cross-section 5.

- The suspended load in cross-section 6 increases significantly in series B2.

- The increase of the loads with the higher waves in series B2 in cross-section 7 is much smaller. The difference in suspended load increases in cross-section 8 and decreases in cross-section 9 in series B2. The increase of the loads with increasing wave height is the result of the larger fluid velocity at the bottom. The increasing orbital velocities lead to stirring up of more sediment.

To get more insight into the influence of the wave height on the distribution of the suspended load over the flume the absolute and relative increase of the load have been calculated in Table 5.5:

L_s : Depth-integrated suspended load (kg/m²)				
Cross-section	L_s series B1 [kg/m²]	L_s series B2 [kg/m²]	Increase B1 -> B2 [kg/m²]	Relative increase B1 -> B2 [%]
1	0.157	0.186	0.029	18.5
2	0.154	0.248	0.094	61.0
3	0.185	0.288	0.103	55.7
4	0.352	0.378	0.026	7.4
5	0.496	0.551	0.055	11.1
6	0.249	0.471	0.222	89.2
7	0.108	0.199	0.091	84.3
8	0.147	0.247	0.100	68.0
9	0.188	0.269	0.081	43.1

Table 5.5 Increase in suspended load with increased wave height

The increasing difference between the loads in the first cross-sections of series B1 and series B2 can be explained with the increasing difference in wave height between the two series, and thus the difference in orbital velocity. Also the percentage breaking waves in series B2 is larger. This leads to stirring up of more sediment.
The smaller increase in series B2 in cross-section 4 and 5 may be explained by the plastering of the bed (see Section 5.3.3).
The increase in suspended load with higher waves in cross-section 6 can be explained by the difference in turbulence intensity between both series.
On the nearshore upsloping part of the sand bed the increase in suspended load is almost constant (absolute), as result of the increase in orbital velocity.

5.5.3 Influence wave height-water depth ratio

The influence of the wave height-water depth ratio on the suspended load will be discussed in this section. Based on the analysis of the Figures 5.5.A1 and 5.5.A2 (Part I), the following conclusion can be drawn:

- An increase in H_s/h leads to an increase in suspended sediment load.

In Figure 5.5.B1 (Part I) the suspended load is presented as function of H_s/h. From this figure the following conclusion can be drawn:

- There seems to be a linear relationship between H_s/h and the suspended load, especially with small values of H_s/h. With larger values of the wave height-water depth ratio this linearity is less pronounced.

- Based on the measurements a relationship between H_s/h and the suspended sediment load can be determined. Using the least square method, the following empirical formulae were found:

$$L_s = -0.171 + 1.220 * (\frac{H_s}{h}) \tag{5.8}$$

and dimensionless:

$$\frac{L_s}{\rho_s * D_{50}} = -0.902 + 5.807 * (\frac{H_s}{h}) \tag{5.9}$$

where

L_s	:	suspended sediment load	(kg/m²)
H_s	:	wave height	(m)
h	:	water depth	(m)
ρ_s	:	mass density of sediment	(kg/m³)
D_{50}	:	grain diameter exceeded by 50% by weight	(m)

These formulae are valid within the limits $0.26 < Hs/h < 0.65$
$0.31 \text{ m} < h < 0.60 \text{ m}$

The parameter H_s/h turns out to be an important parameter for the suspended sediment load. An increase in H_s/h means an increase in fluid velocities at the bottom and more sediment particles are brought into suspension.
The deviation with larger values of H_s/h is the result of the breaking waves, which mainly occurs with larger values of the wave height-water depth ratio.

5.5.4 Influence of percentage breaking waves

Herein the influence of the percentage breaking waves Q_b on the suspended sediment load will be discussed. The Figures 5.5.A1 and 5.5.A2 (Part I) are used for analysis:

- The distribution of the suspended load over the flume is almost the same as the distribution of Q_b over the flume. The peak value of the suspended load in series B1 occurs in cross-section 5, but the peak value of the percentage breaking waves was found in cross-section 6.

- The peak value of the suspended load in series B2 can be found in cross-section 5a, while the peak value of Q_b is located in cross-section 6.

The explanation for this difference may be related to the determination of the percentage of breaking waves (see Section 5.2.4). The 'history' of the wave is not taken into account in the value of the percentage breaking waves, so the influence of Q_b on the suspended sediment load is smaller in cross-section 6.

All suspended sediment loads with the corresponding Q_b have been drawn in Figure 5.5.C1 (Part I). The following became clear:

- Two different processes can be distinguished, one on the upsloping parts and one on the downsloping part of the sand bar.

- On the upsloping part of the bar the relationship between the load and percentage breaking waves seems to be a logarithmic one.

- On the downsloping part of the bar the relationship between the suspended load and the percentage breaking waves is linear.

The logarithmic relation between the suspended sediment load and Q_b has the following consequence: a small magnitude of Q_b leads to a relatively large increase in suspended sediment load, while with more breaking waves the relative increase is smaller.

5.5.5 Comparison A- and B-series

A comparison between the loads of the tests in series A (without current) and series B will be discussed in this section. For both series the averaged values of method 1 and 3 (see Appendix 2) have been calculated. In Figure 5.5.D1 (Part I) the magnitude of the load has been plotted as function of the wave height. The following conclusion can be drawn:

- The magnitude of the loads measured in series A is larger compared to the magnitude of the loads in series B with the same wave height.

The explanation for the larger magnitude of the suspended sediment load in series A is the smaller water depth. This leads to stirring up of more sediment particles compared to a situation with a larger water depth (series B).

5.6 Current-related sediment transport rates

5.6.1 Sediment flux

Herein, only the current-related sediment transport is considered (See also Sections 2.1, 4.7.1 and 4.7.2). In the Figures 5.6.A1 - 5.6.A20 (Part I) the distributions of the transport over the vertical, for different cross-sections along the flume are presented. The calculated values are obtained by multiplication of the time-averaged concentration with the time-averaged fluid velocity for 10 different heights in each cross-section. It shows that:

- The time-averaged sediment transport mainly takes place in the near bed regions.
- In the first cross-sections of the flume the sediment transport in the tests of *series B1* takes place for $z/h < 0.10$. This 'transport' depth increases to $z/h < 0.25$ in cross-section 2. In cross-section 3 the sediment transport takes place for $z/h < 0.10$, in cross-section 4 the transport depth increases to $z/h < 0.40$. In cross-section 5 the transport takes place over the whole depth. In cross-section 6 the 'transport' depth decreases to $z/h < 0.40$. This depth decreases to $z/h < 0.10$ in cross-section 7 and increases to $z/h < 0.30$ in the last cross-sections of the flume.
- In the tests of *series B2* the sediment transport mainly takes place for $z/h < 0.10$ in cross-section 1 and 2. In cross-section 3 the transport depth increases to $z/h < 0.20$. In cross-section 4 the transport takes place over the whole depth. This is also the case for cross-section 5 and 5a, but the magnitude increases here. In cross-section 6 a full 'transport' depth can be noted, but the magnitude decreases. In cross-section 7 and 8 the contribution for $z/h < 0.20$ is significant for the sediment transport. In cross-section 9 the most significant part of the sediment transport takes place for $z/h < 0.3$.
- The time-averaged transport in the flume is predominantly seawards. Sometimes the lowest measurement(s) give(s) a landward sediment transport. This is the case in cross-sections 1, 4, 7 and 8 for the tests of series B1. In cross-section 7 and 8 landward transport takes place in series B2 with higher waves.
- The tests of series B2 have only landward transport results in cross-section 7 and 8 in the near bed zone.

The distribution of the 'transport' depth along the flume is linked with the distribution of the concentration profile over the flume particularly.
The predominantly seaward sediment transport is the result of the return flow induced by the propagating waves.
The landward transport that sometimes occurs in the near bed zone is related to the time-averaged landward velocity, which occurs in the near bed zone of these cross-

sections. The onshore bottom layer drift is known as the Longuet-Higgins-effect (see Section 5.4.2).

5.6.2 Distribution of suspended sediment transport over the flume

This section discusses the current-related depth-integrated sediment transport. The methods of calculation can be found in Appendix 2. The values used for the depth-integrated sediment transport is the mean of method 1 and 3. The sediment transport rate is depending on the location in the flume as follows (see Figures 5.6.B1 - 5.6.B2 and Tables 5.6.1 - 5.6.2, Part I):

- In nearly every cross-section the sediment transport is found to be directed seaward.
- The transport rate reaches its maximum value on top of the bar in series B1 and directly behind the top of the bar in series B2.
- In series B1 the sediment transport that appears is slightly positive (landwards) at the beginning of the sand bed. This was also found in cross-section 7 and 8. For the tests in series B2 only in cross-section 8 a small landward transport was found.

The seaward sediment transport is the result of the return flow.
The peak value in transport rate on top of the sand bar is caused by the combination of a large magnitude of sediment concentration and fluid velocity. The large magnitude of the concentration is a result of the shoaling waves and the increasing percentage breaking waves. The shoaling waves lead to an increase in orbital velocities. A result is the stirring up of more sediment. The breaking waves also introduce turbulence in the flume, and increase the magnitude of the sediment concentration. The large magnitude of the fluid velocity is also a result of the shoaling waves. The return flow increases on the upsloping part of the bar. This combination results in a large magnitude of the suspended sediment transport rate, the product of sediment concentration and fluid velocity.
A landward depth-integrated sediment transport occurs when a combination of time-averaged landward velocity (Longuet-Higgins effect) together with a significant magnitude of the concentration in the near bed zone occurs.

5.6.3 Influence of the wave height

The comparison of Figure 5.6.B1 and Figure 5.6.B2 (Part I), and thus of the sediment transport rate in series B1 and B2, gives some insight in the influence of the wave height on the sediment transport rate. The following observations about sediment transport rate and the wave height can be made:

- The suspended transport rate increases with increasing wave height.
- The influence of the wave height on the sediment transport rate varies strongly over the flume (see Table 5.6). In cross-section 1 the direction of the transport is landward during Series B1. The landward transport in series B1 changes into seaward transport with the increase in wave height. In cross-section 2 and 3 an increase in suspended sediment transport of 61 % respectively 73 % can be noted in series B2. The transport in cross-section 4 increases by a factor 13 as result of the increase in wave height. In cross-section 5 the difference in transport rate decreases to 73 % and in cross-section 6 the depth-integrated sediment transport increases by a factor 3 in series B2. Also in cross-section 7 an enormous increase in transport by a factor 15 with the larger wave height can be noticed. The seaward transport in cross-section 8 becomes a landward sediment transport in series B2. In cross-section 9 an increase in transport of 46 % with the increased wave height can be noted.

S_s : Depth-integrated suspended sediment transport (kg/s.m)				
Cross-section	S_s series B1 [kg/s.m]	S_s series B2 [kg/s.m]	Increase B1 -> B2 [kg/s.m]	Relative increase B1 -> B2 [%]
1	+ 0.00073	- 0.00220	- 0.00293	- 401.4
2	- 0.00120	- 0.00193	- 0.00073	+ 60.8
3	- 0.00166	- 0.00287	- 0.00121	+ 72.9
4	- 0.00096	- 0.01236	- 0.01140	+ 1187.5
5	- 0.01399	- 0.02424	- 0.01025	+ 73.3
6	- 0.00482	- 0.01567	- 0.01085	+ 225.1
7	- 0.00006	- 0.00093	- 0.00087	+ 1450.0
8	- 0.00003	+ 0.00010	+ 0.00013	- 433.3
9	- 0.00225	- 0.00328	- 0.00103	+ 45.8

Table 5.6 Increase in suspended sediment transport with increased wave height

An increase in wave height results in an increase in return flow. Also more sediment is stirred up. This results in an increase in magnitude of the suspended sediment transport.

The reversal of the transport direction with larger wave height is related to the direction of the time-averaged bottom fluid velocity. In cross-section 1 the reversal from the landward to the seaward direction of the time-averaged bottom velocity with larger wave height can be noticed. In combination with the most significant concentrations in the near bed zone this results in the reversal of the transport direction in series B2. In cross-section 8, the time-averaged bottom fluid velocity switches to the landward direction, as a result of the increase in wave height, and so does the sediment transport.
The increase in cross-section 2 and 3 in series B2 is the result of the larger wave height, the larger wave height-water depth ratio and the percentage breaking waves. The result of the increase in the above mentioned parameters is an increase in concentration (stirring effect) and fluid velocity (return flow) and their product, the current-related sediment transport. This process reaches its peak in cross-section 4 with a tremendous increase in transport.
The decrease in bottom concentration in cross-section 5 with larger wave height results in a smaller increase in transport.
In cross-section 6, with larger wave height, a larger magnitude of concentration and fluid velocity can be noted and thus an increase in transport.
In cross-section 7 a tremendous increase in sediment transport with higher waves can be noted, especially as the result of the increase in concentration in the upper layers.
The increase in sediment transport in cross-section 9 with higher waves is the consequence of the larger contribution of the upper layers.

Figure 5.6.C1 (Part I) shows the relation between the wave height and the suspended sediment transport. Based on the measurements the following empirical formula is found:

$$S_s = 64154 * H_s^{9.5} \qquad (5.10)$$

where	S_s	:	seaward suspended sediment transport	(kg/sm)
	H_s	:	wave height	(m)

This formula is valid within the limits 0.15 m $< H_s <$ 0.21 m and 0.31 m $< h <$ 0.60 m. It should be taken into account that this formula has no practical use whatsoever. It only describes the relationship between the measured wave height and the calculated magnitude of the suspended transport based on the measurements in this series. The same form of formula has been chosen as in the earlier 100-μm-basin-study (1992). The difference in the exponents found in series A and B shows the sensibility of this kind of formula to small changes in the magnitude of the wave height and the calculated sediment transport. This makes clear that the reliability of this formula is not very high.

5.6.4 Influence of H_s/h

The Figures 5.6.B1 and 5.6.B2 (Part I) show the influence of H_s/h on the suspended sediment transport. The following can be noticed:

- The similarity between the distribution of H_s/h and the suspended transport.

An increase in H_s/h means an increase in velocity at the bottom. This has two consequences: more sediment is brought into suspension and the mean fluid velocity increases. This results in a larger magnitude of the suspended transport.

In Figure 5.6.D1 (Part I) the suspended sediment transport is shown as a function of H_s/h. Based on the measurements the following empirical formula is found:

$$S_s = 0.425 * (\frac{H_s}{h})^{5.3} \qquad (5.11)$$

where	S_s	:	seaward suspended sediment transport	(kg/sm)
	H_s	:	wave height	(m)
	h	:	water depth	(m)

This formula is valid within the limits $0.26 < H_s/h < 0.65$ and $0.31 \text{ m} < h < 0.60 \text{ m}$. In comparison to Eq. 5.10, a significant change in the exponent can be noticed. However, a comparison with series A shows about the same magnitude in the exponent for both series: 5.2 for series A, 5.3 for series B.

5.6.5 Influence of percentage breaking waves

Herein, the relationship between the suspended transport and the percentage breaking waves is discussed (see Figures 5.6.B1 and 5.6.B2, Part I).

The distribution of the percentage breaking waves Q_b is similar to that of the suspended transport rate, but:

- The peak of Q_b and the peak in sediment transport are not located in the same cross-section. For series B1 the peak of Q_b is in cross-section 6 and the peak of the transport is in cross-section 5.

- In series B2 the peak of the transport is in cross-section 5a, while the peak of the percentage breaking waves is situated in cross-section 6.

This difference may be related to the definition of the percentage breaking waves (see Section 5.2.4). The 'history' of the wave is not taken into account in the value of the percentage breaking waves, so the influence of Q_b on the suspended sediment transport is smaller in cross-section 6.

Figure 5.6.E1 (Part I) shows the transport with the corresponding Q_b. The following conclusions can be drawn:

- Two processes can be distinguished, one on the upsloping parts in the flume and one on the downsloping part (bar trough zone).
- The relation between the suspended sediment transport rate and the percentage breaking waves on the upsloping parts seems to be a logarithmic one.
- The relation between the suspended sediment transport and Q_b on the downsloping part of the bar seems to be an exponential one.

The logarithmic relation between the suspended sediment transport and Q_b shows the decreasing influence of Q_b on the transport with an increasing number of breaking waves. The exponential relationship on the downsloping part of the bar means an increasing influence of the percentage breaking waves on the suspended sediment transport.

5.6.6 Comparison of current-related sediment transport and total sediment transport

In this section two transport rates will be compared: the current-related sediment transport and the total transport rate, which has been calculated from bed level changes.

1. Current-related sediment transport
The current-related transport rate was also used in the previous sections. This method is based on the time-averaged values of the sediment concentration and the fluid velocity. The current-related transport is calculated as follows:

$$S_x = \int_0^h \bar{\bar{u}} * \bar{\bar{c}} \, dz \qquad (5.12)$$

where	S_x	:	current-related sediment transport	(kg/s.m)
	h	:	waterdepth	(m)
	$\bar{\bar{u}}$	:	time-and bed-averaged fluid velocity	(m/s)
	$\bar{\bar{c}}$	:	time- and bed-averaged sediment concentration	(kg/m^3)

The distribution over the flume of the magnitude of the current-related sediment transport rate is presented in Tables 5.6.1 and 5.6.2 (Part I).

2. Total sediment transport
The total sediment transport has been calculated from the observed bed level changes. These changes were determined by comparing bed profiles at different times. The bed profiles were measured at the flume windows. The total sediment transport is calculated as follows:

$$S_{n+1} = S_n + \frac{V * \rho_s * (1-\epsilon)}{\Delta t * b} \qquad (5.13)$$

where				
	S_n	:	suspended sediment transport in a cross-section with number n	(kg/s.m)
	V	:	volume of accreted / eroded sediment between cross-sections n and n+1	(m^3)
	Δt	:	time between two bed level measurements	(s)
	b	:	width flume	(m)
	ρ_s	:	mass density of sediment	(kg/m^3)
	ϵ	:	voids ratio	(-)

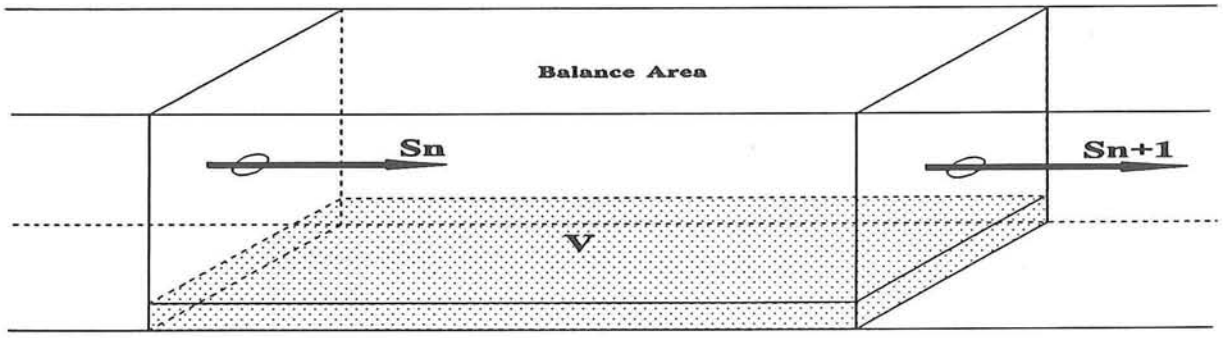

Figure 5.3 Balance area for sediment transport

The unknown parameter is S_0, the suspended transport at x=0. As an approximation $S_0 = 0$ is assumed, although a small amount of sediment was found between the wave board and cross-section 1.
The distribution over the flume of the magnitude of the bed changes is presented in Table 5.6.3 (Part I).

The transport for both series can be found in Figures 5.6.F1 and 5.6.F2 (Part I). It shows that, especially around the sand top of the bar, the current-related sediment transport rate is larger than the total sediment transport.
The difference can be explained by the fact that the wave-related sediment transport that occurs as a result of the asymmetry of the waves is not taken into account. It looks like that the wave-related sediment transport decreases the current related transport. This means a predominantly landward wave-related sediment transport rate, while the current-related sediment transport is predominantly seaward. The wave-related sediment transport

will be considered in a later study.
Figures 5.6.F3 and 5.6.F4 and Table 5.6.3 (Part I) show the bed profiles before and after the test and the difference between the two for both series. The most important conclusion from these figures and the table is the fact that the sand bar moves seaward.
The sand balance for the flume has also been checked for both series using the results of the bed level change measurements. It shows that in series B1 the bed level decreases overall with only 0.10 cm and in series B2 the bed level increases overall with 0.15 cm. The decrease in bed level in series B1 can be explained by the losses under the wave damping structure and in front of cross-section 1. The increase in bed level in series B2 can be explained by the dumping of sand in front of the wave damping structure, which was necessary, because the sediment was eroded there. This was a consequence of the periodic flushing of the flume, which was necessary for clearing the system of the smallest sediment particles floating in the water. For equal conditions in all experiments sediment was added in front of the wave damping structure.

5.6.7 Comparison A- and B-series

In Figure 5.6.G1 (Part I) a comparison is made between the the suspended sediment transport for all tests in series A without current and series B, as a function of H_s. The magnitude of the suspended sediment transport is calculated as the average of method 1 and 3 (see Appendix 2). From this figure the following conclusion can be drawn:

- The suspended sediment transport in series A is larger compared to the suspended sediment transport in series B.

The explanation may be that the water depth in series A is smaller compared to the water depth in series B. This leads to stirring up of more sediment compared to a situation with a larger water depth. The return flow is however smaller, because the wave height is smaller in series A. The combination still leads to a larger transport rate in series A compared to the suspended sediment transport in series B with the same wave height.

5.7 Ripple parameters

5.7.1 General

During each experiment the mean bed level was determined and a plot was made with the pen recorder. Based on these plots, the ripple parameters have been determined, such as ripple height and ripple length. From these parameters the ripple steepness can be calculated. The moving carriage moved over a small distance of 15 cm. A consequence of this small moving distance is that the parameters of only 2 or 3 ripples can be determined. The mean values of these parameters have been calculated. This section discusses these averaged parameters as function of the distance from the wave board.

During the experiments the following bed forms occured, defined as:

- 2-dimensional ripples: regular ripple-shaped bed, with ripples in wave direction.
- 2.5-dimensional ripples: semi-regular ripple-shaped bed, with some ripples not in wave direction.

Other forms, like "dunes" or a "flat bed" were not observed in this series. The bed form for each experiment is listed in the tables with experimental data under "BFT bedf type:".

5.7.2 Ripple height

The ripple height fluctuates slightly over the sand bar in the flume. Series B1 showed mean ripple heights between 0.005 and 0.013 m; in series B2 mean ripple heights ranging from 0.005 to 0.011 m were found. No clear pattern can be observed in either series (see Figures 5.7.A1 - 5.7.A2, Part I).

5.7.3 Ripple length

The ripple length does seem to have a certain distribution over the flume. In the first cross-section the ripple length is relatively large, the length decreases up to cross-section 3. Then the ripple length increases to cross-section 6 in series B1 and cross-section 5 in series B2. A decrease in ripple length can be noticed up to cross-section 8 and an increase in ripple length for the last cross-sections occurs. This can also be seen in Figures 5.7.A1 and 5.7.A2 (Part I). Series B1 showed mean ripple lengths between 0.046 and 0.073 m, in series B2 mean ripple lengths ranging from 0.038 to 0.083 m were found.

5.7.4 Ripple steepness

The ripple steepness has a quite different distribution for series B1 and B2. See Figures 5.7.B1 and 5.7.B2 (Part I). The steepness for series B1 shows a fluctuating behaviour and no clear relation can be found.
But in series B2 there is a quite smooth pattern. After a small increase in cross-section 3 the ripple steepness decreases up to cross-section 5. In cross-section 5a the steepness becomes much larger. The steepness is smaller in cross-section 6 and in cross-section 7 the ripple steepness grows. The last cross-section shows a somewhat smaller steepness. In series B2 mean ripple lengths ranging from 0.038 to 0.083 m were found.

5.8 Size of the suspended sediment

5.8.1 General

In each experiment ten water-sediment samples were obtained. These samples were added together to make a bulk sample. Each bulk sample was analysed in the Visual Accumulation Tube at DELFT HYDRAULICS to determine the fall velocity distribution and the suspended material size D_s. The Experimental Data Tables (Part I) present the measured fall velocity and the suspended sediment size distribution. In this section the distribution of the size of the suspended sediment will be discussed.

5.8.2 Distribution of the sediment size over the flume

The subject of this section is the distribution of the sediment size along the flume. In Figures 5.8.A1 and 5.8.A2 (Part I) the suspended sediment sizes as measured in series B1 and B2 have been plotted. It can be observed that:

- In series B1 the sediment size is small in cross-section 4 and cross-section 8. At a distance of 16 m there is a maximum in sediment size.
- In series B2 the minimum size is in cross-section 4 and the maximum size in cross-section 5a.

The relatively small sediment size in cross-section 4 can be explained as follows: the waves break mostly in cross-section 5. This has as a consequence a large amount of stirred up sediment in cross-section 5. The smallest sediment particles reach the highest fluid layers. The return flow transports these small sediment particles to cross-section 4 and increase the contribution in small sediment particles.
The relative maxima that occur at 16 m (series B1) and cross-section 5a (series B2) may also be explained with the breaking process. If the vortices of the breaking waves reach the sand bed, this also means that the larger sediment particles are stirred up. Their contribution is larger, so D_{50} increases.
The relative minimum sediment size in cross-section 8 in series B1 is a result of the decreasing rate of turbulence in the flume and the decreasing wave height. This means that less and smaller sediment particles are brought into suspension.
In the last cross-section the contribution of the larger sediment particles grows, because of the increase in wave height, and wave height-water depth ratio. More sediment particles of larger size are stirred up.

5.8.3 Distribution over the depth

For one measurement the distribution of the sediment size as function of the depth has

been determined. This has been done for cross-section 1 in series B1. It is certainly not said that this distribution is representative for the sediments in the whole flume. Most likely this is not the case. Figure 5.8.A3 (Part I) shows the results:

- The sediment size is largest at the bottom and decreases upwards.
- A relative minimum occurs at z/h $\approx$ 0.20. Going upwards, the sediment size increases.
- A relative maximum can be found at z/h $\approx$ 0.33. Going upwards, the sediment size decreases.

This distribution is not a very logical one. A distribution with a decreasing sediment size going upwards would be expected. It seems rewarding to do some experiments to examine this phenomenon.

6 Models for sediment transport

6.1 General

In this chapter two existing sediment transport prediction models will be discussed. The models are used to compare the predicted results with the experimental results of the A series. The models used are:

- Van Rijn model. Computer model TRANSPOR (March 1994)
- Bijker model (1967,1971). Computer model BAAK (May 1987)

The Van Rijn model (3rd edition) is partly based on the results from the earlier 100-μm-flume-study (1988) and 100-μm-basin-study (1992). Both models give an explicit estimation of the concentration and fluid velocity profiles. The precise description of the formulae are given in Appendix 4 (Bijker model) and Appendix 5 (Van Rijn model). Their results will be compared to the experimental results. As in the earlier 100-μm-flume-study and 100-μm-basin-study two classes of transport rates will be distinguished:

- small transport rates ($S_s < 0.01$ kg/sm)
- large transport rates ($S_s > 0.03$ kg/sm)

The parameters needed for calculation of the transport rates will be given in the next paragraph. A precise comparison of formula results and experimental results is not always possible, because the use of the input parameters are subjective. Therefore some assumptions have to be made to accomplish a reasonable comparison.

6.2 Parameters for transport models

6.2.1 General

The parameters, needed for the calculation of the transport rates, will be discussed in this paragraph. These parameters are: wave period (T_z, T_p'), wave height (H_s), bedroughness (K_s), mean fluid velocity (U_m), diameter of sediment (D_{50},D_{90},D_{ss}). In all computations the following parameters were kept constant:

-	mass density of water:	ρ_w	:	1000 kg/m^3
-	mass density of sediment:	ρ_s	:	2650 kg/m^3
-	porosity:	p	:	0.4
-	acceleration of gravity	g	:	9.81 m/s^2
-	viscosity	υ	:	1e-6 m^2/s
-	ratio of sediment and fluid mixing coefficient	ß	:	1.0

6.2.2 Wave period

The available parameters for the wave period are:

- Relative zero crossing period T_z
- Relative wave spectrum peak period T_p'

According to the conclusions in the earlier 100-μm-flume-study (1988) the use of the relative peak period T_p' as the characteristic parameter should give the best results, because of the fact that in case of regular waves, the energy wave spectrum shows that most energy is concentrated around this period. To account for the presence of the current, the relative peak period T_p' and the corresponding wave length L were used in all computations.

6.2.3 Bed roughness

The bedroughness parameter K_s is of great importance for sediment transport computation. For both models the following value for the bed roughness has been chosen:

- bed roughness: $K_{s,w}=K_{s,c}$: 3*r

Where $K_{s,w}$ is the wave-related physical roughness height, $K_{s,c}$ is the current-related physical roughness height and r is the mean ripple height. Other parameters related to the bed roughness are the thickness of the wave mixing layer δb and the reference level a. In both models the following values have been chosen for these parameters:

- thickness wave mixing layer: δb : 3*r
- reference level: a : 0.5*r

6.3 Van Rijn transport model

6.3.1 General

For the velocity profile, in the Van Rijn formula a distinction is made between the velocity distribution outside and inside the wave-boudary layer. Outside this layer the velocity distribution is based on the apparent roughness $K_{s,app}$, inside also on the physical roughness $K_{s,phys}$. The concentration has a constant value below the reference level, while above this level a concentration gradient is computed.

The Van Rijn formula is based on the time-averaged convection-diffusion equation, with relationships for current-related and wave-related mixing coefficients. The current-related mixing coefficient is described as:

$$\varepsilon_{s,c} = \beta * \phi * \varepsilon_{f,c} \tag{6.4}$$

The ϕ-factor in this formula expresses the influence of the sediment particles on the turbulent structure of the fluid (damping effects). Using measured concentration profiles, Van Rijn assumed a concentration-dependent ϕ-factor. For the wave-related sediment mixing coefficient, Van Rijn related the vertical distribution of the sediment mixing coefficient to basic wave parameters. (See Handbook Sediment Transport by currents and waves 2nd edition, by Van Rijn).

A parameter that needs attention in this model is the apparent roughness $K_{s,app}$. This roughness is based on the physical roughness $K_{s,phys}$. According to Van Rijn (1988) this relation can be described by:

$$\frac{K_{s,app}}{K_{s,phys}} = e^{(\gamma \frac{U_b}{U_m})} \tag{6.5}$$

with γ : coefficient dependent on the angle between the current and the waves, in case of following waves $\gamma=0.75$.

Although in the present study a value of $\gamma=0.54$ was found, the correlation between the measured and the calculated values was not very high. In section 4.10.8 it was found that, for the present study, the relation between $K_{s,app}/K_{s,phys}$ and $\hat{U}_{b,on}/U_m$ is not exponential. This has its influence on the computed velocities and concentrations.

6.3.2 Comparison Van Rijn model with measured transport

In this section a comparison between the results from Van Rijn computations with the results from the measurements will be made. From Table 6.3.1 (part I) it can be concluded that compared to the experimental data:

- The transport rates computed with the Van Rijn formula are small compared to the measured values (measured values are on an average 3.2 times larger compared to the calculated values).

In the Figures 6.3.A.1 and 6.3.A.2 (Part I) the influence of the wave height H_s on the measured - and calculated transport rates is presented. From these figures it can be seen that compared to the measured transports:

- The increase in sediment transport with increasing wave height is less pronounced for the Van Rijn formula than the measurements show. This difference is more pronounced with increasing current strength.

In the Figures 6.3.B.1 - 6.3.B.3 (Part I) the influence of the current strength U_m on the measured - and calculated transports is presented. From these figures it can be seen that compared to the measured transports:

- The increase in sediment transport with increasing current strength is less pronounced for the Van Rijn formula than the measurements show. This difference is more pronounced with increasing wave height.

6.3.3 Comparison Van Rijn model with measured concentration profile

For $K_{s,w}=K_{s,c}=3*r_m$ the concentration profile is computed and compared with the measured concentration profile. From the Tables 6.3.2 - 6.3.5 and Figures 6.3.C.1 - 6.3.C.7 (Part I) the following conclusions can be made; compared with the measurements:

- The concentration profile is predicted too uniform by the Van Rijn model, especially in the lower part of the profile ($z/h<0.5$). This difference is less pronounced with increasing current strength.

- The concentrations in the near bed zone are predicted too small by the Van Rijn model, especially in case of a large wave height and a weak current.

- Compared to the measurements, the increase in concentrations with increasing wave height is less pronounced for the Van Rijn formula.

6.3.4 Comparison Van Rijn model with measured velocity profile

In the Figures 6.3.D.1 - 6.3.D.7 (Part I) a comparison is made between the computed - and the measured velocity profiles. From these figures the following conclusions can be made; compared with the measured velocity profile:

- In the upper part of the profile the velocities predicted by the Van Rijn model are too large.
- In case of a small wave height and a strong current the lower part ($z/h < 0.5$) of the computed profile agrees reasonably well with the measured velocities.

As was mentioned in section 6.3.1 an explanation for the differences between the measured and the computed velocities may be found in the relation between $K_{s,app}/K_{s,phys}$ and the ratio U_b/U_m. In the Van Rijn model, the relation between $K_{s,app}/K_{s,phys}$ and U_b/U_m is assumed to be exponential. In the present study a different relation for the prediction of $K_{s,app}/K_{s,phys}$ was found (see section 4.10.8). This has its influence on the computed velocities.

6.4 Bijker transport model

6.4.1 General

The Bijker formula is a typical longshore transport formula, based on bed friction forces. The formula only estimates the current related part of the sediment transport.

The Bijker model computes a total sediment transport, devided in a bed load transport and a suspended load transport. As the bed load transport was not determined in the present study, this part will not be considered now. For computing the suspended sediment transport however, it is necessary to know the concentration in the bed load layer. This concentration can be computed from the bed load transport.

The concentration profile is approximated by a Rouse/Einstein concentration distribution, in which the mixing coefficient is assumed to be parabolic:

$$\varepsilon_s(z) = 4 * \varepsilon_{s,max} * \frac{z}{h} * \frac{h-z}{h} \qquad (6.6)$$

The bed layer concentration is used as reference concentration. The velocity profile is assumed to be logarithmic. The suspended load transport follows from multiplication of the concentration and velocity profile. When comparing the computed and the measured suspended transport it should be noticed that Bijker defined the suspended transport in the zone from $z=K_s$ to $z=h$, while the measured suspended sediment is defined between $z=2*D_{50}$ and $z=h$.

Some parameters in the Bijker formula need attention, especially the dimensionless empirical parameter B. Values between 1 and 5 have been suggested for this parameter. For computation of longshore transport *in the breaker-zone* this parameter is usually taken equal to 5. Although in the present study breaking wave are involved, to be consistent with the earlier 200-μm-flume-study (1987), the earlier 100-μm-flume-study (1988) and the earlier 100-μm-basin-study (1992), the parameter B was taken equal 1. Besides, this factor gives good results considering the concentrations near the bed.

6.4.2 Comparison Bijker model with measured transport

In this section a comparison between the results from Bijker computations with the results from the measurements will be made. From Table 6.4.1 (part I) it can be concluded that compared to the experimental data:

- In case of a small wave height ($H_s<0.16$ m) and a weak current ($U_m\leq0.10$ m/s) the transport rates are rather good predicted by the Bijker formula.

7 Conclusions and Recommendations

Conclusions

Series A

1. Wave influence on the fluid velocities

Compared with the current-alone situation, the velocities measured when current and waves are present are:

- Relatively small in the near bed zone ($z/h < 0.3$)
- Still small but the difference is less in the middle layer ($0.3 < z/h < 0.6$)
- Relatively small in the upper layer ($0.6 < z/h < 0.8$)

The influence of the wave height and current strength on the observed differences is summarized as follows:

- Increasing the current strength U_m with a constant wave height leads to a decrease of the differences.

- Increasing the significant wave height H_s with a constant current velocity leads to an increase of the differences.

- The differences are largest in case of large wave height in combination with a weak current.

The influence of the current-wave-angle:

- At a current-wave-angle of $\phi = 0°$ waves superimposed on a current lead to a decrease in velocities in the upper layer ($0.5 < z/h < 0.8$) compared to the current alone situation.

- At a current-wave-angle of $\phi = 60°$ waves superimposed on a current lead to an increase in velocities in the upper layer ($0.5 < z/h < 0.8$) compared to the current alone situation.

- From $\phi = 60°$ to $\phi = 180°$, the increase in velocities in the upper layer ($0.5 < z/h < 0.8$) compared to the current alone situation becomes more pronounced with increasing current-wave-angle.

- At every current-wave-angle, waves superimposed on a current lead to decreasing velocities in the near bed zone ($z/h < 0.3$) compared to the current alone situation. The extent of this decrease depends on the

complicated interaction between the waves, the current and the generated ripple pattern.

The influence of the wave steepness:

- An increasing wave steepness H_s/L leads to an increasing wave asymmetry (asymmetry in the velocity signal).

2. Wave influence on sediment concentrations

- Increasing the significant wave height, H_s, leads to an increase in concentrations. The increasing orbital velocities lead to the stirring up of more sediment.

- Increasing the significant wave height, H_s, leads to a slightly more uniform concentration profile. The turbulence caused by increasing orbital velocities and breaking of waves leads to a more uniform concentration profile. This can easily be seen from the mass balance described by Eq.4.26. An increasing diffusion coefficient implies a decreasing concentration gradiënt. This effect may however be small because an increasing wave height also causes a decrease of the ripple height and additional less vortices.

3. Current velocity influence on sediment concentrations

With a significant wave height of $H_s = 0.100$ m

- An increasing current strength leads to smaller concentration magnitudes in the near bed zone and increasing concentrations in the upper layers. The current induced mixing becomes apparently more important with increasing current velocities, resulting in an increasing vertical transport of sediment particles to the upper layers.

With a significant wave height of $H_s = 0.140$ m

- An increase in current strength from $U_m = 0$ m/s to $U_m = 0.10$ m/s leads to a less uniform profile and decreasing concentrations, especially in the upper part of the profile ($z/h > 0.3$). This may be caused by a decreasing wave steepness and thus less breaking waves.

- An increase in current strength from $U_m = 0.10$ m/s to $U_m = 0.20$ m/s leads to increasing concentrations and a somewhat more uniform profile in spite of a decrease in the number of breaking waves, probably because current related mixing becomes more important.

- An increase in current strength from U_m = 0.20 m/s to U_m = 0.30 m/s leads to increasing concentrations, because current related mixing becomes more important.

With a significant wave height of H_s = 0.156 m

- A stronger current causes a slight increase in concentrations in the upper part of the profile, smaller concentrations magnitudes in the near bed zone and a slightly more uniform profile caused by current induced mixing.

4. Influence fraction of breaking waves Q_b on sediment concentrations

- One could carefully say that more breaking waves lead to a more uniform concentration profile, especially in the upper part of the profile.

5. Influence current strength U_m on the suspended sediment loads L_s

With a significant wave height of H_s = 0.10 m:

- The decrease of the loads with increasing current velocity is caused by a decrease of the concentrations in the near bed zone. The decrease of the loads is related to the wave-induced changes of the velocity distribution in the near bed zone. The interaction between waves and current results in an increasing turbulence which leads to an increasing shear stress, higher ripples and a decrease of the velocities in the near bed zone, especially in the onshore direction.

- In the earlier 100-μm-flume-study (1988) and the 100-μm-basin-study (1992) it was also found that a weak current ($U_m \approx 0.1$ m/s) superimposed on the waves leads to a decrease of the loads. This phenomenon is related with the velocity decrease in the near bed zone ($z/h < 0.3$) caused by waves superimposed on a current. In the earlier 200-μm-flume-study (1987) a weak current hardly changed the loads.

With a significant wave height of H_s = 0.14 m:

- The decrease of the loads with increasing depth averaged velocity from U_m=0.00 to 0.10 m/s is caused by a less uniform concentration profile and decreasing concentrations, especially in the upper part of the profile. Less breaking waves and a decrease of the velocity in the near bed zone, especially in the offshore direction might be a reason.

- The increase of the loads with increasing depth averaged velocity from U_m

= 0.10 to 0.30 m/s is caused by increasing concentrations and a more uniform concentration profile. An increase of the velocity in the near bed zone both in the on- and offshore direction might be a reason (Table 4.4).

With a significant wave height of H_s = 0.16 m:

- A stronger current causes a slight increase in concentrations in the upper part of the profile, smaller concentrations magnitudes in the near bed zone and a slightly more uniform profile caused by current induced mixing. These effects hardly influence the sediment load. The relatively large velocities in the near bed zone are not influenced by the depth-averaged velocity U_m.

- In the earlier 200-μm-flume-study (1987) and the 100-μm-flume-study (1988) it was also found that a large significant wave height causes a less pronounced increase of the suspended load L_s with increasing current strength.

6. Influence H_s/h ratio on suspended sediment loads L_s

- An increasing H_s/h leads to increasing sediment loads.

- When no current is present (U_m = 0.0 m/s) the influence of the water depth h on the sediment load L_s is more pronounced compared to the current and waves situation.

7. Influence velocity on suspended sediment transport S_s

- The relationship between the suspended sediment transport S_s and the depth-averaged velocity U_m can be described by:

$$S_s = \beta * U_m^y$$

- In case of a strong current (U_m=0.20 m/s) the value for q found in the present study (q=2.8) is relatively large compared to the earlier 100-μm-basin-study (1992) (q=2.0). This means a more pronounced influence of the wave height on the sediment transport.

8. Influence wave height H_s on suspended sediment transport S_s

- The relation between the suspended sediment transport S_s and the

significant wave height H_s (for constant U_m) can be described by:

$$S_s = \alpha * H_s^q$$

- The values for y found in the present study are relatively small compared to the earlier 100-μm-basin-study, especially in case of a small wave height. This means a less pronounced influence of the current strength on the suspended sediment transport.

- The difference between the two studies may be related to the difference in wave-induced changes of the velocity distribution in the near bed zone. In the earlier 100-μm-basin-study the wave height to water depth ratio varied from $H_s/h = 0.16$ to 0.35, while in the present study this parameter varies from $H_s/h = 0.33$ to 0.55. This will have its effect on the velocities in the near bed zone, especially on the asymmetry (onshore velocity larger than offshore).

9. Influence H_s/h ratio on suspended sediment transport S_s

- An increasing H_s/h ratio leads to a decreasing influence of the depth averaged velocity U_m on the suspended sediment transport S_s.

- An increasing H_s/h ratio leads to an increasing influence of the onshore orbital peak velocity $\hat{U}_{b,on,tot}$ and a decreasing influence of the offshore orbital peak velocity $\hat{U}_{b,off,tot}$ on the suspended sediment transport S_s.

- The influence of H_s/h on the suspended sediment transport is important, especially for the stirring up of sediment to the middle and upper layers.

10. Influence fraction breaking waves Q_b on suspended sediment transport S_s

- The influence of the fraction of breaking waves Q_b on the suspended sediment transport is of some importance, especially for the stirring up of sediment to the middle and upper layers.

11. Influence orbital peak velocities on the ripples

- Increase of the on- and offshore orbital peak velocities leads to a decrease of the relative ripple height (due to erosion of the ripple crest) and to a decrease of the ripple length.

12. Influence current velocity on the ripples

- Increase of U_m leads to an increase of the relative ripple height and ripple length. The ripples become higher and more three dimensional.

13. Influence wave steepness on the ripples

- Increase of the wave steepness leads to a decrease of the relative ripple height and a decrease of the ripple length.

14. Influence waves on the bed roughness

- Waves superimposed on a current lead to an apparent increase in bed roughness. In the present study values for z_1/z_0 from 1.7 to 11.4 are found. The increase of the zero velocity level becomes less significant with increasing value of $\hat{U}_{b,on,tot}/U_m$ and $\hat{U}_{b,off,tot}/U_m$.

- The increase in bed shear velocity by wave influence is less pronounced than the increase in zero velocity level. Values for U_{*cw}/U_{*c} from 1 to 2 are found.

15. Comparison Van Rijn transport model with measured values

- The transport rates computed with the Van Rijn formula are small compared to the measured values (measured values are on average 3.2 times larger compared to the calculated values).

- The increase in sediment transport with increasing wave height is less pronounced for the Van Rijn formula than the measurements show. This difference is more pronounced with increasing current strength.

- The increase in sediment transport with increasing current strength is less pronounced for the Van Rijn formula than the measurements show. This difference is more pronounced with increasing wave height.

- The concentration profile is predicted too uniform by the Van Rijn model, especially in the lower part of the profile ($z/h < 0.5$). This difference is less pronounced with increasing current strength.

- The concentrations in the near bed zone are predicted too small by the Van Rijn model, especially in case of a large wave height and a weak current.

- Compared to the measurements, the increase in concentrations with increasing wave height is less pronounced for the Van Rijn formula.

- In case of a small wave height and a strong current the lower part ($z/h < 0.5$) of the computed profile agrees reasonably well with the measured velocities.

16. Comparison Bijker transport model with measured values

- In case of a small wave height ($H_s < 0.16$ m) and a weak current ($U_m < 0.10$ m/s) the transport rates are rather good predicted by the Bijker formula.

- In case of a strong current ($U_m \geq .20$ m/s) the transport rates computed with the Bijker formula are small compared to the measured values (measured values are on average 138 % larger than computed values).

- The increase in sediment transport with increasing wave height is less pronounced for the Bijker formula. This difference is more pronounced with increasing current strength.

- The concentration profile is predicted too uniform by the Bijker model. This difference is less pronounced with increasing current strength.

- In case of a small wave height ($H_s < 0.14$ m) with a weak current ($U_m \leq 0.20$ m/s) the concentrations in the near bed zone are predicted rather good by the Bijker model.

- In case of a large wave height ($H_s > 0.14$ m) with a strong current ($U_m > 0.20$ m/s) the concentrations in the near bed zone computed with the Bijker model are small compared to the measured values.

- Compared to the measurements, the increase in concentrations with increasing wave height is less pronounced for the Bijker formula.

Series B

1. Distribution of the concentration over the flume

- In front of the top of the bar and with the water depth becoming shallower the concentrations in general show an increase.

- In front of the top of the bar and with the water depth becoming shallower

the concentration profile becomes more uniform.

- Behind the top of the bar the sediment concentration decreases.
- Behind the top of the bar the concentration profile becomes less uniform.

2. Wave height influence on concentration profile

- An increase in wave height leads, in general, to an increase in concentrations in one cross-section.
- In front of the top of the bar and with the water depth becoming shallower the concentration profile becomes more and more uniform with higher waves.

3. Influence of H_s/h on concentration profile

- The relative increase of the sediment concentration in the upper layers is larger than the relative increase in the near bed zone with increasing H_s/h. This means a more uniform profile with increasing H_s/h.

4. Influence of Q_b on concentration profile

- An increase in Q_b leads to an increase of the concentrations in the upper layers of the profile ($z/h > 0.2$), especially for larger values of Q_b.

5. Bottom concentration

- The in/decreasing bottom sediment concentration is the result of the in/decreasing orbital velocity in the near bed zone. The relation between the peak orbital velocity at the bottom and the bottom concentration seems to be a logarithmic one.

6. Distribution of the fluid velocity over the flume

- The averaged fluid velocity is mainly seawards, especially in the upper layers of the profile.
- The fluid velocity increases in front of the top of the sand bar and with the water depth becoming shallower.

- The velocity profile becomes more uniform in front of the top of the sand bar and with the water depth becoming shallower.
- The fluid velocity decreases directly behind the top of the bar.
- Behind the top of the bar the velocity profile becomes less uniform.

7. Return flow and approximations

- The depth-averaged fluid velocity is in seaward direction in every cross-section; the return flow.
- The depth-averaged fluid velocity increases in both series up to the top of the sand bar.
- Behind the bar the depth-averaged fluid velocity decreases.
- The velocity increases on the landward upsloping part of the sand bed.
- The calculated magnitude of the return flow using the *Svendsen*-formula has the same distribution over the flume as the measured one, but predicts too small values for the return flow.
- The calculated magnitude of the return flow using the *Stive and Wind*-formula has the same distribution over the flume as the measured one, but predicts too large values for the return flow.
- The formula developed by *van Rijn* gives the best results for the first and last cross-sections in the flume, but around the top of the bar the calculated return flow is found to be a factor 2 larger compared to the measured one.

8. Wave height influence on the velocity profile

- The velocity increases with increasing wave height in series B2.
- The difference between the time- and bed-averaged fluid velocity of series B1 (low waves) and B2 (higher waves) increases in front of the top of the sand bar on the upsloping part of the bar.
- Behind the bar the difference between the magnitude of the velocity of both series decreases.

9. Influence of H_s/h on the velocity profile

- An increasing H_s/h ratio leads to increasing velocities.

10. Asymmetry in fluid velocity signal at the bottom

- The asymmetry in the fluid velocity signal reaches it peak at the top of the sand bar.

11. Distribution of the suspended sediment load over the flume

- The sediment loads in front of the top of the bar and with the water depth becoming shallower strongly increase. The sediment load behind this point decreases.

12. Wave height influence on suspended load

- An increasing wave height leads to increasing suspended sediment loads.
- An increase in wave height has the largest influence on the suspended load behind the bar (cross-section 6).

13. Influence wave height-water depth ratio on suspended load

- An increase in H_s/h leads to an increase in suspended sediment load.
- There seems to be a linear relationship between H_s/h and the suspended load, especially with small values of H_s/h. With larger values of the wave height-water depth ratio this linearity is less pronounced.

14. Influence of percentage breaking waves on suspended load

- Two different processes can be distinguished, one on the upsloping parts and one on the downsloping part of the sand bar.
- On the upsloping part of the bar the relationship between the load and percentage breaking waves seems to be a logarithmic one.
- On the downsloping part of the bar the relationship between the suspended load and the percentage breaking waves is linear.

15. Sediment flux

- The depth over which significant sediment transport takes place increases with decreasing water depth.
- The time-averaged transport in the flume is predominantly seawards. Sometimes the lowest measurement(s) give(s) a landward sediment transport.

16. Distribution of current-related suspended sediment transport over the flume

- In nearly every cross-section the sediment transport is found to be directed seaward.
- The peak value of the current-related transport depends on the wave height. The transport rate reaches its peak value on top of the bar with low waves and directly behind the top of the bar with higher waves.

17. Influence of the wave height on the current-related sediment transport rate

- The suspended transport rate increases with increasing wave height.
- An increase in wave height has the largest influence on the sediment transport in the cross-sections arounhd the top of the bar.

18. Influence of H_s/h on current-related sediment transport rate

- An increase in H_s/h leads to an increase in sediment transport.

19. Influence of percentage breaking waves on current-related sediment transport

- Two processes can be distinguished, one on the upsloping parts in the flume and one on the downsloping part.
- The relation between the suspended sediment transport rate and the percentage breaking waves on the upsloping parts seems to be a logarithmic one.
- The relation between the suspended sediment transport and Q_b on the downsloping part of the bar seems to be an exponential one.

20. Comparison of current-related sediment transport and total sediment transport

- Especially around the sand top of the bar, the current-related sediment transport rate is larger than the total sediment transport.

Recommendations

- Large instantaneous sediment concentrations near the bed (compared to time averaged values) were observed when two or more large breaking waves were passing the measuring section. It might be meaningfull in a next study to make video images to get more insight in the mechanisms that play a role in the stirring up of sediment, especially in the stirring up of these large instantaneous concentrations near the bed.

- In addition to the above, it might be usefull to study whether a time-averaged convection-diffusion equation like in the Van Rijn transport model gives an adequate solution to the phenomena observed. A detailed study on the transportmechanisms near the bed (relations between: orbital velocities, ripple height, ripple length, turbulent eddies, beginning of movement of sediment etc.) should be conducted.

- In the present study the horizontal fluid velocities were measured (x-direction). In a next study it might be usefull to take into account the influence of vertical orbital velocities (z-direction).

- From the present study it appeares that the orbital on - and offshore peak velocities are important parameters in determining the suspended sediment transport. In a following study it might be usefull to investigate the importance of these parameters.

- For well graded material, D_{50} will change with the height above the bed. Smaller particles are brought into suspension more easily and reach higher levels more easily. In a next study more attention should be paid to the distribution of the sediment size over the vertical.

References

Battjes, J.A. (1982)
'Windgolven'
Lecture notes
Delft University of Technology

Battjes, J.A., Beji, S. (1992)
'Experimental investigation of wave propagation over a bar'
Published in Coastal Engineering, 19: 151-162

Bosman, J.J. (1982)
'Concentration measurements under oscillating water motion'
Report on model investigation (M1965-II)
Delft Hydraulics Laboratory

Bosman, J.J. (1985)
'Concentration measurements in model and prototype'
Concept
Delft Hydraulics Laboratory

Bosman, J.J., Velden, E.T.J.M. van der, Hulsbergen, C.H. ('87)
'Sediment concentration measurements by transverse suction'
Published in Coastal Engineering, December 1987

'Coastal Engineering', january 1989
Lecture notes
Delft University of Technology

Havinga, F.J. (1992)
'Sediment concentrations and sediment transport in case of irregular non-breaking waves with a current'
Report
Delft University of Technology

Kaay, Th. van der, Nieuwjaar, M.W.C. (1987)
'Sediment concentrations and sediment transport in case of irregular non-breaking waves with a current'
Report
Delft University of Technology

Kampen, H.F.A. van, E.N. Nap (1988)
'Sediment concentrations and sediment transport in case of irregular non-breaking waves with a current'
Report
Delft University of Technology

Longuet-Higgins, M.S. (1953)
'Mass transport in water waves'
Phill. Trans. Roy. Soc. London, Series A, Vol. 245, no. 903
pp 535-581

Rijn, L.C. van (1993)
'Principles of sediment transport in rivers, estuaries and coastal seas'
Aqua Publications, Amsterdam

Shore Protection Manual, fourth edition, second printing, 1984
Coastal Engineering Research Center
Department of the Army

Appendix

Mass transport and return flow

Water particles are predicted to move in closed orbits by linear wave theory; i.e., each particle returns to its initial position after each wave cycle. Morison and Crooke (1953) compared laboratory measurements of particel orbits with wave theory and found, as had others, that particle orbits were not completely closed. This difference is due to the mass transport phenomenon, which is discussed in this section. The action of mass transport, extended over a long period, can be important in carrying sediment onshore or offshore, particularly seaward of the breaker position.

The massflux between wave-through and wave-crest can be denoted by:

$$m = Q_b * m_b + (1-Q_b) * m_{nb} \qquad (1)$$

where	m_x	:	mass flux contribution by breaking (b) and non-breaking (nb) waves	(kg/sm)
	Q_b	:	percentage breaking waves	(%)

According to Svendsen (1984) the contribution of breaking waves to the total mass flux is given by:

$$m_b = (1 + 7 * \frac{h}{L}) * \frac{E}{c} \qquad (2)$$

where	c	:	wave celerity	(m/s)
	E	:	$\frac{1}{8}\rho g(H_{rms})^2$, wave energy per unit surface area	(kg/s^2)
	h	:	water depth	(m)
	L	:	wave length	(m)

The contribution of non-breaking waves to the total mass flux is given by:

$$m_{nb} = \frac{E}{c} \qquad (3)$$

Substitution of Eq.2 and Eq.3 in Eq.1 gives:

$$m = (1 + 7 * \frac{h}{L} * Q_b) * \frac{E}{c} \qquad (4)$$

To balance the mass transported in the direction of the wave travel the return flow $U_{mean,return}$ is found to be:

$$U_{mean\ return} = \frac{m}{\rho * h} \tag{5}$$

$$U_{mean,return} = (1 + 7 * \frac{h}{L} * Q_b) * \frac{\frac{1}{8} * \rho * g * H_{rms}^2}{\rho * h * c} \tag{6}$$

$$U_{mean,return} = \frac{1}{8} * (1 + 7 * \frac{h}{L} * Q_b) * \frac{g * H_{rms}^2}{h * c} \tag{7}$$

For relatively shallow water Eq.7 becomes Eq.8. Besides this formula of Svendsen two other expressions for the return flow are given below.

Svendsen (1984):

$$U_{mean,return} = \frac{1}{8} * (1 + 7 * \frac{h}{L} * Q_b) * (\frac{H_{rms}}{h})^2 * c \tag{8}$$

Stive and Wind (1986):

$$U_{mean,return} = 0.1 * (\frac{g}{h})^{0.5} * H_{rms} \tag{9}$$

Van Rijn (1990):

$$U_{mean,return} = 0.125 * (\frac{g}{h})^{0.5} * \frac{H_s^2}{h_t} \tag{10}$$

where

g	:	acceleration of gravity	(m/s^2)
h	:	water depth	(m)
h_t	:	water depth below wave trough	(m)
H_{rms}	:	root mean square wave height	(m)
H_s	:	significant wave height	(m)
L	:	wave length	(m)
Q_b	:	percentage breaking waves	(%)

Extrapolation of concentrations in unmeasured zones

To compute the sediment load, the concentrations in the zones below the lowest and above the highest measuring point must be known. This was done by extrapolation. Three extrapolation methods were used (Fig.2.1):

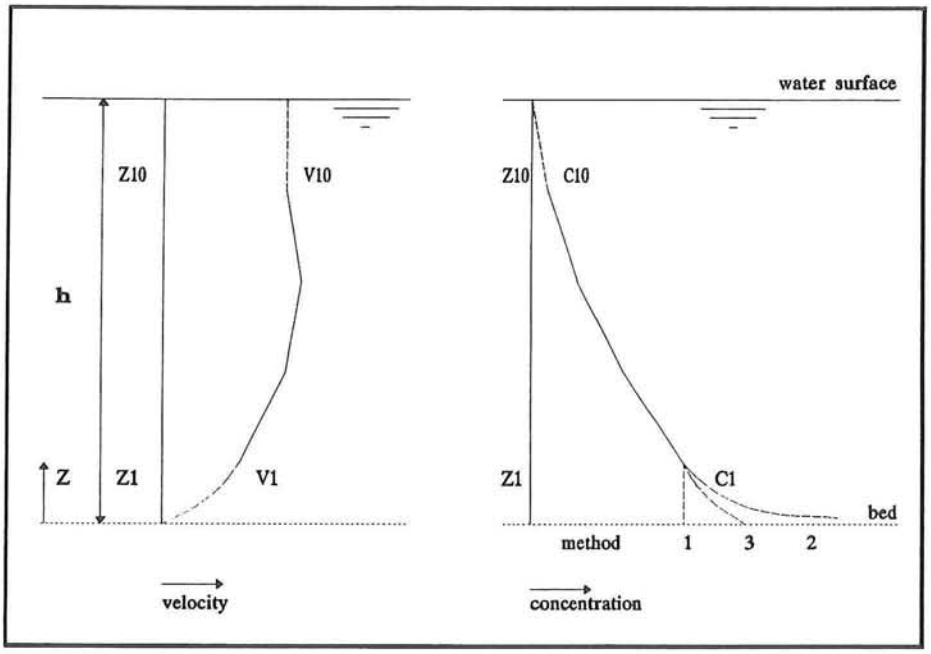

Fig.2.1 Extrapolation of profiles

method 1

The sediment concentrations between the bed (z = 0 m) and the first measuring point (z = z_1) are assumed to be equal to the concentration in the first measuring point. This method is used to give an underlimit.

$$c = c_1 \qquad \textit{for } 0 < z < z_1 \tag{11}$$

method 2

The sediment concentrations between the bed (z = 0.001 m) and the first measuring point are computed by:

$$c = A * Y^B \qquad \text{for } 0.001 < z < z_1 \tag{12}$$

where

Y	:	(h-z)/z = dimensionless vertical coordinate	(-)
z	:	vertical coordinate	(m)
h	:	water depth	(m)
A,B	:	coefficients	(-)

The A and B coefficients are determined by a regression method applying the measured concentrations of the first three measuring points above the bed, as follows:

- select:

$$B = 0.1 \tag{13}$$

- compute:

$$A = \frac{\sum_{1}^{3} (Y_k^B * c_k)}{\sum_{1}^{3} (Y_k^B * Y_k^B)} \tag{14}$$

- compute:

$$T = \sum_{1}^{3} (A * Y_k^B - c_k) \tag{15}$$

- select:

$$B = 0.2 \tag{16}$$

- repeat procedure (B is varied over the range 0.1 to 5)

Finally, the A and B coefficients corresponding to a minimum T-value are selected as the "best" coefficients. Applying Eq.12, the sediment concentrations are computed in 50 equidistant points between the bed (defined at $z = 2 * D_{50}$) and the first measuring point ($z = z_1$). The maximum concentration is assumed to be 1590 kg/m^3. This method is supposed to give an upper limit.

method 3

The sediment concentrations between the bed and the first measuring point are represented by:

$$c = e^{Az + B} \qquad \textit{for } 0 < z < z_1 \tag{17}$$

where z : height above bed (m)
A,B : coefficients (-)

The A and B coefficients are determined by a linear regression method applying the measured concentration of the first three measuring points above the bed, as follows:

$$A = \frac{3 \sum_{1}^{3}(z_k \ln c_k) - \sum_{1}^{3}(z_k) \sum_{1}^{3}(\ln c_k)}{3 \sum_{1}^{3}(z_k z_k) - (\sum_{1}^{3} z_k)^2} \tag{18}$$

$$B = \frac{\sum_{1}^{3}(z_k z_k)\sum_{1}^{3}(\ln c_k) - \sum_{1}^{3}(z_k)\sum_{1}^{3}(z_k \ln c_k)}{3\sum_{1}^{3}(z_k z_k) - (\sum_{1}^{3} z_k)^2} \tag{19}$$

Applying Eq.17, the sediment concentration is computed in 50 equidistant points between the bed (defined at $z = 2 * D_{50}$) and first measuring point ($z = z_1$). The maximum concentration is assumed to be 1590 kg/m^3.

Determination of the bedroughness

In a uniform stationary current in shallow water the velocity is affected by the bottom friction over the entire depth. The bottom shear stress in case of a current alone can be denoted by:

$$\tau_c = \rho * g * \frac{U_m^2}{C^2} \tag{20}$$

Jonsson (1966) carried out experiments to determine the bed shear stress under waves. He found that this shear stress τ_w could be described in terms of the near bed velocity and the wave friction factor:

$$\tau_w = \frac{1}{2} * \rho * f_w * \hat{U}_b^2 * \sin^2(\omega t) \tag{21}$$

$$\hat{\tau}_w = \frac{1}{2} * \rho * f_w * \hat{U}_b^2 \tag{22}$$

where	τ	:	bottom shear stress for waves	(N/m^2)
	f_w	:	friction factor	
	$\hat{U}_b$	:	maximum horizontal velocity component just outside the boundary layer	(m/s)
	ω	:	wave frequency, $2\pi/T_p$	(s^{-1})

Wave friction factors depend on the Reynolds $U*A_b/\upsilon$ as well as the relative roughness A_b/K_s. When the Reynolds number is small this friction factor depends only on this Reynolds number. However, the Reynolds number dependence is commonly ignored since prototype conditions can be expected to be fully turbulent (and thus have a high Re-number).

The original relation for f_w (Jonsson (1966)), in terms of the relative roughness as rewritten by Swart (1976) in a more practical expression, is:

for $A_b/K_s > 1.59$:

$$f_w = \exp\left(-5.977 + 5.213 * \left(\frac{A_b}{K_s}\right)^{-0.194}\right) \qquad (23)$$

for $A_b/K_s < 1.59$:

$$f_w = 0.30 \qquad (24)$$

where

f_w	:	friction factor	
K_s	:	bottom roughness	(m)
A_b	:	maximum horizontal displacement of water particles just outside the boundary layer	(m)

This relation is only valid for $A_b/K_s < 3000$. The upper limit of f_w, of 0.30, is arbitrary and probably too low since both Carstens et al. (1969) and Lofquist (1980) have found wave friction factors between 0.30 and 0.40 in several experiments. Sleath (1984) even suggested there is no upper limit; he suggests that the wave friction factor remains proportional to A_b/K_s.

The Bijker formula

The approach of Bijker (1971) was to introduce the wave influence via a modification of the bottom shear stress in an existing sediment transport formula for currents. He devided the total load transport S_t into two parts, the bed load transport S_b and the suspended load transport S_s. The bed load transport is calculated with the Kalinske-Frijlink formula, in which the combined action of waves and current is accounted for by a modification of the bed shear stress:

$$S_b = \frac{B * D_{50} * U_m * \sqrt{g}}{C} * \exp\left(\frac{-0.27 * \Delta * D_{50} * \rho * g}{\mu * \bar{\tau}_{cw}}\right) \qquad (25)$$

where

S_b	:	bed load transport	(m^3/sm)
B	:	coefficient	(-)
D_{50}	:	grain daimeter exceeded by 50% of the bed material by weight	(m)
U_m	:	depth-averaged fluid velocity	(m/s)
g	:	acceleration of gravity	(m/s^2)
C	:	Chezy coefficient	($m^{1/2}/s$)
Δ	:	relative sediment density	(-)
ρ	:	density of fluid	(kg/m^3)
μ	:	ripple factor	(-)
τ_{cw}	:	bottom shear stress in case of current and waves	(N/m^2)

The bed load transport according to Eq.25 is expressed in m^3/sm and includes the voids. After multiplying Eq.25 with a factor (1-p)*ρ_s, with p=porosity (-) and ρ_s=sediment density (kg/m^3), the bed load transport is expressed in kg/sm and no longer includes the voids.

The coefficient B might reflect the influence of the breaking of waves. In the breaker zone, B is usually taken equal to 5 and outside the breaker zone equal to 1.

The Chezy coefficient is denoted by:

$$C = 18 \log\left(\frac{12\ h}{K_s}\right) \qquad (26)$$

where	h	:	water depth	(m)
	K_s	:	bed-roughness	(m)

The bed-roughness predictors used in combination with the Bijker formula are:

- The Van Rijn formula (1982) as a minimum approximation:

$$K_s = 3 * D_{90} + 1.1 * r * (1 - \exp(-25 * \frac{r}{\lambda})) \quad (27)$$

- The Swart formula (1976) as a maximum approximation:

$$K_s = 25 * r * \frac{r}{\lambda} \quad (28)$$

where	D_{90}	:	grain diameter exceeded by 10% of the bed material by weight	(m)
	r	:	ripple height	(m)
	λ	:	ripple length	(m)

The ripple factor is denoted by:

$$\mu = (\frac{C}{C_{90}})^{\frac{3}{2}} \quad (29)$$

The Chezy coefficient based upon D_{90} is denoted by:

$$C_{90} = 18 \log (\frac{12\ h}{D_{90}}) \quad (30)$$

The bottom shear stress in case of current and waves is denoted by: :

$$\overline{\tau}_{cw} = \tau_c + \frac{1}{2}\hat{\tau}_w \quad (31)$$

where	τ_c	:	bottom shear stress in case of a current	(N/m^2)
	τ_w	:	bottom shear stress in case of waves (see also Appendix 3)	(N/m^2)

Bijker assumed that the bed load transport takes place in a bed load layer having a thickness of the bed-roughness K_s. The concentration in this layer is assumed to be constant over this layer:

where	c_b	:	concentration in the bed load layer	(kg/m^3)

$$c_b = \frac{S_b}{6.34 * \sqrt{\frac{\tau_c}{\rho}} * K_s} \qquad (32)$$

The suspended load transport S_s is calculated as:

$$S_s = \int_{z-K_s}^{h} c(z) * U(z)\, dz \qquad (33)$$

where	c(z)	:	concentration at height z above the bed	(kg/m^3)
	U(z)	:	velocity at height z above the bed	(m/s)

To compute the suspended load transport S_s, the velocities are approximated by the Prandtl-Von Karman logarithmic velocity distribution:

$$U(z) = \frac{U^*}{\kappa} * \ln\left(\frac{z}{z_0}\right) \qquad (34)$$

where	U(z)	:	velocity at height z above the bed	(m/s)
	U^*	:	shear velocity	(m/s)
	κ	:	Von Karman coefficient (=0.4)	(-)
	z	:	height above mean bed level	(m)
	z_0	:	roughness length scale ($=K_s/33$)	(m)

The concentration magnitudes at height z above the bed are approximated by an Einstein (1950) concentration distribution:

$$c(z) = c_b * \left(\frac{h-z}{z} * \frac{K_s}{h-K_s}\right)^{z_*} \qquad (35)$$

The exponential part is defined by:

$$z_* = \frac{w_{50} * \sqrt{\rho}}{\kappa * \sqrt{\tau_{cw}}} \qquad (36)$$

where w_{50} : median fall velocity of bed material (m/s)

After substitution of Eq.34 and Eq.35 into Eq.33 and after using the Einstein terms (I_1 and I_2) for the integral in Eq.33 it can be shown that:

$$S_s = 1.83 * (I_1 * \ln(\frac{33\ h}{K_s}) + I_2) * S_b \tag{37}$$

In which I_1 and I_2 are the Einstein integrals defined as:

$$I_1 = 0.216 * \frac{A^{(z_*-1)}}{(1-A)^{z_*}} * \int_{\zeta=A}^{1} (\frac{1-\zeta}{\zeta})^{z_*}\ d\zeta \tag{38}$$

$$I_2 = 0.216 * \frac{A^{(z_*-1)}}{(1-A)^{z_*}} * \int_{\zeta=A}^{1} (\frac{1-\zeta}{\zeta})^{z_*} \ln(\zeta)\ d\zeta \tag{39}$$

where A : dimensionless roughness = r/h (-)
ζ : dimensionless elevation = z/h (-)

These integral are solved using the binomium of Newton (Bogaard, 1977).

Once the bed load transport S_b (Eq.25) and the suspended load transport S_s (Eq.37) are known the total transport S_t follows by adding S_s to S_b:

$$S_t = S_s + S_b \tag{40}$$

The Van Rijn formula

The concentration profile can be obtained from numerical integration of the time-averaged convection-difussion equation (Eq.41) applying Eq.42 as reference concentration.

$$\frac{dc}{dz} = -\frac{c\ w_{s,m}}{\epsilon_{s,cw}} \tag{41}$$

$$c_a = 0.015\ \rho_s\ \frac{D_{50}}{a}\ \frac{T_a^{1.5}}{D_*^{0.3}} \tag{42}$$

where				
	c	:	time-averaged concentration at height z above the bed	(kg/m^3)
	$w_{s,m}$	:	$(1\text{-}c^5)w_s$ = particle fall velocity of suspended sediment in fluid-sediment mixture	(m/s)
	w_s	:	particle velocity of suspended sediment in clear water	(m/s)
	$\epsilon_{s,cw}$	:	$(\epsilon_{s,c}^2 + \epsilon_{s,w}^2)^{0.5}$ = sediment mixing coefficient in combined currents and waves	(m^2/s)
	ρ_s	:	sediment density $\approx$2650	(kg/m^3)
	a	:	reference level	(m)
	D_{50}	:	median particle diameter of bed material	(m)
	T_a	:	bed-shear stress parameter	(-)
	D_*	:	particle parameter	(-)

The sediment mixing coefficient in combined currents and waves is assumed to be given by the sum of the squares of the current-related and the wave-related values. Thus: $\epsilon_{s,cw}^2 = \epsilon_{s,c}^2 + \epsilon_{s,w}^2$. Since $\epsilon \approx 1\ k^{0.5}$ with k=kinetic energy and l=length scale, this approach corresponds to the summation of the kinetic energy of both types of motions, which seems to be more realistic than assuming $\epsilon_{s,cw} = \epsilon_{s,c} + \epsilon_{s,w}$.

The reference level is assumed to be equal to $a=K_{s,w}$ or $a=0.5$ r in case of a rippled bed (r=ripple height) or $a=\delta_w$ in case of a plane sheet flow bed (δ_w=wave boundary layer thickness).

The variables are specified below.

1. Input

$\underline{h}$	=	water depth	(m)
$\overline{v_R}$	=	depth-averaged velocity in main current direction	(m/s)
$\overline{u_r}$	=	time-averaged and depth-averaged return velocity below wave trough compensating the mass transport between wave crest and trough (- in backward or offshore direction)	(m/s)
u_b	=	time-averaged near-bed velocity due to waves, wind or density gradient (+ in forward direction, - in backward direction)	
H_s	=	significant wave height	(m)
T_p	=	(absolute) wave period of peak of spectrum	(s)
Φ	=	angle between wave and main current direction	(-)
D_{50}	=	median diameter of bed material	(m)
D_{90}	=	grain daimeter exceeded by 10% of the bed material by weight	(m)
D_s	=	representative diameter of suspended material	(m)
$K_{s,c}$	=	current-related bed roughness height (minimum $K_{s,c}$=0.01 m)	(m)
$K_{s,w}$	=	wave-related bed roughness height (minimum $K_{s,w}$=0.01 m)	(m)
T_e	=	fluid temperature	(°C)
SA	=	fluid salinity	(‰)

Remarks

A The representative particle size (D_s) of the suspended sediment will be in the range of: D_s = 0.6 to 1) $D_{50,bed}$. A reasonable estimate is D_s = 0.8 $D_{50,bed}$

B The wave-related bed roughness height in the ripple regime will be in the range $K_{s,w}$ = (1 to 3) r with values from 0.01 to 0.1 m.

The wave-related bed roughness height in the sheet flow regime will be: $K_{s,w} = 0.01$ m.

The current-related bed roughness height will be in the range $K_{s,c} = 0.01$ to 1 m.

C The constant of Von Karman is assumed to be $\kappa = 0.1$. The sediment density is $\rho_s = 2650$ kg/m^3.

2. Compute General parameters

Chloridity : $CL = \dfrac{(SA - 0.03)}{1.805}$

Fluid density : $\rho = 1000 + 1.455\ CL - 0.0065\ (T_e - 4 + 0.4\ CL)^2$

Kinematic viscosity : $\nu = \dfrac{4}{20 + T_e}\ 10^{-5}$

Fall velocity

for $1 < D \leq 100\ \mu$m : $w_s = \dfrac{(s-1)\ g\ D^2}{18\ \nu}$

for $100 < D < 1000\ \mu$m : $w_s = \dfrac{10\ \nu}{D}\left(\sqrt{1 + \dfrac{0.01\ (s-1)\ g\ D^3}{\nu^2}} - 1\right)$

for $D \geq 1000\ \mu$m : $w_s = 1.1\ \sqrt{(s-1)\ g\ D}$

where

D	:	sieve diameter	(m)
s	:	specific gravity (= 2.65)	(-)
υ	:	kinematic viscosity coefficient	(m^2/s)

3. Compute sediment characteristics

Relative density		: s	$= \rho_s/\rho$
Particle diameter		: D_*	$= D_{50}\ [\ (s\text{-}1)\ g/\upsilon^2\ ]^{1/3}$
Shields parameter	$1 < D_* \leq 4$	: Θ_{cr}	$= 0.24\ D_*^{-1}$
	$4 < D_* \leq 10$	: Θ_{cr}	$= 0.14\ D_*^{-0.64}$
	$10 < D_* \leq 20$	: Θ_{cr}	$= 0.04\ D_*^{-0.1}$
	$20 < D_* \leq 150$	: Θ_{cr}	$= 0.013\ D_*^{0.29}$
	$D_* > 150$	: Θ_{cr}	$= 0.055$
Critical bed shear stress		: τ_{cr}	$= (\rho_s\text{-}\rho)\ g\ D_{50}\ \Theta_{cr}$
Critical depth-averaged velocity		: $\overline{u_{cr}}$	$= 5.75[(s\text{-}1)g\ D_{50}]^{0.5}\ \Theta_{cr}^{0.5}\ \log(4h/D_{90})$
Critical peak orbital velocity (Komar)			
	$D_{50} < 0.0005$ m	: $\hat{U}_c$	$= [0.12(s\text{-}1)g\ D_{50}^{0.5}\ T_p^{0.5}]^{2/3}$
	$D_{50} \geq 0.0005$ m	: $\hat{U}_c$	$= [1.09(s\text{-}1)g\ D_{50}^{0.75}\ T_p^{0.25}]^{0.571}$

4. Compute wave length

Wave length modified by currents : $(\frac{L'}{T_p} - \overline{v_R} \cos \phi)^2 = \frac{g\ L'}{2\pi} \tanh (\frac{2\pi h}{L'})$

5. Compute relative wave period

The relative wave period is : $T_p' = \frac{T_p}{1 - (\overline{v_R}\ T_p \cos \phi)/L'}$

6. Compute wave parameters

Near-bed peak orbital excursion : $\hat{A}_\delta = \frac{H_s}{2 \sinh (2\pi h/L')}$

Near-bed peak orbital velocity : $\hat{U}_\delta = \frac{\pi\ H_s}{T_p' \sinh (2\pi h/L')}$

Wave-boundary layer thickness : $\delta_w = 0.072\ \hat{A}_\delta\ (\hat{A}_\delta/K_{s,w})^{0.25}$

Near-bed peak orbital velocity in forward direction

$h \geq 0.01\ g\ T_p^2$: $\hat{U}_\delta = \hat{U}_\delta + \frac{3\ \pi^2\ H_s^2}{4\ T_p'\ L'(\sinh (2\pi h/L')^4}$

$h < 0.01\ g\ T_p^2$: $\hat{U}_\delta = \alpha\ \hat{U}_\delta$

$\alpha = 1 + 0.3\ \frac{H_s}{h}$

Near orbital velocity in backward direction

$h \geq 0.01\ g\ T_p^2$: $\hat{U}_\delta = \hat{U}_\delta - \frac{3\ \pi^2\ H_s^2}{4\ T_p'\ L'(\sinh (2\pi h/L')^4}$

$h < 0.01\ g\ T_p^2$: $\hat{U}_\delta = (2-\alpha)\ \hat{U}_\delta$

Return velocity mass transport : $\overline{u_r} = -0.125 \sqrt{\frac{g}{h}} \frac{H_s^2}{h_t}$

$$h_t = (0.95 - 0.35 \frac{H_s}{h})\ h$$

Near bed wave-induced velocity : $u_b = (0.05 - (\alpha_s - 0.5))\ \hat{U}_\delta$

$$\alpha_s = \frac{\hat{U}_{\delta,f}}{\hat{U}_{\delta,f} + \hat{U}_{\delta,b}}$$

7. Compute apparent bed roughness

$$K_s = K_{s,c} \exp\left(\gamma \frac{\hat{U}_\delta}{\sqrt{(\overline{v_R})^2 + (\overline{u_r})^2}}\right)$$

$$\gamma = 0.8 + \beta - 0.3\ \beta^2$$

$$\beta = \frac{\phi}{360^\circ}\ 2\pi$$

8. Compute friction factors

Current : $C' = 18 \log\left(\frac{12h}{3D_{90}}\right)$

$$C = 18 \log\left(\frac{12h}{K_{s,c}}\right)$$

$$f_c' = 0.24 \log^{-2}\left(\frac{12h}{3D_{90}}\right)$$

$$f_c = 0.24 \log^{-2}\left(\frac{12h}{K_{s,c}}\right)$$

$$f_a = 0.24 \log^{-2}\left(\frac{12h}{K_a}\right)$$

Waves : $f_w' = \exp\left[-6 + 5.2\left(\frac{\hat{A}_\delta}{3D_{90}}\right)^{-0.19}\right]$

$$f_w = \exp\left[-6 + 5.2\left(\frac{\hat{A}_\delta}{K_{s,w}}\right)^{-0.19}\right]$$

$$f_{w,\max} = 0.3$$

9. Compute effective time-averaged bed-shear stresses

Efficiency factor current : $\mu_c = \frac{f_c'}{f_c}$

Efficiency factor waves : $\mu_w = \frac{f_w'}{f_w}$

$$\mu_{w,a} = \frac{0.6}{D_*}$$

Wave-current interaction coefficient : $\alpha_{cw} = \left[\frac{\ln(90\delta_w/K_a)}{\ln(90\delta_w/K_{s,c})}\right]^2 \left[\frac{-1 + \ln(30h/K_{s,c})}{-1 + \ln(30h/K_a)}\right]^2$

$$\alpha_{cw,\max} = 1$$

Bed-shear stress current : $\tau_c = \frac{1}{8}\rho f_w \sqrt{(\overline{v_R})^2 + (\overline{u_r})}$

Bed-shear stress waves : $\tau_w = \frac{1}{4}\rho f_w (\hat{U}_\delta)^2$

Bed-shear stress current-waves : $\tau_{cw} = \tau_c + \tau_w$

Effective bed-shear velocity current : $u_{*,c}' = \sqrt{\frac{\alpha_{cw}\,\mu_c\,\tau_c}{\rho}}$

10. Compute bed-shear stress parameters

Dimensionless bed-shear stress for

bed load transport : $$T = \frac{(\alpha\ \mu_c\ \tau_c + \mu_w\ \tau_w) - \tau_{cr}}{\tau_{cr}}$$

Dimensionless bed-shear stress for

reference concentration at z=a : $$T_a = \frac{(\alpha\ \mu_c\ \tau_c + \mu_{w,a}\ \tau_w) - \tau_{cr}}{\tau_{cr}}$$

T = 0 if T < 0

11. Compute velocity distribution over the depth

Outside wave-boundary layer, $z \geq 3\delta_w$: $$\nu_{R,z} = \frac{\overline{\nu_R}\ \ln\ (30\ z\ /\ K_a)}{-1 + \ln\ (30\ h\ /\ K_a)}$$

Inside wave-boundary layer, $z < 3\delta_w$: $$\nu_{R,z} = \frac{\nu_\delta\ \ln\ (\ 30\ z\ /\ K_{s,c})}{\ln\ (\ 90\ \delta_w\ /\ K_{s,c})}$$

$$\nu_\delta = \frac{\overline{\nu_R}\ \ln\ (\ 90\ \delta_w\ /\ K_a)}{-1 + \ln\ (\ 30\ h\ /\ K_a)}$$

12. Compute sediment mixing coefficient distribution over the depth

Current, $z < 0.5\ h$: $$\epsilon_{s,c} = \kappa\ \beta\ u_{*,c}\ z\ (1 - \frac{z}{h})$$

$z \geq 0.5\ h$: $$\epsilon_{s,c} = 0.25\ \kappa\ \beta\ u_{*,c}\ h$$

$$u_{*,c} = \frac{\sqrt{g}}{C}\ \sqrt{(\overline{v_R})^2 + (\overline{u_r})^2}$$

$$\beta = 1 + 2\ (\frac{w_s}{u_{*,c}})^2$$

$$\beta_{max} = 1.5$$

Waves, $z \leq \delta_s$: $\epsilon_{s,w} = \epsilon_{s,bed} = 0.004\, D_*\, \delta_s\, \hat{U}_\delta$

$z \geq 0.5\ h$: $\epsilon_{s,w} = \epsilon_{s,\max} = 0.035\, h\, \frac{H_s}{T_p}$

$\delta_s < z < 0.5\ h$: $\epsilon_{s,w} = \epsilon_{s,bed} + [\epsilon_{s,\max} - \epsilon_{s,bed}]\, \frac{z - \delta_s}{0.5h - \delta_s}$

$\delta_s = 0.3\, h \sqrt{\frac{H_s}{h}}$

$\delta_{s,\min} = 0.05\ m, \quad \delta_{s,\max} = 0.2\ m$

Current and waves, : $\epsilon_{s,w} = \sqrt{\epsilon_{s,c}^2 + \epsilon_{s,w}^2}$

13. Compute concentration distribution over the depth by numerical integration

Reference level : $a = maximum(K_{s,c}, K_{s,w})$

Concentration gradient $(z < a)$: $\frac{dc}{dz} = -\frac{(1 - c)^5\, c\, w_s}{\epsilon_{s,cw}\, (\, 1 + (\frac{c}{c_0})^{0.8} - 2\, (\frac{c}{c_0})^{0.4}\,)}$

Bed concentration $(z \leq a)$: $c_a = 0.015\, \frac{D_{50}}{a}\, \frac{T_a^{1.5}}{D_*^{0.3}}$

$c_0 =$ 0.65 = *maximum volume concentration*

$w_s =$ *fall velocity of suspended sediment*

14. Compute time-averaged suspended load transport rates

Current direction : $q_s = \rho_s \int_a^h v_R\, c\, dz$

Wave direction : $q_s = \rho_s \int_a^h u_r\, c\, dz$

Sediment concentrations

and

Sediment transport

in case of

Irregular breaking waves

"Experimental results series A and B"

Part I: Tables and figures

August 1995

Bart Grasmeijer
Rico Sies

Experimental Data Tables

CODE	Grasmeijer/Sies 1	ID	938
MODEL	TU-flume	SET	Series A
TEST	T 10 00	DATE	23-02-1994
LOCATION	18 m, test 1	TIME	

H	waterdepth	(m)	0.300
WS	water surface slope	(-)	
Hsig	sign wave height	(m)	0.1022
Hm	mean wave height	(m)	0.0646
Hrms	rms wave height	(m)	0.0724
Tz	zero-cross period	(s)	1.63
Tp	peak period	(s)	2.30
Um	mean vel // shore	(m/s)	
Vm	mean vel L shore	(m/s)	
Vmr	mean result vel	(m/s)	
Vprof	mean vel profile	(m/s)	-0.0221
Urms	rms vel at bed	(m/s)	
Umax	max vel at bed	(m/s)	
U15	vel exceed by 15%	(m/s)	
PHI	angle flow-waves	(degr)	0
BT	br. type :	Non breaking	
DMB	distance between meas. loc. and breakerline	(m)	
Urms,on	rms vel. at bed in onsh. dir.	(m/s)	
Urms,off	rms vel. at bed in offsh. dir.	(m/s)	
Te	water temp	(o C)	18.6
BS	local bed slope normal to shore	(-)	0.010000

D10	bed mat size	(um)	76
D50	bed mat size	(um)	95
D90	bed mat size	(um)	131
Ds -mean	susp mat size	(um)	88
-min	susp mat size	(um)	69
-max	susp mat size	(um)	130
WSB	fall vel bed	(m/s)	
WSS-mean	fall vel sus	(m/s)	0.0068
-min	fall vel sus	(m/s)	0.0041
-max	fall vel sus	(m/s)	0.0123
Cbed1	bed concent.	(kg/m3)	2.76000
Cbed2	bed concent.	(kg/m3)	1590.00000
Cbed3	bed concent.	(kg/m3)	9.09068
Lb	bed load	(kg/m2)	
Ls1	sus load	(kg/m2)	0.108155
Ls2	sus load	(kg/m2)	0.937051
Ls3	sus load	(kg/m2)	0.159291
Sb	bed transp	(kg/sm)	
Ss1	sus transp	(kg/sm)	-0.001199
Ss2	sus transp	(kg/sm)	-0.006680
Ss3	sus transp	(kg/sm)	-0.001936
BFH-mean	bedform height	(m)	0.008
-min	bedform height	(m)	0.002
-max	bedform height	(m)	0.013
BFL-mean	bedform length	(m)	0.049
-min	bedform length	(m)	0.028
-max	bedform length	(m)	0.076
BFT	bedf type:		2.5-D ripples

Z (m) height	C concentration (kg/m3) mean	min	max	Z (m) height	Vr result velocity (m/s) mean	min	max	Z (m) height	D50 (um)
0.020	2.760	2.560	2.870	0.020	-0.014				
0.030	1.660	1.640	1.680	0.030	-0.014				
0.040	0.851	0.829	0.873	0.040	-0.017				
0.055	0.349	0.329	0.369	0.055	-0.015				
0.080	0.117	0.112	0.122	0.080	-0.021				
0.110	0.032	0.031	0.033	0.110	-0.017				
0.145	0.009	0.009	0.010	0.145	-0.022				
0.180	0.004	0.004	0.004	0.180	-0.021				
0.220	0.003	0.003	0.003	0.220	-0.031				
0.270	0.002	0.002	0.002	0.270	-0.029				

Vm,Vmr,Vr + : landwards
Vm,Vmr,Vr - : seawards
0 < PHI < 180

CODE	Grasmeijer/Sies 2	ID	939
MODEL	TU-flume	SET	Series A
TEST	T 10 00	DATE	23-02-1994
LOCATION	18 m, test 2	TIME	

H	waterdepth (m)	0.300	
WS	water surface slope (-)		
Hsig	sign wave height (m)	0.1027	
Hm	mean wave height (m)	0.0646	
Hrms	rms wave height (m)	0.0726	
Tz	zero-cross period (s)	1.63	
Tp	peak period (s)	2.30	
Um	mean vel // shore (m/s)		
Vm	mean vel L shore (m/s)		
Vmr	mean result vel (m/s)		
Vprof	mean vel profile (m/s)	-0.0225	
Urms	rms vel at bed (m/s)		
Umax	max vel at bed (m/s)		
U15	vel exceed by 15% (m/s)		
PHI	angle flow-waves (degr)	0	
BT	br. type :	Non breaking	
DMB	distance between meas. loc. and breakerline (m)		
Urms,on	rms vel. at bed in onsh. dir. (m/s)		
Urms,off	rms vel. at bed in offsh. dir. (m/s)		
Te	water temp (o C)	18.9	
BS	local bed slope normal to shore (-)	0.010000	

D10	bed mat size (um)	76
D50	bed mat size (um)	95
D90	bed mat size (um)	131
Ds -mean	susp mat size (um)	89
-min	susp mat size (um)	70
-max	susp mat size (um)	126
WSB	fall vel bed (m/s)	
WSS-mean	fall vel sus (m/s)	0.0069
-min	fall vel sus (m/s)	0.0043
-max	fall vel sus (m/s)	0.0116
Cbed1	bed concent. (kg/m3)	2.71000
Cbed2	bed concent. (kg/m3)	1268.02000
Cbed3	bed concent. (kg/m3)	7.96902
Lb	bed load (kg/m2)	
Ls1	sus load (kg/m2)	0.109140
Ls2	sus load (kg/m2)	0.739887
Ls3	sus load (kg/m2)	0.151868
Sb	bed transp (kg/sm)	
Ss1	sus transp (kg/sm)	-0.001184
Ss2	sus transp (kg/sm)	-0.005427
Ss3	sus transp (kg/sm)	-0.001834
BFH-mean	bedform height (m)	0.009
-min	bedform height (m)	0.005
-max	bedform height (m)	0.013
BFL-mean	bedform length (m)	0.053
-min	bedform length (m)	0.041
-max	bedform length (m)	0.071
BFT	bedf type:	2.5-D ripples

Z (m) height	C concentration (kg/m3) mean	min	max
0.020	2.710		
0.030	1.620		
0.040	0.920		
0.055	0.387		
0.080	0.128		
0.110	0.045		
0.145	0.015		
0.180	0.007		
0.220	0.004		
0.270	0.000		

Z (m) height	Vr result velocity (m/s) mean	min	max
0.020	-0.014		
0.030	-0.013		
0.040	-0.015		
0.055	-0.015		
0.080	-0.017		
0.110	-0.021		
0.145	-0.025		
0.180	-0.024		
0.220	-0.034		
0.270	-0.025		

Z (m) height	D50 (um)

Vm,Vmr,Vr + : landwards
Vm,Vmr,Vr - : seawards
0 < PHI < 180

CODE	Grasmeijer/Sies 3	ID	940
MODEL	TU-flume	SET	Series A
TEST	T 14 00	DATE	28-02-1994
LOCATION	18 m, test 1	TIME	

H	waterdepth (m)	0.300	
WS	water surface slope (-)		
Hsig	sign wave height (m)	0.1412	
Hm	mean wave height (m)	0.0895	
Hrms	rms wave height (m)	0.1004	
Tz	zero-cross period (s)	1.47	
Tp	peak period (s)	2.30	
Um	mean vel // shore (m/s)		
Vm	mean vel L shore (m/s)		
Vmr	mean result vel (m/s)		
Vprof	mean vel profile (m/s)	-0.0308	
Urms	rms vel at bed (m/s)		
Umax	max vel at bed (m/s)		
U15	vel exceed by 15% (m/s)		
PHI	angle flow-waves (degr)	0	
BT	br. type :Breaking:	5.5 %	
DMB	distance between meas. loc. and breakerline(m)		
Urms,on	rms vel. at bed in onsh. dir. (m/s)		
Urms,off	rms vel. at bed in offsh. dir. (m/s)		
Te	water temp (o C)	17.1	
BS	local bed slope normal to shore (-)	0.010000	

D10	bed mat size (um)	76
D50	bed mat size (um)	95
D90	bed mat size (um)	131
Ds -mean	susp mat size (um)	85
-min	susp mat size (um)	67
-max	susp mat size (um)	118
WSB	fall vel bed (m/s)	
WSS-mean	fall vel sus (m/s)	0.0066
-min	fall vel sus (m/s)	0.0041
-max	fall vel sus (m/s)	0.0107
Cbed1	bed concent.(kg/m3)	6.29500
Cbed2	bed concent.(kg/m3)	1590.00000
Cbed3	bed concent.(kg/m3)	18.80264
Lb	bed load (kg/m2)	
Ls1	sus load (kg/m2)	0.256796
Ls2	sus load (kg/m2)	1.192072
Ls3	sus load (kg/m2)	0.356058
Sb	bed transp (kg/sm)	
Ss1	sus transp (kg/sm)	-0.004423
Ss2	sus transp (kg/sm)	-0.012237
Ss3	sus transp (kg/sm)	-0.006125
BFH-mean	bedform height (m)	0.006
-min	bedform height (m)	0.001
-max	bedform height (m)	0.013
BFL-mean	bedform length (m)	0.040
-min	bedform length (m)	0.024
-max	bedform length (m)	0.055
BFT	bedf type:	2.5-D ripples

Z (m) height	C concentration (kg/m3) mean	min	max	Z (m) height	Vr result velocity (m/s) mean	min	max	Z (m) height	D50 (um)
0.019	6.295	5.540	7.050	0.019	-0.016				
0.029	4.105	4.050	4.160	0.029	-0.027				
0.039	2.060	2.040	2.080	0.039	-0.022				
0.054	0.770	0.738	0.802	0.054	-0.034				
0.079	0.319	0.289	0.348	0.079	-0.029				
0.109	0.160	0.141	0.179	0.109	-0.034				
0.144	0.103	0.086	0.120	0.144	-0.034				
0.179	0.065	0.054	0.075	0.179	-0.037				
0.219	0.049	0.040	0.058	0.219	-0.039				
0.269	0.032	0.023	0.040	0.269	-0.026				

Vm,Vmr,Vr + : landwards
Vm,Vmr,Vr - : seawards
0 < PHI < 180

CODE	Grasmeijer/Sies 4	ID	941
MODEL	TU-flume	SET	Series A
TEST	T 14 00	DATE	01-03-1994
LOCATION	18 m, test 2	TIME	

H	waterdepth	(m)	0.300	D10	bed mat size	(um)	76
WS	water surface slope	(-)		D50	bed mat size	(um)	95
Hsig	sign wave height	(m)	0.1404	D90	bed mat size	(um)	131
Hm	mean wave height	(m)	0.0899	Ds -mean	susp mat size	(um)	86
Hrms	rms wave height	(m)	0.1002	-min	susp mat size	(um)	66
Tz	zero-cross period	(s)	1.45	-max	susp mat size	(um)	122
Tp	peak period	(s)	2.30	WSB	fall vel bed	(m/s)	
Um	mean vel // shore	(m/s)		WSS-mean	fall vel sus	(m/s)	0.0067
Vm	mean vel L shore	(m/s)		-min	fall vel sus	(m/s)	0.0040
Vmr	mean result vel	(m/s)		-max	fall vel sus	(m/s)	0.0114
Vprof	mean vel profile	(m/s)	-0.0316	Cbed1	bed concent.	(kg/m3)	6.68000
Urms	rms vel at bed	(m/s)		Cbed2	bed concent.	(kg/m3)	1590.00000
Umax	max vel at bed	(m/s)		Cbed3	bed concent.	(kg/m3)	18.12893
U15	vel exceed by 15%	(m/s)		Lb	bed load	(kg/m2)	
PHI	angle flow-waves	(degr)	0	Ls1	sus load	(kg/m2)	0.277681
BT	br. type :Breaking:		6.3 %	Ls2	sus load	(kg/m2)	1.240233
DMB	distance between meas. loc. and breakerline	(m)		Ls3	sus load	(kg/m2)	0.366986
Urms,on	rms vel. at bed in onsh. dir.	(m/s)		Sb	bed transp	(kg/sm)	
Urms,off	rms vel. at bed in offsh. dir.	(m/s)		Ss1	sus transp	(kg/sm)	-0.005117
				Ss2	sus transp	(kg/sm)	-0.015228
				Ss3	sus transp	(kg/sm)	-0.007143
				BFH-mean	bedform height	(m)	0.006
				-min	bedform height	(m)	0.001
				-max	bedform height	(m)	0.011
				BFL-mean	bedform length	(m)	0.046
				-min	bedform length	(m)	0.022
				-max	bedform length	(m)	0.083
Te	water temp	(o C)	18.0	BFT	bedf type:		2.5-D ripples
BS	local bed slope normal to shore	(-)	0.010000				

Z (m) height	C concentration (kg/m3) mean	min	max	Z (m) height	Vr result velocity (m/s) mean	min	max	Z (m) height	D50 (um)
0.019	6.680	6.130	7.230	0.019	-0.020				
0.029	4.010	3.840	4.180	0.029	-0.020				
0.039	2.325	2.120	2.530	0.039	-0.030				
0.054	0.942	0.853	1.030	0.054	-0.026				
0.079	0.393	0.372	0.414	0.079	-0.035				
0.109	0.199	0.181	0.217	0.109	-0.029				
0.144	0.123	0.119	0.127	0.144	-0.039				
0.179	0.095	0.081	0.108	0.179	-0.036				
0.219	0.064	0.059	0.069	0.219	-0.041				
0.269	0.033	0.026	0.039	0.269	-0.027				

Vm,Vmr,Vr + : landwards
Vm,Vmr,Vr - : seawards
0 < PHI < 180

CODE	Grasmeijer/Sies 5	ID	942
MODEL	TU-flume	SET	Series A
TEST	T 14 00	DATE	16-03-1994
LOCATION	18 m, test 3	TIME	

H	waterdepth	(m)	0.300	D10	bed mat size	(um)	76
WS	water surface slope	(-)		D50	bed mat size	(um)	95
Hsig	sign wave height	(m)	0.1432	D90	bed mat size	(um)	131
Hm	mean wave height	(m)	0.0909	Ds -mean	susp mat size	(um)	91
Hrms	rms wave height	(m)	0.1018	-min	susp mat size	(um)	66
Tz	zero-cross period	(s)	1.47	-max	susp mat size	(um)	137
Tp	peak period	(s)	2.30	WSB	fall vel bed	(m/s)	
Um	mean vel // shore	(m/s)		WSS-mean	fall vel sus	(m/s)	0.0076
Vm	mean vel L shore	(m/s)		-min	fall vel sus	(m/s)	0.0040
Vmr	mean result vel	(m/s)		-max	fall vel sus	(m/s)	0.0141
Vprof	mean vel profile	(m/s)	-0.0324	Cbed1	bed concent.	(kg/m3)	6.56000
Urms	rms vel at bed	(m/s)		Cbed2	bed concent.	(kg/m3)	1590.00000
Umax	max vel at bed	(m/s)		Cbed3	bed concent.	(kg/m3)	18.66321
U15	vel exceed by 15%	(m/s)		Lb	bed load	(kg/m2)	
PHI	angle flow-waves	(degr)	0	Ls1	sus load	(kg/m2)	0.268145
BT	br. type :Breaking:		5.1 %	Ls2	sus load	(kg/m2)	1.435996
DMB	distance between meas. loc. and breakerline	(m)		Ls3	sus load	(kg/m2)	0.362674
				Sb	bed transp	(kg/sm)	
Urms,on	rms vel. at bed in onsh. dir.	(m/s)		Ss1	sus transp	(kg/sm)	-0.004876
				Ss2	sus transp	(kg/sm)	-0.016483
Urms,off	rms vel. at bed in offsh. dir.	(m/s)		Ss3	sus transp	(kg/sm)	-0.006858
				BFH-mean	bedform height	(m)	0.007
Te	water temp	(o C)	19.5	-min	bedform height	(m)	0.001
BS	local bed slope normal to shore	(-)	0.010000	-max	bedform height	(m)	0.014
				BFL-mean	bedform length	(m)	0.048
				-min	bedform length	(m)	0.028
				-max	bedform length	(m)	0.069
				BFT	bedf type:		2.5-D ripples

Z (m) height	C concentration (kg/m3) mean	min	max	Z (m) height	Vr result velocity (m/s) mean	min	max	Z (m) height	D50 (um)
0.019	6.560	6.180	6.940	0.019	-0.019				
0.029	3.980	3.810	4.150	0.029	-0.027				
0.039	2.195	2.130	2.260	0.039	-0.020				
0.054	0.925	0.920	0.930	0.054	-0.034				
0.079	0.365	0.336	0.394	0.079	-0.029				
0.109	0.181	0.152	0.210	0.109	-0.032				
0.144	0.094	0.076	0.112	0.144	-0.037				
0.179	0.073	0.052	0.094	0.179	-0.036				
0.219	0.041	0.035	0.046	0.219	-0.044				
0.269	0.029	0.020	0.037	0.269	-0.030				

Vm,Vmr,Vr + : landwards
Vm,Vmr,Vr - : seawards
0 < PHI < 180

CODE	Grasmeijer/Sies 6	ID	943
MODEL	TU-flume	SET	Series A
TEST	T 16 00	DATE	24-02-1994
LOCATION	18 m, test 1	TIME	

H	waterdepth (m)	0.290	
WS	water surface slope (-)		
Hsig	sign wave height (m)	0.1661	
Hm	mean wave height (m)	0.1132	
Hrms	rms wave height (m)	0.1238	
Tz	zero-cross period (s)	1.37	
Tp	peak period (s)	2.30	
Um	mean vel // shore (m/s)		
Vm	mean vel L shore (m/s)		
Vmr	mean result vel (m/s)		
Vprof	mean vel profile (m/s)	-0.0353	
Urms	rms vel at bed (m/s)		
Umax	max vel at bed (m/s)		
U15	vel exceed by 15% (m/s)		
PHI	angle flow-waves (degr)	0	
BT	br. type :Breaking:	21.0 %	
DMB	distance between meas. loc. and breakerline (m)		
Urms,on	rms vel. at bed in onsh. dir. (m/s)		
Urms,off	rms vel. at bed in offsh. dir. (m/s)		
Te	water temp (o C)	18.7	
BS	local bed slope normal to shore (-)	0.010000	

D10	bed mat size (um)	76
D50	bed mat size (um)	95
D90	bed mat size (um)	131
Ds -mean	susp mat size (um)	84
-min	susp mat size (um)	66
-max	susp mat size (um)	117
WSB	fall vel bed (m/s)	
WSS-mean	fall vel sus (m/s)	0.0066
-min	fall vel sus (m/s)	0.0040
-max	fall vel sus (m/s)	0.0107
Cbed1	bed concent.(kg/m3)	9.51500
Cbed2	bed concent.(kg/m3)	1590.00000
Cbed3	bed concent.(kg/m3)	26.71893
Lb	bed load (kg/m2)	
Ls1	sus load (kg/m2)	0.391971
Ls2	sus load (kg/m2)	1.852125
Ls3	sus load (kg/m2)	0.519475
Sb	bed transp (kg/sm)	
Ss1	sus transp (kg/sm)	-0.011846
Ss2	sus transp (kg/sm)	-0.042000
Ss3	sus transp (kg/sm)	-0.017236
BFH-mean	bedform height (m)	0.006
-min	bedform height (m)	0.001
-max	bedform height (m)	0.011
BFL-mean	bedform length (m)	0.047
-min	bedform length (m)	0.021
-max	bedform length (m)	0.076
BFT	bedf type:	2.5-D ripples

Z (m) height	C concentration (kg/m3) mean	min	max	Z (m) height	Vr result velocity (m/s) mean	min	max	Z (m) height	D50 (um)
0.018	9.515	8.960	10.070	0.018	-0.038				
0.028	5.650	5.590	5.710	0.028	-0.036				
0.038	3.040			0.038	-0.040				
0.053	1.270	1.260	1.280	0.053	-0.044				
0.078	0.596	0.576	0.615	0.078	-0.046				
0.108	0.349	0.314	0.383	0.108	-0.034				
0.143	0.247	0.234	0.260	0.143	-0.048				
0.178	0.180	0.167	0.192	0.178	-0.037				
0.218	0.146	0.145	0.147	0.218	-0.042				
0.268	0.098	0.095	0.101	0.268	-0.009				

Vm,Vmr,Vr + : landwards
Vm,Vmr,Vr - : seawards
0 < PHI < 180

CODE	Grasmeijer/Sies 7	ID	944
MODEL	TU-flume	SET	Series A
TEST	T 16 00	DATE	25-02-1994
LOCATION	18 m, test 2	TIME	

H	waterdepth	(m)	0.300	D10	bed mat size	(um)	76
WS	water surface slope	(-)		D50	bed mat size	(um)	95
Hsig	sign wave height	(m)	0.1683	D90	bed mat size	(um)	131
Hm	mean wave height	(m)	0.1154	Ds -mean	susp mat size	(um)	82
Hrms	rms wave height	(m)	0.1258	-min	susp mat size	(um)	64
Tz	zero-cross period	(s)	1.37	-max	susp mat size	(um)	112
Tp	peak period	(s)	2.30	WSB	fall vel bed	(m/s)	
Um	mean vel // shore	(m/s)		WSS-mean	fall vel sus	(m/s)	0.0063
Vm	mean vel L shore	(m/s)		-min	fall vel sus	(m/s)	0.0038
Vmr	mean result vel	(m/s)		-max	fall vel sus	(m/s)	0.0100
Vprof	mean vel profile	(m/s)	-0.0333	Cbed1	bed concent.	(kg/m3)	10.46000
Urms	rms vel at bed	(m/s)		Cbed2	bed concent.	(kg/m3)	1590.00000
Umax	max vel at bed	(m/s)		Cbed3	bed concent.	(kg/m3)	32.94638
U15	vel exceed by 15%	(m/s)		Lb	bed load	(kg/m2)	
PHI	angle flow-waves	(degr)	0	Ls1	sus load	(kg/m2)	0.425109
BT	br. type :Breaking:		20.6 %	Ls2	sus load	(kg/m2)	2.512955
DMB	distance between meas. loc. and breakerline	(m)		Ls3	sus load	(kg/m2)	0.595564
				Sb	bed transp	(kg/sm)	
Urms,on	rms vel. at bed in onsh. dir.	(m/s)		Ss1	sus transp	(kg/sm)	-0.011161
				Ss2	sus transp	(kg/sm)	-0.049238
Urms,off	rms vel. at bed in offsh. dir.	(m/s)		Ss3	sus transp	(kg/sm)	-0.017265
				BFH-mean	bedform height	(m)	0.006
Te	water temp	(o C)	18.8	-min	bedform height	(m)	0.001
BS	local bed slope normal to shore	(-)	0.010000	-max	bedform height	(m)	0.009
				BFL-mean	bedform length	(m)	0.043
				-min	bedform length	(m)	0.024
				-max	bedform length	(m)	0.071
				BFT	bedf type:		2.5-D ripples

Z (m) height	C concentration (kg/m3) mean	min	max	Z (m) height	Vr result velocity (m/s) mean	min	max	Z (m) height	D50 (um)
0.019	10.460	10.060	10.860	0.019	-0.034				
0.029	5.755	5.600	5.910	0.029	-0.031				
0.039	3.100	2.940	3.260	0.039	-0.035				
0.054	1.255	1.190	1.320	0.054	-0.033				
0.079	0.566	0.519	0.612	0.079	-0.042				
0.109	0.329	0.280	0.377	0.109	-0.038				
0.144	0.244	0.207	0.280	0.144	-0.041				
0.179	0.178	0.158	0.198	0.179	-0.044				
0.219	0.148	0.133	0.162	0.219	-0.045				
0.269	0.112	0.104	0.119	0.269	-0.007				

Vm,Vmr,Vr + : landwards
Vm,Vmr,Vr - : seawards
0 < PHI < 180

CODE	Grasmeijer/Sies 8	ID	945
MODEL	TU-flume	SET	Series A
TEST	T 16 00	DATE	15-03-1994
LOCATION	18 m, test 3	TIME	

H	waterdepth (m)	0.300	
WS	water surface slope (-)		
Hsig	sign wave height (m)	0.1546	
Hm	mean wave height (m)	0.1002	
Hrms	rms wave height (m)	0.1111	
Tz	zero-cross period (s)	1.42	
Tp	peak period (s)	2.30	
Um	mean vel // shore (m/s)		
Vm	mean vel L shore (m/s)		
Vmr	mean result vel (m/s)		
Vprof	mean vel profile (m/s)	-0.0380	
Urms	rms vel at bed (m/s)		
Umax	max vel at bed (m/s)		
U15	vel exceed by 15% (m/s)		
PHI	angle flow-waves (degr)	0	
BT	br. type :Breaking:	10.2 %	
DMB	distance between meas. loc. and breakerline (m)		
Urms,on	rms vel. at bed in onsh. dir. (m/s)		
Urms,off	rms vel. at bed in offsh. dir. (m/s)		
Te	water temp (o C)	19.2	
BS	local bed slope normal to shore (-)	0.010000	

D10	bed mat size (um)	76
D50	bed mat size (um)	95
D90	bed mat size (um)	131
Ds -mean	susp mat size (um)	95
-min	susp mat size (um)	70
-max	susp mat size (um)	134
WSB	fall vel bed (m/s)	
WSS-mean	fall vel sus (m/s)	0.0084
-min	fall vel sus (m/s)	0.0046
-max	fall vel sus (m/s)	0.0138
Cbed1	bed concent. (kg/m3)	9.32500
Cbed2	bed concent. (kg/m3)	1590.00000
Cbed3	bed concent. (kg/m3)	23.97859
Lb	bed load (kg/m2)	
Ls1	sus load (kg/m2)	0.369850
Ls2	sus load (kg/m2)	1.446232
Ls3	sus load (kg/m2)	0.473005
Sb	bed transp (kg/sm)	
Ss1	sus transp (kg/sm)	-0.008879
Ss2	sus transp (kg/sm)	-0.023109
Ss3	sus transp (kg/sm)	-0.011783
BFH-mean	bedform height (m)	0.007
-min	bedform height (m)	0.002
-max	bedform height (m)	0.013
BFL-mean	bedform length (m)	0.048
-min	bedform length (m)	0.031
-max	bedform length (m)	0.072
BFT	bedf type:	2.5-D ripples

Z (m) height	C concentration (kg/m3) mean	min	max	Z (m) height	Vr result velocity (m/s) mean	min	max	Z (m) height	D50 (um)
0.017	9.325	8.740	9.910	0.017	-0.024				
0.027	5.470	5.120	5.820	0.027	-0.029				
0.037	3.060	2.900	3.220	0.037	-0.033				
0.052	1.375	1.300	1.450	0.052	-0.041				
0.077	0.576	0.570	0.581	0.077	-0.039				
0.107	0.296	0.290	0.301	0.107	-0.048				
0.142	0.181	0.179	0.182	0.142	-0.044				
0.177	0.139	0.138	0.140	0.177	-0.045				
0.217	0.101	0.100	0.102	0.217	-0.050				
0.267	0.065	0.063	0.067	0.267	-0.023				

Vm,Vmr,Vr + : landwards
Vm,Vmr,Vr - : seawards
0 < PHI < 180

CODE	Grasmeijer/Sies 9	ID	946
MODEL	TU-flume	SET	Series A
TEST	T 10 10	DATE	21-02-1994
LOCATION	18 m, test 1	TIME	

H	waterdepth (m)	0.300	
WS	water surface slope (-)		
Hsig	sign wave height (m)	0.1013	
Hm	mean wave height (m)	0.0629	
Hrms	rms wave height (m)	0.0714	
Tz	zero-cross period (s)	1.62	
Tp	peak period (s)	2.30	
Um	mean vel // shore (m/s)		
Vm	mean vel L shore (m/s)		
Vmr	mean result vel (m/s)		
Vprof	mean vel profile (m/s)	0.1014	
Urms	rms vel at bed (m/s)		
Umax	max vel at bed (m/s)		
U15	vel exceed by 15% (m/s)		
PHI	angle flow-waves (degr)	0	
BT	br. type :	Non breaking	
DMB	distance between meas. loc. and breakerline (m)		
Urms,on	rms vel. at bed in onsh. dir. (m/s)		
Urms,off	rms vel. at bed in offsh. dir. (m/s)		
Te	water temp (o C)	19.0	
BS	local bed slope normal to shore (-)	0.010000	

D10	bed mat size (um)	76	
D50	bed mat size (um)	95	
D90	bed mat size (um)	131	
Ds -mean	susp mat size (um)	94	
-min	susp mat size (um)	76	
-max	susp mat size (um)	130	
WSB	fall vel bed (m/s)		
WSS-mean	fall vel sus (m/s)	0.0079	
-min	fall vel sus (m/s)	0.0052	
-max	fall vel sus (m/s)	0.0125	
Cbed1	bed concent. (kg/m3)	2.58500	
Cbed2	bed concent. (kg/m3)	1590.00000	
Cbed3	bed concent. (kg/m3)	8.08440	
Lb	bed load (kg/m2)		
Ls1	sus load (kg/m2)	0.127110	
Ls2	sus load (kg/m2)	1.162218	
Ls3	sus load (kg/m2)	0.181513	
Sb	bed transp (kg/sm)		
Ss1	sus transp (kg/sm)	0.005442	
Ss2	sus transp (kg/sm)	0.023025	
Ss3	sus transp (kg/sm)	0.007564	
BFH-mean	bedform height (m)	0.009	
-min	bedform height (m)	0.003	
-max	bedform height (m)	0.015	
BFL-mean	bedform length (m)	0.059	
-min	bedform length (m)	0.048	
-max	bedform length (m)	0.069	
BFT	bedf type:	2.5-D ripples	

Z (m) height	C concentration (kg/m3) mean	min	max	Z (m) height	Vr result velocity (m/s) mean	min	max	Z (m) height	D50 (um)
0.025	2.585	2.570	2.600	0.025	0.037				
0.035	1.560	1.500	1.620	0.035	0.053				
0.045	1.020	1.010	1.030	0.045	0.067				
0.060	0.533	0.528	0.537	0.060	0.087				
0.085	0.217	0.200	0.234	0.085	0.101				
0.115	0.077	0.074	0.080	0.115	0.121				
0.150	0.026	0.025	0.027	0.150	0.125				
0.185	0.015	0.012	0.018	0.185	0.123				
0.225	0.011	0.011	0.012	0.225	0.120				
0.275	0.003	0.002	0.005	0.275	0.106				

Vm,Vmr,Vr + : landwards
Vm,Vmr,Vr - : seawards
0 < PHI < 180

CODE	Grasmeijer/Sies 10	ID	947
MODEL	TU-flume	SET	Series A
TEST	T 10 10	DATE	21-02-1994
LOCATION	18 m, test 2	TIME	

H	waterdepth (m)	0.300	
WS	water surface slope (-)		
Hsig	sign wave height (m)	0.1008	
Hm	mean wave height (m)	0.0624	
Hrms	rms wave height (m)	0.0709	
Tz	zero-cross period (s)	1.61	
Tp	peak period (s)	2.30	
Um	mean vel // shore (m/s)		
Vm	mean vel L shore (m/s)		
Vmr	mean result vel (m/s)		
Vprof	mean vel profile (m/s)	0.1043	
Urms	rms vel at bed (m/s)		
Umax	max vel at bed (m/s)		
U15	vel exceed by 15% (m/s)		
PHI	angle flow-waves (degr)	0	
BT	br. type :	Non breaking	
DMB	distance between meas. loc. and breakerline (m)		
Urms,on	rms vel. at bed in onsh. dir. (m/s)		
Urms,off	rms vel. at bed in offsh. dir. (m/s)		
Te	water temp (o C)	19.1	
BS	local bed slope normal to shore (-)	0.010000	

D10	bed mat size (um)	76
D50	bed mat size (um)	95
D90	bed mat size (um)	131
Ds -mean	susp mat size (um)	91
-min	susp mat size (um)	74
-max	susp mat size (um)	129
WSB	fall vel bed (m/s)	
WSS-mean	fall vel sus (m/s)	0.0073
-min	fall vel sus (m/s)	0.0048
-max	fall vel sus (m/s)	0.0121
Cbed1	bed concent. (kg/m3)	1.97000
Cbed2	bed concent. (kg/m3)	257.60640
Cbed3	bed concent. (kg/m3)	4.74426
Lb	bed load (kg/m2)	
Ls1	sus load (kg/m2)	0.098300
Ls2	sus load (kg/m2)	0.302250
Ls3	sus load (kg/m2)	0.125122
Sb	bed transp (kg/sm)	
Ss1	sus transp (kg/sm)	0.004454
Ss2	sus transp (kg/sm)	0.008380
Ss3	sus transp (kg/sm)	0.005563
BFH-mean	bedform height (m)	0.009
-min	bedform height (m)	0.003
-max	bedform height (m)	0.015
BFL-mean	bedform length (m)	0.059
-min	bedform length (m)	0.048
-max	bedform length (m)	0.069
BFT	bedf type:	2.5-D ripples

Z (m) height	C concentration (kg/m3) mean	min	max	Z (m) height	Vr result velocity (m/s) mean	min	max	Z (m) height	D50 (um)
0.023	1.970			0.023	0.034				
0.033	1.360	1.280	1.440	0.033	0.053				
0.043	0.915	0.849	0.980	0.043	0.069				
0.058	0.406	0.298	0.513	0.058	0.085				
0.083	0.201	0.199	0.203	0.083	0.110				
0.113	0.072	0.066	0.078	0.113	0.122				
0.148	0.027	0.025	0.029	0.148	0.122				
0.183	0.012	0.010	0.014	0.183	0.121				
0.223	0.010	0.009	0.011	0.223	0.118				
0.273	0.007	0.006	0.007	0.273	0.121				

Vm,Vmr,Vr + : landwards
Vm,Vmr,Vr - : seawards
0 < PHI < 180

CODE	Grasmeijer/Sies 11	ID	948
MODEL	TU-flume	SET	Series A
TEST	T 10 10	DATE	02-03-1994
LOCATION	18 m, test 3	TIME	

H	waterdepth	(m)	0.300
WS	water surface slope	(-)	
Hsig	sign wave height	(m)	0.0999
Hm	mean wave height	(m)	0.0626
Hrms	rms wave height	(m)	0.0706
Tz	zero-cross period	(s)	1.57
Tp	peak period	(s)	2.30
Um	mean vel // shore	(m/s)	
Vm	mean vel L shore	(m/s)	
Vmr	mean result vel	(m/s)	
Vprof	mean vel profile	(m/s)	0.0922
Urms	rms vel at bed	(m/s)	
Umax	max vel at bed	(m/s)	
U15	vel exceed by 15%	(m/s)	
PHI	angle flow-waves	(degr)	0
BT	br. type :	Non breaking	
DMB	distance between meas. loc. and breakerline	(m)	
Urms,on	rms vel. at bed in onsh. dir.	(m/s)	
Urms,off	rms vel. at bed in offsh. dir.	(m/s)	
Te	water temp	(o C)	19.0
BS	local bed slope normal to shore	(-)	0.010000

D10	bed mat size	(um)	76
D50	bed mat size	(um)	95
D90	bed mat size	(um)	131
Ds -mean	susp mat size	(um)	91
-min	susp mat size	(um)	72
-max	susp mat size	(um)	129
WSB	fall vel bed	(m/s)	
WSS-mean	fall vel sus	(m/s)	0.0073
-min	fall vel sus	(m/s)	0.0047
-max	fall vel sus	(m/s)	0.0124
Cbed1	bed concent.	(kg/m3)	2.18000
Cbed2	bed concent.	(kg/m3)	636.62520
Cbed3	bed concent.	(kg/m3)	5.44658
Lb	bed load	(kg/m2)	
Ls1	sus load	(kg/m2)	0.098822
Ls2	sus load	(kg/m2)	0.458304
Ls3	sus load	(kg/m2)	0.125627
Sb	bed transp	(kg/sm)	
Ss1	sus transp	(kg/sm)	0.004333
Ss2	sus transp	(kg/sm)	0.010380
Ss3	sus transp	(kg/sm)	0.005390
BFH-mean	bedform height	(m)	0.009
-min	bedform height	(m)	0.001
-max	bedform height	(m)	0.019
BFL-mean	bedform length	(m)	0.056
-min	bedform length	(m)	0.031
-max	bedform length	(m)	0.083
BFT	bedf type:		2.5-D ripples

Z (m) height	C concentration (kg/m3) mean	min	max	Z (m) height	Vr result velocity (m/s) mean	min	max	Z (m) height	D50 (um)
0.020	2.180	2.170	2.190	0.020	0.033				
0.030	1.330	1.280	1.380	0.030	0.049				
0.040	0.857	0.832	0.881	0.040	0.064				
0.055	0.482	0.482	0.482	0.055	0.079				
0.080	0.207	0.199	0.215	0.080	0.106				
0.110	0.092	0.086	0.097	0.110	0.112				
0.145	0.028	0.023	0.033	0.145	0.115				
0.180	0.013	0.011	0.015	0.180	0.109				
0.220	0.008	0.007	0.008	0.220	0.102				
0.270	0.004	0.004	0.004	0.270	0.088				

Vm,Vmr,Vr + : landwards
Vm,Vmr,Vr - : seawards
0 < PHI < 180

CODE	Grasmeijer/Sies 12	ID	949
MODEL	TU-flume	SET	Series A
TEST	T 14 10	DATE	03-03-1994
LOCATION	18 m, test 1	TIME	

H	waterdepth (m)	0.300	
WS	water surface slope (-)		
Hsig	sign wave height (m)	0.1393	
Hm	mean wave height (m)	0.0866	
Hrms	rms wave height (m)	0.0979	
Tz	zero-cross period (s)	1.39	
Tp	peak period (s)	2.30	
Um	mean vel // shore (m/s)		
Vm	mean vel L shore (m/s)		
Vmr	mean result vel (m/s)		
Vprof	mean vel profile (m/s)	0.0779	
Urms	rms vel at bed (m/s)		
Umax	max vel at bed (m/s)		
U15	vel exceed by 15% (m/s)		
PHI	angle flow-waves (degr)	0	
BT	br. type :Breaking:	3.9 %	
DMB	distance between meas. loc. and breakerline (m)		
Urms,on	rms vel. at bed in onsh. dir. (m/s)		
Urms,off	rms vel. at bed in offsh. dir. (m/s)		
Te	water temp (o C)	19.2	
BS	local bed slope normal to shore (-)	0.010000	

D10	bed mat size (um)	76
D50	bed mat size (um)	95
D90	bed mat size (um)	131
Ds -mean	susp mat size (um)	89
-min	susp mat size (um)	74
-max	susp mat size (um)	120
WSB	fall vel bed (m/s)	
WSS-mean	fall vel sus (m/s)	0.0074
-min	fall vel sus (m/s)	0.0051
-max	fall vel sus (m/s)	0.0112
Cbed1	bed concent. (kg/m3)	4.83500
Cbed2	bed concent. (kg/m3)	1418.50100
Cbed3	bed concent. (kg/m3)	12.50468
Lb	bed load (kg/m2)	
Ls1	sus load (kg/m2)	0.210000
Ls2	sus load (kg/m2)	1.011425
Ls3	sus load (kg/m2)	0.273466
Sb	bed transp (kg/sm)	
Ss1	sus transp (kg/sm)	0.006367
Ss2	sus transp (kg/sm)	0.014946
Ss3	sus transp (kg/sm)	0.007920
BFH-mean	bedform height (m)	0.007
-min	bedform height (m)	0.001
-max	bedform height (m)	0.018
BFL-mean	bedform length (m)	0.047
-min	bedform length (m)	0.024
-max	bedform length (m)	0.096
BFT	bedf type:	2.5-D ripples

Z (m) height	C concentration (kg/m3) mean	min	max	Z (m) height	Vr result velocity (m/s) mean	min	max	Z (m) height	D50 (um)
0.020	4.835	4.480	5.190	0.020	0.021				
0.030	3.035	2.870	3.200	0.030	0.037				
0.040	1.860	1.770	1.950	0.040	0.047				
0.055	0.855	0.840	0.870	0.055	0.063				
0.080	0.345	0.332	0.358	0.080	0.076				
0.110	0.143	0.132	0.154	0.110	0.095				
0.145	0.050	0.040	0.060	0.145	0.090				
0.180	0.030	0.024	0.035	0.180	0.094				
0.220	0.019	0.015	0.022	0.220	0.088				
0.270	0.014	0.012	0.015	0.270	0.089				

Vm,Vmr,Vr + : landwards
Vm,Vmr,Vr - : seawards
0 < PHI < 180

CODE	Grasmeijer/Sies 13	ID	950
MODEL	TU-flume	SET	Series A
TEST	T 14 10	DATE	03-03-1994
LOCATION	18 m, test 2	TIME	

H	waterdepth	(m)	0.300	D10	bed mat size	(um)	76
WS	water surface slope	(-)		D50	bed mat size	(um)	95
Hsig	sign wave height	(m)	0.1403	D90	bed mat size	(um)	131
Hm	mean wave height	(m)	0.0881	Ds -mean	susp mat size	(um)	91
Hrms	rms wave height	(m)	0.0992	-min	susp mat size	(um)	74
Tz	zero-cross period	(s)	1.37	-max	susp mat size	(um)	127
Tp	peak period	(s)	2.30	WSB	fall vel bed	(m/s)	
Um	mean vel // shore	(m/s)		WSS-mean	fall vel sus	(m/s)	0.0077
Vm	mean vel L shore	(m/s)		-min	fall vel sus	(m/s)	0.0051
Vmr	mean result vel	(m/s)		-max	fall vel sus	(m/s)	0.0125
Vprof	mean vel profile	(m/s)	0.0721	Cbed1	bed concent.	(kg/m3)	4.02000
Urms	rms vel at bed	(m/s)		Cbed2	bed concent.	(kg/m3)	1171.27200
Umax	max vel at bed	(m/s)		Cbed3	bed concent.	(kg/m3)	10.80607
U15	vel exceed by 15%	(m/s)		Lb	bed load	(kg/m2)	
PHI	angle flow-waves	(degr)	0	Ls1	sus load	(kg/m2)	0.173135
BT	br. type :Breaking:		4.0 %	Ls2	sus load	(kg/m2)	0.834333
DMB	distance between meas. loc. and breakerline	(m)		Ls3	sus load	(kg/m2)	0.229014
				Sb	bed transp	(kg/sm)	
Urms,on	rms vel. at bed in onsh. dir.	(m/s)		Ss1	sus transp	(kg/sm)	0.005350
				Ss2	sus transp	(kg/sm)	0.012765
Urms,off	rms vel. at bed in offsh. dir.	(m/s)		Ss3	sus transp	(kg/sm)	0.006750
				BFH-mean	bedform height	(m)	0.007
Te	water temp	(o C)	19.3	-min	bedform height	(m)	0.001
BS	local bed slope normal to shore	(-)	0.010000	-max	bedform height	(m)	0.015
				BFL-mean	bedform length	(m)	0.048
				-min	bedform length	(m)	0.021
				-max	bedform length	(m)	0.072
				BFT	bedf type:		2.5-D ripples

Z (m) height	C concentration (kg/m3) mean	min	max	Z (m) height	Vr result velocity (m/s) mean	min	max	Z (m) height	D50 (um)
0.020	4.020			0.020	0.022				
0.030	2.490			0.030	0.040				
0.040	1.490			0.040	0.050				
0.055	0.693			0.055	0.062				
0.080	0.279			0.080	0.075				
0.110	0.130			0.110	0.089				
0.145	0.043			0.145	0.088				
0.180	0.023			0.180	0.086				
0.220	0.013			0.220	0.089				
0.270	0.010			0.270	0.066				

Vm,Vmr,Vr + : landwards
Vm,Vmr,Vr - : seawards
0 < PHI < 180

CODE	Grasmeijer/Sies 14	ID	951
MODEL	TU-flume	SET	Series A
TEST	T 14 10	DATE	17-03-1994
LOCATION	18 m, test 3	TIME	

H	waterdepth	(m)	0.300	D10	bed mat size	(um)	76
WS	water surface slope	(-)		D50	bed mat size	(um)	95
Hsig	sign wave height	(m)	0.1442	D90	bed mat size	(um)	131
Hm	mean wave height	(m)	0.0898	Ds -mean	susp mat size	(um)	96
Hrms	rms wave height	(m)	0.1018	-min	susp mat size	(um)	76
Tz	zero-cross period	(s)	1.44	-max	susp mat size	(um)	132
Tp	peak period	(s)	2.30	WSB	fall vel bed	(m/s)	
Um	mean vel // shore	(m/s)		WSS-mean	fall vel sus	(m/s)	0.0086
Vm	mean vel L shore	(m/s)		-min	fall vel sus	(m/s)	0.0053
Vmr	mean result vel	(m/s)		-max	fall vel sus	(m/s)	0.0134
Vprof	mean vel profile	(m/s)	0.0775	Cbed1	bed concent.	(kg/m3)	4.74000
Urms	rms vel at bed	(m/s)		Cbed2	bed concent.	(kg/m3)	1590.00000
Umax	max vel at bed	(m/s)		Cbed3	bed concent.	(kg/m3)	14.30713
U15	vel exceed by 15%	(m/s)		Lb	bed load	(kg/m2)	
PHI	angle flow-waves	(degr)	0	Ls1	sus load	(kg/m2)	0.198545
BT	br. type :Breaking:		4.5 %	Ls2	sus load	(kg/m2)	1.236415
DMB	distance between meas. loc. and breakerline	(m)		Ls3	sus load	(kg/m2)	0.279953
				Sb	bed transp	(kg/sm)	
Urms,on	rms vel. at bed in onsh. dir.	(m/s)		Ss1	sus transp	(kg/sm)	0.006283
				Ss2	sus transp	(kg/sm)	0.021846
Urms,off	rms vel. at bed in offsh. dir.	(m/s)		Ss3	sus transp	(kg/sm)	0.008899
				BFH-mean	bedform height	(m)	0.007
Te	water temp	(o C)	20.0	-min	bedform height	(m)	0.003
BS	local bed slope normal to shore	(-)	0.010000	-max	bedform height	(m)	0.015
				BFL-mean	bedform length	(m)	0.046
				-min	bedform length	(m)	0.021
				-max	bedform length	(m)	0.072
				BFT	bedf type:		2.5-D ripples

Z (m) height	C concentration (kg/m3) mean	min	max	Z (m) height	Vr result velocity (m/s) mean	min	max	Z (m) height	D50 (um)
0.021	4.740	4.670	4.810	0.021	0.030				
0.031	2.885	2.830	2.940	0.031	0.040				
0.041	1.655	1.610	1.700	0.041	0.049				
0.056	0.716	0.678	0.753	0.056	0.0				
0.081	0.243	0.224	0.261	0.081	0.080				
0.111	0.088	0.079	0.096	0.111	0.095				
0.146	0.027	0.023	0.031	0.146	0.094				
0.181	0.013	0.012	0.014	0.181	0.095				
0.221	0.007	0.006	0.007	0.221	0.084				
0.271	0.004	0.004	0.004	0.271	0.081				

Vm,Vmr,Vr + : landwards
Vm,Vmr,Vr - : seawards
0 < PHI < 180

CODE	Grasmeijer/Sies 15	ID	952
MODEL	TU-flume	SET	Series A
TEST	T 14 10	DATE	17-03-1994
LOCATION	18 m, test 4	TIME	

H	waterdepth	(m)	0.310	D10	bed mat size	(um)	76
WS	water surface slope	(-)		D50	bed mat size	(um)	95
Hsig	sign wave height	(m)	0.1438	D90	bed mat size	(um)	131
Hm	mean wave height	(m)	0.0895	Ds -mean	susp mat size	(um)	103
Hrms	rms wave height	(m)	0.1013	-min	susp mat size	(um)	79
Tz	zero-cross period	(s)	1.47	-max	susp mat size	(um)	138
Tp	peak period	(s)	2.30	WSB	fall vel bed	(m/s)	
Um	mean vel // shore	(m/s)		WSS-mean	fall vel sus	(m/s)	0.0091
Vm	mean vel L shore	(m/s)		-min	fall vel sus	(m/s)	0.0058
Vmr	mean result vel	(m/s)		-max	fall vel sus	(m/s)	0.0144
Vprof	mean vel profile	(m/s)	0.0802	Cbed1	bed concent.	(kg/m3)	4.07000
Urms	rms vel at bed	(m/s)		Cbed2	bed concent.	(kg/m3)	1590.00000
Umax	max vel at bed	(m/s)		Cbed3	bed concent.	(kg/m3)	11.84683
U15	vel exceed by 15%	(m/s)		Lb	bed load	(kg/m2)	
PHI	angle flow-waves	(degr)	0	Ls1	sus load	(kg/m2)	0.165031
BT	br. type :Breaking:		4.0 %	Ls2	sus load	(kg/m2)	1.050986
DMB	distance between meas. loc. and breakerline	(m)		Ls3	sus load	(kg/m2)	0.228501
				Sb	bed transp	(kg/sm)	
Urms,on	rms vel. at bed in onsh. dir.	(m/s)		Ss1	sus transp	(kg/sm)	0.005327
				Ss2	sus transp	(kg/sm)	0.019726
Urms,off	rms vel. at bed in offsh. dir.	(m/s)		Ss3	sus transp	(kg/sm)	0.007612
				BFH-mean	bedform height	(m)	0.007
Te	water temp	(o C)	20.0	-min	bedform height	(m)	0.001
BS	local bed slope normal to shore	(-)	0.010000	-max	bedform height	(m)	0.016
				BFL-mean	bedform length	(m)	0.046
				-min	bedform length	(m)	0.024
				-max	bedform length	(m)	0.076
				BFT	bedf type:		2.5-D ripples

Z (m) height	C concentration (kg/m3) mean	min	max
0.020	4.070		
0.030	2.470		
0.040	1.400		
0.055	0.582		
0.080	0.208		
0.110	0.070		
0.145	0.022		
0.180	0.007		
0.220	0.006		
0.270	0.0032		

Z (m) height	Vr result velocity (m/s) mean	min	max
0.020	0.033		
0.030	0.036		
0.040	0.051		
0.055	0.061		
0.080	0.080		
0.110	0.102		
0.145	0.090		
0.180	0.099		
0.220	0.087		
0.270	0.087		

Z (m) height	D50 (um)

Vm,Vmr,Vr + : landwards
Vm,Vmr,Vr - : seawards
0 < PHI < 180

CODE	Grasmeijer/Sies 16	ID	953
MODEL	TU-flume	SET	Series A
TEST	T 16 10	DATE	08-03-1994
LOCATION	18 m, test 1	TIME	

H	waterdepth	(m)	0.300
WS	water surface slope	(-)	
Hsig	sign wave height	(m)	0.1559
Hm	mean wave height	(m)	0.1062
Hrms	rms wave height	(m)	0.1161
Tz	zero-cross period	(s)	1.29
Tp	peak period	(s)	2.30
Um	mean vel // shore	(m/s)	
Vm	mean vel L shore	(m/s)	
Vmr	mean result vel	(m/s)	
Vprof	mean vel profile	(m/s)	0.0717
Urms	rms vel at bed	(m/s)	
Umax	max vel at bed	(m/s)	
U15	vel exceed by 15%	(m/s)	
PHI	angle flow-waves	(degr)	0
BT	br. type :Breaking:		19.6 %
DMB	distance between meas. loc. and breakerline	(m)	
Urms,on	rms vel. at bed in onsh. dir.	(m/s)	
Urms,off	rms vel. at bed in offsh. dir.	(m/s)	
Te	water temp	(o C)	19.4
BS	local bed slope normal to shore	(-)	0.010000

D10	bed mat size	(um)	76
D50	bed mat size	(um)	95
D90	bed mat size	(um)	131
Ds -mean	susp mat size	(um)	93
-min	susp mat size	(um)	76
-max	susp mat size	(um)	128
WSB	fall vel bed	(m/s)	
WSS-mean	fall vel sus	(m/s)	0.0081
-min	fall vel sus	(m/s)	0.0054
-max	fall vel sus	(m/s)	0.0127
Cbed1	bed concent.	(kg/m3)	7.76500
Cbed2	bed concent.	(kg/m3)	1590.00000
Cbed3	bed concent.	(kg/m3)	21.22073
Lb	bed load	(kg/m2)	
Ls1	sus load	(kg/m2)	0.361995
Ls2	sus load	(kg/m2)	1.576124
Ls3	sus load	(kg/m2)	0.478280
Sb	bed transp	(kg/sm)	
Ss1	sus transp	(kg/sm)	0.010837
Ss2	sus transp	(kg/sm)	0.024371
Ss3	sus transp	(kg/sm)	0.013590
BFH-mean	bedform height	(m)	0.008
-min	bedform height	(m)	0.001
-max	bedform height	(m)	0.018
BFL-mean	bedform length	(m)	0.045
-min	bedform length	(m)	0.024
-max	bedform length	(m)	0.065
BFT	bedf type:		2.5-D ripples

Z (m) height	C concentration (kg/m3) mean	min	max	Z (m) height	Vr result velocity (m/s) mean	min	max	Z (m) height	D50 (um)
0.021	7.765	7.030	8.500	0.021	0.021				
0.031	4.910	4.550	5.270	0.031	0.030				
0.041	2.975	2.860	3.090	0.041	0.043				
0.056	1.395	1.390	1.400	0.056	0.058				
0.081	0.611	0.591	0.630	0.081	0.066				
0.111	0.311	0.297	0.325	0.111	0.081				
0.146	0.189	0.181	0.197	0.146	0.094				
0.181	0.142	0.132	0.151	0.181	0.089				
0.221	0.100	0.091	0.109	0.221	0.092				
0.271	0.065	0.060	0.070	0.271	0.071				

Vm,Vmr,Vr + : landwards
Vm,Vmr,Vr - : seawards
0 < PHI < 180

CODE	Grasmeijer/Sies 17	ID	954
MODEL	TU-flume	SET	Series A
TEST	T 16 10	DATE	08-03-1994
LOCATION	18 m, test 2	TIME	

H	waterdepth	(m)	0.300	D10	bed mat size	(um)	76
WS	water surface slope	(-)		D50	bed mat size	(um)	95
Hsig	sign wave height	(m)	0.1571	D90	bed mat size	(um)	131
Hm	mean wave height	(m)	0.1068	Ds -mean	susp mat size	(um)	93
Hrms	rms wave height	(m)	0.1165	-min	susp mat size	(um)	77
Tz	zero-cross period	(s)	1.24	-max	susp mat size	(um)	128
Tp	peak period	(s)	2.30	WSB	fall vel bed	(m/s)	
Um	mean vel // shore	(m/s)		WSS-mean	fall vel sus	(m/s)	0.0081
Vm	mean vel L shore	(m/s)		-min	fall vel sus	(m/s)	0.0056
Vmr	mean result vel	(m/s)		-max	fall vel sus	(m/s)	0.0128
Vprof	mean vel profile	(m/s)	0.0710	Cbed1	bed concent.	(kg/m3)	7.26000
Urms	rms vel at bed	(m/s)		Cbed2	bed concent.	(kg/m3)	1590.00000
Umax	max vel at bed	(m/s)		Cbed3	bed concent.	(kg/m3)	20.68686
U15	vel exceed by 15%	(m/s)		Lb	bed load	(kg/m2)	
PHI	angle flow-waves	(degr)	0	Ls1	sus load	(kg/m2)	0.343694
BT	br. type :Breaking:		20.0 %	Ls2	sus load	(kg/m2)	1.561764
DMB	distance between meas. loc. and breakerline	(m)		Ls3	sus load	(kg/m2)	0.464578
				Sb	bed transp	(kg/sm)	
Urms,on	rms vel. at bed in onsh. dir.	(m/s)		Ss1	sus transp	(kg/sm)	0.010843
				Ss2	sus transp	(kg/sm)	0.026815
Urms,off	rms vel. at bed in offsh. dir.	(m/s)		Ss3	sus transp	(kg/sm)	0.014171
				BFH-mean	bedform height	(m)	0.008
Te	water temp	(o C)	19.6	-min	bedform height	(m)	0.001
BS	local bed slope normal to shore	(-)	0.010000	-max	bedform height	(m)	0.018
				BFL-mean	bedform length	(m)	0.054
				-min	bedform length	(m)	0.024
				-max	bedform length	(m)	0.114
				BFT	bedf type:		2.5-D ripples

Z (m) height	C concentration (kg/m3) mean	min	max	Z (m) height	Vr result velocity (m/s) mean	min	max	Z (m) height	D50 (um)
0.022	7.260			0.022	0.025				
0.032	4.620			0.032	0.035				
0.042	2.800			0.042	0.043				
0.057	1.350			0.057	0.062				
0.082	0.579			0.082	0.072				
0.112	0.274			0.112	0.082				
0.147	0.148			0.147	0.092				
0.182	0.107			0.182	0.092				
0.222	0.077			0.222	0.083				
0.272	0.051			0.272	0.067				

Vm,Vmr,Vr + : landwards
Vm,Vmr,Vr - : seawards
0 < PHI < 180

CODE	Grasmeijer/Sies 18	ID	955
MODEL	TU-flume	SET	Series A
TEST	T 10 20	DATE	14-03-1994
LOCATION	18 m, test 1	TIME	

H	waterdepth	(m)	0.300
WS	water surface slope	(-)	
Hsig	sign wave height	(m)	0.0987
Hm	mean wave height	(m)	0.0616
Hrms	rms wave height	(m)	0.0696
Tz	zero-cross period	(s)	1.65
Tp	peak period	(s)	2.30
Um	mean vel // shore	(m/s)	
Vm	mean vel L shore	(m/s)	
Vmr	mean result vel	(m/s)	
Vprof	mean vel profile	(m/s)	0.1824
Urms	rms vel at bed	(m/s)	
Umax	max vel at bed	(m/s)	
U15	vel exceed by 15%	(m/s)	
PHI	angle flow-waves	(degr)	0
BT	br. type :	Non breaking	
DMB	distance between meas. loc. and breakerline	(m)	
Urms,on	rms vel. at bed in onsh. dir.	(m/s)	
Urms,off	rms vel. at bed in offsh. dir.	(m/s)	
Te	water temp	(o C)	19.9
BS	local bed slope normal to shore	(-)	0.010000

D10	bed mat size	(um)	76
D50	bed mat size	(um)	95
D90	bed mat size	(um)	131
Ds -mean	susp mat size	(um)	113
-min	susp mat size	(um)	83
-max	susp mat size	(um)	149
WSB	fall vel bed	(m/s)	
WSS-mean	fall vel sus	(m/s)	0.0098
-min	fall vel sus	(m/s)	0.0062
-max	fall vel sus	(m/s)	0.0161
Cbed1	bed concent.	(kg/m3)	1.54500
Cbed2	bed concent.	(kg/m3)	232.64490
Cbed3	bed concent.	(kg/m3)	3.33283
Lb	bed load	(kg/m2)	
Ls1	sus load	(kg/m2)	0.097067
Ls2	sus load	(kg/m2)	0.290713
Ls3	sus load	(kg/m2)	0.116428
Sb	bed transp	(kg/sm)	
Ss1	sus transp	(kg/sm)	0.010958
Ss2	sus transp	(kg/sm)	0.022583
Ss3	sus transp	(kg/sm)	0.013760
BFH-mean	bedform height	(m)	0.009
-min	bedform height	(m)	0.002
-max	bedform height	(m)	0.019
BFL-mean	bedform length	(m)	0.064
-min	bedform length	(m)	0.038
-max	bedform length	(m)	0.093
BFT	bedf type:		2.5-D ripples

Z (m) height	C concentration (kg/m3) mean	min	max	Z (m) height	Vr result velocity (m/s) mean	min	max	Z (m) height	D50 (um)
0.026	1.545	1.470	1.620	0.026	0.109				
0.036	1.075	1.050	1.100	0.036	0.124				
0.046	0.839	0.825	0.852	0.046	0.142				
0.061	0.571	0.563	0.579	0.061	0.159				
0.086	0.308	0.297	0.318	0.086	0.189				
0.116	0.145	0.145	0.145	0.116	0.207				
0.151	0.049	0.048	0.050	0.151	0.217				
0.186	0.024	0.023	0.024	0.186	0.220				
0.226	0.011	0.010	0.012	0.226	0.208				
0.276	0.006	0.006	0.006	0.276	0.175				

Vm,Vmr,Vr + : landwards
Vm,Vmr,Vr - : seawards
0 < PHI < 180

CODE	Grasmeijer/Sies 20	ID	957
MODEL	TU-flume	SET	Series A
TEST	T 14 20	DATE	10-03-1994
LOCATION	18 m, test 1	TIME	

H	waterdepth	(m)	0.300	D10	bed mat size	(um)	76
WS	water surface slope	(-)		D50	bed mat size	(um)	95
Hsig	sign wave height	(m)	0.1391	D90	bed mat size	(um)	131
Hm	mean wave height	(m)	0.0886	Ds -mean	susp mat size	(um)	92
Hrms	rms wave height	(m)	0.0990	-min	susp mat size	(um)	74
Tz	zero-cross period	(s)	1.48	-max	susp mat size	(um)	128
Tp	peak period	(s)	2.30	WSB	fall vel bed	(m/s)	
Um	mean vel // shore	(m/s)		WSS-mean	fall vel sus	(m/s)	0.0079
Vm	mean vel L shore	(m/s)		-min	fall vel sus	(m/s)	0.0051
Vmr	mean result vel	(m/s)		-max	fall vel sus	(m/s)	0.0127
Vprof	mean vel profile	(m/s)	0.1684	Cbed1	bed concent.	(kg/m3)	3.66000
Urms	rms vel at bed	(m/s)		Cbed2	bed concent.	(kg/m3)	646.10680
Umax	max vel at bed	(m/s)		Cbed3	bed concent.	(kg/m3)	8.44355
U15	vel exceed by 15%	(m/s)		Lb	bed load	(kg/m2)	
PHI	angle flow-waves	(degr)	0	Ls1	sus load	(kg/m2)	0.242770
BT	br. type :Breaking:		3.5 %	Ls2	sus load	(kg/m2)	0.813010
DMB	distance between meas. loc. and breakerline	(m)		Ls3	sus load	(kg/m2)	0.302841
				Sb	bed transp	(kg/sm)	
Urms,on	rms vel. at bed in onsh. dir.	(m/s)		Ss1	sus transp	(kg/sm)	0.024588
				Ss2	sus transp	(kg/sm)	0.052534
Urms,off	rms vel. at bed in offsh. dir.	(m/s)		Ss3	sus transp	(kg/sm)	0.031508
				BFH-mean	bedform height	(m)	0.012
Te	water temp	(o C)	19.9	-min	bedform height	(m)	0.001
BS	local bed slope normal to shore	(-)	0.010000	-max	bedform height	(m)	0.027
				BFL-mean	bedform length	(m)	0.082
				-min	bedform length	(m)	0.048
				-max	bedform length	(m)	0.124
				BFT	bedf type:		2.5-D ripples

Z (m) height	C concentration (kg/m3) mean	min	max	Z (m) height	Vr result velocity (m/s) mean	min	max	Z (m) height	D50 (um)
0.030	3.660	3.540	3.780	0.030	0.092				
0.040	2.675	2.580	2.770	0.040	0.114				
0.050	2.075	2.000	2.150	0.050	0.136				
0.065	1.255	1.190	1.320	0.065	0.160				
0.090	0.660	0.640	0.679	0.090	0.191				
0.120	0.286	0.268	0.304	0.120	0.206				
0.155	0.112	0.098	0.126	0.155	0.217				
0.190	0.063	0.054	0.072	0.190	0.205				
0.230	0.046	0.045	0.046	0.230	0.196				
0.280	0.031	0.029	0.033	0.280	0.128				

Vm,Vmr,Vr + : landwards
Vm,Vmr,Vr - : seawards
0 < PHI < 180

CODE	Grasmeijer/Sies 21	ID	958
MODEL	TU-flume	SET	Series A
TEST	T 16 20	DATE	09-03-1994
LOCATION	18 m, test 1	TIME	

H	waterdepth	(m)	0.300	D10	bed mat size	(um)	76
WS	water surface slope	(-)		D50	bed mat size	(um)	95
Hsig	sign wave height	(m)	0.1562	D90	bed mat size	(um)	131
Hm	mean wave height	(m)	0.1029	Ds -mean	susp mat size	(um)	96
Hrms	rms wave height	(m)	0.1139	-min	susp mat size	(um)	80
Tz	zero-cross period	(s)	1.26	-max	susp mat size	(um)	131
Tp	peak period	(s)	2.30	WSB	fall vel bed	(m/s)	
Um	mean vel // shore	(m/s)		WSS-mean	fall vel sus	(m/s)	0.0087
Vm	mean vel L shore	(m/s)		-min	fall vel sus	(m/s)	0.0060
Vmr	mean result vel	(m/s)		-max	fall vel sus	(m/s)	0.0132
Vprof	mean vel profile	(m/s)	0.1627	Cbed1	bed concent.	(kg/m3)	6.38500
Urms	rms vel at bed	(m/s)		Cbed2	bed concent.	(kg/m3)	534.88200
Umax	max vel at bed	(m/s)		Cbed3	bed concent.	(kg/m3)	14.16586
U15	vel exceed by 15%	(m/s)		Lb	bed load	(kg/m2)	
PHI	angle flow-waves	(degr)	0	Ls1	sus load	(kg/m2)	0.394334
BT	br. type :Breaking:		21.2 %	Ls2	sus load	(kg/m2)	0.900123
DMB	distance between meas. loc. and breakerline	(m)		Ls3	sus load	(kg/m2)	0.473970
				Sb	bed transp	(kg/sm)	
Urms,on	rms vel. at bed in onsh. dir.	(m/s)		Ss1	sus transp	(kg/sm)	0.039724
				Ss2	sus transp	(kg/sm)	0.066482
Urms,off	rms vel. at bed in offsh. dir.	(m/s)		Ss3	sus transp	(kg/sm)	0.048645
				BFH-mean	bedform height	(m)	0.007
Te	water temp	(o C)	19.6	-min	bedform height	(m)	0.002
BS	local bed slope normal to shore	(-)	0.010000	-max	bedform height	(m)	0.014
				BFL-mean	bedform length	(m)	0.059
				-min	bedform length	(m)	0.028
				-max	bedform length	(m)	0.100
				BFT	bedf type:		2.5-D ripples

Z (m) height	C concentration (kg/m3) mean	min	max	Z (m) height	Vr result velocity (m/s) mean	min	max	Z (m) height	D50 (um)
0.024	6.385	6.110	6.660	0.024	0.087				
0.034	4.630	4.390	4.870	0.034	0.094				
0.044	3.280	3.130	3.430	0.044	0.126				
0.059	2.105	1.890	2.320	0.059	0.137				
0.084	1.170	1.030	1.310	0.084	0.175				
0.114	0.585	0.521	0.649	0.114	0.201				
0.149	0.306	0.256	0.354	0.149	0.206				
0.184	0.210	0.172	0.248	0.184	0.199				
0.224	0.147	0.116	0.178	0.224	0.205				
0.274	0.089	0.068	0.109	0.274	0.122				

Vm,Vmr,Vr + : landwards
Vm,Vmr,Vr - : seawards
0 < PHI < 180

CODE	Grasmeijer/Sies 22	ID	959
MODEL	TU-flume	SET	Series A
TEST	T 16 20	DATE	09-03-1994
LOCATION	18 m, test 2	TIME	

H	waterdepth	(m)	0.300	D10	bed mat size	(um)	76
WS	water surface slope	(-)		D50	bed mat size	(um)	95
Hsig	sign wave height	(m)	0.1595	D90	bed mat size	(um)	131
Hm	mean wave height	(m)	0.1050	Ds -mean	susp mat size	(um)	97
Hrms	rms wave height	(m)	0.1161	-min	susp mat size	(um)	79
Tz	zero-cross period	(s)	1.27	-max	susp mat size	(um)	135
Tp	peak period	(s)	2.30	WSB	fall vel bed	(m/s)	
Um	mean vel // shore	(m/s)		WSS-mean	fall vel sus	(m/s)	0.0090
Vm	mean vel L shore	(m/s)		-min	fall vel sus	(m/s)	0.0059
Vmr	mean result vel	(m/s)		-max	fall vel sus	(m/s)	0.0142
Vprof	mean vel profile	(m/s)	0.1588	Cbed1	bed concent.	(kg/m3)	5.81100
Urms	rms vel at bed	(m/s)		Cbed2	bed concent.	(kg/m3)	1590.00000
Umax	max vel at bed	(m/s)		Cbed3	bed concent.	(kg/m3)	14.57163
U15	vel exceed by 15%	(m/s)		Lb	bed load	(kg/m2)	
PHI	angle flow-waves	(degr)	0	Ls1	sus load	(kg/m2)	0.381694
BT	br. type :Breaking:		21.2 %	Ls2	sus load	(kg/m2)	1.601878
DMB	distance between meas. loc. and breakerline	(m)		Ls3	sus load	(kg/m2)	0.487207
				Sb	bed transp	(kg/sm)	
Urms,on	rms vel. at bed in onsh. dir.	(m/s)		Ss1	sus transp	(kg/sm)	0.036713
				Ss2	sus transp	(kg/sm)	0.090292
Urms,off	rms vel. at bed in offsh. dir.	(m/s)		Ss3	sus transp	(kg/sm)	0.047689
				BFH-mean	bedform height	(m)	0.010
Te	water temp	(o C)	19.8	-min	bedform height	(m)	0.001
BS	local bed slope normal to shore	(-)	0.010000	-max	bedform height	(m)	0.021
				BFL-mean	bedform length	(m)	0.060
				-min	bedform length	(m)	0.041
				-max	bedform length	(m)	0.089
				BFT	bedf type:		2.5-D ripples

Z (m) height	C concentration (kg/m3) mean	min	max	Z (m) height	Vr result velocity (m/s) mean	min	max	Z (m) height	D50 (um)
0.029	5.811			0.029	0.088				
0.039	4.160			0.039	0.100				
0.049	3.060			0.049	0.111				
0.064	1.840			0.064	0.169				
0.089	1.010			0.089	0.164				
0.119	0.549			0.119	0.198				
0.154	0.245			0.154	0.190				
0.189	0.157			0.189	0.194				
0.229	0.109			0.229	0.191				
0.279	0.070			0.279	0.129				

Vm,Vmr,Vr + : landwards
Vm,Vmr,Vr - : seawards
0 < PHI < 180

CODE	Grasmeijer/Sies 23	ID	960
MODEL	TU-flume	SET	Series A
TEST	T 14 30	DATE	18-03-1994
LOCATION	18 m, test 1	TIME	

H	waterdepth (m)	0.320	
WS	water surface slope (-)		
Hsig	sign wave height (m)	0.1406	
Hm	mean wave height (m)	0.0885	
Hrms	rms wave height (m)	0.0996	
Tz	zero-cross period (s)	1.53	
Tp	peak period (s)	2.30	
Um	mean vel // shore (m/s)		
Vm	mean vel L shore (m/s)		
Vmr	mean result vel (m/s)		
Vprof	mean vel profile (m/s)	0.2433	
Urms	rms vel at bed (m/s)		
Umax	max vel at bed (m/s)		
U15	vel exceed by 15% (m/s)		
PHI	angle flow-waves (degr)	0	
BT	br. type :Breaking:	3.1 %	
DMB	distance between meas. loc. and breakerline(m)		
Urms,on	rms vel. at bed in onsh. dir. (m/s)		
Urms,off	rms vel. at bed in offsh. dir. (m/s)		
Te	water temp (o C)	20.2	
BS	local bed slope normal to shore (-)	0.010000	

D10	bed mat size (um)	76
D50	bed mat size (um)	95
D90	bed mat size (um)	131
Ds -mean	susp mat size (um)	104
-min	susp mat size (um)	78
-max	susp mat size (um)	138
WSB	fall vel bed (m/s)	
WSS-mean	fall vel sus (m/s)	0.0091
-min	fall vel sus (m/s)	0.0058
-max	fall vel sus (m/s)	0.0145
Cbed1	bed concent.(kg/m3)	2.80000
Cbed2	bed concent.(kg/m3)	1571.02100
Cbed3	bed concent.(kg/m3)	8.66127
Lb	bed load (kg/m2)	
Ls1	sus load (kg/m2)	0.269962
Ls2	sus load (kg/m2)	1.776387
Ls3	sus load (kg/m2)	0.389345
Sb	bed transp (kg/sm)	
Ss1	sus transp (kg/sm)	0.043549
Ss2	sus transp (kg/sm)	0.150134
Ss3	sus transp (kg/sm)	0.064537
BFH-mean	bedform height (m)	0.021
-min	bedform height (m)	0.004
-max	bedform height (m)	0.041
BFL-mean	bedform length (m)	0.129
-min	bedform length (m)	0.076
-max	bedform length (m)	0.292
BFT	bedf type:	2.5-D ripples

Z (m) height	C concentration (kg/m3) mean	min	max	Z (m) height	Vr result velocity (m/s) mean	min	max	Z (m) height	D50 (um)
0.050	2.800	2.490	3.110	0.050	0.168				
0.060	2.290	2.070	2.510	0.060	0.217				
0.070	1.785	1.690	1.880	0.070	0.232				
0.085	1.245	1.160	1.330	0.085	0.251				
0.110	0.742	0.672	0.811	0.110	0.277				
0.140	0.381	0.359	0.402	0.140	0.295				
0.175	0.172	0.168	0.176	0.175	0.301				
0.210	0.087	0.076	0.098	0.210	0.296				
0.250	0.056	0.048	0.064	0.250	0.286				
0.300	0.036	0.030	0.041	0.300	0.189				

Vm,Vmr,Vr + : landwards
Vm,Vmr,Vr - : seawards
0 < PHI < 180

CODE	Grasmeijer/Sies 25	ID	985
MODEL	TU-flume	SET	Series B1
TEST	T 16 00 01	DATE	31-03-1994
LOCATION	5.0 m, section 1, test 2	TIME	

H	waterdepth (m)	0.600	
WS	water surface slope (-)		
Hsig	sign wave height (m)	0.1596	
Hm	mean wave height (m)		
Hrms	rms wave height (m)	0.1127	
Tz	zero-cross period (s)		
Tp	peak period (s)		
Um	mean vel // shore (m/s)		
Vm	mean vel L shore (m/s)		
Vmr	mean result vel (m/s)		
Vprof	mean vel profile (m/s)	-0.0248	
Urms	rms vel at bed (m/s)		
Umax	max vel at bed (m/s)		
U15	vel exceed by 15% (m/s)		
PHI	angle flow-waves (degr)		
BT	br. type :Non breaking		
DMB	distance between meas. loc. and breakerline (m)	9.000	
Urms,on	rms vel. at bed in onsh. dir. (m/s)		
Urms,off	rms vel. at bed in offsh. dir. (m/s)		
Te	water temp (o C)	20.0	
BS	local bed slope normal to shore (-)		

D10	bed mat size (um)	76
D50	bed mat size (um)	95
D90	bed mat size (um)	131
Ds -mean	susp mat size (um)	87
-min	susp mat size (um)	66
-max	susp mat size (um)	124
WSB	fall vel bed (m/s)	
WSS-mean	fall vel sus (m/s)	0.0066
-min	fall vel sus (m/s)	0.0038
-max	fall vel sus (m/s)	0.0111
Cbed1	bed concent. (kg/m3)	3.22500
Cbed2	bed concent. (kg/m3)	1590.00000
Cbed3	bed concent. (kg/m3)	10.95302
Lb	bed load (kg/m2)	
Ls1	sus load (kg/m2)	0.126612
Ls2	sus load (kg/m2)	1.189917
Ls3	sus load (kg/m2)	0.188240
Sb	bed transp (kg/sm)	
Ss1	sus transp (kg/sm)	0.000482
Ss2	sus transp (kg/sm)	0.004583
Ss3	sus transp (kg/sm)	0.000983
BFH-mean	bedform height (m)	0.007
-min	bedform height (m)	0.002
-max	bedform height (m)	0.012
BFL-mean	bedform length (m)	0.068
-min	bedform length (m)	0.061
-max	bedform length (m)	0.075
BFT	bedf type:2.5-D ripples	

Z (m) height	C concentration (kg/m3) mean	min	max	Z (m) height	Vr result velocity (m/s) mean	min	max	Z (m) height	D50 (um)
0.020	3.225	2.810	3.640	0.020	0.008				
0.030	1.855	1.750	1.960	0.030	0.009				
0.040	0.956	0.871	1.040	0.040	0.009				
0.055	0.399	0.361	0.437	0.055	-0.012				
0.080	0.115	0.099	0.131	0.080	0.009				
0.110	0.042	0.034	0.049	0.110	-0.018				
0.145	0.014	0.008	0.020	0.145	-0.024				
0.180	0.010	0.004	0.015	0.180	-0.026				
0.220	0.009	0.003	0.015	0.220	-0.025				
0.270	0.009	0.003	0.014	0.270	-0.033				

Vm,Vmr,Vr + : landwards
Vm,Vmr,Vr - : seawards
0 < PHI < 180

CODE	Grasmeijer/Sies 26	ID	986
MODEL	TU-flume	SET	Series B1
TEST	T 16 00 02	DATE	05-04-1994
LOCATION	8.0 m, section 2	TIME	

H	waterdepth (m)	0.590	
WS	water surface slope (-)		
Hsig	sign wave height (m)	0.1560	
Hm	mean wave height (m)		
Hrms	rms wave height (m)	0.1105	
Tz	zero-cross period (s)		
Tp	peak period (s)		
Um	mean vel // shore (m/s)		
Vm	mean vel L shore (m/s)		
Vmr	mean result vel (m/s)		
Vprof	mean vel profile (m/s)	-0.0266	
Urms	rms vel at bed (m/s)		
Umax	max vel at bed (m/s)		
U15	vel exceed by 15% (m/s)		
PHI	angle flow-waves (degr)		
BT	br. type :Non breaking		
DMB	distance between meas. loc. and breakerline (m)	6.000	
Urms,on	rms vel. at bed in onsh. dir. (m/s)		
Urms,off	rms vel. at bed in offsh. dir. (m/s)		
Te	water temp (o C)	19.1	
BS	local bed slope normal to shore (-)		

D10	bed mat size (um)	76
D50	bed mat size (um)	95
D90	bed mat size (um)	131
Ds -mean	susp mat size (um)	87
-min	susp mat size (um)	66
-max	susp mat size (um)	123
WSB	fall vel bed (m/s)	
WSS-mean	fall vel sus (m/s)	0.0066
-min	fall vel sus (m/s)	0.0038
-max	fall vel sus (m/s)	0.0111
Cbed1	bed concent. (kg/m3)	2.98000
Cbed2	bed concent. (kg/m3)	1590.00000
Cbed3	bed concent. (kg/m3)	11.54736
Lb	bed load (kg/m2)	
Ls1	sus load (kg/m2)	0.119351
Ls2	sus load (kg/m2)	1.757253
Ls3	sus load (kg/m2)	0.189007
Sb	bed transp (kg/sm)	
Ss1	sus transp (kg/sm)	-0.000960
Ss2	sus transp (kg/sm)	-0.006441
Ss3	sus transp (kg/sm)	-0.001431
BFH-mean	bedform height (m)	0.010
-min	bedform height (m)	0.009
-max	bedform height (m)	0.011
BFL-mean	bedform length (m)	0.047
-min	bedform length (m)	0.047
-max	bedform length (m)	0.047
BFT	bedf type:2.5-D ripples	

Z (m) height	C concentration (kg/m3) mean	min	max	Z (m) height	Vr result velocity (m/s) mean	min	max	Z (m) height	D50 (um)
0.021	2.980	2.830	3.130	0.021	-0.007				
0.031	1.620	1.480	1.760	0.031	-0.010				
0.041	0.820	0.719	0.920	0.041	-0.014				
0.056	0.370	0.330	0.409	0.056	-0.019				
0.081	0.123	0.117	0.129	0.081	-0.020				
0.111	0.041	0.040	0.042	0.111	-0.020				
0.146	0.017	0.013	0.021	0.146	-0.026				
0.181	0.016	0.010	0.021	0.181	-0.028				
0.221	0.010	0.006	0.014	0.221	-0.031				
0.271	0.009	0.007	0.011	0.271	-0.030				

Vm,Vmr,Vr + : landwards
Vm,Vmr,Vr - : seawards
0 < PHI < 180

CODE	Grasmeijer/Sies 27	ID	987
MODEL	TU-flume	SET	Series B1
TEST	T 16 00 03	DATE	06-04-1994
LOCATION	10.0 m, section 3	TIME	

H	waterdepth	(m)	0.500	D10	bed mat size	(um)	76
WS	water surface slope	(-)		D50	bed mat size	(um)	95
Hsig	sign wave height	(m)	0.1563	D90	bed mat size	(um)	131
Hm	mean wave height	(m)		Ds -mean	susp mat size	(um)	84
Hrms	rms wave height	(m)	0.1106	-min	susp mat size	(um)	61
Tz	zero-cross period	(s)		-max	susp mat size	(um)	116
Tp	peak period	(s)		WSB	fall vel bed	(m/s)	
Um	mean vel // shore	(m/s)		WSS-mean	fall vel sus	(m/s)	0.0060
Vm	mean vel L shore	(m/s)		-min	fall vel sus	(m/s)	0.0032
Vmr	mean result vel	(m/s)		-max	fall vel sus	(m/s)	0.0099
Vprof	mean vel profile	(m/s)	-0.0252	Cbed1	bed concent.	(kg/m3)	3.32000
Urms	rms vel at bed	(m/s)		Cbed2	bed concent.	(kg/m3)	1590.00000
Umax	max vel at bed	(m/s)		Cbed3	bed concent.	(kg/m3)	18.16748
U15	vel exceed by 15%	(m/s)		Lb	bed load	(kg/m2)	
PHI	angle flow-waves	(degr)		Ls1	sus load	(kg/m2)	0.129221
BT	br. type :Non breaking			Ls2	sus load	(kg/m2)	3.183819
DMB	distance between meas. loc. and breakerline	(m)	4.000	Ls3	sus load	(kg/m2)	0.241598
				Sb	bed transp	(kg/sm)	
Urms,on	rms vel. at bed in onsh. dir.	(m/s)		Ss1	sus transp	(kg/sm)	-0.001215
				Ss2	sus transp	(kg/sm)	-0.015100
Urms,off	rms vel. at bed in offsh. dir.	(m/s)		Ss3	sus transp	(kg/sm)	-0.002099
				BFH-mean	bedform height	(m)	0.007
Te	water temp	(o C)	19.3	-min	bedform height	(m)	0.005
BS	local bed slope normal to shore	(-)	0.050000	-max	bedform height	(m)	0.009
				BFL-mean	bedform length	(m)	0.050
				-min	bedform length	(m)	0.049
				-max	bedform length	(m)	0.051
				BFT	bedf type:2.5-D ripples		

Z (m) height	C concentration (kg/m3) mean	min	max	Z (m) height	Vr result velocity (m/s) mean	min	max	Z (m) height	D50 (um)
0.021	3.320	3.260	3.380	0.021	-0.009				
0.031	1.490	1.480	1.500	0.031	-0.012				
0.041	0.651	0.623	0.679	0.041	-0.015				
0.056	0.291	0.274	0.308	0.056	-0.015				
0.081	0.144	0.137	0.151	0.081	-0.022				
0.111	0.075	0.070	0.079	0.111	-0.025				
0.146	0.043	0.040	0.046	0.146	-0.029				
0.181	0.032	0.030	0.033	0.181	-0.028				
0.221	0.023	0.019	0.027	0.221	-0.032				
0.271	0.028	0.027	0.028	0.271	-0.027				

Vm,Vmr,Vr + : landwards
Vm,Vmr,Vr - : seawards
0 < PHI < 180

CODE	Grasmeijer/Sies 28	ID	988
MODEL	TU-flume	SET	Series B1
TEST	T17 00 04	DATE	06-04-1994
LOCATION	12.0 m, section 4	TIME	

H	waterdepth (m)	0.400	
WS	water surface slope (-)		
Hsig	sign wave height (m)	0.1652	
Hm	mean wave height (m)		
Hrms	rms wave height (m)	0.1163	
Tz	zero-cross period (s)		
Tp	peak period (s)		
Um	mean vel // shore (m/s)		
Vm	mean vel L shore (m/s)		
Vmr	mean result vel (m/s)		
Vprof	mean vel profile (m/s)	-0.0319	
Urms	rms vel at bed (m/s)		
Umax	max vel at bed (m/s)		
U15	vel exceed by 15% (m/s)		
PHI	angle flow-waves (degr)		
BT	br. type :Breaking:	0.4 %	
DMB	distance between meas. loc. and breakerline (m)	2.000	
Urms,on	rms vel. at bed in onsh. dir. (m/s)		
Urms,off	rms vel. at bed in offsh. dir. (m/s)		
Te	water temp (o C)	19.2	
BS	local bed slope normal to shore (-)	0.050000	

D10	bed mat size (um)	76
D50	bed mat size (um)	95
D90	bed mat size (um)	131
Ds -mean	susp mat size (um)	75
-min	susp mat size (um)	55
-max	susp mat size (um)	111
WSB	fall vel bed (m/s)	
WSS-mean	fall vel sus (m/s)	0.0053
-min	fall vel sus (m/s)	0.0029
-max	fall vel sus (m/s)	0.0099
Cbed1	bed concent. (kg/m3)	7.39000
Cbed2	bed concent. (kg/m3)	1590.00000
Cbed3	bed concent. (kg/m3)	33.64647
Lb	bed load (kg/m2)	
Ls1	sus load (kg/m2)	0.263829
Ls2	sus load (kg/m2)	3.378634
Ls3	sus load (kg/m2)	0.440699
Sb	bed transp (kg/sm)	
Ss1	sus transp (kg/sm)	-0.001695
Ss2	sus transp (kg/sm)	0.013364
Ss3	sus transp (kg/sm)	-0.000229
BFH-mean	bedform height (m)	0.012
-min	bedform height (m)	0.011
-max	bedform height (m)	0.014
BFL-mean	bedform length (m)	0.048
-min	bedform length (m)	0.045
-max	bedform length (m)	0.051
BFT	bedf type:2.5-D ripples	

Z (m) height	C concentration (kg/m3) mean	min	max	Z (m) height	Vr result velocity (m/s) mean	min	max	Z (m) height	D50 (um)
0.018	7.390	6.970	7.810	0.018	0.009				
0.028	3.290	3.260	3.320	0.028	-0.021				
0.038	1.365	1.320	1.410	0.038	-0.026				
0.053	0.572	0.562	0.582	0.053	-0.031				
0.078	0.298	0.280	0.315	0.078	-0.034				
0.108	0.182	0.178	0.185	0.108	-0.038				
0.143	0.127	0.123	0.131	0.143	-0.034				
0.178	0.100	0.094	0.106	0.178	-0.034				
0.218	0.080	0.079	0.081	0.218	-0.033				
0.268	0.072	0.068	0.076	0.268	-0.036				

Vm,Vmr,Vr + : landwards
Vm,Vmr,Vr - : seawards
0 < PHI < 180

CODE	Grasmeijer/Sies 29	ID	989
MODEL	TU-flume	SET	Series B1
TEST	T 18 00 05	DATE	07-04-1994
LOCATION	14.0 m, section 5	TIME	

H	waterdepth (m)	0.320	
WS	water surface slope (-)		
Hsig	sign wave height (m)	0.1769	
Hm	mean wave height (m)		
Hrms	rms wave height (m)	0.1231	
Tz	zero-cross period (s)		
Tp	peak period (s)		
Um	mean vel // shore (m/s)		
Vm	mean vel L shore (m/s)		
Vmr	mean result vel (m/s)		
Vprof	mean vel profile (m/s)	-0.0472	
Urms	rms vel at bed (m/s)		
Umax	max vel at bed (m/s)		
U15	vel exceed by 15% (m/s)		
PHI	angle flow-waves (degr)		
BT	br. type :Breaking:	6.3 %	
DMB	distance between meas. loc. and breakerline (m)	0.000	
Urms,on	rms vel. at bed in onsh. dir. (m/s)		
Urms,off	rms vel. at bed in offsh. dir. (m/s)		
Te	water temp (o C)	19.9	
BS	local bed slope normal to shore (-)	0.000000	

D10	bed mat size (um)	76
D50	bed mat size (um)	95
D90	bed mat size (um)	131
Ds -mean	susp mat size (um)	81
-min	susp mat size (um)	60
-max	susp mat size (um)	120
WSB	fall vel bed (m/s)	
WSS-mean	fall vel sus (m/s)	0.0063
-min	fall vel sus (m/s)	0.0034
-max	fall vel sus (m/s)	0.0114
Cbed1	bed concent. (kg/m3)	9.79500
Cbed2	bed concent. (kg/m3)	1590.00000
Cbed3	bed concent. (kg/m3)	27.40594
Lb	bed load (kg/m2)	
Ls1	sus load (kg/m2)	0.431902
Ls2	sus load (kg/m2)	1.899975
Ls3	sus load (kg/m2)	0.560817
Sb	bed transp (kg/sm)	
Ss1	sus transp (kg/sm)	-0.012118
Ss2	sus transp (kg/sm)	-0.032891
Ss3	sus transp (kg/sm)	-0.015865
BFH-mean	bedform height (m)	0.008
-min	bedform height (m)	0.005
-max	bedform height (m)	0.011
BFL-mean	bedform length (m)	0.051
-min	bedform length (m)	0.047
-max	bedform length (m)	0.055
BFT	bedf type:3-D ripples	

Z (m) height	C concentration (kg/m3) mean	min	max	Z (m) height	Vr result velocity (m/s) mean	min	max	Z (m) height	D50 (um)
0.018	9.795	9.290	10.300	0.018	-0.026				
0.028	5.555	5.060	6.050	0.028	-0.035				
0.038	3.095	2.840	3.350	0.038	-0.033				
0.053	1.500	1.430	1.570	0.053	-0.045				
0.078	0.795	0.793	0.797	0.078	-0.041				
0.108	0.532	0.516	0.547	0.108	-0.049				
0.143	0.366	0.344	0.387	0.143	-0.050				
0.178	0.300	0.285	0.315	0.178	-0.050				
0.218	0.231	0.215	0.246	0.218	-0.054				
0.268	0.172	0.163	0.180						

Vm,Vmr,Vr + : landwards
Vm,Vmr,Vr - : seawards
0 < PHI < 180

CODE	Grasmeijer/Sies 30	ID	990
MODEL	TU-flume	SET	Series B1
TEST	T 15 00 06	DATE	08-04-1994
LOCATION	16.5 m, section 6	TIME	

H	waterdepth (m)	0.420	
WS	water surface slope (-)		
Hsig	sign wave height (m)	0.1493	
Hm	mean wave height (m)		
Hrms	rms wave height (m)	0.1058	
Tz	zero-cross period (s)		
Tp	peak period (s)		
Um	mean vel // shore (m/s)		
Vm	mean vel L shore (m/s)		
Vmr	mean result vel (m/s)		
Vprof	mean vel profile (m/s)	-0.0343	
Urms	rms vel at bed (m/s)		
Umax	max vel at bed (m/s)		
U15	vel exceed by 15% (m/s)		
PHI	angle flow-waves (degr)		
BT	br. type :Breaking:	14.9 %	
DMB	distance between meas. loc. and breakerline (m)	2.500	
Urms,on	rms vel. at bed in onsh. dir. (m/s)		
Urms,off	rms vel. at bed in offsh. dir. (m/s)		
Te	water temp (o C)	19.8	
BS	local bed slope normal to shore (-)	-.040000	

D10	bed mat size (um)	76
D50	bed mat size (um)	95
D90	bed mat size (um)	131
Ds -mean	susp mat size (um)	87
-min	susp mat size (um)	66
-max	susp mat size (um)	122
WSB	fall vel bed (m/s)	
WSS-mean	fall vel sus (m/s)	0.0071
-min	fall vel sus (m/s)	0.0041
-max	fall vel sus (m/s)	0.0117
Cbed1	bed concent. (kg/m3)	3.23000
Cbed2	bed concent. (kg/m3)	1590.00000
Cbed3	bed concent. (kg/m3)	11.44166
Lb	bed load (kg/m2)	
Ls1	sus load (kg/m2)	0.204466
Ls2	sus load (kg/m2)	1.494655
Ls3	sus load (kg/m2)	0.292981
Sb	bed transp (kg/sm)	
Ss1	sus transp (kg/sm)	-0.004162
Ss2	sus transp (kg/sm)	-0.013244
Ss3	sus transp (kg/sm)	-0.005481
BFH-mean	bedform height (m)	0.007
-min	bedform height (m)	0.005
-max	bedform height (m)	0.009
BFL-mean	bedform length (m)	0.061
-min	bedform length (m)	0.052
-max	bedform length (m)	0.071
BFT	bedf type:2.5-D ripples	

Z (m) height	C concentration (kg/m3) mean	min	max	Z (m) height	Vr result velocity (m/s) mean	min	max	Z (m) height	D50 (um)
0.027	3.230	3.220	3.240	0.027	-0.015				
0.037	2.185	2.040	2.330	0.037	-0.025				
0.047	1.280	1.230	1.330	0.047	-0.024				
0.062	0.753	0.727	0.779	0.062	-0.035				
0.087	0.431	0.386	0.476	0.087	-0.037				
0.117	0.264	0.220	0.307	0.117	-0.041				
0.152	0.200	0.164	0.236	0.152	-0.037				
0.187	0.145	0.119	0.171	0.187	-0.037				
0.227	0.124	0.096	0.151	0.227	-0.037				
0.277	0.101	0.081	0.121	0.277	-0.036				

Vm,Vmr,Vr + : landwards
Vm,Vmr,Vr - : seawards
0 < PHI < 180

CODE	Grasmeijer/Sies	ID	991
MODEL	TU-flume	SET	Series B1
TEST	T 14 00 07	DATE	08-04-1994
LOCATION	19.0 m, section 7	TIME	

H	waterdepth	(m)	0.500	D10	bed mat size	(um)	76
WS	water surface slope	(-)		D50	bed mat size	(um)	95
Hsig	sign wave height	(m)	0.1398	D90	bed mat size	(um)	131
Hm	mean wave height	(m)		Ds -mean	susp mat size	(um)	87
Hrms	rms wave height	(m)	0.0998	-min	susp mat size	(um)	67
Tz	zero-cross period	(s)		-max	susp mat size	(um)	123
Tp	peak period	(s)		WSB	fall vel bed	(m/s)	
Um	mean vel // shore	(m/s)		WSS-mean	fall vel sus	(m/s)	0.0069
Vm	mean vel L shore	(m/s)		-min	fall vel sus	(m/s)	0.0042
Vmr	mean result vel	(m/s)		-max	fall vel sus	(m/s)	0.0117
Vprof	mean vel profile	(m/s)	-0.0270	Cbed1	bed concent.	(kg/m3)	2.15500
Urms	rms vel at bed	(m/s)		Cbed2	bed concent.	(kg/m3)	360.64840
Umax	max vel at bed	(m/s)		Cbed3	bed concent.	(kg/m3)	4.99202
U15	vel exceed by 15%	(m/s)		Lb	bed load	(kg/m2)	
PHI	angle flow-waves	(degr)		Ls1	sus load	(kg/m2)	0.096370
BT	br. type :Breaking:		2.7 %	Ls2	sus load	(kg/m2)	0.326188
DMB	distance between meas. loc. and breakerline	(m)	5.000	Ls3	sus load	(kg/m2)	0.119177
				Sb	bed transp	(kg/sm)	
Urms,on	rms vel. at bed in onsh. dir.	(m/s)		Ss1	sus transp	(kg/sm)	-0.000133
				Ss2	sus transp	(kg/sm)	0.000501
Urms,off	rms vel. at bed in offsh. dir.	(m/s)		Ss3	sus transp	(kg/sm)	0.000010
				BFH-mean	bedform height	(m)	0.010
Te	water temp	(o C)	19.9	-min	bedform height	(m)	0.005
BS	local bed slope normal to shore	(-)	0.000000	-max	bedform height	(m)	0.015
				BFL-mean	bedform length	(m)	0.046
				-min	bedform length	(m)	0.038
				-max	bedform length	(m)	0.055
				BFT	bedf type:2.5-D ripples		

Z (m) height	C concentration (kg/m3) mean	min	max	Z (m) height	Vr result velocity (m/s) mean	min	max	Z (m) height	D50 (um)
0.019	2.155	2.080	2.230	0.019	0.005				
0.029	1.420	1.340	1.500	0.029	0.005				
0.039	0.890	0.858	0.921	0.039	-0.008				
0.054	0.464	0.453	0.474	0.054	-0.008				
0.079	0.167	0.164	0.169	0.079	-0.013				
0.119	0.069	0.065	0.072	0.119	-0.025				
0.144	0.026	0.023	0.028	0.144	-0.025				
0.179	0.013	0.011	0.015	0.179	-0.030				
0.219	0.009	0.007	0.011	0.219	-0.029				
0.269	0.005	0.003	0.007	0.269	-0.035				

Vm,Vmr,Vr + : landwards
Vm,Vmr,Vr - : seawards
0 < PHI < 180

CODE	Grasmeijer/Sies 32	ID	992
MODEL	TU-flume	SET	Series B1
TEST	T 13 00 08	DATE	12-04-1994
LOCATION	22.0 m, section 8	TIME	

H	waterdepth	(m)	0.450	D10	bed mat size	(um)	76
WS	water surface slope	(-)		D50	bed mat size	(um)	95
Hsig	sign wave height	(m)	0.1339	D90	bed mat size	(um)	131
Hm	mean wave height	(m)		Ds -mean	susp mat size	(um)	82
Hrms	rms wave height	(m)	0.0980	-min	susp mat size	(um)	61
Tz	zero-cross period	(s)		-max	susp mat size	(um)	114
Tp	peak period	(s)		WSB	fall vel bed	(m/s)	
Um	mean vel // shore	(m/s)		WSS-mean	fall vel sus	(m/s)	0.0063
Vm	mean vel L shore	(m/s)		-min	fall vel sus	(m/s)	0.0036
Vmr	mean result vel	(m/s)		-max	fall vel sus	(m/s)	0.0104
Vprof	mean vel profile	(m/s)	-0.0315	Cbed1	bed concent.	(kg/m3)	3.04000
Urms	rms vel at bed	(m/s)		Cbed2	bed concent.	(kg/m3)	1590.00000
Umax	max vel at bed	(m/s)		Cbed3	bed concent.	(kg/m3)	8.95972
U15	vel exceed by 15%	(m/s)		Lb	bed load	(kg/m2)	
PHI	angle flow-waves	(degr)		Ls1	sus load	(kg/m2)	0.123412
BT	br. type :Non breaking			Ls2	sus load	(kg/m2)	0.985632
DMB	distance between meas. loc. and breakerline	(m)	8.000	Ls3	sus load	(kg/m2)	0.171418
				Sb	bed transp	(kg/sm)	
Urms,on	rms vel. at bed in onsh. dir.	(m/s)		Ss1	sus transp	(kg/sm)	-0.000215
				Ss2	sus transp	(kg/sm)	0.002664
Urms,off	rms vel. at bed in offsh. dir.	(m/s)		Ss3	sus transp	(kg/sm)	0.000150
				BFH-mean	bedform height	(m)	0.005
Te	water temp	(o C)	19.2	-min	bedform height	(m)	0.001
BS	local bed slope normal to shore	(-)	0.015900	-max	bedform height	(m)	0.008
				BFL-mean	bedform length	(m)	0.047
				-min	bedform length	(m)	0.036
				-max	bedform length	(m)	0.058
				BFT	bedf type:2.5-D ripples		

Z (m) height	C concentration (kg/m3) mean	min	max	Z (m) height	Vr result velocity (m/s) mean	min	max	Z (m) height	D50 (um)
0.020	3.040	3.000	3.080	0.020	0.007				
0.030	1.805	1.730	1.880	0.030	-0.007				
0.040	1.028	0.955	1.100	0.040	-0.012				
0.055	0.494	0.469	0.518	0.055	-0.012				
0.080	0.162	0.159	0.164	0.080	-0.018				
0.110	0.045	0.043	0.046	0.110	-0.021				
0.145	0.009	0.009	0.009	0.145	-0.029				
0.180	0.004	0.004	0.004	0.180	-0.034				
0.220	0.003	0.003	0.003	0.220	-0.035				
0.270	0.001	0.001	0.001	0.270	-0.043				

Vm,Vmr,Vr + : landwards
Vm,Vmr,Vr - : seawards
0 < PHI < 180

CODE	Grasmeijer/Sies 33	ID	993
MODEL	TU-flume	SET	Series B1
TEST	T 14 00 09	DATE	12-04-1994
LOCATION	25.0 m, section 9	TIME	

H	waterdepth (m)	0.410	
WS	water surface slope (-)		
Hsig	sign wave height (m)	0.1367	
Hm	mean wave height (m)		
Hrms	rms wave height (m)	0.1000	
Tz	zero-cross period (s)		
Tp	peak period (s)		
Um	mean vel // shore (m/s)		
Vm	mean vel L shore (m/s)		
Vmr	mean result vel (m/s)		
Vprof	mean vel profile (m/s)	-0.0344	
Urms	rms vel at bed (m/s)		
Umax	max vel at bed (m/s)		
U15	vel exceed by 15% (m/s)		
PHI	angle flow-waves (degr)		
BT	br. type :Non breaking		
DMB	distance between meas. loc. and breakerline (m)	11.000	
Urms,on	rms vel. at bed in onsh. dir. (m/s)		
Urms,off	rms vel. at bed in offsh. dir. (m/s)		
Te	water temp (o C)	19.3	
BS	local bed slope normal to shore (-)	0.015900	

D10	bed mat size (um)	76
D50	bed mat size (um)	95
D90	bed mat size (um)	131
Ds -mean	susp mat size (um)	90
-min	susp mat size (um)	68
-max	susp mat size (um)	128
WSB	fall vel bed (m/s)	
WSS-mean	fall vel sus (m/s)	0.0077
-min	fall vel sus (m/s)	0.0045
-max	fall vel sus (m/s)	0.0129
Cbed1	bed concent. (kg/m3)	4.30000
Cbed2	bed concent. (kg/m3)	1590.00000
Cbed3	bed concent. (kg/m3)	13.78169
Lb	bed load (kg/m2)	
Ls1	sus load (kg/m2)	0.154362
Ls2	sus load (kg/m2)	1.315201
Ls3	sus load (kg/m2)	0.221838
Sb	bed transp (kg/sm)	
Ss1	sus transp (kg/sm)	-0.001830
Ss2	sus transp (kg/sm)	-0.008800
Ss3	sus transp (kg/sm)	-0.002678
BFH-mean	bedform height (m)	0.011
-min	bedform height (m)	0.009
-max	bedform height (m)	0.016
BFL-mean	bedform length (m)	0.053
-min	bedform length (m)	0.040
-max	bedform length (m)	0.066
BFT	bedf type:2.5-D ripples	

Z (m) height	C concentration (kg/m3) mean	min	max
0.018	4.300	3.980	4.620
0.028	2.220	2.180	2.260
0.038	1.160	1.130	1.190
0.053	0.520	0.515	0.524
0.078	0.179	0.176	0.181
0.108	0.054	0.050	0.058
0.143	0.020	0.019	0.020
0.178	0.010	0.010	0.010
0.218	0.005	0.004	0.006
0.268	0.004	0.003	0.004

Z (m) height	Vr result velocity (m/s) mean	min	max
0.018	-0.012		
0.028	-0.018		
0.038	-0.017		
0.053	-0.021		
0.078	-0.028		
0.108	-0.026		
0.143	-0.030		
0.178	-0.034		
0.218	-0.039		
0.268	-0.044		

Z (m) height	D50 (um)

Vm,Vmr,Vr + : landwards
Vm,Vmr,Vr - : seawards
0 < PHI < 180

CODE	Grasmeijer/Sies 34	ID	994
MODEL	TU-flume	SET	series B1
TEST	T 13 00 10	DATE	13-04-1994
LOCATION	28.0 m, section 10	TIME	

H	waterdepth	(m)	0.360	D10	bed mat size	(um)	76
WS	water surface slope	(-)		D50	bed mat size	(um)	95
Hsig	sign wave height	(m)	0.1322	D90	bed mat size	(um)	131
Hm	mean wave height	(m)		Ds -mean	susp mat size	(um)	96
Hrms	rms wave height	(m)	0.0963	-min	susp mat size	(um)	77
Tz	zero-cross period	(s)		-max	susp mat size	(um)	134
Tp	peak period	(s)		WSB	fall vel bed	(m/s)	
Um	mean vel // shore	(m/s)		WSS-mean	fall vel sus	(m/s)	0.0088
Vm	mean vel L shore	(m/s)		-min	fall vel sus	(m/s)	0.0056
Vmr	mean result vel	(m/s)		-max	fall vel sus	(m/s)	0.0140
Vprof	mean vel profile	(m/s)	-0.0364	Cbed1	bed concent.	(kg/m3)	5.69000
Urms	rms vel at bed	(m/s)		Cbed2	bed concent.	(kg/m3)	1590.00000
Umax	max vel at bed	(m/s)		Cbed3	bed concent.	(kg/m3)	24.07619
U15	vel exceed by 15%	(m/s)		Lb	bed load	(kg/m2)	
PHI	angle flow-waves	(degr)		Ls1	sus load	(kg/m2)	0.228390
BT	br. type :Non breaking			Ls2	sus load	(kg/m2)	3.450923
DMB	distance between meas. loc. and breakerline	(m)	14.000	Ls3	sus load	(kg/m2)	0.387001
				Sb	bed transp	(kg/sm)	
Urms,on	rms vel. at bed in onsh. dir.	(m/s)		Ss1	sus transp	(kg/sm)	-0.002495
				Ss2	sus transp	(kg/sm)	-0.022328
Urms,off	rms vel. at bed in offsh. dir.	(m/s)		Ss3	sus transp	(kg/sm)	-0.004283
				BFH-mean	bedform height	(m)	0.013
Te	water temp	(o C)	20.0	-min	bedform height	(m)	0.011
BS	local bed slope normal to shore	(-)	0.015900	-max	bedform height	(m)	0.016
				BFL-mean	bedform length	(m)	0.073
				-min	bedform length	(m)	0.067
				-max	bedform length	(m)	0.079
				BFT	bedf type:2.5-D ripples		

Z (m) height	C concentration (kg/m3) mean	min	max	Z (m) height	Vr result velocity (m/s) mean	min	max	Z (m) height	D50 (um)
0.023	5.690	5.260	6.120	0.023	-0.012				
0.033	2.905	2.890	2.920	0.033	-0.015				
0.043	1.590	1.510	1.670	0.043	-0.022				
0.058	0.677	0.634	0.720	0.058	-0.024				
0.083	0.183	0.169	0.197	0.083	-0.024				
0.113	0.036	0.032	0.040	0.113	-0.030				
0.148	0.007	0.007	0.007	0.148	-0.036				
0.183	0.003	0.003	0.003	0.183	-0.037				
0.223	0.001	0.001	0.001	0.223	-0.043				
0.273	0.000	0.000	0.000	0.273	-0.051				

Vm,Vmr,Vr + : landwards
Vm,Vmr,Vr - : seawards
0 < PHI < 180

CODE	Grasmeijer/Sies 35	ID	995
MODEL	TU-flume	SET	Series B2
TEST	T 19 00 01	DATE	26-04-1994
LOCATION	5.0 m, section 1	TIME	

H	waterdepth (m)	0.600	
WS	water surface slope (-)		
Hsig	sign wave height (m)	0.1890	
Hm	mean wave height (m)		
Hrms	rms wave height (m)	0.1334	
Tz	zero-cross period (s)		
Tp	peak period (s)		
Um	mean vel // shore (m/s)		
Vm	mean vel L shore (m/s)		
Vmr	mean result vel (m/s)		
Vprof	mean vel profile (m/s)	-0.0363	
Urms	rms vel at bed (m/s)		
Umax	max vel at bed (m/s)		
U15	vel exceed by 15% (m/s)		
PHI	angle flow-waves (degr)		
BT	br. type :Breaking:	0.4 %	
DMB	distance between meas. loc. and breakerline (m)	9.000	
Urms,on	rms vel. at bed in onsh. dir. (m/s)		
Urms,off	rms vel. at bed in offsh. dir. (m/s)		
Te	water temp (o C)	19.5	
BS	local bed slope normal to shore (-)	0.000000	

D10	bed mat size (um)	76	
D50	bed mat size (um)	95	
D90	bed mat size (um)	131	
Ds -mean	susp mat size (um)	93	
-min	susp mat size (um)	72	
-max	susp mat size (um)	130	
WSB	fall vel bed (m/s)		
WSS-mean	fall vel sus (m/s)	0.0076	
-min	fall vel sus (m/s)	0.0045	
-max	fall vel sus (m/s)	0.0123	
Cbed1	bed concent. (kg/m3)	4.65500	
Cbed2	bed concent. (kg/m3)	1590.00000	
Cbed3	bed concent. (kg/m3)	15.61474	
Lb	bed load (kg/m2)		
Ls1	sus load (kg/m2)	0.150797	
Ls2	sus load (kg/m2)	1.200458	
Ls3	sus load (kg/m2)	0.221214	
Sb	bed transp (kg/sm)		
Ss1	sus transp (kg/sm)	-0.001694	
Ss2	sus transp (kg/sm)	-0.009176	
Ss3	sus transp (kg/sm)	-0.002705	
BFH-mean	bedform height (m)	0.011	
-min	bedform height (m)	0.009	
-max	bedform height (m)	0.013	
BFL-mean	bedform length (m)	0.083	
-min	bedform length (m)	0.083	
-max	bedform length (m)	0.083	
BFT	bedf type:	2.5-D ripples	

Z (m) height	C concentration (kg/m3) mean	min	max
0.016	4.655	4.400	4.910
0.026	2.415	2.310	2.520
0.036	1.046	1.018	1.073
0.051	0.416	0.393	0.439
0.076	0.125	0.118	0.132
0.106	0.040	0.033	0.046
0.141	0.016	0.011	0.020
0.176	0.012	0.008	0.015
0.216	0.009	0.005	0.012
0.266	0.007	0.005	0.009

Z (m) height	Vr result velocity (m/s) mean	min	max
0.016	-0.014		
0.026	-0.013		
0.036	-0.016		
0.051	-0.015		
0.076	-0.020		
0.106	-0.022		
0.141	-0.028		
0.176	-0.035		
0.216	-0.034		
0.266	-0.038		
0.396	-0.046		

Z (m) height	D50 (um)

Vm,Vmr,Vr + : landwards
Vm,Vmr,Vr - : seawards
0 < PHI < 180

CODE	Grasmeijer/Sies 36	ID	996
MODEL	TU-flume	SET	Series B2
TEST	T 19 00 02	DATE	25-04-1994
LOCATION	8.0 m, section 2	TIME	

H	waterdepth	(m)	0.590	D10	bed mat size	(um)	76
WS	water surface slope	(-)		D50	bed mat size	(um)	95
Hsig	sign wave height	(m)	0.1875	D90	bed mat size	(um)	131
Hm	mean wave height	(m)		Ds -mean	susp mat size	(um)	89
Hrms	rms wave height	(m)	0.1331	-min	susp mat size	(um)	70
Tz	zero-cross period	(s)		-max	susp mat size	(um)	123
Tp	peak period	(s)		WSB	fall vel bed	(m/s)	
Um	mean vel // shore	(m/s)		WSS-mean	fall vel sus	(m/s)	0.0070
Vm	mean vel L shore	(m/s)		-min	fall vel sus	(m/s)	0.0043
Vmr	mean result vel	(m/s)		-max	fall vel sus	(m/s)	0.0110
Vprof	mean vel profile	(m/s)	-0.0349	Cbed1	bed concent.	(kg/m3)	4.35500
Urms	rms vel at bed	(m/s)		Cbed2	bed concent.	(kg/m3)	1590.00000
Umax	max vel at bed	(m/s)		Cbed3	bed concent.	(kg/m3)	24.81644
U15	vel exceed by 15%	(m/s)		Lb	bed load	(kg/m2)	
PHI	angle flow-waves	(degr)		Ls1	sus load	(kg/m2)	0.166504
BT	br. type :Breaking:		0.6 %	Ls2	sus load	(kg/m2)	3.837272
DMB	distance between meas. loc. and breakerline	(m)	6.000	Ls3	sus load	(kg/m2)	0.329313
				Sb	bed transp	(kg/sm)	
Urms,on	rms vel. at bed in onsh. dir.	(m/s)		Ss1	sus transp	(kg/sm)	-0.001370
				Ss2	sus transp	(kg/sm)	-0.016569
Urms,off	rms vel. at bed in offsh. dir.	(m/s)		Ss3	sus transp	(kg/sm)	-0.002496
				BFH-mean	bedform height	(m)	0.006
Te	water temp	(o C)	19.2	-min	bedform height	(m)	0.003
BS	local bed slope normal to shore	(-)	0.000000	-max	bedform height	(m)	0.009
				BFL-mean	bedform length	(m)	0.044
				-min	bedform length	(m)	0.040
				-max	bedform length	(m)	0.048
				BFT	bedf type:		2.5-D ripples

Z (m) height	C concentration (kg/m3) mean	min	max	Z (m) height	Vr result velocity (m/s) mean	min	max	Z (m) height	D50 (um)
0.022	4.355	4.340	4.370	0.022	-0.008				
0.032	2.125	2.030	2.220	0.032	-0.010				
0.042	0.902	0.798	1.006	0.042	-0.018				
0.057	0.349	0.320	0.377	0.057	-0.018				
0.082	0.120	0.108	0.131	0.082	-0.021				
0.112	0.061	0.051	0.070	0.112	-0.027				
0.147	0.024	0.023	0.024	0.147	-0.030				
0.182	0.017	0.016	0.017	0.182	-0.034				
0.222	0.014	0.013	0.014	0.222	-0.036				
0.272	0.011	0.009	0.012	0.272	-0.033				
				0.402	-0.045				

Vm,Vmr,Vr + : landwards
Vm,Vmr,Vr - : seawards
0 < PHI < 180

CODE	Grasmeijer/Sies 37	ID	997
MODEL	TU-flume	SET	Series B2
TEST	T 19 00 03	DATE	25-04-1994
LOCATION	10.0 m, section 3	TIME	

H	waterdepth	(m)	0.510	D10	bed mat size	(um)	76
WS	water surface slope	(-)		D50	bed mat size	(um)	95
Hsig	sign wave height	(m)	0.1875	D90	bed mat size	(um)	131
Hm	mean wave height	(m)		Ds -mean	susp mat size	(um)	83
Hrms	rms wave height	(m)	0.1335	-min	susp mat size	(um)	65
Tz	zero-cross period	(s)		-max	susp mat size	(um)	121
Tp	peak period	(s)		WSB	fall vel bed	(m/s)	
Um	mean vel // shore	(m/s)		WSS-mean	fall vel sus	(m/s)	0.0060
Vm	mean vel L shore	(m/s)		-min	fall vel sus	(m/s)	0.0037
Vmr	mean result vel	(m/s)		-max	fall vel sus	(m/s)	0.0108
Vprof	mean vel profile	(m/s)	-0.0373	Cbed1	bed concent.	(kg/m3)	4.72000
Urms	rms vel at bed	(m/s)		Cbed2	bed concent.	(kg/m3)	1590.00000
Umax	max vel at bed	(m/s)		Cbed3	bed concent.	(kg/m3)	27.74803
U15	vel exceed by 15%	(m/s)		Lb	bed load	(kg/m2)	
PHI	angle flow-waves	(degr)		Ls1	sus load	(kg/m2)	0.193882
BT	br. type :Breaking:		0.6 %	Ls2	sus load	(kg/m2)	4.626162
DMB	distance between meas. loc. and breakerline	(m)	4.000	Ls3	sus load	(kg/m2)	0.381446
Urms,on	rms vel. at bed in onsh. dir.	(m/s)		Sb	bed transp	(kg/sm)	
Urms,off	rms vel. at bed in offsh. dir.	(m/s)		Ss1	sus transp	(kg/sm)	-0.002224
				Ss2	sus transp	(kg/sm)	-0.020925
				Ss3	sus transp	(kg/sm)	-0.003512
Te	water temp	(o C)	19.2	BFH-mean	bedform height	(m)	0.007
BS	local bed slope normal to shore	(-)	0.050000	-min	bedform height	(m)	0.004
				-max	bedform height	(m)	0.009
				BFL-mean	bedform length	(m)	0.045
				-min	bedform length	(m)	0.040
				-max	bedform length	(m)	0.050
				BFT	bedf type:		2.5-D ripples

Z (m) height	C concentration (kg/m3) mean	min	max	Z (m) height	Vr result velocity (m/s) mean	min	max	Z (m) height	D50 (um)
0.023	4.720	4.630	4.810	0.023	-0.008				
0.033	2.140	2.040	2.240	0.033	-0.021				
0.043	0.995	0.890	1.100	0.043	-0.013				
0.058	0.392	0.370	0.413	0.058	-0.031				
0.083	0.193	0.184	0.202	0.083	-0.033				
0.113	0.105	0.104	0.106	0.113	-0.036				
0.148	0.069	0.068	0.069	0.148	-0.034				
0.183	0.048	0.046	0.050	0.183	-0.039				
0.223	0.040	0.036	0.043	0.223	-0.035				
0.273	0.037	0.037	0.037	0.273	-0.044				

Vm,Vmr,Vr + : landwards
Vm,Vmr,Vr - : seawards
0 < PHI < 180

CODE	Grasmeijer/Sies 38	ID	998
MODEL	TU-flume	SET	Series B2
TEST	T 20 00 04	DATE	22-04-1994
LOCATION	12.0 m, section 4	TIME	

H	waterdepth	(m)	0.390	D10	bed mat size	(um)	76
WS	water surface slope	(-)		D50	bed mat size	(um)	95
Hsig	sign wave height	(m)	0.2011	D90	bed mat size	(um)	131
Hm	mean wave height	(m)		Ds -mean	susp mat size	(um)	69
Hrms	rms wave height	(m)	0.1416	-min	susp mat size	(um)	50
Tz	zero-cross period	(s)		-max	susp mat size	(um)	97
Tp	peak period	(s)		WSB	fall vel bed	(m/s)	
Um	mean vel // shore	(m/s)		WSS-mean	fall vel sus	(m/s)	0.0042
Vm	mean vel L shore	(m/s)		-min	fall vel sus	(m/s)	0.0022
Vmr	mean result vel	(m/s)		-max	fall vel sus	(m/s)	0.0081
Vprof	mean vel profile	(m/s)	-0.0491	Cbed1	bed concent.	(kg/m3)	8.72000
Urms	rms vel at bed	(m/s)		Cbed2	bed concent.	(kg/m3)	1590.00000
Umax	max vel at bed	(m/s)		Cbed3	bed concent.	(kg/m3)	35.83846
U15	vel exceed by 15%	(m/s)		Lb	bed load	(kg/m2)	
PHI	angle flow-waves	(degr)		Ls1	sus load	(kg/m2)	0.296350
BT	br. type :Breaking:		1.6 %	Ls2	sus load	(kg/m2)	3.280787
DMB	distance between meas. loc. and breakerline	(m)	2.000	Ls3	sus load	(kg/m2)	0.459637
				Sb	bed transp	(kg/sm)	
Urms,on	rms vel. at bed in onsh. dir.	(m/s)		Ss1	sus transp	(kg/sm)	-0.009243
				Ss2	sus transp	(kg/sm)	-0.074694
Urms,off	rms vel. at bed in offsh. dir.	(m/s)		Ss3	sus transp	(kg/sm)	-0.015475
				BFH-mean	bedform height	(m)	0.005
Te	water temp	(o C)	20.0	-min	bedform height	(m)	0.001
BS	local bed slope normal to shore	(-)	0.050000	-max	bedform height	(m)	0.009
				BFL-mean	bedform length	(m)	0.038
				-min	bedform length	(m)	0.036
				-max	bedform length	(m)	0.040
				BFT	bedf type:		2.5-D ripples

Z (m) height	C concentration (kg/m3) mean	min	max	Z (m) height	Vr result velocity (m/s) mean	min	max	Z (m) height	D50 (um)
0.016	8.720	7.840	9.600	0.016	-0.040				
0.026	3.505	3.150	3.860	0.026	-0.034				
0.036	1.450	1.360	1.540	0.036	-0.035				
0.051	0.684	0.668	0.699	0.051	-0.043				
0.076	0.373	0.367	0.379	0.076	-0.051				
0.106	0.240	0.238	0.241	0.106	-0.047				
0.141	0.175	0.158	0.192	0.141	-0.043				
0.176	0.177	0.170	0.184	0.176	-0.050				
0.216	0.133	0.119	0.146	0.216	-0.044				
0.266	0.110	0.092	0.128	0.266	-0.057				

Vm,Vmr,Vr + : landwards
Vm,Vmr,Vr - : seawards
0 < PHI < 180

CODE	Grasmeijer/Sies 39	ID	999
MODEL	TU-flume	SET	Series B2
TEST	T 20 00 05	DATE	21-04-1994
LOCATION	14.0 m, section 5	TIME	

H	waterdepth (m)	0.310	
WS	water surface slope (-)		
Hsig	sign wave height (m)	0.2010	
Hm	mean wave height (m)		
Hrms	rms wave height (m)	0.1421	
Tz	zero-cross period (s)		
Tp	peak period (s)		
Um	mean vel // shore (m/s)		
Vm	mean vel L shore (m/s)		
Vmr	mean result vel (m/s)		
Vprof	mean vel profile (m/s)	-0.0539	
Urms	rms vel at bed (m/s)		
Umax	max vel at bed (m/s)		
U15	vel exceed by 15% (m/s)		
PHI	angle flow-waves (degr)		
BT	br. type :Breaking:	10.0 %	
DMB	distance between meas. loc. and breakerline (m)	0.000	
Urms,on	rms vel. at bed in onsh. dir. (m/s)		
Urms,off	rms vel. at bed in offsh. dir. (m/s)		
Te	water temp (o C)	20.5	
BS	local bed slope normal to shore (-)	0.000000	

D10	bed mat size (um)	76
D50	bed mat size (um)	95
D90	bed mat size (um)	131
Ds -mean	susp mat size (um)	85
-min	susp mat size (um)	62
-max	susp mat size (um)	123
WSB	fall vel bed (m/s)	
WSS-mean	fall vel sus (m/s)	0.0063
-min	fall vel sus (m/s)	0.0034
-max	fall vel sus (m/s)	0.0111
Cbed1	bed concent. (kg/m3)	8.93500
Cbed2	bed concent. (kg/m3)	1590.00000
Cbed3	bed concent. (kg/m3)	21.08138
Lb	bed load (kg/m2)	
Ls1	sus load (kg/m2)	0.509323
Ls2	sus load (kg/m2)	1.540388
Ls3	sus load (kg/m2)	0.592705
Sb	bed transp (kg/sm)	
Ss1	sus transp (kg/sm)	-0.021834
Ss2	sus transp (kg/sm)	-0.047818
Ss3	sus transp (kg/sm)	-0.026648
BFH-mean	bedform height (m)	0.006
-min	bedform height (m)	0.003
-max	bedform height (m)	0.011
BFL-mean	bedform length (m)	0.069
-min	bedform length (m)	0.057
-max	bedform length (m)	0.081
BFT	bedf type:	3-D ripples

Z (m) height	C concentration (kg/m3) mean	min	max
0.017	8.935	8.600	9.270
0.027	4.885	4.680	5.090
0.037	3.120	2.950	3.290
0.052	1.990	1.830	2.150
0.077	1.435	1.290	1.580
0.107	1.118	1.016	1.220
0.142	0.844	0.780	0.907
0.177	0.735	0.687	0.783
0.217	0.631	0.598	0.663
0.267	0.512	0.477	0.547

Z (m) height	Vr result velocity (m/s) mean	min	max
0.017	-0.046		
0.027	-0.042		
0.037	-0.043		
0.052	-0.055		
0.077	-0.048		
0.107	-0.065		
0.142	-0.050		
0.177	-0.064		
0.217	-0.055		

Z (m) height	D50 (um)

Vm,Vmr,Vr + : landwards
Vm,Vmr,Vr - : seawards
0 < PHI < 180

CODE	Grasmeijer/Sies 40	ID	1000
MODEL	TU-flume	SET	Series B2
TEST	T 19 00 5a	DATE	20-04-1994
LOCATION	15.0 m, section 5a	TIME	

H	waterdepth (m)	0.330	
WS	water surface slope (-)		
Hsig	sign wave height (m)	0.1866	
Hm	mean wave height (m)		
Hrms	rms wave height (m)	0.1336	
Tz	zero-cross period (s)		
Tp	peak period (s)		
Um	mean vel // shore (m/s)		
Vm	mean vel L shore (m/s)		
Vmr	mean result vel (m/s)		
Vprof	mean vel profile (m/s)	-0.0591	
Urms	rms vel at bed (m/s)		
Umax	max vel at bed (m/s)		
U15	vel exceed by 15% (m/s)		
PHI	angle flow-waves (degr)		
BT	br. type :Breaking:	18.6 %	
DMB	distance between meas. loc. and breakerline (m)	1.000	
Urms,on	rms vel. at bed in onsh. dir. (m/s)		
Urms,off	rms vel. at bed in offsh. dir. (m/s)		
Te	water temp (o C)	20.6	
BS	local bed slope normal to shore (-)	-.040000	

D10	bed mat size (um)	76
D50	bed mat size (um)	95
D90	bed mat size (um)	131
Ds -mean	susp mat size (um)	89
-min	susp mat size (um)	66
-max	susp mat size (um)	134
WSB	fall vel bed (m/s)	
WSS-mean	fall vel sus (m/s)	0.0069
-min	fall vel sus (m/s)	0.0038
-max	fall vel sus (m/s)	0.0130
Cbed1	bed concent. (kg/m3)	7.25000
Cbed2	bed concent. (kg/m3)	1590.00000
Cbed3	bed concent. (kg/m3)	19.08018
Lb	bed load (kg/m2)	
Ls1	sus load (kg/m2)	0.561864
Ls2	sus load (kg/m2)	1.778773
Ls3	sus load (kg/m2)	0.688660
Sb	bed transp (kg/sm)	
Ss1	sus transp (kg/sm)	-0.023745
Ss2	sus transp (kg/sm)	-0.040156
Ss3	sus transp (kg/sm)	-0.027534
BFH-mean	bedform height (m)	0.011
-min	bedform height (m)	0.009
-max	bedform height (m)	0.014
BFL-mean	bedform length (m)	0.054
-min	bedform length (m)	0.053
-max	bedform length (m)	0.055
BFT	bedf type:	3-D ripples

Z (m) height	C concentration (kg/m3) mean	min	max	Z (m) height	Vr result velocity (m/s) mean	min	max	Z (m) height	D50 (um)
0.026	7.250	6.840	7.660	0.026	-0.026				
0.036	4.950	4.580	5.320	0.036	-0.052				
0.046	3.420	3.160	3.680	0.046	-0.048				
0.061	2.250	2.120	2.380	0.061	-0.062				
0.086	1.595	1.510	1.680	0.086	-0.067				
0.116	1.200	1.120	1.280	0.116	-0.069				
0.151	0.912	0.856	0.968	0.151	-0.050				
0.186	0.779	0.737	0.821	0.186	-0.075				
0.226	0.673	0.595	0.751	0.226	-0.063				
0.276	0.492	0.430	0.554						

Vm,Vmr,Vr + : landwards
Vm,Vmr,Vr - : seawards
0 < PHI < 180

CODE	Grasmeijer/Sies 41	ID	1001
MODEL	TU-flume	SET	Series B2
TEST	T 16 00 06	DATE	19-04-1994
LOCATION	16.5 m, section 6	TIME	

H	waterdepth (m)	0.400	
WS	water surface slope (-)		
Hsig	sign wave height (m)	0.1631	
Hm	mean wave height (m)		
Hrms	rms wave height (m)	0.1184	
Tz	zero-cross period (s)		
Tp	peak period (s)		
Um	mean vel // shore (m/s)		
Vm	mean vel L shore (m/s)		
Vmr	mean result vel (m/s)		
Vprof	mean vel profile (m/s)	-0.0478	
Urms	rms vel at bed (m/s)		
Umax	max vel at bed (m/s)		
U15	vel exceed by 15% (m/s)		
PHI	angle flow-waves (degr)		
BT	br. type :Breaking:	27.6 %	
DMB	distance between meas. loc. and breakerline (m)	2.500	
Urms,on	rms vel. at bed in onsh. dir. (m/s)		
Urms,off	rms vel. at bed in offsh. dir. (m/s)		
Te	water temp (o C)	19.9	
BS	local bed slope normal to shore (-)	-.040000	

D10	bed mat size (um)	76
D50	bed mat size (um)	95
D90	bed mat size (um)	131
Ds -mean	susp mat size (um)	85
-min	susp mat size (um)	65
-max	susp mat size (um)	122
WSB	fall vel bed (m/s)	
WSS-mean	fall vel sus (m/s)	0.0064
-min	fall vel sus (m/s)	0.0037
-max	fall vel sus (m/s)	0.0111
Cbed1	bed concent. (kg/m3)	6.60500
Cbed2	bed concent. (kg/m3)	1590.00000
Cbed3	bed concent. (kg/m3)	21.65455
Lb	bed load (kg/m2)	
Ls1	sus load (kg/m2)	0.400044
Ls2	sus load (kg/m2)	2.793687
Ls3	sus load (kg/m2)	0.542954
Sb	bed transp (kg/sm)	
Ss1	sus transp (kg/sm)	-0.013315
Ss2	sus transp (kg/sm)	-0.052030
Ss3	sus transp (kg/sm)	-0.018031
BFH-mean	bedform height (m)	0.007
-min	bedform height (m)	0.005
-max	bedform height (m)	0.009
BFL-mean	bedform length (m)	0.055
-min	bedform length (m)	0.051
-max	bedform length (m)	0.058
BFT	bedf type:	2.5-D ripples

Z (m) height	C concentration (kg/m3) mean	min	max	Z (m) height	Vr result velocity (m/s) mean	min	max	Z (m) height	D50 (um)
0.024	6.605	6.510	6.700	0.024	-0.032				
0.034	3.970	3.930	4.010	0.034	-0.036				
0.044	2.430	2.410	2.450	0.044	-0.044				
0.059	1.375	1.370	1.380	0.059	-0.051				
0.084	0.829	0.825	0.833	0.084	-0.045				
0.114	0.587	0.580	0.593	0.114	-0.055				
0.149	0.457	0.443	0.471	0.149	-0.042				
0.184	0.388	0.381	0.394	0.184	-0.070				
0.224	0.312	0.299	0.325	0.224	-0.042				
0.274	0.278	0.251	0.305	0.274	-0.049				

Vm,Vmr,Vr + : landwards
Vm,Vmr,Vr - : seawards
0 < PHI < 180

CODE	Grasmeijer/Sies 42	ID	1002
MODEL	TU-flume	SET	Series B2
TEST	T 15 00 07	DATE	18-04-1994
LOCATION	19.0 m, section 7	TIME	

H	waterdepth (m)	0.510	
WS	water surface slope (-)		
Hsig	sign wave height (m)	0.1539	
Hm	mean wave height (m)		
Hrms	rms wave height (m)	0.1116	
Tz	zero-cross period (s)		
Tp	peak period (s)		
Um	mean vel // shore (m/s)		
Vm	mean vel L shore (m/s)		
Vmr	mean result vel (m/s)		
Vprof	mean vel profile (m/s)	-0.0303	
Urms	rms vel at bed (m/s)		
Umax	max vel at bed (m/s)		
U15	vel exceed by 15% (m/s)		
PHI	angle flow-waves (degr)		
BT	br. type :Breaking:	8.2 %	
DMB	distance between meas. loc. and breakerline (m)	5.000	
Urms,on	rms vel. at bed in onsh. dir. (m/s)		
Urms,off	rms vel. at bed in offsh. dir. (m/s)		
Te	water temp (o C)	18.8	
BS	local bed slope normal to shore (-)	0.000000	

D10	bed mat size (um)	76
D50	bed mat size (um)	95
D90	bed mat size (um)	131
Ds -mean	susp mat size (um)	85
-min	susp mat size (um)	63
-max	susp mat size (um)	122
WSB	fall vel bed (m/s)	
WSS-mean	fall vel sus (m/s)	0.0063
-min	fall vel sus (m/s)	0.0036
-max	fall vel sus (m/s)	0.0111
Cbed1	bed concent.(kg/m3)	3.53500
Cbed2	bed concent.(kg/m3)	1119.78300
Cbed3	bed concent.(kg/m3)	8.95344
Lb	bed load (kg/m2)	
Ls1	sus load (kg/m2)	0.174798
Ls2	sus load (kg/m2)	0.829275
Ls3	sus load (kg/m2)	0.223903
Sb	bed transp (kg/sm)	
Ss1	sus transp (kg/sm)	-0.001072
Ss2	sus transp (kg/sm)	0.000560
Ss3	sus transp (kg/sm)	-0.000782
BFH-mean	bedform height (m)	0.010
-min	bedform height (m)	0.009
-max	bedform height (m)	0.011
BFL-mean	bedform length (m)	0.054
-min	bedform length (m)	0.051
-max	bedform length (m)	0.057
BFT	bedf type:	2.5-D ripples

Z (m) height	C concentration (kg/m3) mean	min	max	Z (m) height	Vr result velocity (m/s) mean	min	max	Z (m) height	D50 (um)
0.022	3.535	3.390	3.680	0.022	0.005				
0.032	2.265	2.190	2.340	0.032	-0.012				
0.042	1.500	1.470	1.530	0.042	-0.012				
0.057	0.815	0.801	0.828	0.057	-0.016				
0.082	0.309	0.305	0.312	0.082	-0.022				
0.112	0.135	0.135	0.135	0.112	-0.027				
0.147	0.067	0.057	0.076	0.147	-0.029				
0.182	0.046	0.040	0.052	0.182	-0.031				
0.222	0.034	0.030	0.037	0.222	-0.035				
0.272	0.022	0.019	0.025	0.272	-0.037				

Vm,Vmr,Vr + : landwards
Vm,Vmr,Vr - : seawards
0 < PHI < 180

CODE	Grasmeijer/Sies 43	ID	1003
MODEL	TU-flume	SET	Series B2
TEST	T 15 00 08	DATE	15-04-1994
LOCATION	22.0 m, section 8	TIME	

H	waterdepth (m)	0.460	
WS	water surface slope (-)		
Hsig	sign wave height (m)	0.1478	
Hm	mean wave height (m)		
Hrms	rms wave height (m)	0.1091	
Tz	zero-cross period (s)		
Tp	peak period (s)		
Um	mean vel // shore (m/s)		
Vm	mean vel L shore (m/s)		
Vmr	mean result vel (m/s)		
Vprof	mean vel profile (m/s)	-0.0311	
Urms	rms vel at bed (m/s)		
Umax	max vel at bed (m/s)		
U15	vel exceed by 15% (m/s)		
PHI	angle flow-waves (degr)		
BT	br. type : Non breaking		
DMB	distance between meas. loc. and breakerline (m)	8.000	
Urms,on	rms vel. at bed in onsh. dir. (m/s)		
Urms,off	rms vel. at bed in offsh. dir. (m/s)		
Te	water temp (o C)	20.3	
BS	local bed slope normal to shore (-)	0.015900	

D10	bed mat size (um)	76	
D50	bed mat size (um)	95	
D90	bed mat size (um)	131	
Ds -mean	susp mat size (um)	84	
-min	susp mat size (um)	63	
-max	susp mat size (um)	118	
WSB	fall vel bed (m/s)		
WSS-mean	fall vel sus (m/s)	0.0063	
-min	fall vel sus (m/s)	0.0036	
-max	fall vel sus (m/s)	0.0105	
Cbed1	bed concent. (kg/m3)	3.98500	
Cbed2	bed concent. (kg/m3)	1590.00000	
Cbed3	bed concent. (kg/m3)	16.77958	
Lb	bed load (kg/m2)		
Ls1	sus load (kg/m2)	0.184209	
Ls2	sus load (kg/m2)	2.743785	
Ls3	sus load (kg/m2)	0.310057	
Sb	bed transp (kg/sm)		
Ss1	sus transp (kg/sm)	-0.000192	
Ss2	sus transp (kg/sm)	0.006017	
Ss3	sus transp (kg/sm)	0.000398	
BFH-mean	bedform height (m)	0.006	
-min	bedform height (m)	0.002	
-max	bedform height (m)	0.009	
BFL-mean	bedform length (m)	0.038	
-min	bedform length (m)	0.020	
-max	bedform length (m)	0.055	
BFT	bedf type:	2.5-D ripples	

Z (m) height	C concentration (kg/m3) mean	min	max	Z (m) height	Vr result velocity (m/s) mean	min	max	Z (m) height	D50 (um)
0.026	3.985	3.710	4.260	0.026	0.005				
0.036	2.260	2.070	2.450	0.036	0.006				
0.046	1.305	1.180	1.430	0.046	-0.014				
0.061	0.611	0.573	0.649	0.061	-0.019				
0.086	0.197	0.187	0.207	0.086	-0.021				
0.116	0.075	0.074	0.076	0.116	-0.023				
0.151	0.022	0.021	0.023	0.151	-0.028				
0.186	0.011	0.009	0.012	0.186	-0.036				
0.226	0.006	0.006	0.006	0.226	-0.038				
0.276	0.002	0.001	0.003	0.276	-0.041				

Vm,Vmr,Vr + : landwards
Vm,Vmr,Vr - : seawards
0 < PHI < 180

CODE	Grasmeijer/Sies 44	ID	1004
MODEL	TU-flume	SET	Series B2
TEST	T 15 00 09	DATE	14-04-1994
LOCATION	25.0 m, section 9	TIME	

H	waterdepth	(m)	0.400	D10	bed mat size	(um)	76
WS	water surface slope	(-)		D50	bed mat size	(um)	95
Hsig	sign wave height	(m)	0.1514	D90	bed mat size	(um)	131
Hm	mean wave height	(m)		Ds -mean	susp mat size	(um)	86
Hrms	rms wave height	(m)	0.1115	-min	susp mat size	(um)	64
Tz	zero-cross period	(s)		-max	susp mat size	(um)	122
Tp	peak period	(s)		WSB	fall vel bed	(m/s)	
Um	mean vel // shore	(m/s)		WSS-mean	fall vel sus	(m/s)	0.0065
Vm	mean vel L shore	(m/s)		-min	fall vel sus	(m/s)	0.0037
Vmr	mean result vel	(m/s)		-max	fall vel sus	(m/s)	0.0111
Vprof	mean vel profile	(m/s)	-0.0378	Cbed1	bed concent.	(kg/m3)	6.39000
Urms	rms vel at bed	(m/s)		Cbed2	bed concent.	(kg/m3)	1590.00000
Umax	max vel at bed	(m/s)		Cbed3	bed concent.	(kg/m3)	17.42752
U15	vel exceed by 15%	(m/s)		Lb	bed load	(kg/m2)	
PHI	angle flow-waves	(degr)		Ls1	sus load	(kg/m2)	0.231892
BT	br. type :	Non breaking		Ls2	sus load	(kg/m2)	1.421941
DMB	distance between meas. loc. and breakerline	(m)	11.000	Ls3	sus load .	(kg/m2)	0.306974
				Sb	bed transp	(kg/sm)	
Urms,on	rms vel. at bed in onsh. dir.	(m/s)		Ss1	sus transp	(kg/sm)	-0.002763
				Ss2	sus transp	(kg/sm)	-0.010229
Urms,off	rms vel. at bed in offsh. dir.	(m/s)		Ss3	sus transp	(kg/sm)	-0.003790
				BFH-mean	bedform height	(m)	0.008
Te	water temp	(o C)	19.5	-min	bedform height	(m)	0.003
BS	local bed slope normal to shore	(-)	0.015900	-max	bedform height	(m)	0.012
				BFL-mean	bedform length	(m)	0.049
				-min	bedform length	(m)	0.034
				-max	bedform length	(m)	0.063
				BFT	bedf type:		2.5-D ripples

Z (m) height	C concentration (kg/m3) mean	min	max	Z (m) height	Vr result velocity (m/s) mean	min	max	Z (m) height	D50 (um)
0.017	6.390	6.240	6.540	0.017	-0.012				
0.027	3.320	3.300	3.340	0.027	-0.014				
0.037	1.900	1.870	1.920	0.037	-0.016				
0.052	0.892	0.867	0.916	0.052	-0.019				
0.077	0.294	0.291	0.296	0.077	-0.029				
0.107	0.111	0.106	0.116	0.107	-0.029				
0.142	0.047	0.046	0.048	0.142	-0.039				
0.177	0.028	0.026	0.029	0.177	-0.040				
0.217	0.021	0.019	0.022	0.217	-0.044				
0.267	0.013	0.012	0.013	0.267	-0.048				

Vm,Vmr,Vr + : landwards
Vm,Vmr,Vr - : seawards
0 < PHI < 180

Tables

H_s : Significant wave height
T_p' : Wave spectrum peak period relative to current
L : Wave length
U_m : Depth-averaged velocity
$\hat{U}_{b,on,tot}$: Amplitude of orbital horizontal velocity (significant onshore velocity)
$\hat{A}_{b,on,tot}$: Amplitude of orbital horizontal displacement ($T_p'/2\pi * \hat{U}_{b,on,tot}$).

exp	H_s [m]	T_p' [sec]	L [m]	U_m [m/s]	$\hat{U}_{b,on,tot}$ [m/s]	$\hat{A}_{b,on,tot}$ [m]
T 10 00 1	0.1022	2.300	3.800	0.0000	0.279	0.102
T 10 00 2	0.1027	2.300	3.800	0.0000	0.286	0.105
T 14 00 1	0.1412	2.300	3.800	0.0000	0.326	0.119
T 14 00 2	0.1404	2.300	3.800	0.0000	0.377	0.138
T 14 00 3	0.1432	2.300	3.800	0.0000	0.355	0.130
T 16 00 1	0.1661	2.300	3.740	0.0000	0.402	0.147
T 16 00 2	0.1683	2.300	3.800	0.0000	0.417	0.153
T 16 00 3	0.1546	2.300	3.800	0.0000	0.392	0.143
T 10 10 1	0.1013	2.440	4.045	0.1106	0.270	0.105
T 10 10 2	0.1008	2.440	4.052	0.1111	0.249	0.097
T 10 10 3	0.0999	2.430	4.023	0.1007	0.274	0.106
T 14 10 1	0.1393	2.410	3.988	0.0973	0.383	0.147
T 14 10 2	0.1403	2.400	3.973	0.0973	0.361	0.138
T 14 10 3	0.1442	2.410	3.987	0.0988	0.313	0.120
T 14 10 4	0.1438	2.410	3.993	0.0993	0.309	0.119
T 16 10 1	0.1559	2.400	3.972	0.1036	0.402	0.154
T 16 10 2	0.1571	2.400	3.971	0.1033	0.416	0.159
T 10 20 1	0.0987	2.550	4.243	0.1952	0.256	0.104
T 10 20 2	0.0979	2.550	4.245	0.1957	0.255	0.103
T 14 20 1	0.1391	2.530	4.209	0.1970	0.377	0.152
T 16 20 1	0.1562	2.530	4.195	0.2046	0.366	0.147
T 16 20 2	0.1595	2.520	4.186	0.2021	0.427	0.171
T 14 30 1	0.1406	2.640	4.391	0.2790	0.390	0.164

m_b : mass flux contribution by breaking waves
m_{nb} : mass flux contribution by non-breaking waves
m : total mass flux
Q_b : percentage breaking waves
U_{return} : return flow

exp	m_b [kg/sm]	m_{nb} [kg/sm]	Q_b [%]	m [kg/sm]	U_{return} Svendsen [m/s]	U_{return} Stive/ Wind [m/s]	U_{return} Van Rijn [m/s]	U_{return} measured [m/s]
T 10 00 1	5.82	3.75	0.0	3.75	-0.012	-0.041	-0.030	-0.022
T 10 00 2	5.85	3.77	0.0	3.77	-0.013	-0.042	-0.030	-0.023
T 14 00 1	11.19	7.21	5.5	7.42	-0.025	-0.057	-0.062	-0.031
T 14 00 2	11.14	7.18	6.3	7.43	-0.025	-0.057	-0.061	-0.032
T 14 00 3	11.50	7.41	5.1	7.62	-0.025	-0.058	-0.064	-0.032
T 16 00 1	17.19	11.14	21.0	12.41	-0.043	-0.072	-0.097	-0.035
T 16 00 2	17.56	11.31	20.6	12.60	-0.042	-0.072	-0.094	-0.033
T 16 00 3	13.70	8.82	10.2	9.32	-0.031	-0.064	-0.077	-0.038
T 10 10 1	5.54	3.64	0.0	3.64	-0.012	-0.041	-0.029	-0.009
T 10 10 2	5.46	3.59	0.0	3.59	-0.012	-0.041	-0.029	-0.007
T 10 10 3	5.42	3.56	0.0	3.56	-0.012	-0.040	-0.029	-0.009
T 14 10 1	10.46	6.85	3.9	6.99	-0.023	-0.056	-0.060	-0.019
T 14 10 2	10.75	7.03	4.0	7.18	-0.024	-0.057	-0.061	-0.025
T 14 10 3	11.31	7.41	4.5	7.58	-0.025	-0.058	-0.065	-0.021
T 14 10 4	11.14	7.22	4.0	7.37	-0.024	-0.057	-0.061	-0.019
T 16 10 1	14.73	9.63	19.6	10.63	-0.035	-0.066	-0.078	-0.032
T 16 10 2	14.83	9.70	20.0	10.73	-0.036	-0.067	-0.080	-0.032
T 10 20 1	5.18	3.46	0.0	3.46	-0.012	-0.040	-0.028	-0.013
T 10 20 2	5.15	3.44	0.0	3.44	-0.011	-0.040	-0.027	-0.013
T 14 20 1	10.50	7.01	3.5	7.13	-0.024	-0.057	-0.060	-0.029
T 16 20 1	13.92	9.27	21.2	10.26	-0.034	-0.065	-0.079	-0.042
T 16 20 2	14.47	9.63	21.2	10.66	-0.036	-0.066	-0.083	-0.043
T 14 30 1	10.37	6.87	3.1	6.97	-0.022	-0.055	-0.055	-0.036

exp.	height (cm)	velocity signal		high frequency		low frequency	
		$\hat{U}_{b,off,tot}$	$\hat{U}_{b,on,tot}$	$\hat{U}_{b,off,high}$	$\hat{U}_{b,on,high}$	$\hat{U}_{b,off,low}$	$\hat{U}_{b,on,low}$
T 10 00 1	2.0	0.195	0.279	0.174	0.279	0.074	0.061
	3.0	0.185	0.236	0.158	0.238	0.076	0.057
	4.0	0.188	0.257	0.161	0.255	0.068	0.069
T 10 00 2	2.0	0.199	0.286	0.175	0.294	0.071	0.060
	3.0	0.181	0.267	0.161	0.268	0.073	0.067
	4.0	0.188	0.269	0.159	0.264	0.076	0.072
T 14 00 1	1.9	0.242	0.326	0.206	0.333	0.094	0.092
	2.9	0.254	0.355	0.216	0.352	0.111	0.107
	3.9	0.226	0.324	0.190	0.317	0.118	0.086
T 14 00 2	2.0	0.252	0.377	0.212	0.379	0.110	0.101
	3.0	0.230	0.333	0.194	0.330	0.107	0.087
	4.0	0.233	0.346	0.195	0.339	0.117	0.104
T 14 00 3	1.9	0.300	0.355	0.250	0.350	0.097	0.078
	2.9	0.252	0.380	0.210	0.373	0.119	0.110
	3.9	0.239	0.337	0.203	0.334	0.128	0.105
T 16 00 1	1.8	0.268	0.402	0.233	0.398	0.125	0.126
	2.8	0.245	0.400	0.212	0.383	0.118	0.137
	3.8	0.254	0.400	0.214	0.375	0.140	0.135
T 16 00 2	2.0	0.275	0.417	0.228	0.402	0.150	0.134
	3.0	0.257	0.403	0.221	0.387	0.126	0.123
	4.0	0.251	0.406	0.222	0.378	0.119	0.133
T 16 00 3	1.7	0.277	0.392	0.234	0.400	0.112	0.100
	2.7	0.281	0.433	0.228	0.423	0.132	0.133
	3.7	0.259	0.409	0.218	0.392	0.146	0.138

r : Ripple height
λ : Ripple length
$K_{s,app}$: Apparent roughness in presence of waves
$K_{s,phys}$: Physical roughness in case of no waves

exp	r	$K_{s,app}$ Measured	$K_{s,phys}$ Measured	$K_{s,phys}/r$ Measured	$K_{s,phys}/r$ Van Rijn	$K_{s,phys}/r$ Swart	$K_{s,phys}/r$ Grant/ Madsen
	[m]	[m]	[m]	[-]	[-]	[-]	[-]
T 10 00 1	0.008				3.3	4.1	2.2
T 10 00 2	0.009				3.4	4.2	2.1
T 14 00 1	0.006				3.0	3.8	2.6
T 14 00 2	0.006				2.6	3.3	2.6
T 14 00 3	0.007				2.9	3.6	2.4
T 16 00 1	0.006				2.6	3.2	2.7
T 16 00 2	0.006				2.8	3.5	2.9
T 16 00 3	0.007				2.9	3.6	2.6
T 10 10 1	0.009	0.29	0.067	7.4	3.1	3.8	1.9
T 10 10 2	0.009	0.26	0.067	7.4	3.1	3.8	1.9
T 10 10 3	0.009	0.19	0.037	4.1	3.2	4.0	2.0
T 14 10 1	0.007	0.28	0.048	6.9	3.0	3.7	2.6
T 14 10 2	0.007	0.24	0.048	6.9	2.9	3.6	2.5
T 14 10 3	0.007	0.22	0.047	6.7	3.0	3.8	2.3
T 14 10 4	0.007	0.22	0.047	6.7	3.0	3.8	2.3
T 16 10 1	0.008	0.36	0.066	8.3	3.6	4.4	2.7
T 16 10 2	0.008	0.29	0.066	8.3	3.0	3.7	2.5
T 10 20 1	0.009	0.11	0.104	11.6	2.8	3.5	1.8
T 10 20 2	0.014	0.12	0.104	7.4	3.5	4.4	1.8
T 14 20 1	0.012	0.16	0.025	2.1	2.9	3.7	2.0
T 16 20 1	0.007	0.19	0.060	8.6	2.4	3.0	2.3
T 16 20 2	0.010	0.17	0.060	6.0	3.3	4.2	2.4
T 14 30 1	0.021	0.10	0.032	1.5	3.3	4.1	1.8

U_{*c} : shear velocity by current (m/s)
U_{*cw} : shear velocity by current and waves (m/s)
$K_{s,phys}$: physical bedroughness (m)
$K_{s,app}$: apparent bedroughness (m)

exp	U_{*c} [m/s]	U_{*cw} [m/s]	$K_{s,phys}$ [m]	$K_{s,app}$ [m]	U_{*cw}/U_{*c} [-]	$K_{s,app}/K_{s,phys}$ [-]
T 10 10 1	0.0111	0.0207	0.067	0.29	1.86	4.33
T 10 10 2	0.0111	0.0204	0.067	0.26	1.84	3.88
T 10 10 3	0.0087	0.0180	0.037	0.19	2.07	5.14
T 14 10 1	0.0091	0.0153	0.048	0.28	1.68	5.83
T 14 10 2	0.0091	0.0140	0.048	0.24	1.54	5.00
T 14 10 3	0.0093	0.0147	0.047	0.22	1.58	4.68
T 14 10 4	0.0093	0.0144	0.047	0.22	1.55	4.68
T 16 10 1	0.0101	0.0152	0.066	0.36	1.50	5.45
T 16 10 2	0.0101	0.0146	0.066	0.29	1.45	4.39
T 10 20 1	0.0216	0.0261	0.104	0.11	1.21	1.06
T 10 20 2	0.0216	0.0264	0.104	0.12	1.22	1.15
T 14 20 1	0.0155	0.0318	0.025	0.16	2.05	6.40
T 16 20	0.0196	0.0290	0.060	0.19	1.48	3.17
T 16 20 2	0.0196	0.0282	0.060	0.17	1.44	2.83
T 14 30 1	0.0231	0.0400	0.032	0.10	1.73	3.13

m_0 : 0-order moment spectrum

m_2 : 2nd-order moment spectrum

$T_{0,2}$: Average zero-crossing period = $\sqrt{(m_0/m_2)}$

Experiment series B1	m_0 [cm²]	m_2 [cm².Hz²]	$T_{0,2}$ [s]
Section1	12.8	4.32	1.72
Section2	12.5	4.27	1.71
Section3	13.1	4.23	1.76
Section4	13.4	4.90	1.65
Section5	16.0	8.54	1.37
Section6	10.7	5.06	1.45
Section7	11.1	4.11	1.64
Section8	12.5	4.42	1.68
Section9	11.8	4.63	1.60
Section10	9.9	4.38	1.51

m_0 : 0-order moment spectrum

m_2 : 2nd-order moment spectrum

$T_{0,2}$: Average zero-crossing period = $\sqrt{(m_0/m_2)}$

Experiment series B2	m_0 [cm²]	m_2 [cm².Hz²]	$T_{0,2}$ [s]
Section1	17.4	5.98	1.71
Section2	18.3	6.20	1.72
Section3	17.4	6.05	1.70
Section4	17.2	6.79	1.59
Section5	17.8	9.16	1.39
Section5a	16.0	9.09	1.33
Section6	13.3	6.78	1.40
Section7	13.6	5.56	1.56
Section8	14.2	5.43	1.62
Section9	15.0	6.42	1.53

Q_b : Percentage breaking waves

H_{m0} : Significant wave height calculated from spectrum

$H_{1/3}$: Wave height (average highest 1/3 part of waves)

$H_{1/10}$: Wave height (average highest 1/10 part of waves)

H_{rms} : Wave height (root mean square)

Experiment Series B1	Distance from x=0 [m]	Water depth [m]	Q_b [%]	H_{m0} [m]	$H_{1/3}$ [m]	$H_{1/10}$ [m]	H_{rms} [m]
Section 1	3	0.60	0.0	0.1429	0.1596	0.2004	0.1127
Section 2	6	0.60	0.0	0.1412	0.1560	0.1963	0.1105
Section 3	8	0.50	0.0	0.1448	0.1563	0.1941	0.1106
Section 4	10	0.40	0.4	0.1464	0.1652	0.2090	0.1163
Section 5	12	0.30	6.3	0.1602	0.1769	0.2177	0.1231
Section 6	14.5	0.40	14.9	0.1307	0.1493	0.1739	0.1058
Section 7	17	0.50	2.7	0.1335	0.1398	0.1624	0.0998
Section 8	20	0.45	0.0	0.1413	0.1339	0.1569	0.0980
Section 9	23	0.40	0.0	0.1374	0.1367	0.1624	0.1000
Section 10	26	0.36	0.0	0.1261	0.1322	0.1599	0.0963

Q_b : Percentage breaking waves

H_{m0} : Significant wave height calculated from spectrum

$H_{1/3}$: Wave height (average highest 1/3 part of waves)

$H_{1/10}$: Wave height (average highest 1/10 part of waves)

H_{rms} : Wave heigt (root mean square)

Experiment Series B2	Distance from x=0 [m]	Water-depth [m]	Q_b [%]	H_{m0} [m]	$H_{1/3}$ [m]	$H_{1/10}$ [m]	H_{rms} [m]
Section 1	3	0.60	0.4	0.1668	0.1890	0.2373	0.1334
Section 2	6	0.60	0.6	0.1711	0.1875	0.2372	0.1331
Section 3	8	0.50	0.6	0.1669	0.1875	0.2345	0.1335
Section 4	10	0.40	1.6	0.1657	0.2011	0.2536	0.1416
Section 5	12	0.30	10.0	0.1690	0.2010	0.2411	0.1421
Section 5a	13	0.34	18.6	0.1601	0.1866	0.2191	0.1336
Section 6	14.5	0.40	27.6	0.1459	0.1631	0.1864	0.1184
Section 7	17	0.50	8.2	0.1478	0.1539	0.1769	0.1116
Section 8	20	0.45	0.0	0.1509	0.1478	0.1740	0.1091
Section 9	23	0.40	0.0	0.1551	0.1514	0.1789	0.1115

Test Series B1	H_s [m]	h [m]	H_s/h [-]	L [m]	H_s/L [-]
Section 1	0.1596	0.5963	0.268	4.687	0.034
Section 2	0.1560	0.5864	0.266	4.664	0.033
Section 3	0.1563	0.4961	0.314	4.348	0.036
Section 4	0.1652	0.3941	0.419	3.950	0.042
Section 5	0.1769	0.3154	0.561	3.585	0.049
Section 6	0.1493	0.4188	0.356	4.041	0.037
Section 7	0.1398	0.5049	0.277	4.374	0.032
Section 8	0.1339	0.4503	0.297	4.186	0,032
Section 9	0.1367	0.4090	0.334	4.011	0.034
Section 10	0.1322	0.3627	0.364	3.791	0,035

Table 5.2.5 Wave parameters series B1

Test Series B2	H_s [m]	h [m]	H_s/h [-]	L [m]	H_s/L [-]
Section 1	0.1890	0.5992	0.315	4.710	0.040
Section 2	0.1875	0.5901	0.318	4.664	0.040
Section 3	0.1875	0.5062	0.370	4.399	0.043
Section 4	0.2011	0.3896	0.516	3.920	0.051
Section 5	0.2010	0.3102	0.648	3.548	0.057
Section 5a	0.1866	0.3329	0.561	3.655	0.051
Section 6	0.1631	0.4038	0.404	3.980	0.041
Section 7	0.1539	0.5116	0.301	4.399	0.035
Section 8	0.1478	0.4558	0.324	4.186	0.035
Section 9	0.1514	0.4026	0.376	3.980	0.038

Table 5.2.6 Wave parameters series B2

Q_b : Percentage breaking waves

$T_{1/3}$: Period (average highest 1/3 part of periods)

$T_{1/10}$: Period (average highest 1/10 part of periods)

T_p : Peakperiod (from wave spectra)

Experiment Series B1	Distance from x=0 [m]	Water depth [m]	Q_b [%]	$T_{1/3}$ [s]	$T_{1/10}$ [s]	T_p [s]
Section 1	3	0.60	0.0	2.37	2.57	2.13
Section 2	6	0.60	0.0	2.38	2.62	2.13
Section 3	8	0.50	0.0	2.40	2.63	2.13
Section 4	10	0.40	0.4	2.41	2.65	2.13
Section 5	12	0.30	6.3	2.42	2.69	2.13
Section 6	14.5	0.40	14.9	2.43	2.71	2.13
Section 7	17	0.50	2.7	2.38	2.72	2.13
Section 8	20	0.45	0.0	2.44	2.73	2.13
Section 9	23	0.40	0.0	2.48	2.79	2.13
Section 10	26	0.36	0.0	2.43	2.87	2.13

Q_b : Percentage breaking waves

$T_{1/3}$: Period (average highest 1/3 part of periods)

$T_{1/10}$: Period (average highest 1/10 part of periods)

T_p : Peak period (from wave spectra)

Experiment Series B2	Distance from x=0 [m]	Waterdepth [m]	Q_b [%]	$T_{1/3}$ [s]	$T_{1/10}$ [s]	T_p [s]
Section 1	3	0.60	0.4	2.39	2.61	2.13
Section 2	6	0.60	0.6	2.41	2.66	2.13
Section 3	8	0.50	0.6	2.44	2.69	2.13
Section 4	10	0.40	1.6	2.44	2.69	2.13
Section 5	12	0.30	10.0	2.45	2.73	2.13
Section 5a	13	0.34	18.6	2.44	2.68	2.13
Section 6	14.5	0.40	27.6	2.44	2.68	2.13
Section 7	17	0.50	8.2	2.38	2.79	2.13
Section 8	20	0.45	0.0	2.39	2.71	2.13
Section 9	23	0.40	0.0	2.48	2.80	2.13

$\hat{u}$: peak orbital velocity ($= u_{1/3}$)

Experiment Series B1	Height above bed (cm)	velocity signal (m/s)		high frequency (m/s)		low frequency (m/s)	
		$\hat{u}_{sig,off}$	$\hat{u}_{sig,on}$	$\hat{u}1_{sig,off}$	$\hat{u}1_{sig,on}$	$\hat{u}2_{sig,off}$	$\hat{u}2_{sig,on}$
Section 1	2.0	0.253	0.266	0.236	0.276	0.064	0.058
	3.0	0.233	0.244	0.219	0.255	0.057	0.047
	4.0	0.243	0.258	0.225	0.266	0.069	0.056
Section 2	2.1	0.229	0.243	0.215	0.245	0.048	0.046
	3.1	0.254	0.272	0.235	0.282	0.057	0.051
	4.1	0.233	0.238	0.212	0.254	0.068	0.054
Section 3	2.1	0.270	0.290	0.246	0.290	0.073	0.061
	3.1	0.226	0.252	0.215	0.254	0.057	0.060
	4.1	0.264	0.287	0.241	0.290	0.070	0.072
Section 4	1.8	0.263	0.348	0.253	0.359	0.055	0.059
	2.8	0.316	0.395	0.286	0.417	0.101	0.079
	3.8	0.273	0.334	0.246	0.352	0.094	0.077
Section 5	1.8	0.289	0.393	0.258	0.414	0.098	0.080
	2.8	0.322	0.440	0.282	0.458	0.120	0.112
	3.8	0.288	0.399	0.255	0.415	0.129	0.101
Section 6	2.7	0.219	0.279	0.199	0.294	0.070	0.068
	3.7	0.215	0.300	0.194	0.304	0.097	0.086
	4.7	0.213	0.294	0.180	0.300	0.108	0.087
Section 7	1.9	0.231	0.220	0.216	0.222	0.063	0.061
	2.9	0.235	0.227	0.218	0.226	0.077	0.069
	3.9	0.220	0.223	0.205	0.223	0.066	0.067
Section 8	2.0	0.281	0.289	0.262	0.289	0.070	0.067
	3.0	0.265	0.276	0.241	0.276	0.076	0.065
	4.0	0.260	0.277	0.239	0.271	0.084	0.093
Section 9	1.8	0.255	0.294	0.235	0.305	0.075	0.078
	2.8	0.249	0.291	0.228	0.292	0.087	0.076
	3.8	0.250	0.264	0.218	0.269	0.090	0.090
Section 10	2.3	0.284	0.318	0.259	0.333	0.088	0.094
	3.3	0.285	0.324	0.258	0.332	0.096	0.100
	4.3	0.266	0.305	0.233	0.318	0.107	0.113

$\hat{u}$: peak orbital velocity ($= u_{1/3}$)

Experiment Series B2	Height above bed (cm)	velocity signal (m/s)		high frequency (m/s)		low frequency (m/s)	
		$\hat{u}_{sig,off}$	$\hat{u}_{sig,on}$	$\hat{u}1_{sig,off}$	$\hat{u}1_{sig,on}$	$\hat{u}2_{sig,off}$	$\hat{u}2_{sig,on}$
Section 1	1.6	0.276	0.273	0.259	0.288	0.057	0.055
	2.6	0.287	0.324	0.264	0.333	0.075	0.064
	3.6	0.278	0.288	0.256	0.298	0.079	0.061
Section 2	2.2	0.271	0.297	0.255	0.305	0.062	0.055
	3.2	0.299	0.321	0.272	0.337	0.078	0.068
	4.2	0.277	0.294	0.251	0.308	0.084	0.059
Section 3	2.3	0.281	0.306	0.263	0.328	0.069	0.075
	3.3	0.343	0.359	0.303	0.376	0.094	0.088
	4.3	0.320	0.296	0.071	0.084	0.127	0.043
Section 4	1.6	0.362	0.437	0.324	0.468	0.122	0.099
	2.6	0.339	0.411	0.298	0.444	0.119	0.091
	3.6	0.320	0.389	0.286	0.405	0.098	0.089
Section 5	1.7	0.323	0.452	0.285	0.477	0.117	0.103
	2.7	0.364	0.525	0.322	0.543	0.158	0.134
	3.7	0.319	0.437	0.271	0.444	0.148	0.128
Section 5a	2.6	0.276	0.410	0.238	0.423	0.123	0.102
	3.6	0.308	0.453	0.257	0.427	0.186	0.158
	4.6	0.294	0.433	0.243	0.418	0.207	0.145
Section 6	2.4	0.241	0.361	0.217	0.379	0.094	0.083
	3.4	0.242	0.372	0.209	0.375	0.142	0.098
	4.4	0.236	0.349	0.202	0.347	0.137	0.131
Section 7	2.2	0.247	0.240	0.228	0.245	0.068	0.068
	3.2	0.237	0.257	0.211	0.246	0.092	0.088
	4.2	0.232	0.246	0.212	0.249	0.095	0.083
Section 8	2.6	0.279	0.268	0.256	0.270	0.086	0.094
	3.6	0.283	0.278	0.253	0.270	0.095	0.103
	4.6	0.270	0.281	0.242	0.267	0.094	0.097
Section 9	1.7	0.277	0.311	0.259	0.318	0.082	0.079
	2.7	0.270	0.322	0.252	0.313	0.096	0.107
	3.7	0.276	0.296	0.241	0.302	0.098	0.089

Ls : Suspended load

Ss : Suspended transport + : landward
- : seaward

Test Series B1	Distance from x=0 [m]	Ls [kg/m²]	Ss [kg/sm]
Section 1	3	0.157426	+0.00073
Section 2	6	0.154179	-0.00120
Section 3	8	0.185410	-0.00166
Section 4	10	0.352264	-0.00096
Section 5	12	0.496360	-0.01399
Section 6	14.5	0.248724	-0.00482
Section 7	17	0.107774	-0.00006
Section 8	20	0.147415	-0.00003
Section 9	23	0.188100	-0.00225
Section 10	26	0.307696	-0.00339

Ls : Suspended load

Ss : Suspended transport + : landward
- : seaward

Test Series B2	Distance from x=0 [m]	Ls [kg/m²]	Ss [kg/sm]
Section 1	3	0.186006	-0.00220
Section 2	6	0.247909	-0.00193
Section 3	8	0.287664	-0.00287
Section 4	10	0.377994	-0.01236
Section 5	12	0.551014	-0.02424
Section 5a	13	0.625262	-0.02564
Section 6	14.5	0.471499	-0.01567
Section 7	17	0.199351	-0.00093
Section 8	20	0.247133	+0.00010
Section 9	23	0.269433	-0.00328

x along flume (m)	Bed level before (m)	Bed level change (m)	Bed level after 25500 s (m)	Bed level before (m)	Bed level change (m)	Bed level after 9700 s (m)
0.00	0.058	0	0.058	0.069	0	0.069
0.25	0.058	-0.005	0.053	0.069	-0.016	0.053
0.50	0.064	-0.005	0.059	0.074	-0.012	0.062
0.75	0.071	-0.004	0.067	0.073	-0.005	0.068
1.00	0.068	-0.005	0.063	0.068	0	0.068
1.25	0.069	0	0.069	0.075	-0.003	0.072
1.50	0.073	-0.005	0.068	0.074	0.005	0.079
1.75	0.074	-0.008	0.066	0.076	0.002	0.078
2.00	0.076	-0.003	0.073	0.070	0.005	0.075
2.25	0.073	-0.003	0.070	0.064	0.003	0.067
2.50	0.073	0	0.073	0.066	0.006	0.072
2.75	0.076	-0.002	0.074	0.072	-0.004	0.068
3.00	0.072	0	0.072	0.062	0.006	0.068
3.25	0.074	-0.007	0.067	0.069	0	0.069
3:50	0.072	-0.001	0.071	0.063	0.002	0.065
3.75	0.072	0.004	0.076	0.061	0.005	0.066
4.00	0.067	0.004	0.071	0.065	0.003	0.068
4.25	0.076	-0.003	0.073	0.068	-0.008	0.060
4.50	0.075	-0.008	0.067	0.063	0.003	0.066
4.75	0.071	-0.004	0.067	0.066	0.001	0.067
5.00	0.063	0.007	0.070	0.063	0	0.063
5.25	0.069	0	0.069	0.068	0.007	0.075
5.50	0.070	0	0.070	0.075	-0.001	0.074
5.75	0.078	-0.002	0.076	0.066	0.008	0.074
6.00	0.087	-0.003	0.084	0.070	0.014	0.084

x along flume (m)	Bed level before (m)	Bed level change (m)	Bed level after 25500 s (m)	Bed level before (m)	Bed level change (m)	Bed level after 9700 s (m)
6.25	0.092	-0.003	0.089	0.083	0.010	0.093
6.50	0.102	-0.003	0.099	0.089	0.005	0.094
6.75	0.113	-0.001	0.112	0.102	0.004	0.106
7.00	0.123	-0.001	0.122	0.112	0.008	0.120
7.25	0.138	-0.002	0.136	0.129	0	0.129
7.50	0.152	-0.004	0.148	0.142	0	0.142
7.75	0.163	-0.004	0.159	0.155	0.001	0.156
8.00	0.176	0.002	0.178	0.166	0.002	0.168
8.25	0.187	0.003	0.190	0.181	0.008	0.189
8.50	0.200	0.012	0.212	0.200	-0.002	0.198
8.75	0.213	0.012	0.225	0.211	0.003	0.214
9.00	0.230	0.011	0.241	0.221	0.009	0.230
9.25	0.244	0.014	0.258	0.234	0.007	0.241
9.50	0.254	0.013	0.267	0.243	0.010	0.253
9.75	0.263	0.015	0.278	0.257	0.010	0.267
10.00	0.274	0.022	0.296	0.267	0.011	0.278
10.25	0.292	0.019	0.311	0.278	0.022	0.300
10.50	0.298	0.024	0.322	0.291	0.023	0.314
10.75	0.306	0.026	0.332	0.308	0.016	0.324
11.00	0.330	0.011	0.341	0.322	0.010	0.332
11.25	0.338	0.015	0.353	0.337	0.009	0.346
11.50	0.352	0.006	0.358	0.351	0.013	0.364
11.75	0.359	0.002	0.361	0.358	0.004	0.362
12.00	0.363	0.002	0.365	0.370	-0.006	0.364
12.25	0.365	-0.002	0.363	0.367	-0.003	0.364

x along flume (m)	Bed level before (m)	Bed level change (m)	Bed level after 25500 s (m)	Bed level before (m)	Bed level change (m)	Bed level after 9700 s (m)
12.50	0.352	0.006	0.358	0.357	0.001	0.358
12.75	0.349	0.003	0.352	0.347	-0.008	0.339
13.00	0.341	-0.004	0.337	0.335	-0.004	0.331
13.25	0.322	-0.002	0.320	0.323	-0.007	0.316
13.50	0.314	-0.012	0.302	0.309	-0.011	0.298
13.75	0.301	-0.010	0.291	0.302	-0.015	0.287
14.00	0.286	-0.007	0.279	0.291	-0.018	0.273
14.25	0.270	-0.010	0.260	0.275	-0.015	0.260
14.50	0.252	-0.004	0.248	0.264	-0.009	0.255
14.75	0.248	-0.012	0.236	0.252	-0.018	0.234
15.00	0.250	-0.032	0.218	0.243	-0.022	0.221
15.25	0.244	-0.035	0.209	0.236	-0.024	0.212
15.50	0.231	-0.027	0.204	0.227	-0.023	0.204
15.75	0.217	-0.021	0.196	0.212	-0.017	0.195
16.00	0.213	-0.018	0.195	0.194	-0.009	0.185
16.25	0.203	-0.015	0.188	0.195	-0.017	0.178
16.50	0.198	-0.017	0.181	0.186	-0.022	0.164
16.75	0.184	-0.012	0.172	0.171	-0.007	0.164
17.00	0.170	-0.001	0.169	0.161	-0.005	0.156
17.25	0.173	-0.003	0.170	0.161	-0.006	0.155
17.50	0.182	-0.014	0.168	0.164	-0.009	0.155
17.75	0.187	-0.014	0.173	0.167	-0.007	0.160
18.00	0.192	-0.014	0.178	0.171	-0.008	0.163
18.25	0.197	-0.008	0.189	0.178	-0.007	0.171
18.50	0.202	-0.005	0.197	0.178	0	0.178

x along flume (m)	Bed level before (m)	Bed level change (m)	Bed level after 25500 s (m)	Bed level before (m)	Bed level change (m)	Bed level after 9700 s (m)
18.75	0.204	-0.002	0.202	0.181	0	0.181
19.00	0.204	-0.005	0.199	0.193	-0.004	0.189
19.25	0.208	-0.005	0.203	0.198	-0.006	0.192
19.50	0.211	0.005	0.216	0.207	-0.004	0.203
19.75	0.218	0	0.218	0.215	-0.004	0.211
20.00	0.223	0.003	0.226	0.224	-0.004	0.220
20.25	0.224	0.007	0.231	0.225	-0.004	0.221
20.50	0.228	0.011	0.239	0.228	0	0.228
20.75	0.236	0.002	0.238	0.240	-0.007	0.233
21.00	0.237	0.002	0.239	0.238	-0.001	0.237
21.25	0.242	0.006	0.248	0.236	0.002	0.238
21.50	0.244	0.002	0.246	0.240	0	0.240
21.75	0.249	0.006	0.255	0.243	0.004	0.247
22.00	0.251	0.011	0.262	0.233	0.016	0.249
22.25	0.259	0.011	0.270	0.226	0.027	0.253
22.50	0.264	0.008	0.272	0.251	0.007	0.258
22.75	0.274	0.004	0.278	0.259	-0.001	0.258
23.00	0.272	0.013	0.285	0.261	0.005	0.266
23.25	0.280	0.008	0.288	0.265	-0.002	0.263
23.50	0.289	0.004	0.293	0.271	0.004	0.275
23.75	0.294	0.009	0.303	0.274	0.005	0.279
24.00	0.298	0.005	0.303	0.281	0.006	0.287
24.25	0.305	0.008	0.313	0.284	0	0.284
24.50	0.307	0.004	0.311	0.285	0.001	0.286
24.75	0.308	0.003	0.311	0.287	0.001	0.288

x along flume (m)	Bed level before (m)	Bed level change (m)	Bed level after 25500 s (m)		Bed level before (m)	Bed level change (m)	Bed level after 9700 s (m)
25.00	0.312	0.004	0.316		0.288	0.006	0.294
25.25	0.314	0.006	0.320		0.297	0.003	0.300
25.50	0.316	0.010	0.326		0.305	-0.002	0.303
25.75	0.321	0.007	0.328		0.308	0.003	0.311
26.00	0.329	-0.003	0.326		0.314	-0.005	0.309
26.25	0.334	-0.010	0.324		0.311	-0.005	0.306
26.50	0.337	-0.010	0.327		0.314	-0.011	0.303
26.75	0.344	-0.018	0.326		0.305	-0.005	0.300
27.00	0.341	-0.012	0.329		0.282	0.020	0.302
27.25	0.340	-0.006	0.334		0.266	0.043	0.309
27.50	0.344	-0.007	0.337		0.271	0.037	0.308
27.75	0.355	-0.018	0.337		0.277	0.041	0.318
28.00	0.349	-0.017	0.332		0.279	0.038	0.317
28.25	0.343	-0.023	0.320		0.278	0.045	0.323
28.50	0.334	-0.022	0.312		0.273	0.036	0.309
28.75	0.282	0.003	0.285		0.262	0.012	0.274
29.00	0.138	0.037	0.175		0.163	-0.026	0.137
29.25	0.086	0	0.086				

D_{50}	:	Median grain diameter of sediment:	95 μm
D_{90}	:	Grain diameter exceeded by 10%:	131 μm
D_{ss}	:	Suspended sediment size (see data-tables):	82-114 μm
$K_{s,c}$	:	Current-related physical bedroughness:	3*r
$K_{s,w}$	:	Wave-related physical bedroughness:	3*r

exp	$S_{s,calc}$ Van Rijn [kg/sm]	$S_{s,meas}$ measured [kg/sm]	$S_{s,meas}/S_{s,calc}$ factor [-]
T 10 10 1	0.0016	0.0076	4.75
T 10 10 2	0.0019	0.0056	2.95
T 10 10 3	0.0014	0.0054	3.86
T 14 10 1	0.0029	0.0079	2.72
T 14 10 2	0.0025	0.0068	2.72
T 14 10 3	0.0025	0.0089	3.56
T 14 10 4	0.0026	0.0076	2.92
T 16 10 1	0.0037	0.0136	3.68
T 16 10 2	0.0038	0.0142	3.74
T 10 20 1	0.0041	0.0138	3.37
T 10 20 2	0.0061	0.0111	1.82
T 14 20 1	0.0147	0.0315	2.14
T 16 20 1	0.0110	0.0486	4.42
T 16 20 2	0.0139	0.0478	3.44
T 14 30 1	0.0381	0.0645	1.69

H_s	:	Significant wave height	:	0.10 m	
U_m	:	Depth averaged velocity	:	0.10 m/s	

Calculated concentration profile			Measured concentration profile		
z [m]	z/h [-]	conc [kg/m³]	z [m]	z/h [-]	conc [kg/m³]
0.027	0.090	0.591	0.023	0.075	1.970
0.030	0.101	0.517	0.033	0.108	1.360
0.034	0.114	0.443	0.043	0.141	0.915
0.039	0.131	0.369	0.058	0.190	0.406
0.046	0.154	0.295	0.083	0.272	0.201
0.056	0.187	0.222	0.113	0.371	0.072
0.073	0.244	0.148	0.148	0.485	0.027
0.107	0.355	0.079	0.183	0.600	0.012
0.144	0.480	0.045	0.223	0.732	0.010
0.182	0.605	0.028	0.273	0.896	0.007
0.219	0.730	0.018			
0.257	0.855	0.011			
0.294	0.980	0.007			
0.300	1.000	0.006			

H_s	:	Significant wave height	:	0.14 m	
U_m	:	Depth averaged velocity	:	0.10 m/s	

Calculated concentration profile			Measured concentration profile		
z [m]	z/h [-]	conc [kg/m³]	z [m]	z/h [-]	conc [kg/m³]
0.021	0.070	1.176	0.020	0.066	4.835
0.025	0.084	1.103	0.030	0.099	3.035
0.030	0.100	0.882	0.040	0.132	1.860
0.036	0.120	0.735	0.055	0.182	0.855
0.044	0.146	0.588	0.080	0.265	0.345
0.055	0.182	0.441	0.110	0.364	0.143
0.072	0.239	0.294	0.145	0.480	0.050
0.106	0.353	0.158	0.180	0.596	0.030
0.143	0.478	0.095	0.220	0.728	0.019
0.181	0.603	0.063	0.270	0.894	0.014
0.218	0.728	0.043			
0.256	0.853	0.029			
0.293	0.978	0.020			
0.300	1.000	0.017			

H_s	:	Significant wave height	:	0.16 m	
U_m	:	Depth averaged velocity	:	0.10 m/s	

Calculated concentration profile			Measured concentration profile		
z [m]	z/h [-]	conc [kg/m³]	z [m]	z/h [-]	conc [kg/m³]
0.024	0.080	1.588	0.021	0.071	7.765
0.028	0.095	1.390	0.031	0.105	4.910
0.034	0.112	1.191	0.041	0.138	2.975
0.040	0.133	0.993	0.056	0.189	1.395
0.048	0.161	0.794	0.081	0.273	0.611
0.060	0.200	0.596	0.111	0.374	0.311
0.079	0.262	0.397	0.146	0.492	0.189
0.114	0.379	0.214	0.181	0.610	0.142
0.151	0.504	0.130	0.221	0.745	0.100
0.189	0.629	0.087	0.271	0.914	0.065
0.226	0.754	0.059			
0.264	0.879	0.040			
0.300	1.000	0.024			

H_s	:	Significant wave height	:	0.10 m	
U_m	:	Depth averaged velocity	:	0.20 m/s	

Calculated concentration profile			Measured concentration profile		
z [m]	z/h [-]	conc [kg/m³]	z [m]	z/h [-]	conc [kg/m³]
0.042	0.140	0.712	0.025	0.082	1.290
0.047	0.157	0.623	0.035	0.115	0.913
0.054	0.179	0.534	0.045	0.148	0.702
0.062	0.208	0.445	0.060	0.198	0.476
0.075	0.249	0.356	0.085	0.280	0.260
0.093	0.310	0.267	0.115	0.379	0.128
0.123	0.410	0.178	0.150	0.495	0.049
0.161	0.535	0.111	0.185	0.610	0.021
0.198	0.660	0.071	0.225	0.742	0.010
0.236	0.785	0.045	0.275	0.907	0.005
0.273	0.910	0.029			
0.300	1.000	0.020			

H_s	:	Significant wave height	:	0.14 m	
U_m	:	Depth averaged velocity	:	0.20 m/s	

Calculated concentration profile			Measured concentration profile		
z [m]	z/h [-]	conc [kg/m³]	z [m]	z/h [-]	conc [kg/m³]
0.036	0.120	1.358	0.030	0.099	3.660
0.042	0.140	1.188	0.040	0.132	2.675
0.050	0.166	1.018	0.050	0.165	2.075
0.060	0.201	0.849	0.065	0.214	1.255
0.075	0.251	0.679	0.090	0.297	0.660
0.099	0.328	0.509	0.120	0.395	0.286
0.134	0.448	0.349	0.155	0.511	0.112
0.172	0.573	0.248	0.190	0.626	0.063
0.209	0.698	0.179	0.230	0.758	0.046
0.247	0.823	0.129	0.280	0.923	0.031
0.284	0.948	0.093			
0.300	1.000	0.077			

H_s	:	Significant wave height	:	0.16 m	
U_m	:	Depth averaged velocity	:	0.20 m/s	

Calculated concentration profile			Measured concentration profile		
z [m]	z/h [-]	conc [kg/m³]	z [m]	z/h [-]	conc [kg/m³]
0.030	0.100	1.724	0.029	0.096	5.811
0.036	0.119	1.509	0.039	0.130	4.160
0.043	0.142	1.293	0.049	0.163	3.060
0.052	0.173	1.078	0.064	0.213	1.840
0.065	0.217	0.862	0.089	0.296	1.010
0.085	0.283	0.647	0.119	0.395	0.549
0.119	0.396	0.431	0.154	0.512	0.245
0.156	0.521	0.282	0.189	0.628	0.157
0.194	0.646	0.197	0.229	0.761	0.109
0.231	0.771	0.138	0.279	0.927	0.070
0.269	0.896	0.097			
0.300	1.000	0.063			

H_s	:	Significant wave height	:	0.14 m	
U_m	:	Depth averaged velocity	:	0.30 m/s	

Calculated concentration profile			Measured concentration profile		
z [m]	z/h [-]	conc [kg/m³]	z [m]	z/h [-]	conc [kg/m³]
0.063	0.197	1.662	0.050	0.155	2.800
0.073	0.229	1.454	0.060	0.186	2.290
0.087	0.271	1.246	0.070	0.217	1.785
0.105	0.328	1.039	0.085	0.263	1.245
0.131	0.409	0.831	0.110	0.340	0.742
0.168	0.523	0.625	0.140	0.433	0.381
0.208	0.648	0.458	0.175	0.542	0.172
0.248	0.773	0.337	0.210	0.650	0.087
0.288	0.898	0.248	0.250	0.774	0.056
0.320	1.000	0.194	0.300	0.929	0.036

D_{50}	:	Median grain diameter of sediment:	95 μm
D_{90}	:	Grain diameter exceeded by 10%:	131 μm
$K_{s,c}$	:	Current-related physical bedroughness:	3*r
B	:	Empirical parameter:	1

exp	$S_{s,calc}$ Bijker [kg/sm]	$S_{s,meas}$ measured [kg/sm]	$S_{s,meas}/S_{s,calc}$ factor [-]
T 10 10 1	0.0067	0.0076	1.13
T 10 10 2	0.0074	0.0056	0.76
T 10 10 3	0.0067	0.0054	0.81
T 14 10 1	0.0101	0.0079	0.78
T 14 10 2	0.0091	0.0068	0.75
T 14 10 3	0.0082	0.0089	1.09
T 14 10 4	0.0083	0.0076	0.92
T 16 10 1	0.0097	0.0136	1.40
T 16 10 2	0.0097	0.0142	1.46
T 10 20 1	0.0106	0.0138	1.30
T 10 20 2	0.0096	0.0111	1.16
T 14 20 1	0.0149	0.0315	2.11
T 16 20 1	0.0193	0.0486	2.52
T 16 20 2	0.0166	0.0478	2.88
T 14 30 1	0.0149	0.0645	4.33

H_s : Significant wave height : 0.10 m
U_m : Depth averaged velocity : 0.10 m/s

Calculated concentraton profile			Measured concentration profile		
z [m]	z/h [-]	conc [kg/m³]	z [m]	z/h [-]	conc [kg/m³]
0.0045	0.015	3.250	0.023	0.075	1.970
0.0054	0.018	3.058	0.033	0.108	1.360
0.0064	0.021	2.874	0.043	0.141	0.915
0.0077	0.026	2.693	0.058	0.190	0.406
0.0094	0.031	2.508	0.083	0.272	0.201
0.0118	0.039	2.313	0.113	0.371	0.072
0.0155	0.052	2.091	0.148	0.485	0.027
0.0233	0.078	1.800	0.183	0.600	0.012
0.0518	0.173	1.316	0.223	0.732	0.010
0.0893	0.298	1.030	0.273	0.896	0.007
0.1268	0.423	0.853			
0.1643	0.548	0.717			
0.2018	0.673	0.597			
0.2393	0.798	0.477			

H_s : Significant wave height : 0.14 m
U_m : Depth averaged velocity : 0.10 m/s

Calculated concentraton profile			Measured concentration profile		
z [m]	z/h [-]	conc [kg/m³]	z [m]	z/h [-]	conc [kg/m³]
0.0036	0.012	4.611	0.020	0.066	4.835
0.0043	0.014	4.359	0.030	0.099	3.035
0.0052	0.017	4.121	0.040	0.132	1.860
0.0062	0.021	3.890	0.055	0.182	0.855
0.0075	0.025	3.659	0.080	0.265	0.345
0.0093	0.031	3.416	0.110	0.364	0.143
0.0121	0.040	3.144	0.145	0.480	0.050
0.0174	0.058	2.792	0.180	0.596	0.030
0.0420	0.140	2.071	0.220	0.728	0.019
0.0795	0.265	1.620	0.270	0.894	0.014
0.1170	0.390	1.357			
0.1545	0.515	1.161			
0.1920	0.640	0.990			
0.2295	0.765	0.821			

H_s	:	Significant wave height	:	0.14 m	
U_m	:	Depth averaged velocity	:	0.30 m/s	

Calculated concentration profile			Measured concentration profile		
z [m]	z/h [-]	conc [kg/m³]	z [m]	z/h [-]	conc [kg/m³]
0.0106	0.033	1.821	0.050	0.155	2.800
0.0135	0.042	1.706	0.060	0.186	2.290
0.0174	0.054	1.593	0.070	0.217	1.785
0.0227	0.071	1.480	0.085	0.263	1.245
0.0306	0.096	1.362	0.110	0.340	0.742
0.0433	0.135	1.231	0.140	0.433	0.381
0.0670	0.209	1.076	0.175	0.542	0.172
0.1068	0.334	0.913	0.210	0.650	0.087
0.1468	0.459	0.798	0.250	0.774	0.056
0.1868	0.584	0.701	0.300	0.929	0.036
0.2268	0.709	0.609			
0.2668	0.834	0.505			
0.3068	0.959	0.341			

Figures

Fraction breaking waves

Influence Hs/h and Hs/L

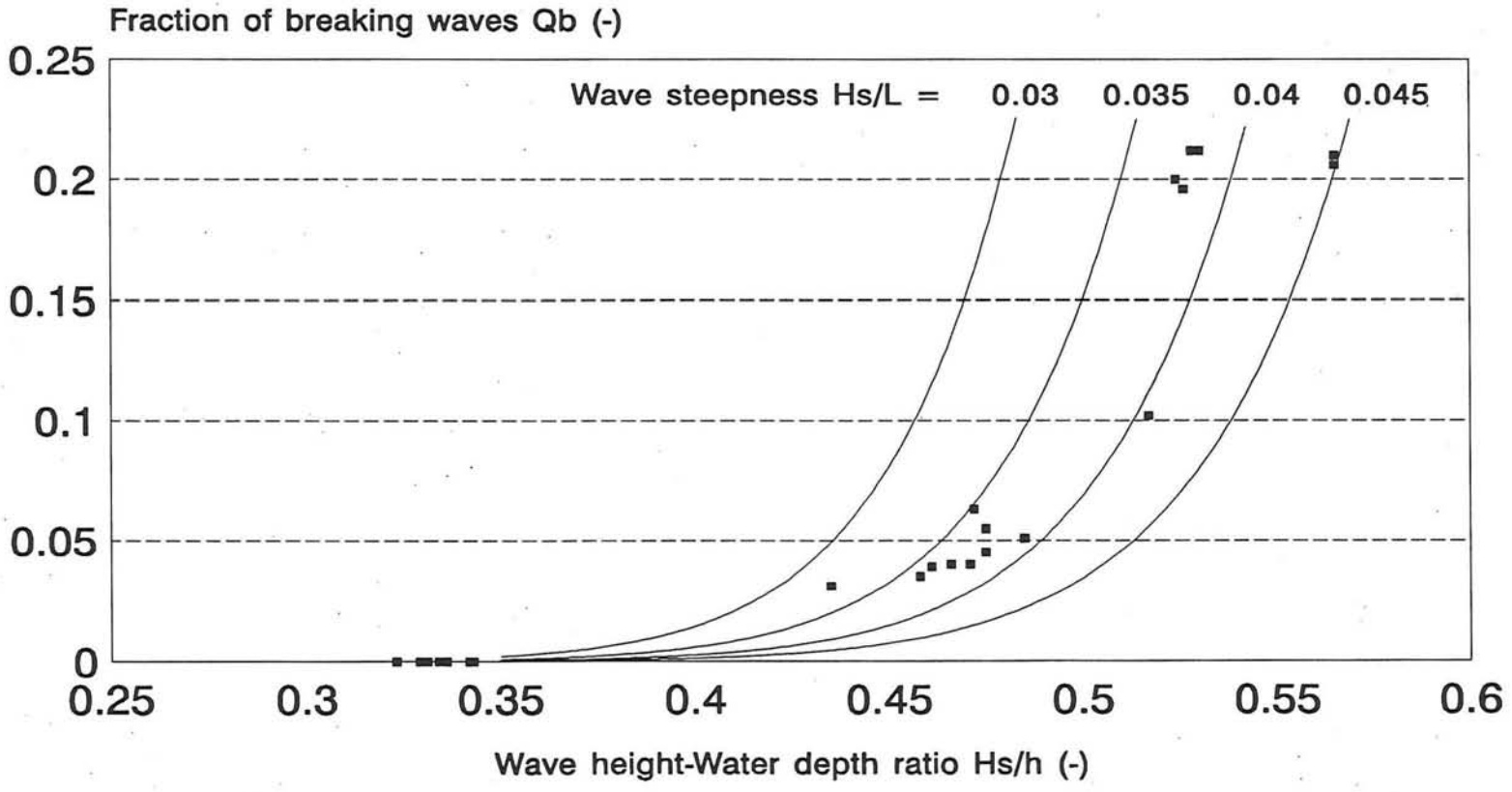

Figure 4.2

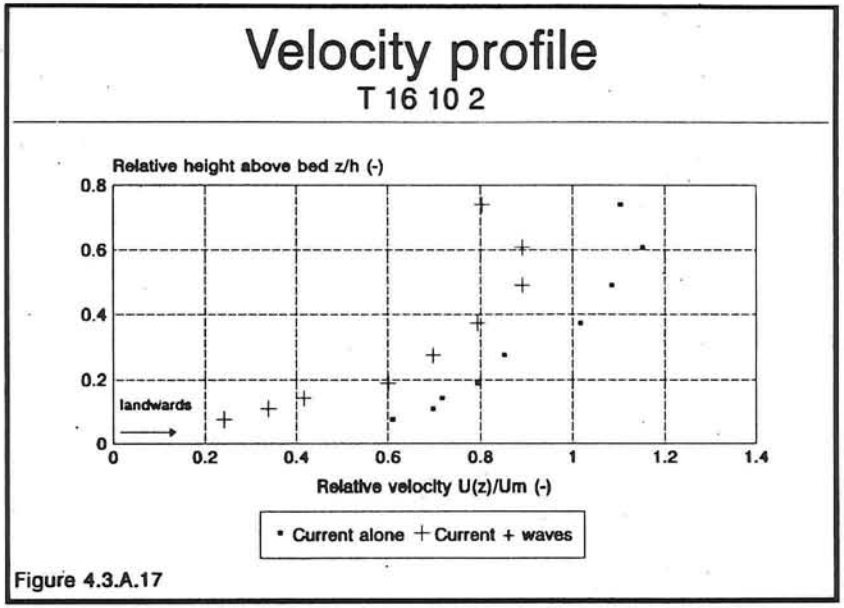

Figure 4.3.A.17

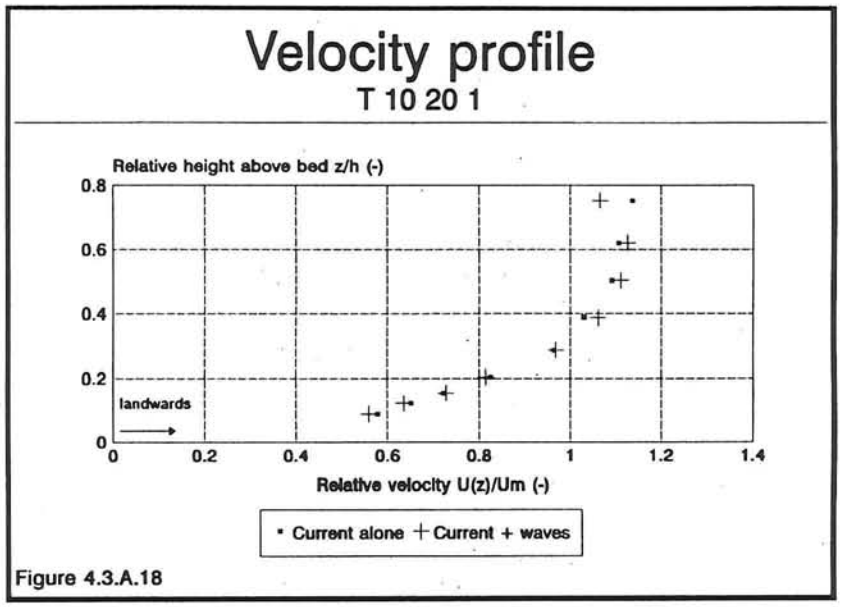

Figure 4.3.A.18

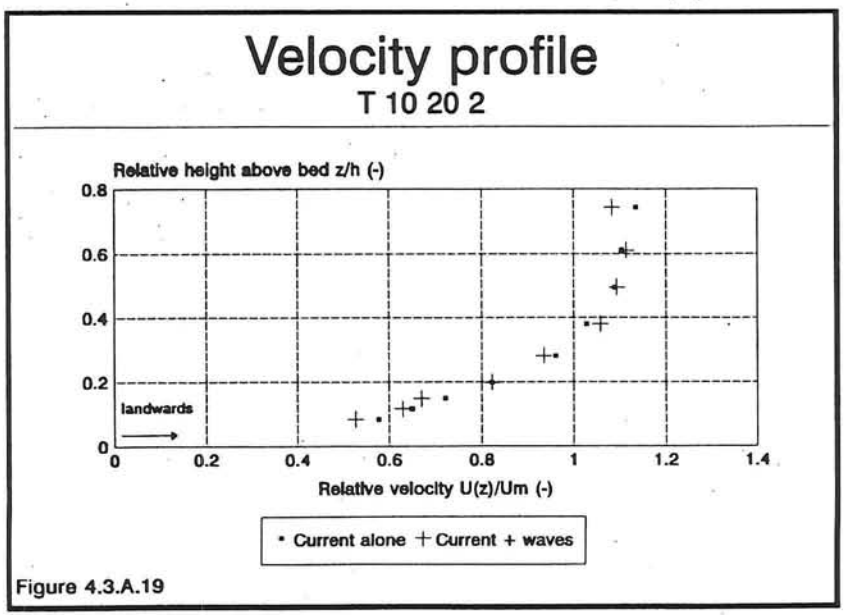

Figure 4.3.A.19

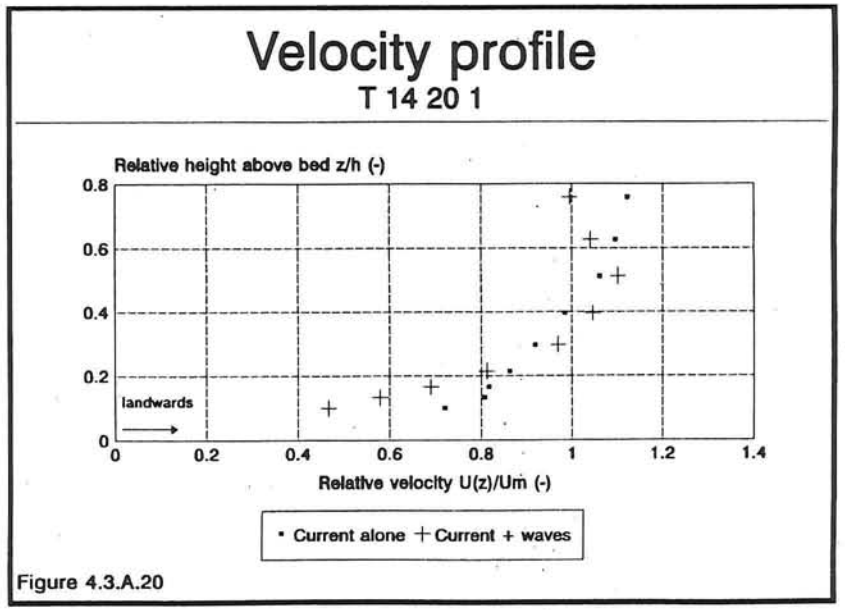

Figure 4.3.A.20

Velocity profile

Influence wave height
Um = 0.10 m/s

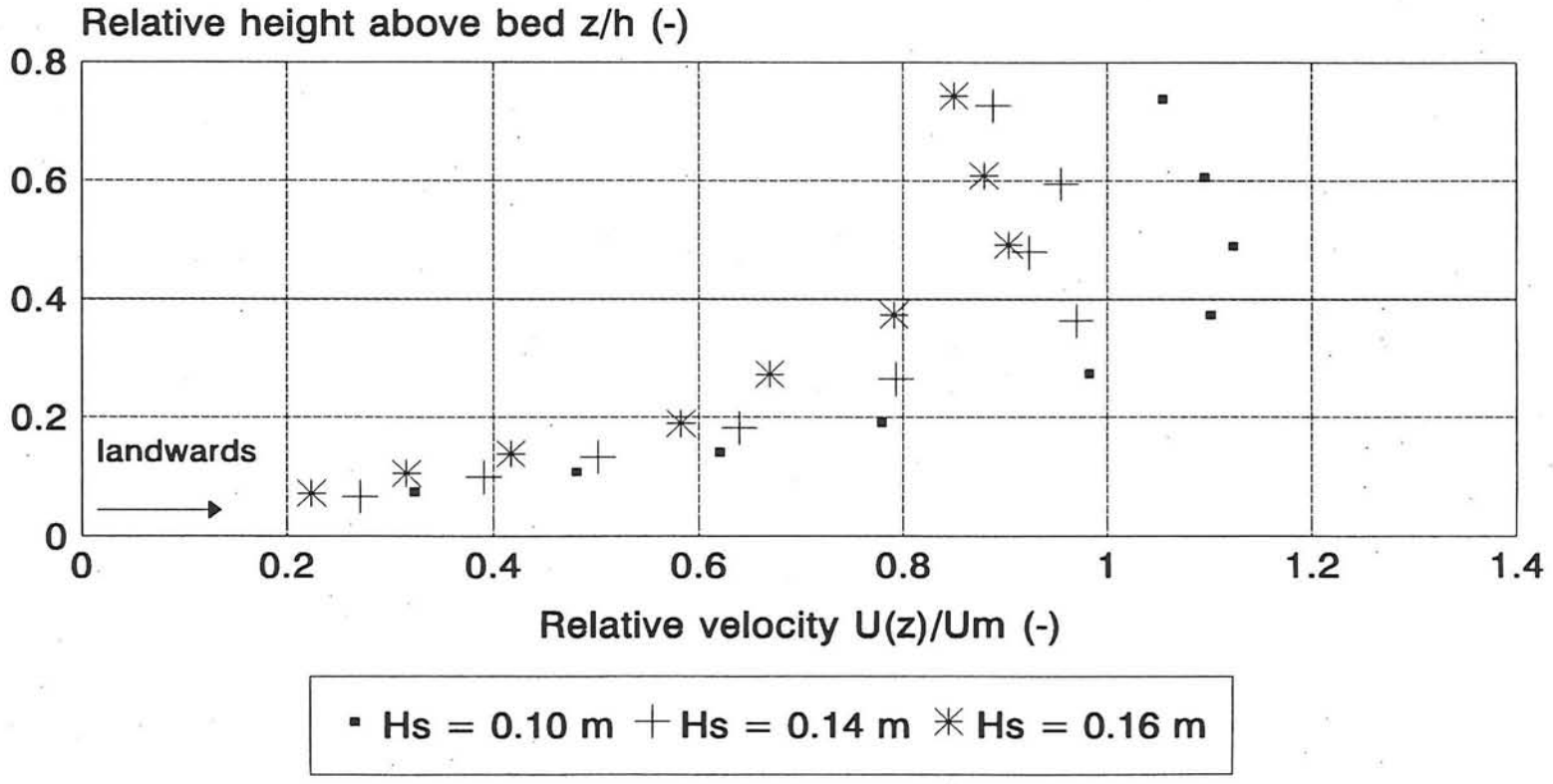

Figure 4.3.C

Velocity profile

Influence wave height
Um = 0.20 m/s

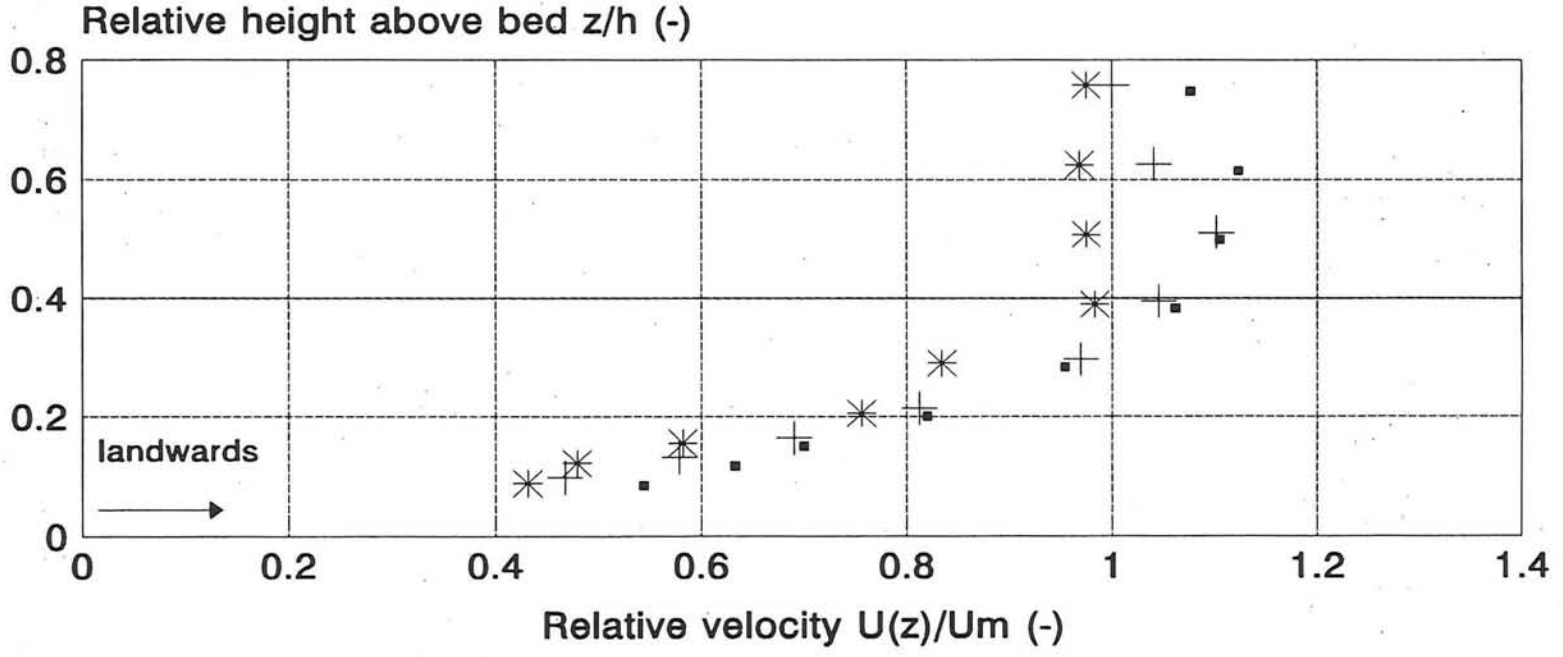

Figure 4.3.D

Return flow

Influence Hs/h

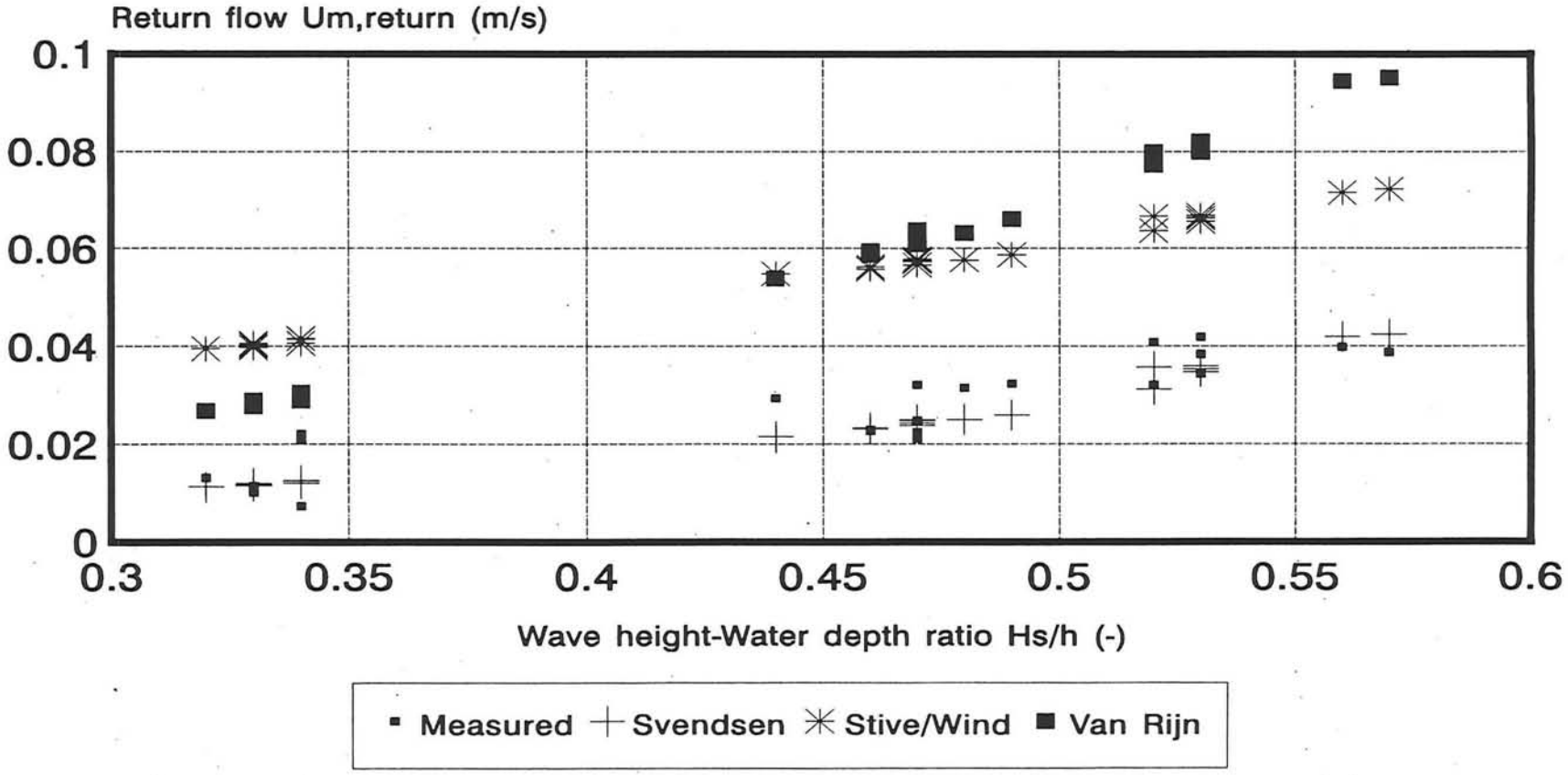

Figure 4.3.E

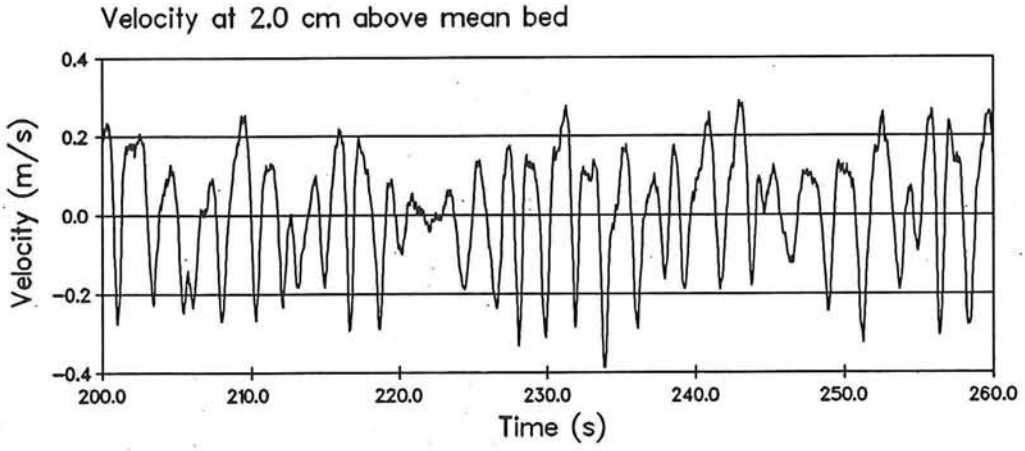

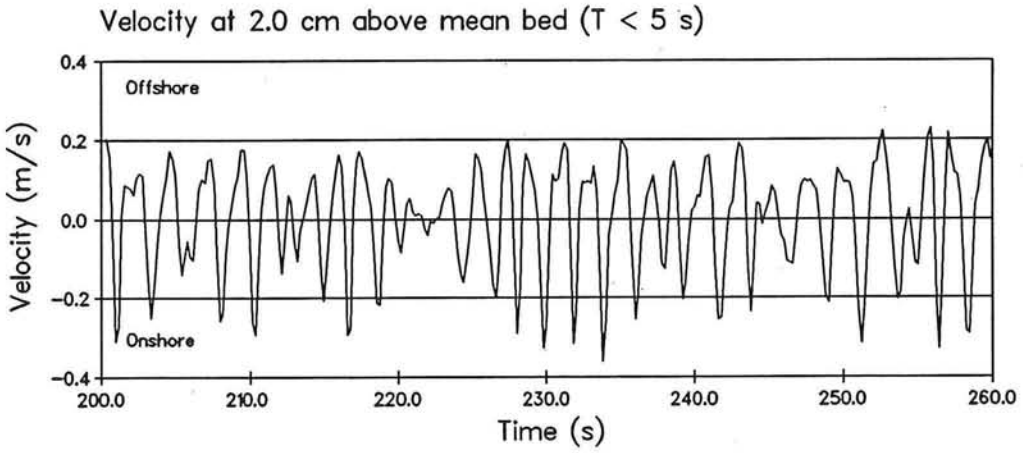

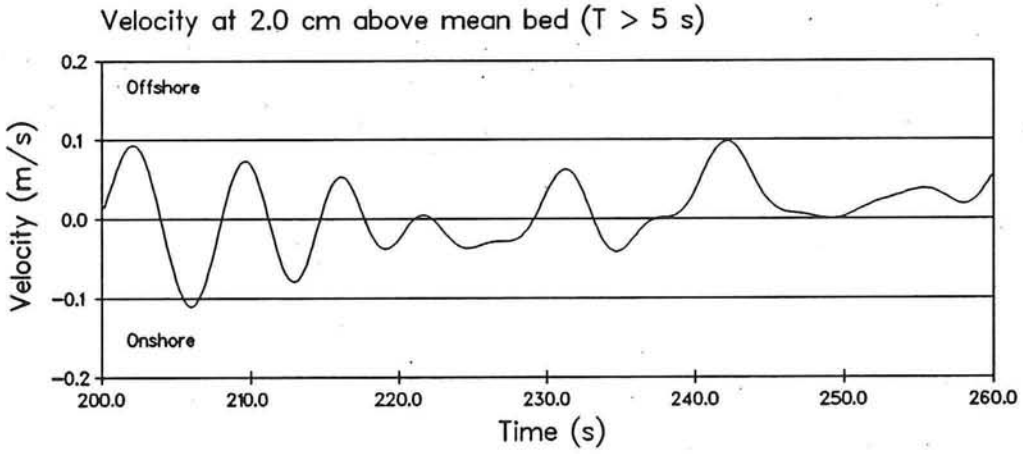

Time series (60 sec) of high– and low frequency velocities.	T 14 10 4	
DELFT HYDRAULICS		FIG. 4.4.A

Velocity asymmetry factor

Influence wave steepness

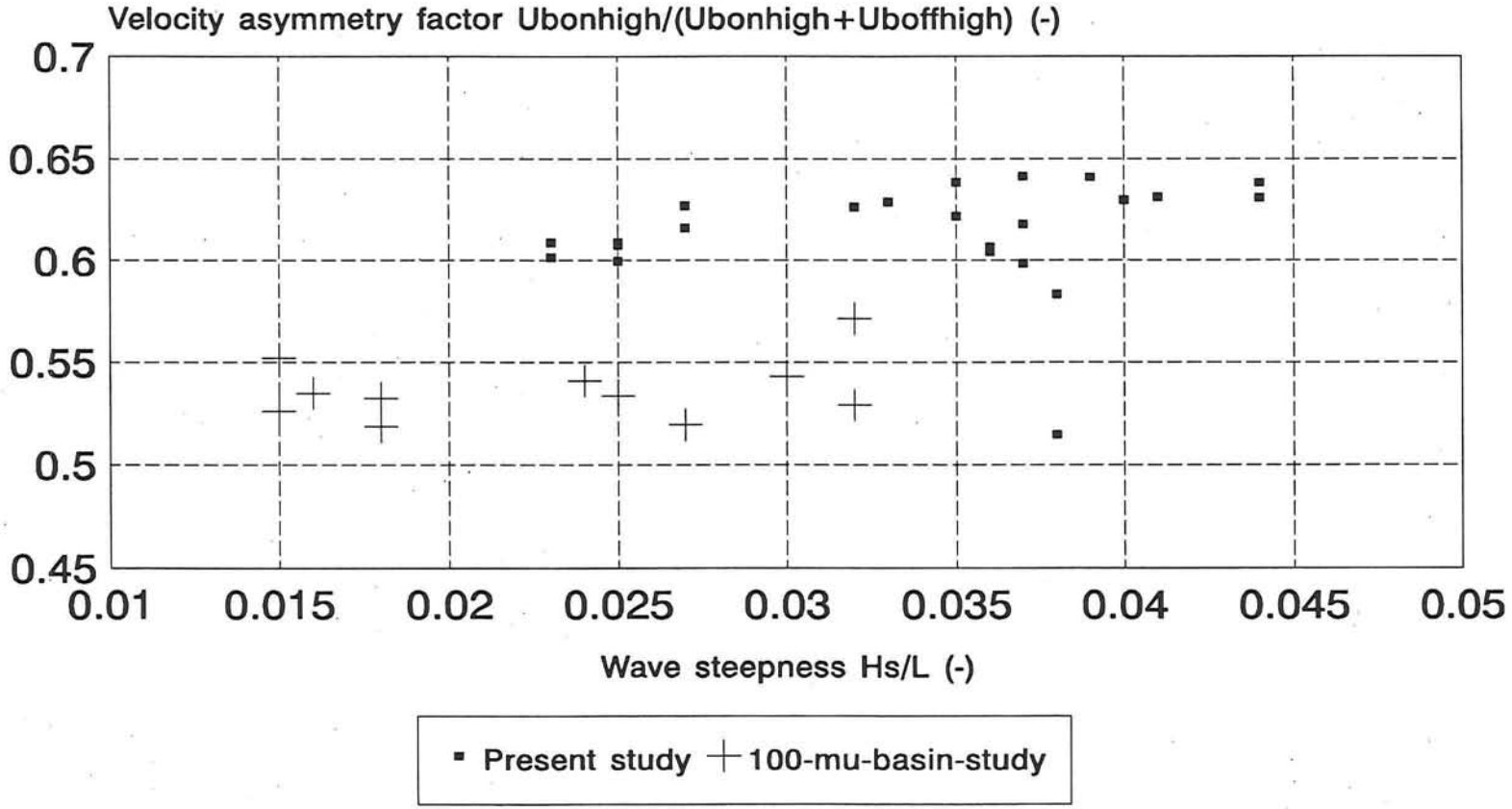

Figure 4.4.B

Velocity asymmetry factor

Influence Hs/h

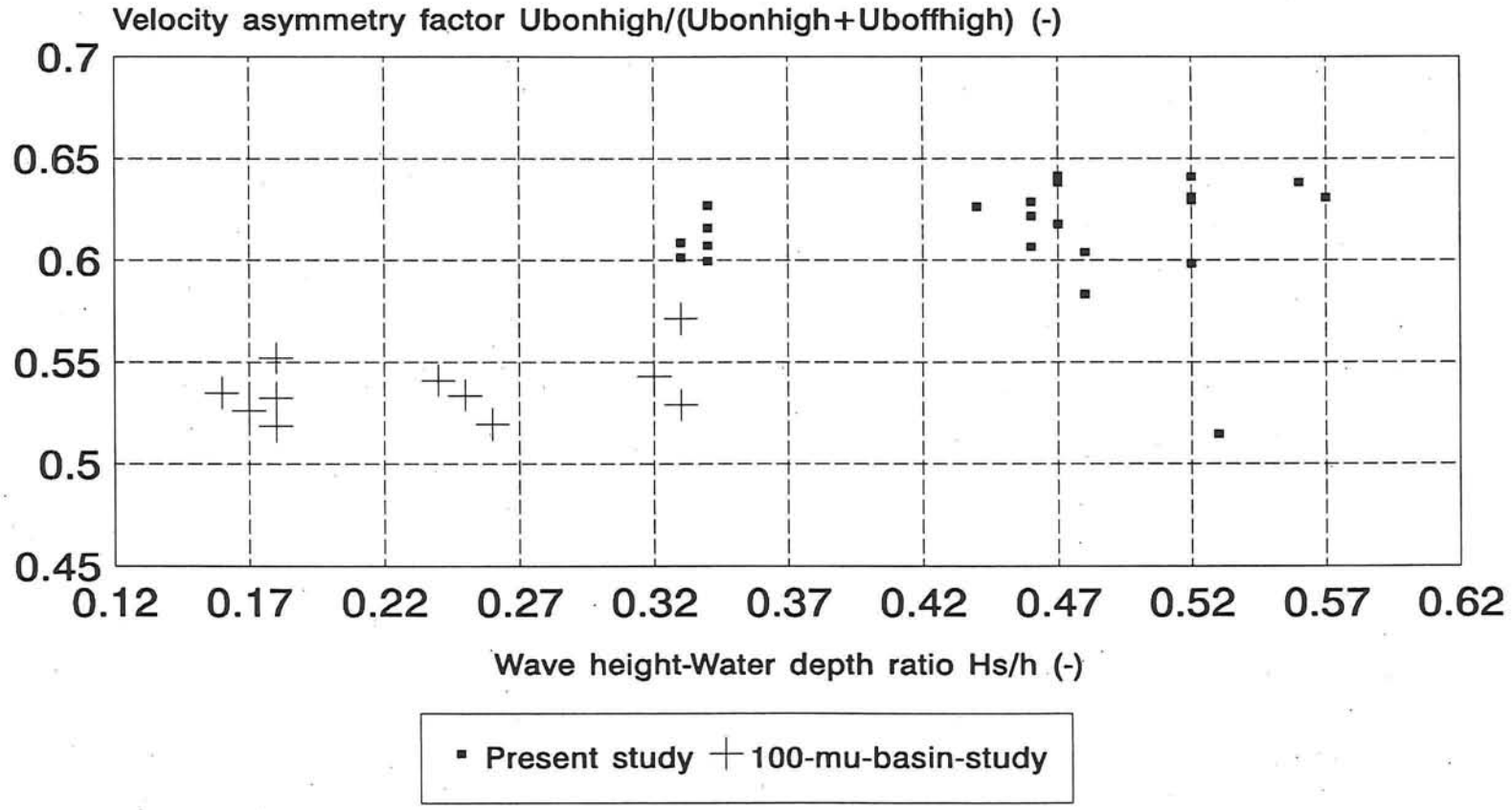

Figure 4.4.C

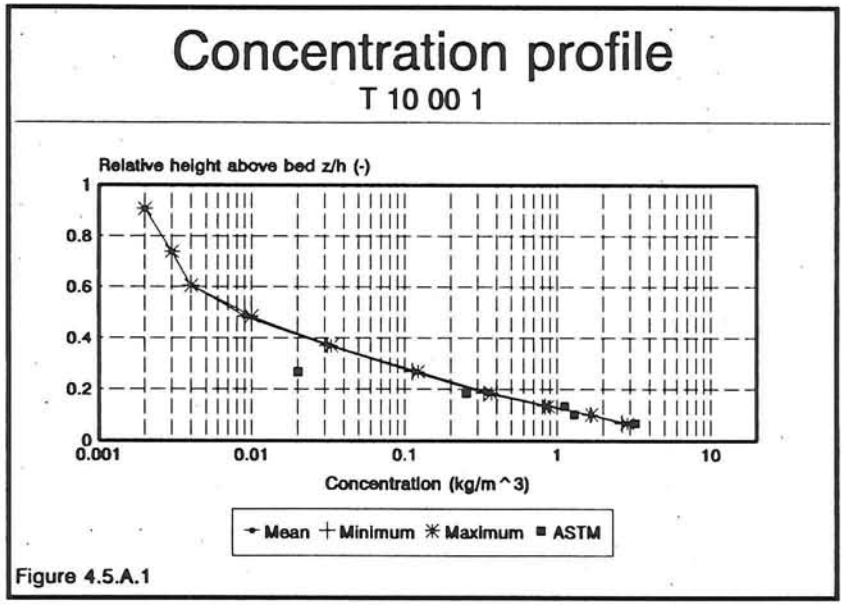

Figure 4.5.A.1

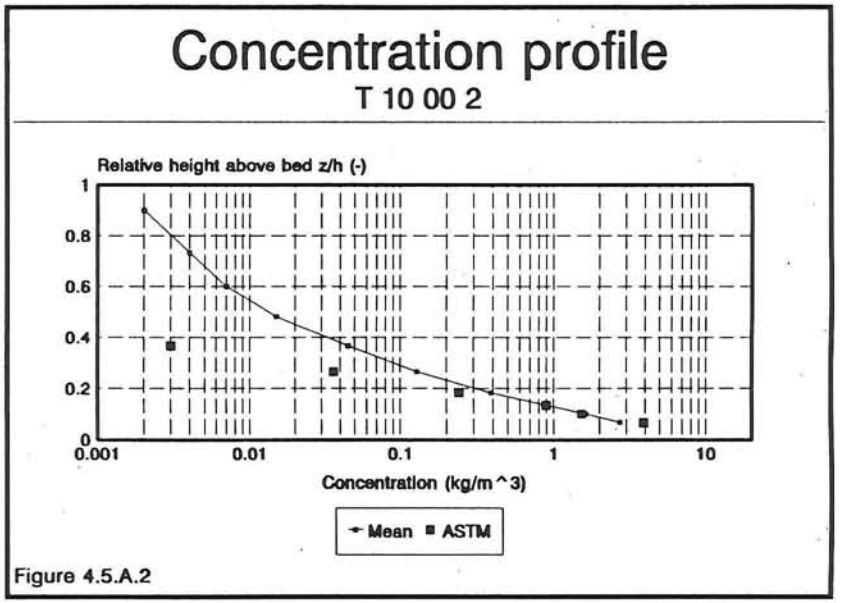

Figure 4.5.A.2

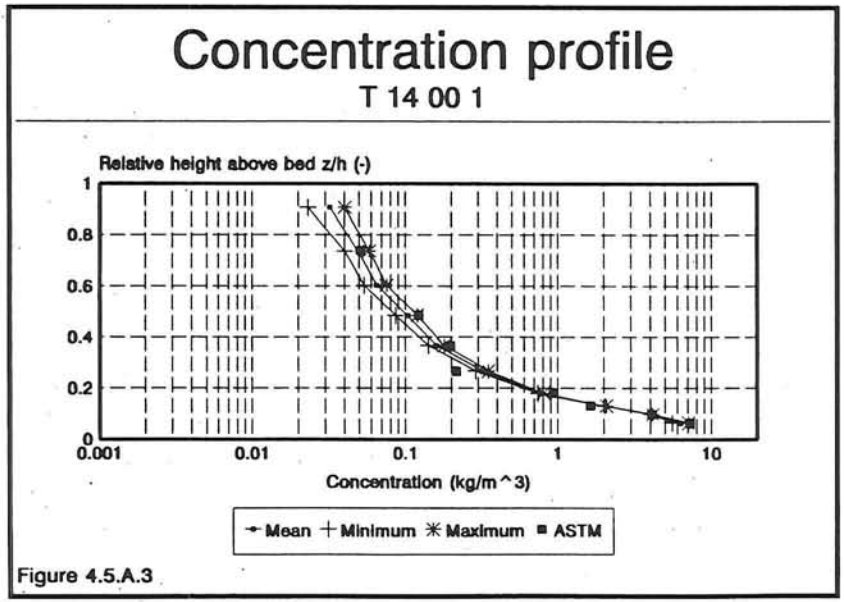

Figure 4.5.A.3

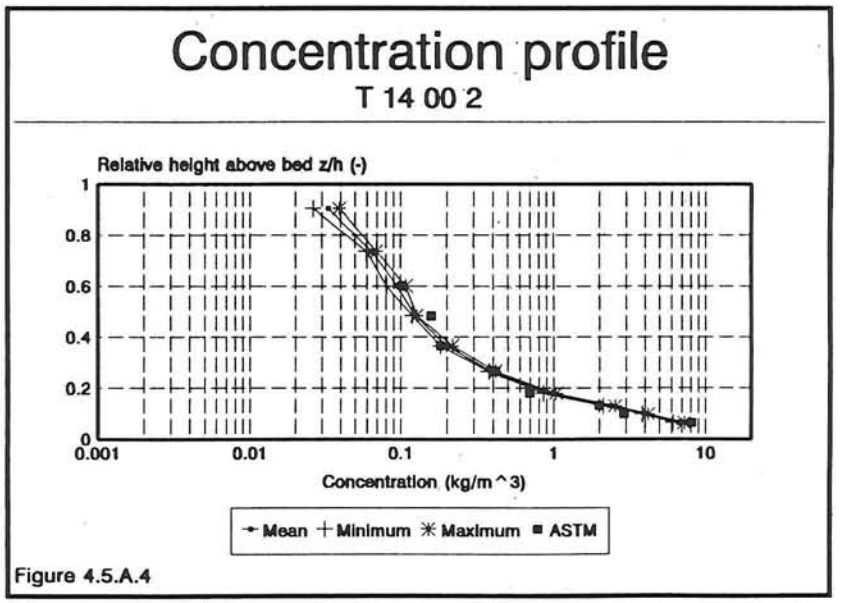

Figure 4.5.A.4

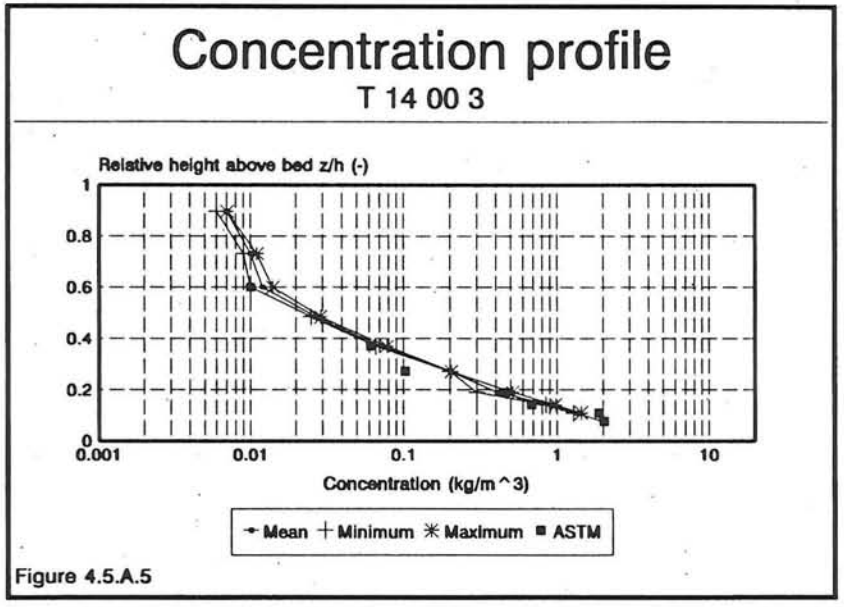

Figure 4.5.A.5

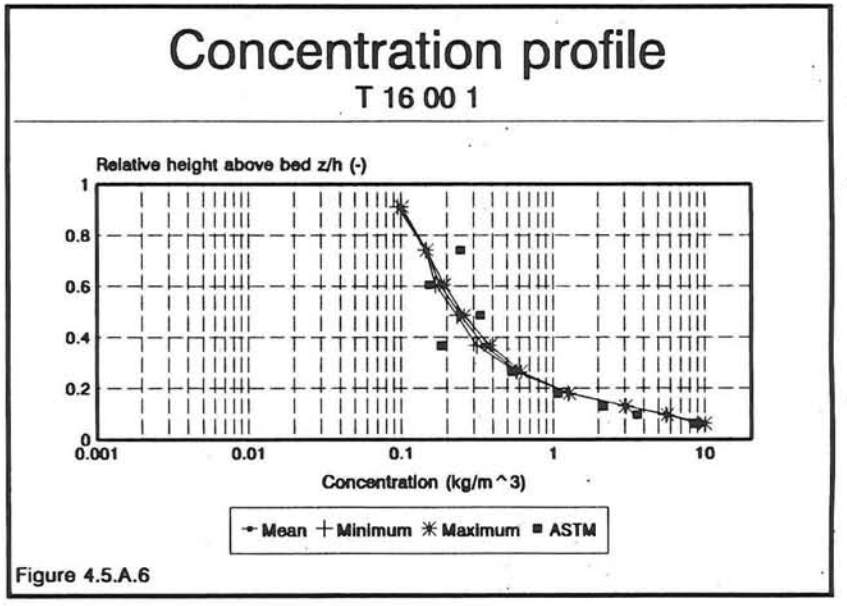

Figure 4.5.A.6

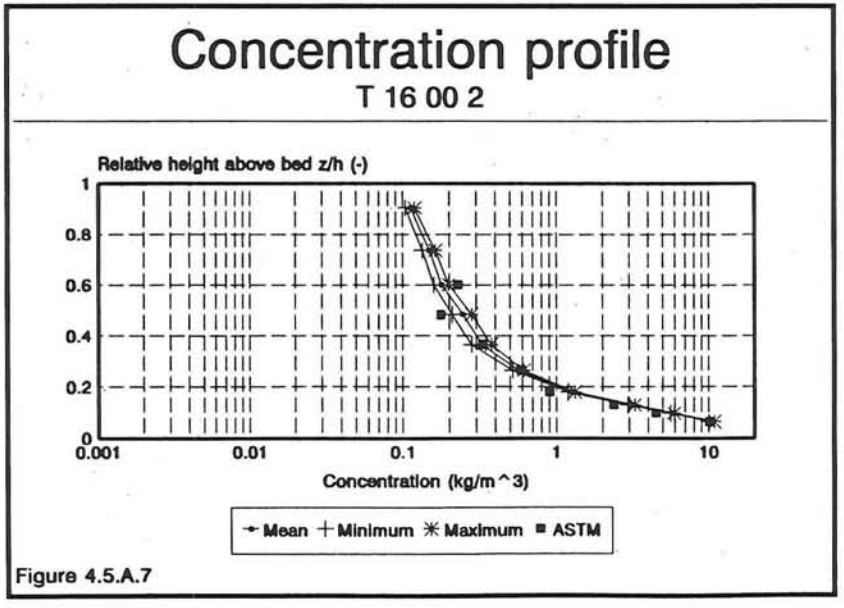

Figure 4.5.A.7

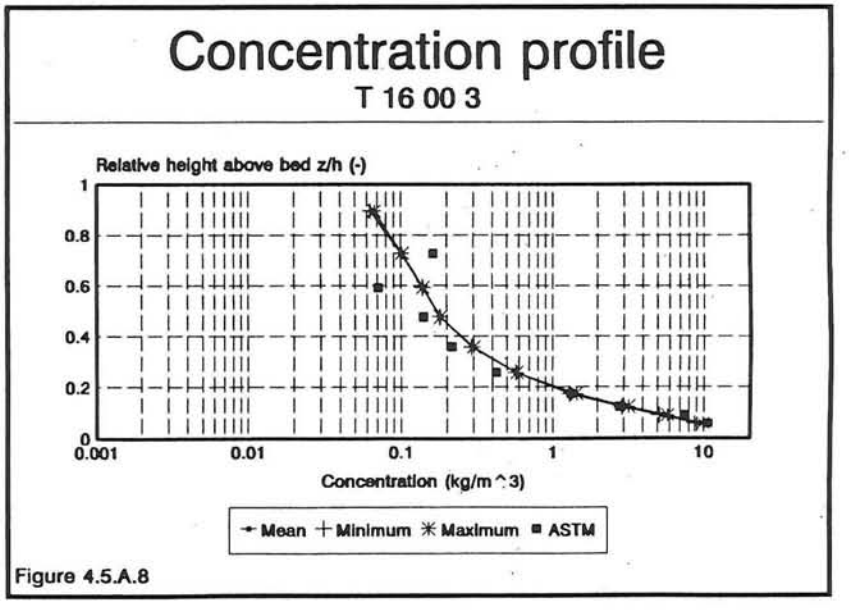

Figure 4.5.A.8

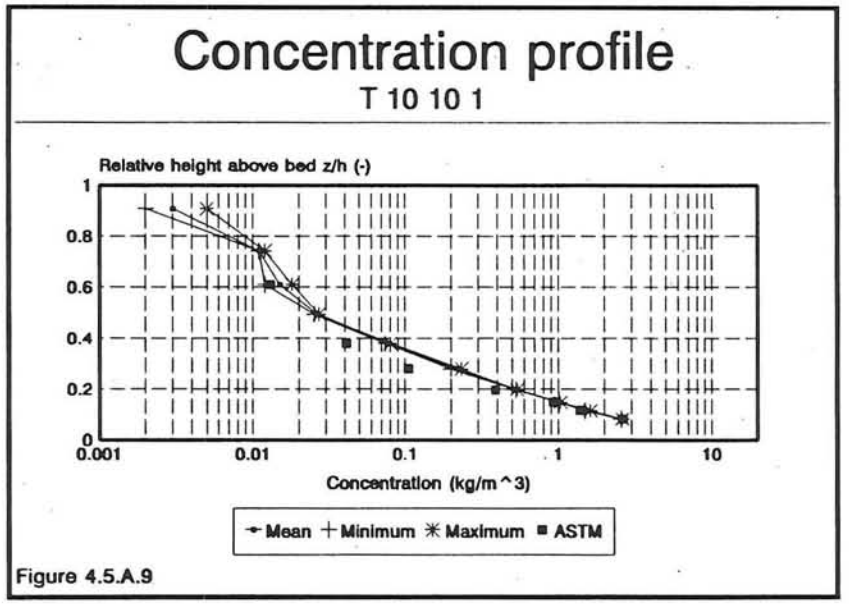

Figure 4.5.A.9

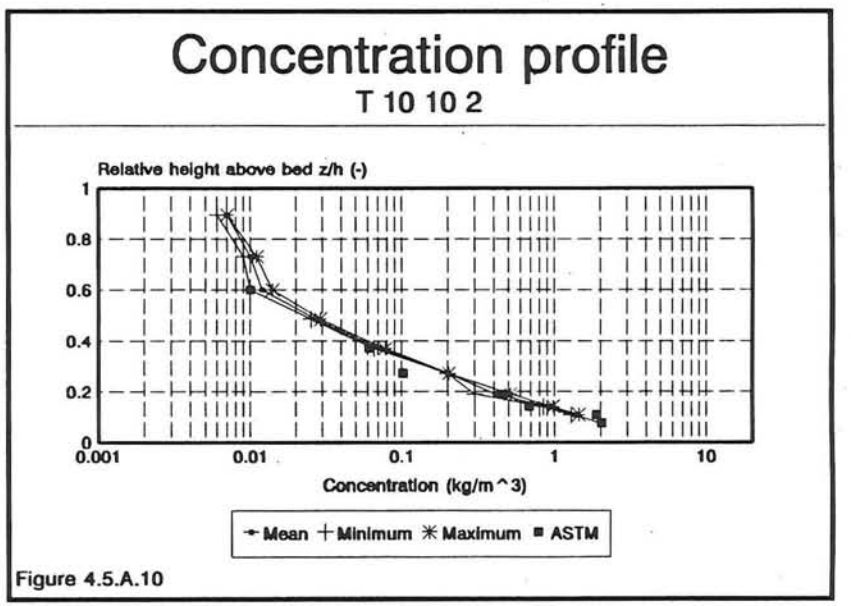

Figure 4.5.A.10

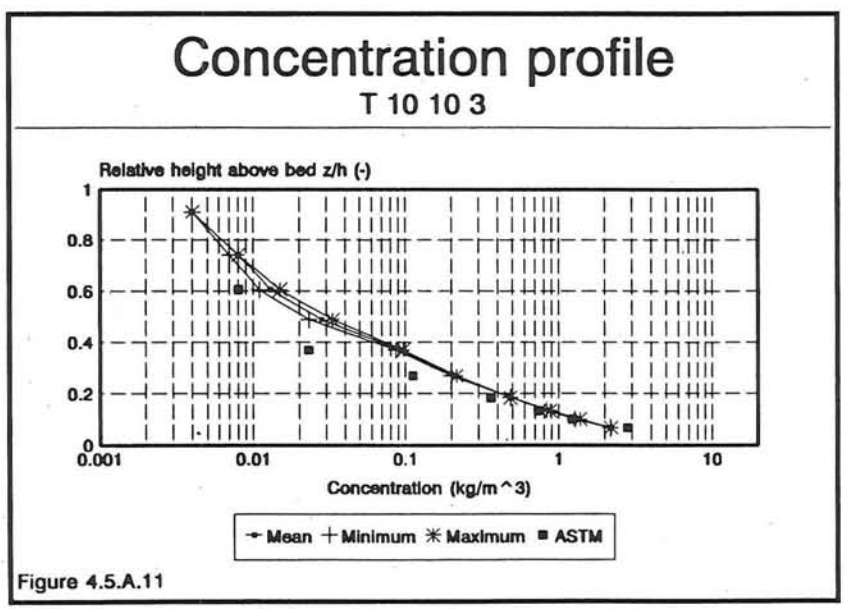

Figure 4.5.A.11

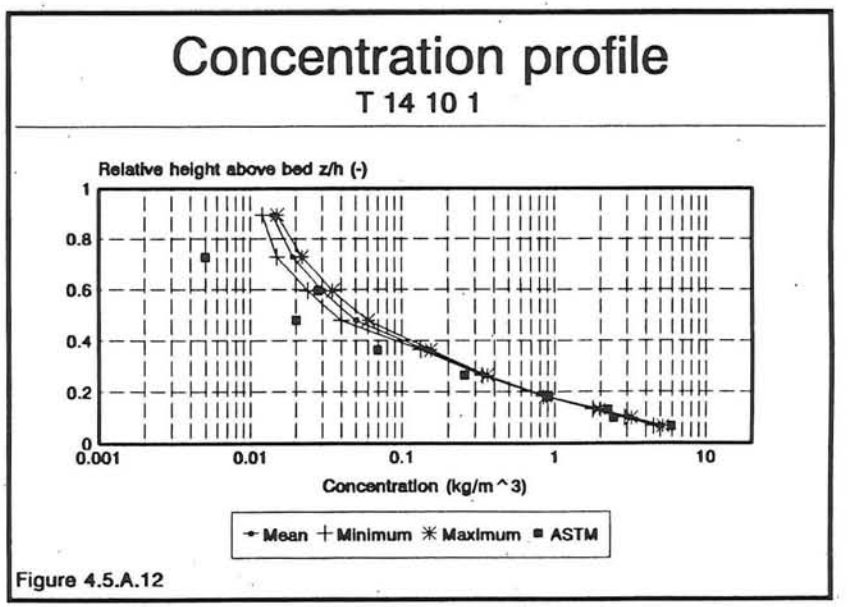

Figure 4.5.A.12

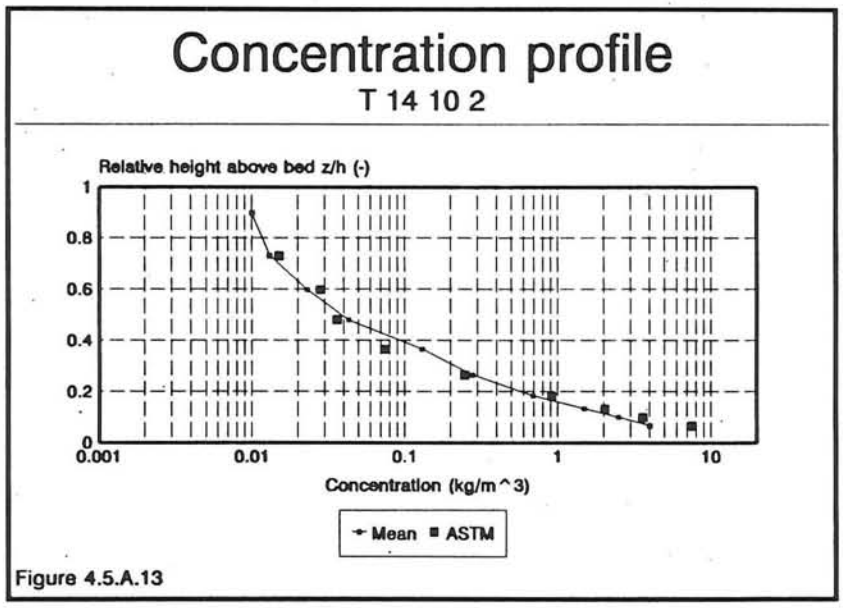

Figure 4.5.A.13

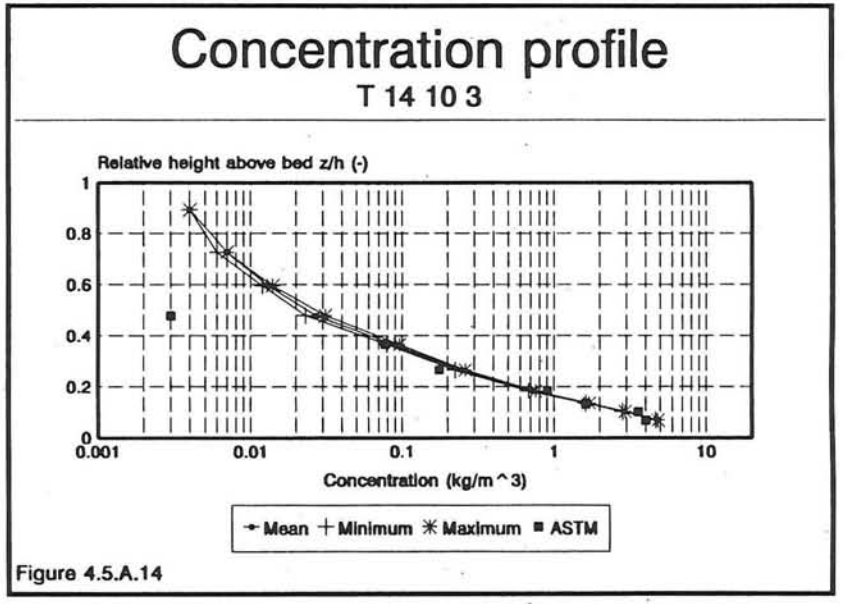

Figure 4.5.A.14

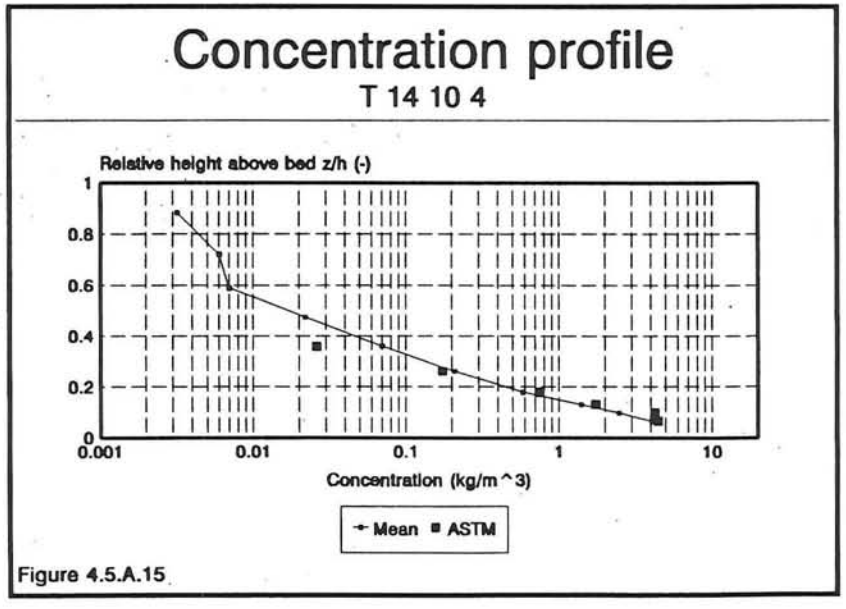

Figure 4.5.A.15

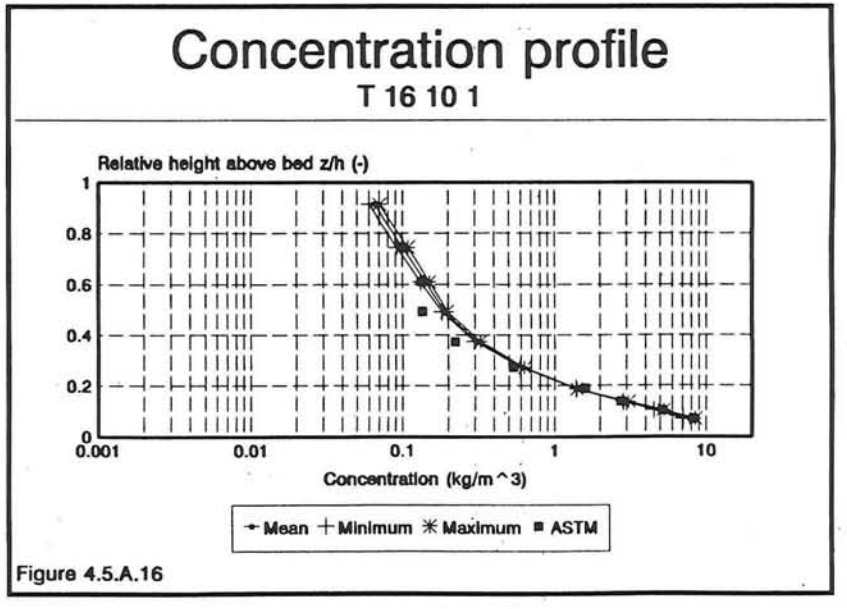

Figure 4.5.A.16

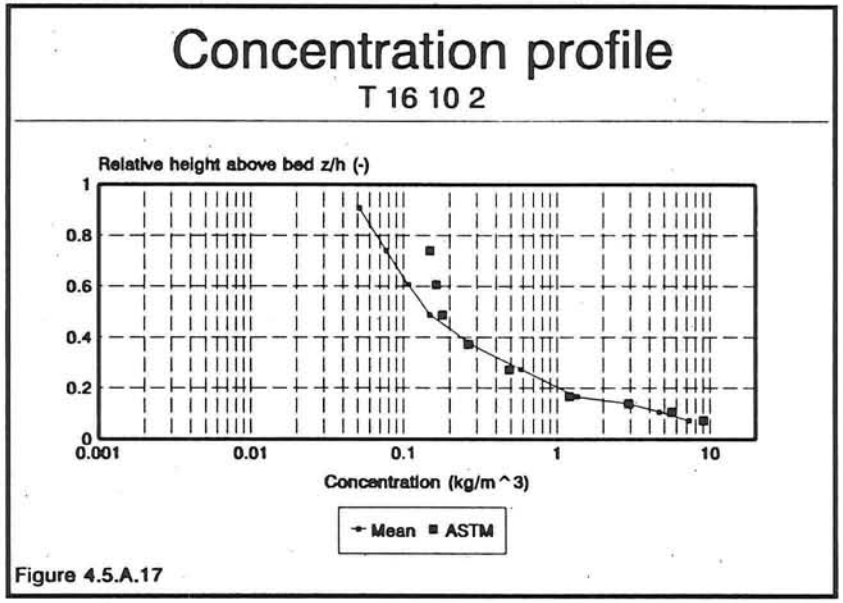

Figure 4.5.A.17

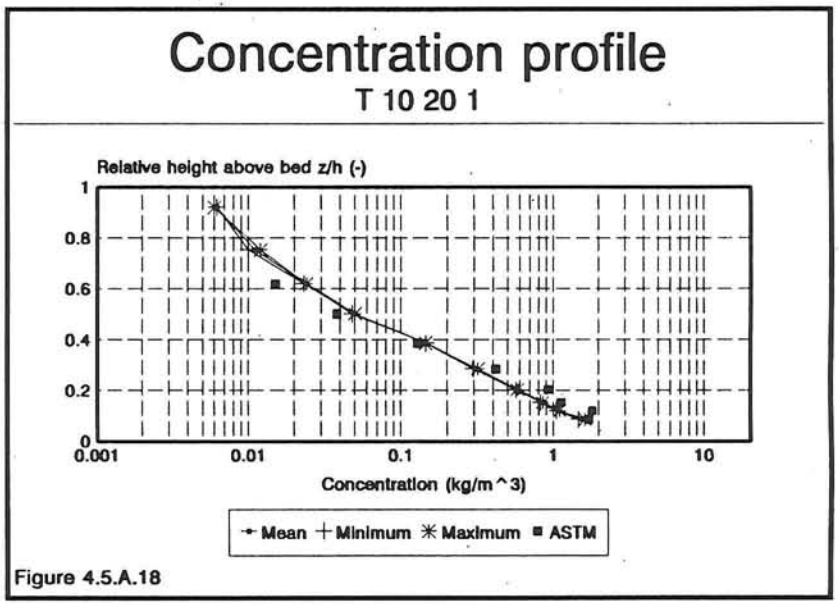

Figure 4.5.A.18

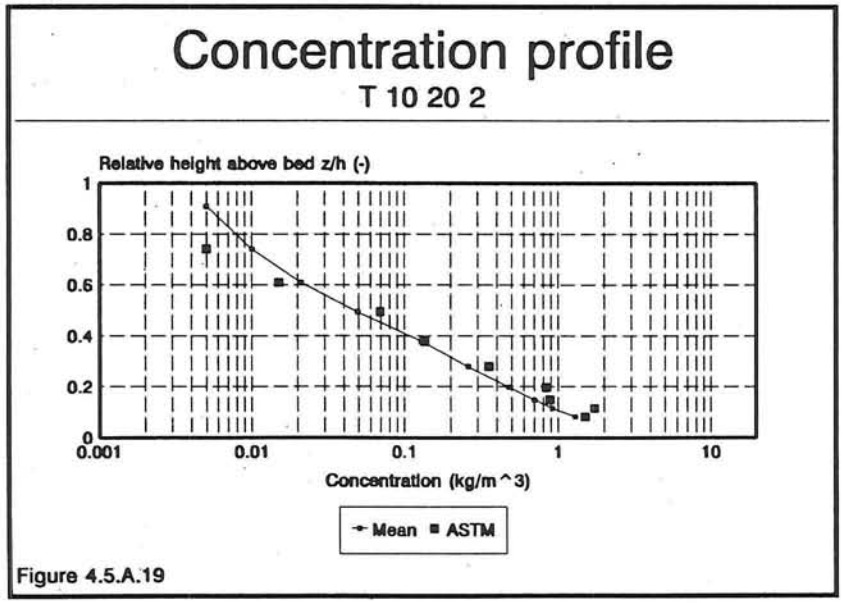

Figure 4.5.A.19

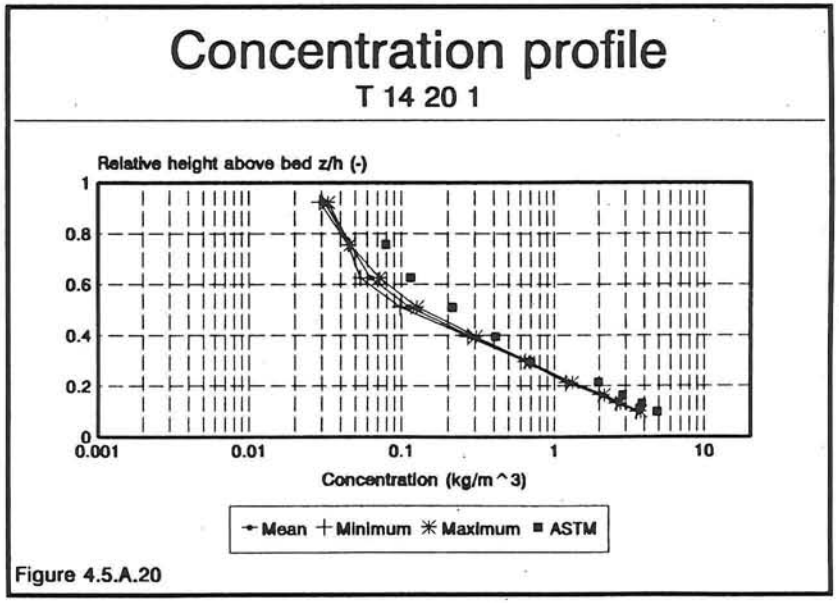

Figure 4.5.A.20

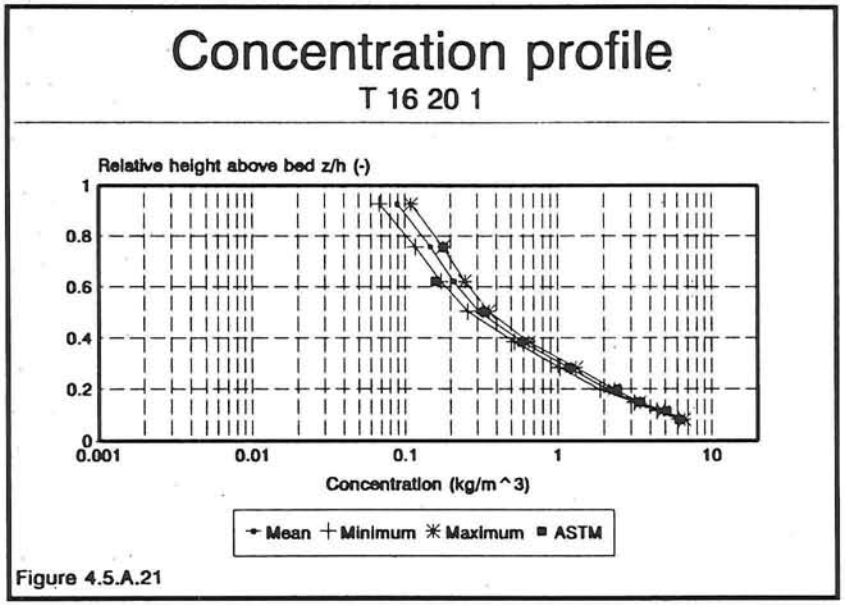

Figure 4.5.A.21

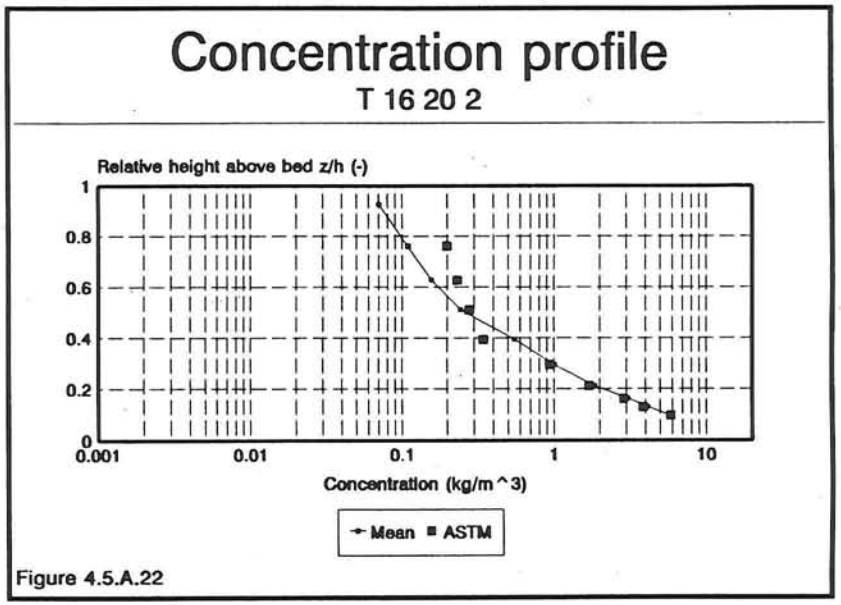

Figure 4.5.A.22

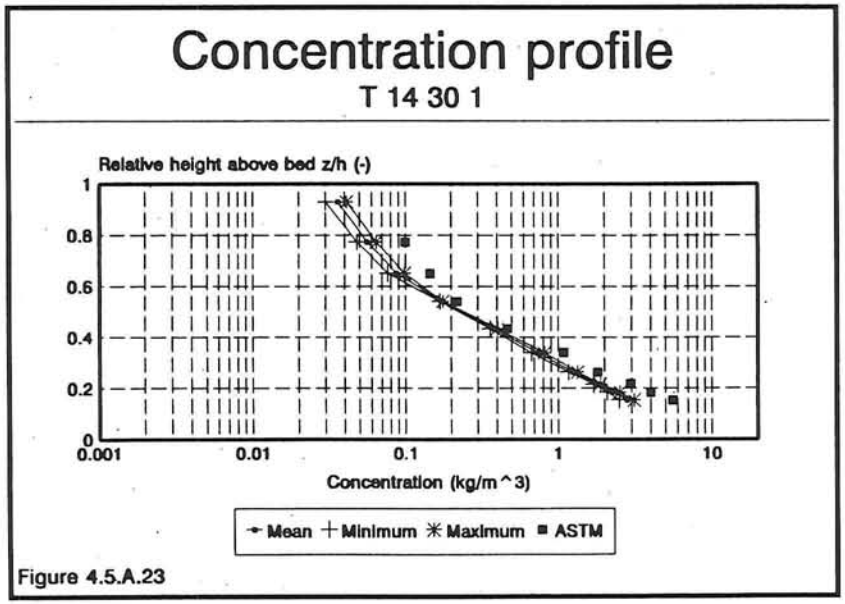

Figure 4.5.A.23

Concentration profile

Influence wave height
Um = 0.0 m/s

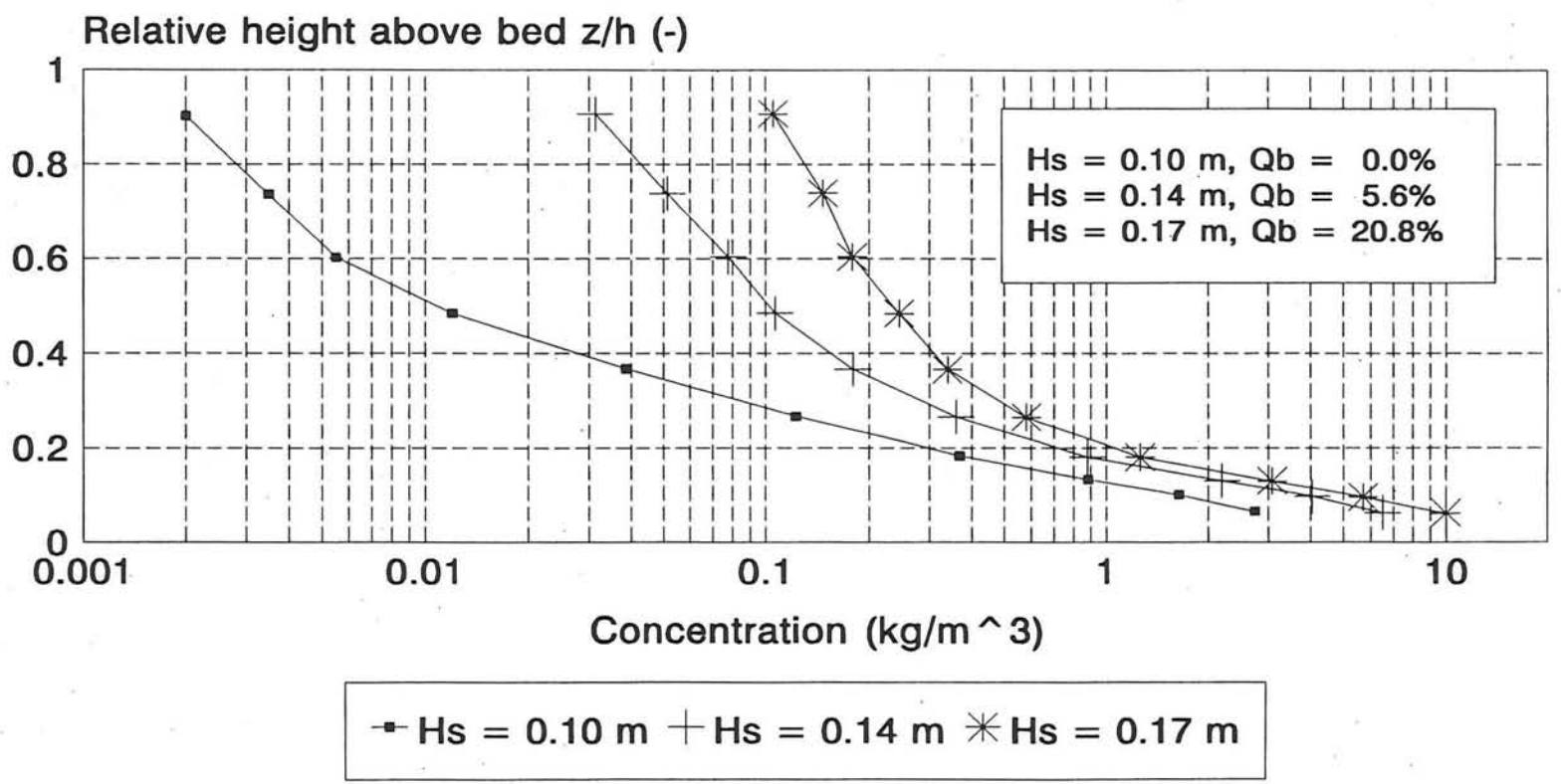

Figure 4.5.B

Concentration profile

Influence wave height
Um = 0.10 m/s

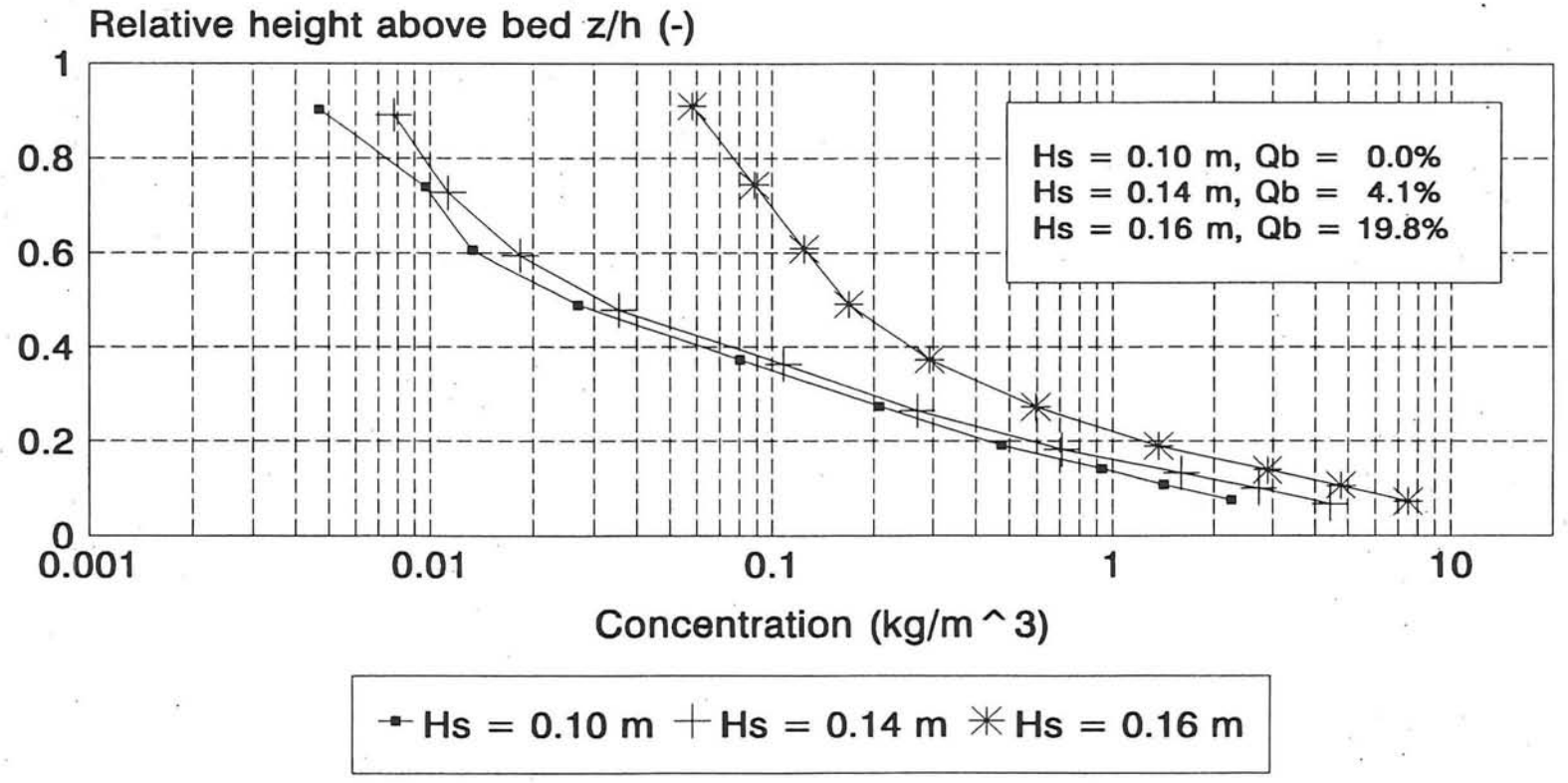

Figure 4.5.C

Concentration profile

Influence wave height
Um = 0.20 m/s

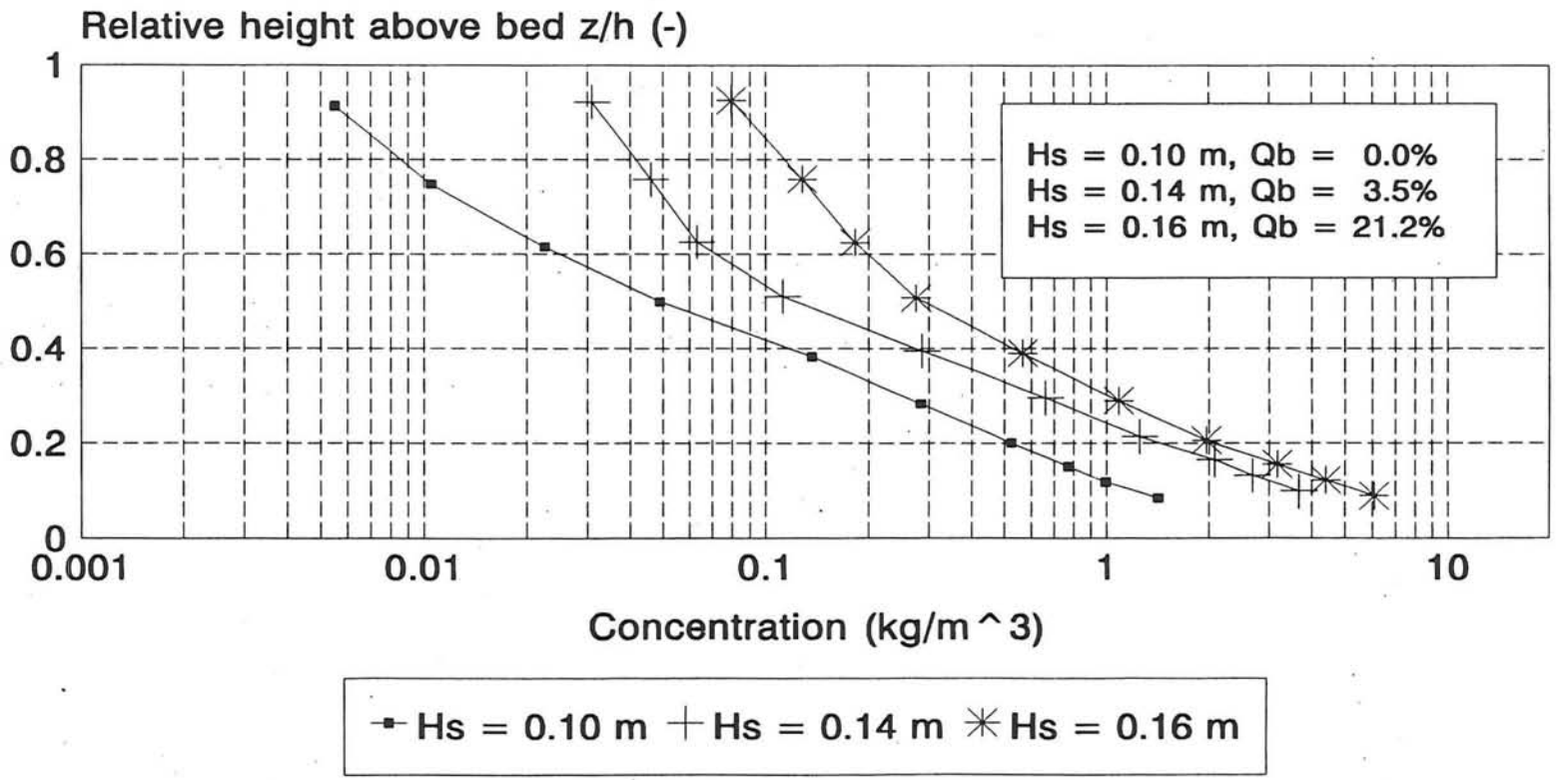

Figure 4.5.D

Concentration profile

Influence current strength
Hs = 0.10 m

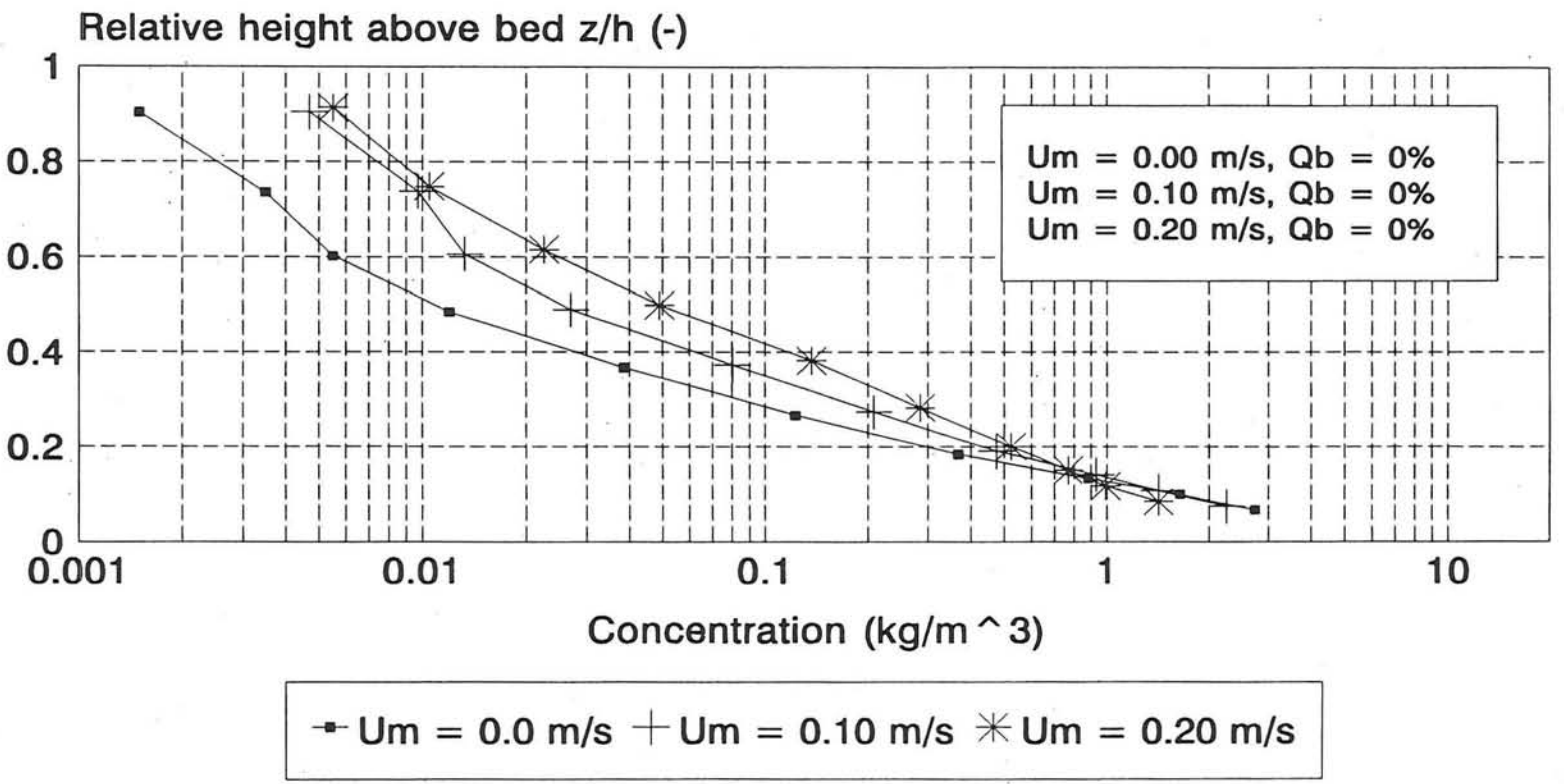

Figure 4.5.E

Concentration profile

Influence current strength
Hs = 0.14 m

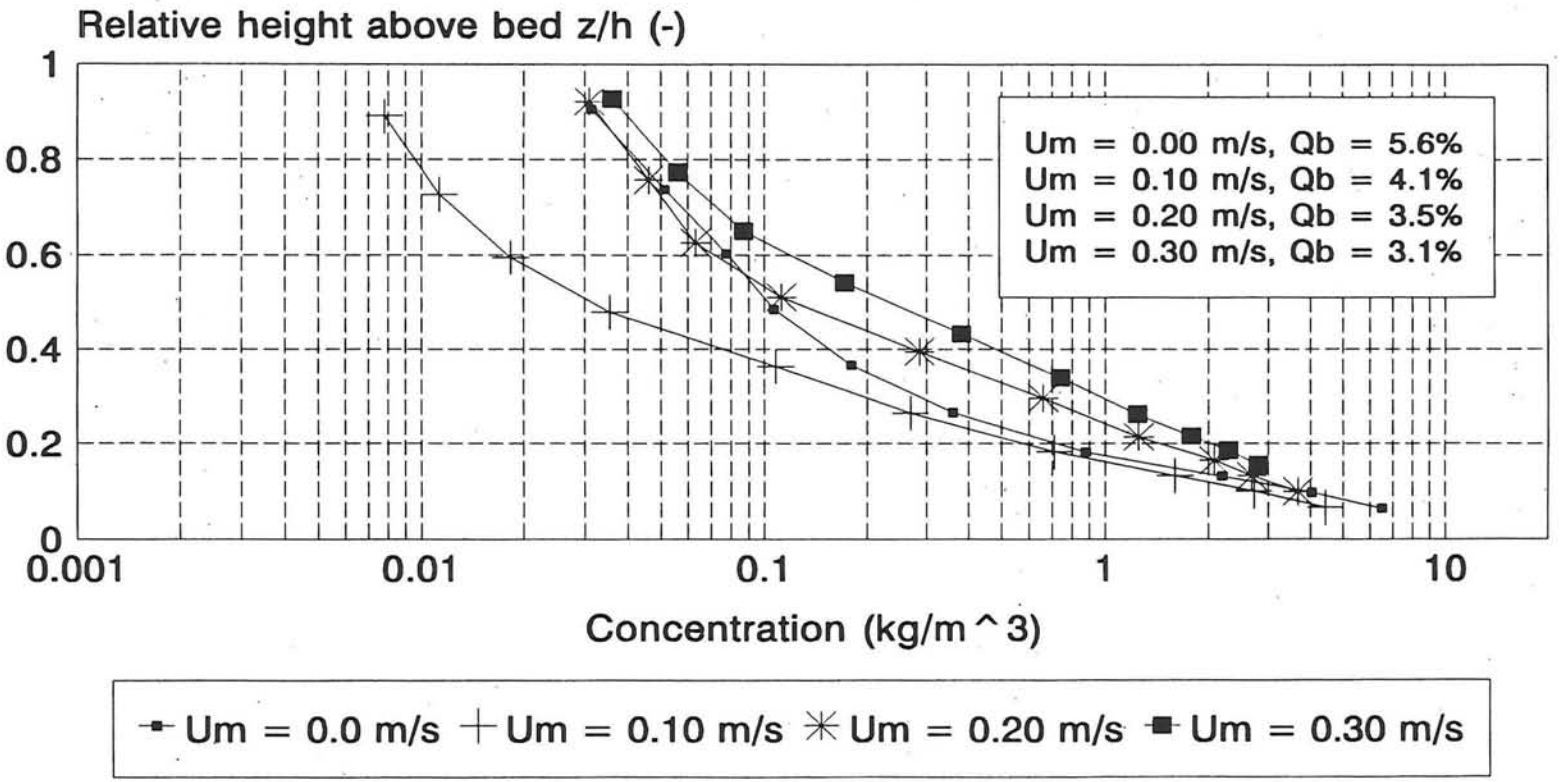

Figure 4.5.F

Concentration profile

Influence current strength
Hs = 0.16 m

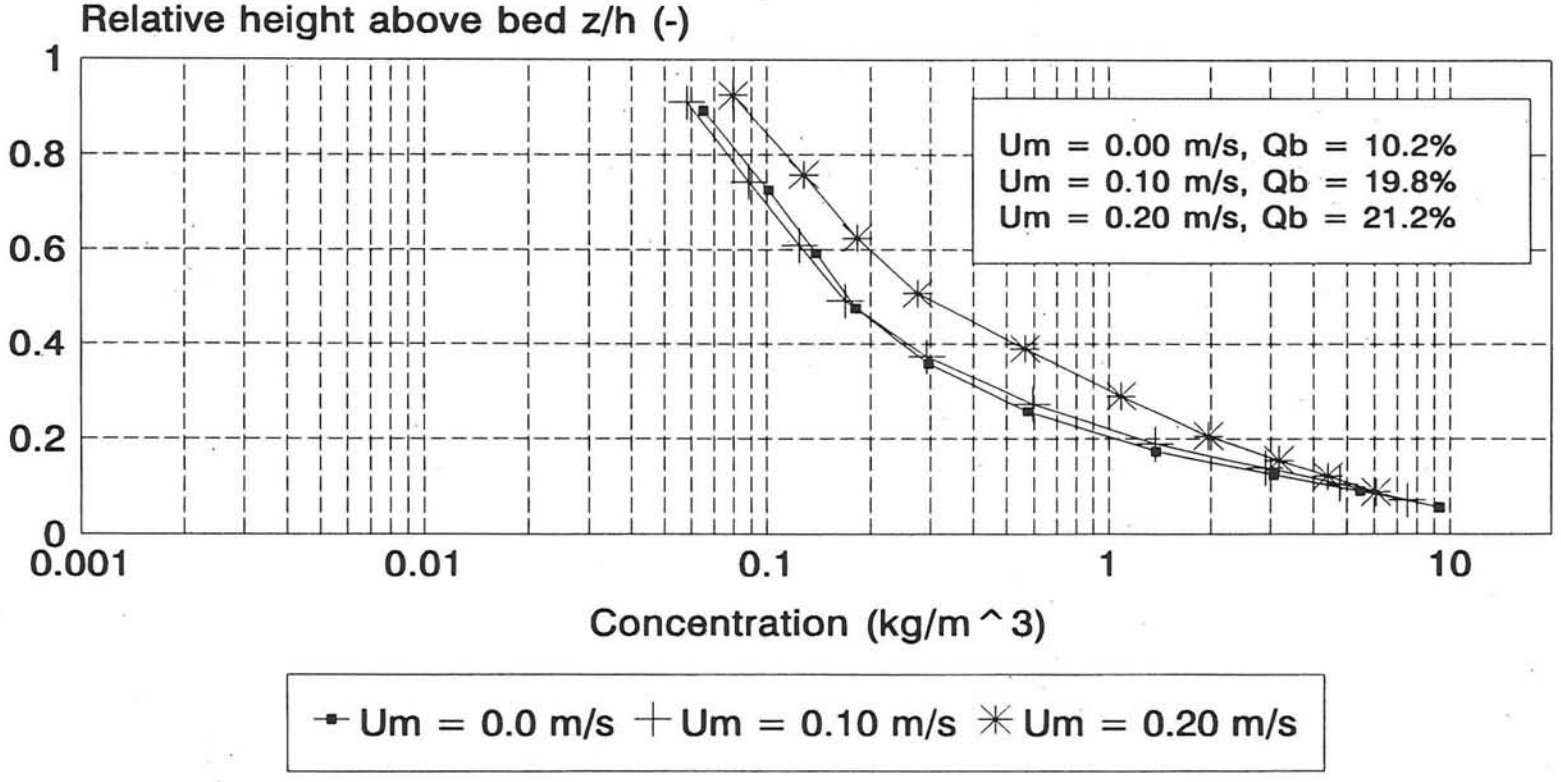

Figure 4.5.G

Suspended Load

Influence wave height

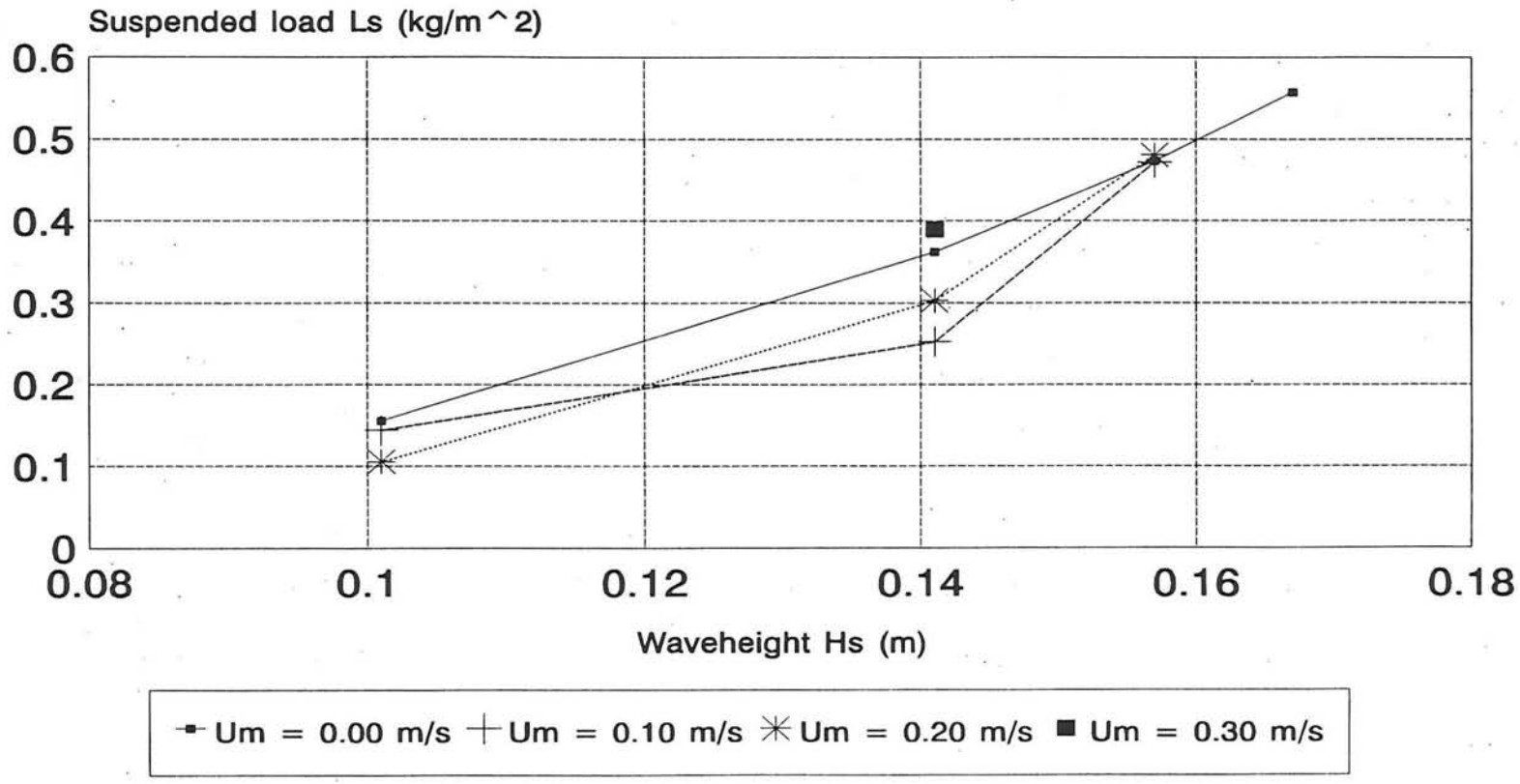

Figure 4.6.A

Suspended Load

Influence current strength

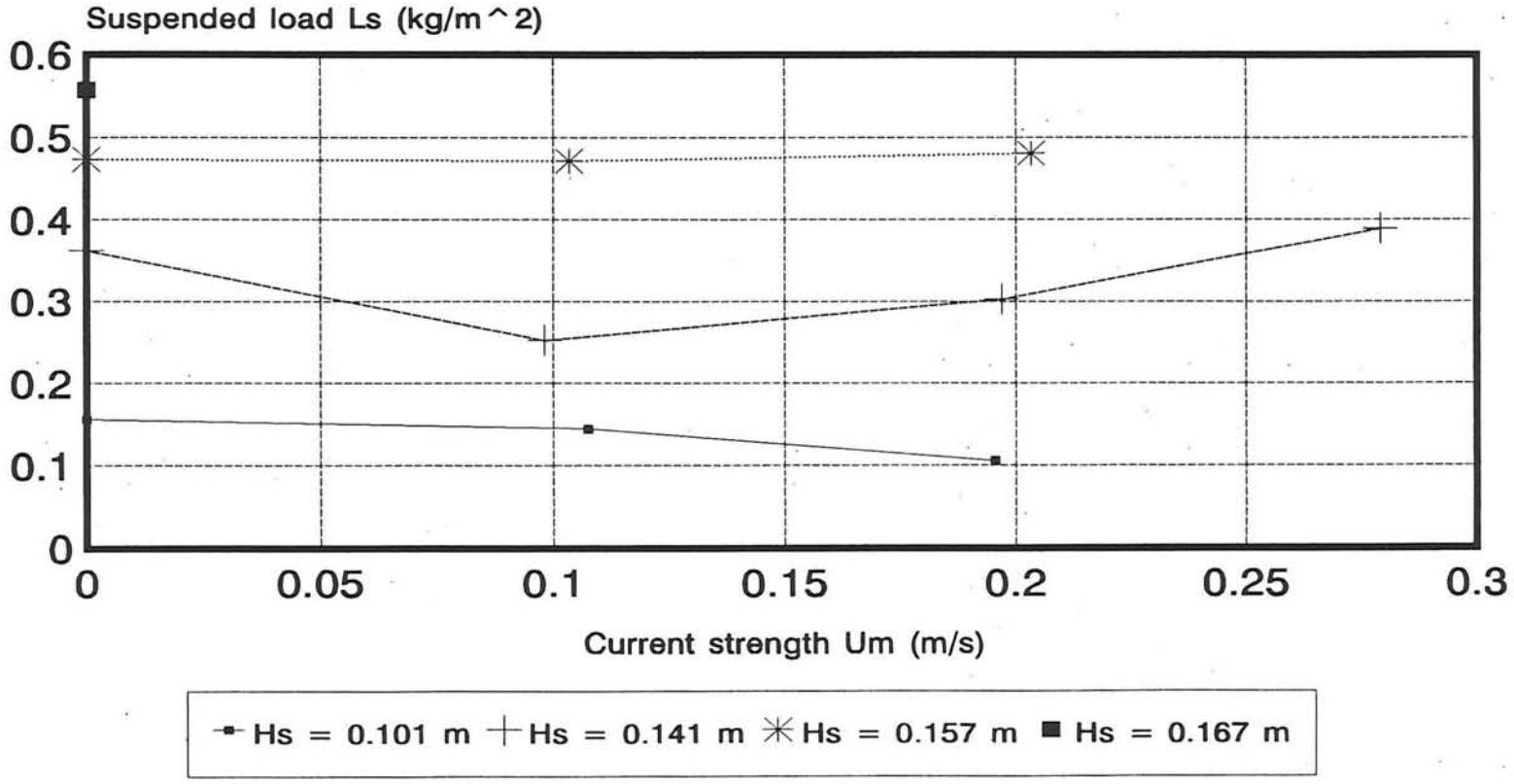

Figure 4.6.B

Suspended Load

Influence breaker index

Um = 0.0 m/s

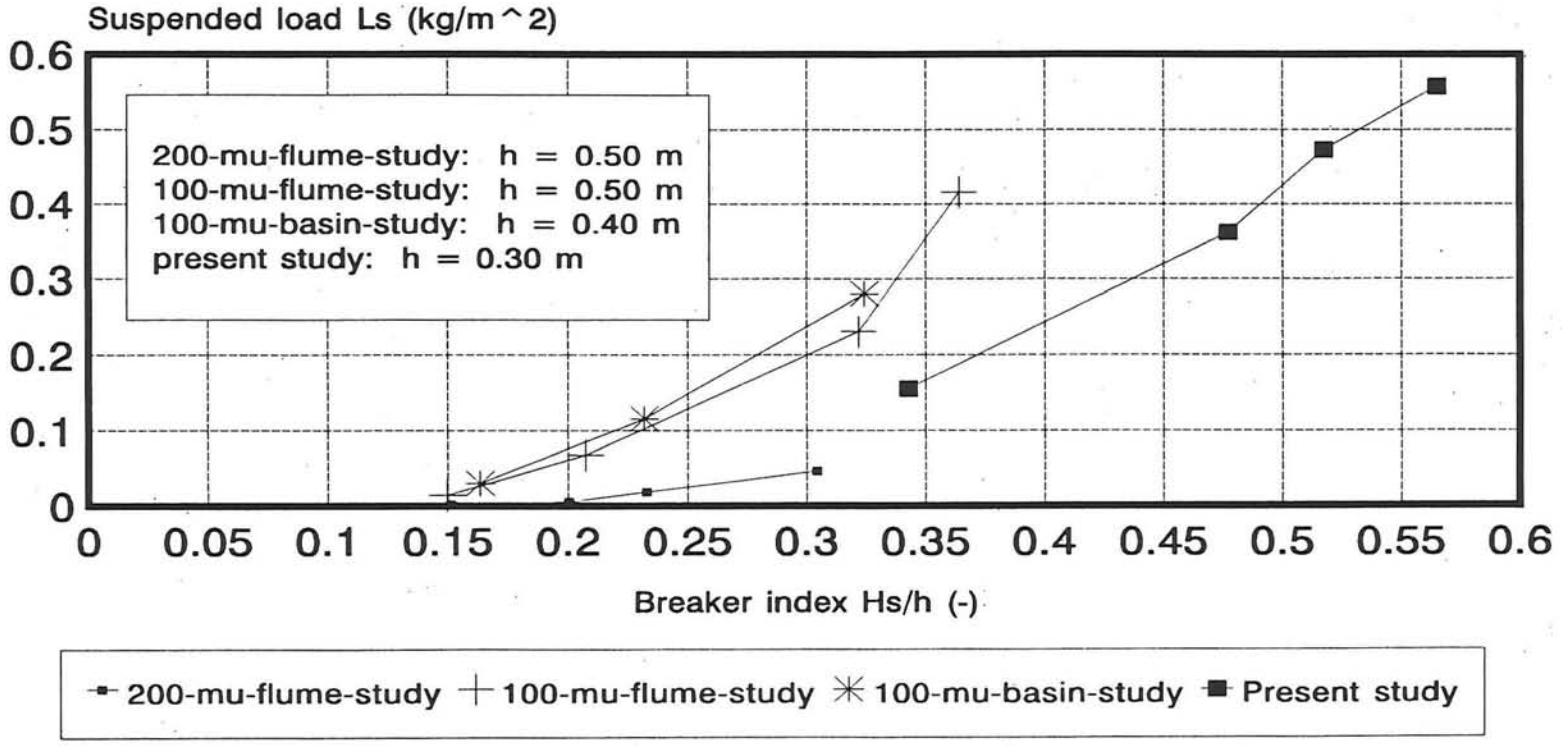

Figure 4.6.C

Suspended Load

Influence breaker index
Um = 0.10 m/s

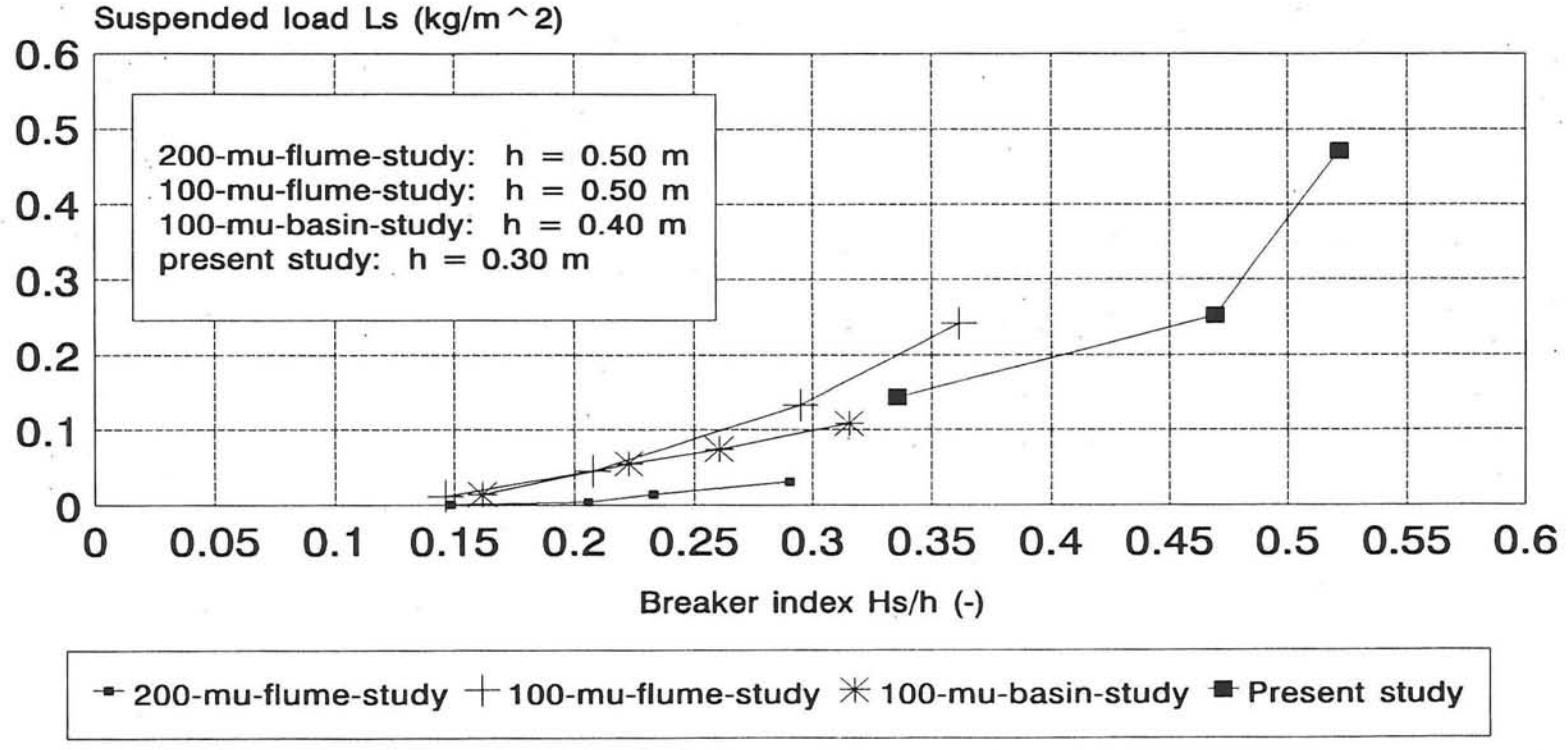

Figure 4.6.D

Suspended Load

Influence breaker index
Um = 0.20 m/s

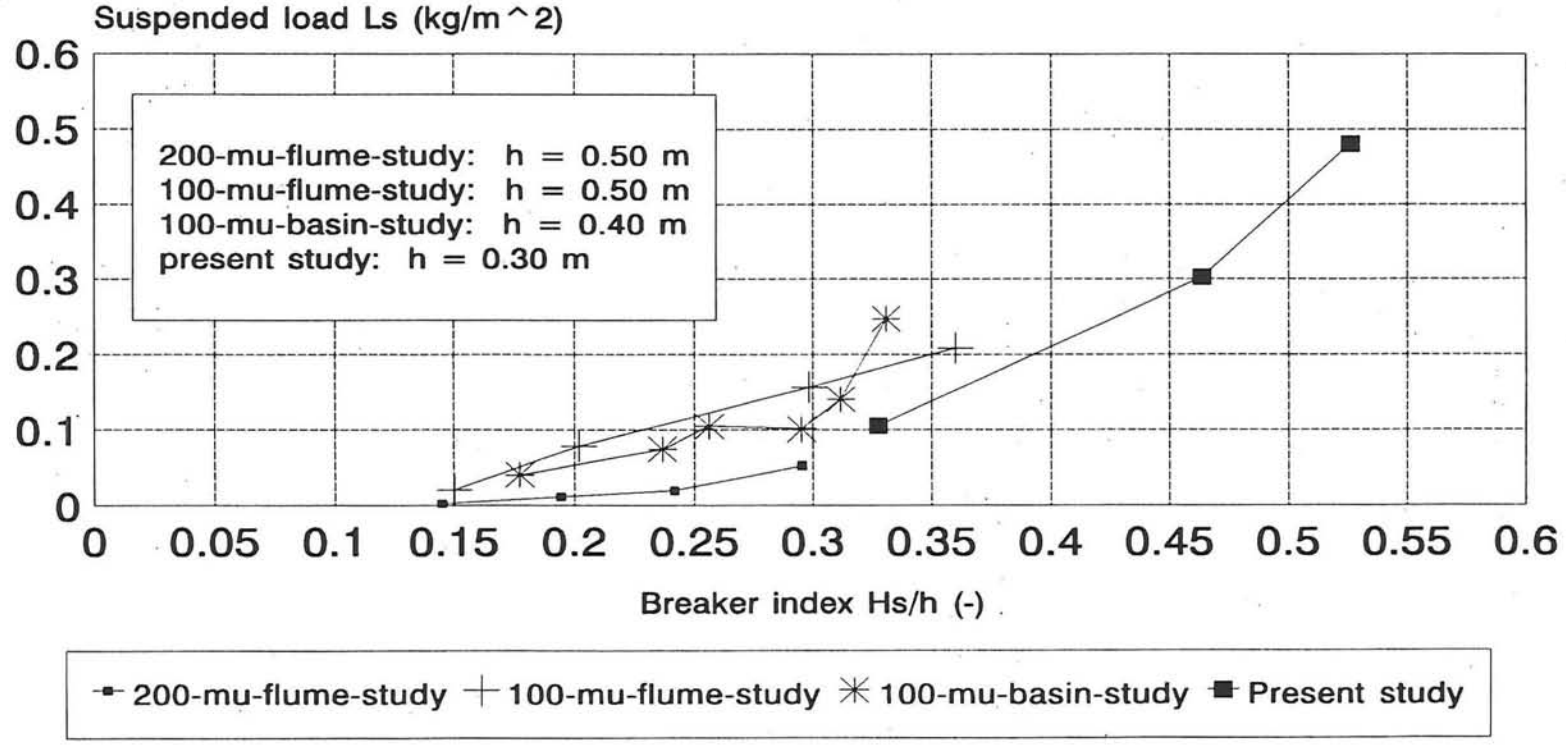

Figure 4.6.E

Suspended Load

Influence Ub,on,tot

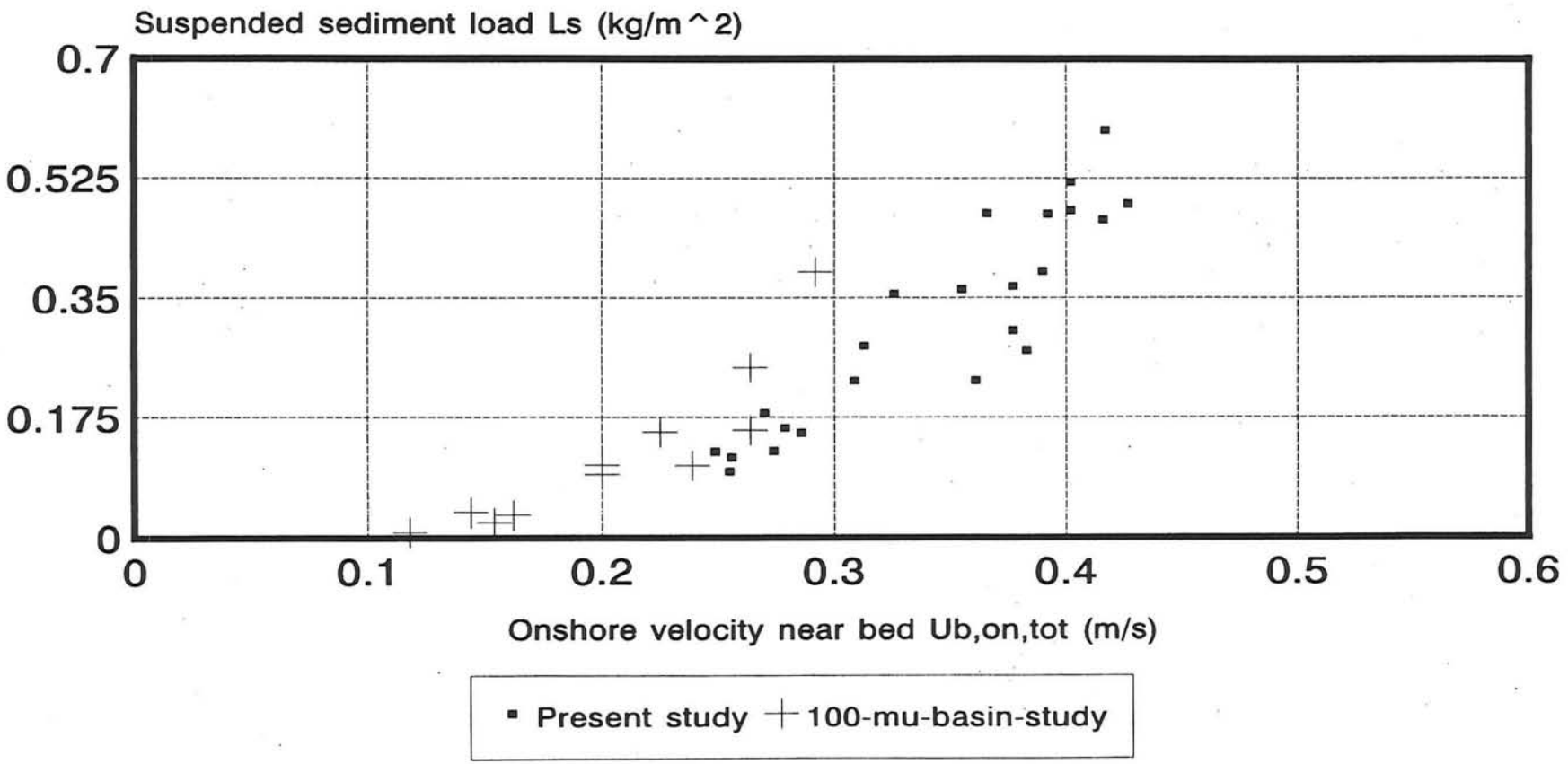

Figure 4.6.F

Suspended Transport

Influence current strength

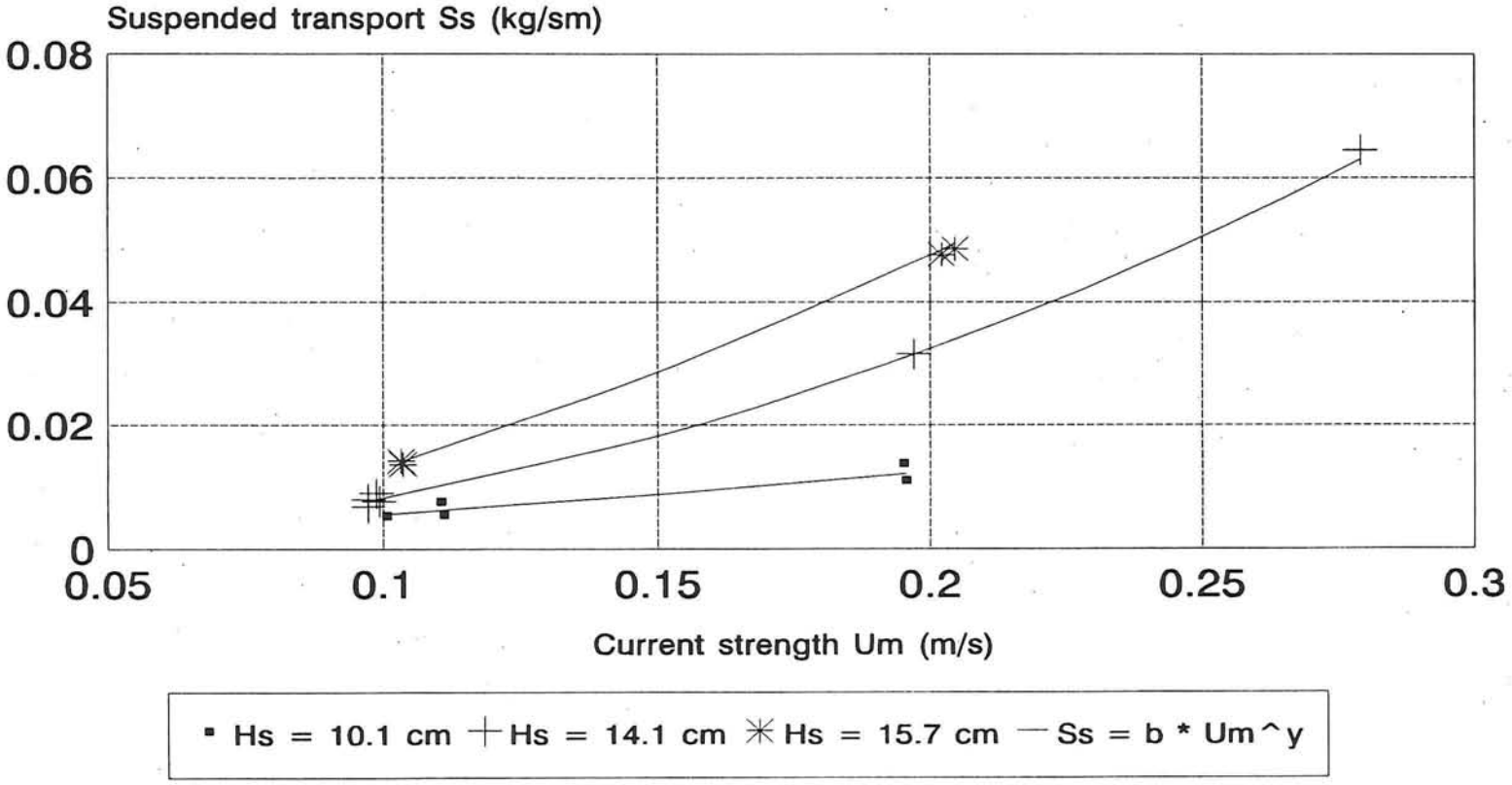

Figure 4.7.B

Suspended Transport

Influence Ub,on,tot

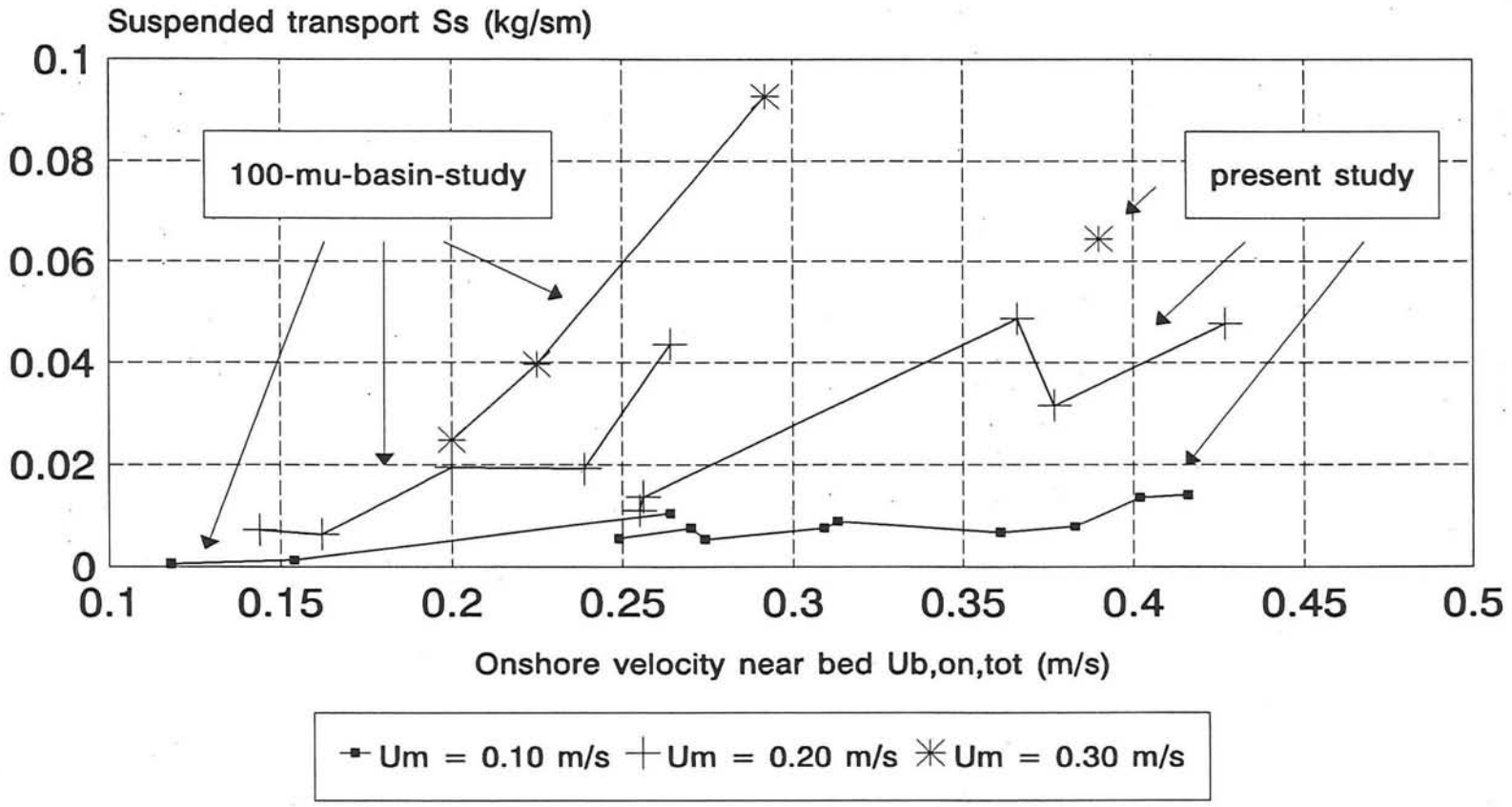

Figure 4.7.C

Suspended Transport

Influence Ub,off,tot

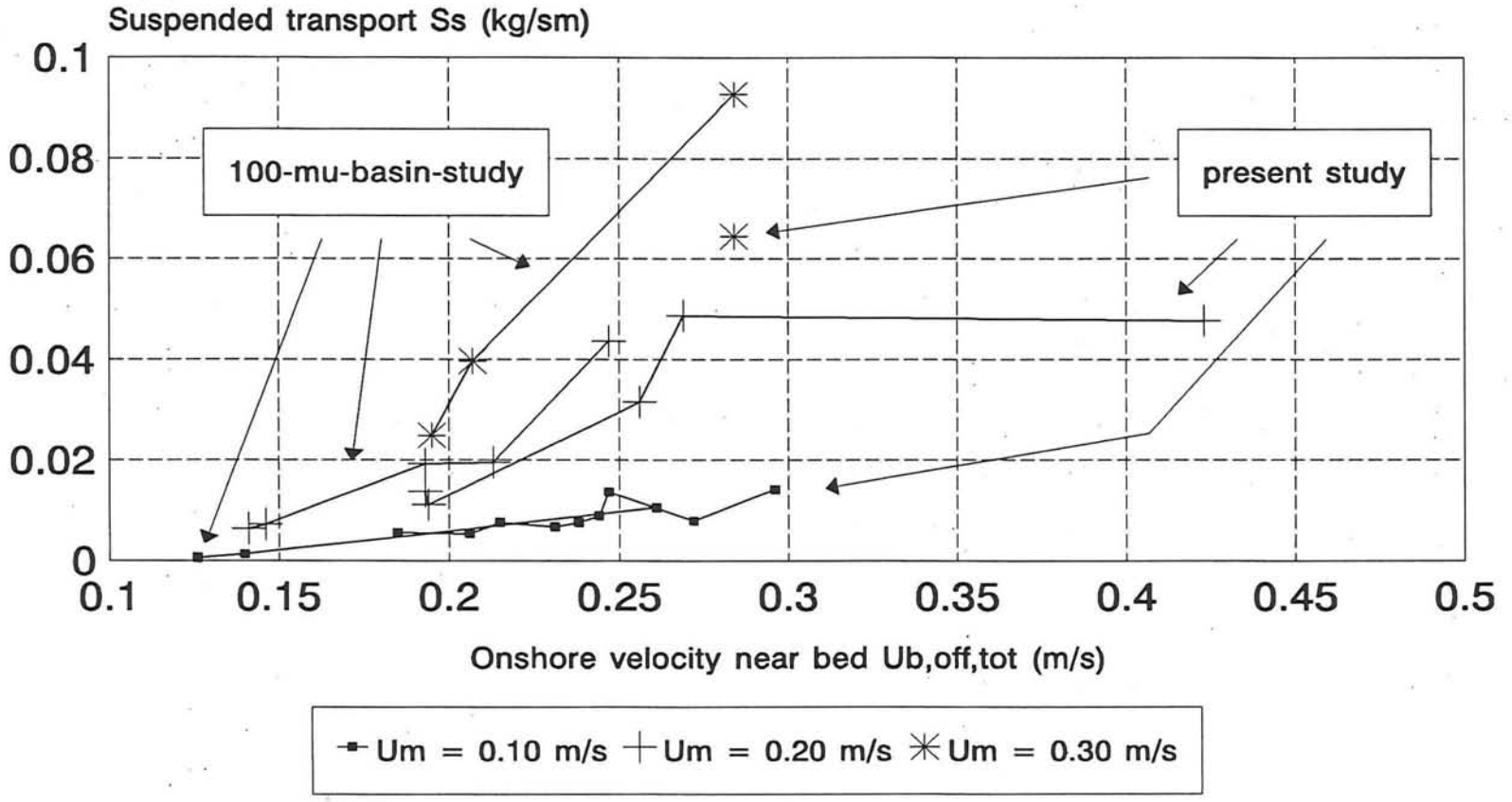

Figure 4.7.D

Relative ripple height

Influence orbital velocity: Ub,on,tot

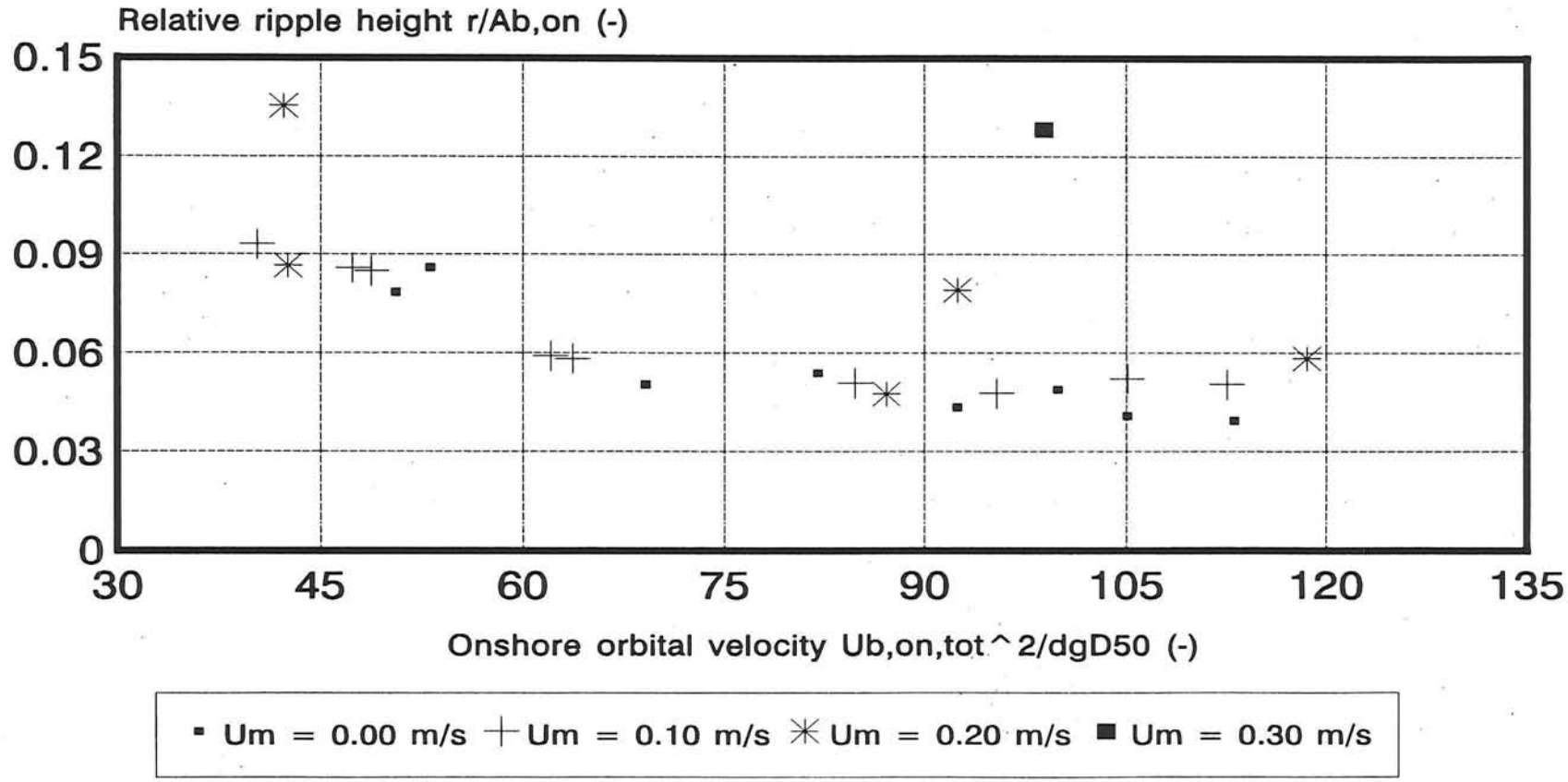

Figure 4.8.A.1

Relative ripple height

Influence orbital velocity: Ub,off,tot

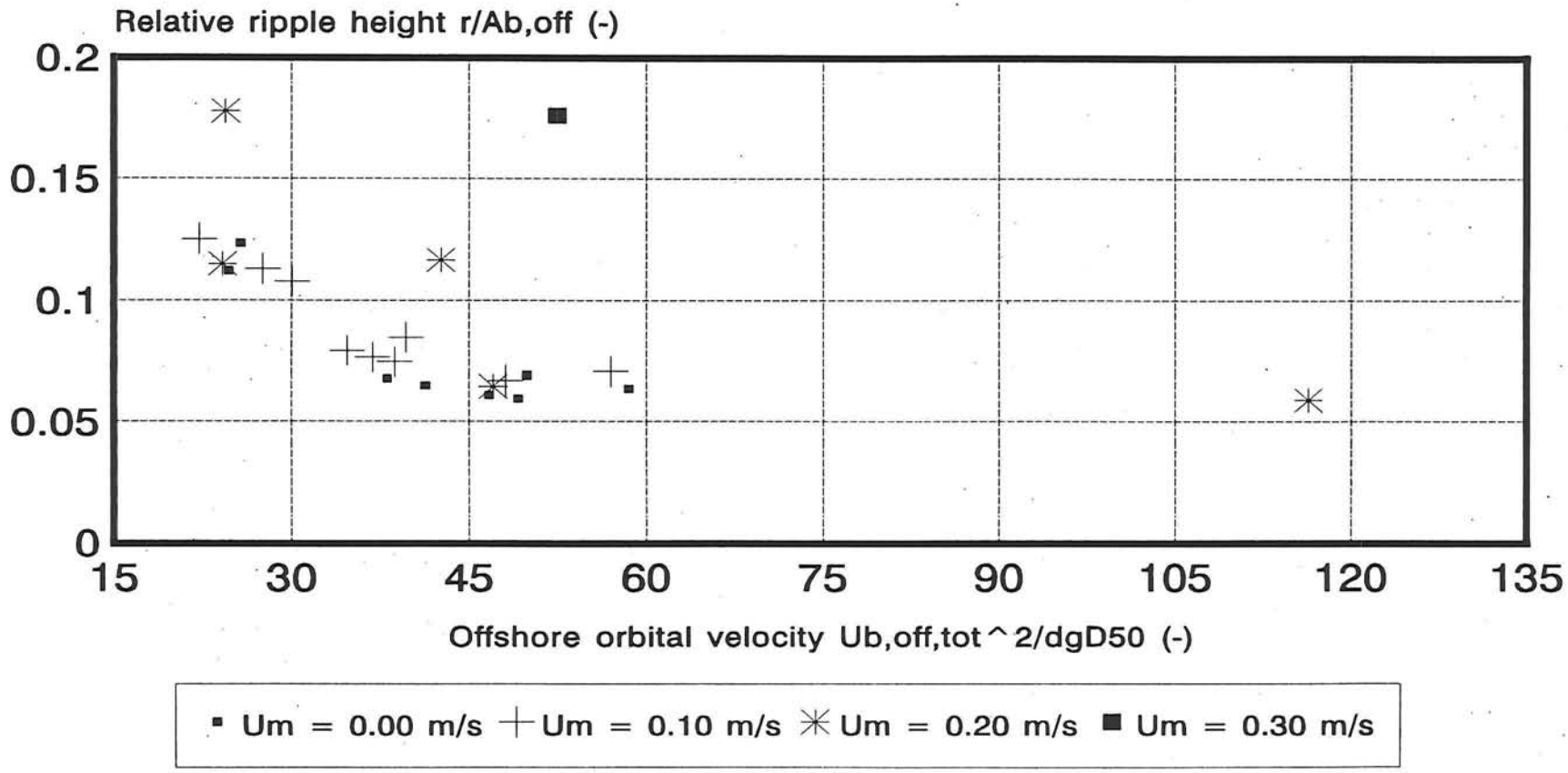

Figure 4.8.A.2

Relative ripple height

Influence current strength

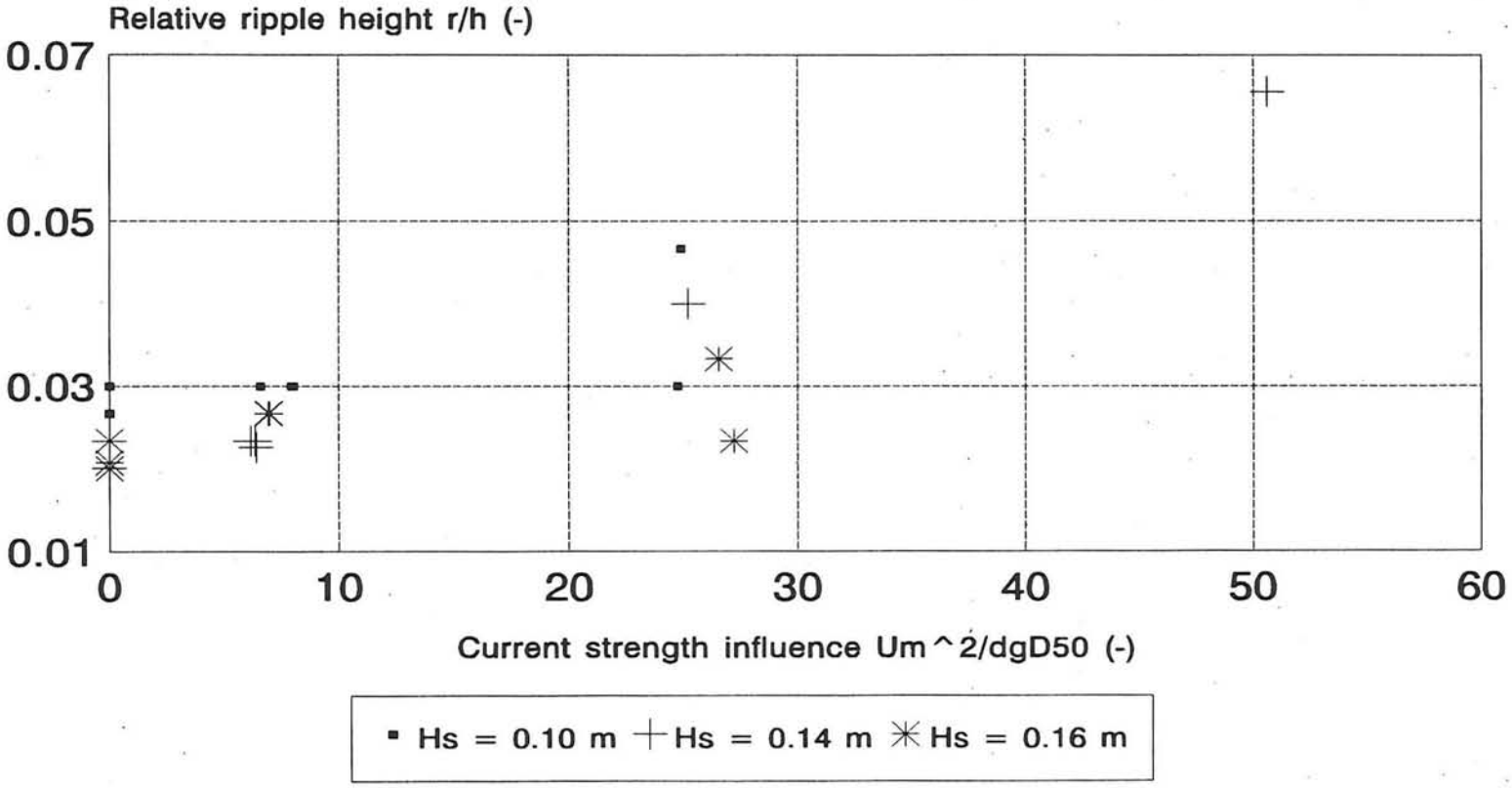

Figure 4.8.B

Relative ripple height

Influence Hs/L

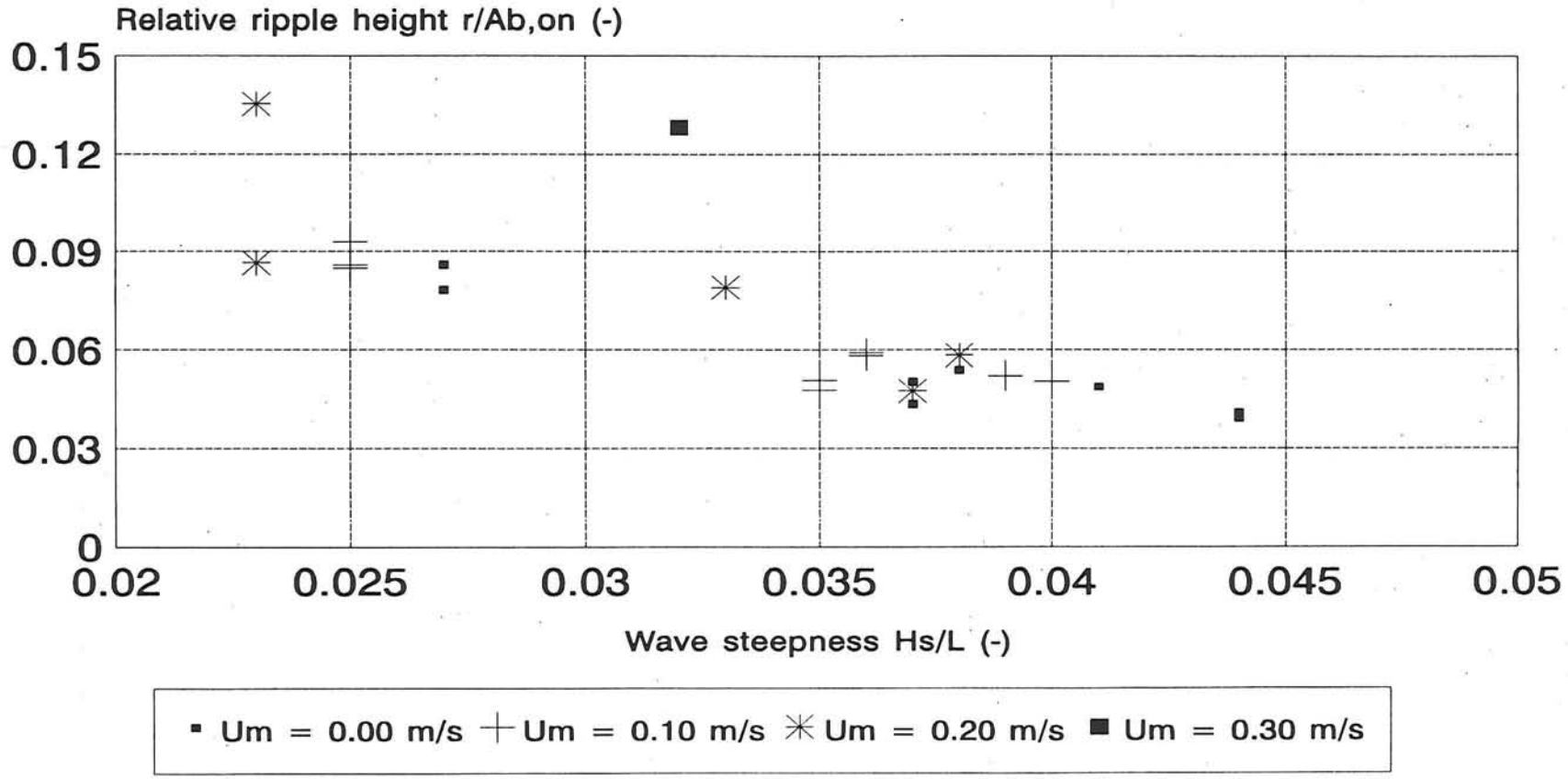

Figure 4.8.C

Relative ripple length

Influence orbital velocity: Ub,on,tot

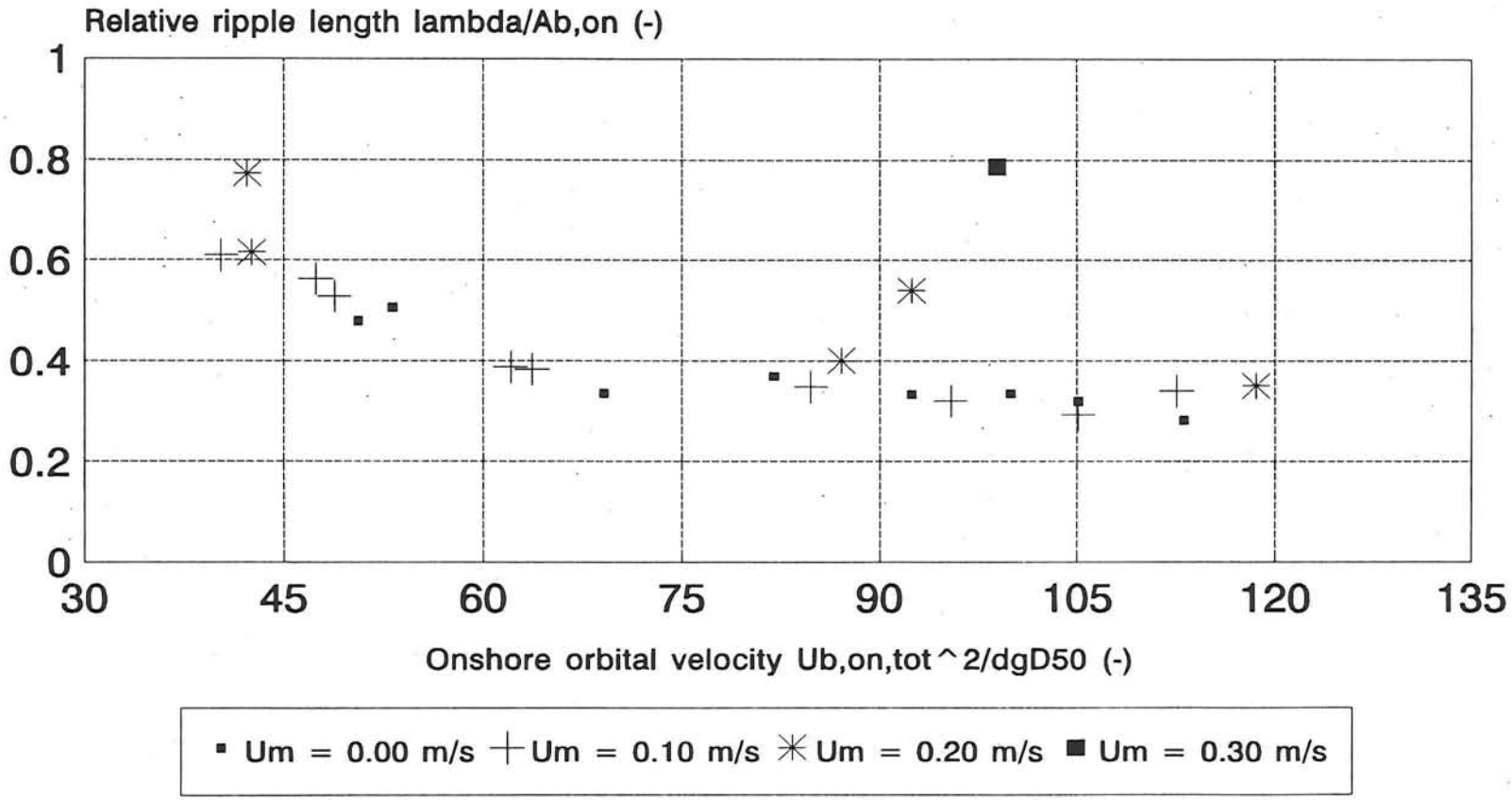

Figure 4.8.D.1

Relative ripple length

Influence orbital velocity: Ub,off,tot

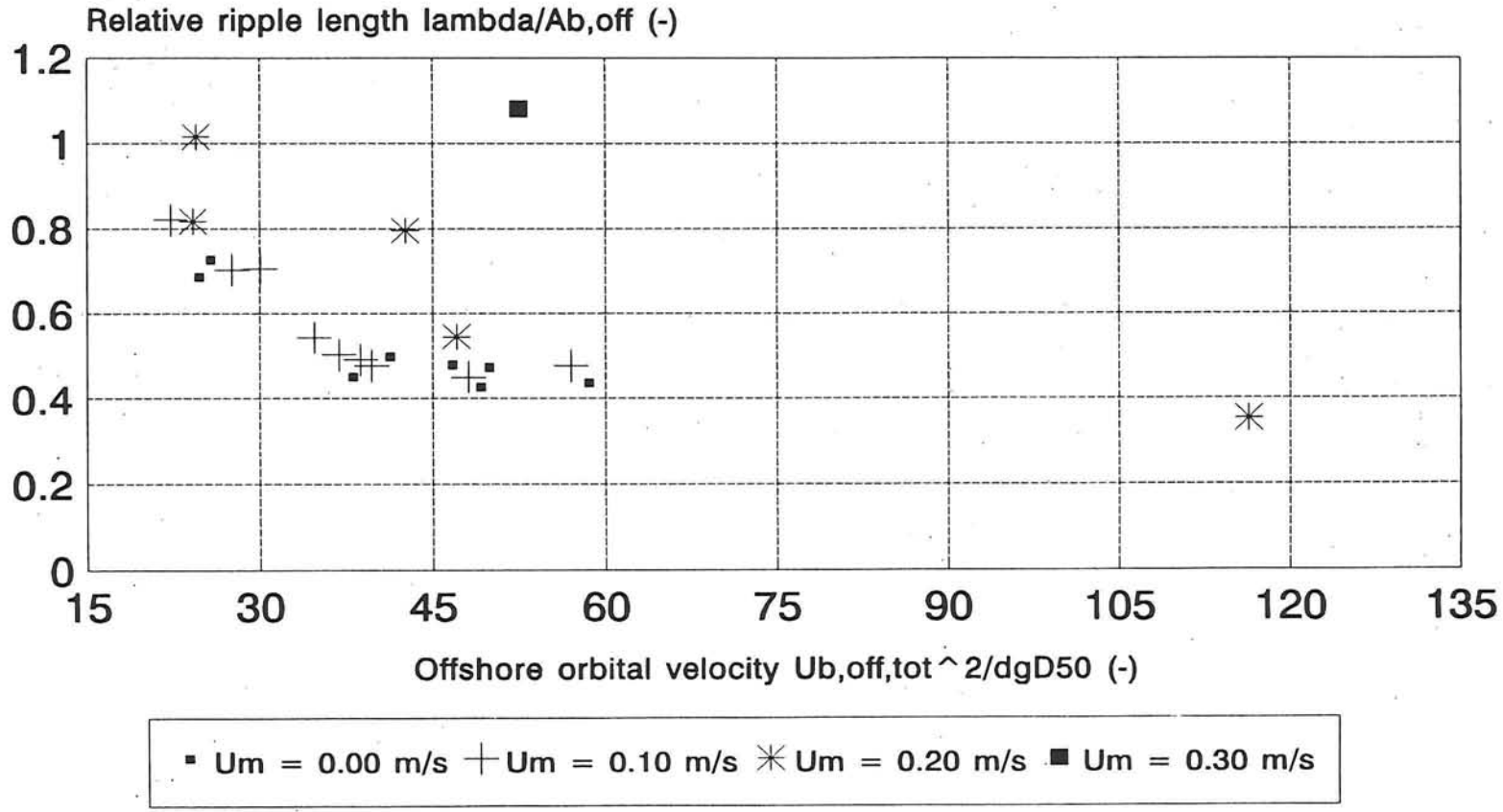

Figure 4.8.D.2

Relative ripple length

Influence current strength

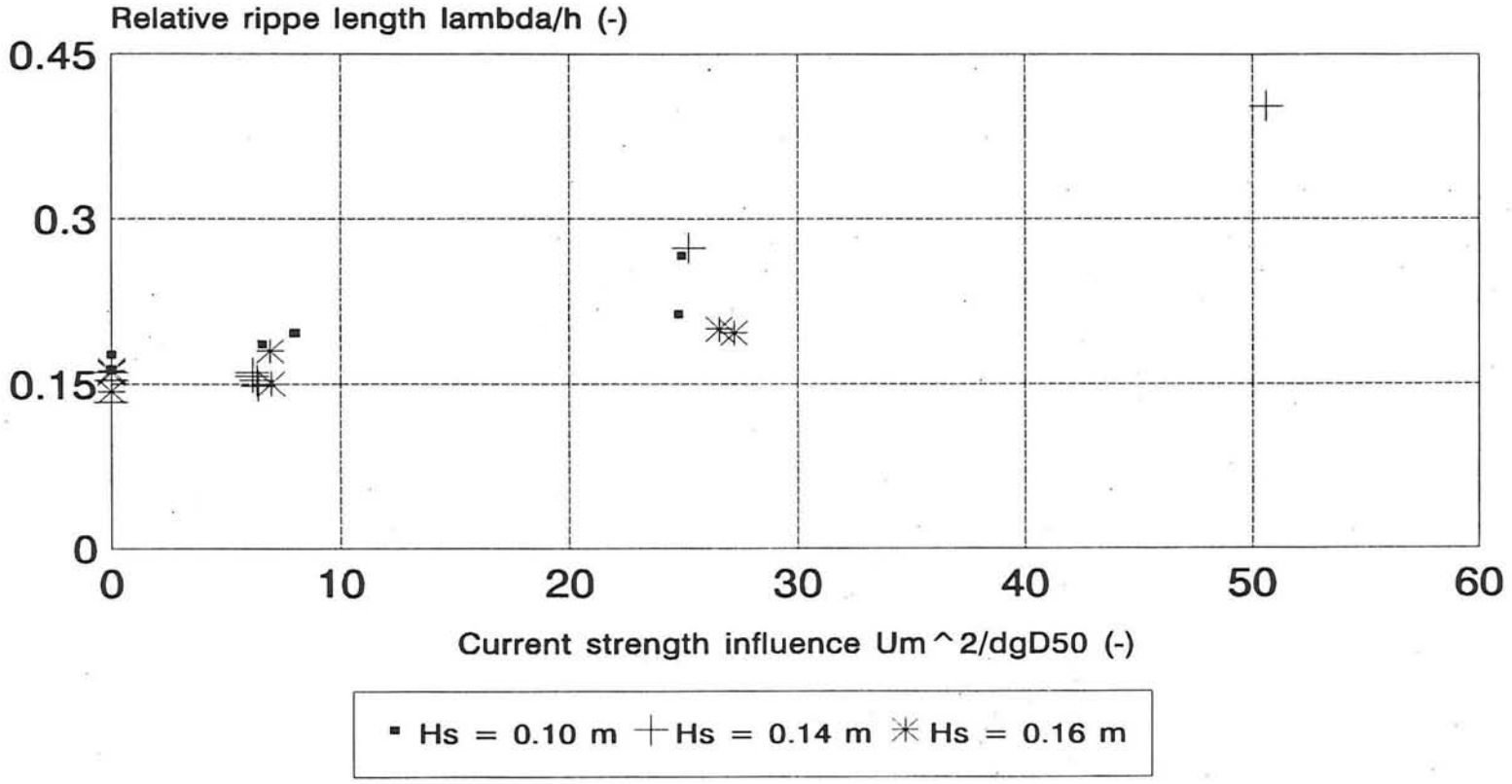

Figure 4.8.E

Relative ripple length

Influence wave steepness

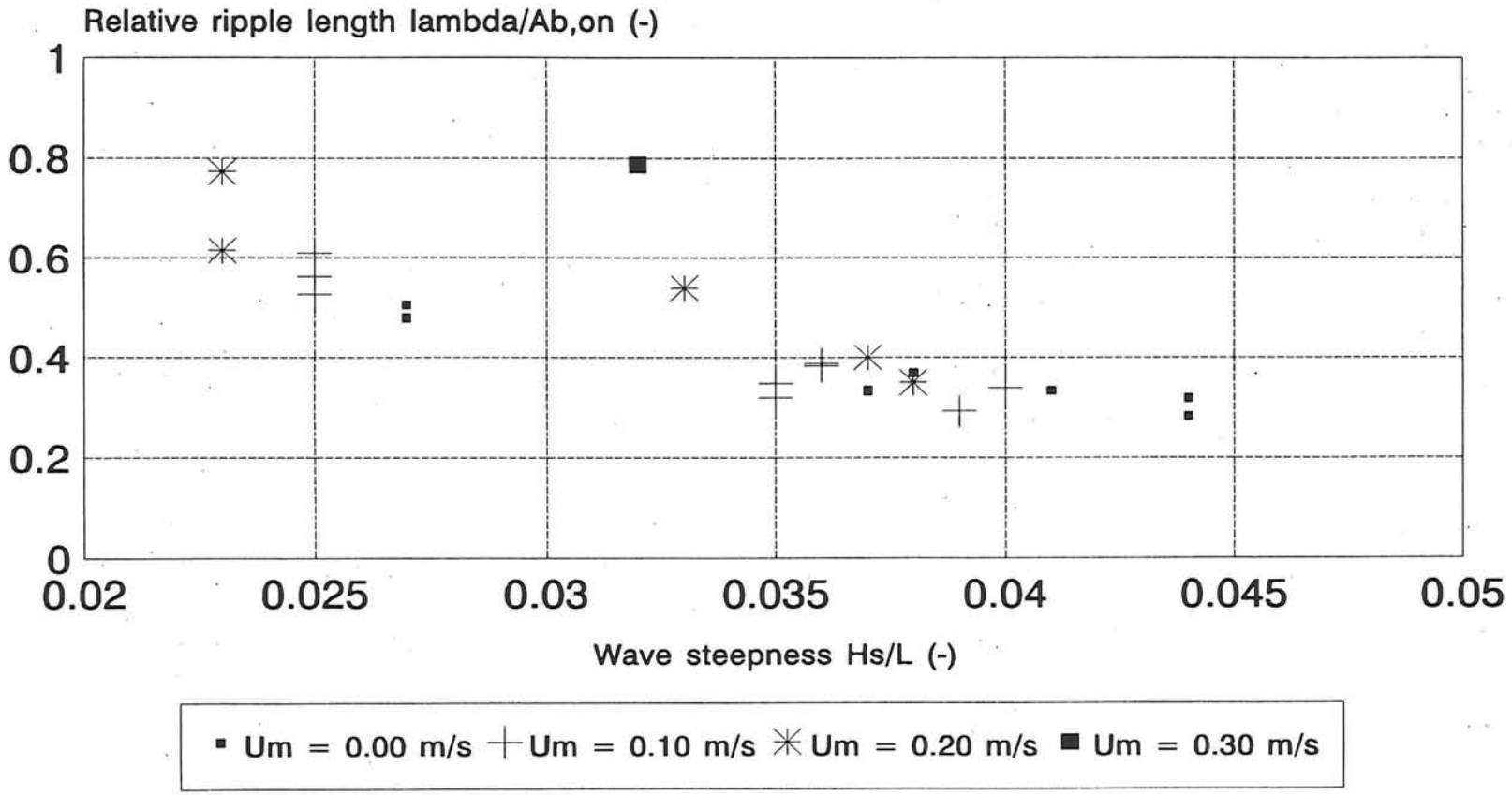

Figure 4.8.F

Ripple steepness

Influence orbital velocity: Ub,on,tot

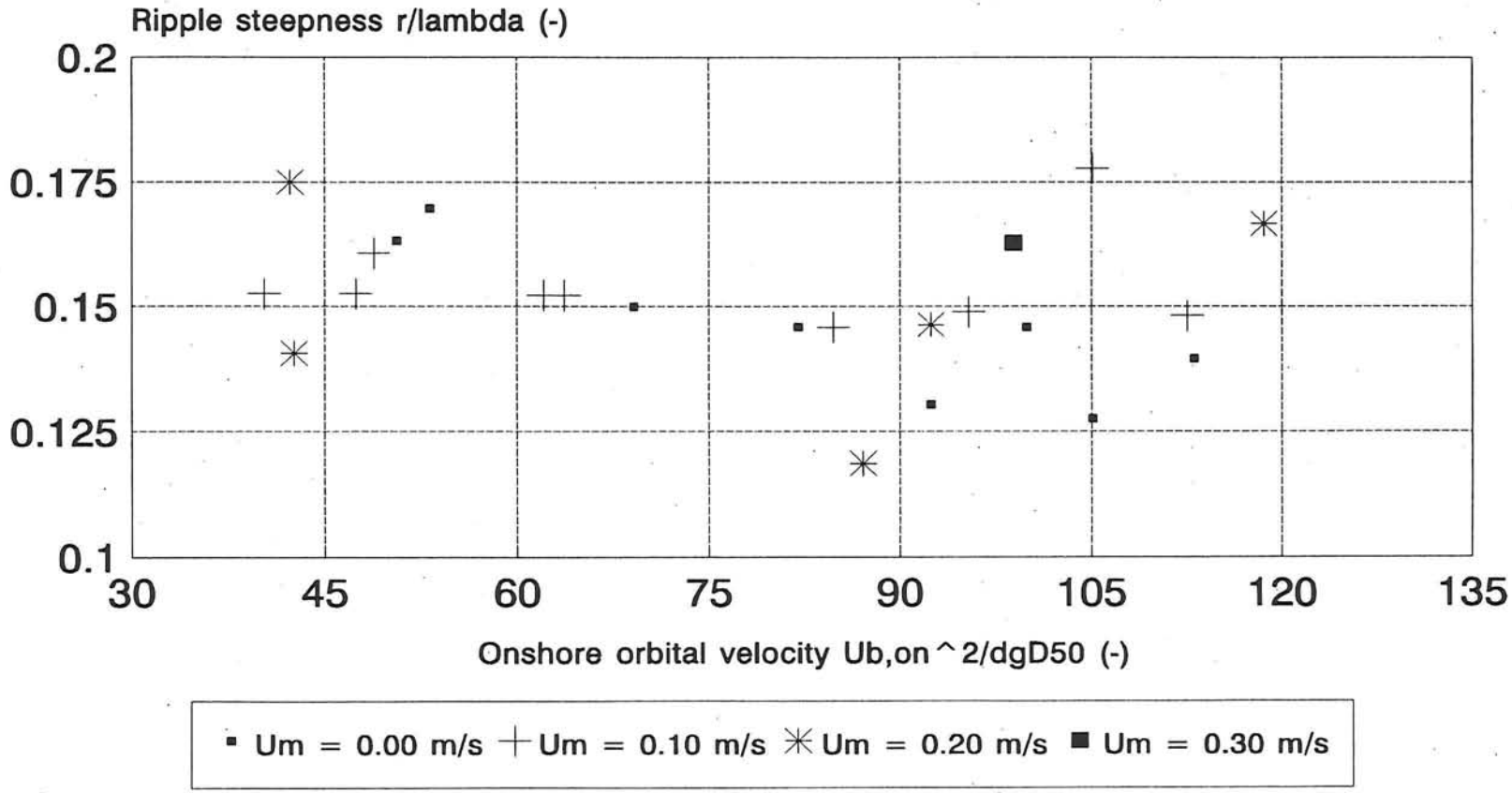

Figure 4.8.G.1

Ripple steepness

Influence orbital velocity: Ub,off,tot

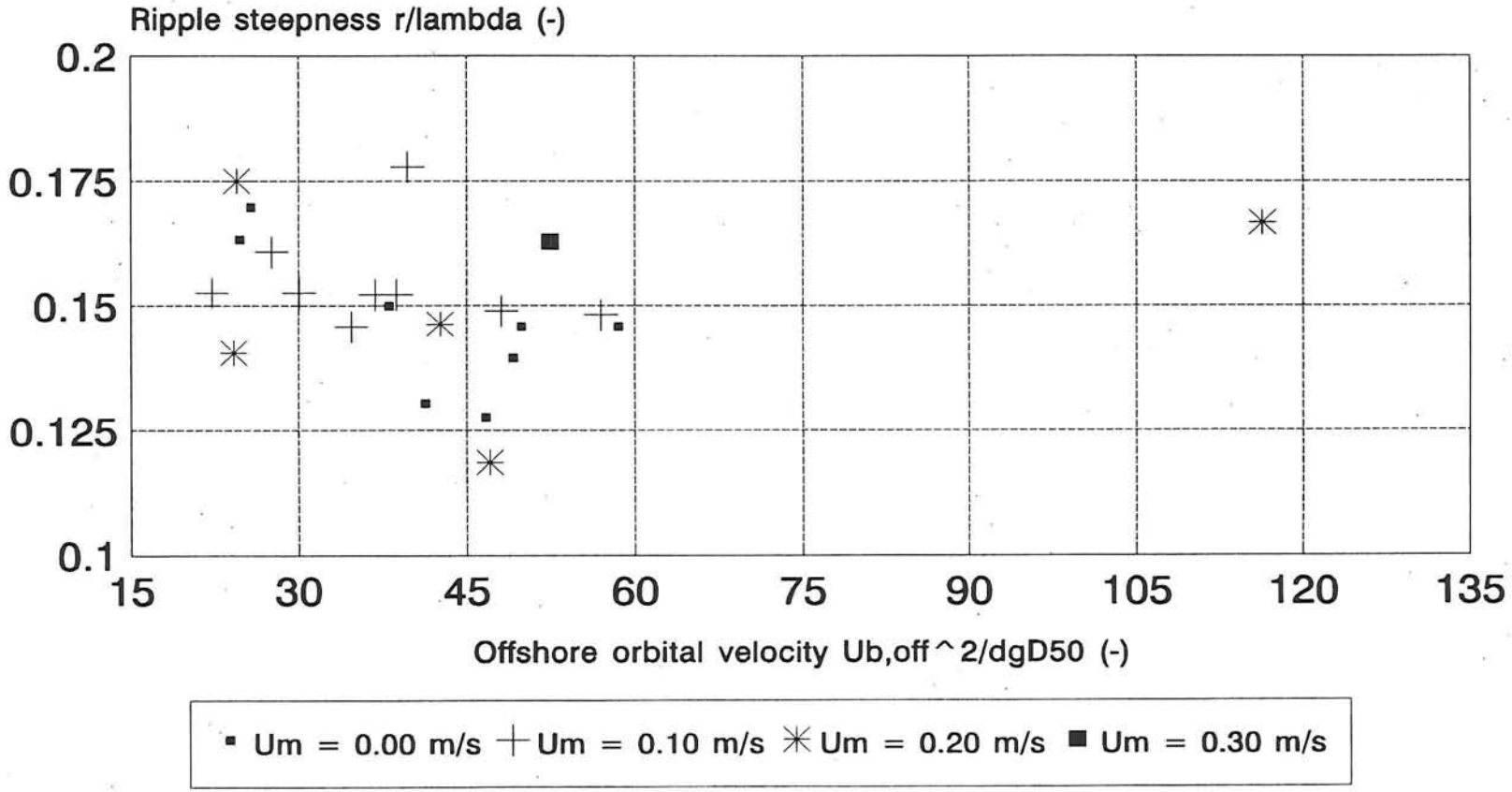

Figure 4.8.G.2

Ripple steepness

Influence current strength

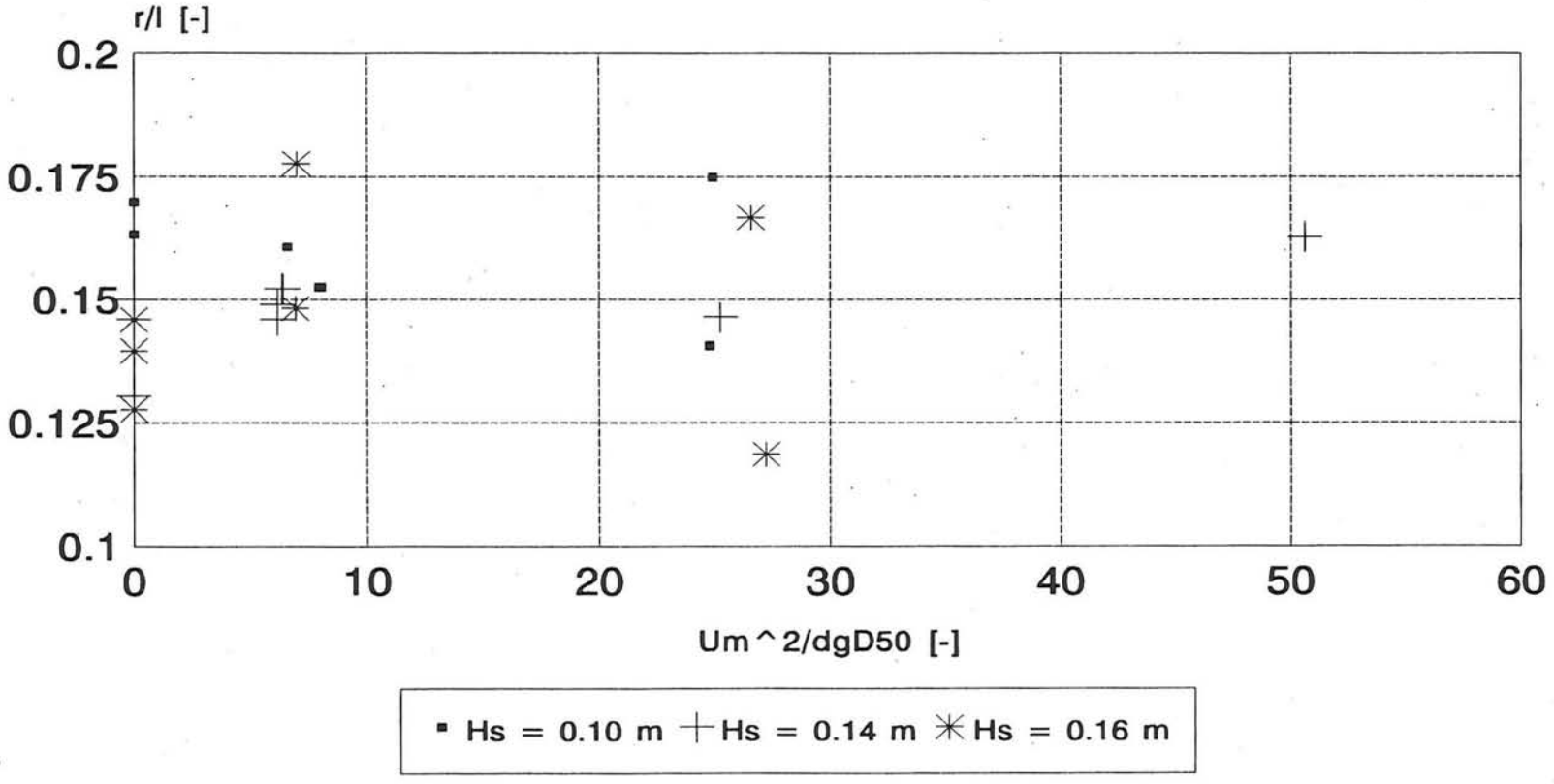

Figure 4.8.H

Ripple steepness

Influence wave steepness

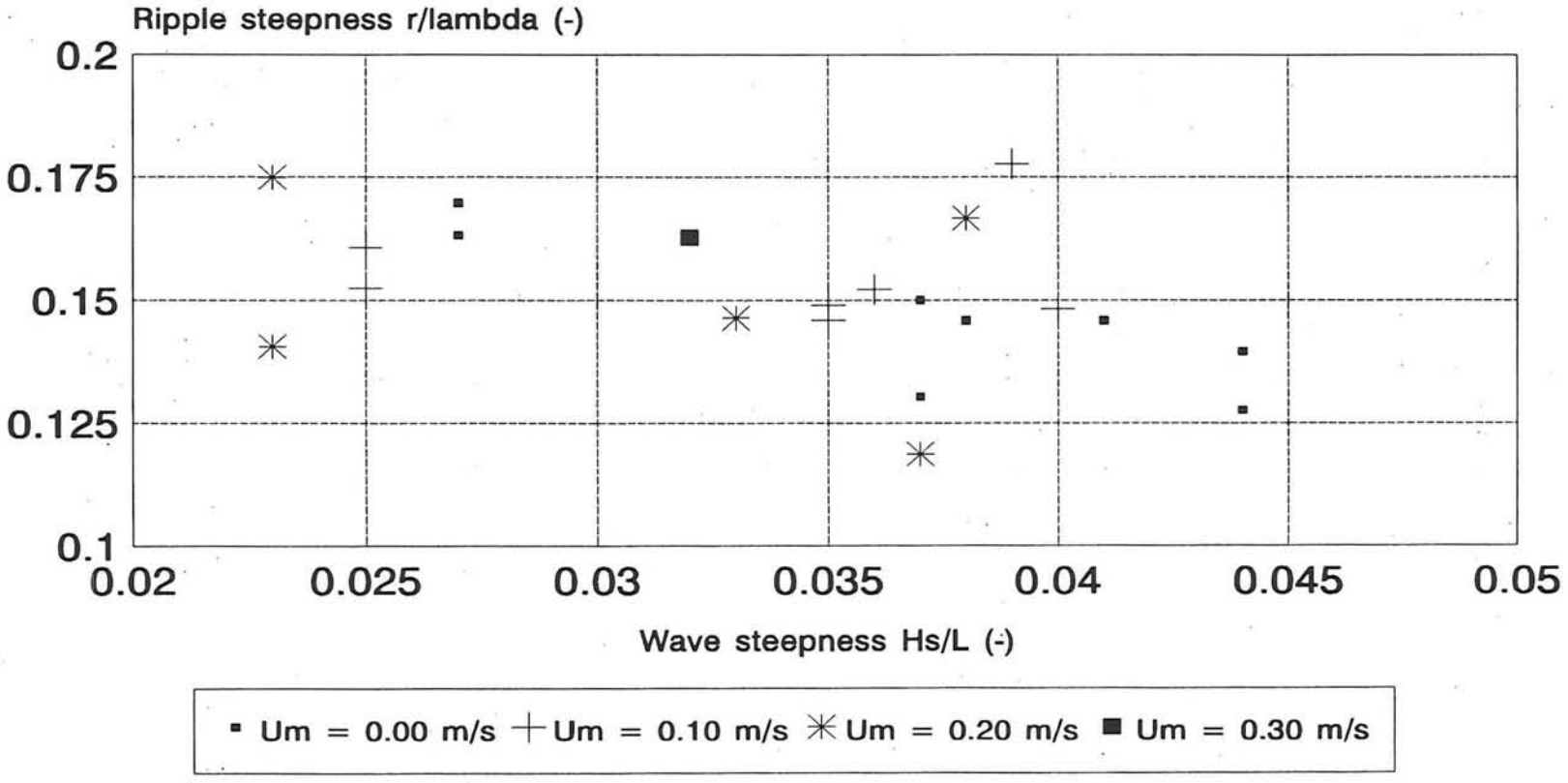

Figure 4.8.I

Physical bed roughness

Influence ripple height

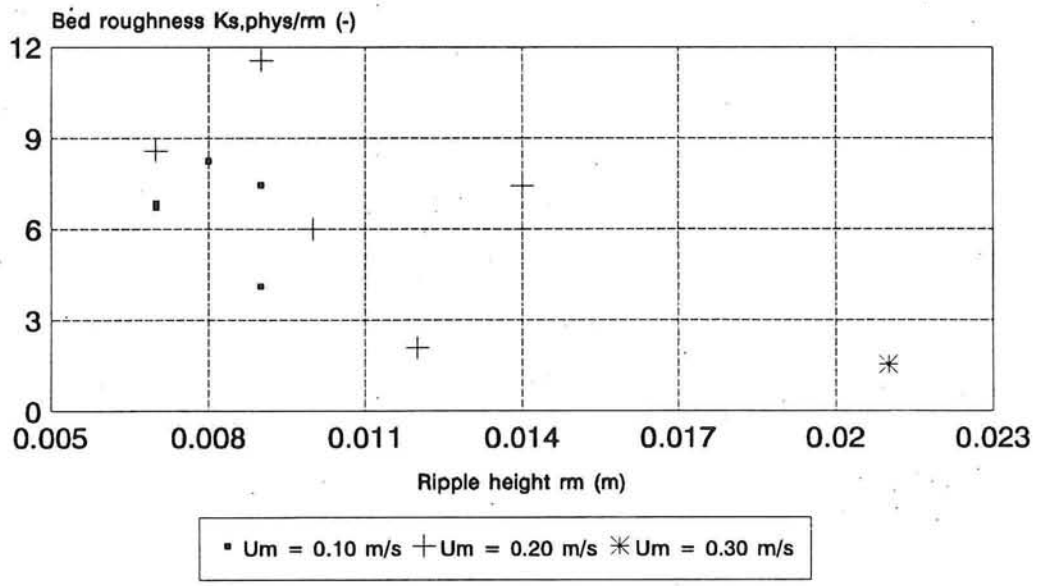

Figure 4.10.A

Physical bed roughness

Influence ripple length

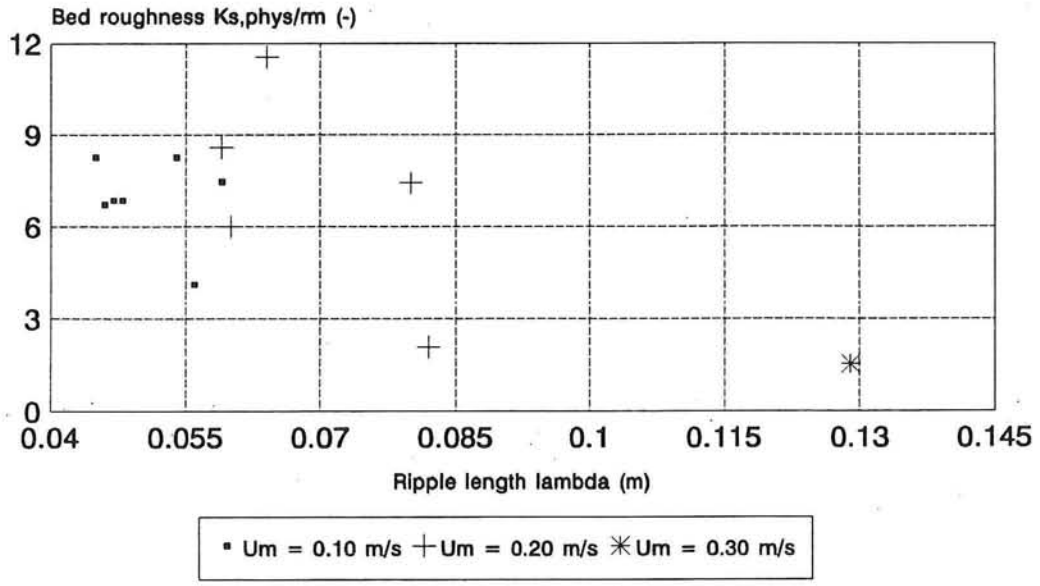

Figure 4.10.B

Physical bed roughness

Influence ripple steepness

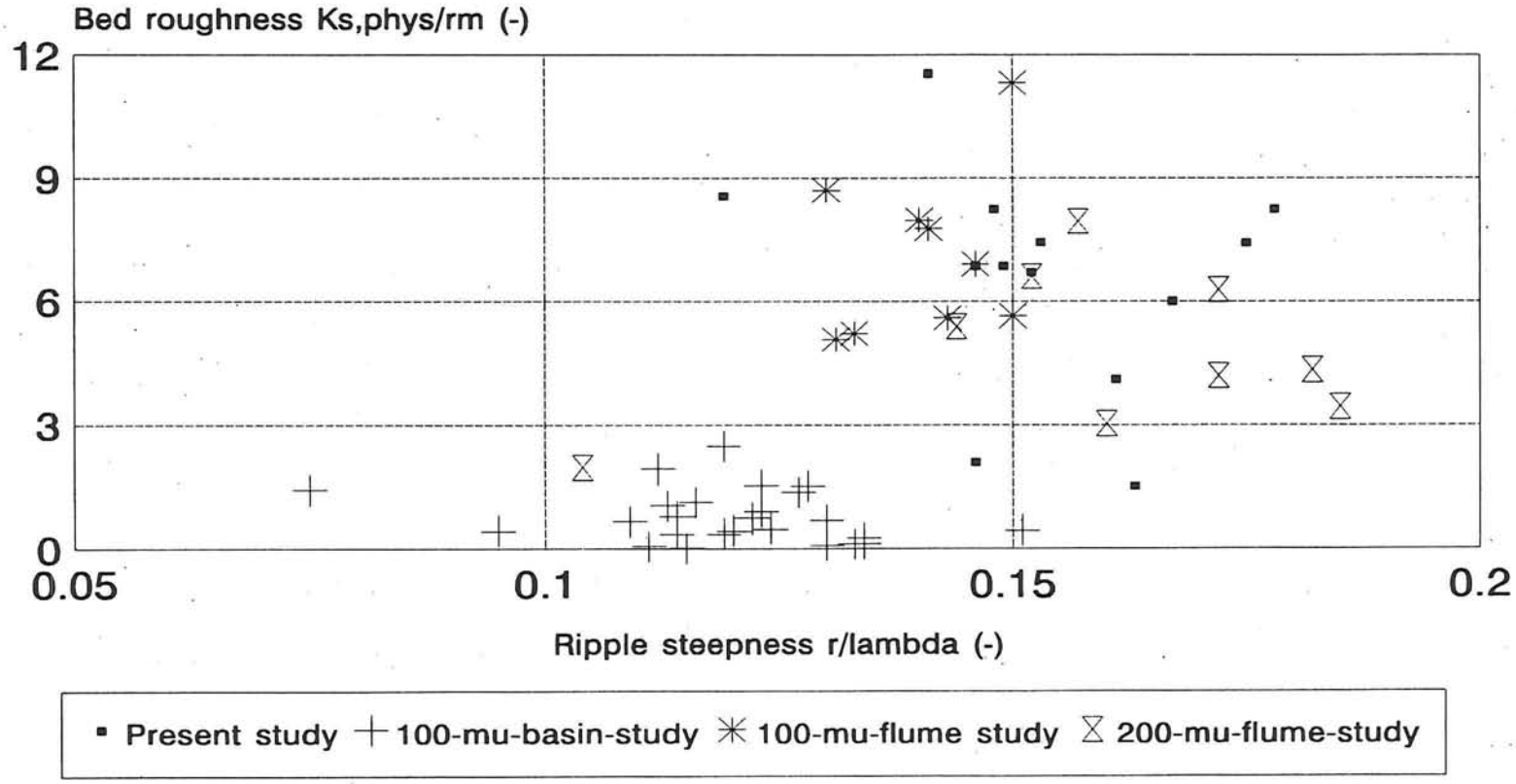

Figure 4.10.C

Physical bed roughness

Influence orbital velocity: Ub,on,tot

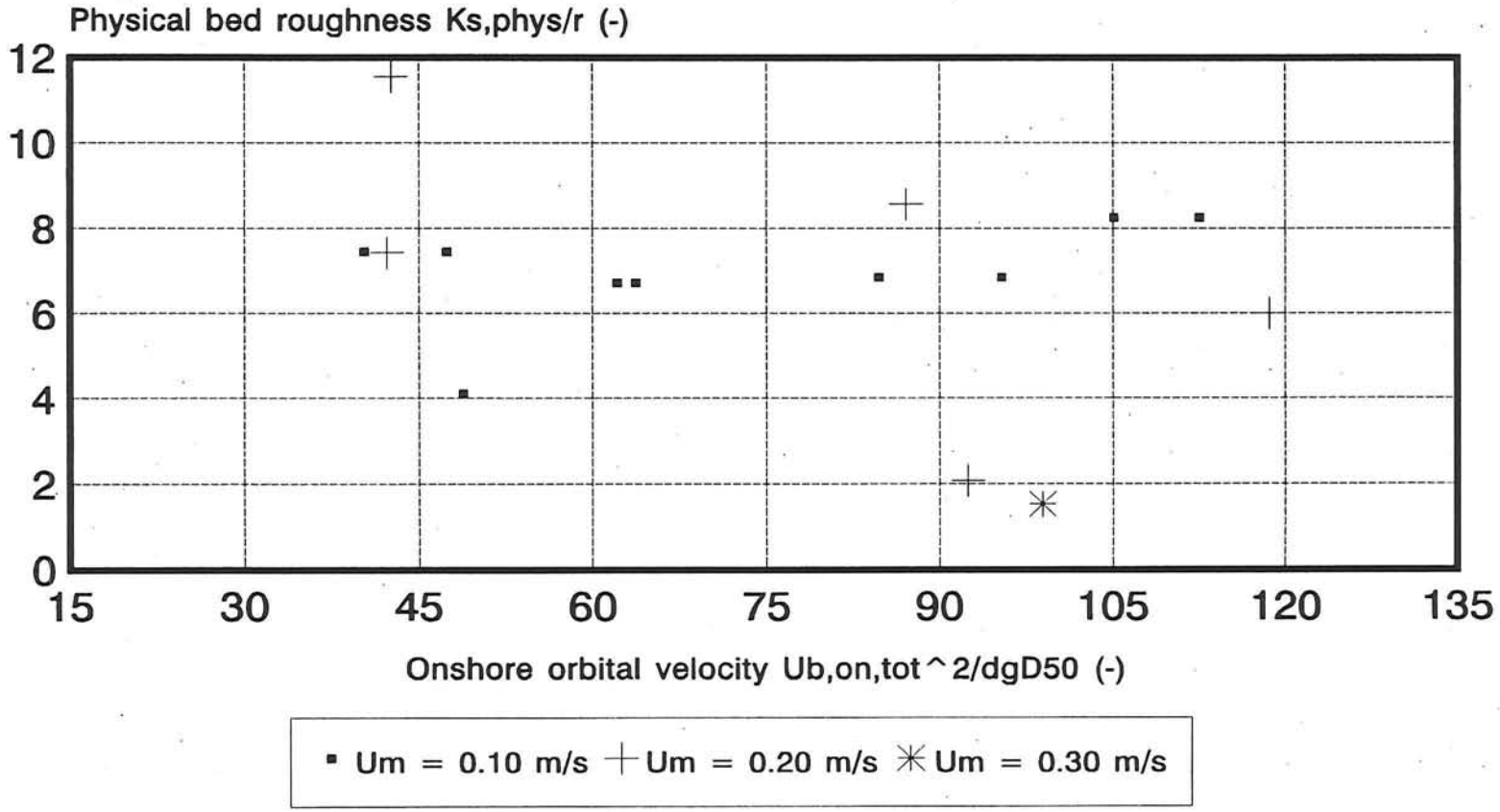

Figure 4.10.D

Physical bed roughness

Influence orbital velocity: Ub,off,tot

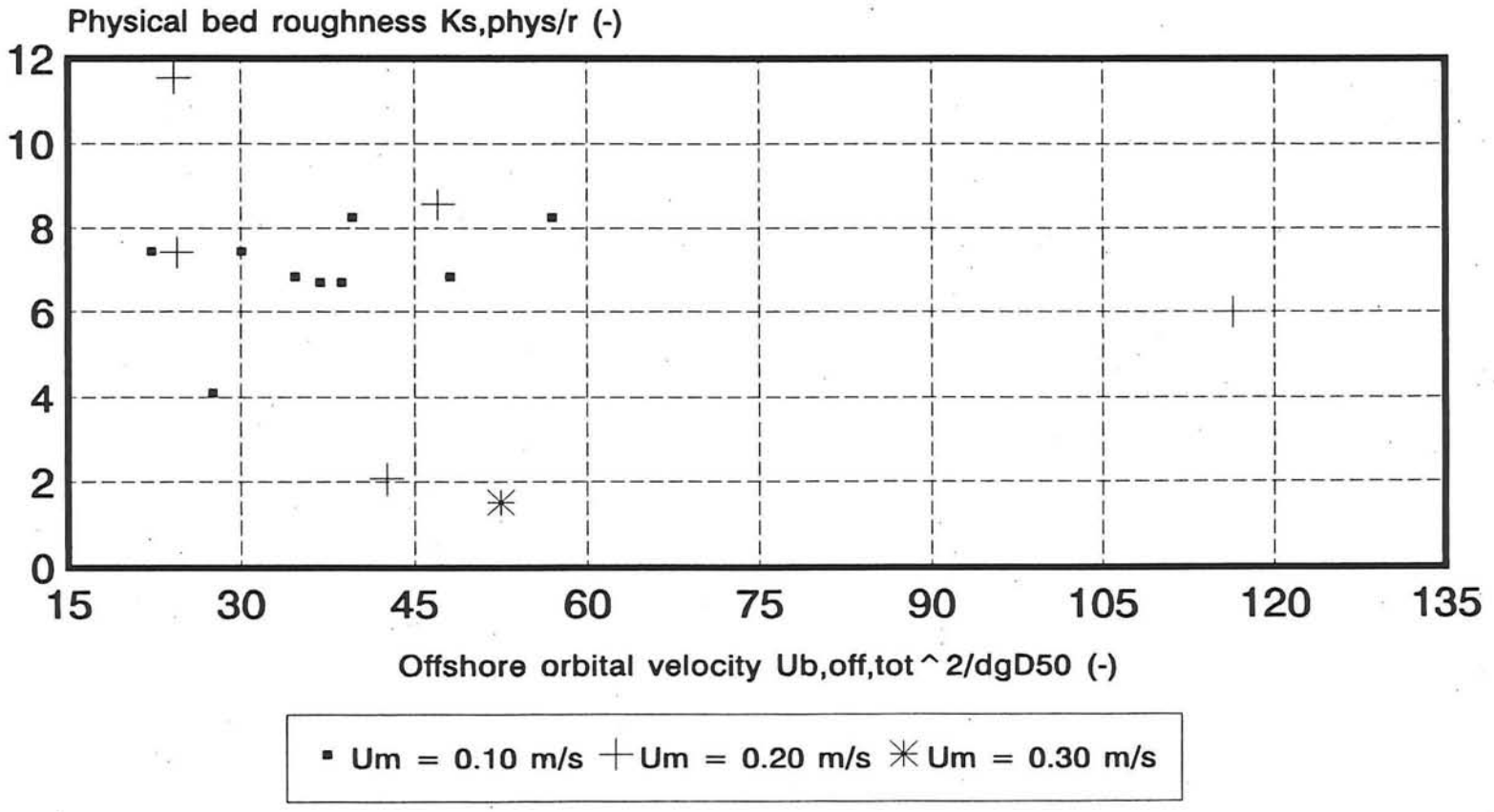

Figure 4.10.E

Physical bed roughness

Influence current strength: Um

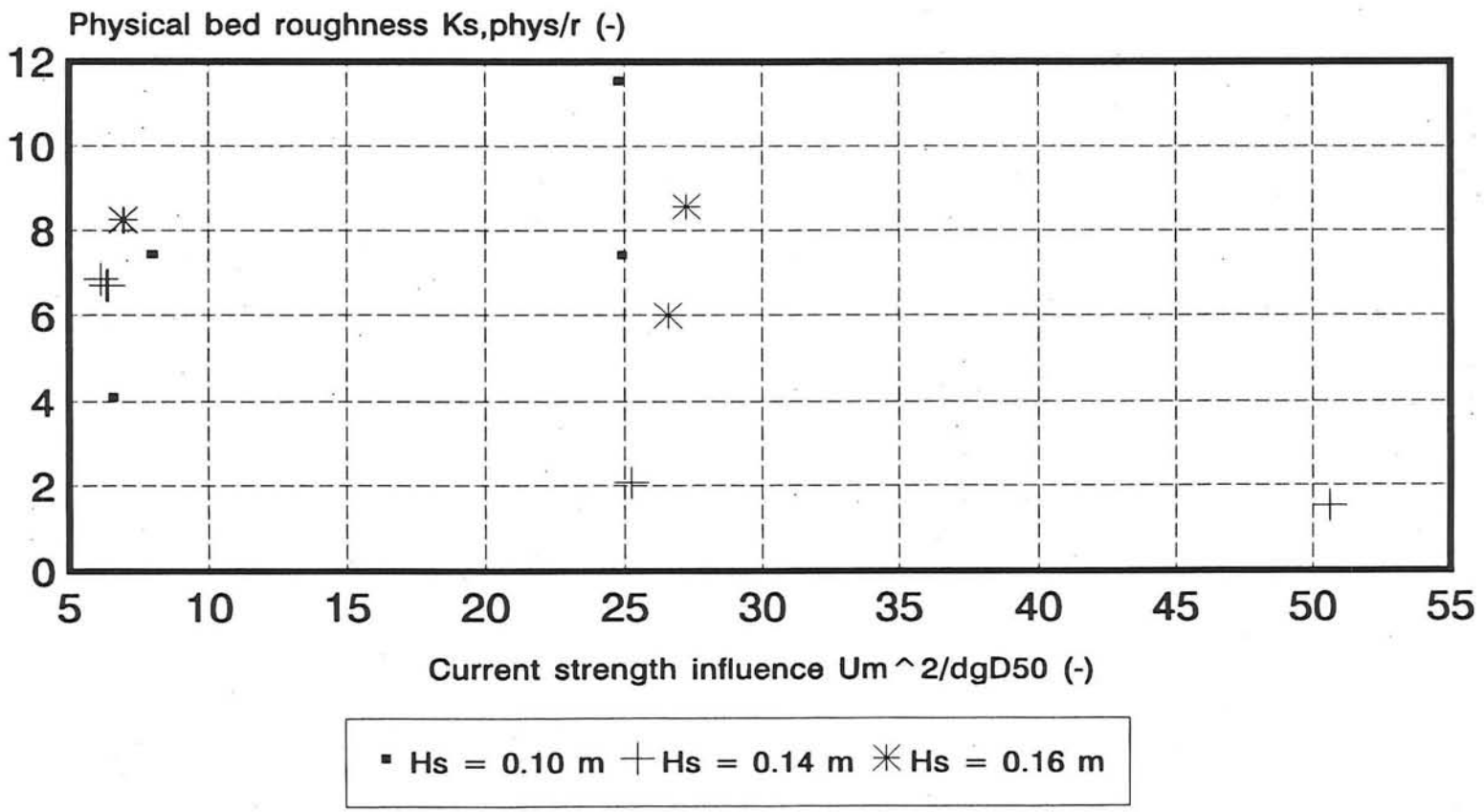

Figure 4.10.F

Physical bed roughness

Influence orbital displacement: Ab,on,tot

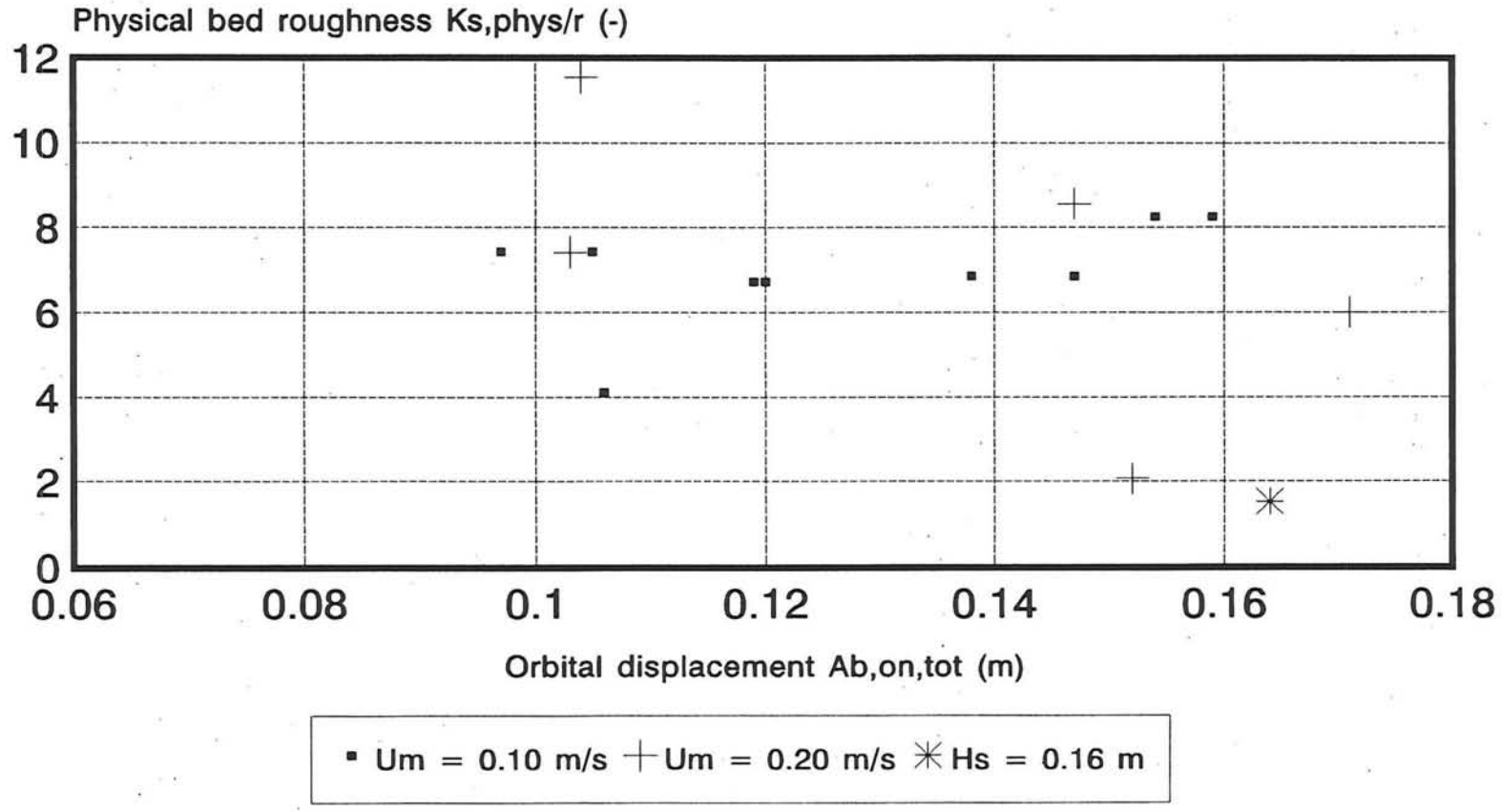

Figure 4.10.G

Physical bed roughness

Influence orbital displacement: Ab,off,tot

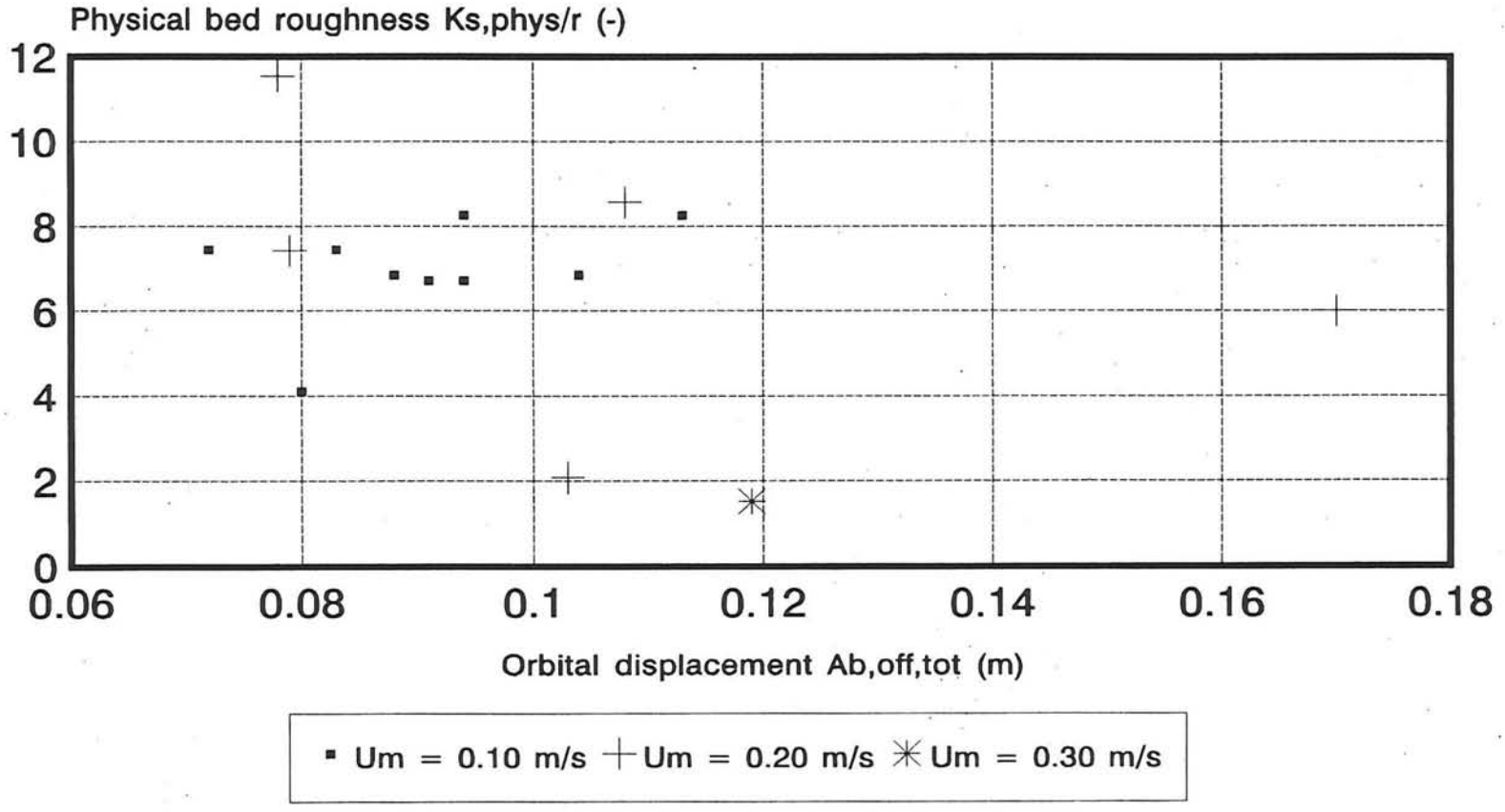

Figure 4.10.H

Zero velocity level increase

Influence Ub,on,tot/Um

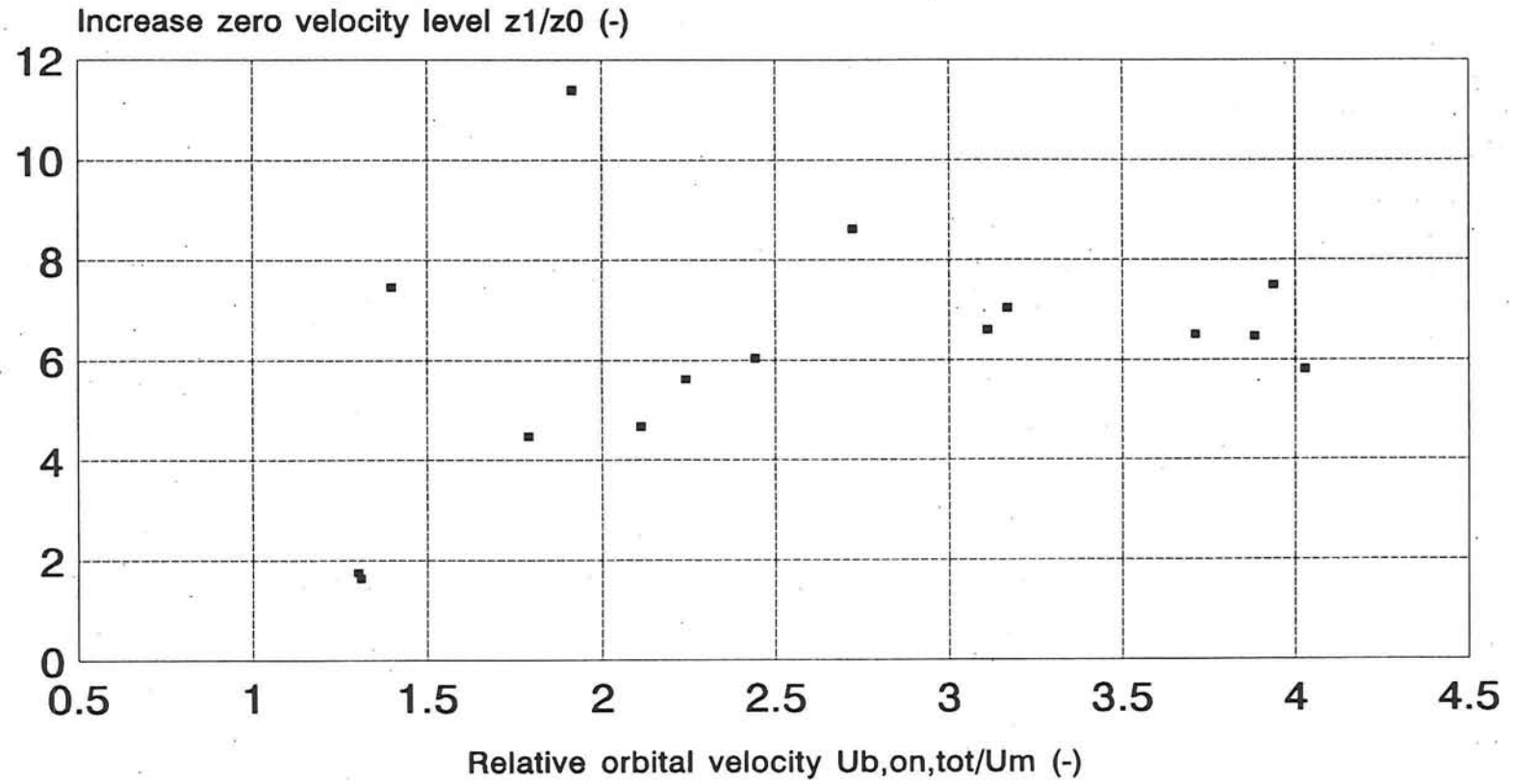

Figure 4.10.I

Zero velocity level increase

Influence Ub,off,tot/Um

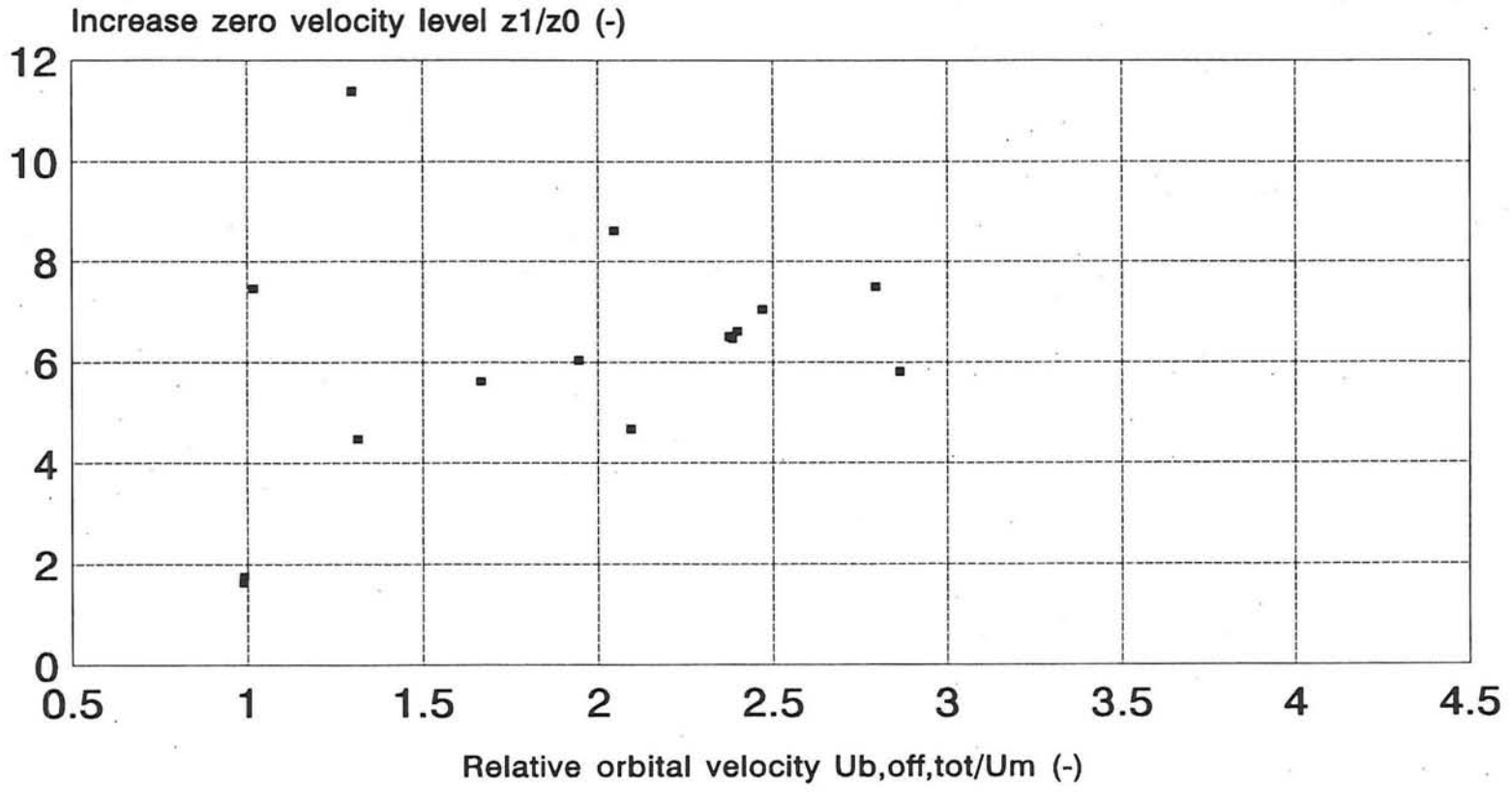

Figure 4.10.J

Bed shear velocity increase

Influence Ub,on,tot/Um

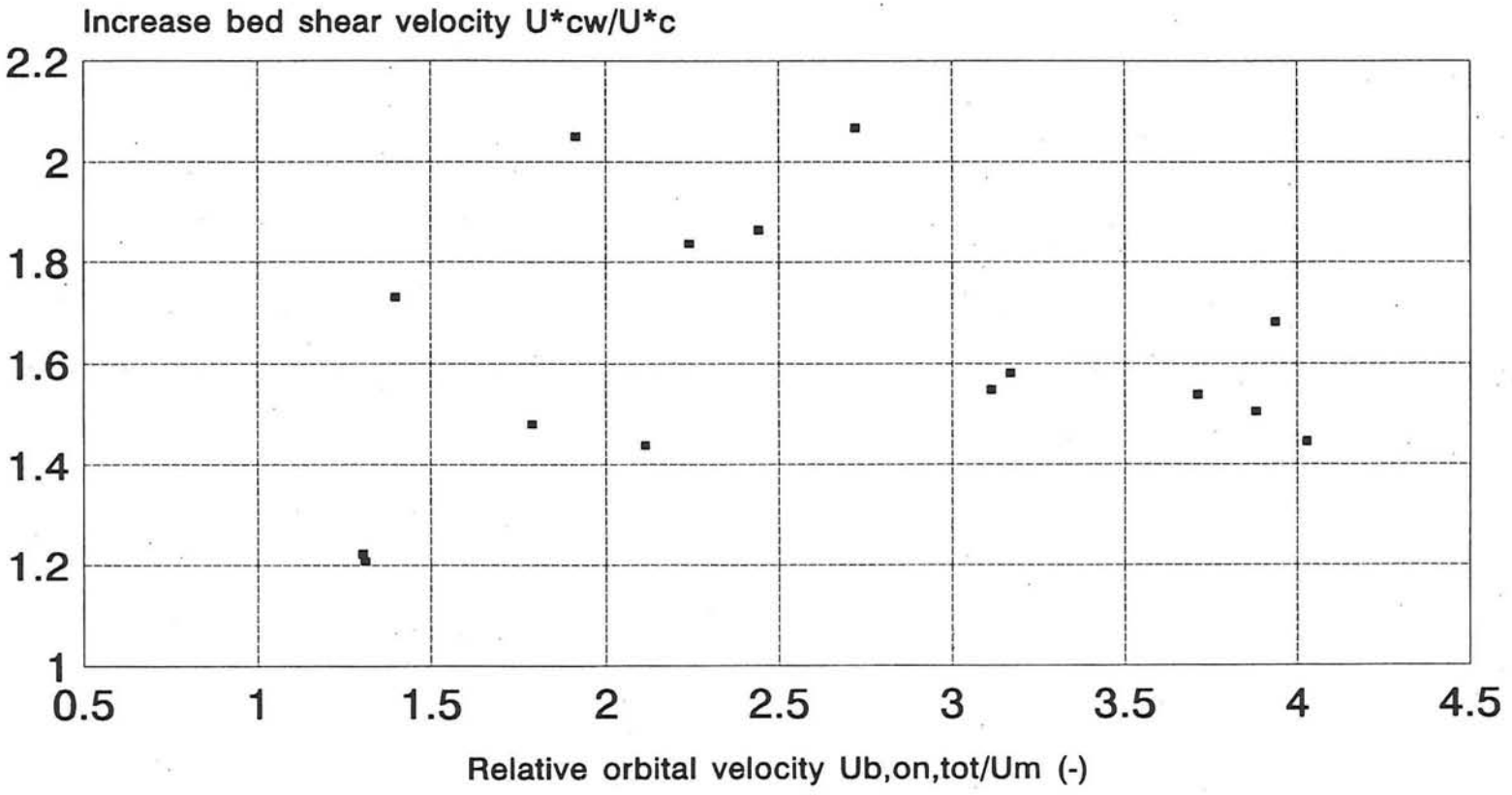

Figure 4.10.K

Bed shear velocity increase

Influence Ub,off,tot/Um

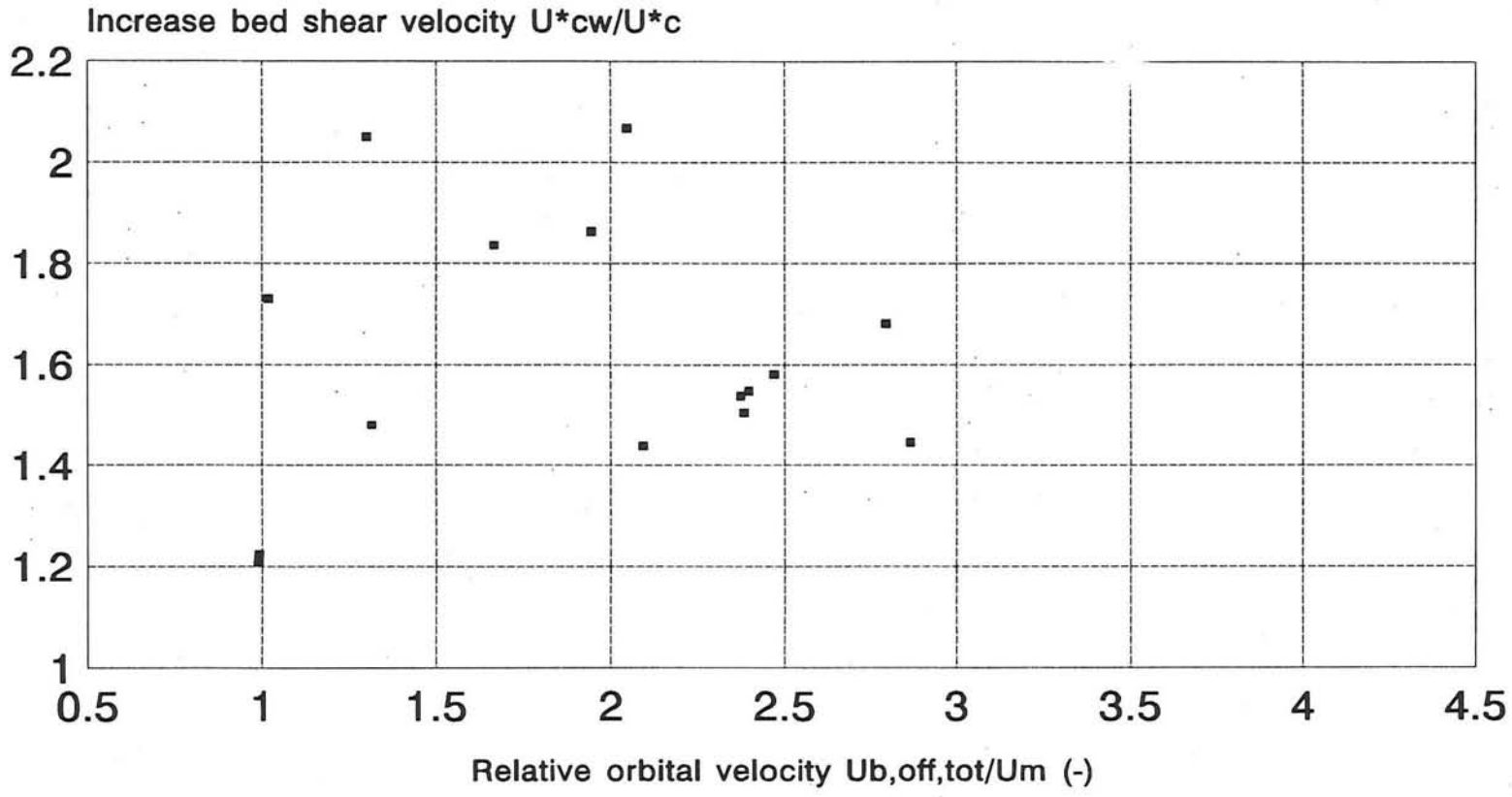

Figure 4.10.L

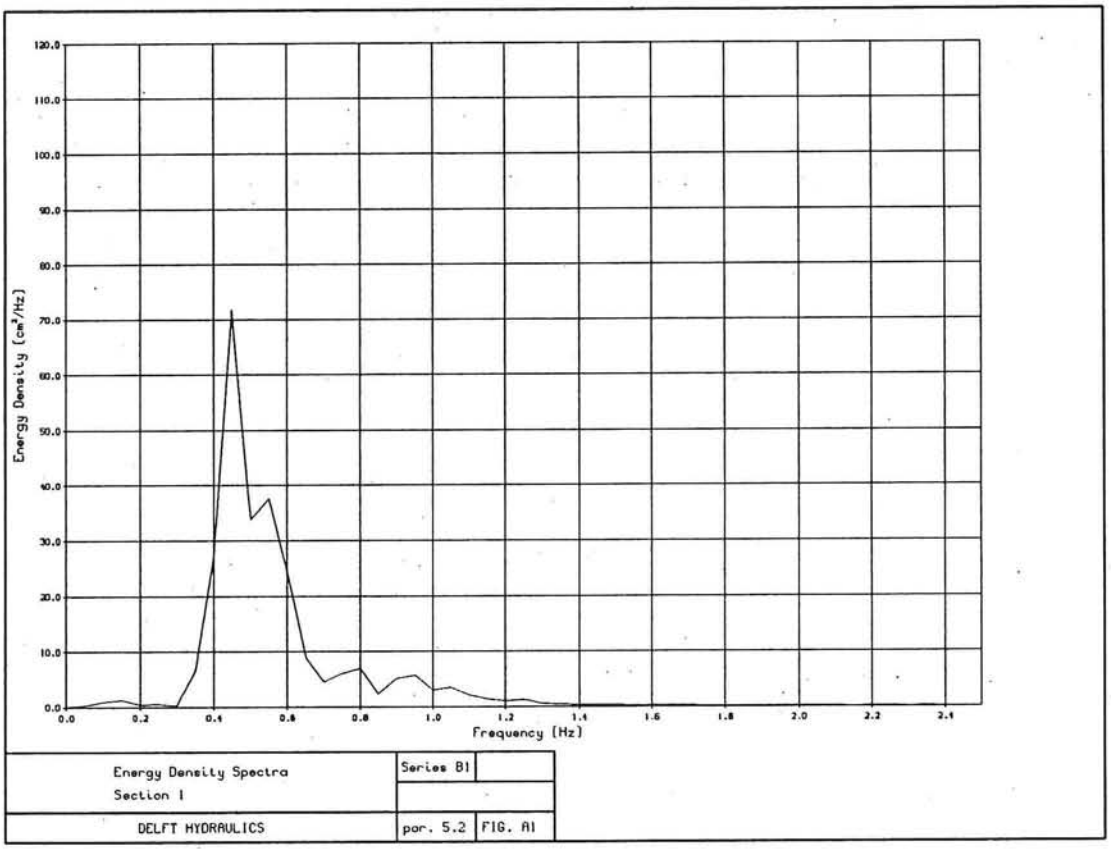

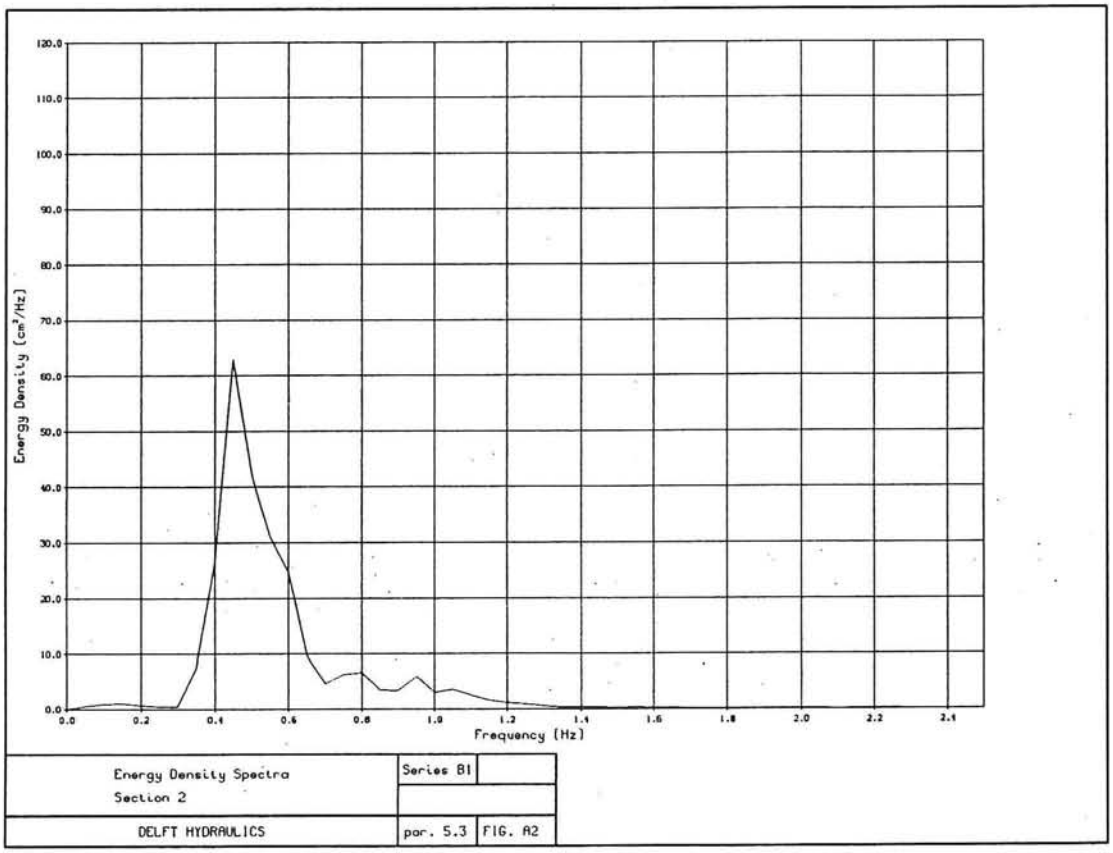

Figure 5.2.A1 - 5.2.A2

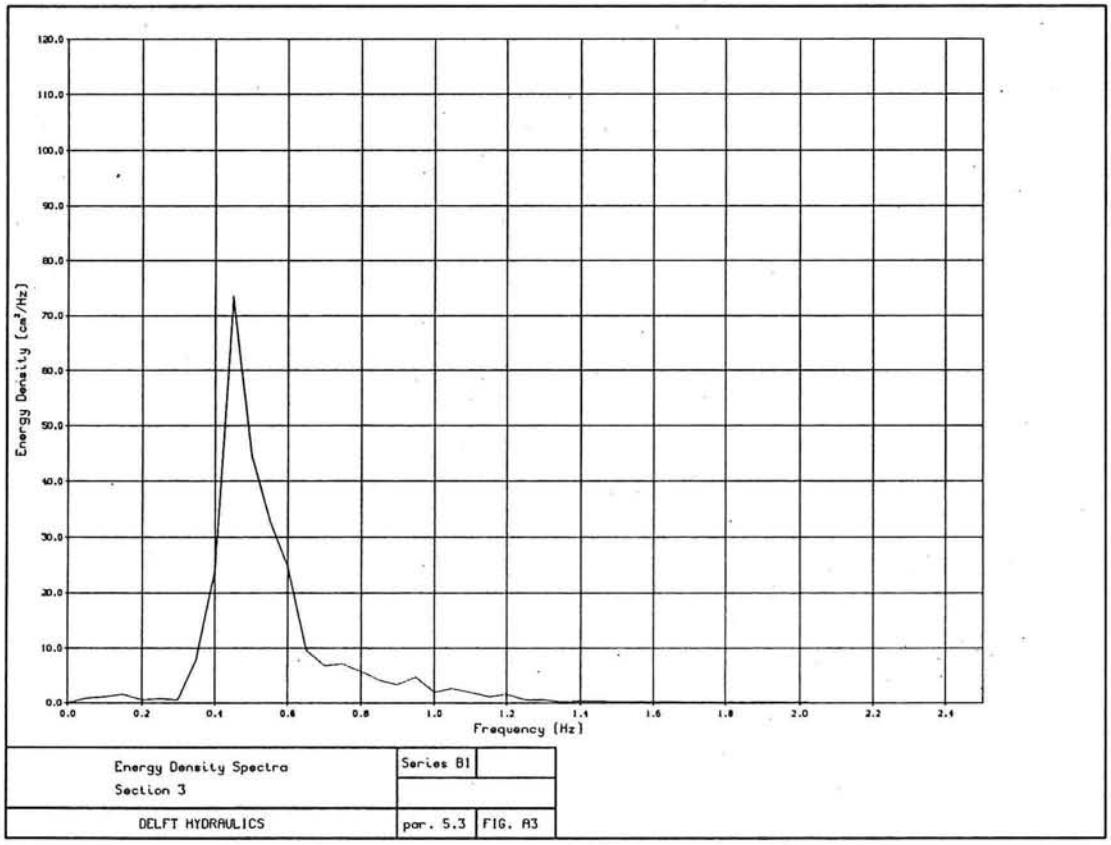

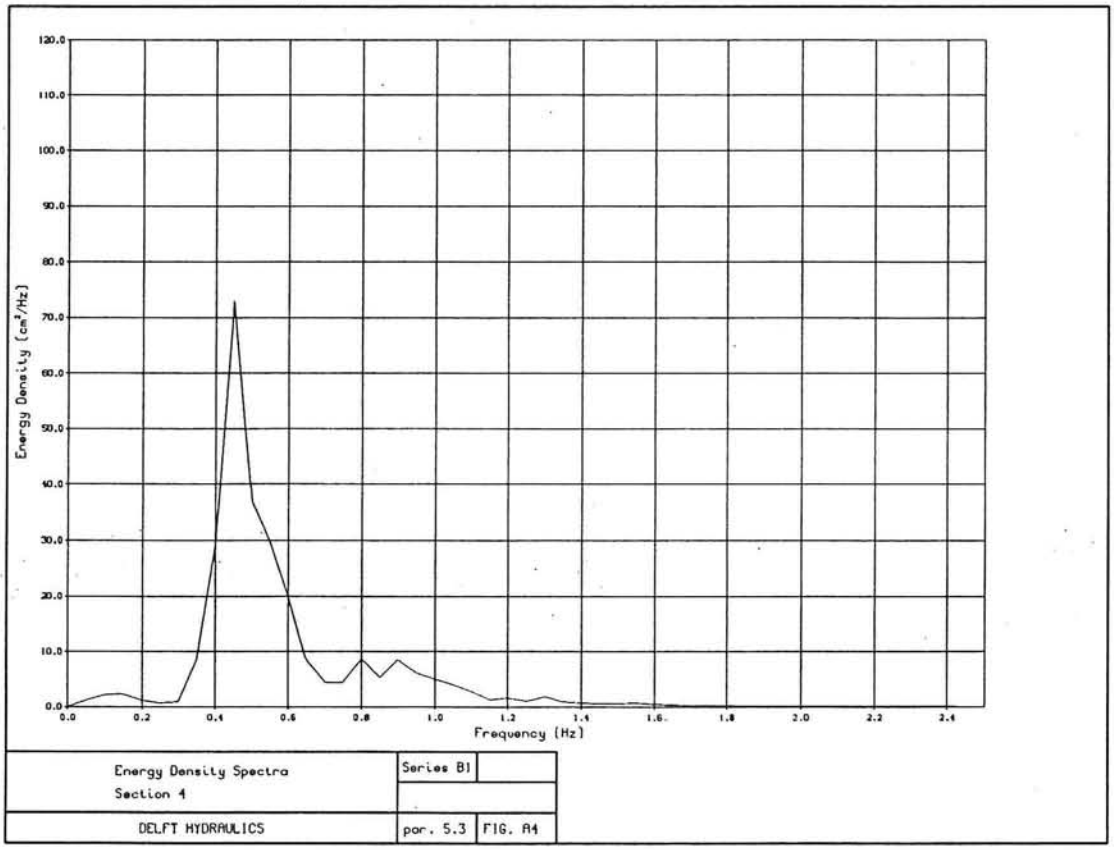

Figure 5.2.A3 - 5.2.A4

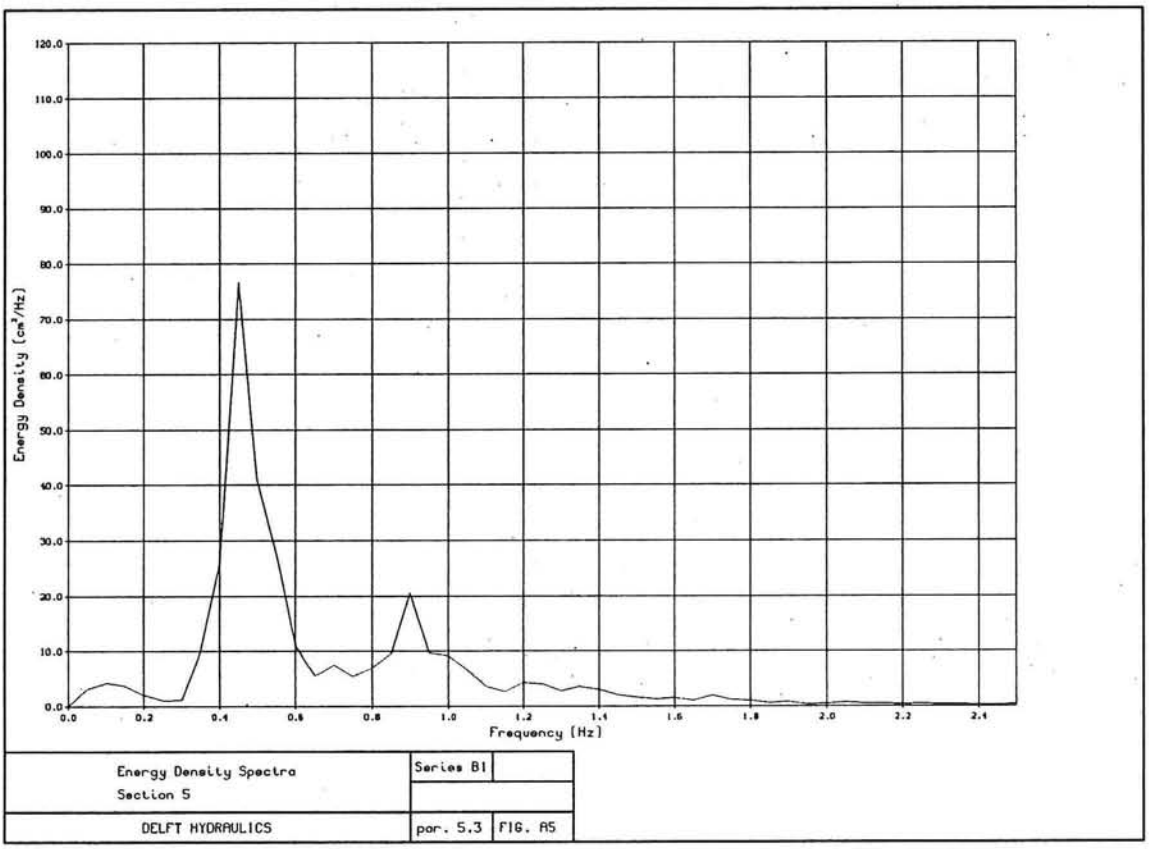

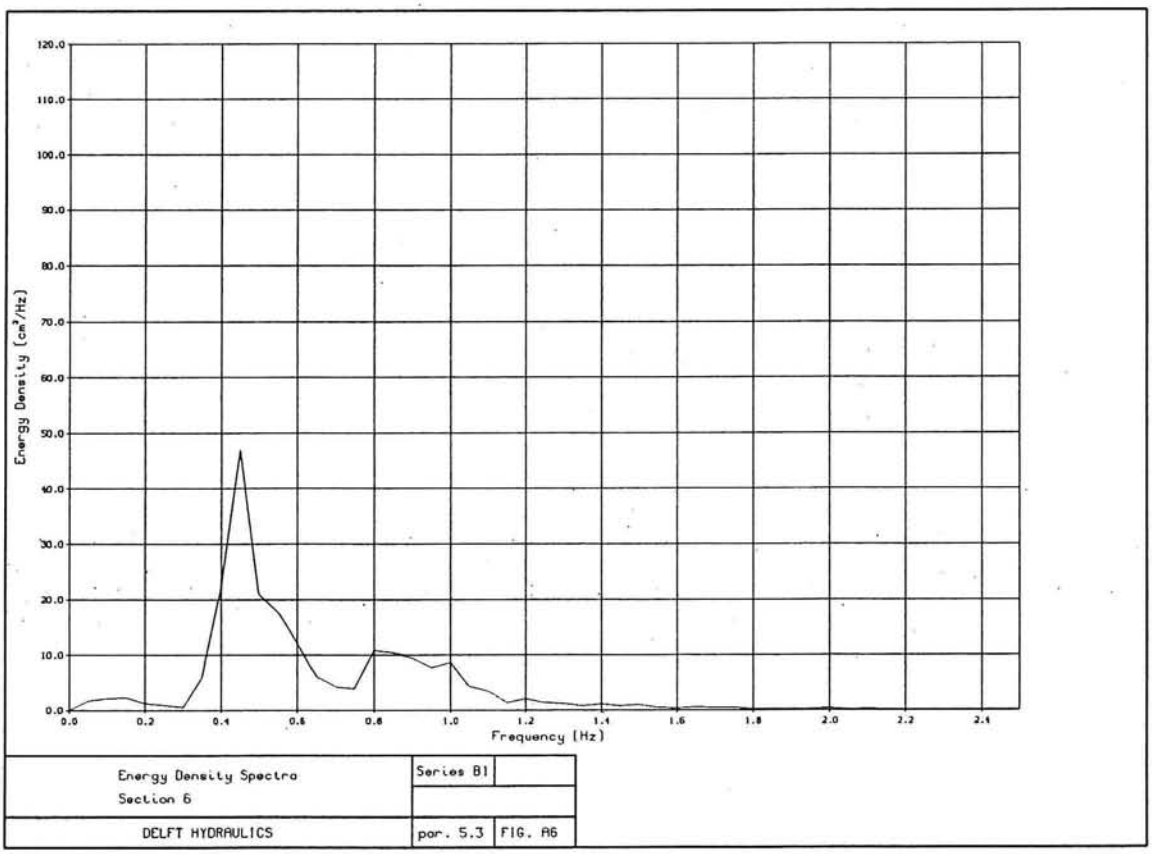

Figure 5.2.A5 - 5.2.A6

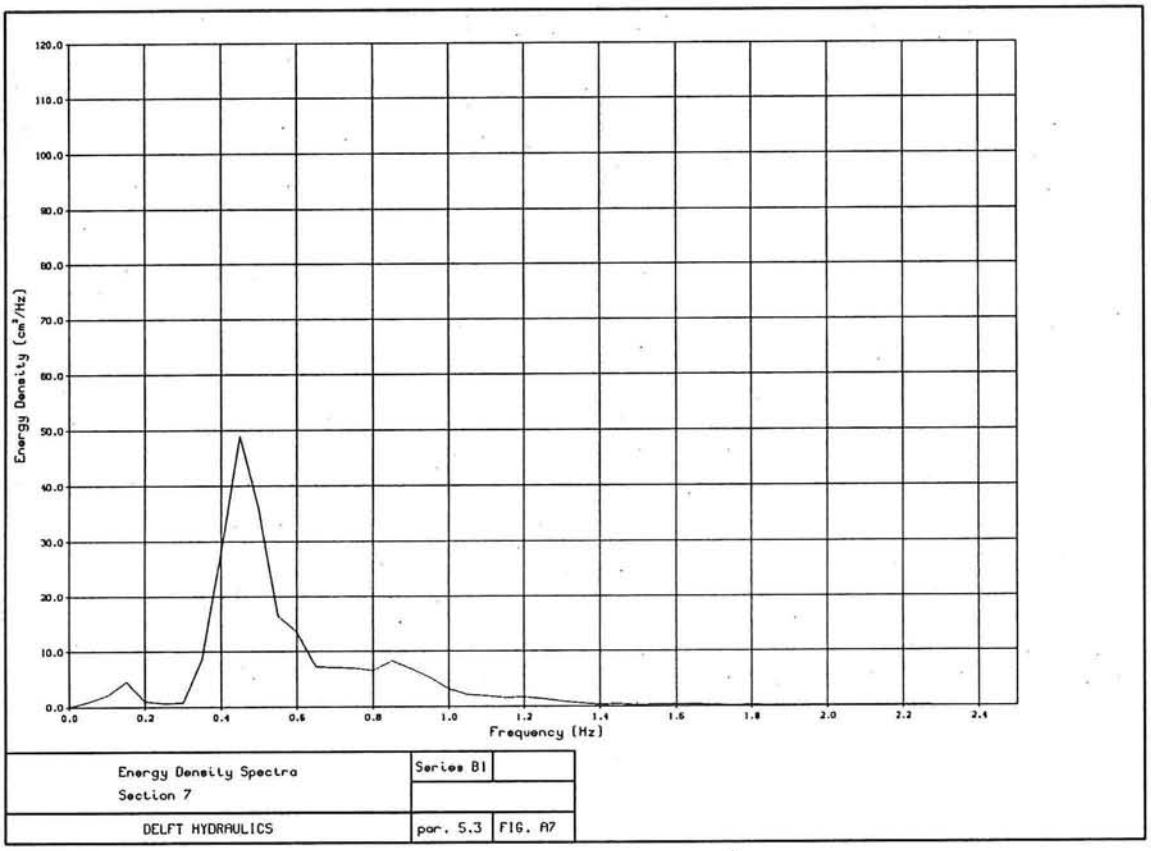

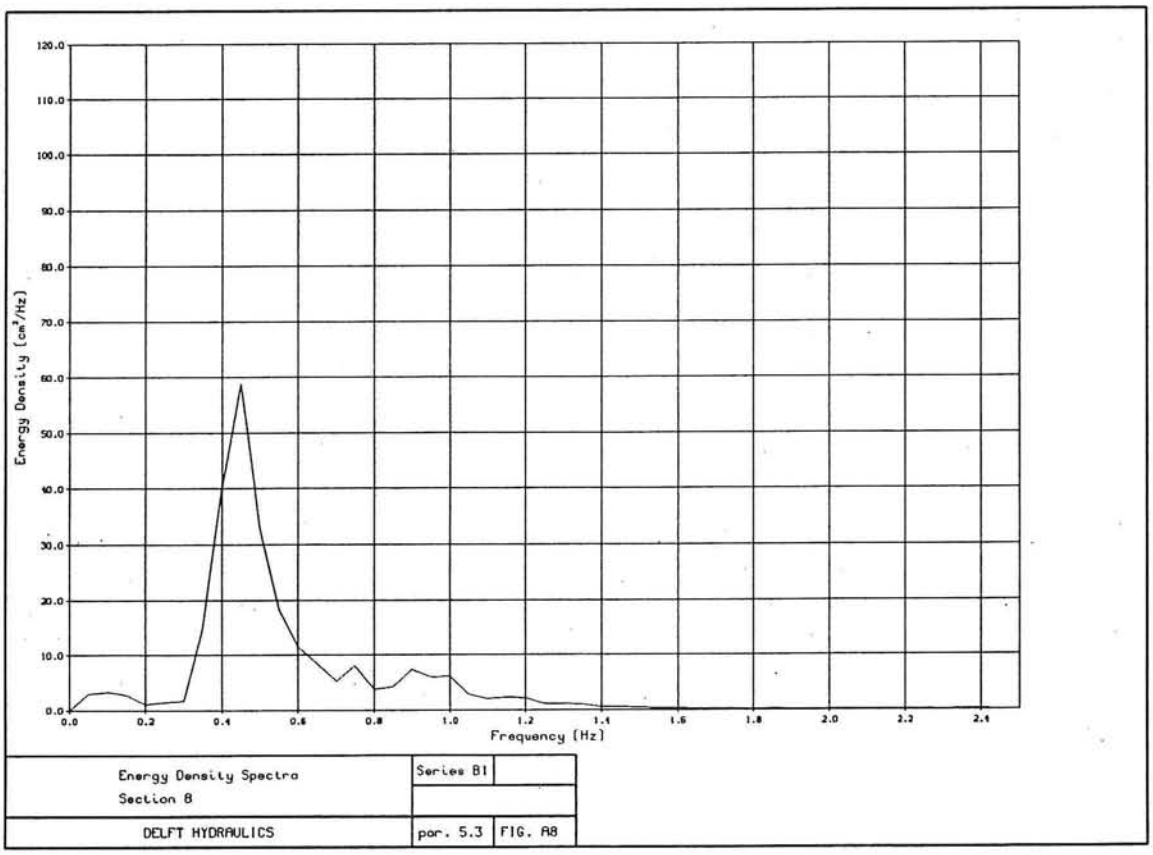

Figure 5.2.A7 - 5.2.A8

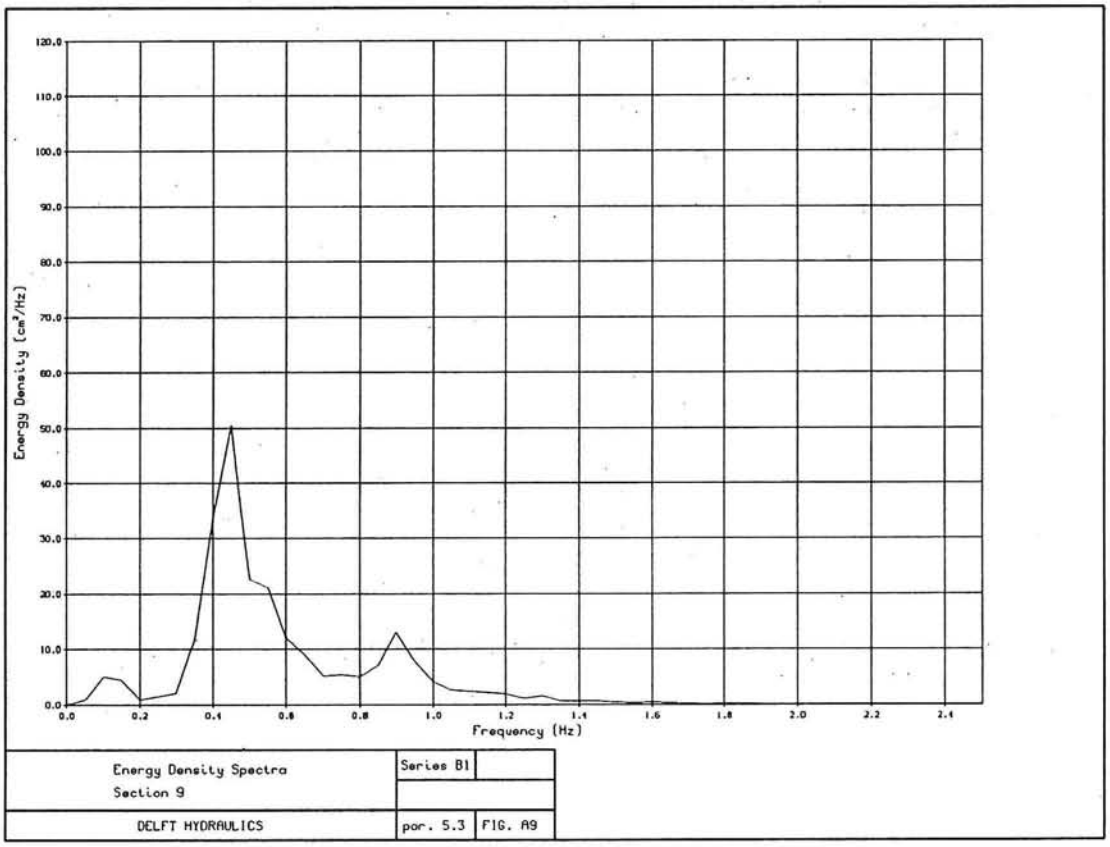

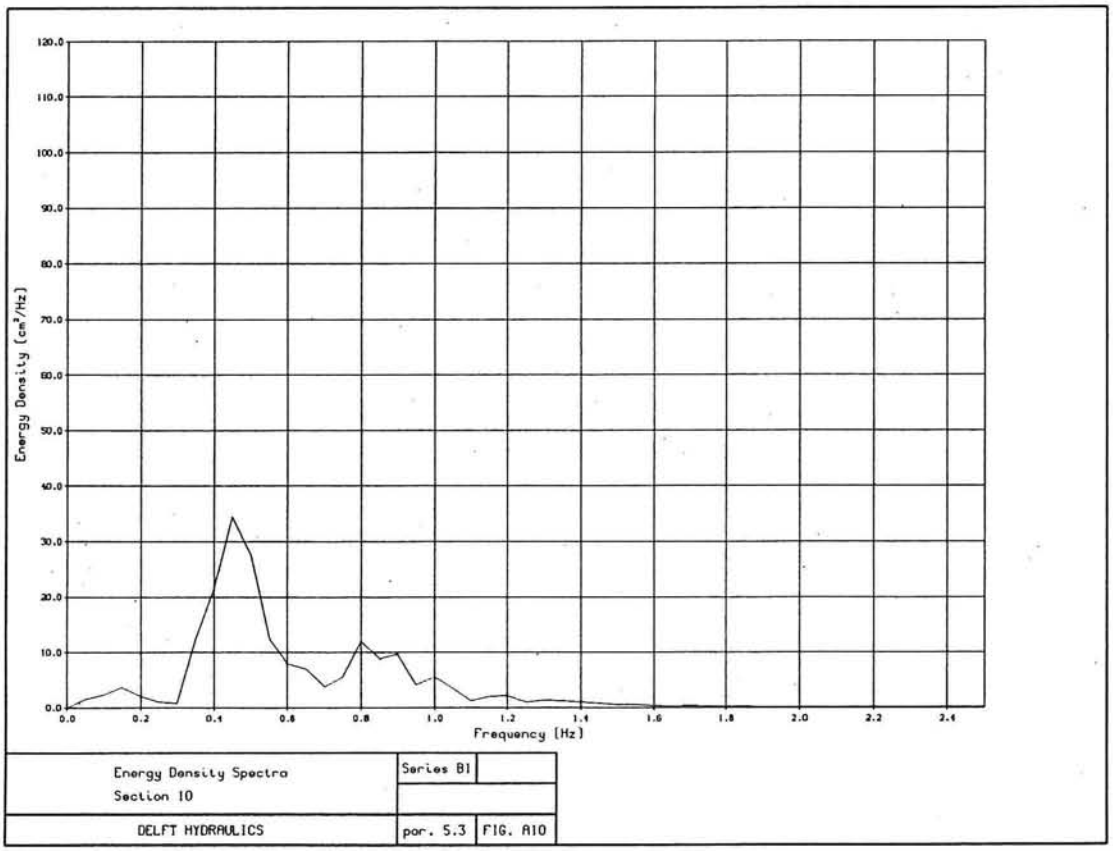

Figure 5.2.A9 - 5.2.A10

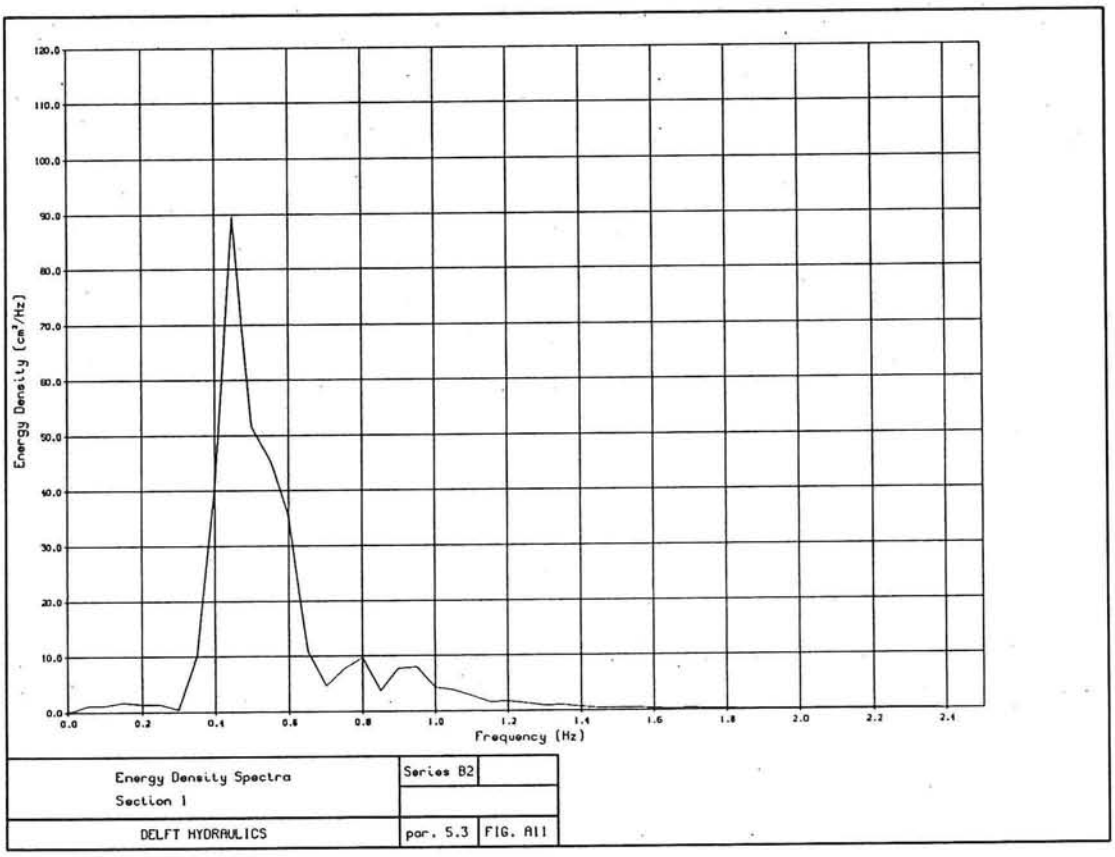

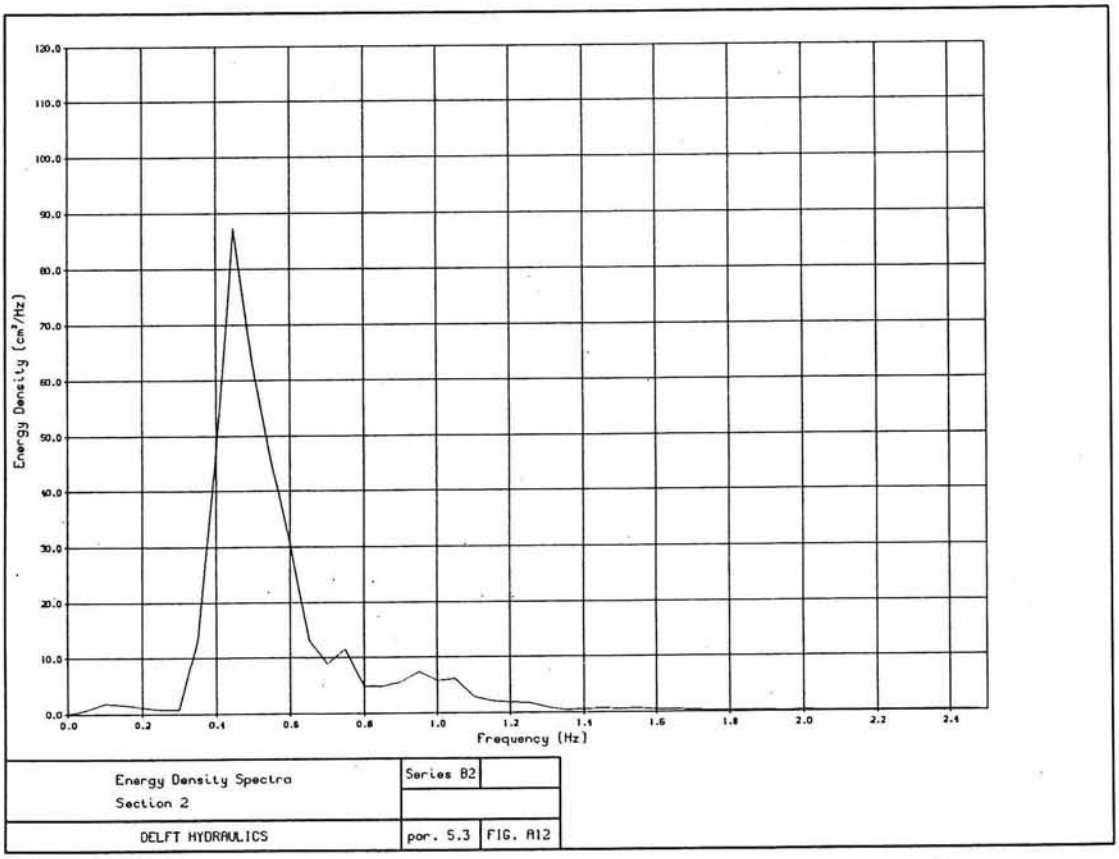

Figure 5.2.A11 - 5.2.A12

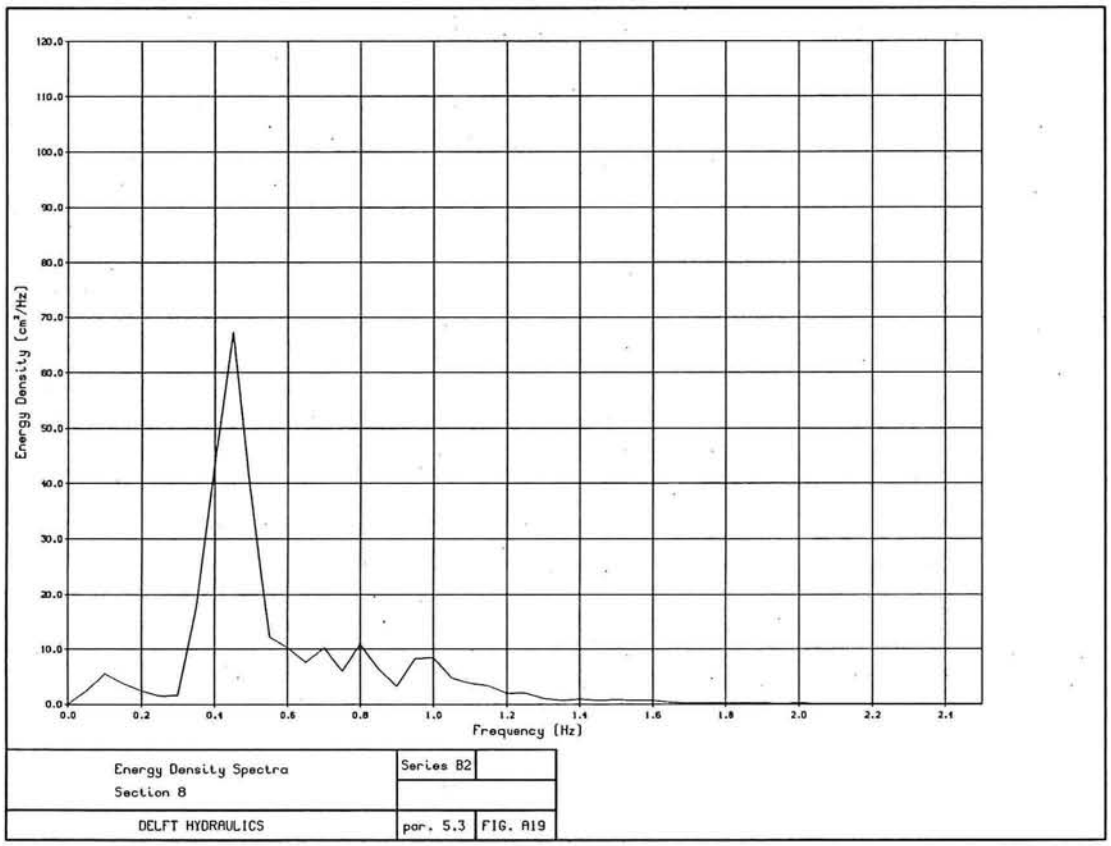

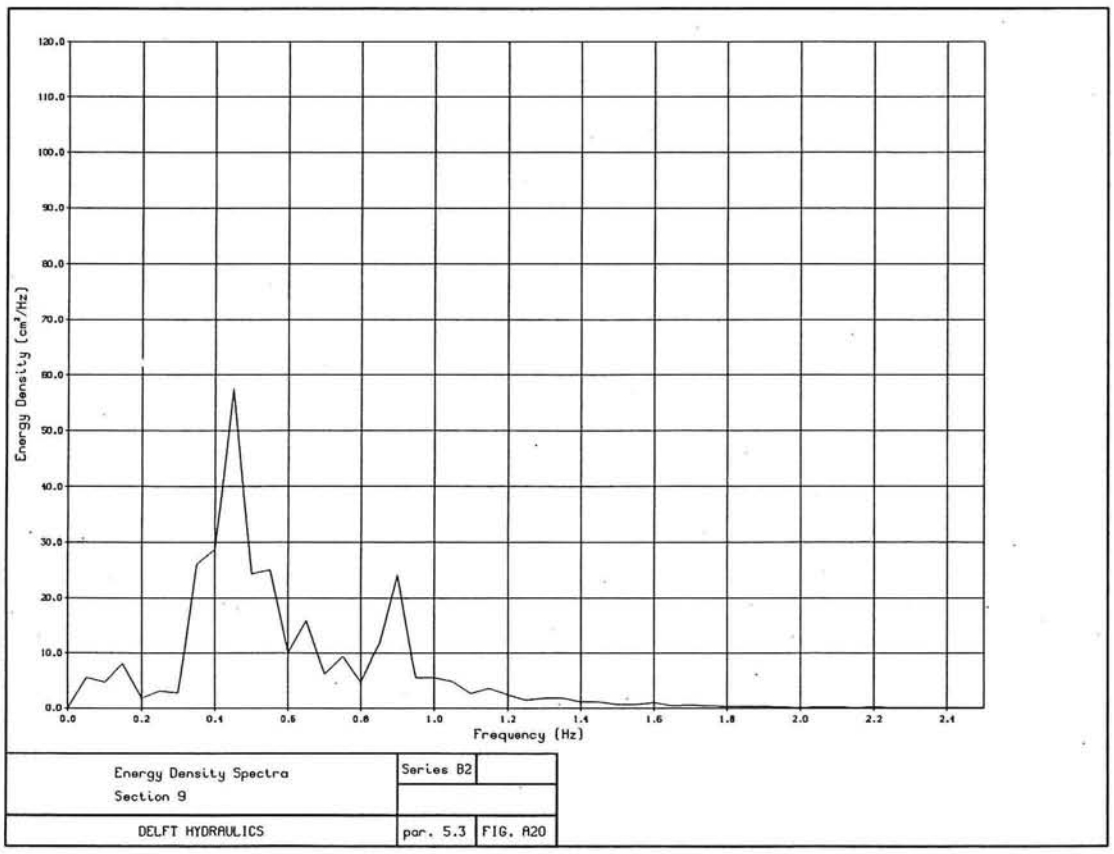

Figure 5.2.A19 - 5.2A20

Wave height Series B1

with parameters Hs/h, Hs/L, Qb

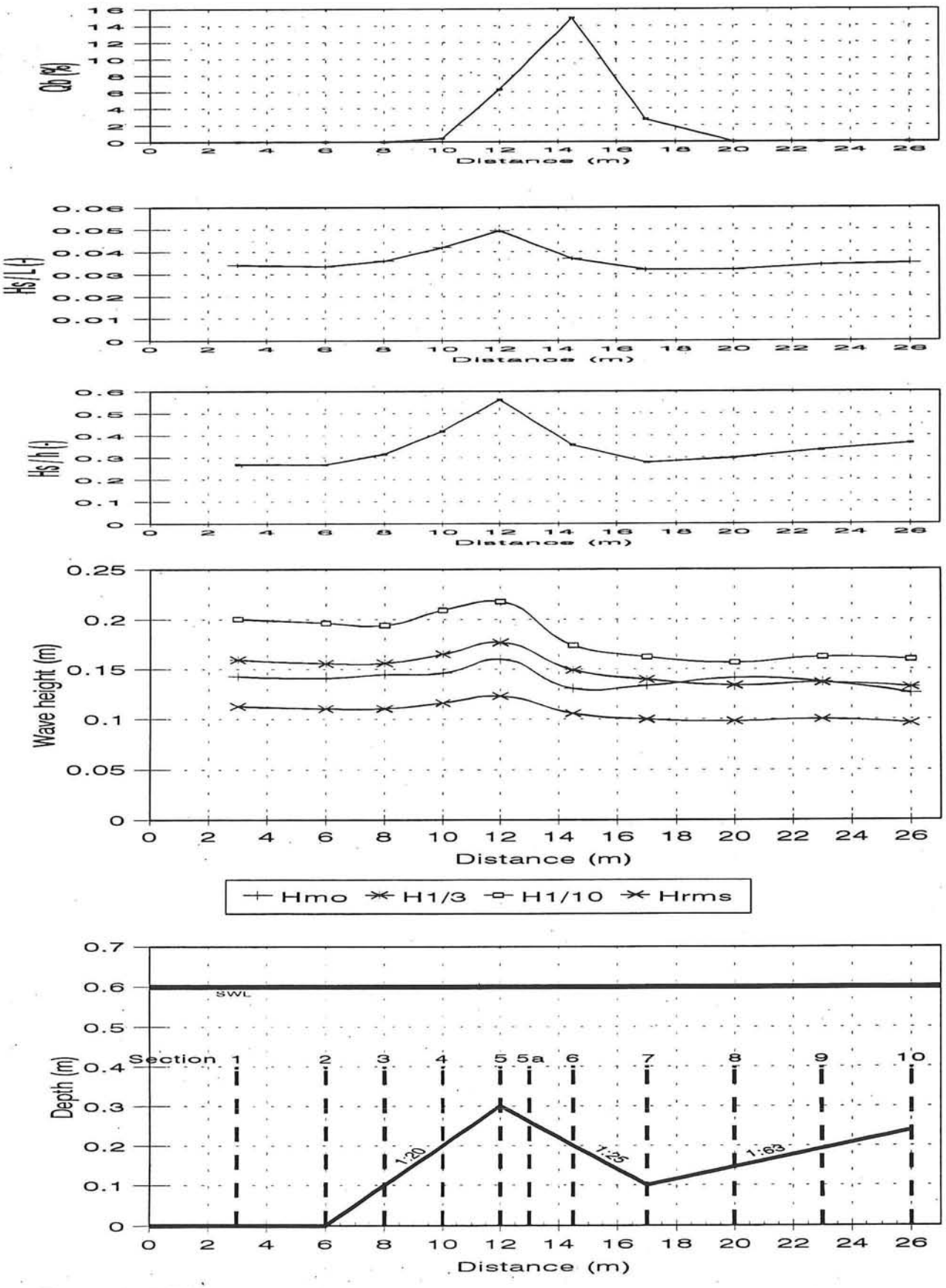

Figure 5.2.B1

Wave height prediction by *Durosta*

and measured values
Series B1

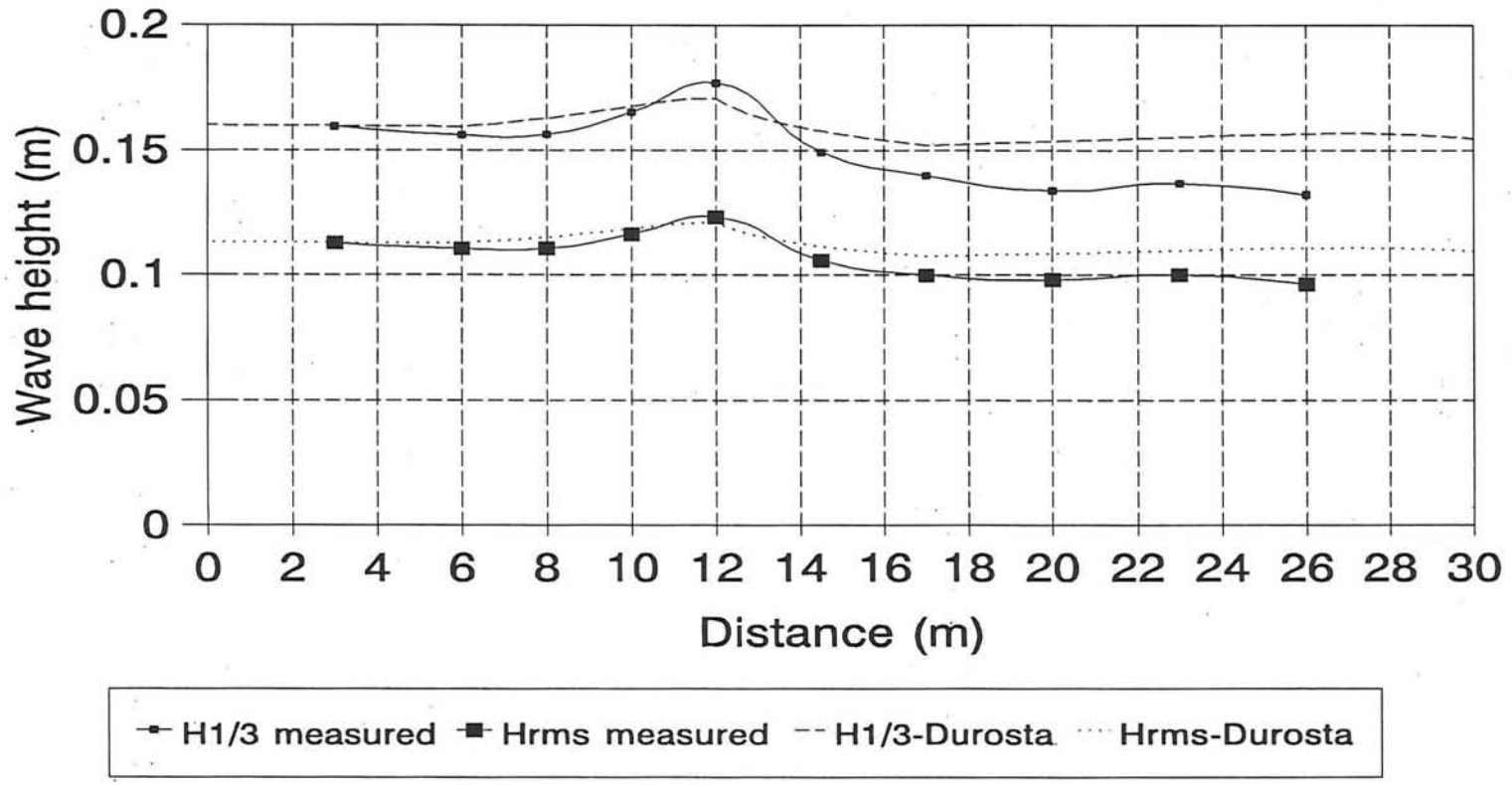

Figure 5.2.B3

Wave height prediction by *Durosta*

and measured values
Series B2

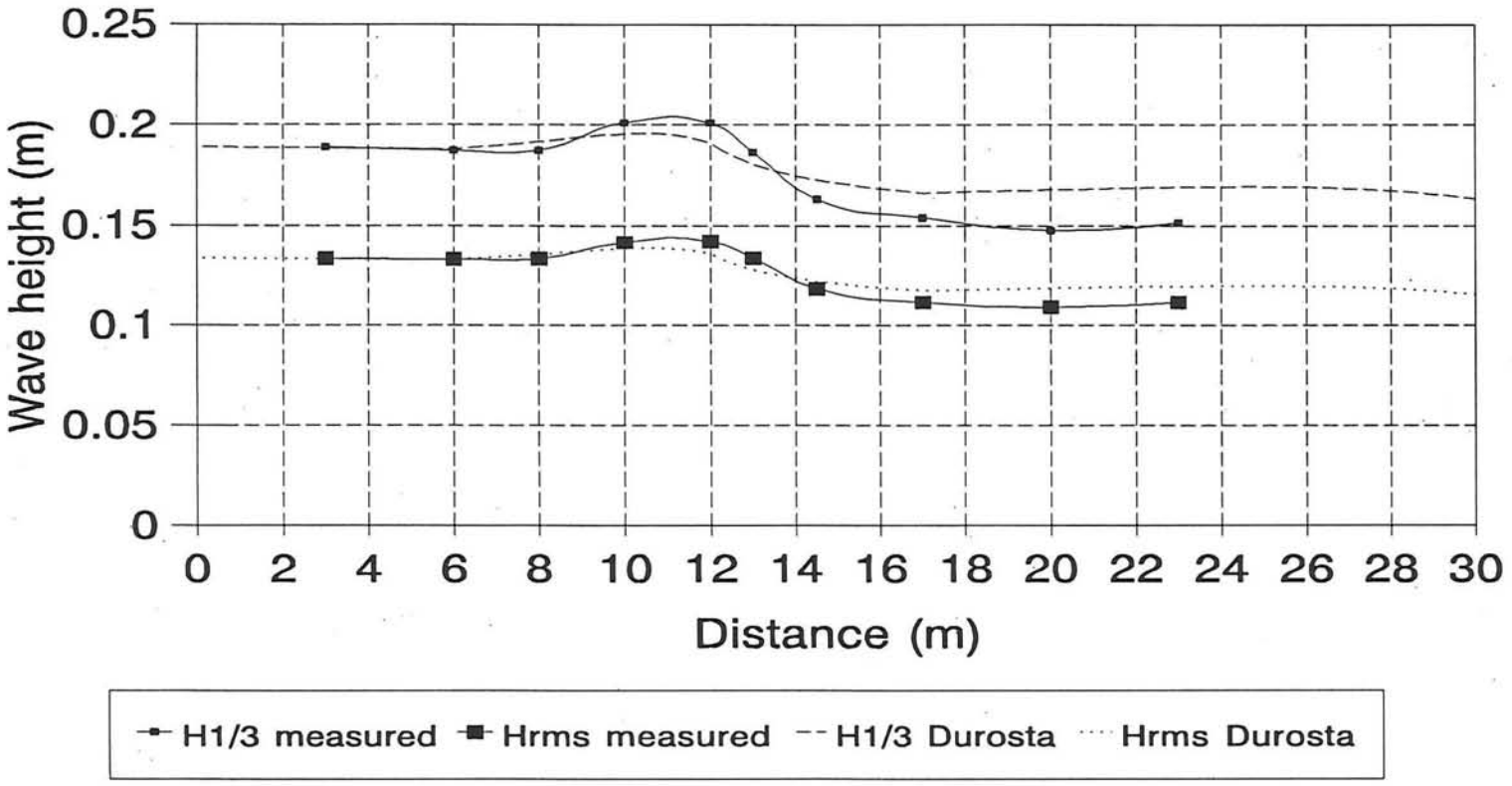

Figure 5.2.B4

Wave length Series B1

with parameters Hs/h, Hs/L, Qb

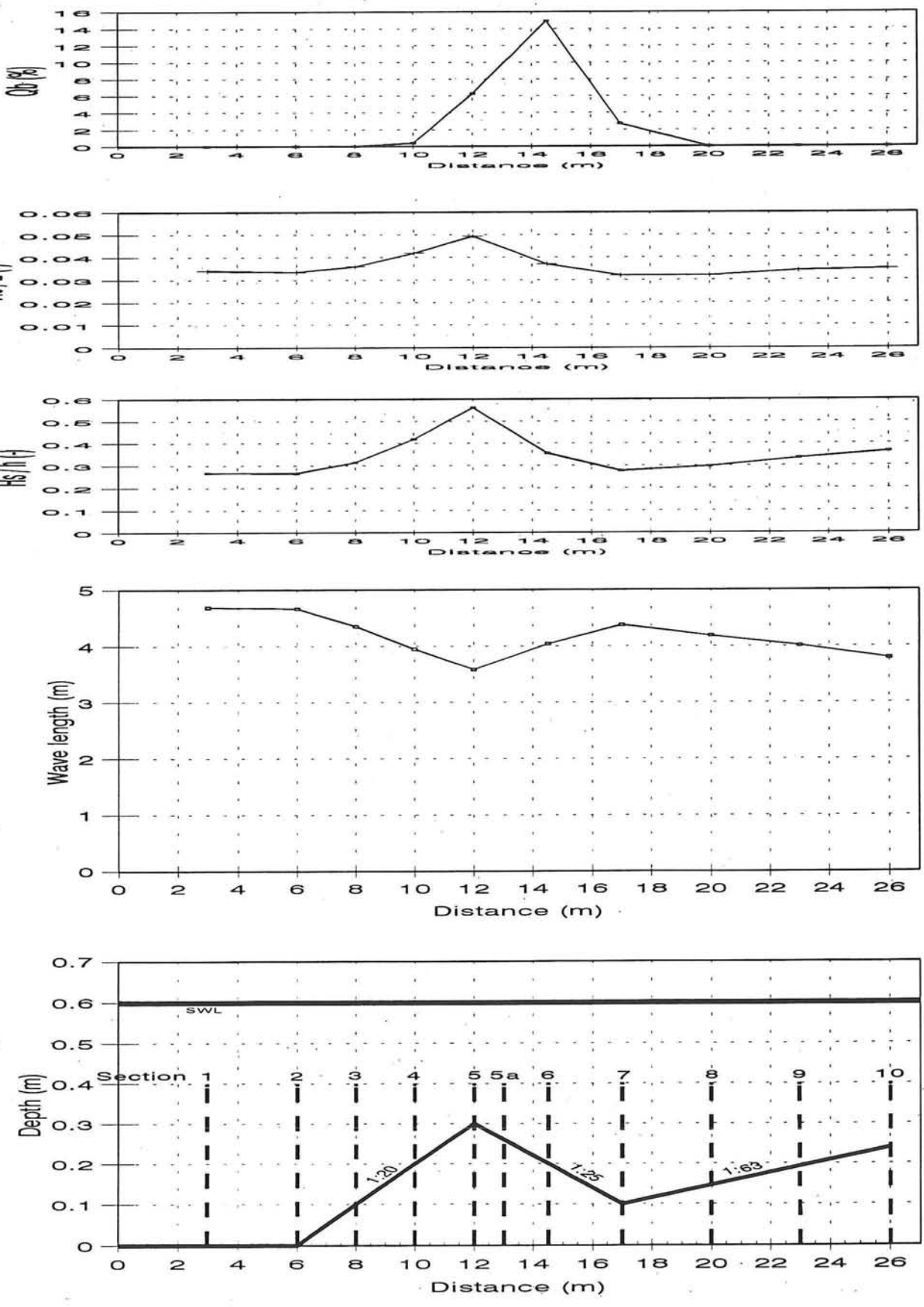

Figure 5.2.C1

Wave length Series B2

with parameters Hs/h, Hs/L, Qb

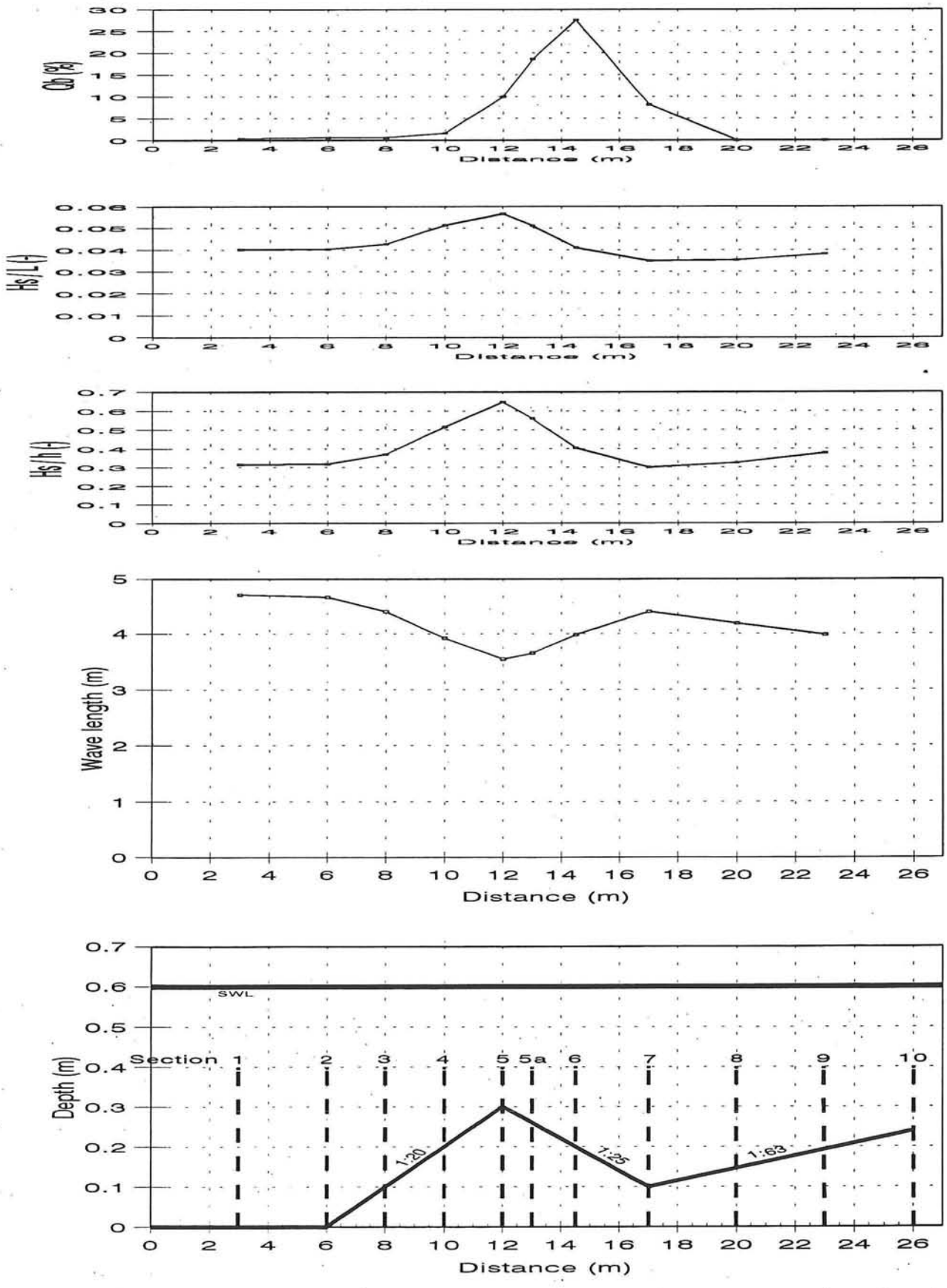

Figure 5.2.C2

Periods Series B1

with parameters Hs/h, Hs/L, Qb

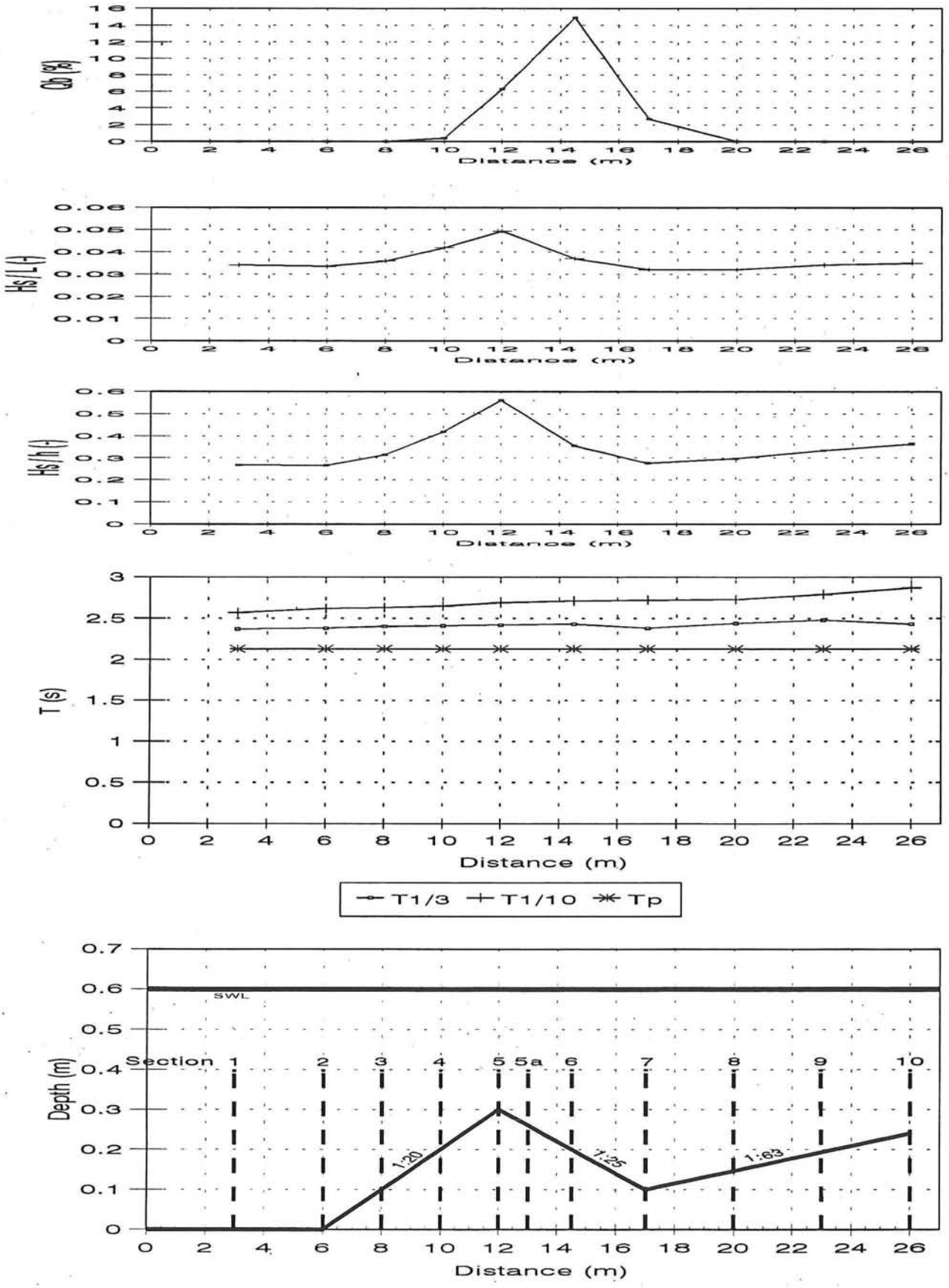

Figure 5.2.C3

Periods Series B2

with parameters Hs/h, Hs/L, Qb

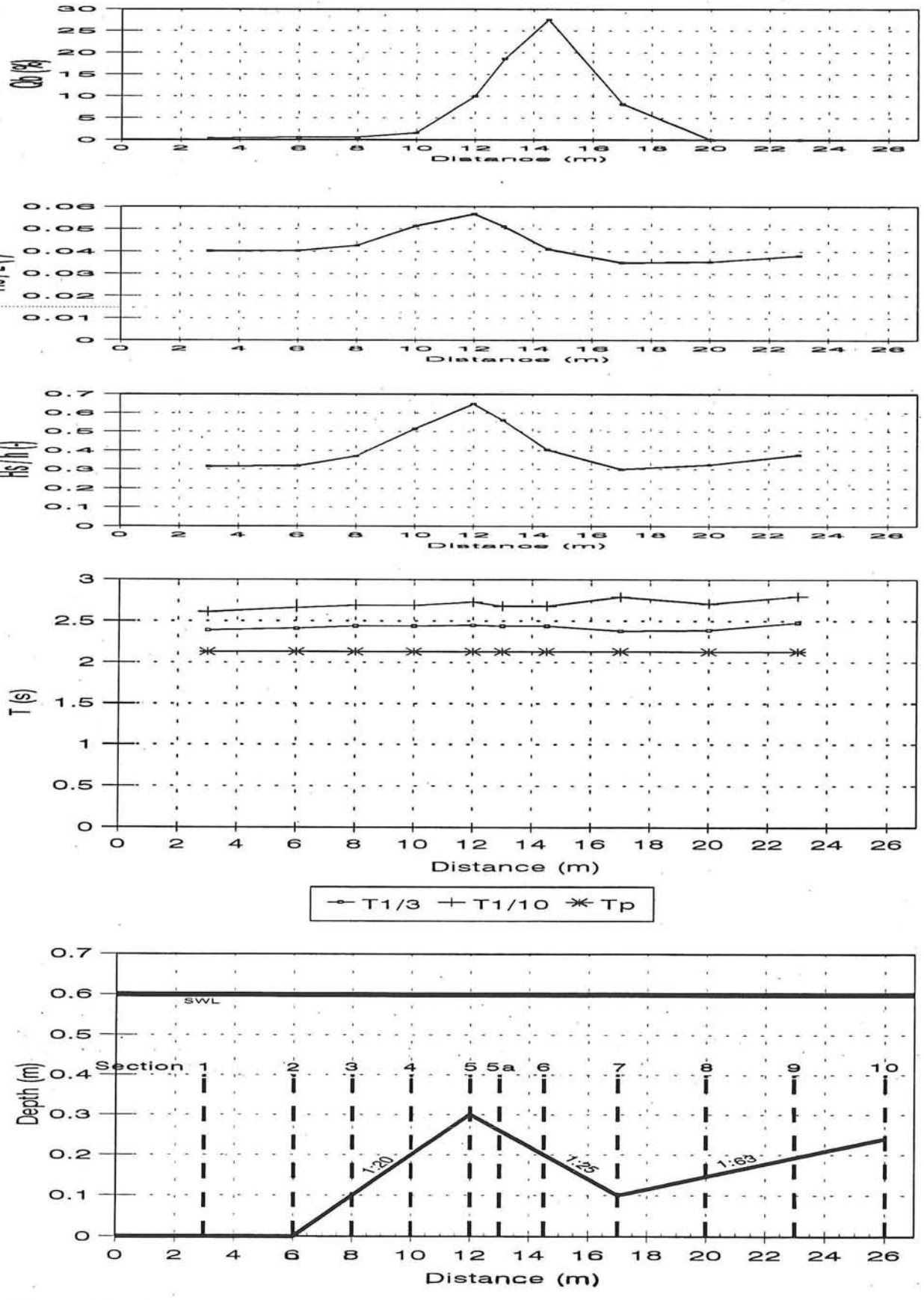

Figure 5.2.C4

Percentage breaking waves Qb

Influence Hs/h

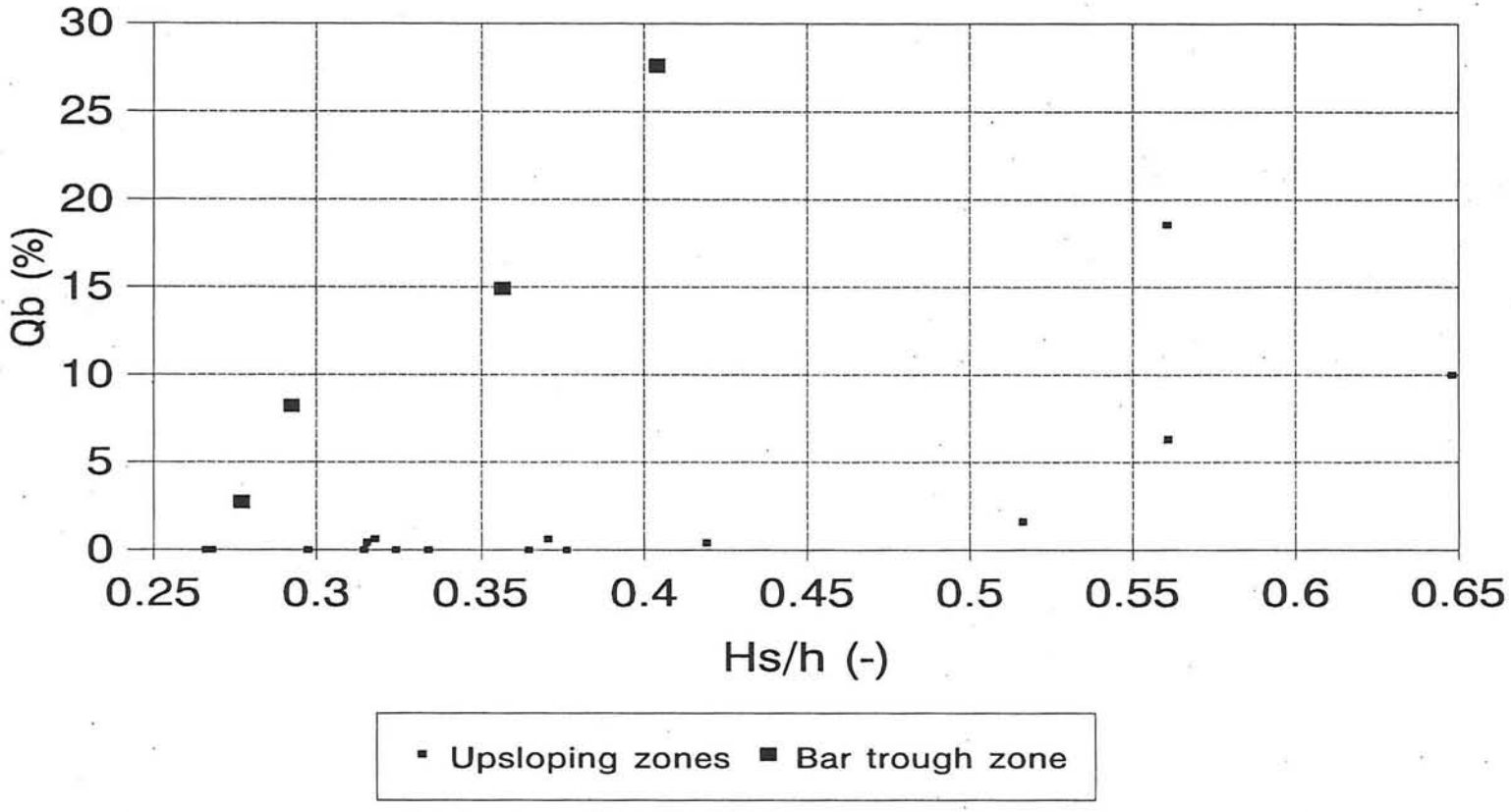

Figure 5.2.D1

Concentration profile series B1

Section 1, Hs = 15.96 cm

T 16 00 01

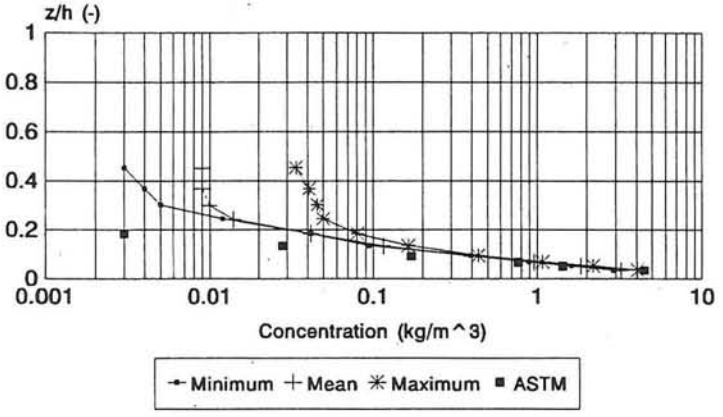

Figure 5.3.A1

Concentration profile series B1

Section 2, Hs = 15.60 cm

T 16 00 02

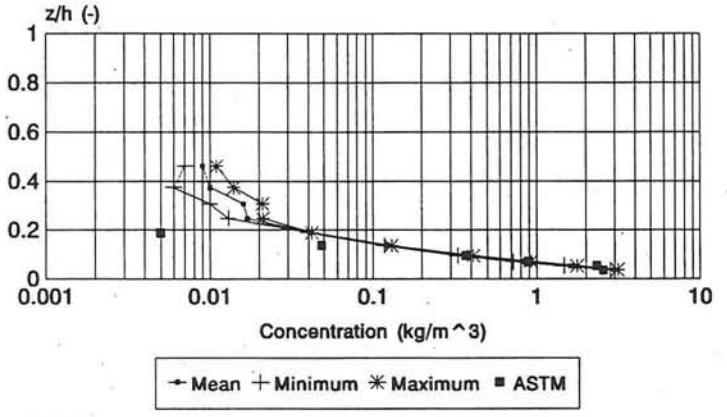

Figure 5.3.A2

Concentration profile series B1

Section 3, Hs = 15.60 cm

T 16 00 03

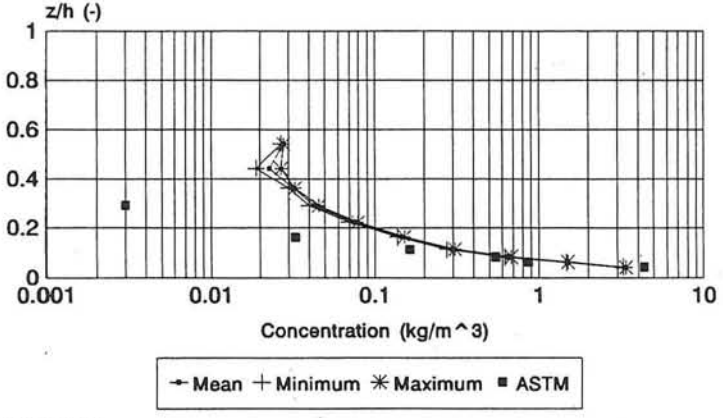

Figure 5.3.A3

Concentration profile series B1

Section 4, Hs = 16.52 cm

T 17 00 04

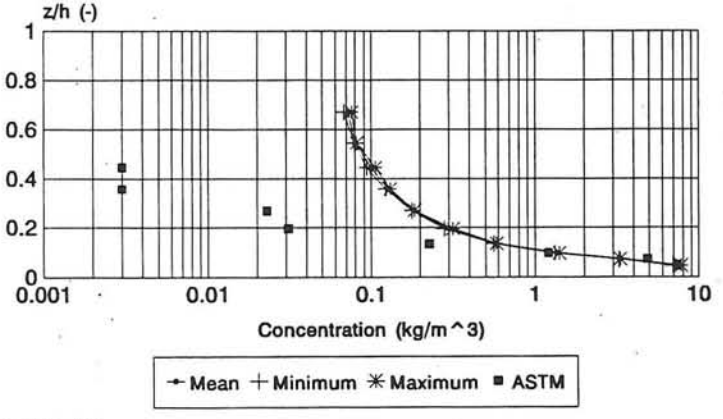

Figure 5.3.A4

Concentration profile series B1

Section 5, Hs = 17.69 cm

T 18 00 05

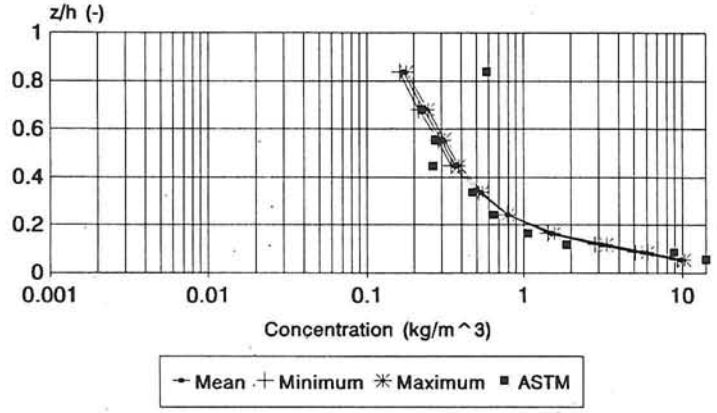

Figure 5.3.A5

Concentration profile series B1

Section 6, Hs = 14.93 cm

T 15 00 06

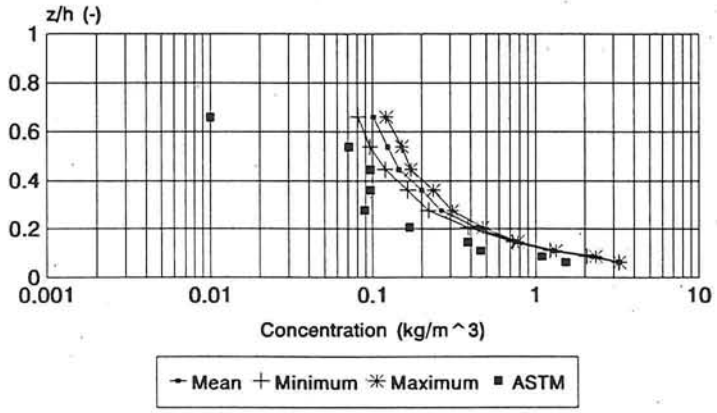

Figure 5.3.A6

Concentration profile series B1

Section 7, Hs = 13.98 cm

T 14 00 07

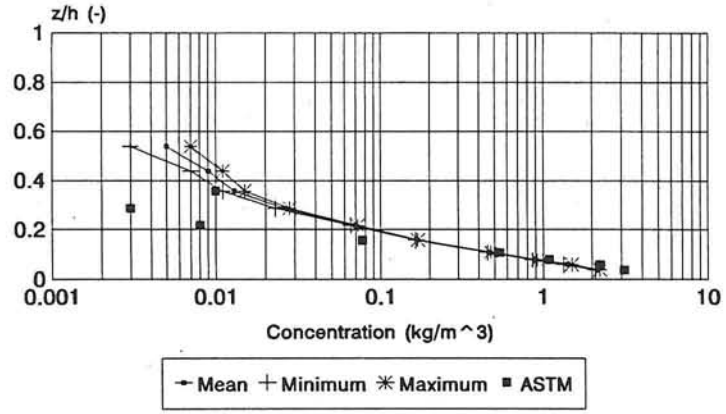

Figure 5.3.A7

Concentration profile series B1

Section 8, Hs = 13.39 cm

T 13 00 08

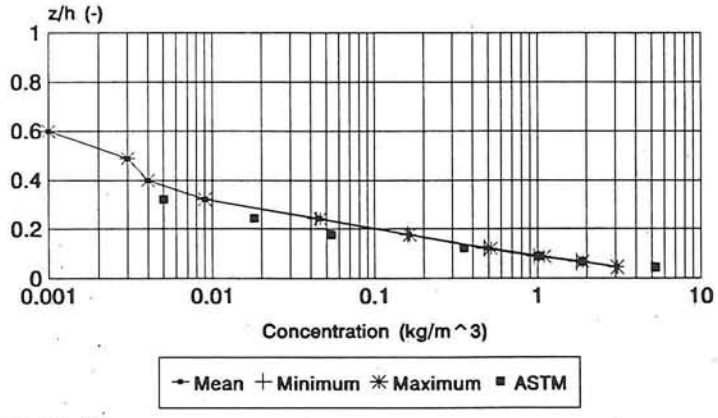

Figure 5.3.A8

Concentration profile series B1

Section 9, Hs = 13.67 cm

T 14 00 09

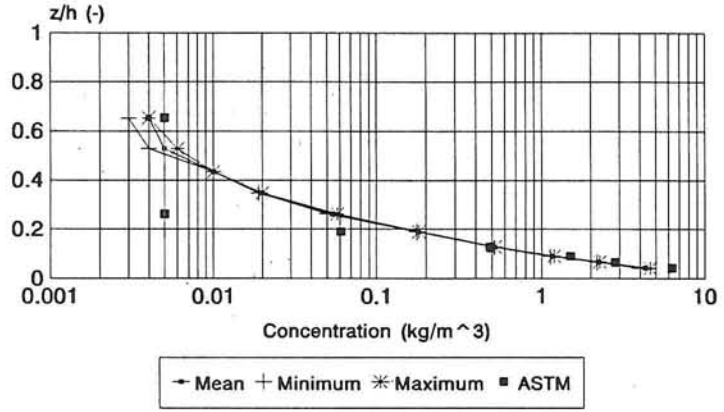

Figure 5.3.A9

Concentration profile series B1

Section 10, Hs = 13.22 cm

T 13 00 10

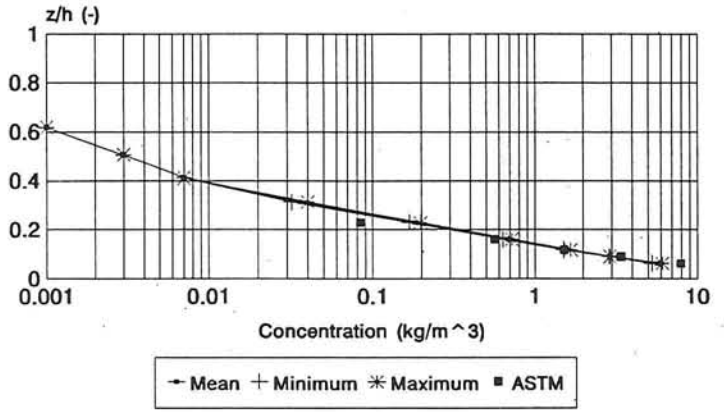

Figure 5.3.A10

Concentration profile series B2

Section 1, Hs = 18.90 cm

T 19 00 01

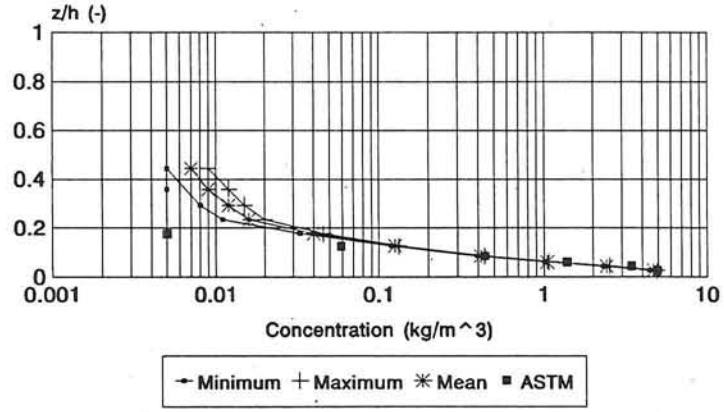

Figure 5.3.A11

Concentration profile series B2

Section 2, Hs = 18.75 cm

T 19 00 02

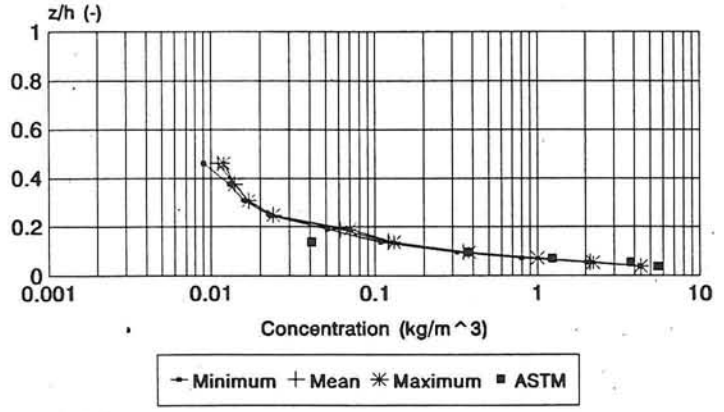

Figure 5.3.A12

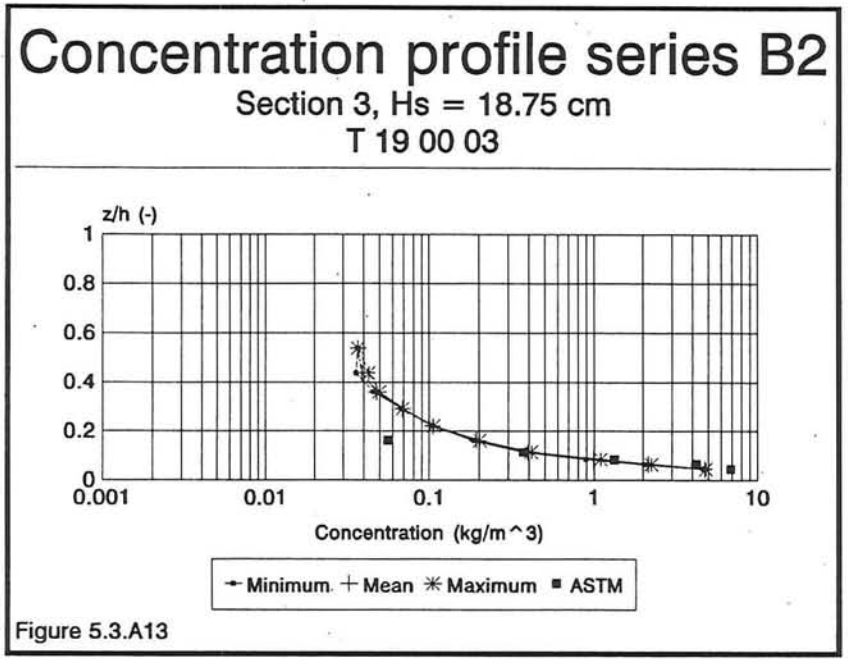

Figure 5.3.A13

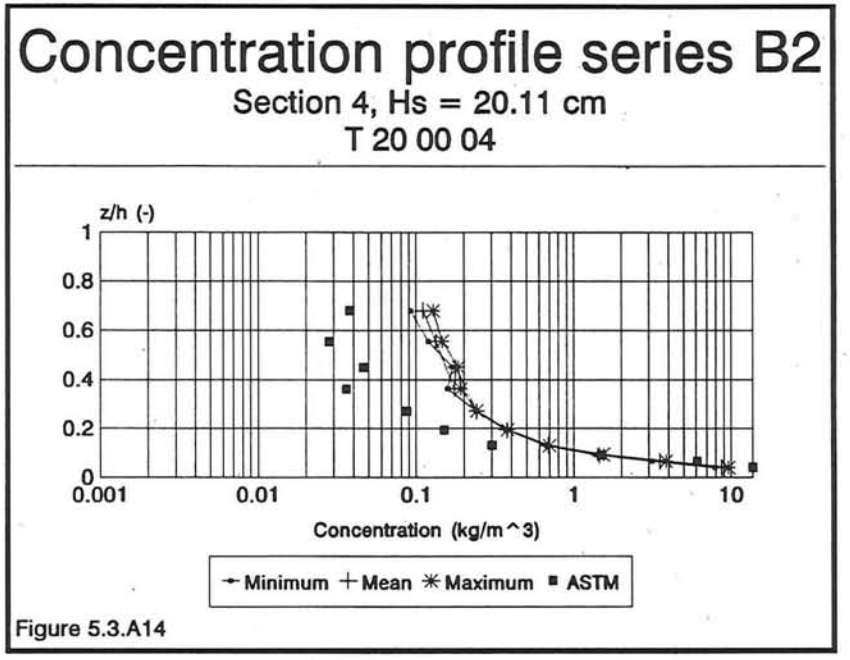

Figure 5.3.A14

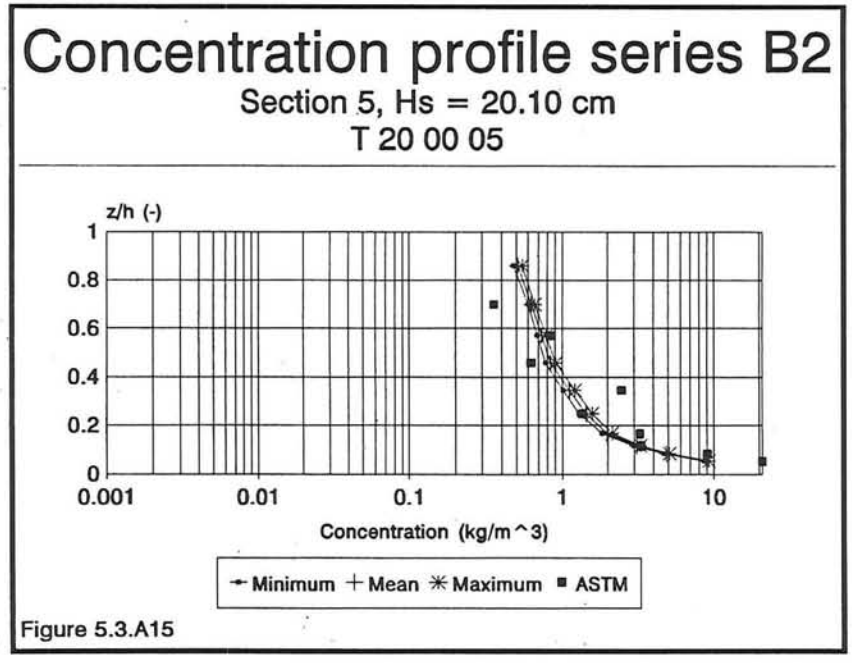

Figure 5.3.A15

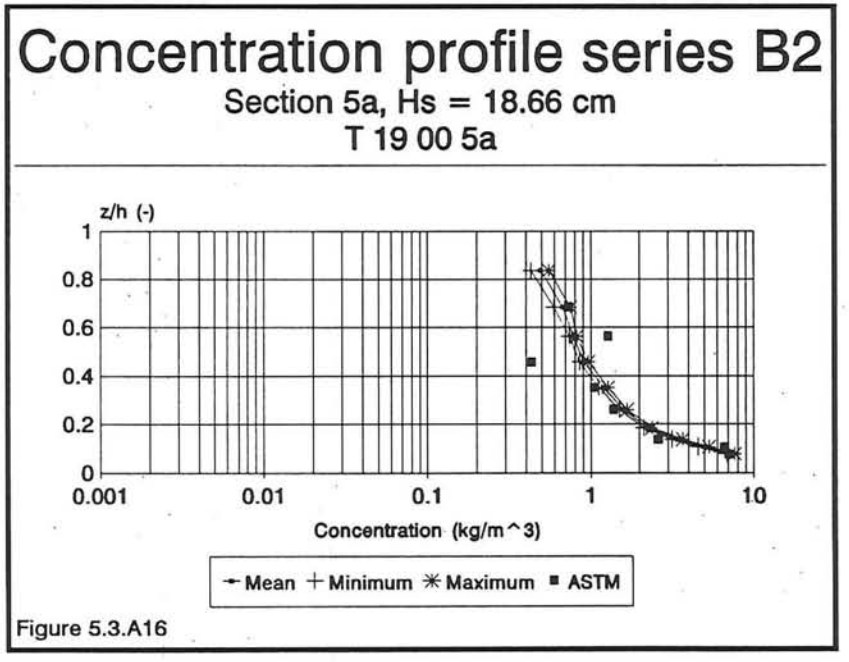

Figure 5.3.A16

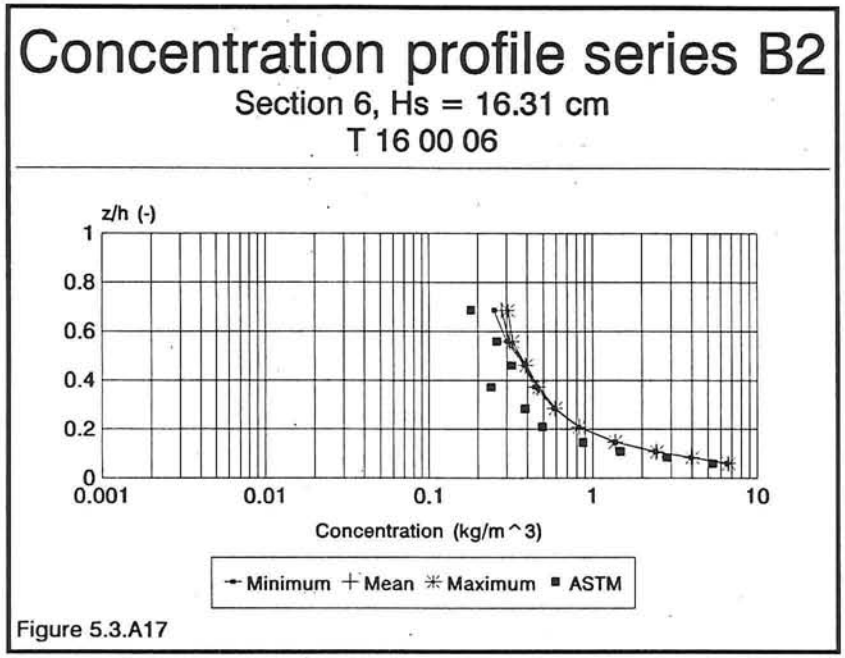

Figure 5.3.A17

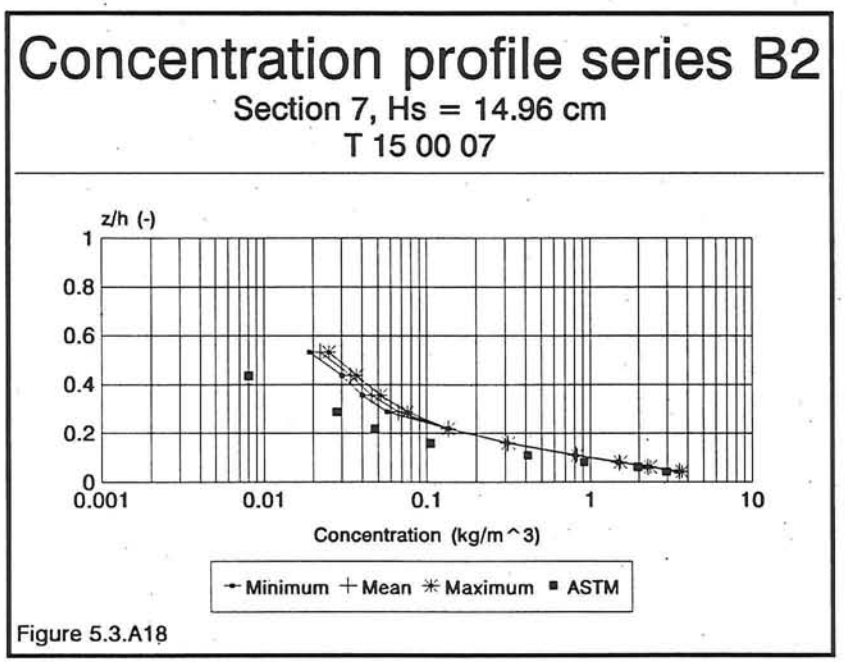

Figure 5.3.A18

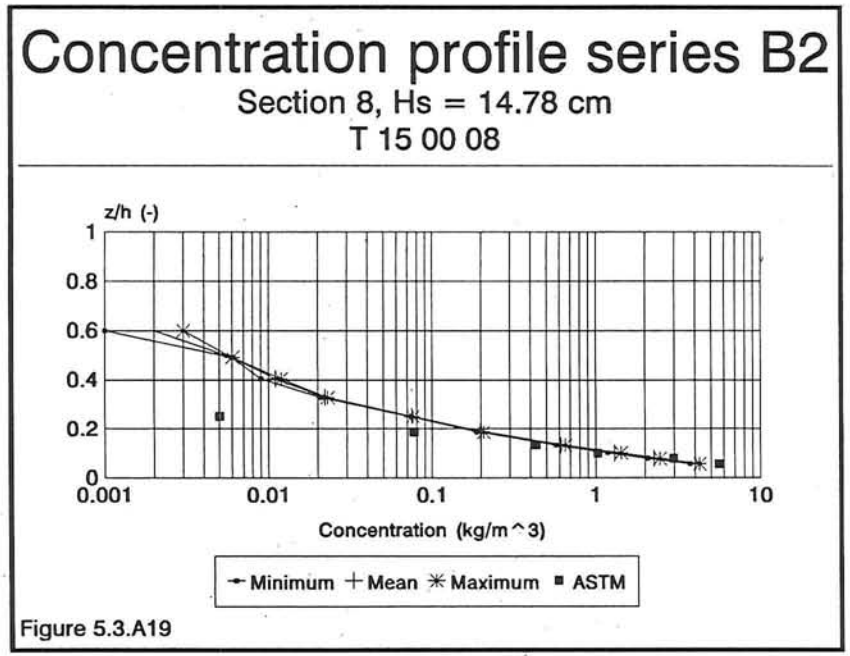

Figure 5.3.A19

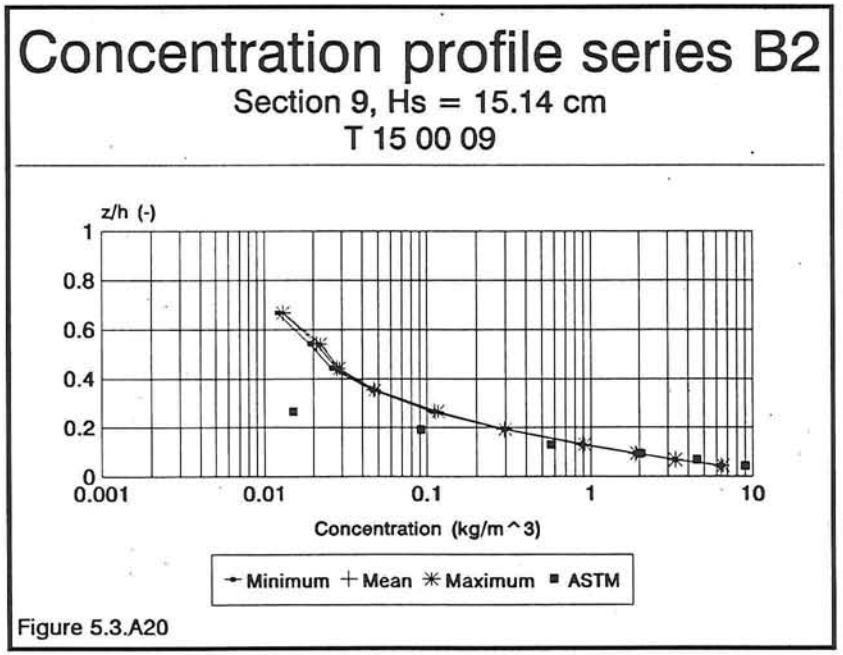

Figure 5.3.A20

Concentration profile section 1

Influence wave height

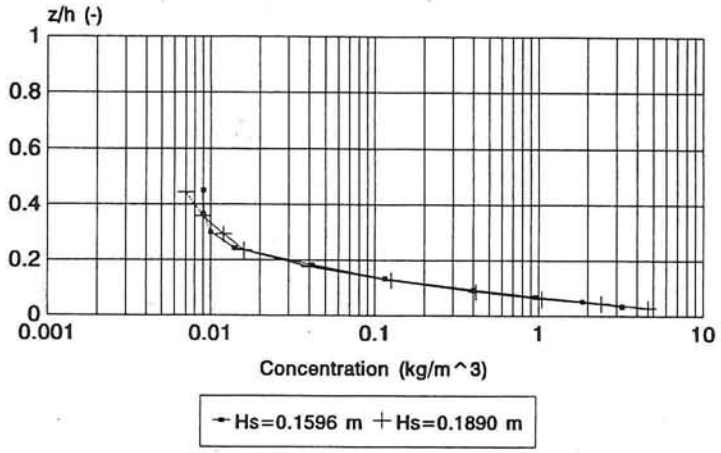

Figure 5.3.B1

Concentration profile section 2

Influence wave height

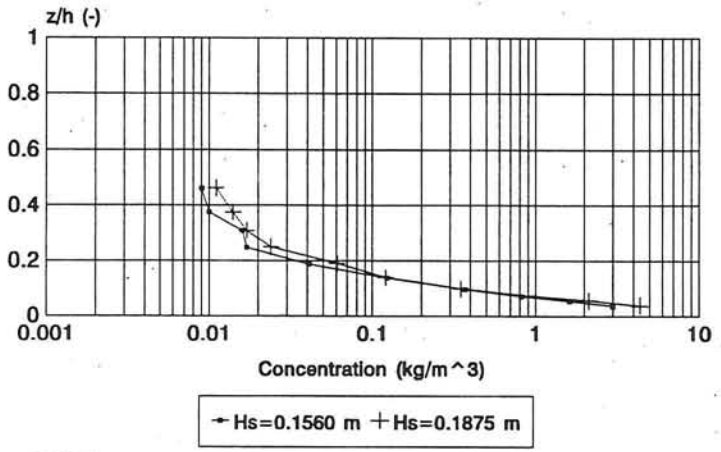

Figure 5.3.B2

Concentration profile section 3

Influence wave height

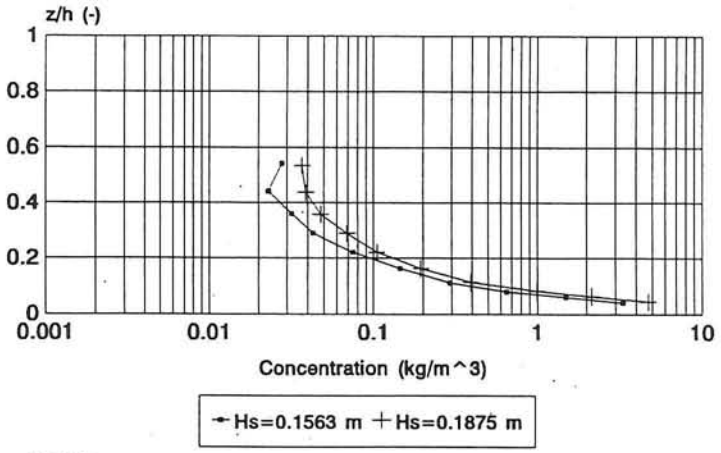

Figure 5.3.B3

Concentration profile section 4

Influence wave height

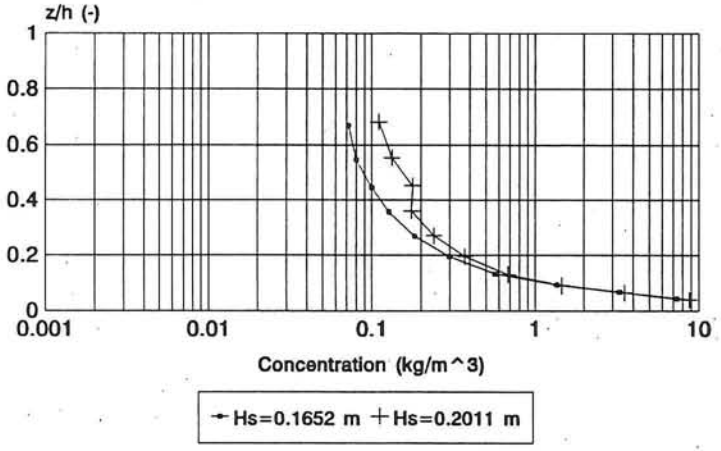

Figure 5.3.B4

Concentration profile section 5

Influence wave height

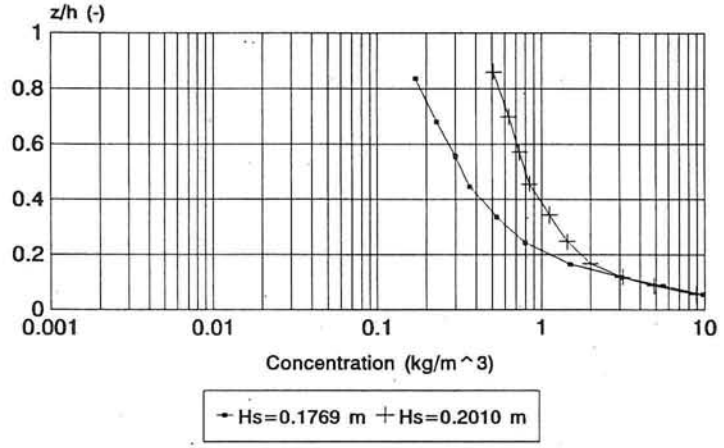

Figure 5.3.B5

Concentration profile section 6

Influence wave height

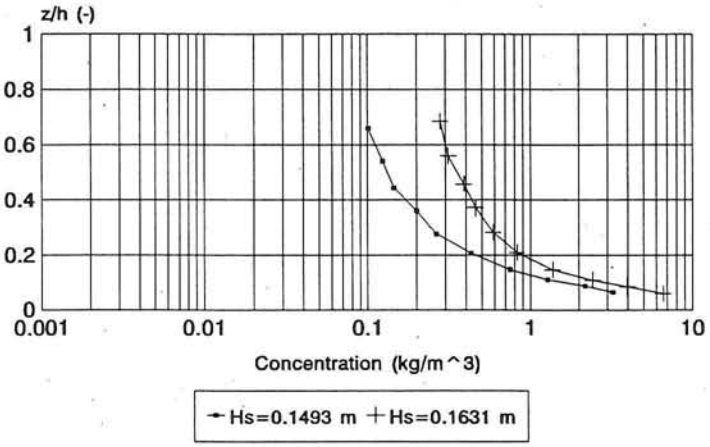

Figure 5.3.B6

Concentration profile section 7

Influence wave height

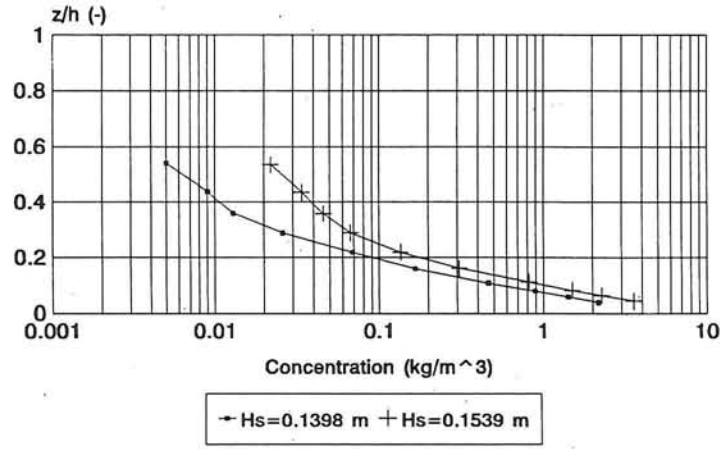

Figure 5.3.B7

Concentration profile section 8

Influence wave height

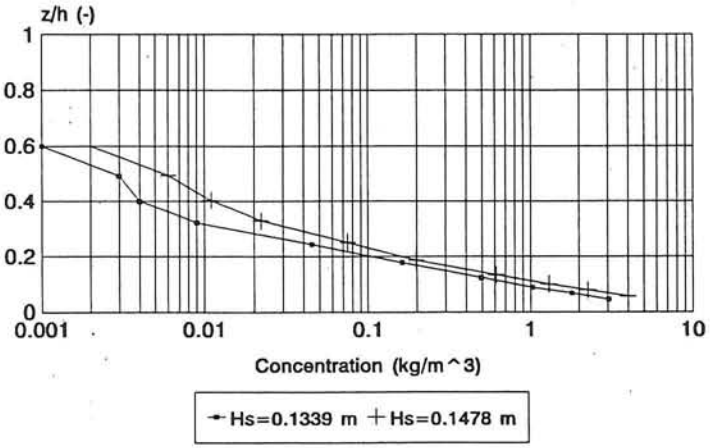

Figure 5.3.B8

Concentration profile section 9

Influence wave height

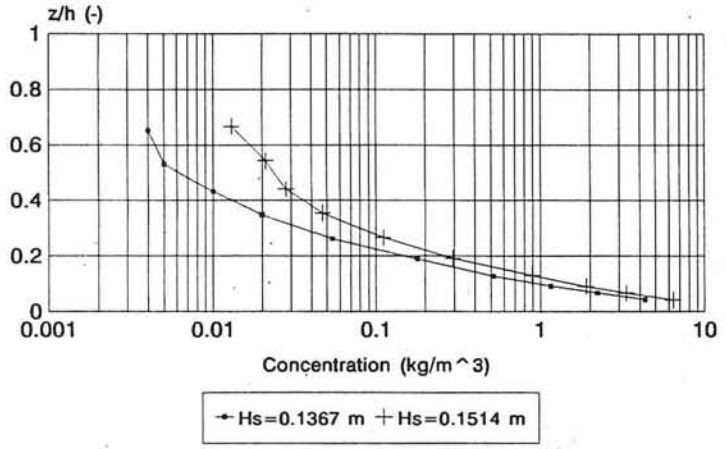

Figure 5.3.B9

Concentration profile

Influence Hs/h and Qb

Hs/h < 0.275

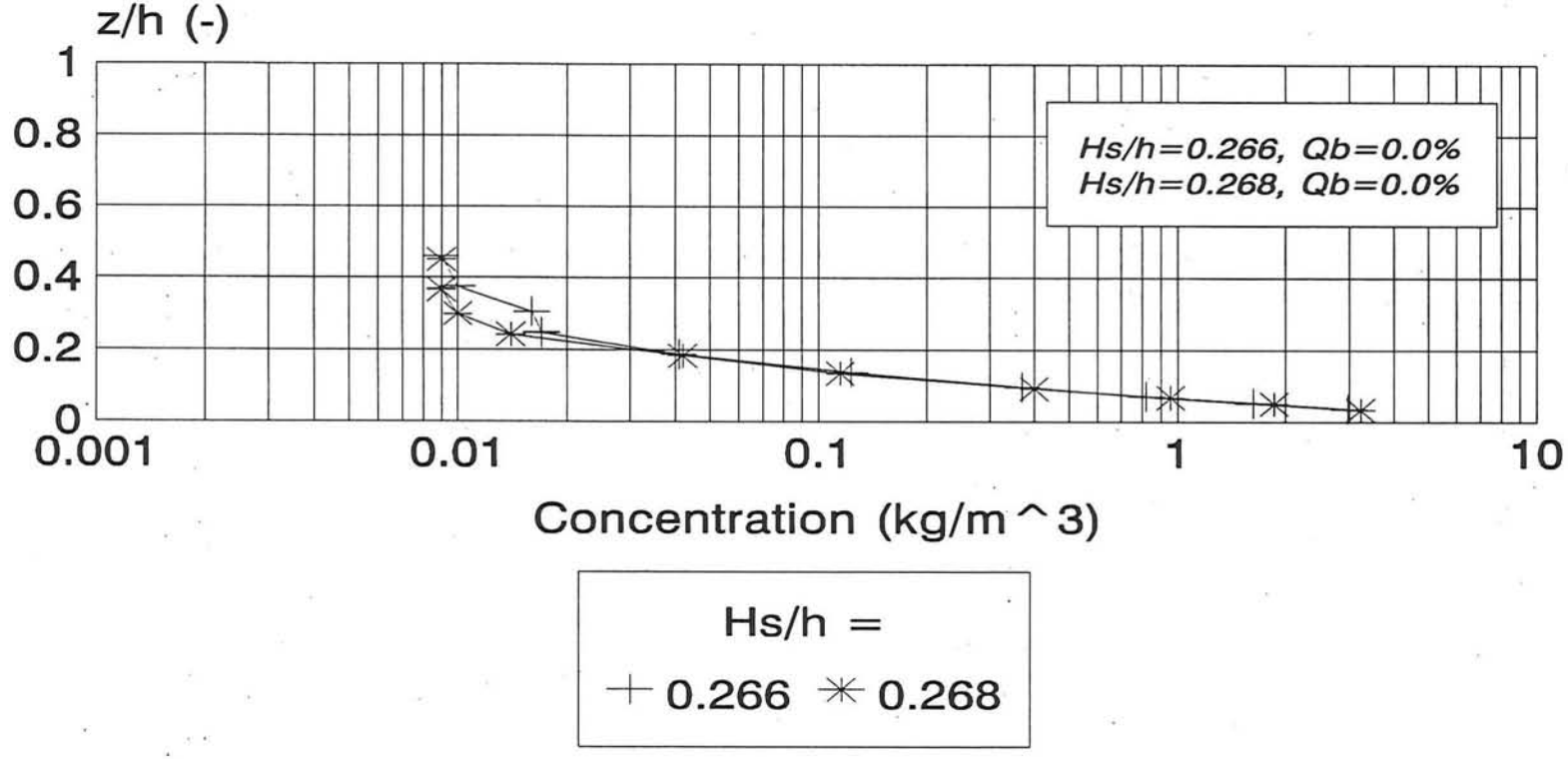

Figure 5.3.C1

Concentration profile

Influence Hs/h and Qb

0.275 < Hs/h < 0.310

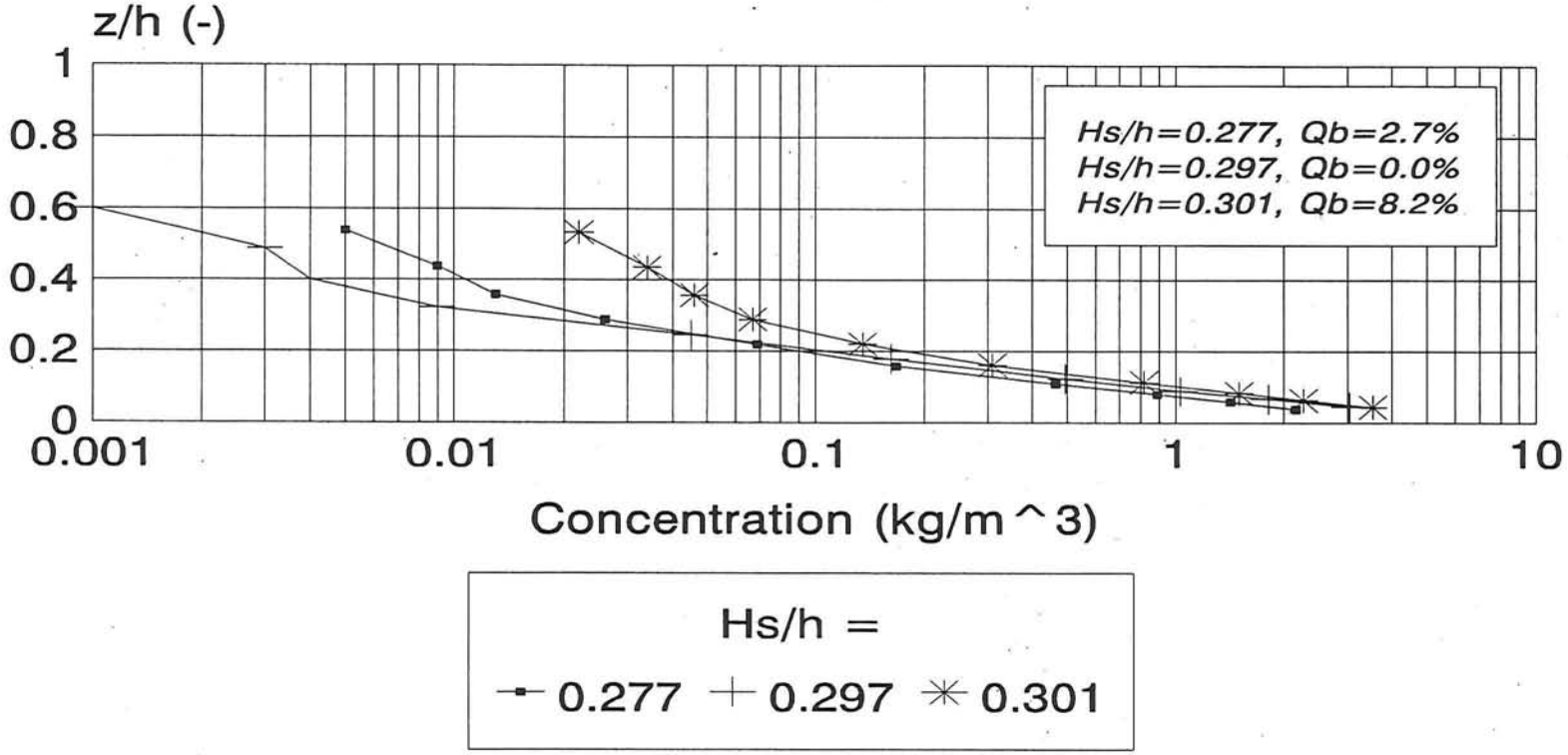

Figure 5.3.C2

Concentration profile

Influence Hs/h and Qb

0.310 < Hs/h < 0.325

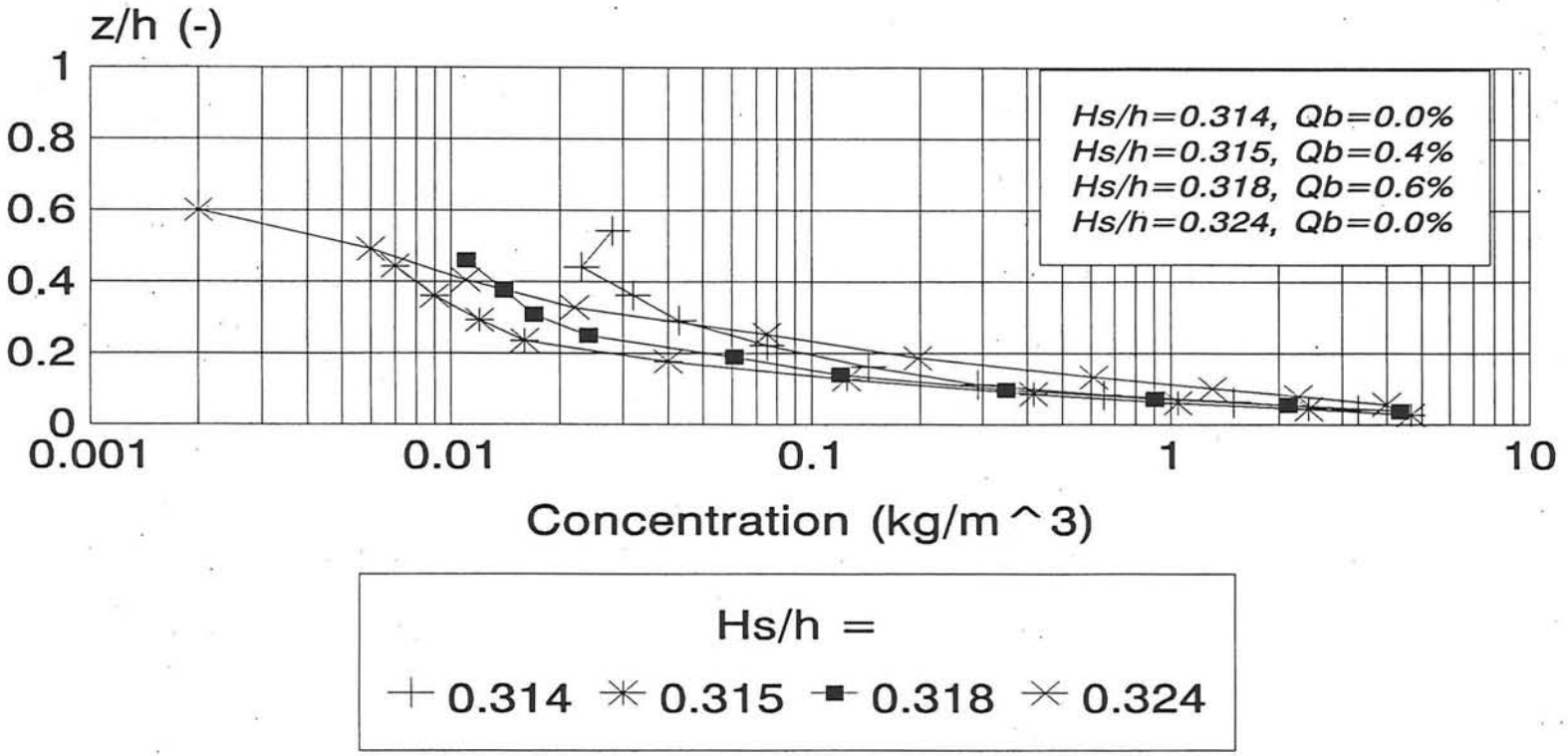

Figure 5.3.C3

Concentration profile

Influence Hs/h and Qb

0.325 < Hs/h < 0.375

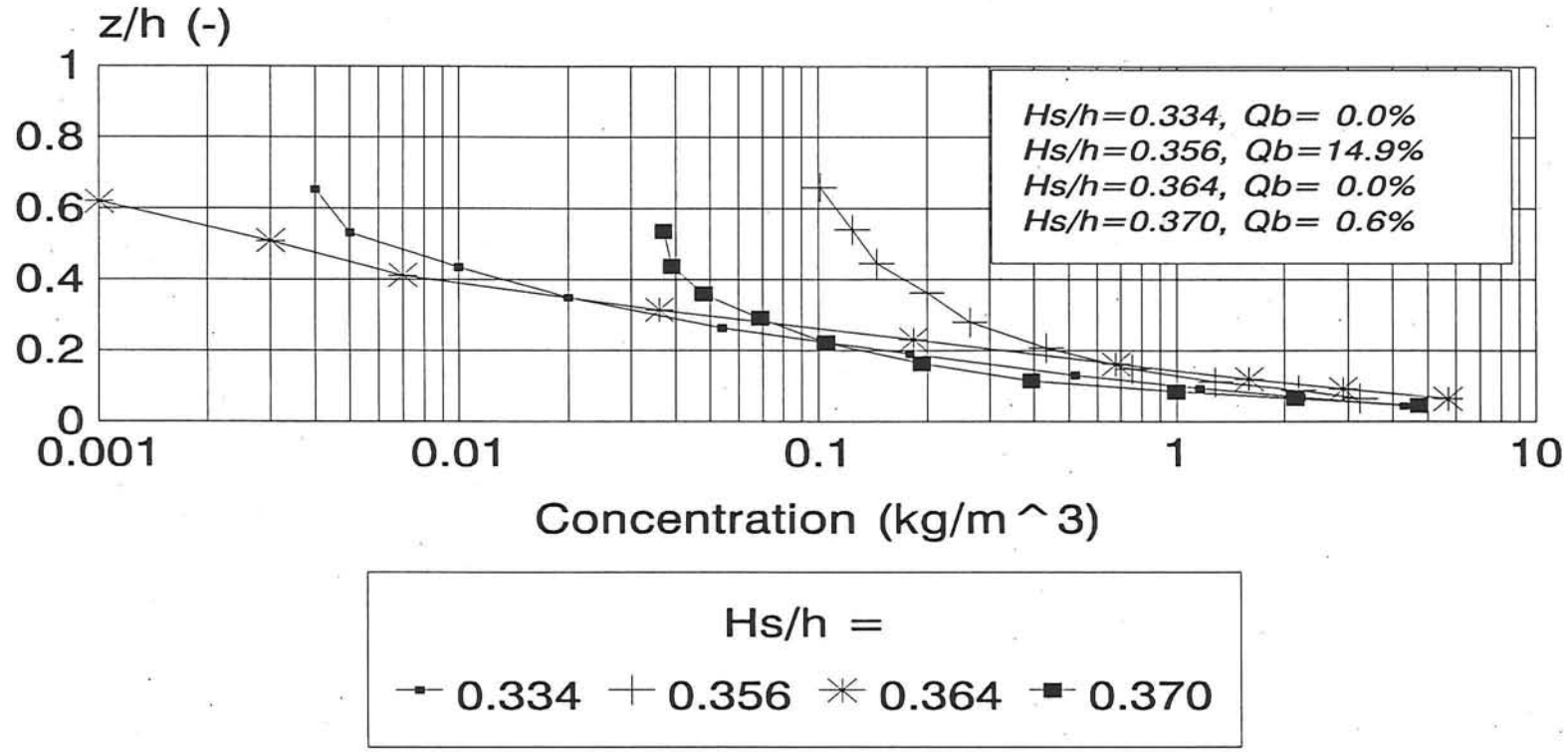

Figure 5.3.C4

Concentration profile

Influence Hs/h and Qb

0.375 < Hs/h < 0.425

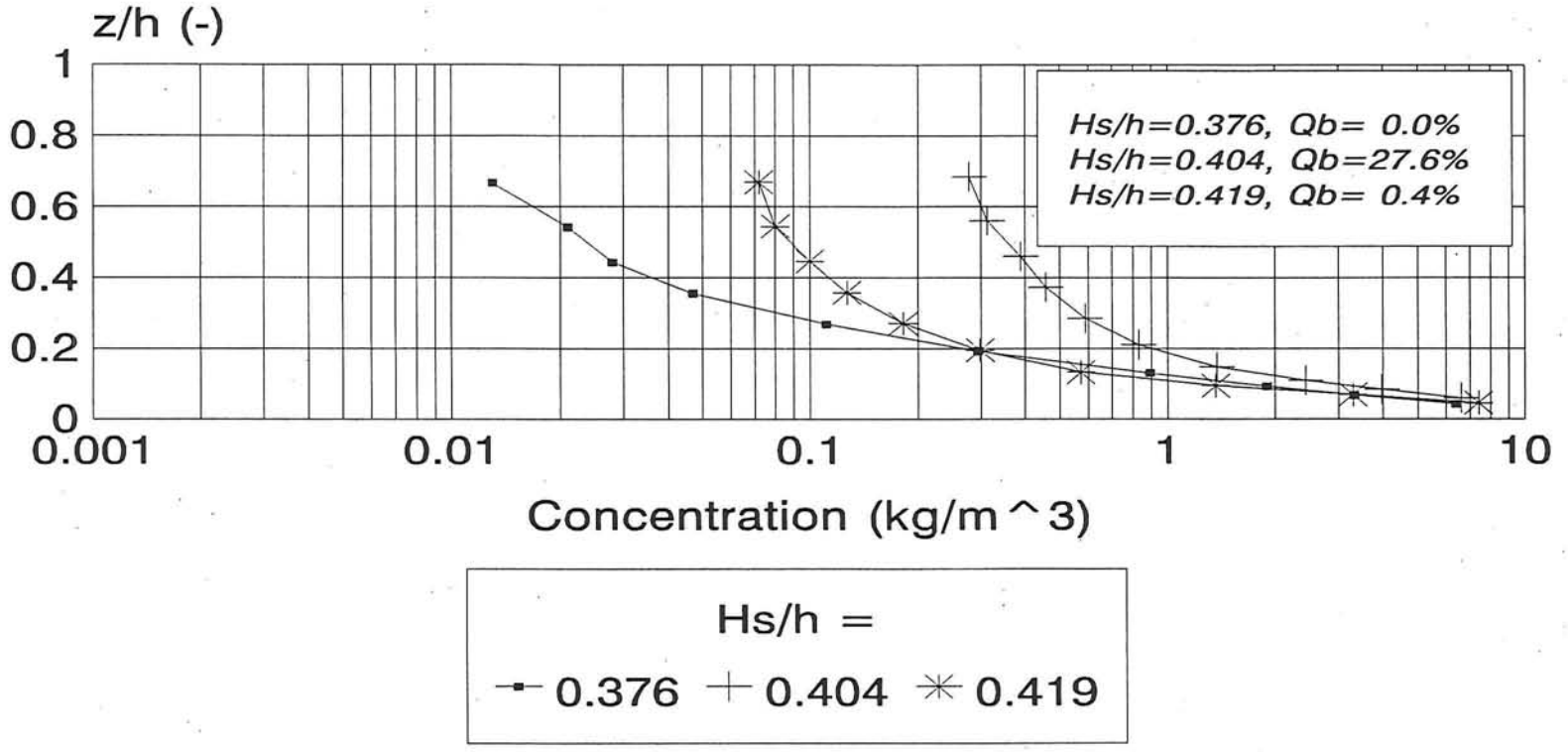

Figure 5.3.C5

Concentration profile

Influence Hs/h and Qb

Hs/h > 0.425

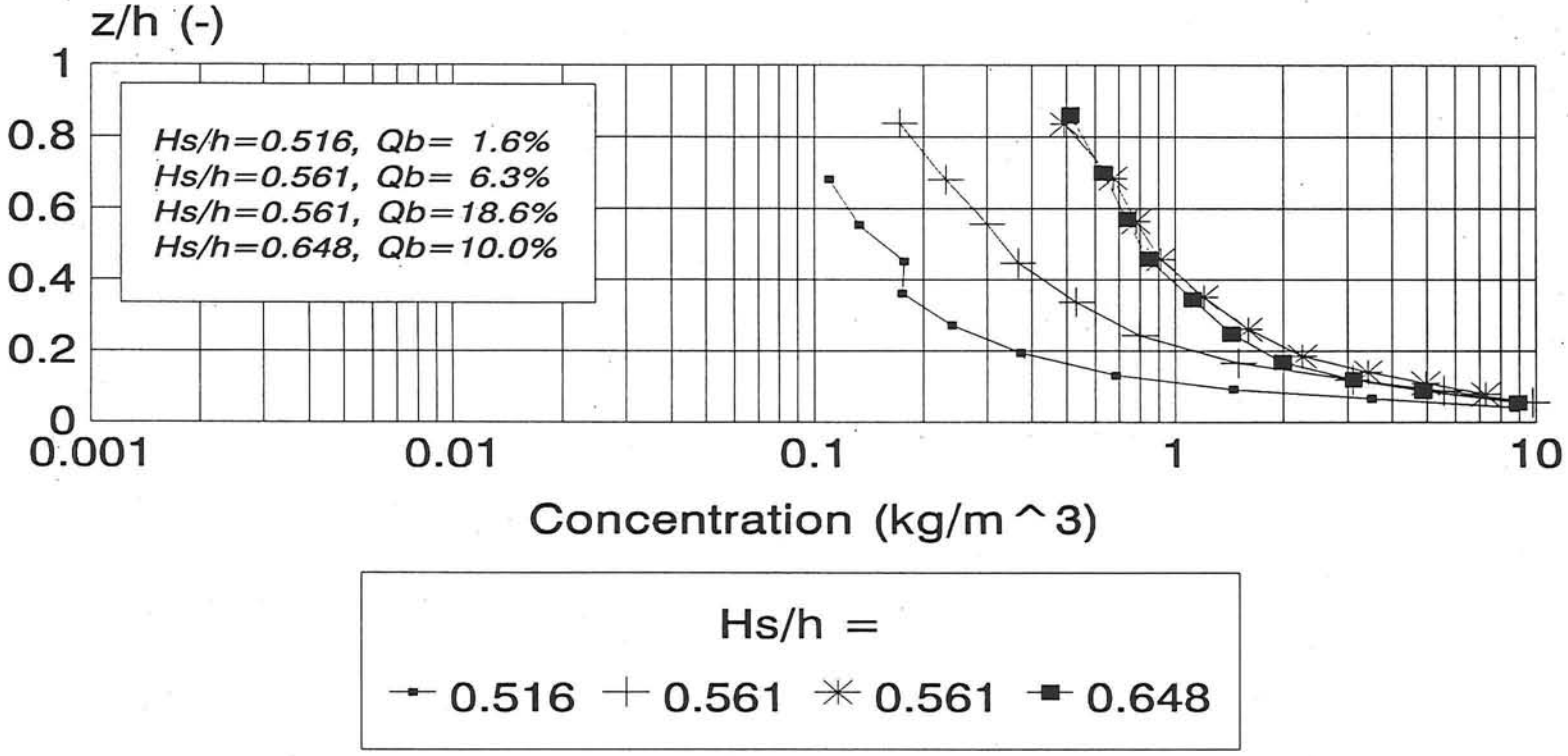

Figure 5.3.C6

Concentration profiles

Comparison averaged values in one class of Hs/h

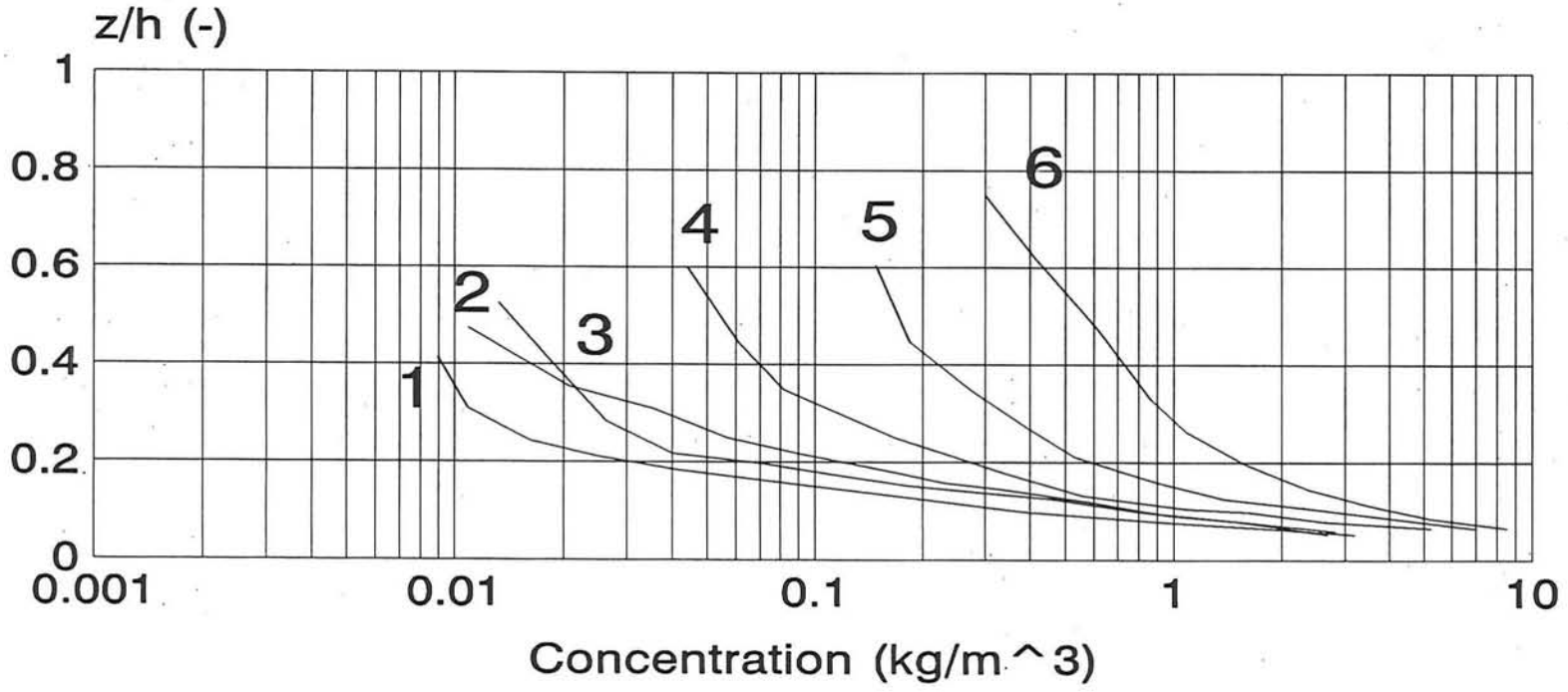

1:<0.275 2:0.275-0.300 3:0.300-0.325 4:0.325-0.375 5:0.375-0.425 6:>0.425

Figure 5.3.C7

Bottom sediment concentration (ripple height)

Influence peak orbital velocity in onshore direction, Qb, ripple height (r)

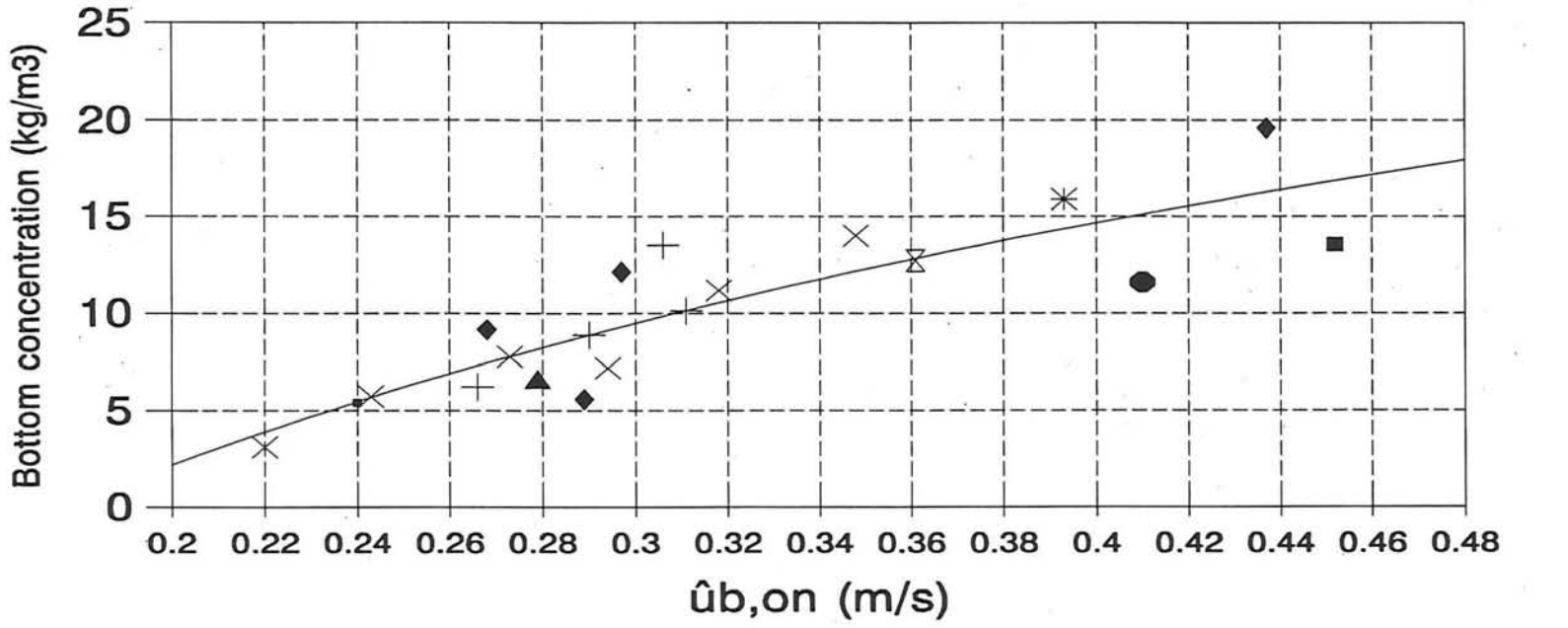

Figure 5.3.D1

Velocity profile series B1

Section 1, Hs = 0.1596 m
T 16 00 01

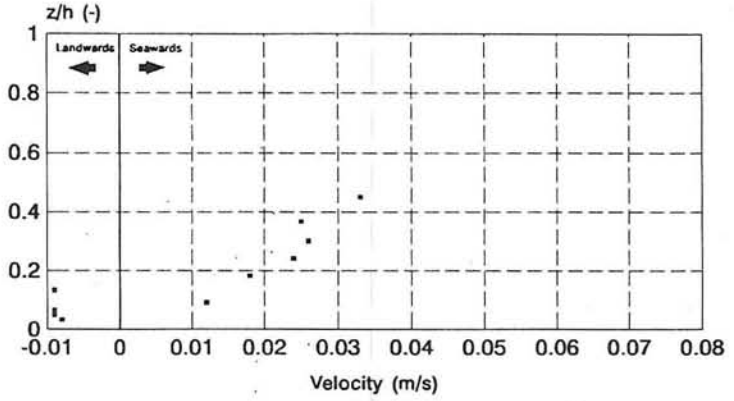

Figure 5.4.A1

Velocity profile series B1

Section 2, Hs = 0.1560 m
T 16 00 02

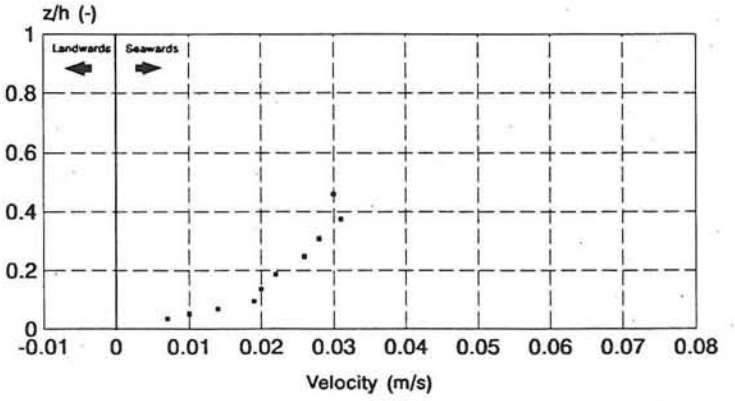

Figure 5.4.A2

Velocity profile series B1

Section 3, Hs = 0.1563 m
T 16 00 03

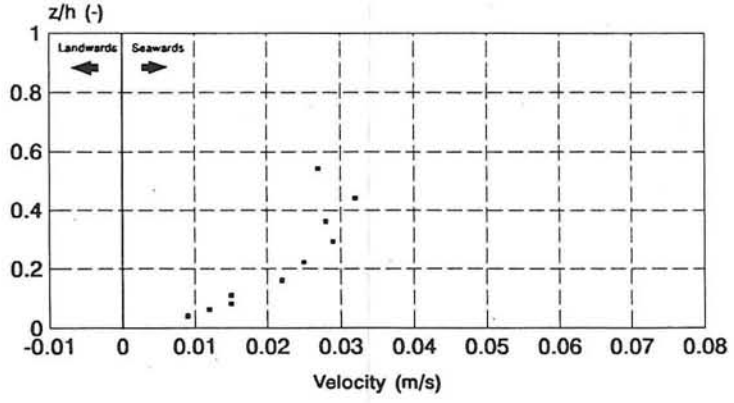

Figure 5.4.A3

Velocity profile series B1

Section 4, Hs = 0.1652 m
T 17 00 04

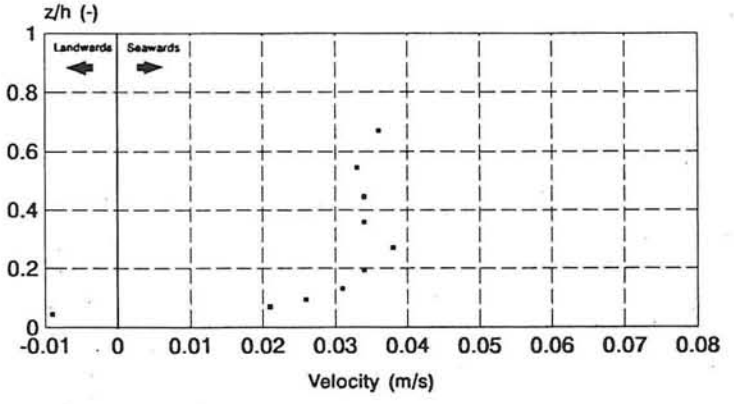

Figure 5.4.A4

Velocity profile series B1

Section 5, Hs = 0.1769 m

T 18 00 05

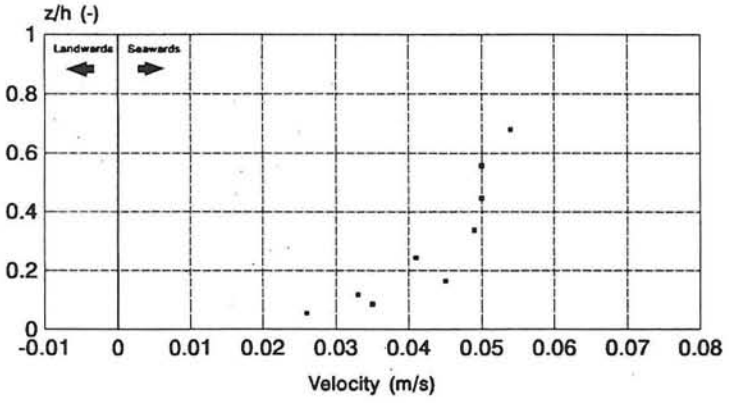

Figure 5.4.A5

Velocity profile series B1

Section 6, Hs = 0.1493 m

T 15 00 06

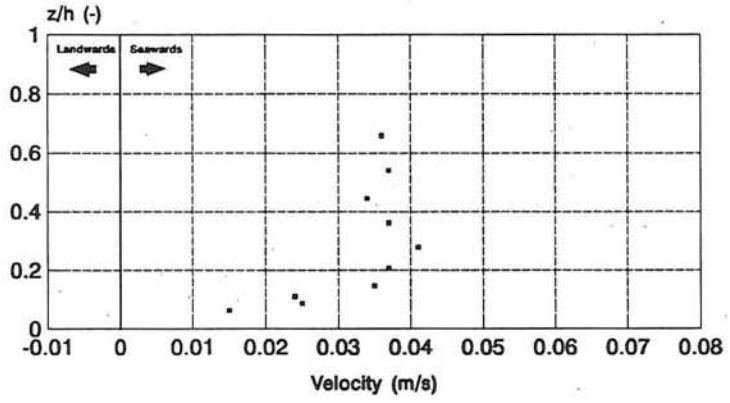

Figure 5.4.A6

Velocity profile series B1

Section 7, Hs = 0.1398 m

T 14 00 07

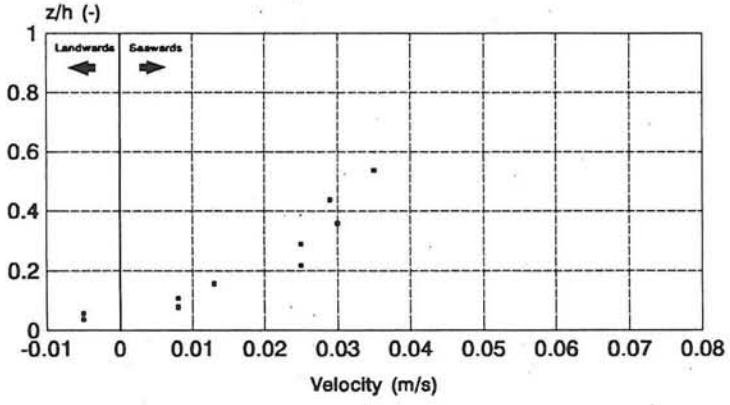

Figure 5.4.A7

Velocity profile series B1

Section 8, Hs = 0.1339 m

T 13 00 08

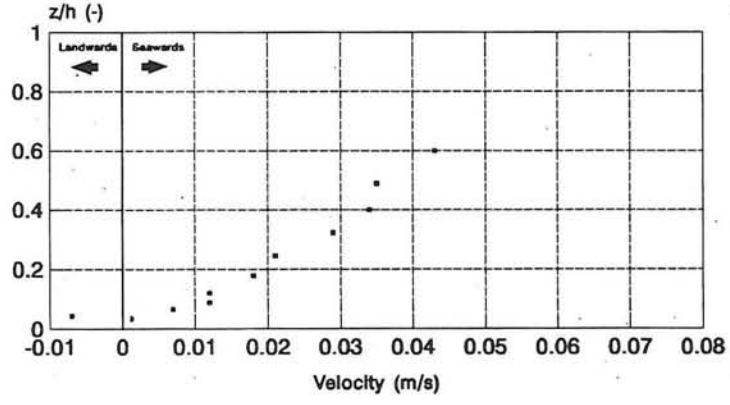

Figure 5.4.A8

Velocity profile series B1

Section 9, Hs = 0.1367 m

T 14 00 09

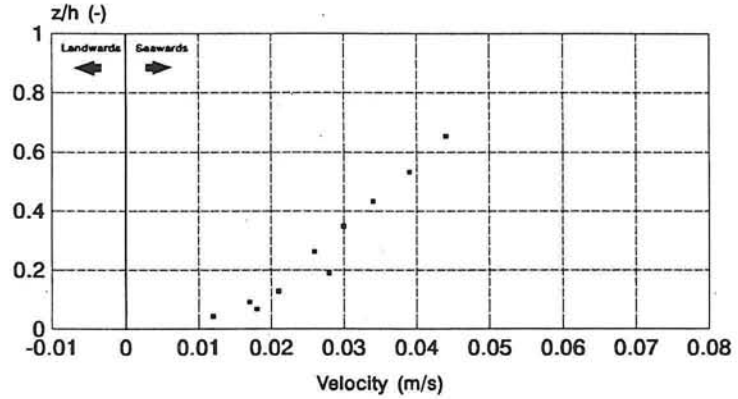

Figure 5.4.A9

Velocity profile series B1

Section 10, Hs = 0.1322 m

T 13 00 10

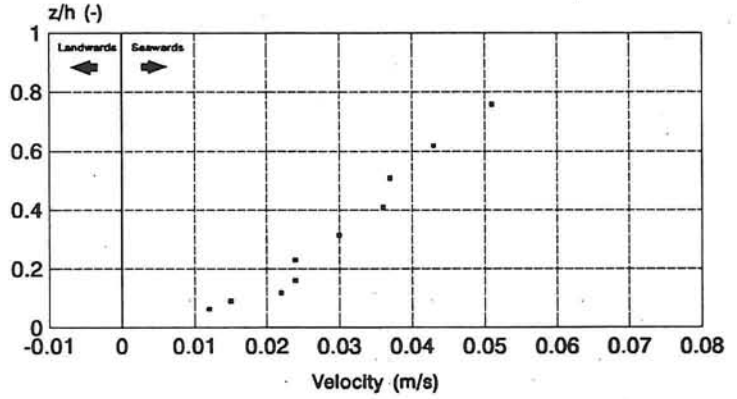

Figure 5.4.A10

Velocity profile series B2

Section 1, Hs = 0.1890 m

T 19 00 01

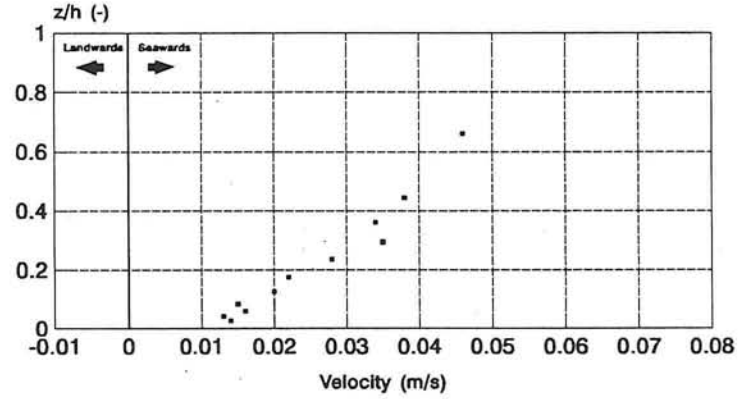

Figure 5.4.A11

Velocity profile series B2

Section 2, Hs = 0.1875 m

T 19 00 02

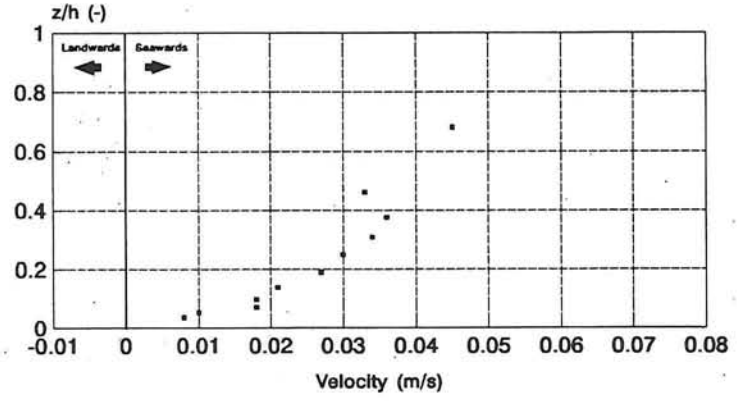

Figure 5.4.A12

Velocity profile series B2

Section 3, Hs = 0.1875 m

T 19 00 03

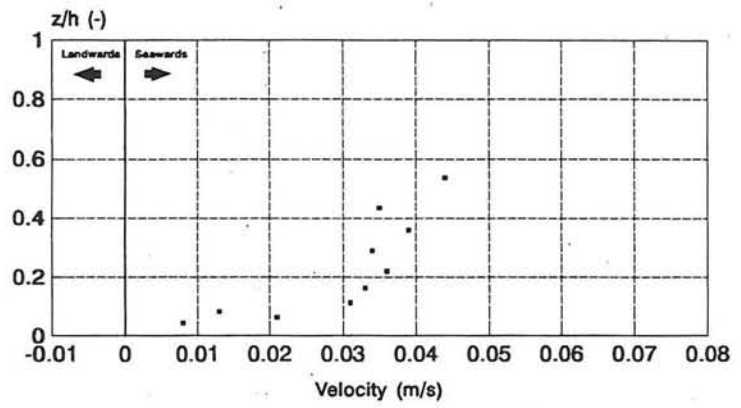

Figure 5.4.A13

Velocity profile series B2

Section 4, Hs = 0.2011 m

T 20 00 04

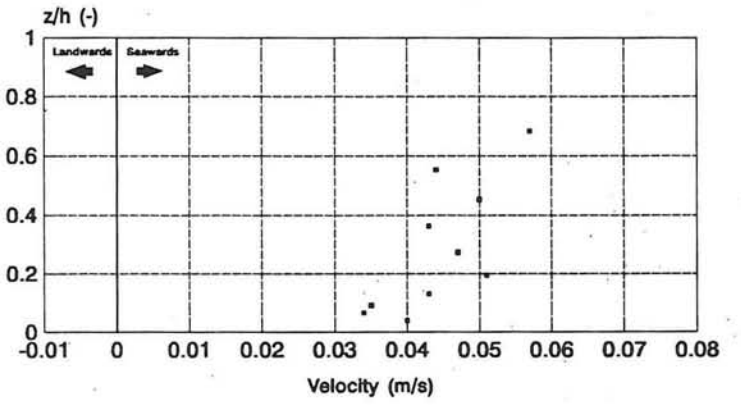

Figure 5.4.A14

Velocity profile series B2

Section 5, Hs = 0.2010 m

T 20 00 05

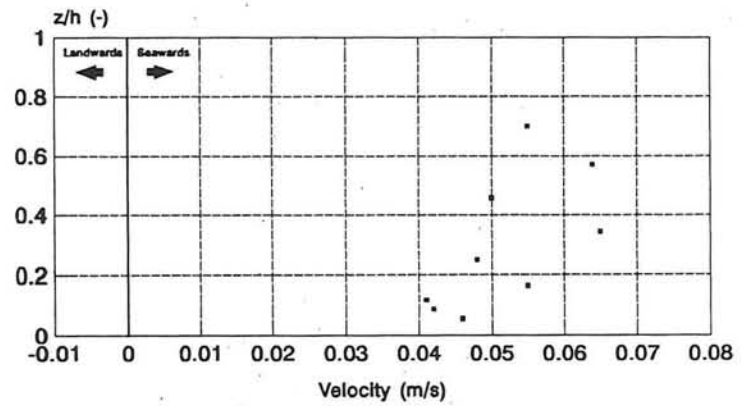

Figure 5.4.A15

Velocity profile series B2

Section 5a, Hs = 0.1866 m

T 19 00 5a

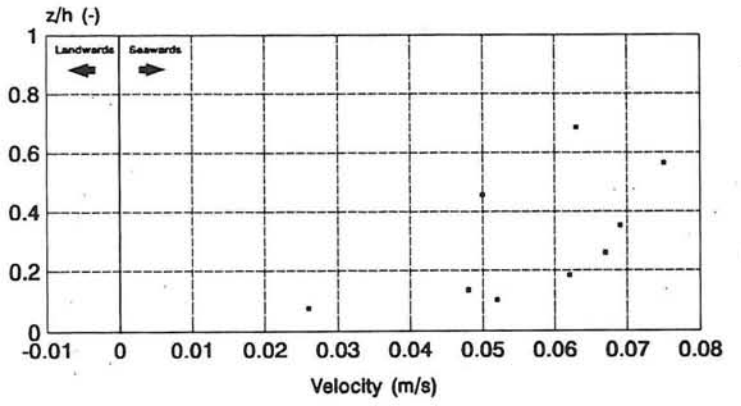

Figure 5.4.A16

Mean velocity section Series B2

with parameters Hs/h, Hs/L, Qb

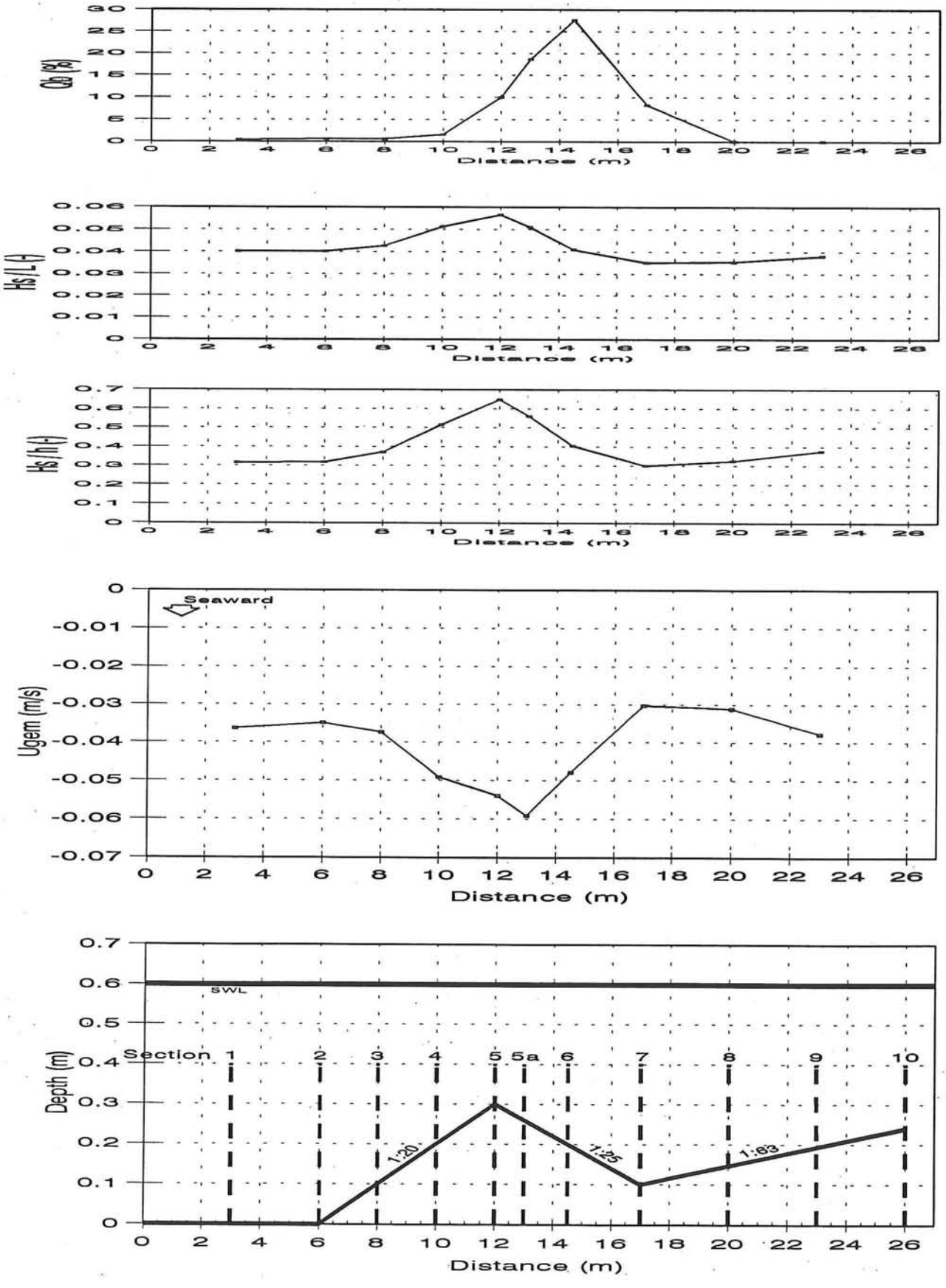

Figure 5.4.B2

Return flow Series B1

Measured values and approximations
with parameters Hs/h, Hs/L, Qb

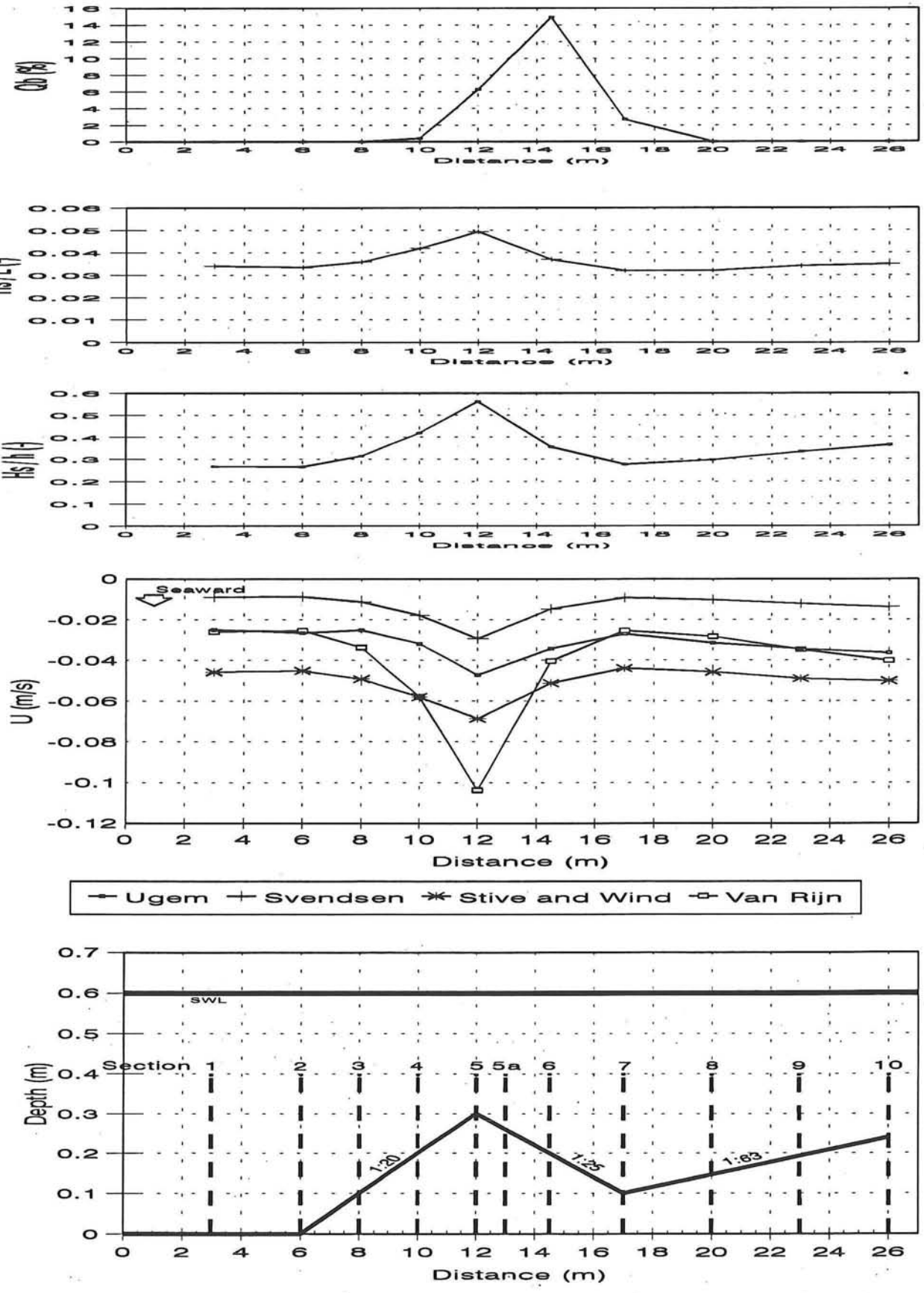

Figure 5.4.B3

Return flow Series B2

Measured values and approximations
with parameters Hs/h, Hs/L, Qb

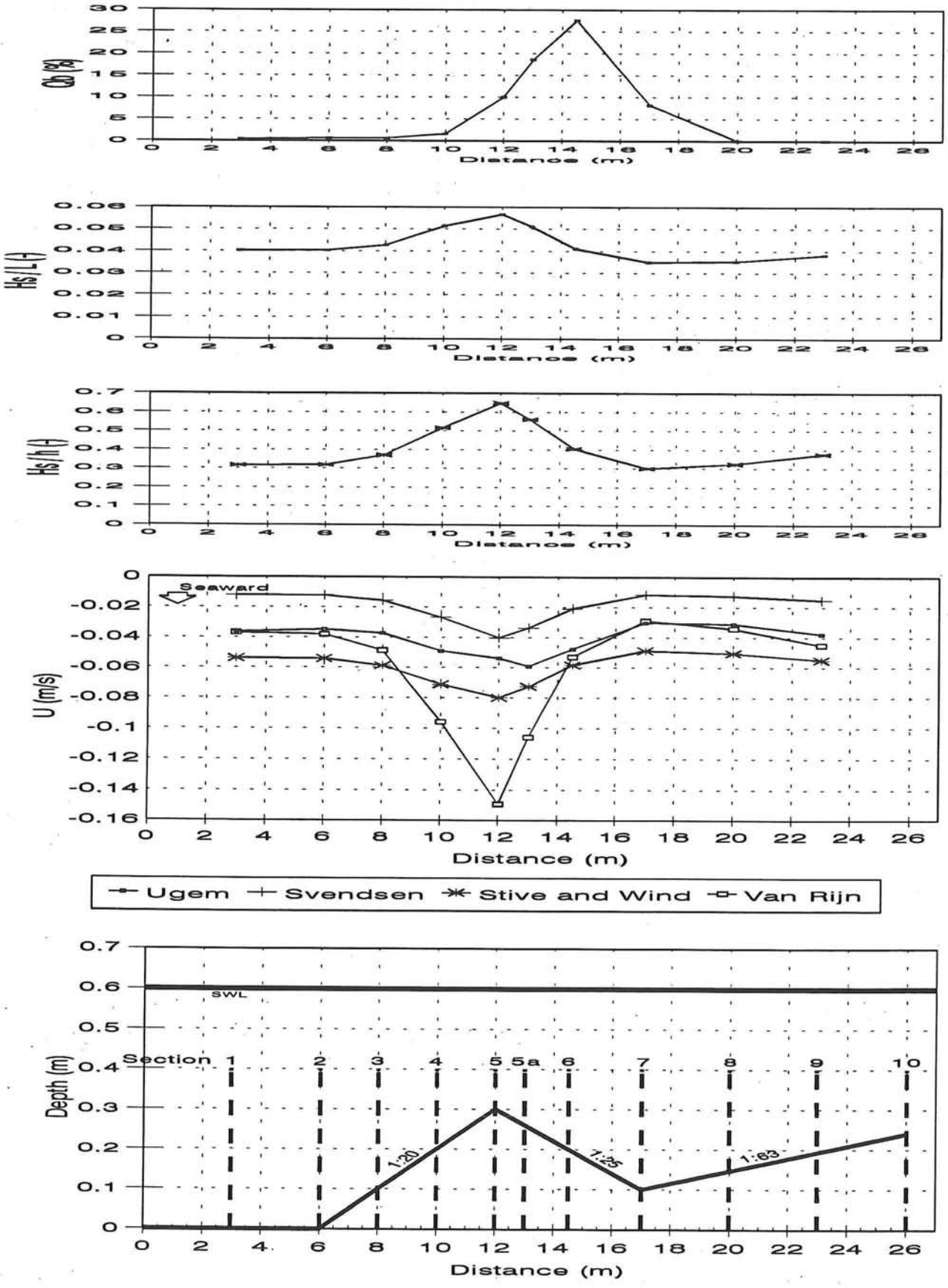

Figure 5.4.B4

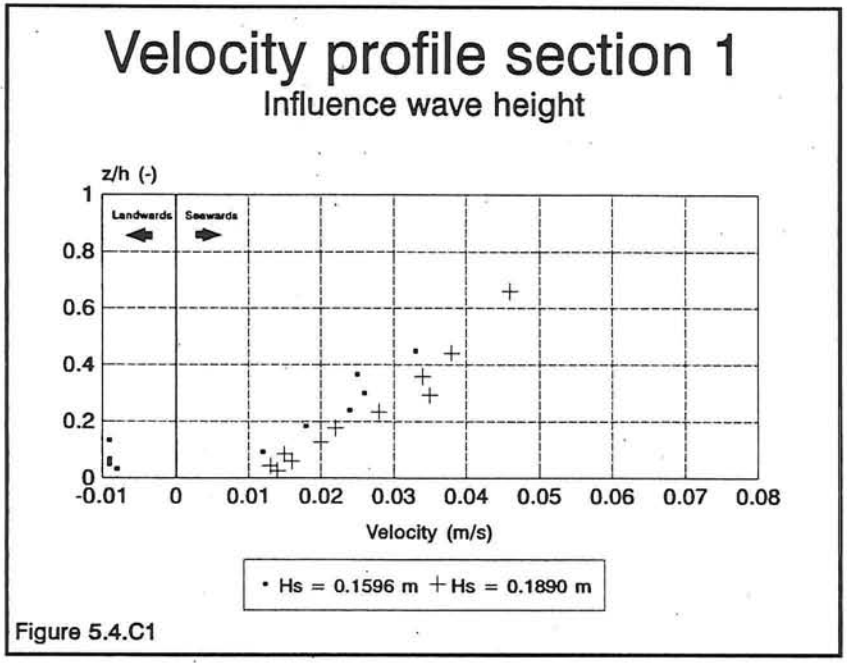

Figure 5.4.C1

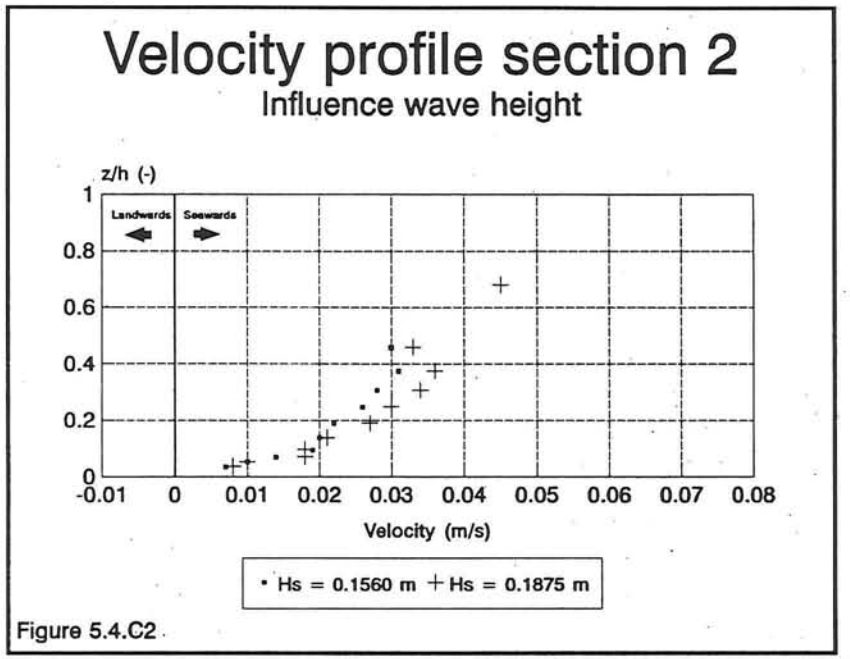

Figure 5.4.C2

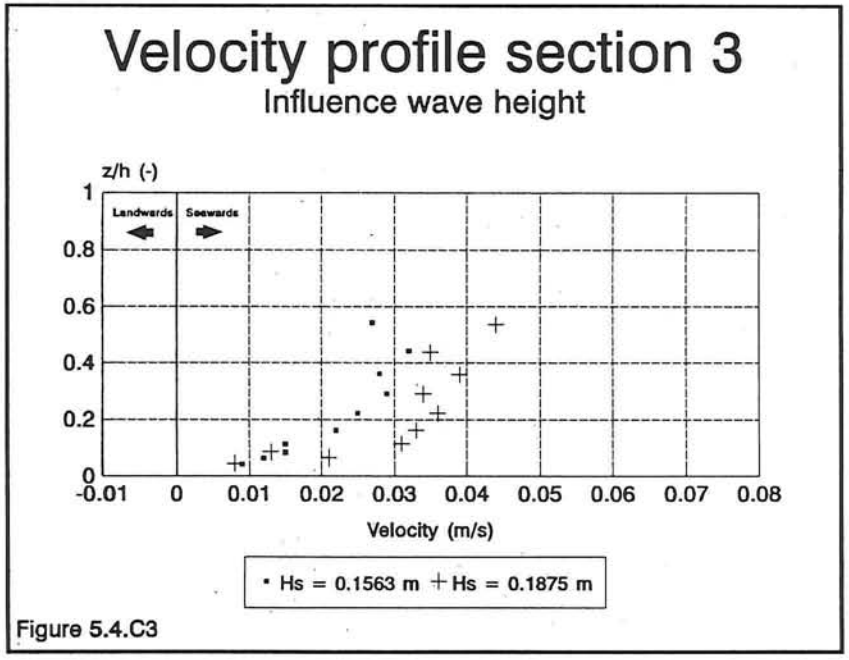

Figure 5.4.C3

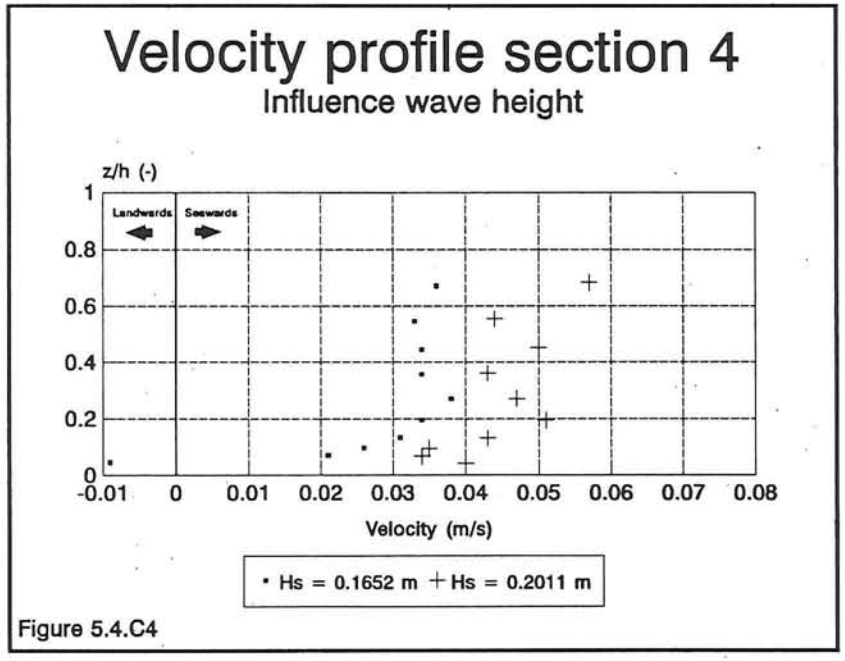

Figure 5.4.C4

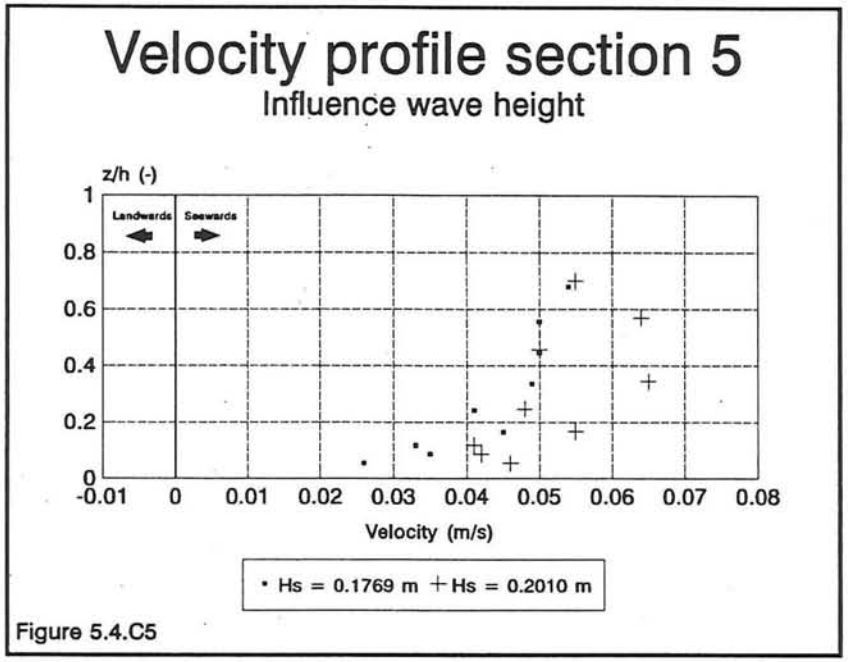

Figure 5.4.C5

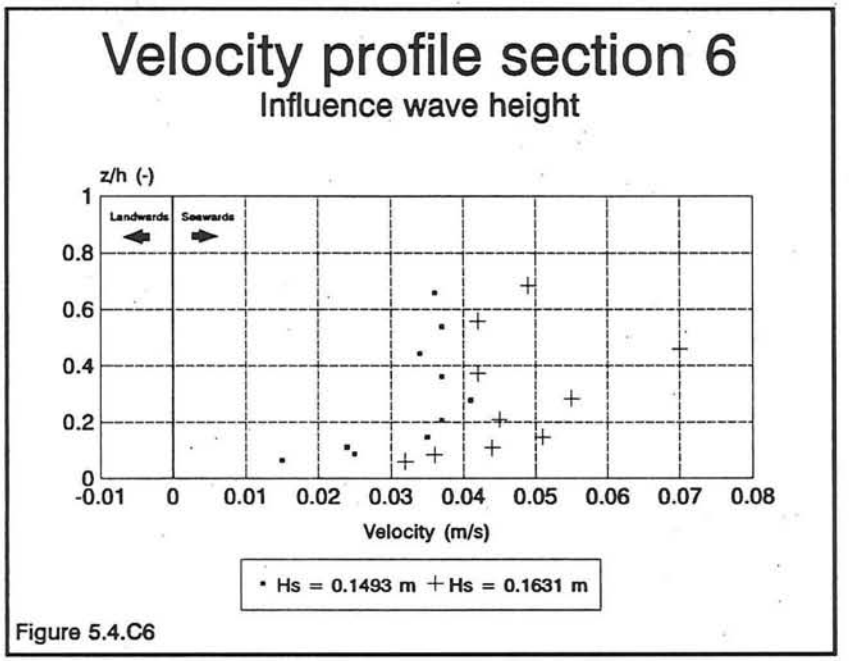

Figure 5.4.C6

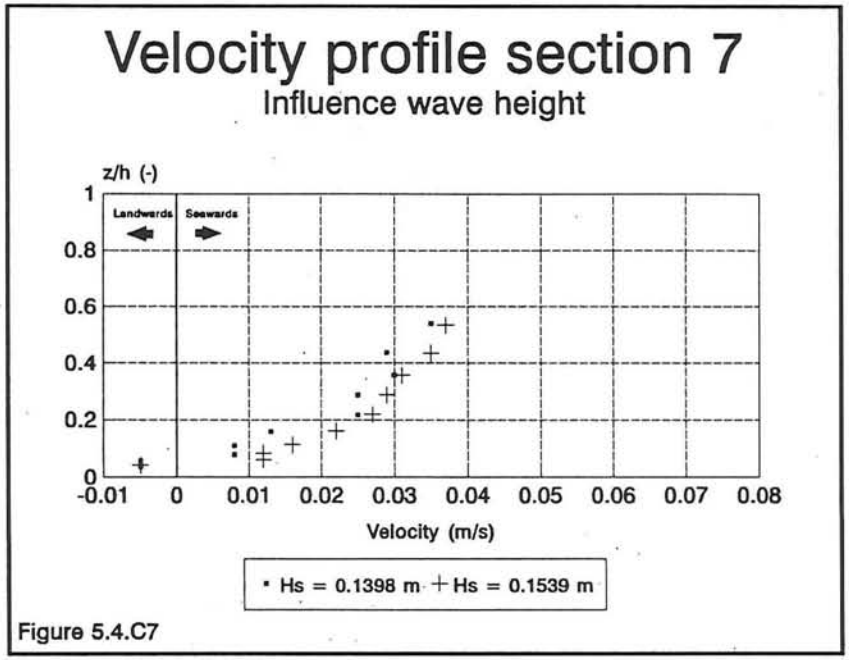

Figure 5.4.C7

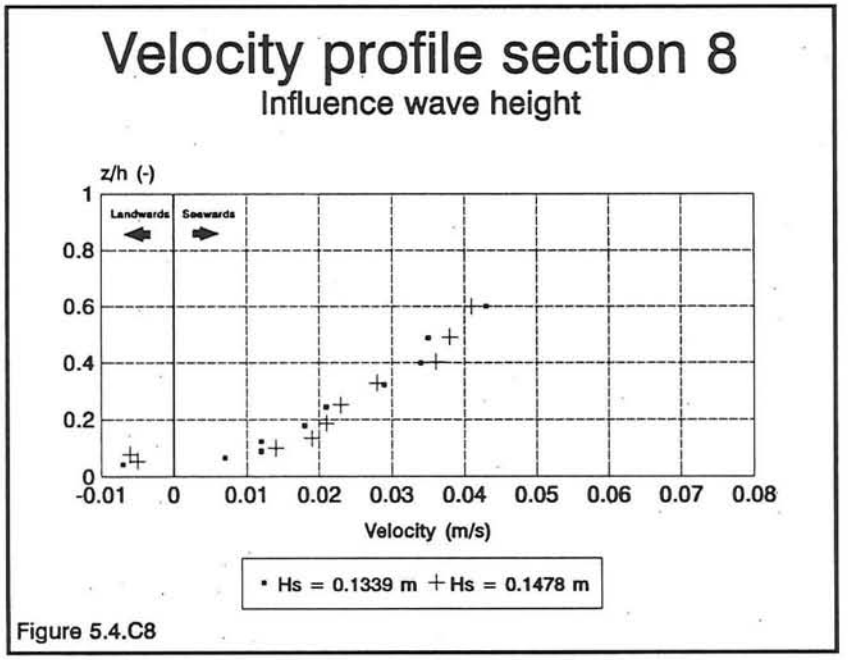

Figure 5.4.C8

Velocity profile section 9

Influence wave height

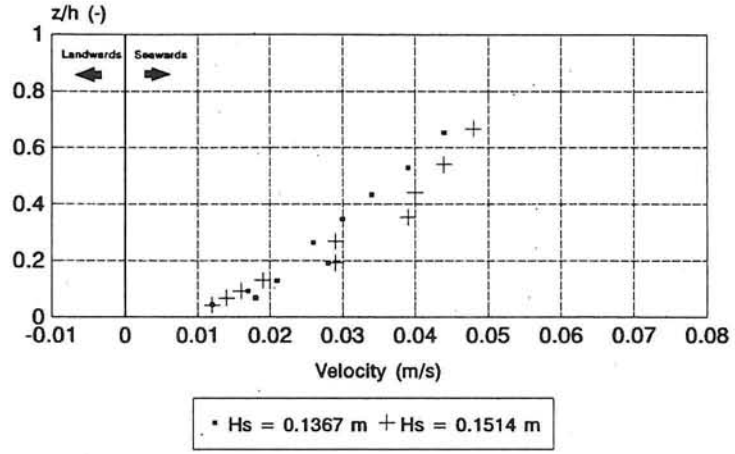

Figure 5.4.C9

Velocity profile

Influence Hs/h and Qb

Hs/h < 0.275

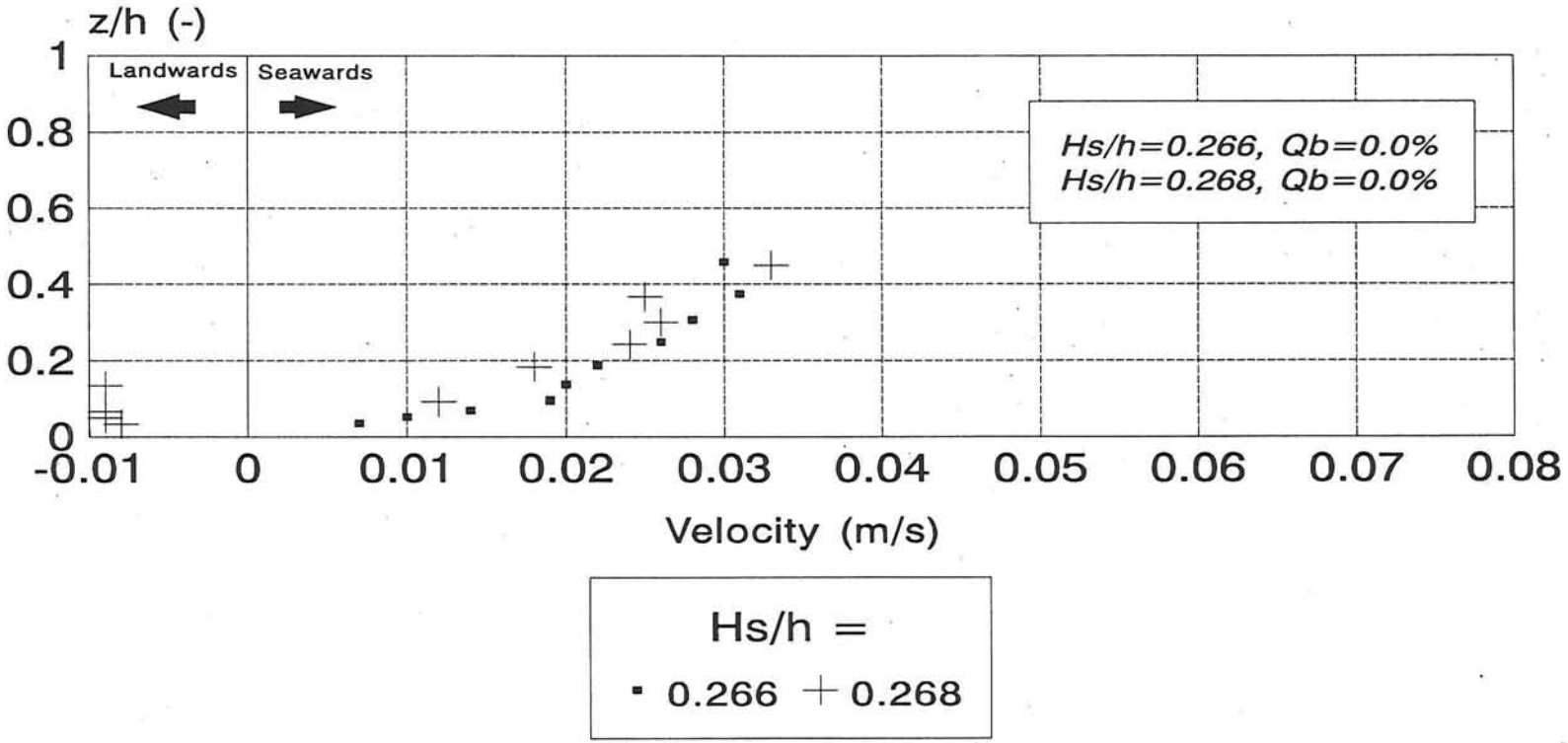

Figure 5.4.D1

Velocity profile

Influence Hs/h and Qb

0.275 < Hs/h < 0.310

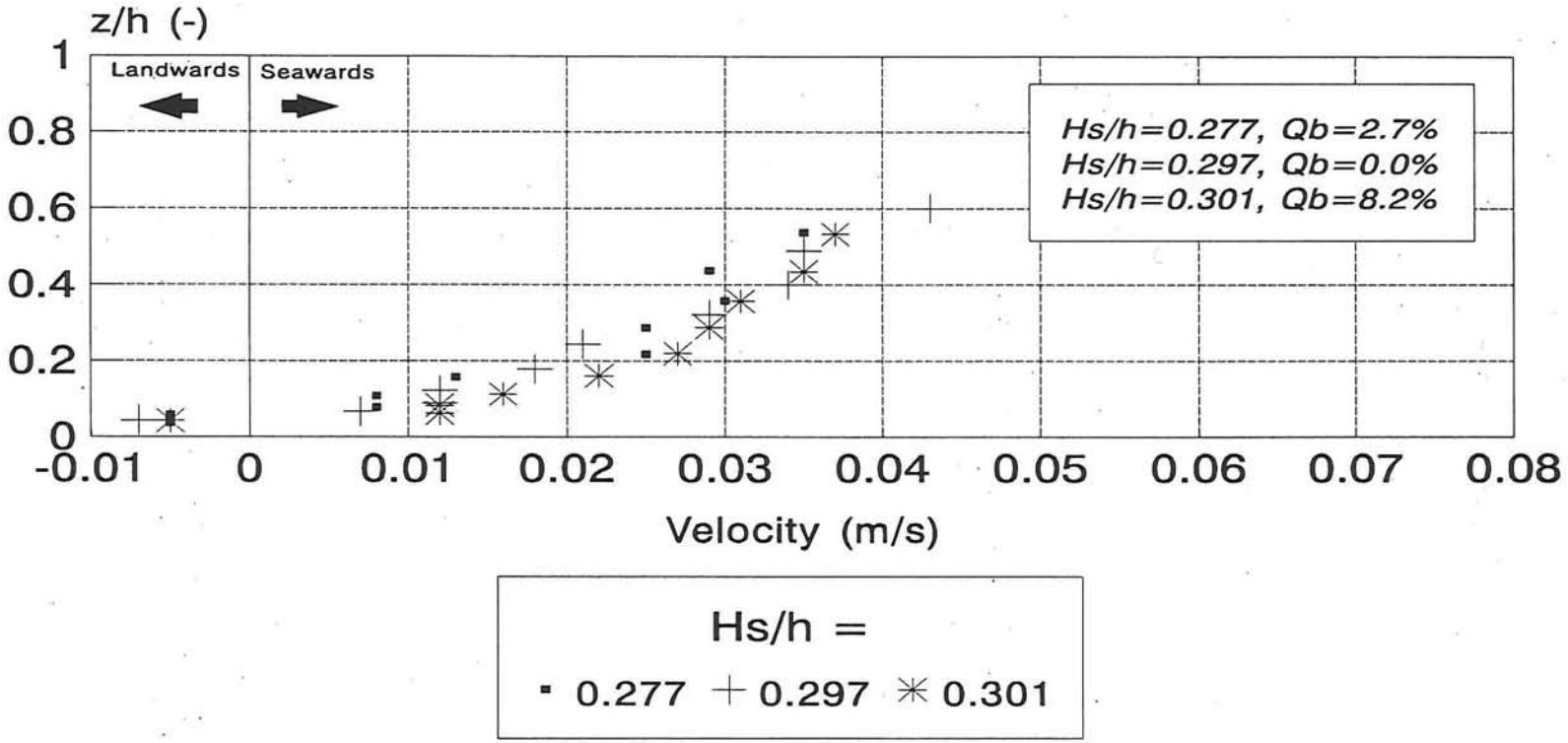

Figure 5.4.D2

Velocity profile

Influence Hs/h and Qb

0.310 < Hs/h < 0.325

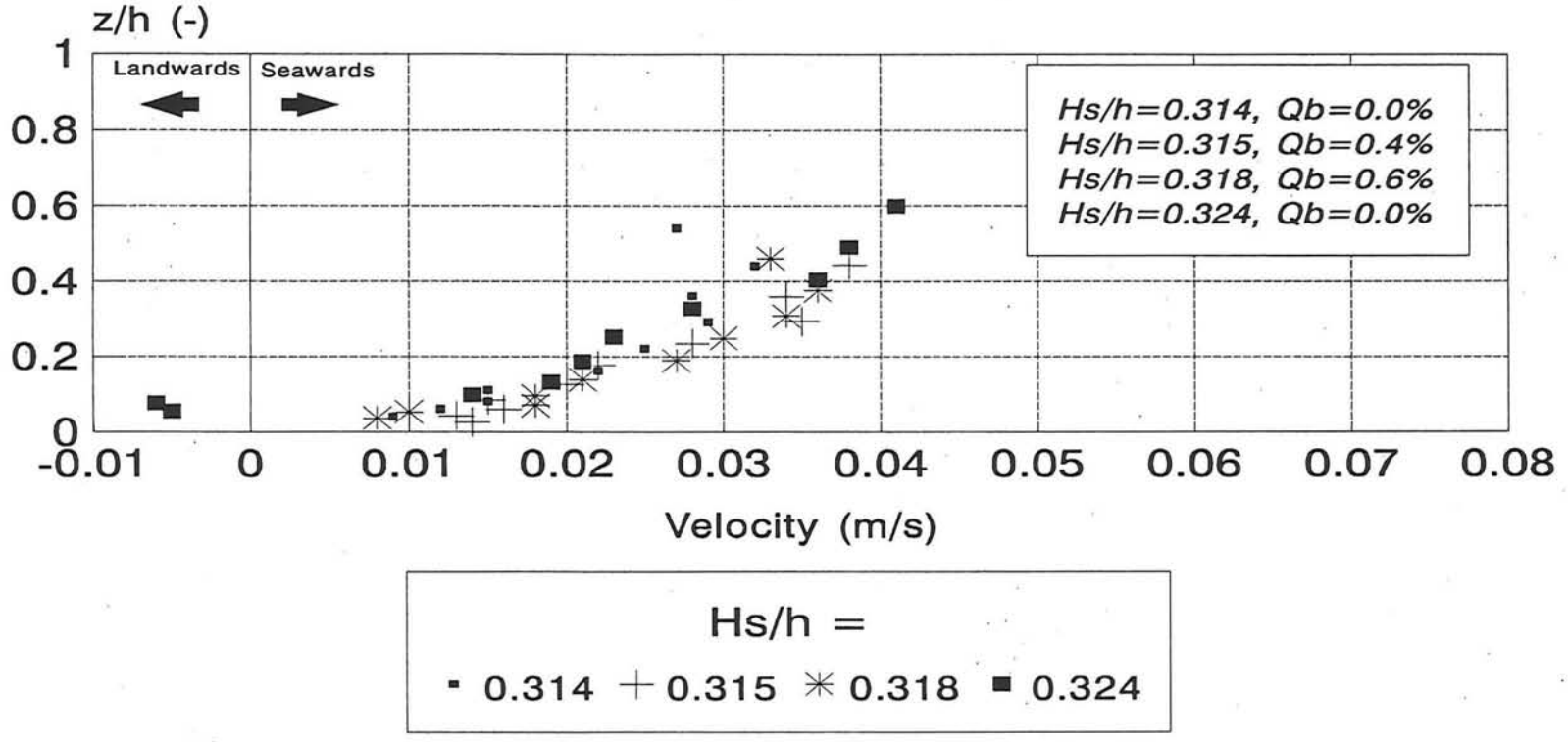

Figure 5.4.D3

Velocity profile

Influence Hs/h and Qb

0.325 < Hs/h < 0.375

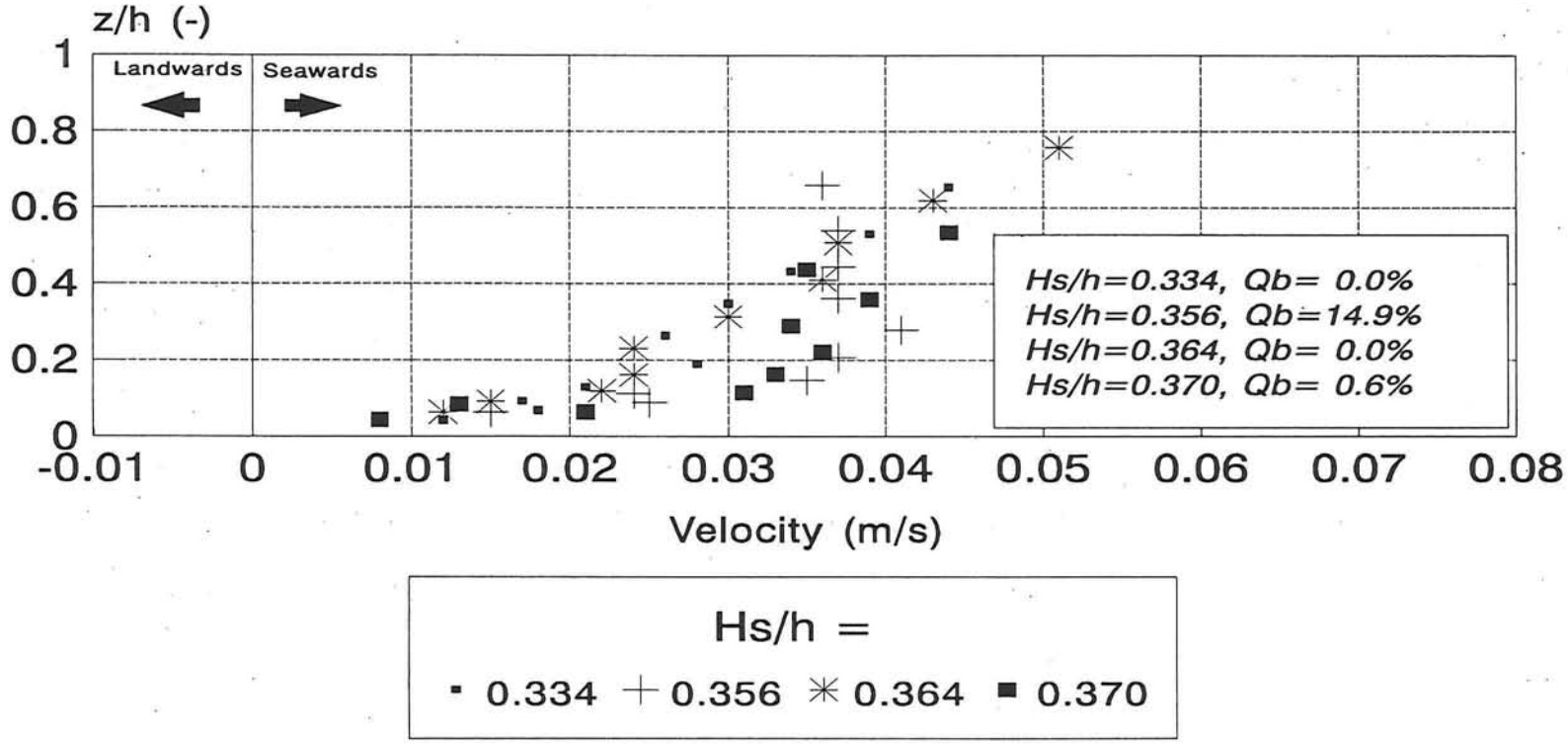

Figure 5.4.D4

Velocity profile

Influence Hs/h

0.375 < Hs/h < 0.425

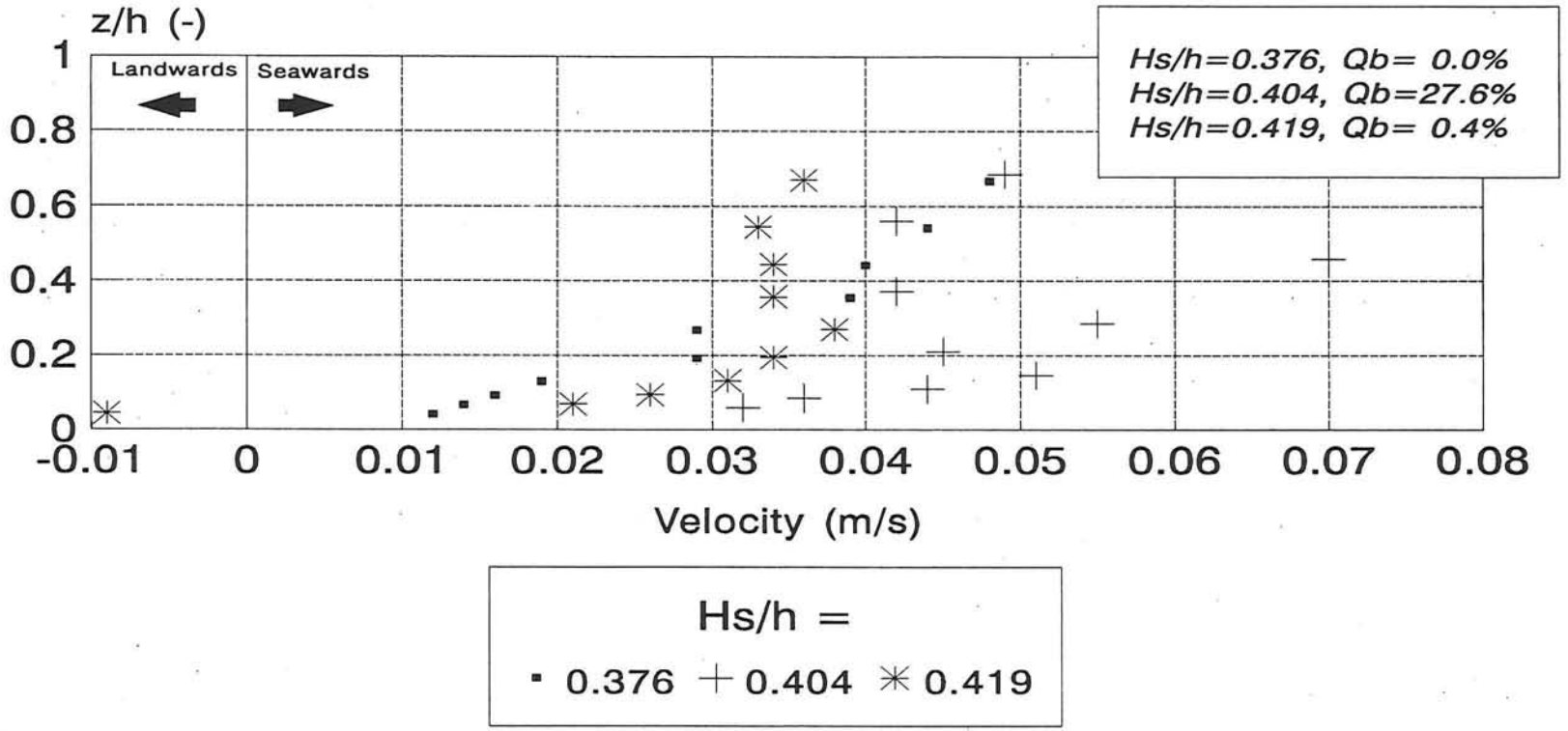

Figure 5.4.D5

Velocity profile

Influence Hs/h and Qb

Hs/h > 0.425

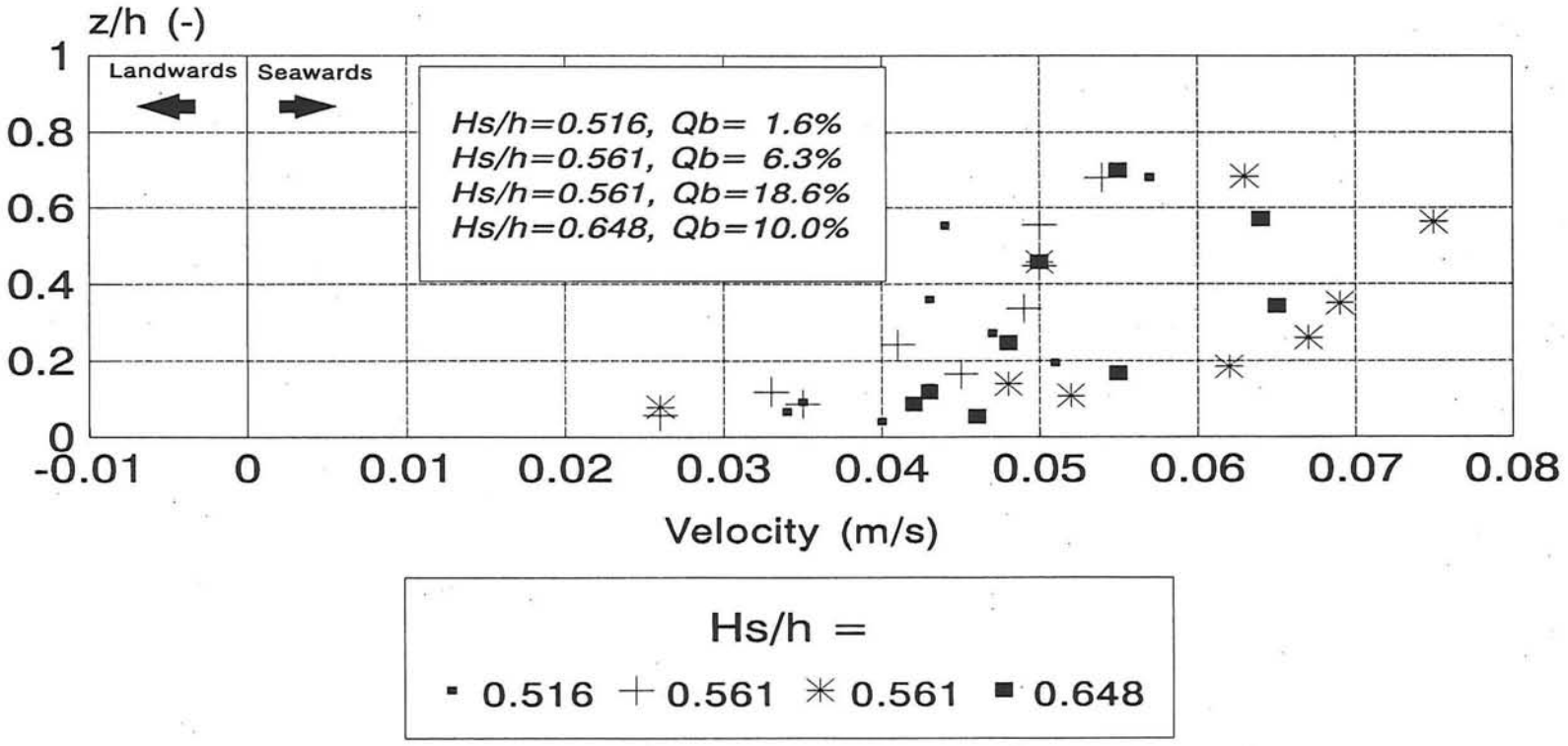

Figure 5.4.D6

Adjusting of velocity signal

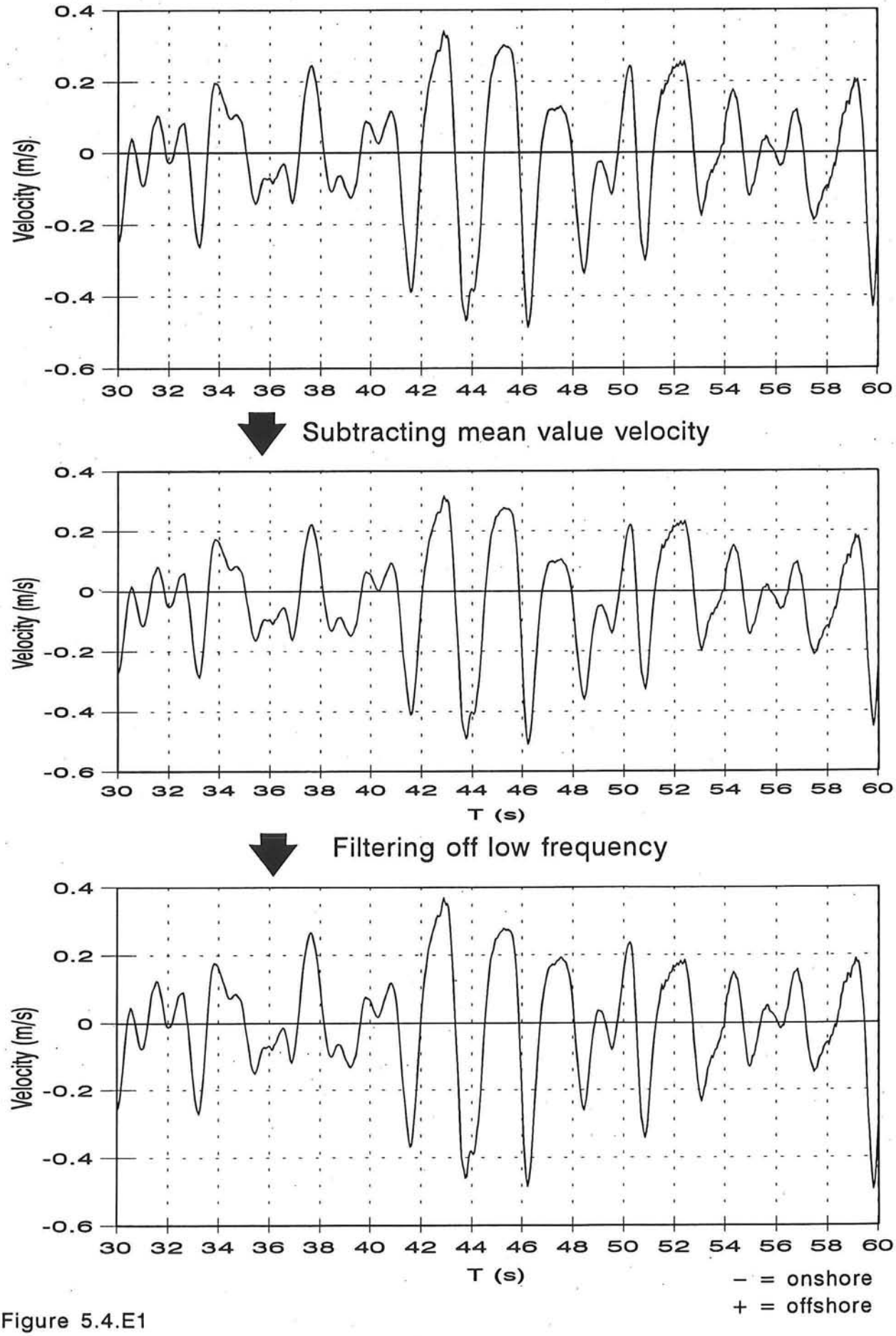

Figure 5.4.E1

Peak orbital velocity in onshore direction for Series B1

with parameters Hs/h, Hs/L, Qb

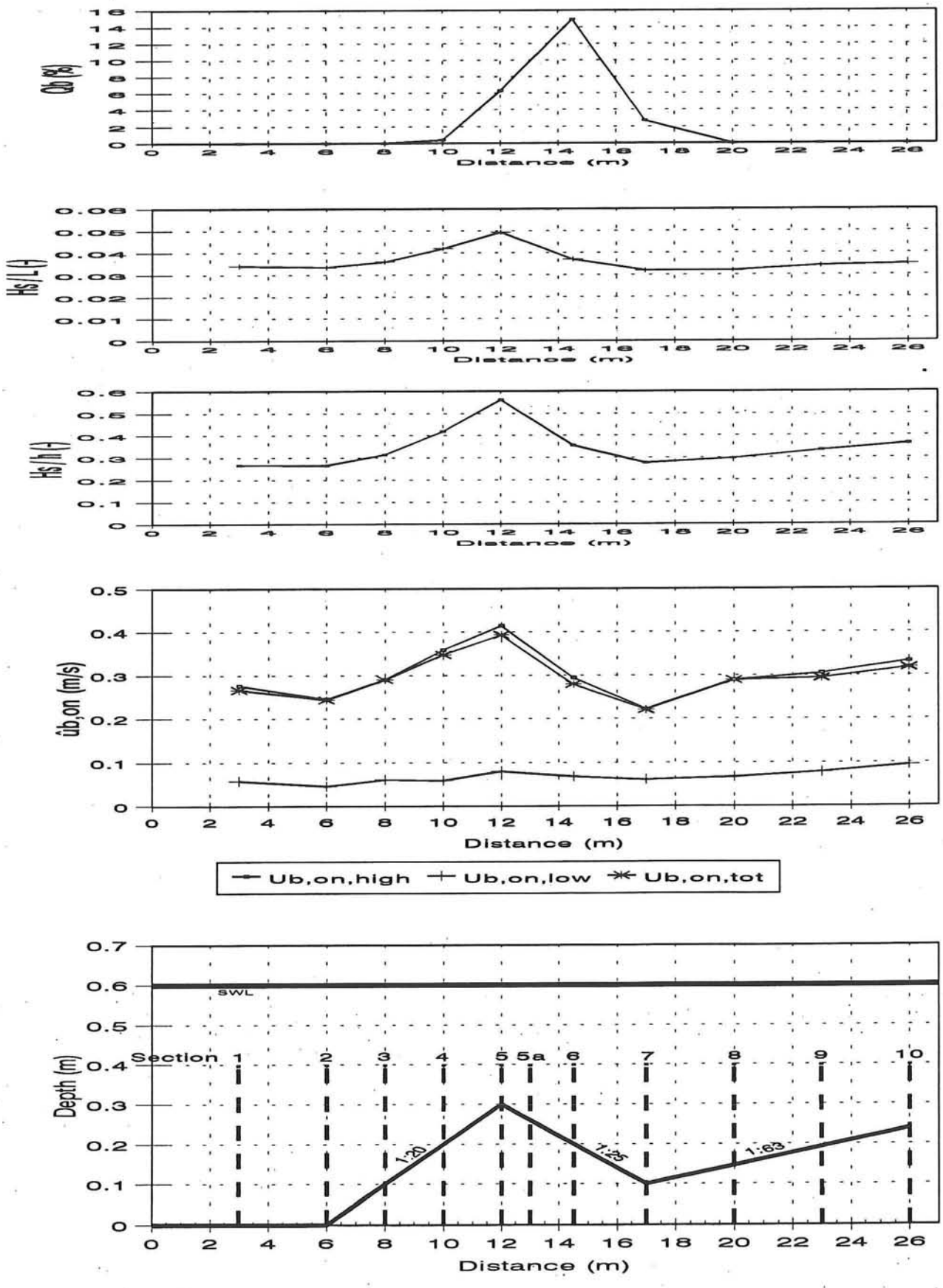

Figure 5.4.E2

Peak orbital velocity in offshore direction for Series B1

with parameters Hs/h, Hs/L, Qb

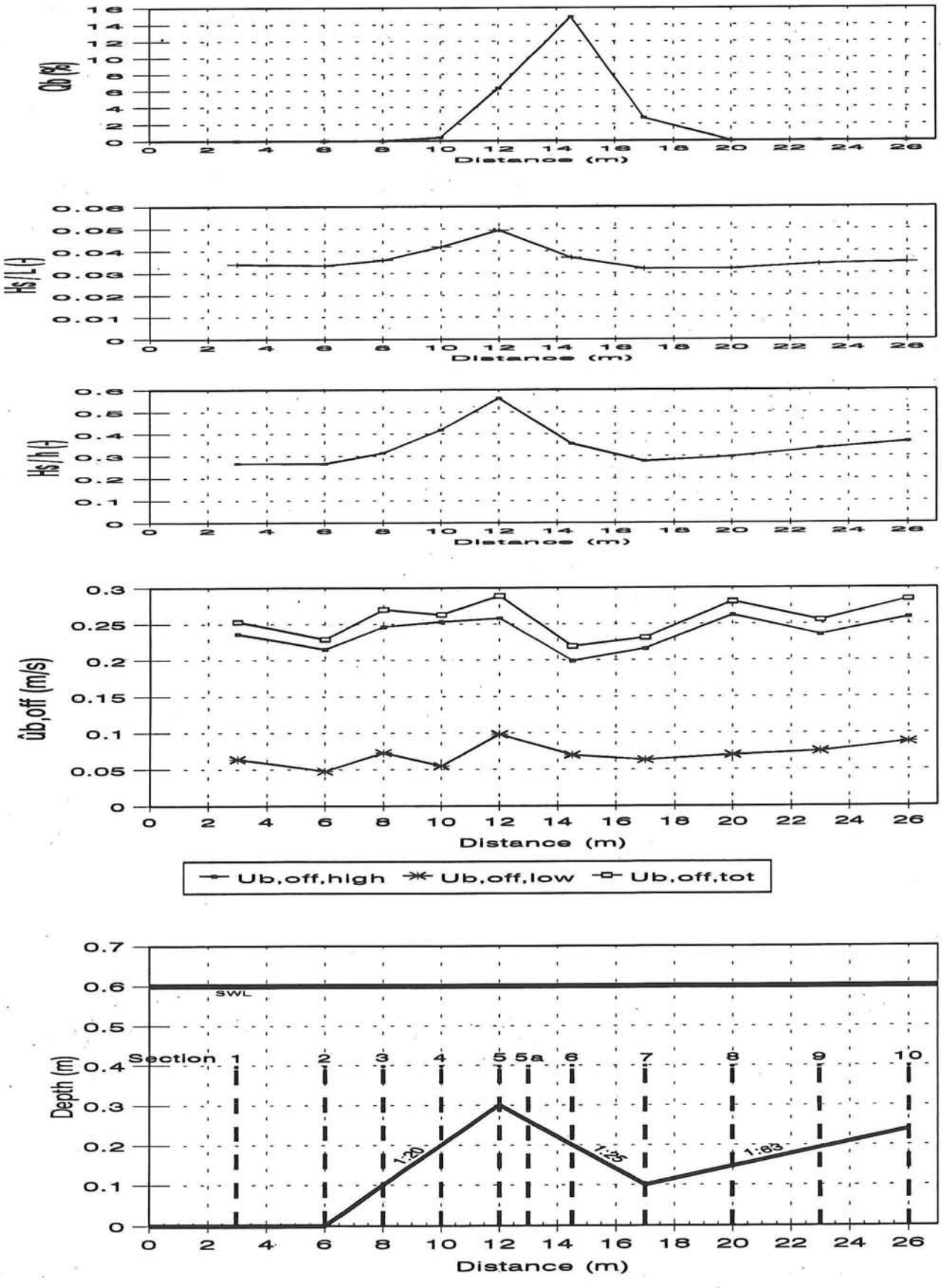

Figure 5.4.E3

Asymmetry velocity signal Series B1

with parameters Hs/h, Hs/L, Qb

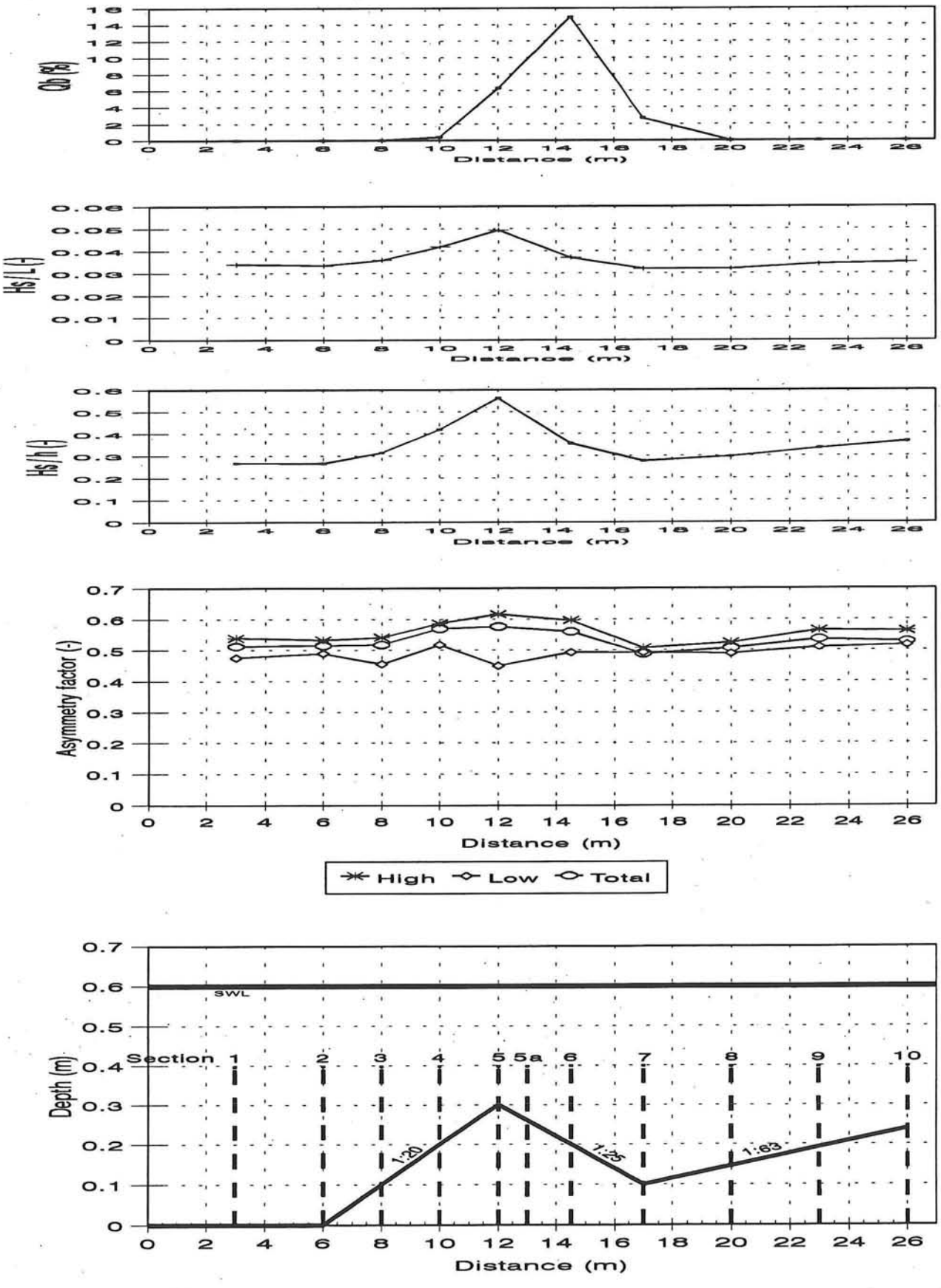

Figure 5.4.E4

Peak orbital velocity in onshore direction for Series B2

with parameters Hs/h, Hs/L, Qb

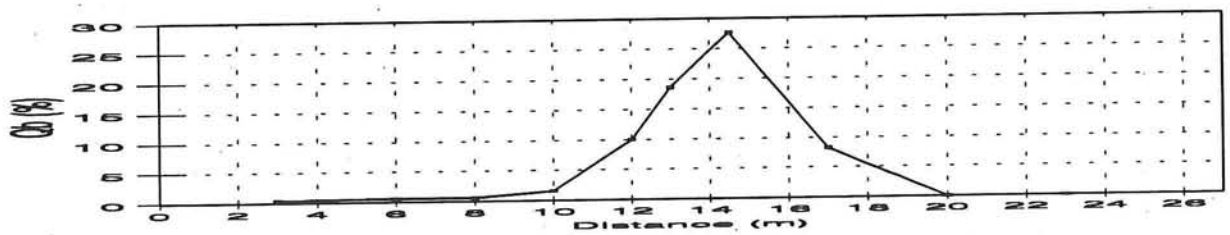

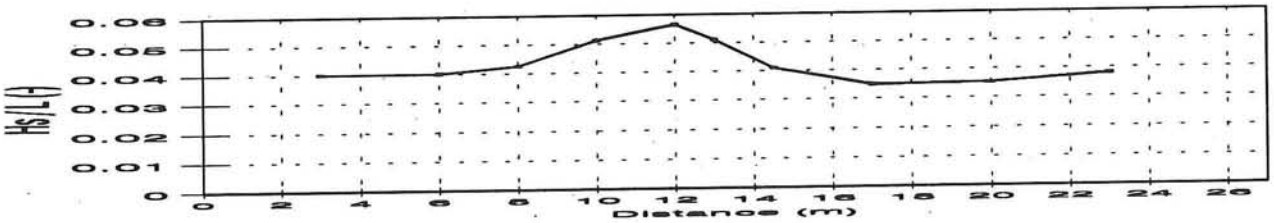

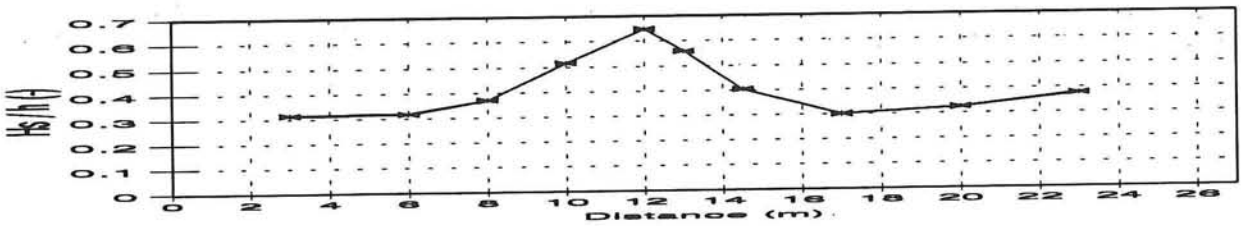

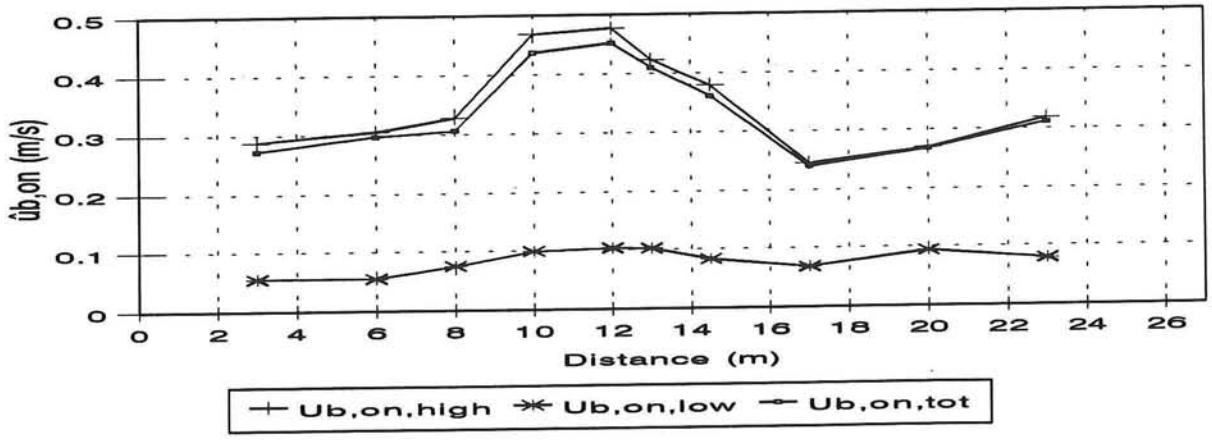

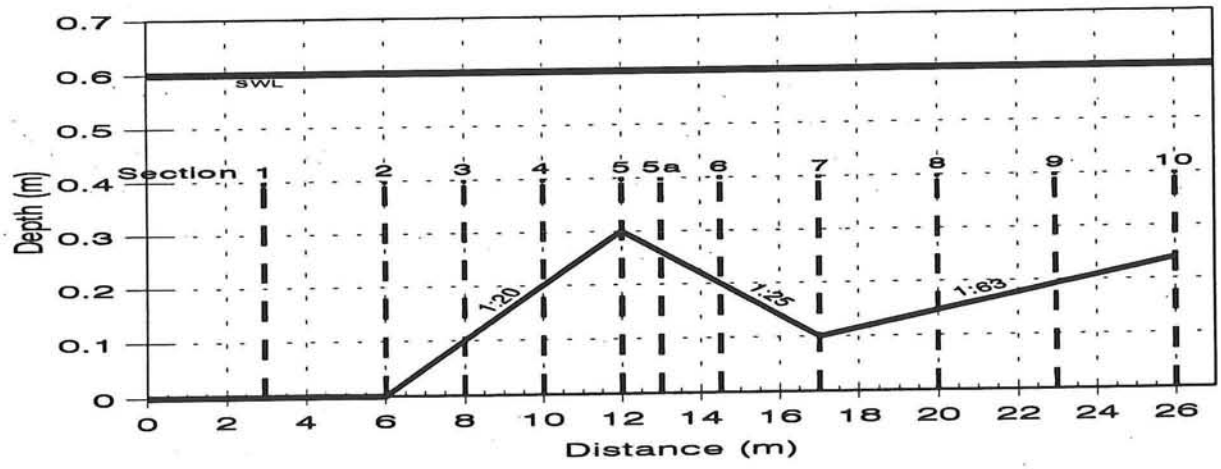

Figure 5.4.E5

Peak orbital velocity in offshore direction for Series B2

with parameters Hs/h, Hs/L, Qb

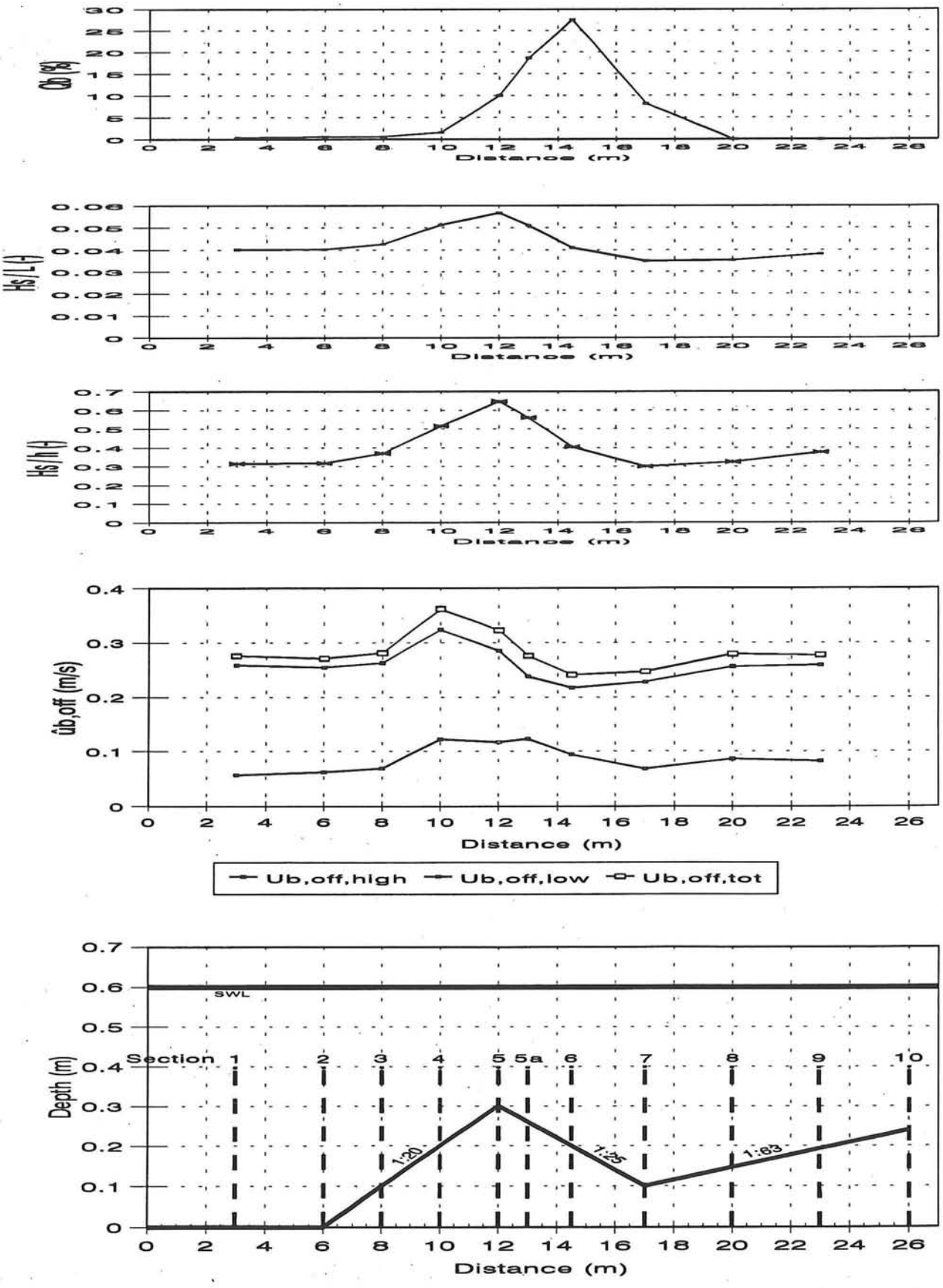

Figure 5.4.E6

Asymmetry Velocity signal Series B2

with parameters Hs/h, Hs/L, Qb

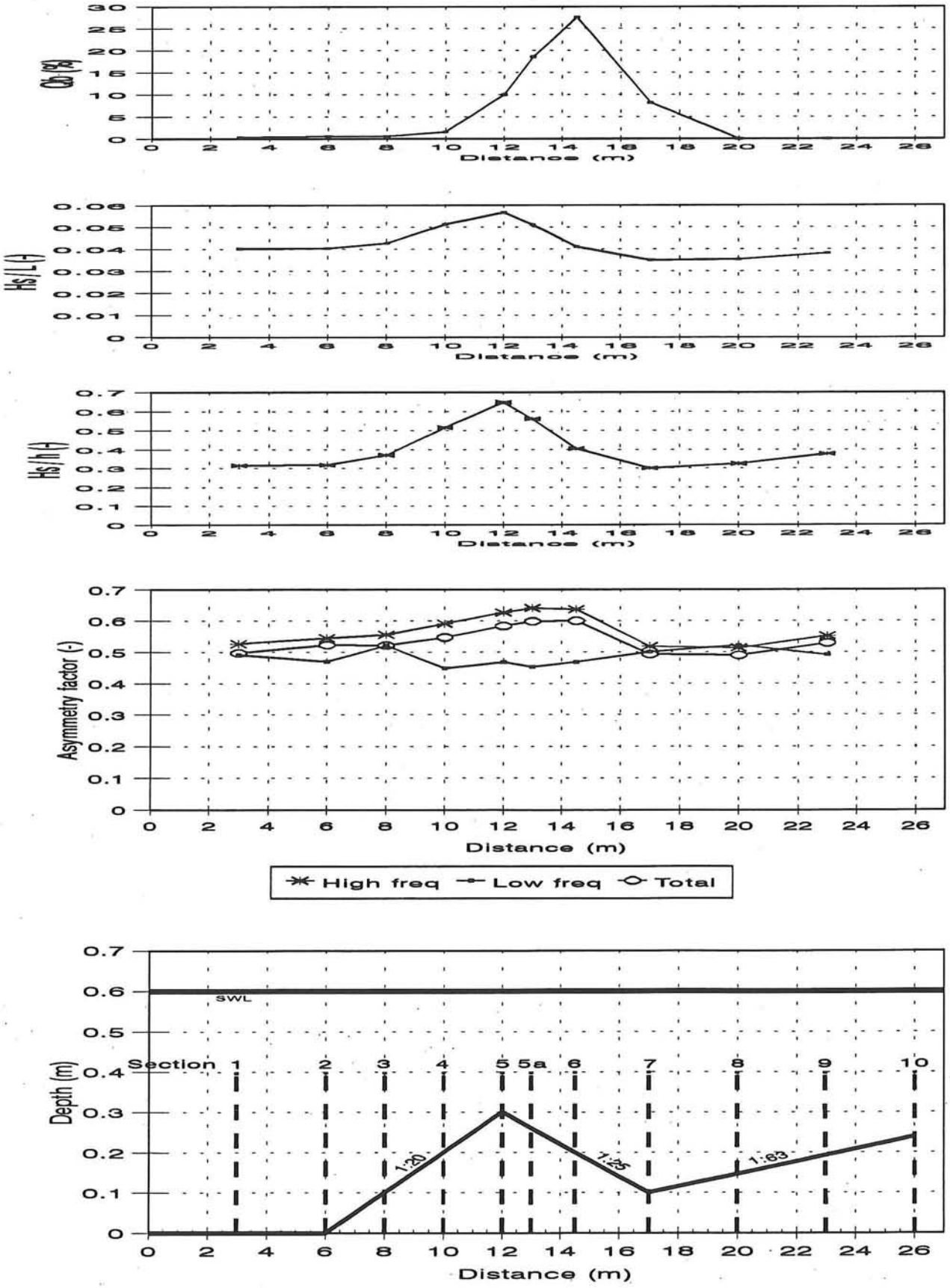

Figure 5.4.E7

Suspended Load Series B1

with parameters Hs/h, Hs/L, Qb

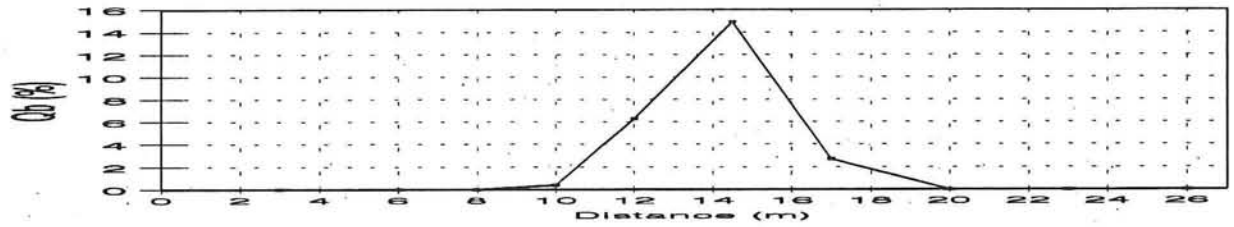

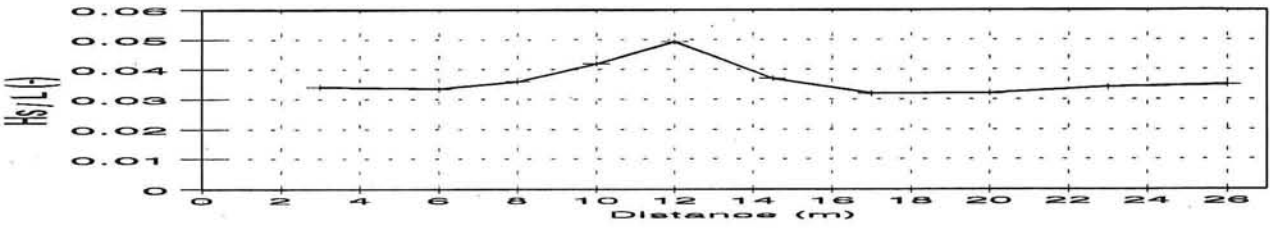

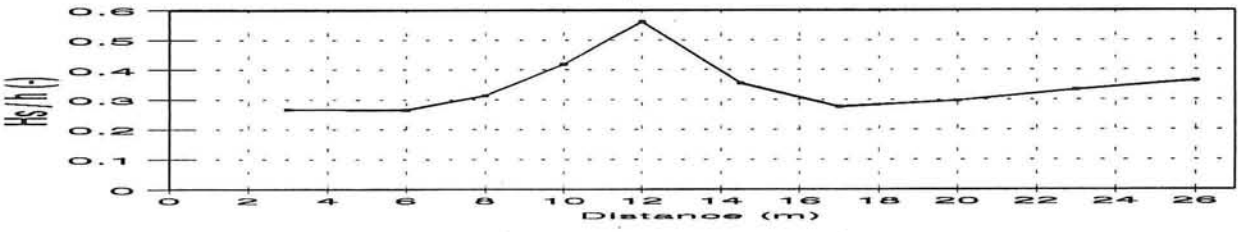

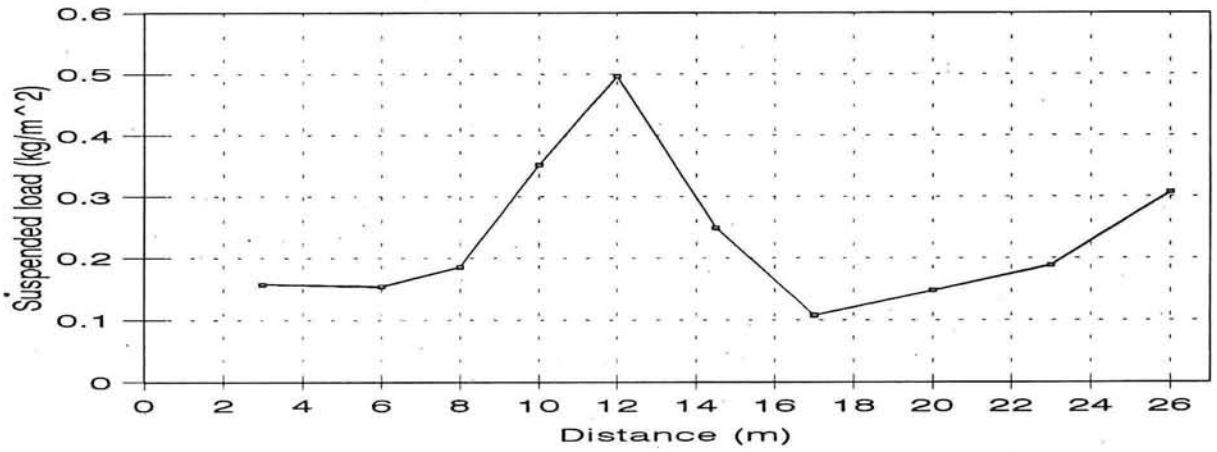

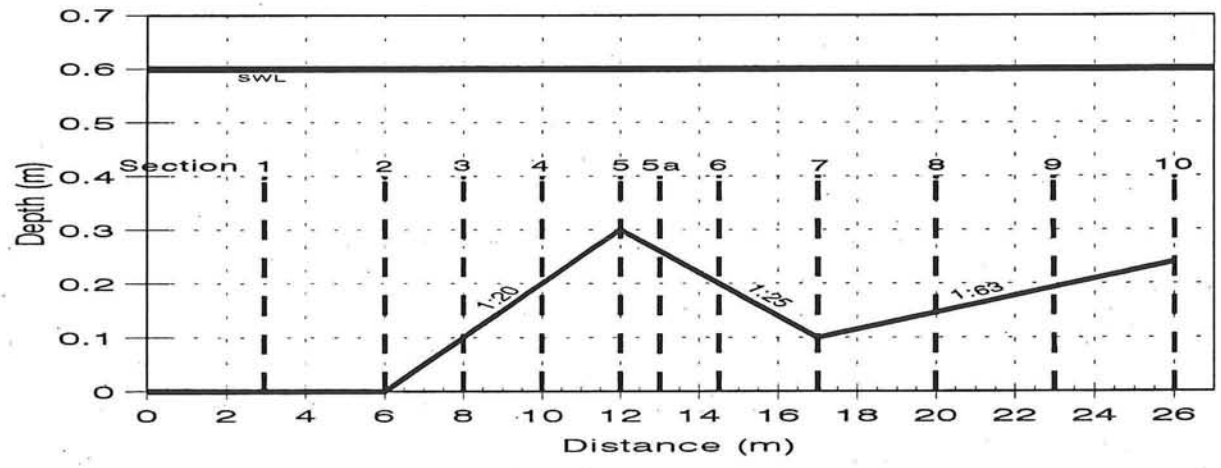

Figure 5.5.A1

Suspended Load Series B2

with parameters Hs/h, Hs/L, Qb

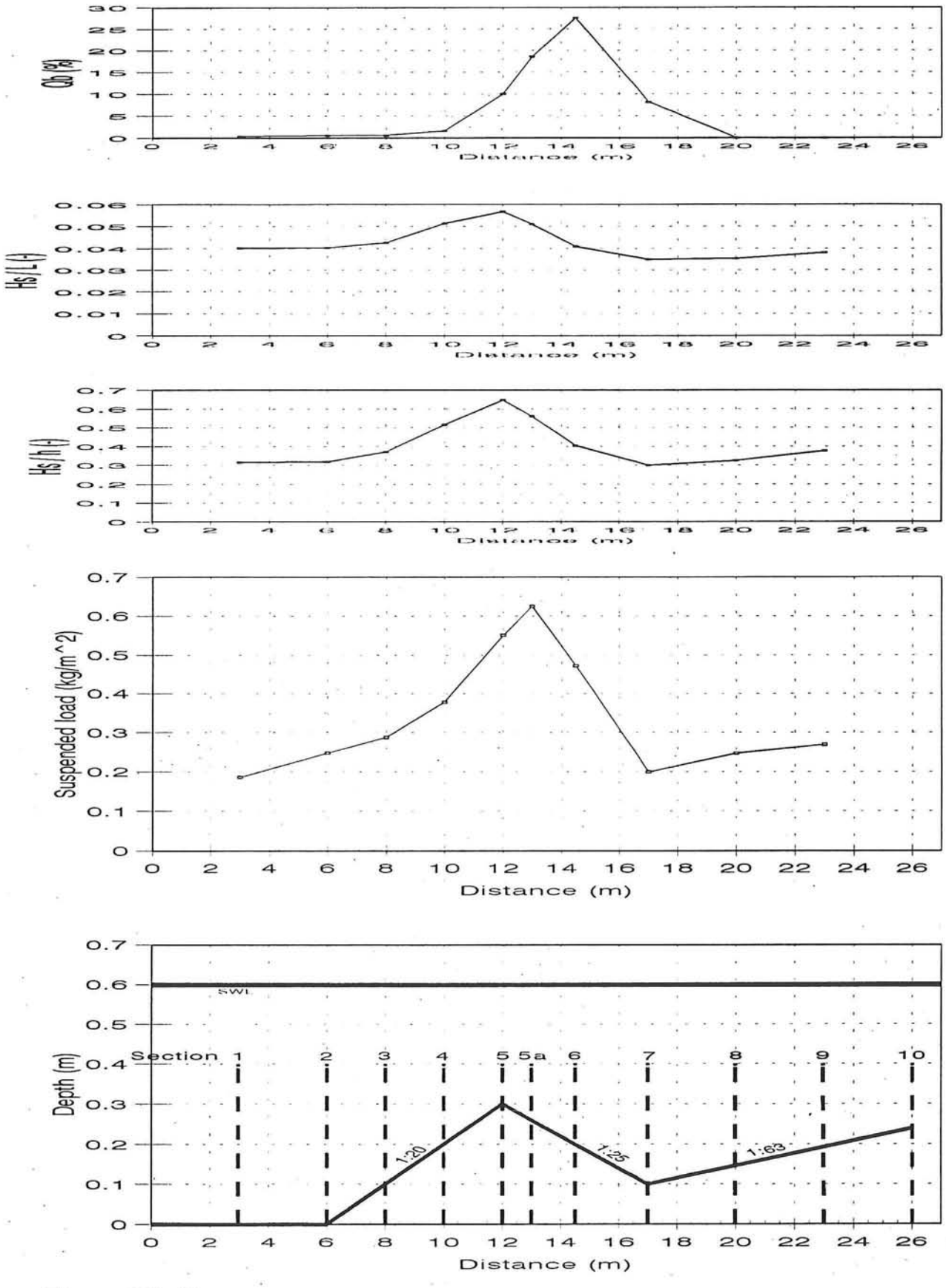

Figure 5.5.A2

Suspended Load

Influence Hs/h, Qb and ripple height (r)

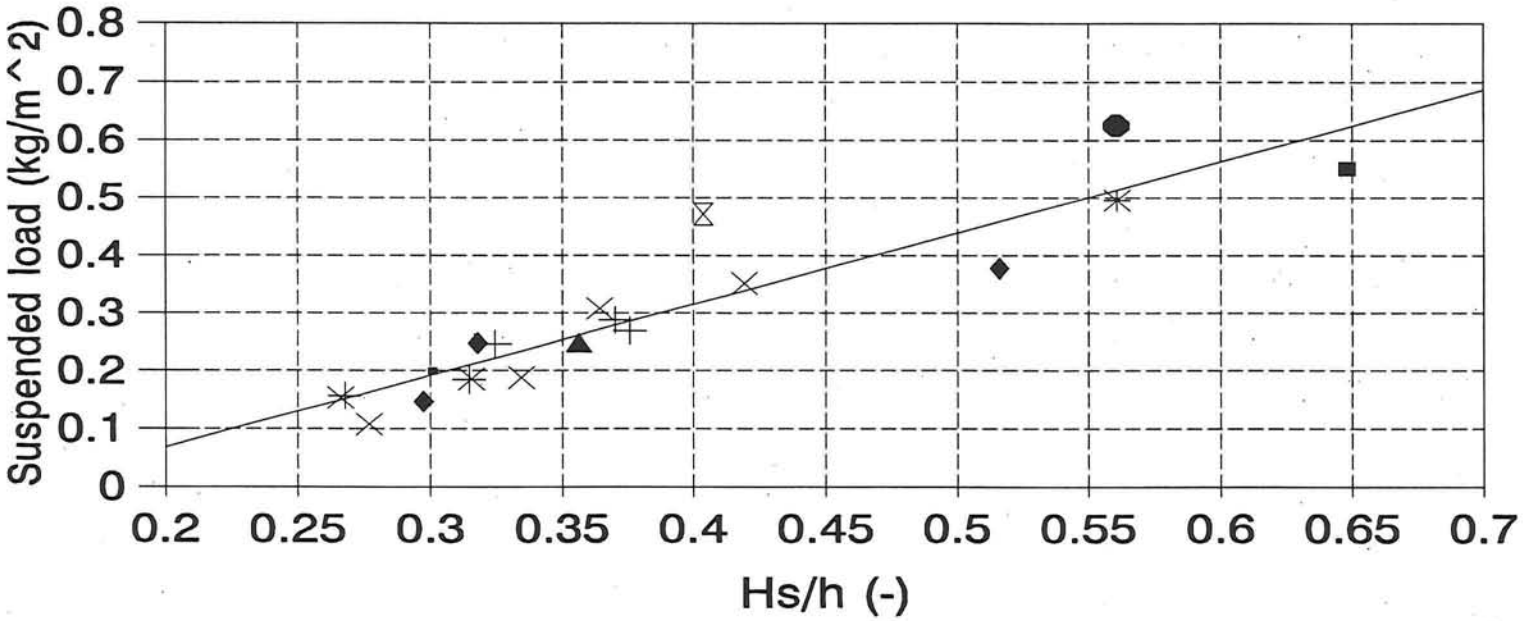

Qb in %; r in mm

Figure 5.5.B1

Suspended Load

Influence Qb

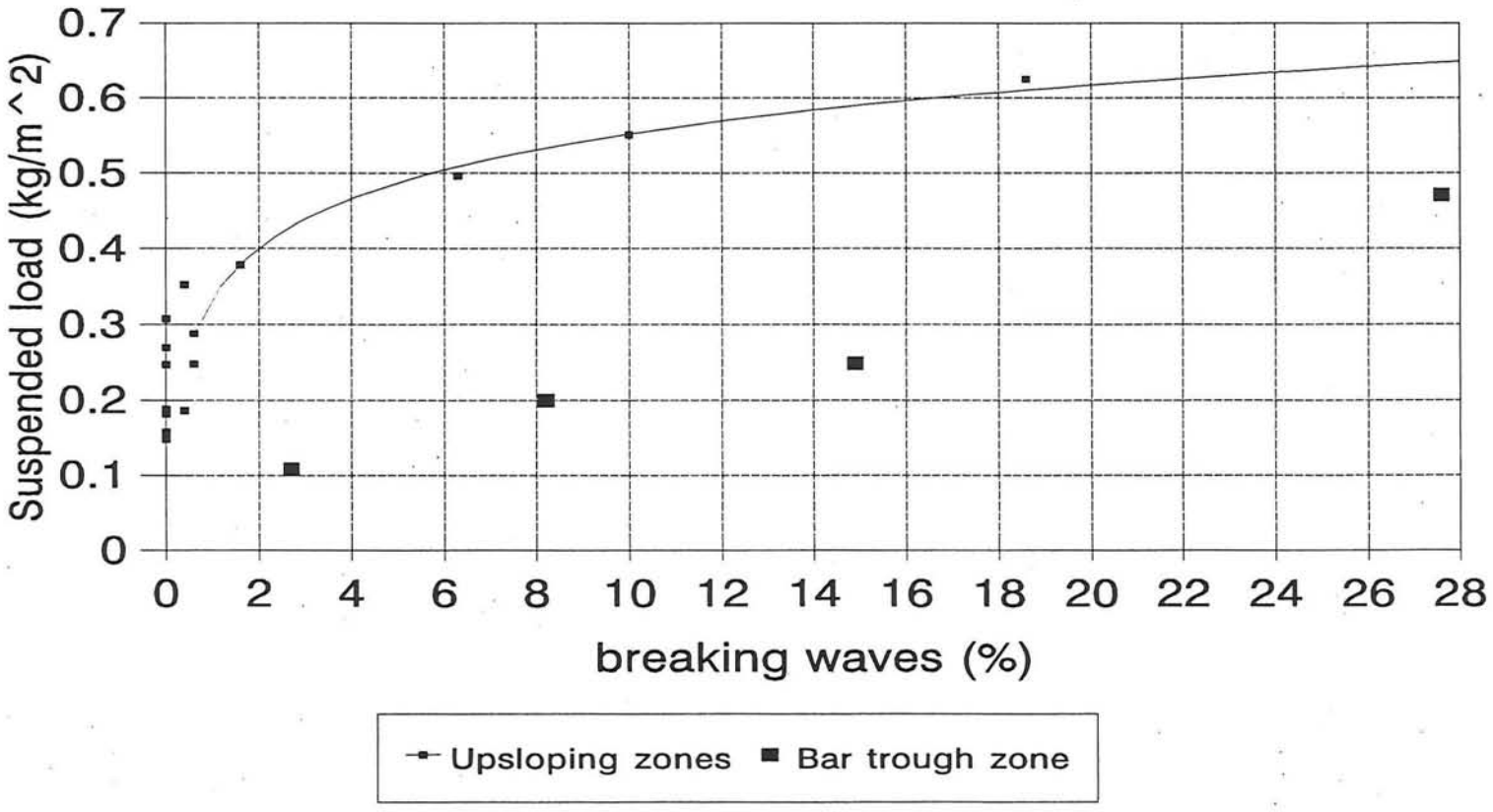

Figure 5.5.C1

Suspended Load

Influence waveheight
Comparison A- and B-series

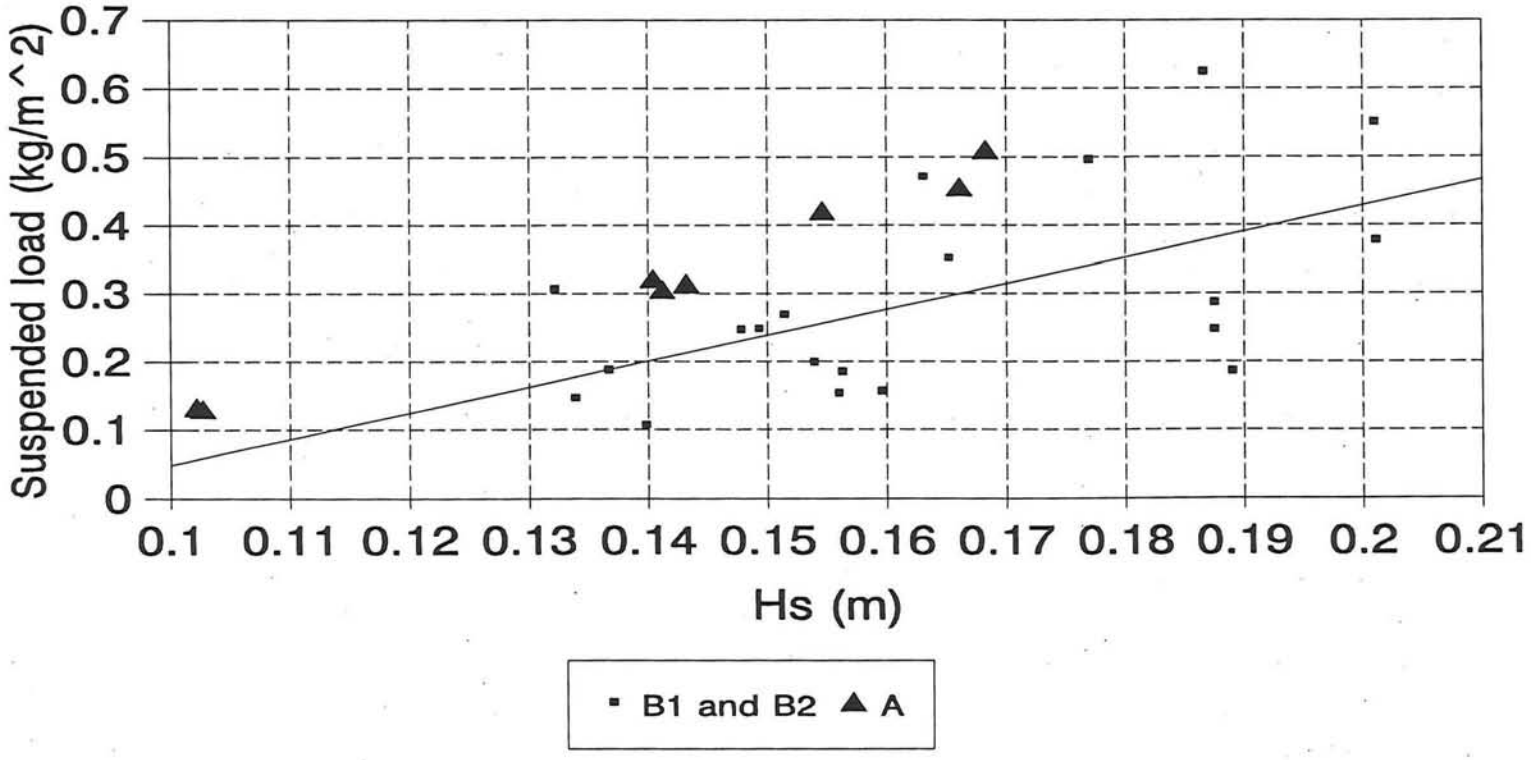

Figure 5.5.D1

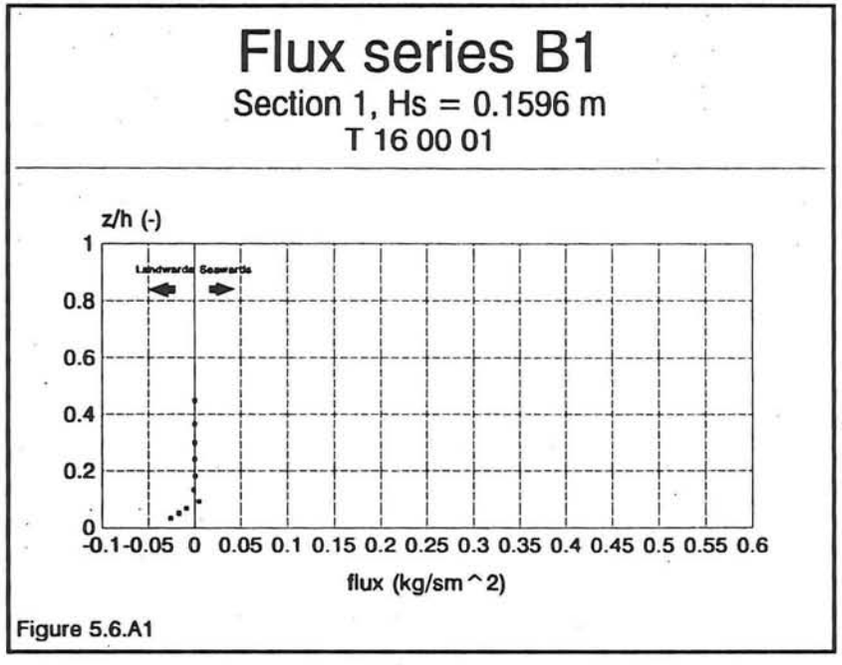

Figure 5.6.A1

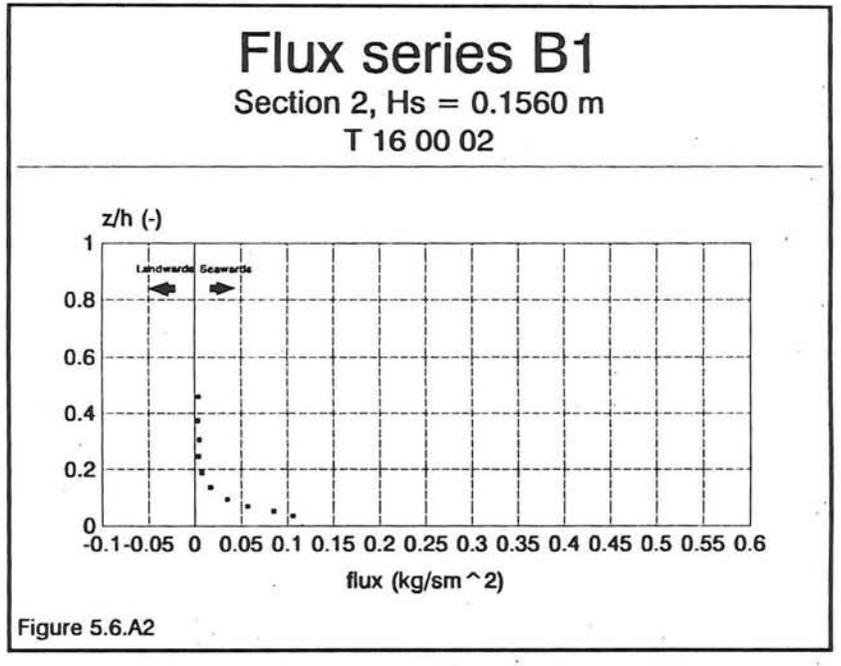

Figure 5.6.A2

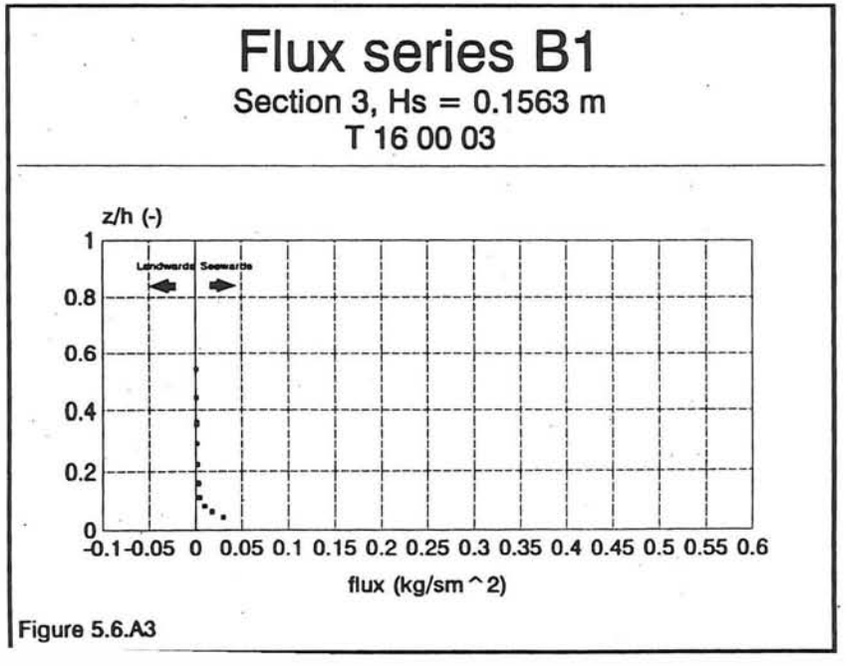

Figure 5.6.A3

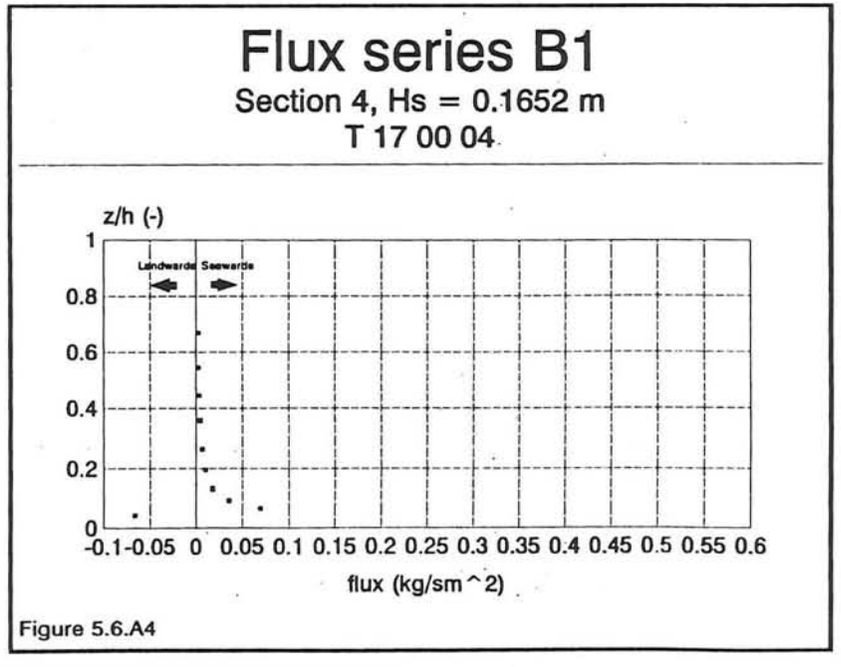

Figure 5.6.A4

Suspended Transport Series B1

with parameters Hs/h, Hs/L, Qb

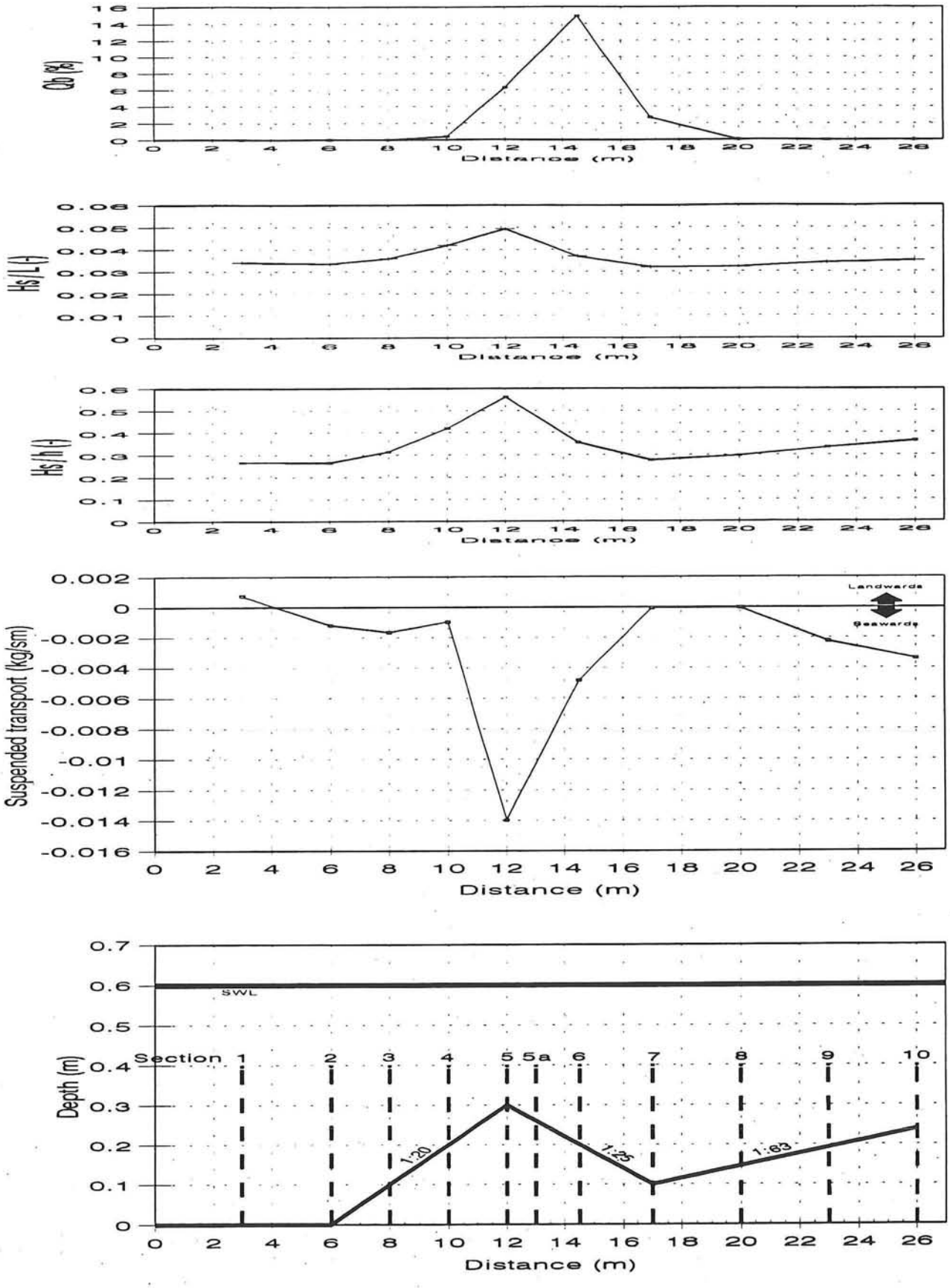

Figure 5.6.B1

Suspended Transport Series B2

with parameters Hs/h, Hs/L, Qb

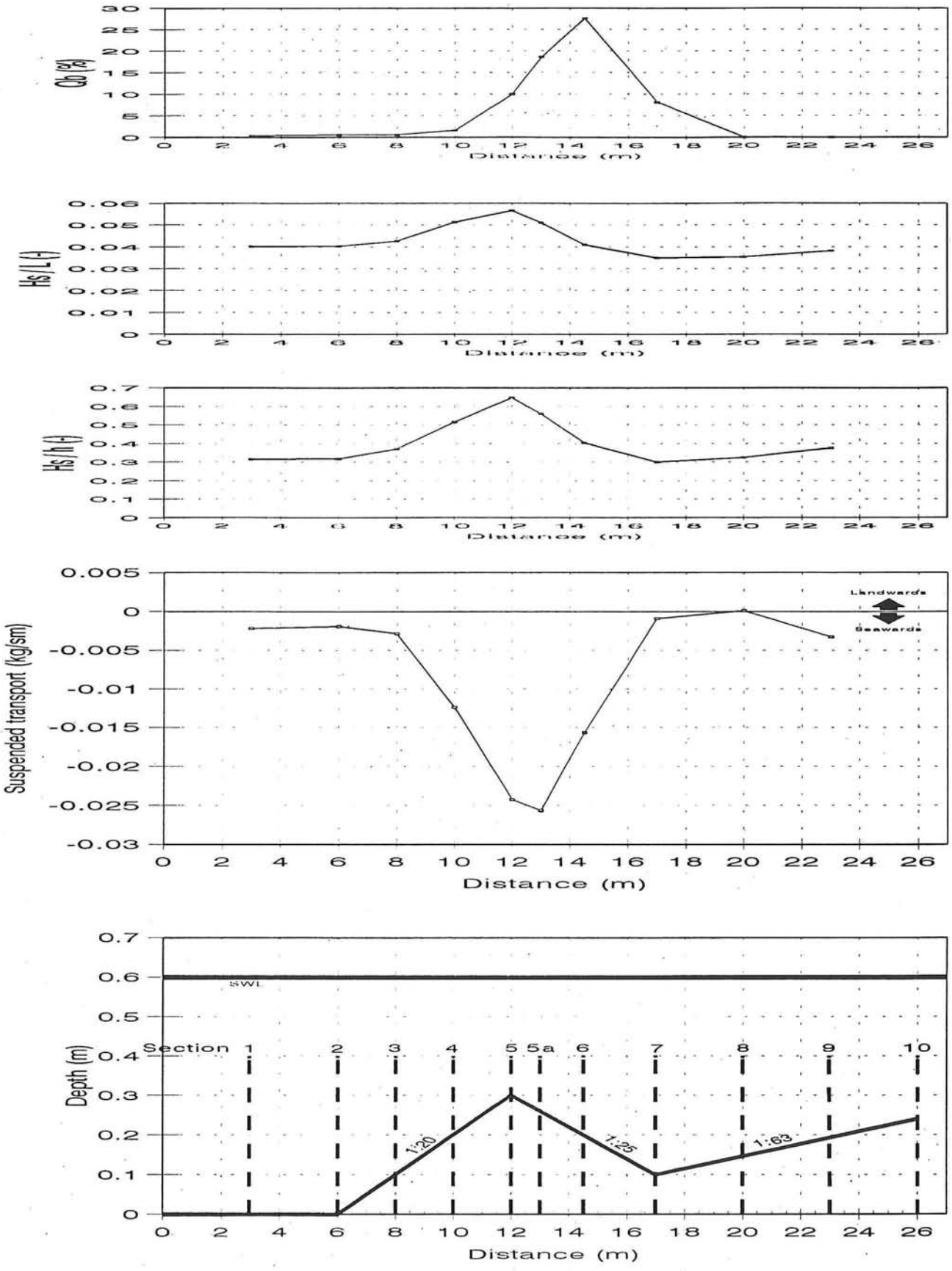

Figure 5.6.B2

Suspended transport

Influence wave height

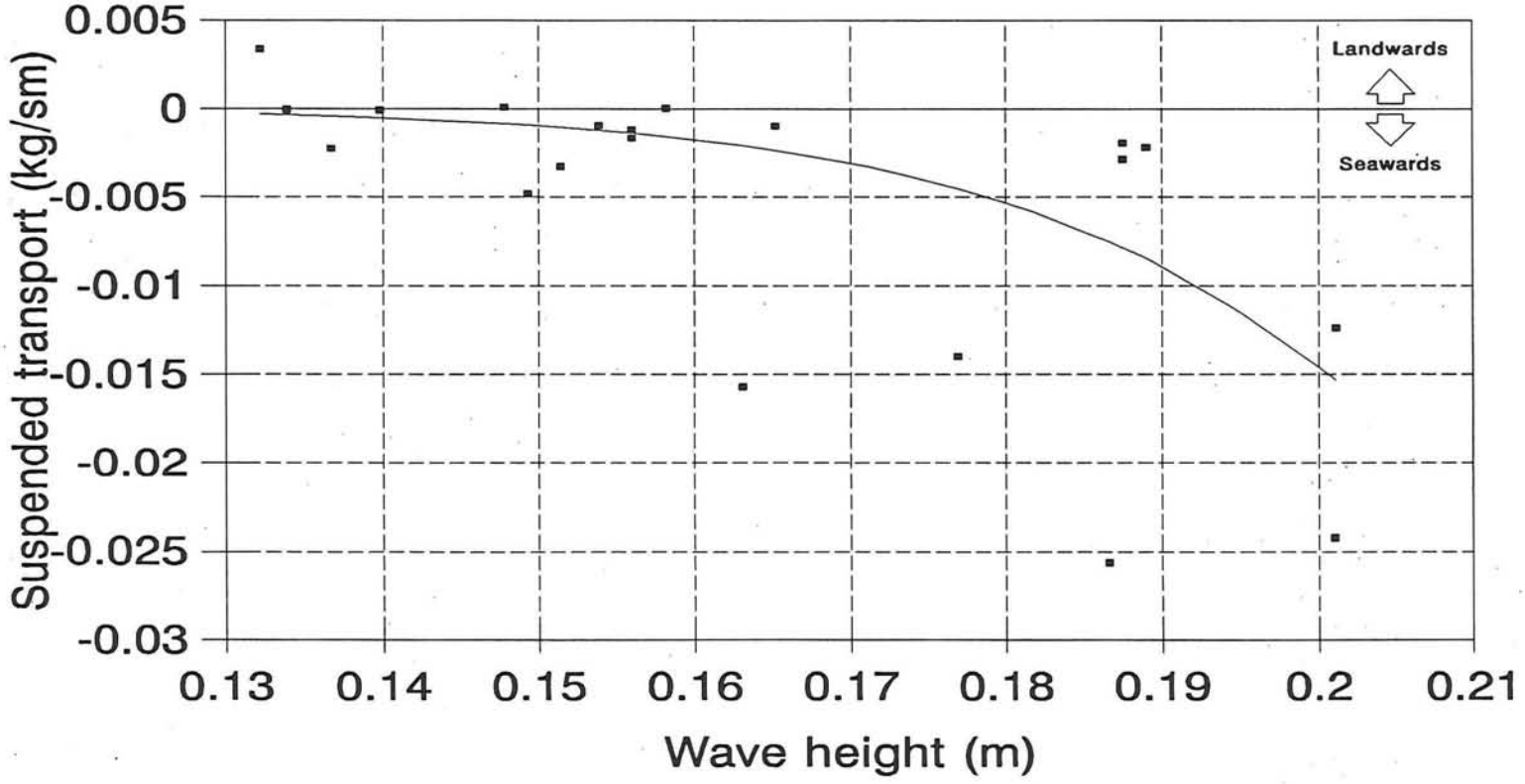

Figure 5.6.C1

Suspended transport

Influence Hs/h

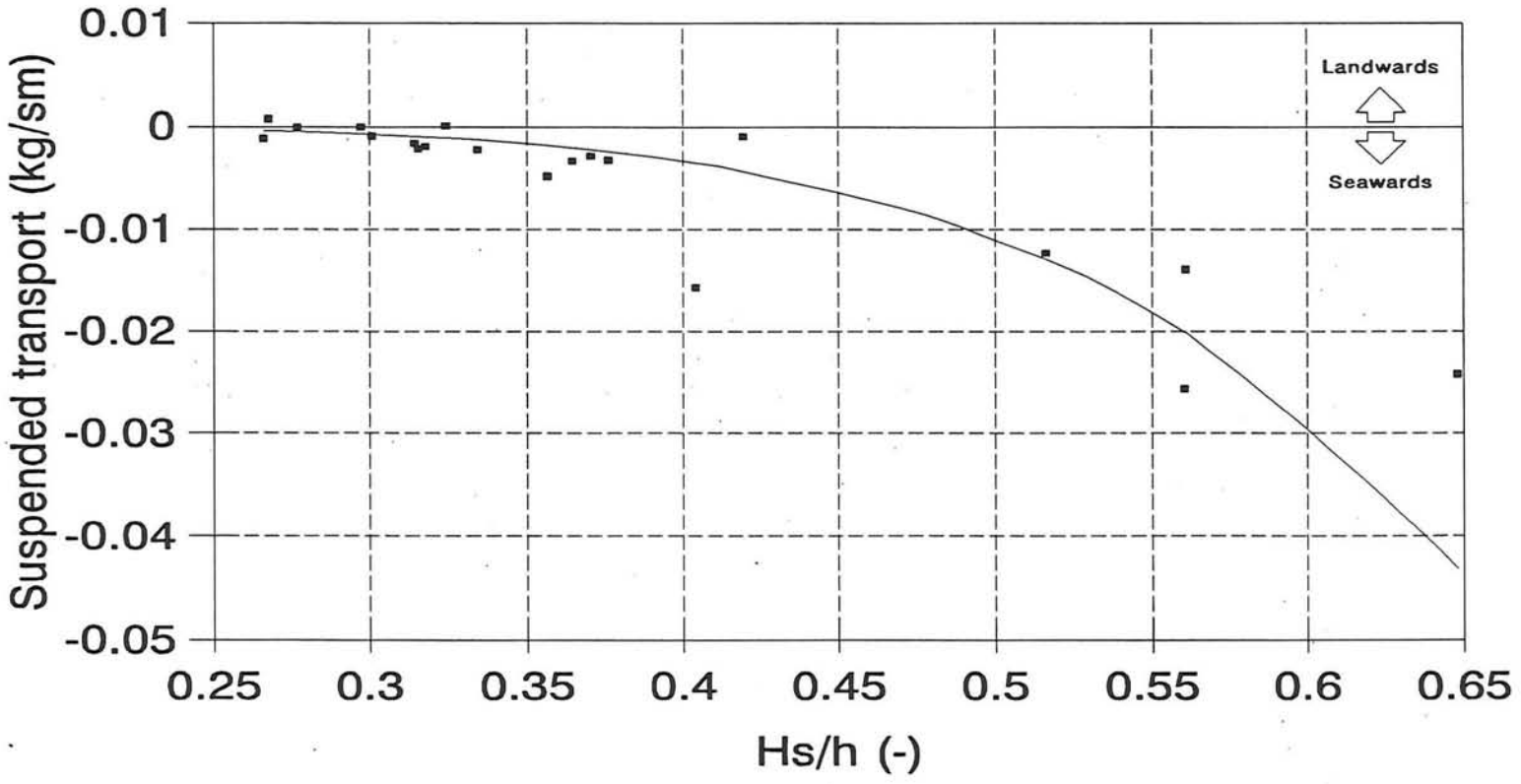

Figure 5.6.D1

Suspended transport

Influence Qb

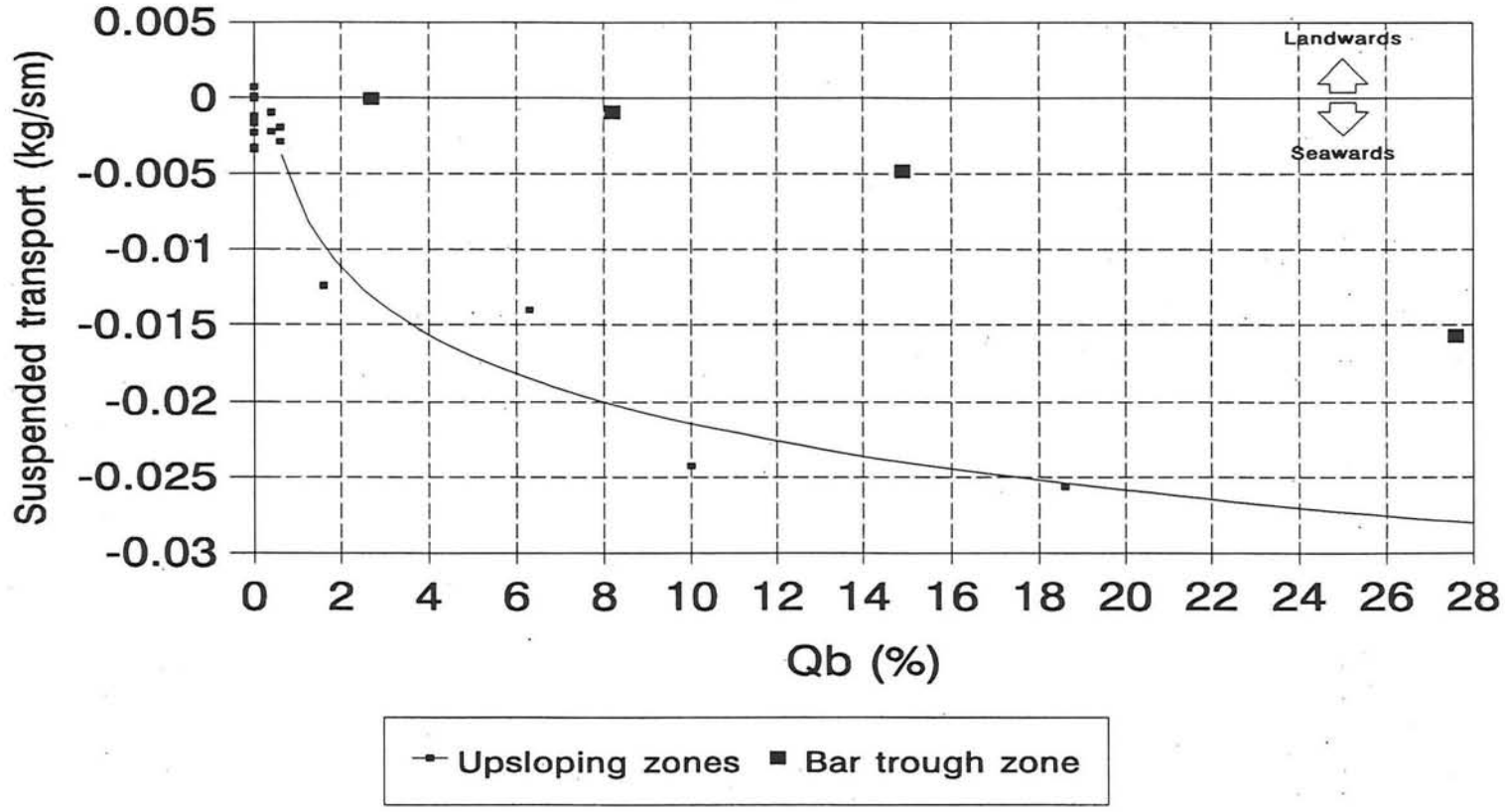

Figure 5.6.E1

Transport series B1

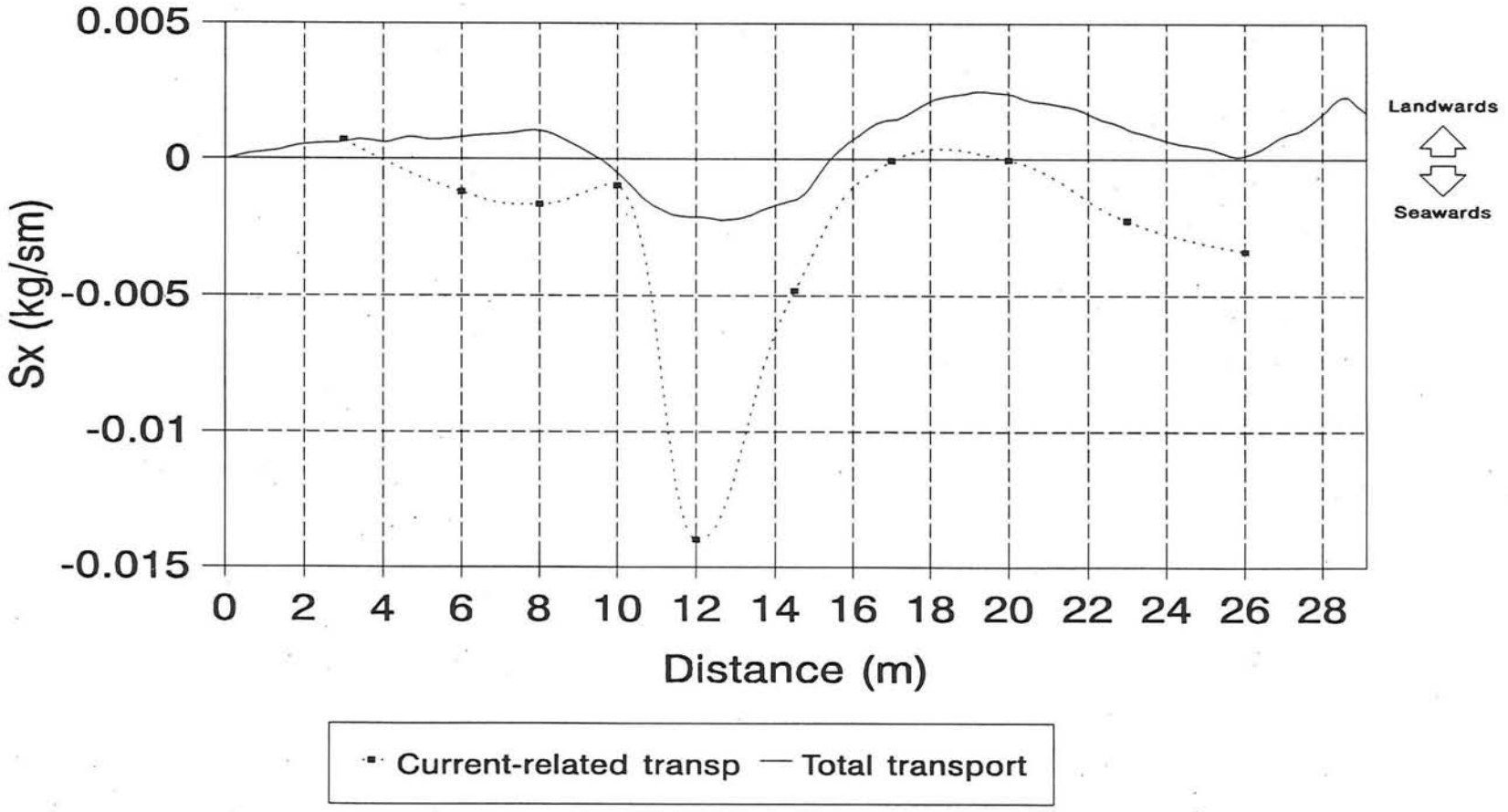

Figure 5.6.F1

Transport Series B2

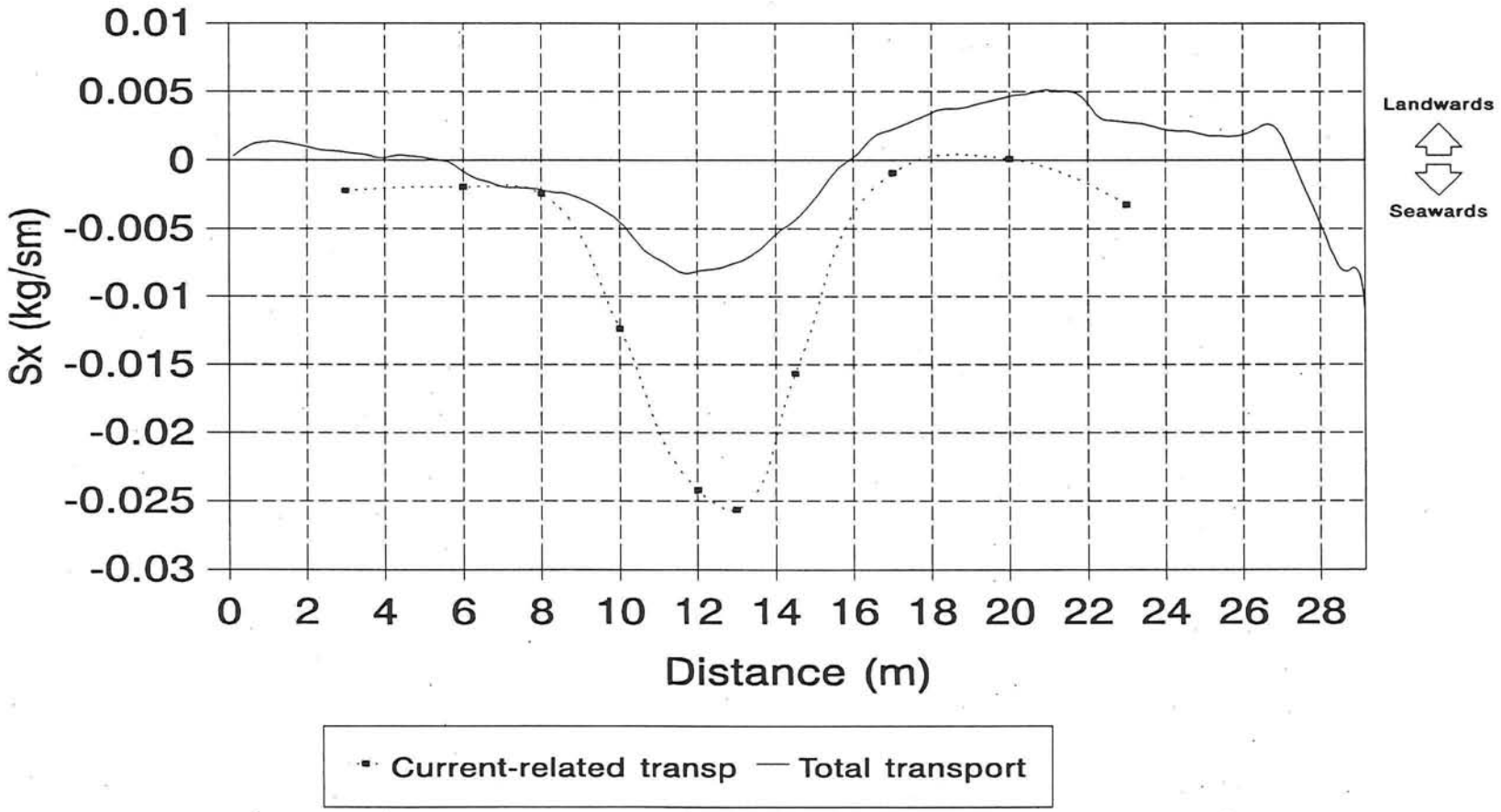

Figure 5.6.F2

Bedheight changes during tests

Series B1

dt = 25500 s

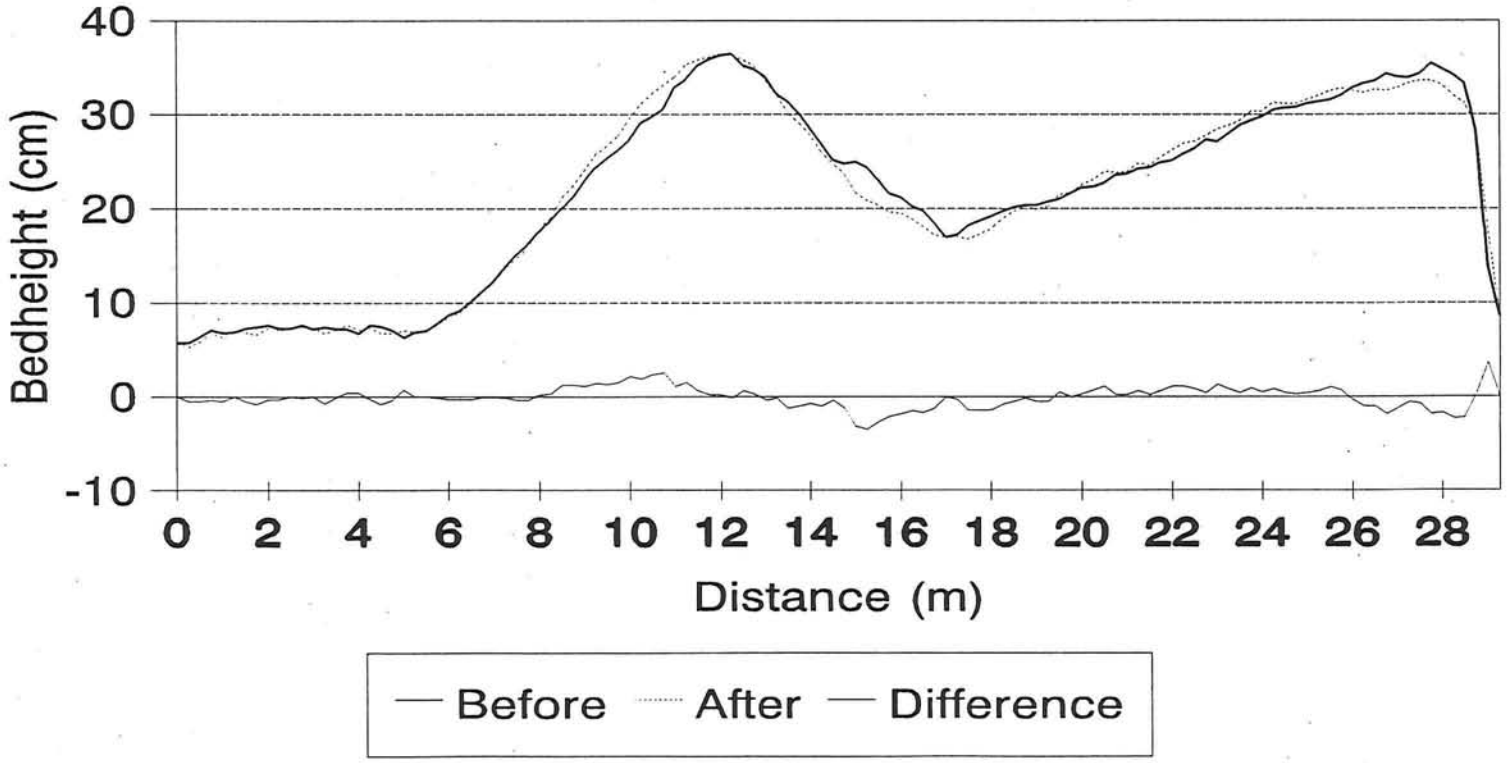

Figure 5.6.F3

Bedheight changes during tests

Series B2

dt = 9700 s

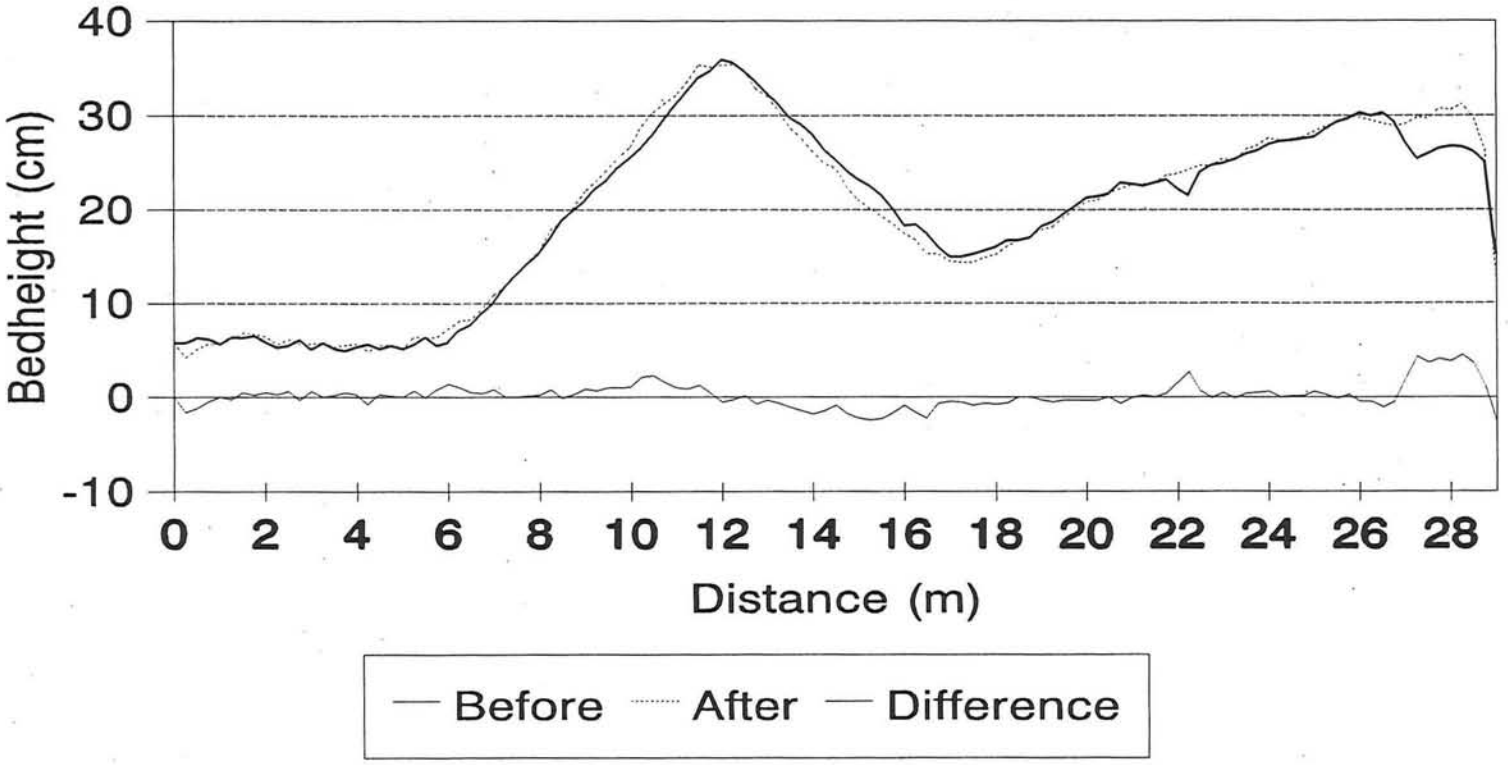

Figure 5.6.F4

Suspended transport

Influence Hs

Comparison A- and B-series

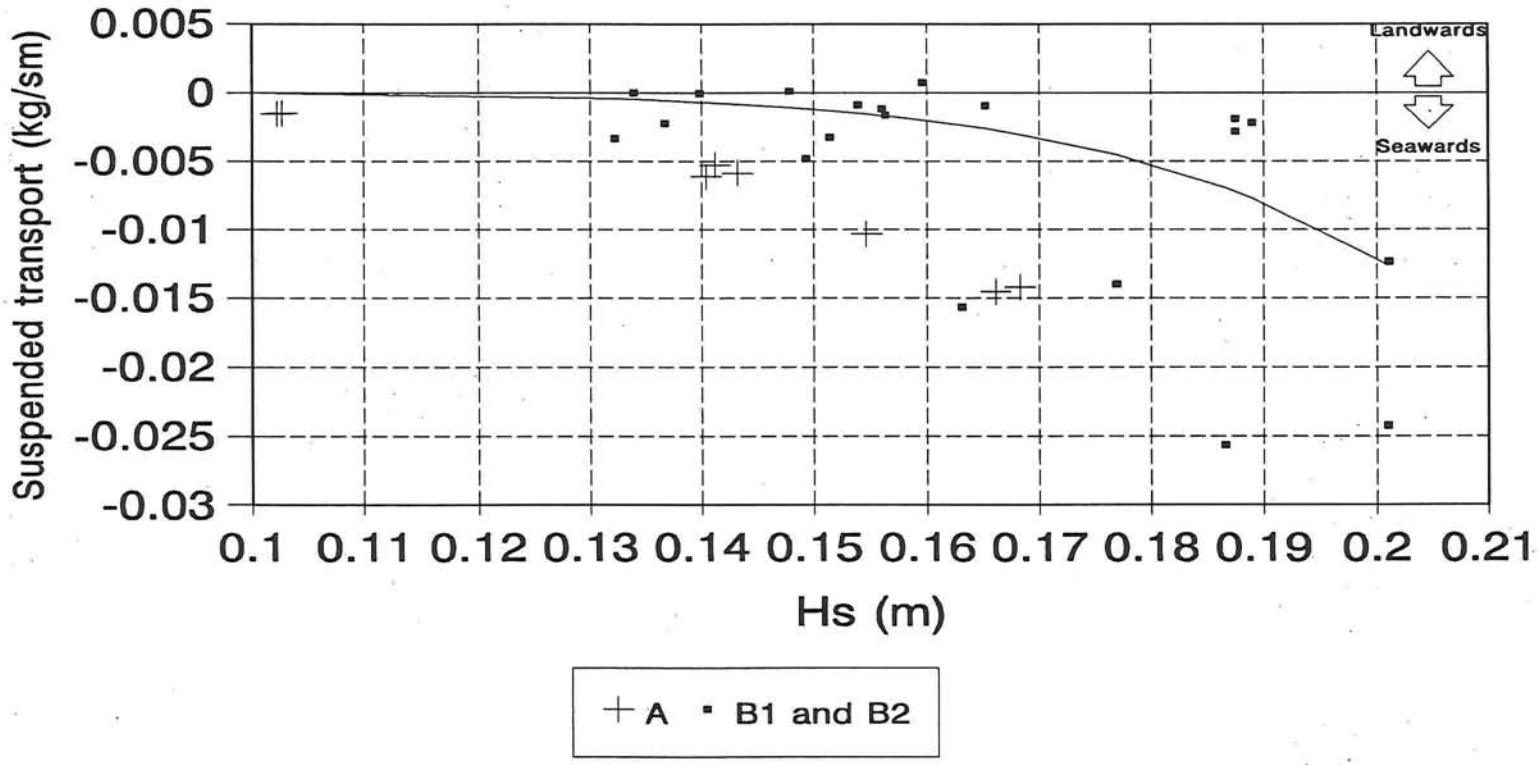

Figure 5.6.G1

Ripple height and length Series B1

with parameters Hs/h, Hs/L, Qb

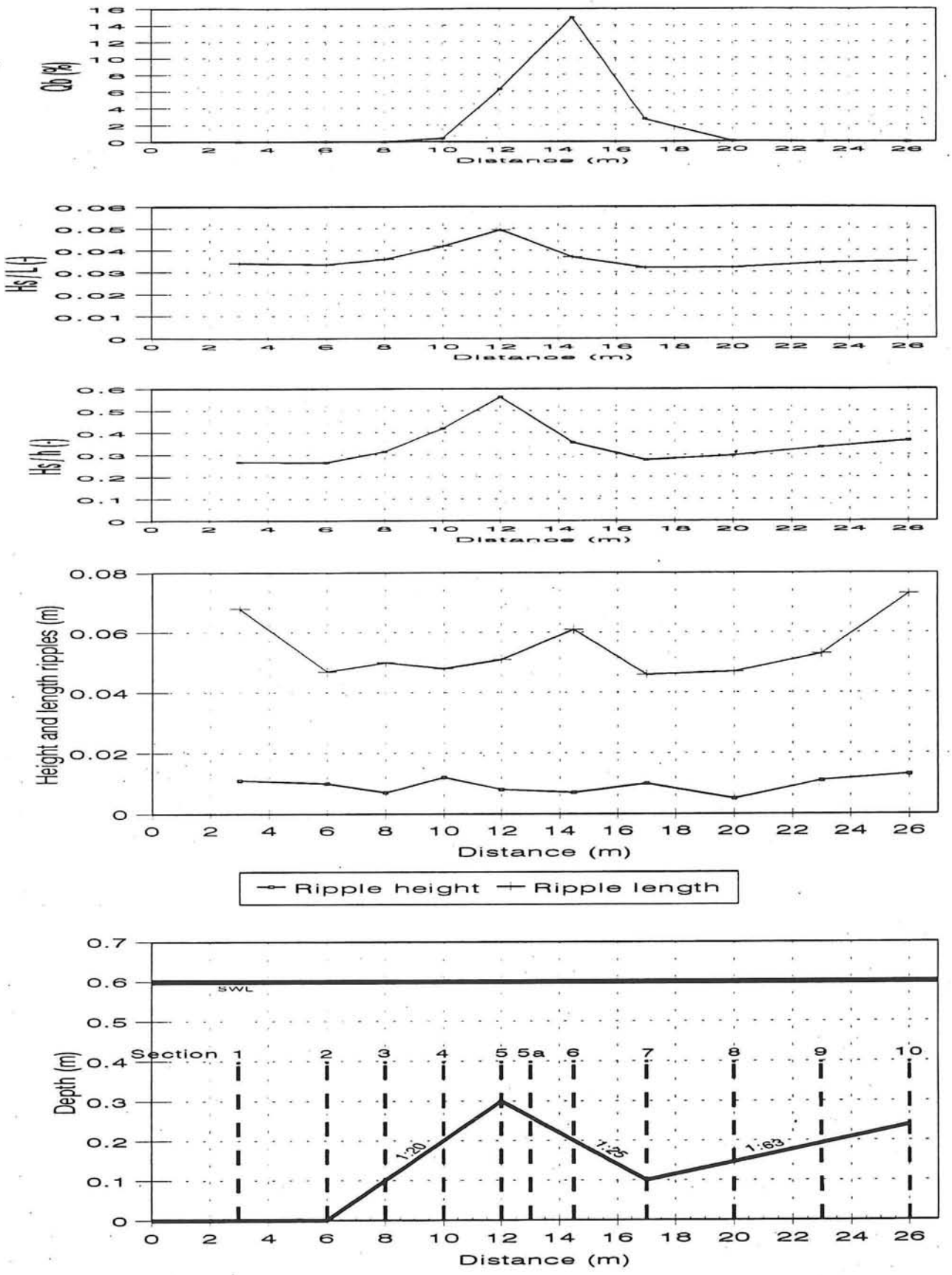

Figure 5.7.A1

Ripple length and height Series B2

with parameters Hs/h, Hs/L, Qb

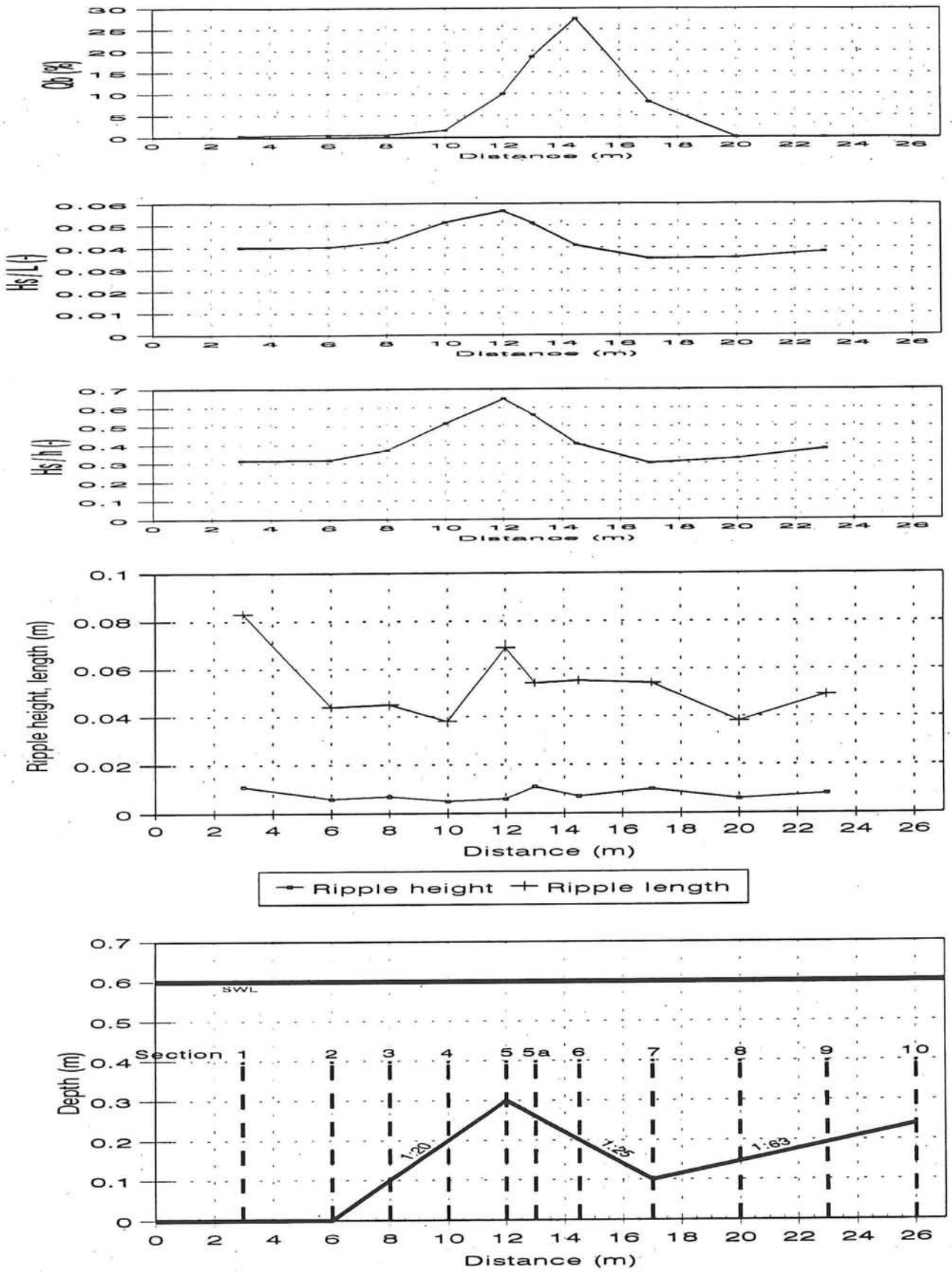

Figure 5.7.A2

Ripple steepness Series B1

with parameters Hs/h, Hs/L, Qb

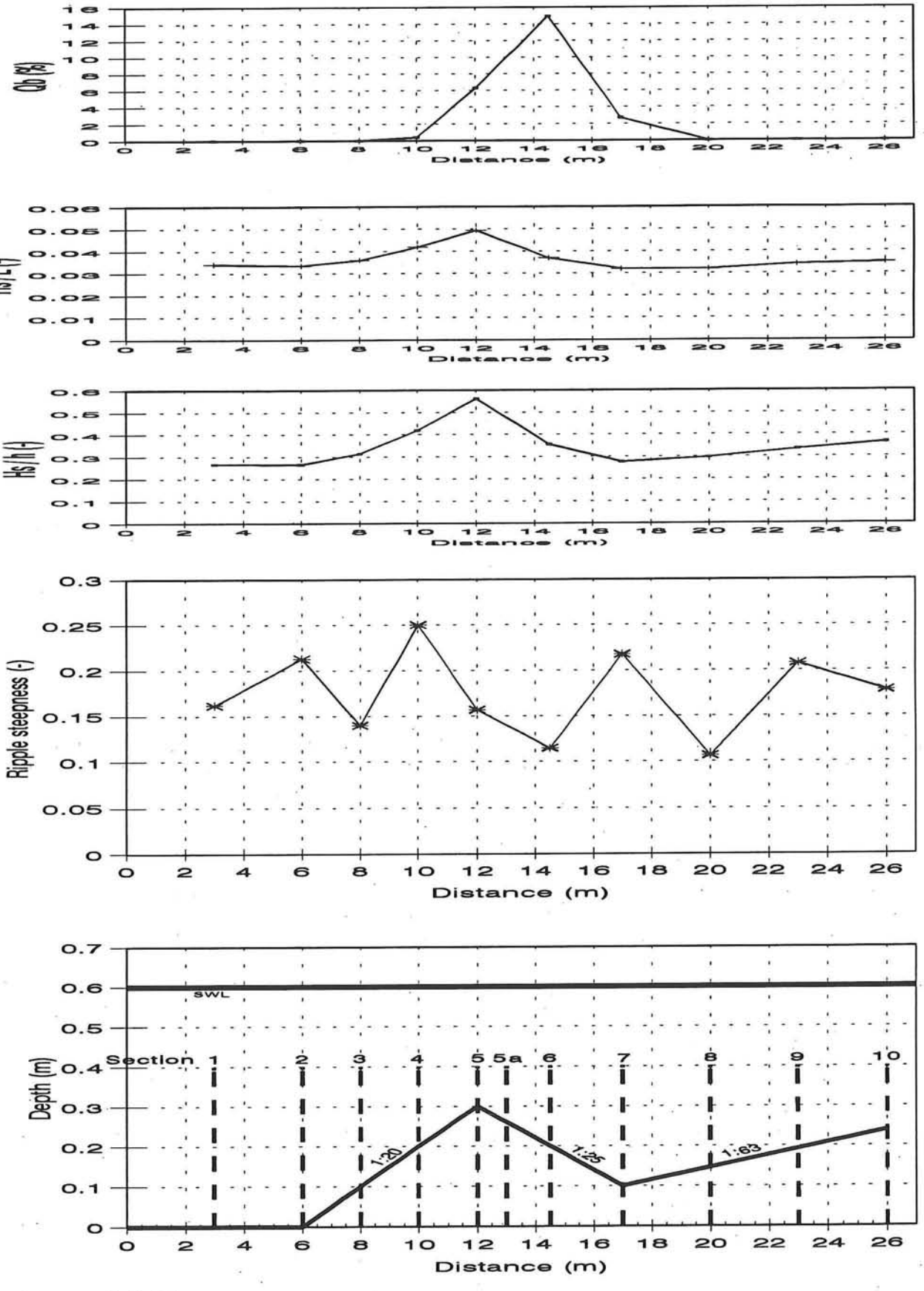

Figure 5.7.B1

Ripple steepness Series B2

with parameters Hs/h, Hs/L, Qb

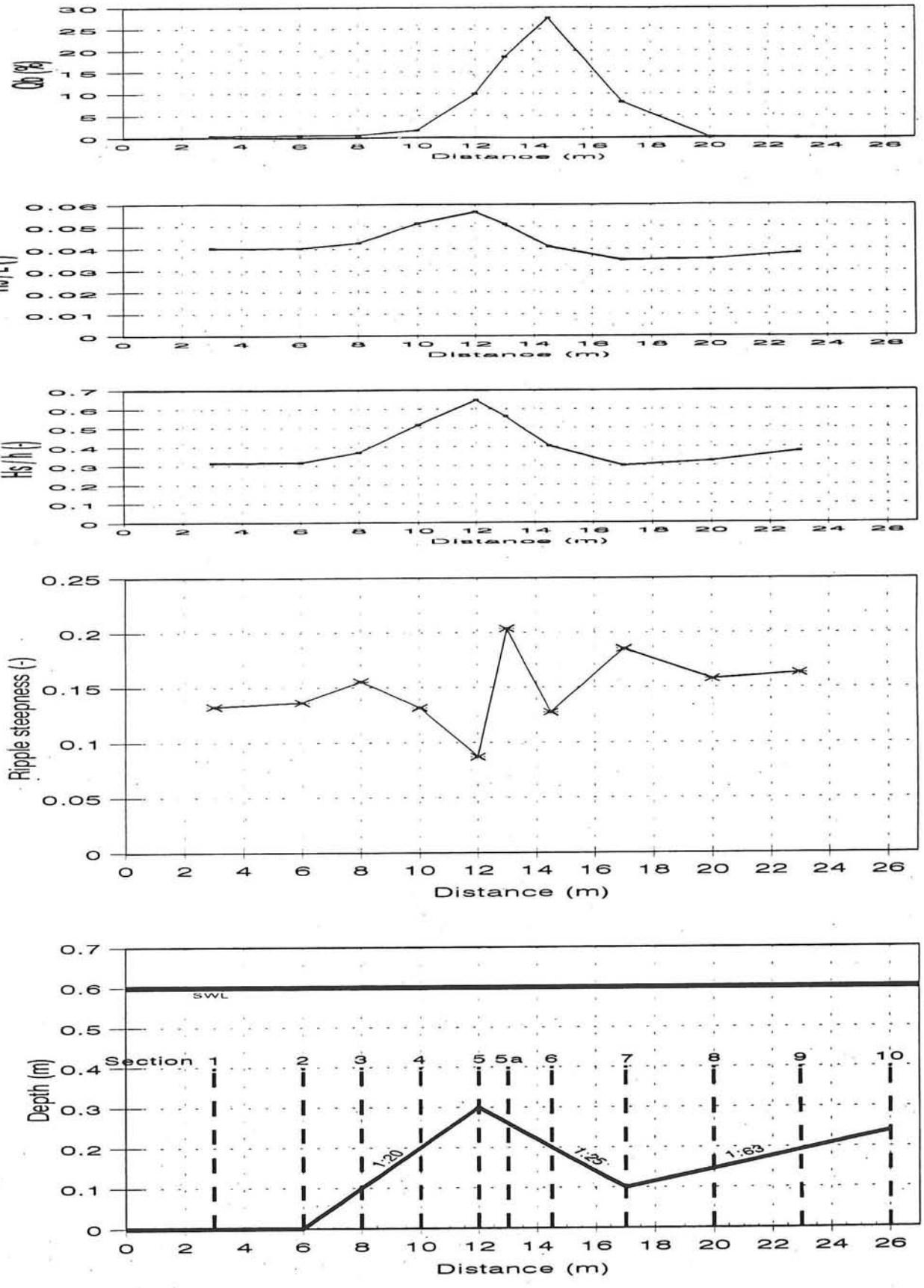

Figure 5.7.B2

Suspended sediment size Series B1

with parameters Hs/h, Hs/L, Qb

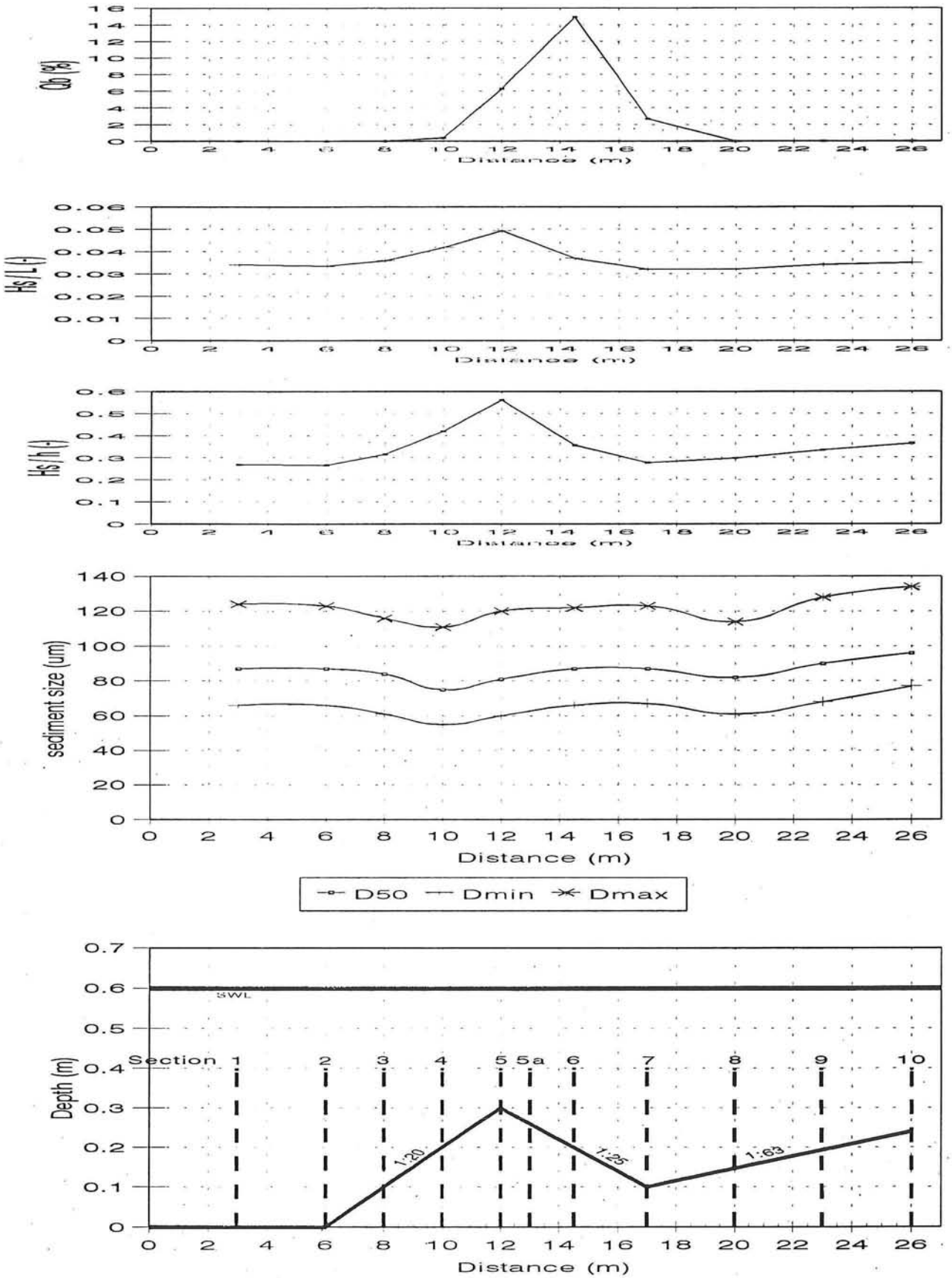

Figure 5.8.A1

Suspended sediment size Series B2

with parameters Hs/h, Hs/L, Qb

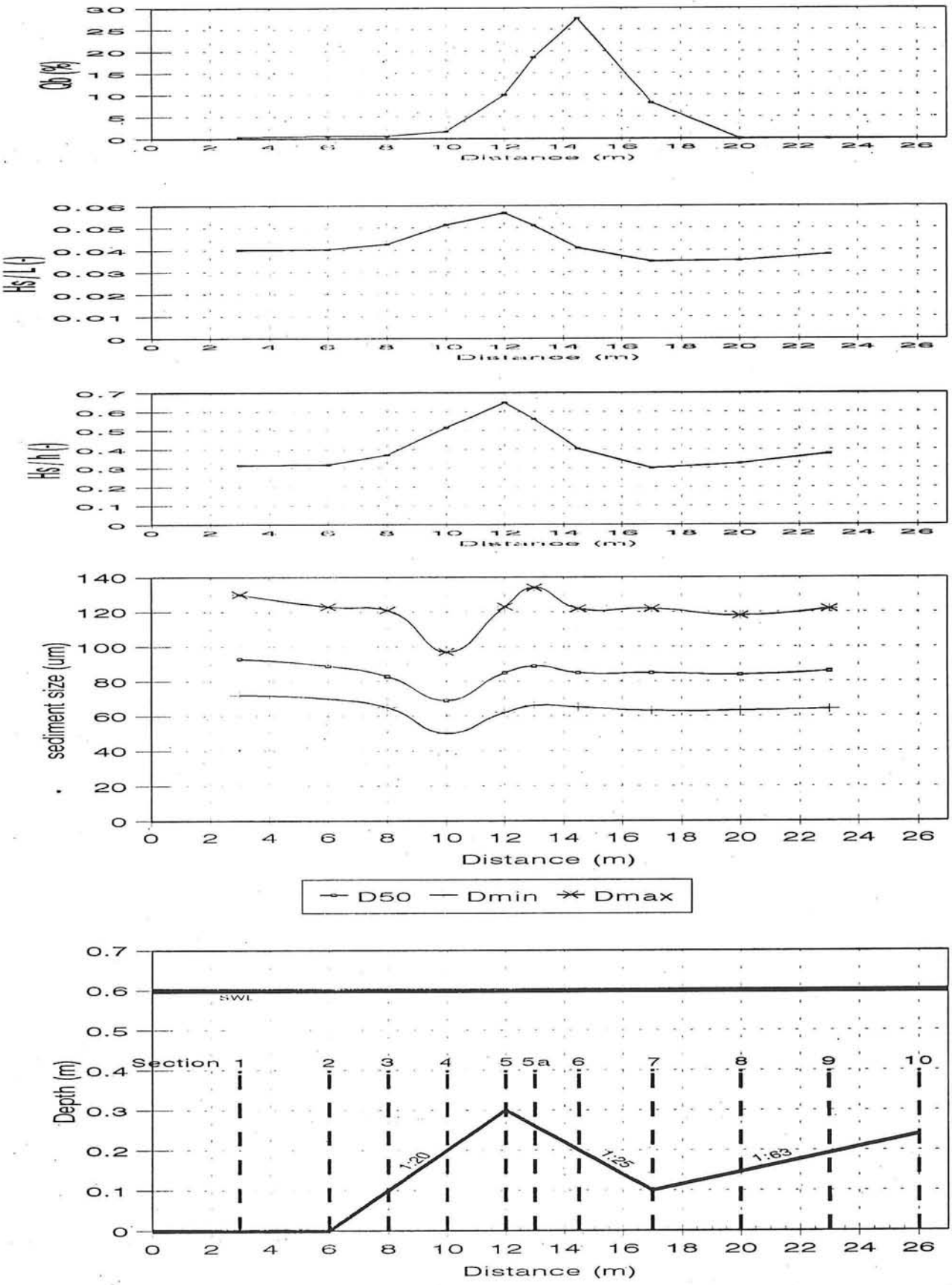

Figure 5.8.A2

Suspended sediment size

Distribution over the depth

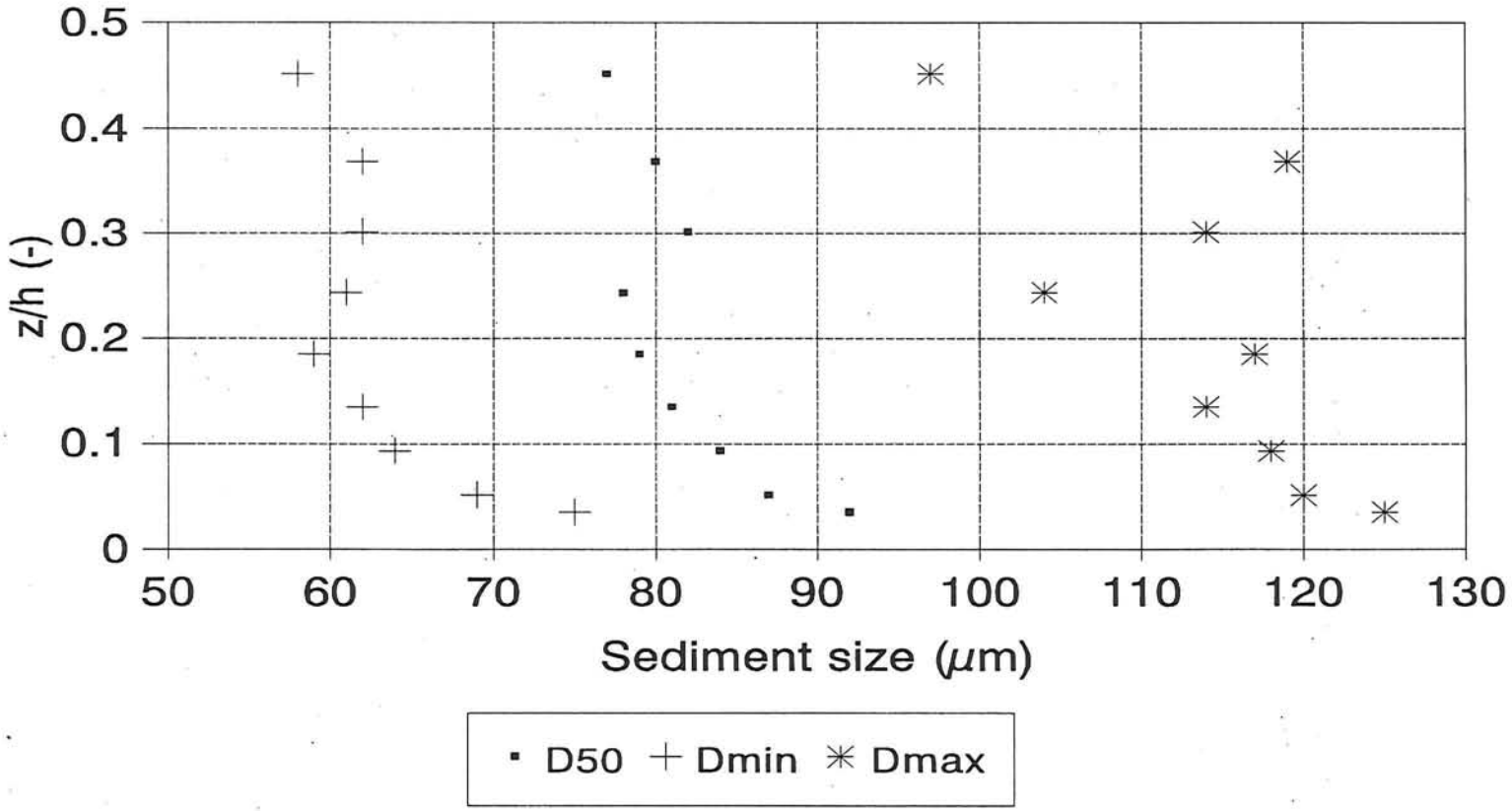

Figure 5.8.A3

Suspended Transport

Comparing models, Um = 0.10 m/s
Influence wave height

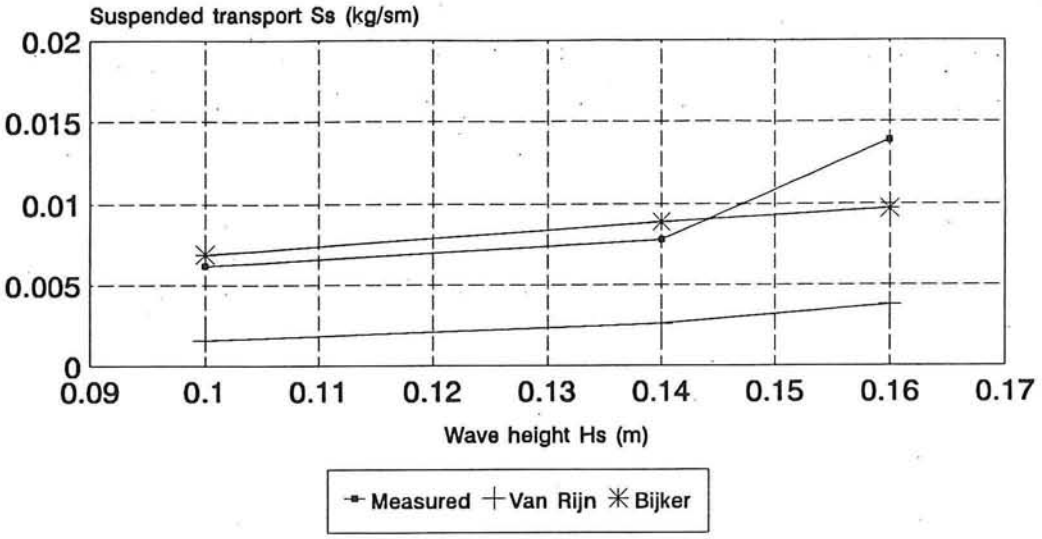

Figure 6.3.A.1

Suspended Transport

Comparing models, Um = 0.20 m/s
Influence wave height

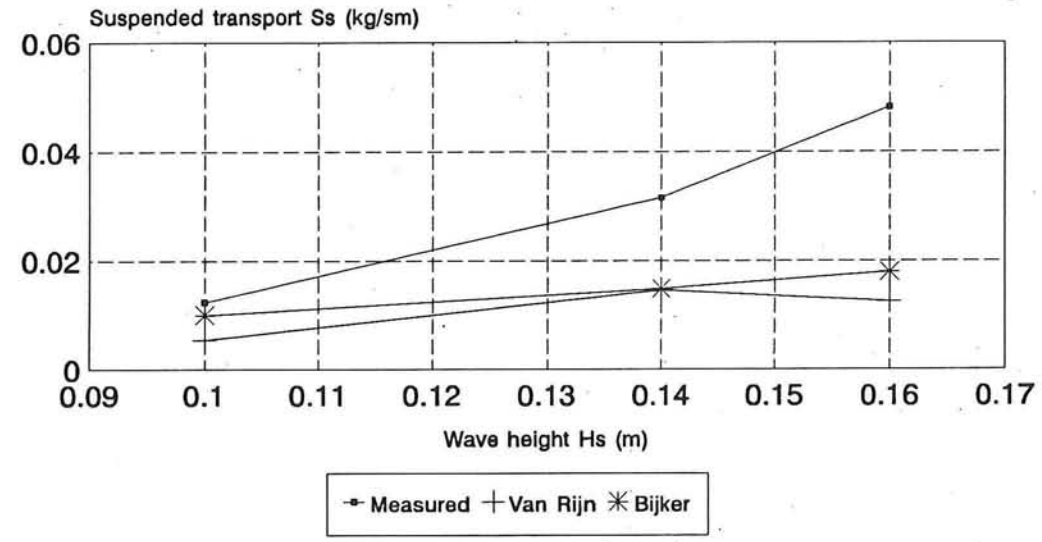

Figure 6.3.A.2

Suspended Transport

Comparing models, Hs = 0.10 m
Influence current strength

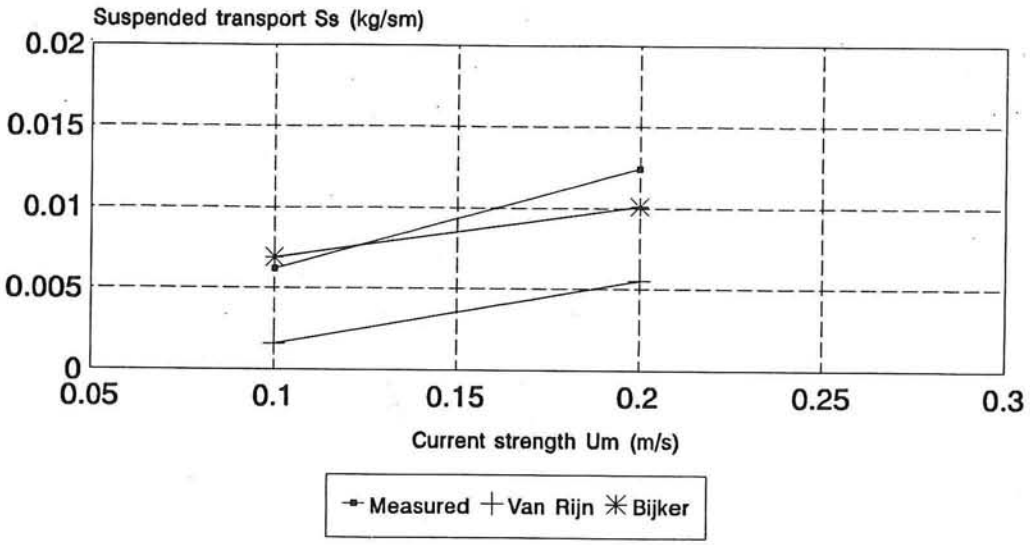

Figure 6.3.B.1

Suspended Transport

Comparing model, Hs = 0.14 m
Influence current strength

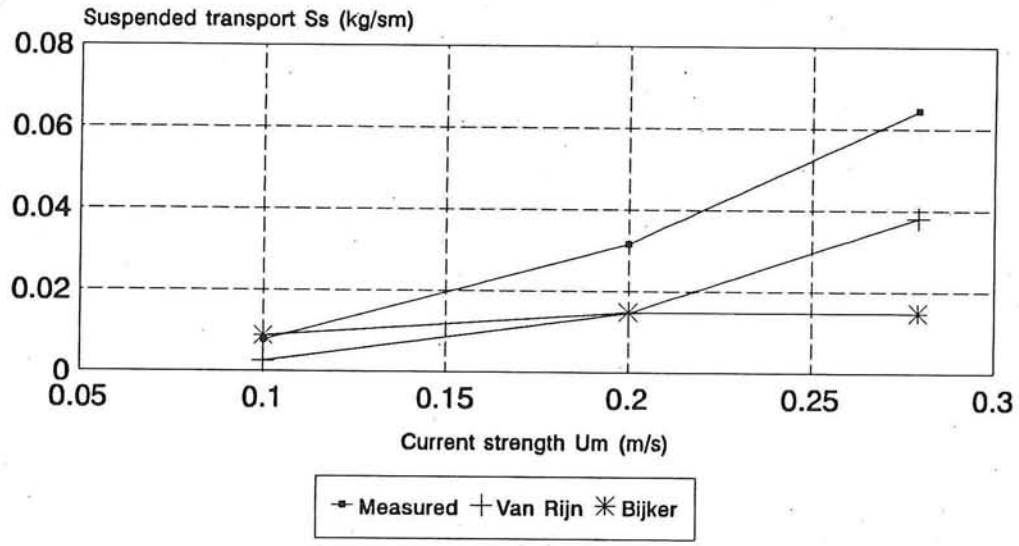

Figure 6.3.B.2

Suspended Transport

Comparing models, Hs = 0.16 m
Influence current strength

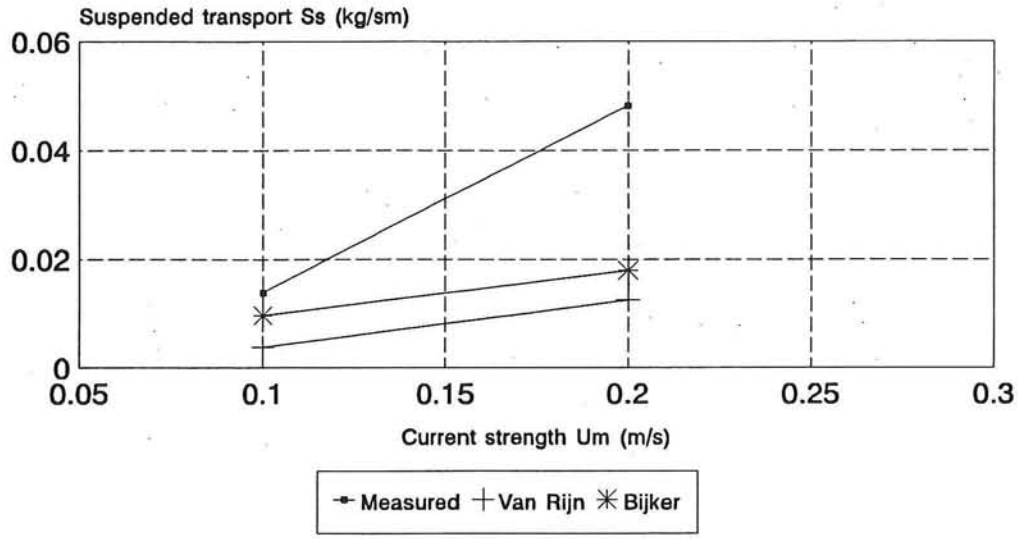

Figure 6.3.B.3

Concentration profile

Comparison of transport models
Hs = 0.10 m, Um = 0.10 m/s

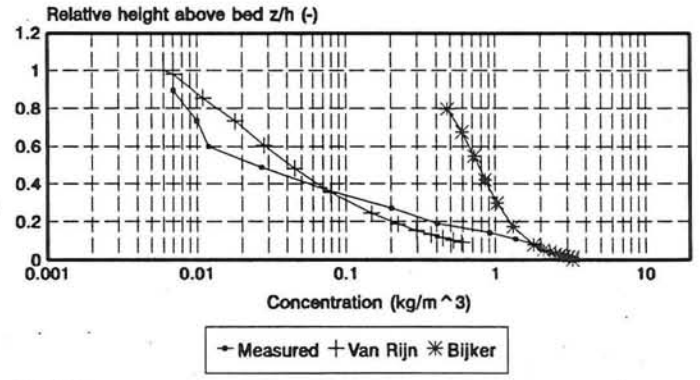

Figure 6.3.C.1

Concentration profile

Comparison of transport models
Hs = 0.14 m, Um = 0.10 m/s

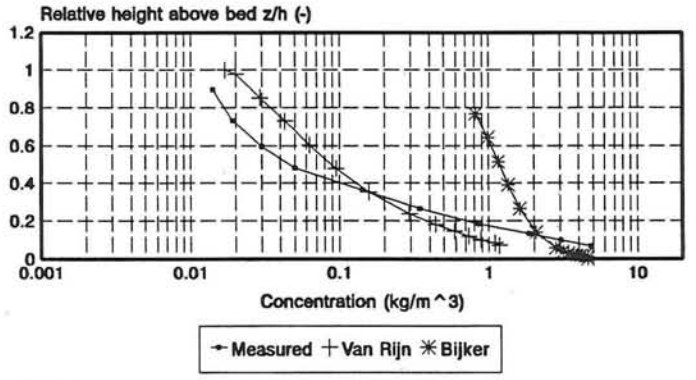

Figure 6.3.C.2

Concentration profile

Comparison of transport models
Hs = 0.16 m, Um = 0.10 m/s

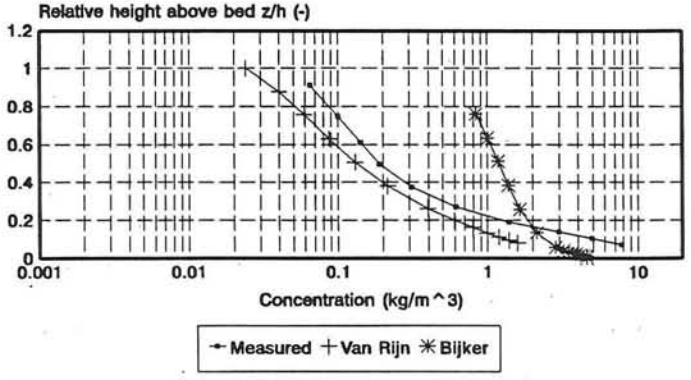

Figure 6.3.C.3

Concentration profile

Comparison of transport models
Hs = 0.10 m, Um = 0.20 m/s

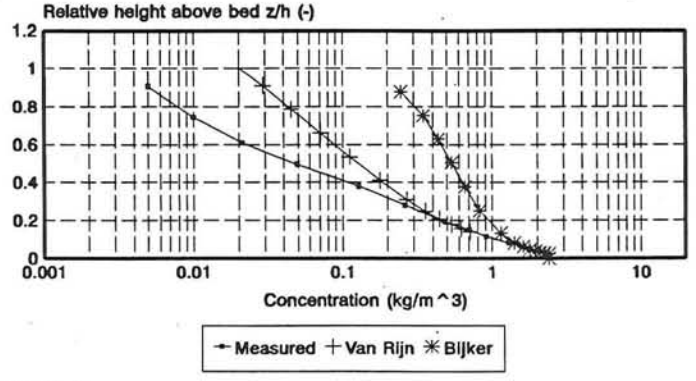

Figure 6.3.C.4

Concentration profile

Comparison of transport models
Hs = 0.14 m, Um = 0.20 m/s

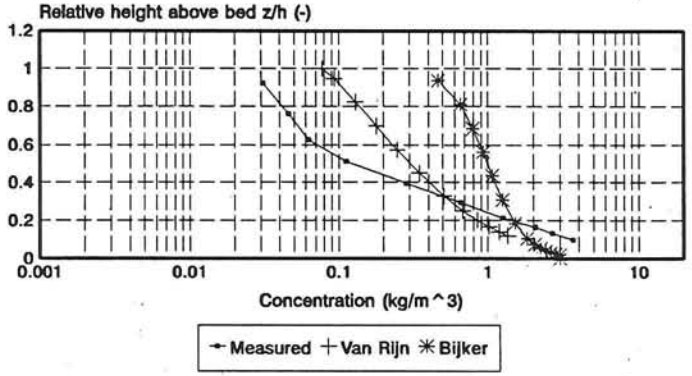

Figure 6.3.C.5

Concentration profile

Comparison of transport models
Hs = 0.16 m, Um = 0.20 m/s

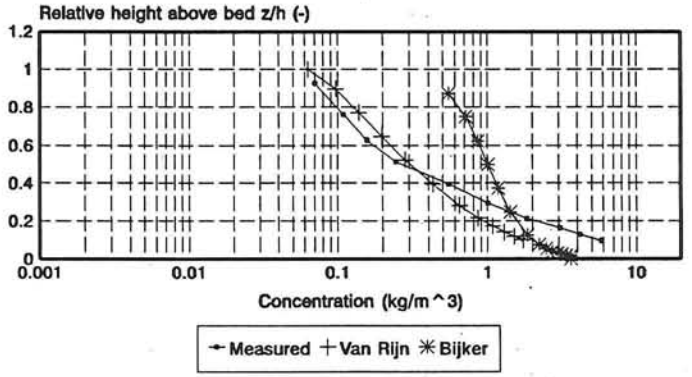

Figure 6.3.C.6

Concentration profile

Comparison of transport models
Hs = 0.14 m, Um = 0.30 m/s

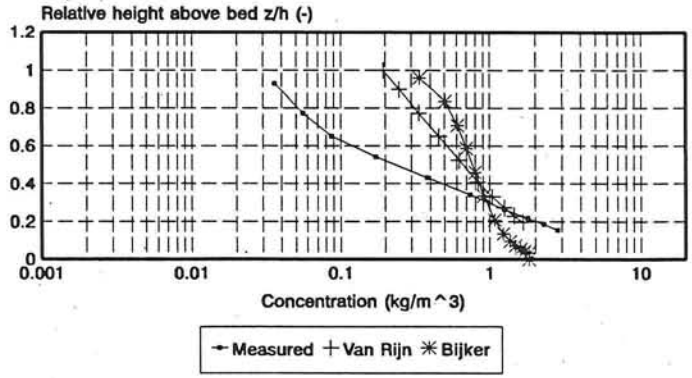

Figure 6.3.C.7

Velocity profile

Hs = 0.10 m, Um = 0.10 m/s
Van Rijn model

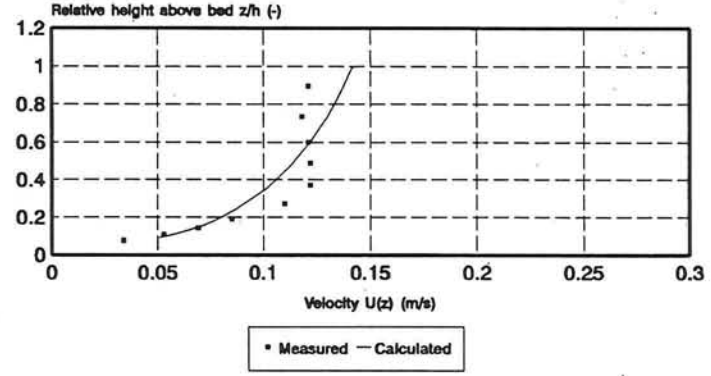

Figure 6.3.D.1

Velocity profile

Hs = 0.14 m, Um = 0.10 m/s
Van Rijn model

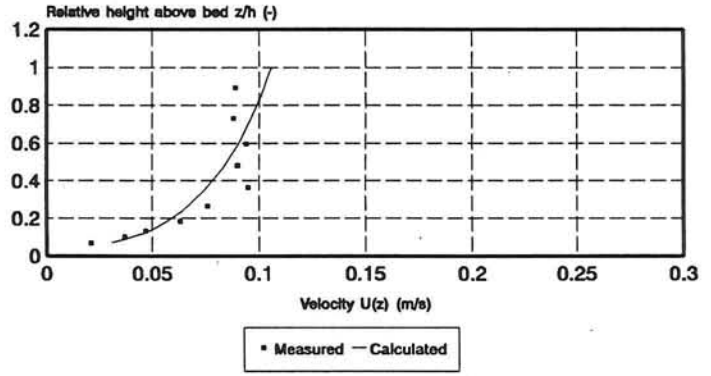

Figure 6.3.D.2

Velocity profile

Hs = 0.16 m, Um = 0.10 m/s
Van Rijn model

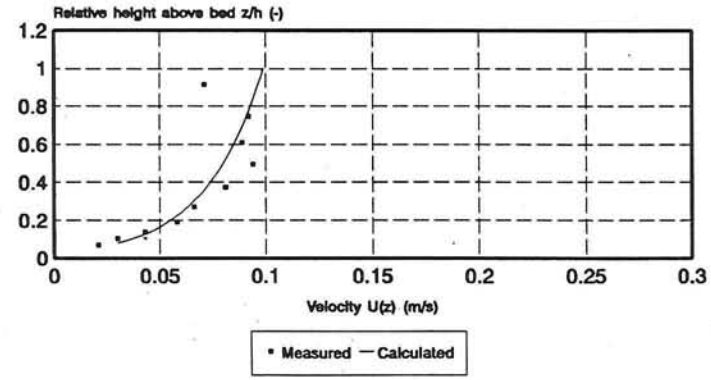

Figure 6.3.D.3

Velocity profile

Hs = 0.10 m, Um = 0.20 m/s
Van Rijn model

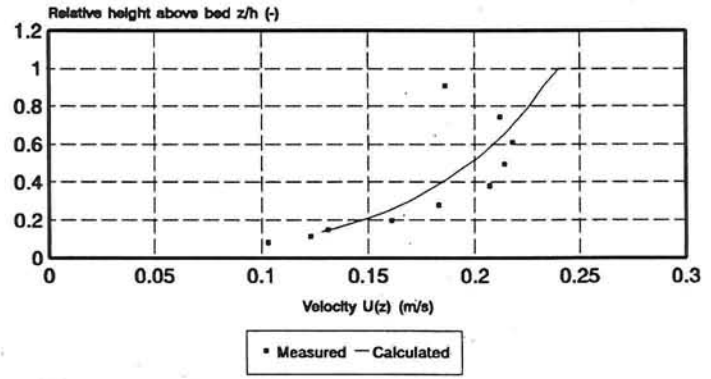

Figure 6.3.D.4

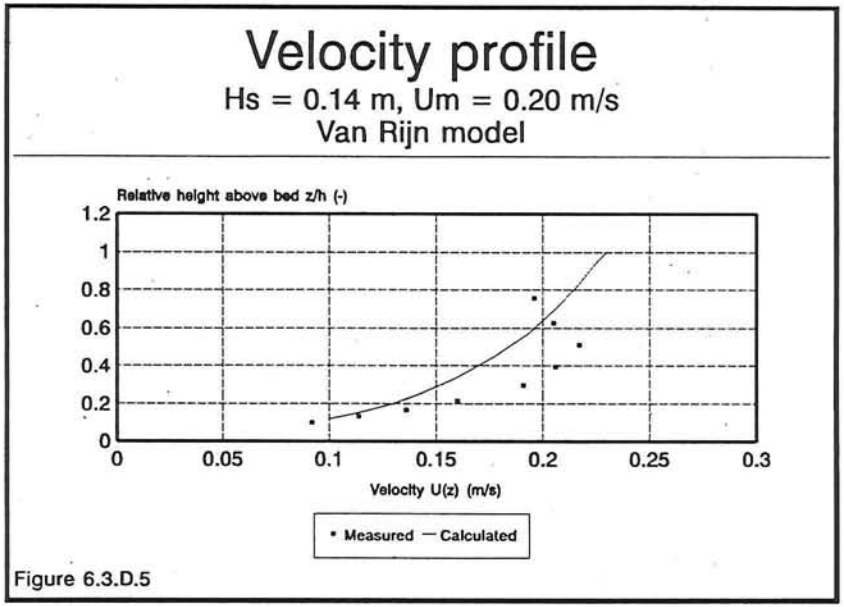

Figure 6.3.D.5

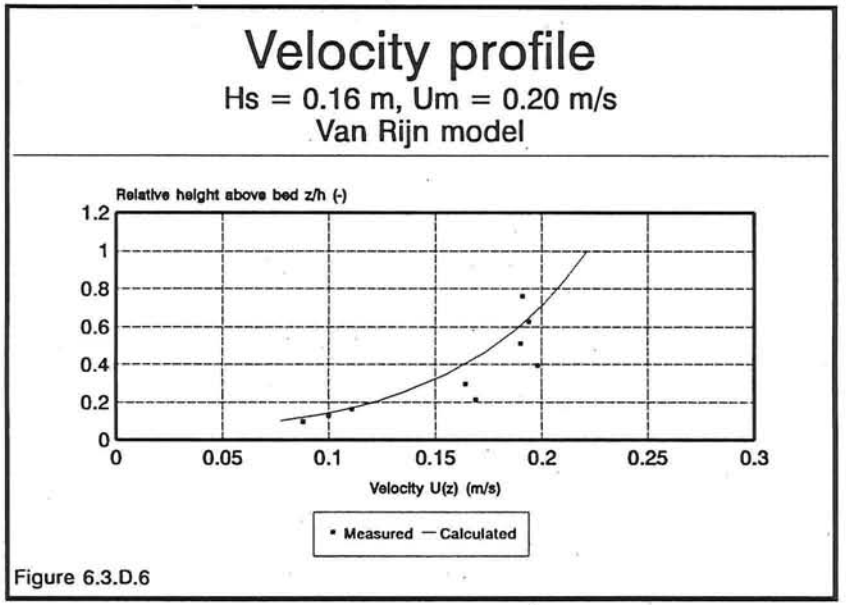

Figure 6.3.D.6

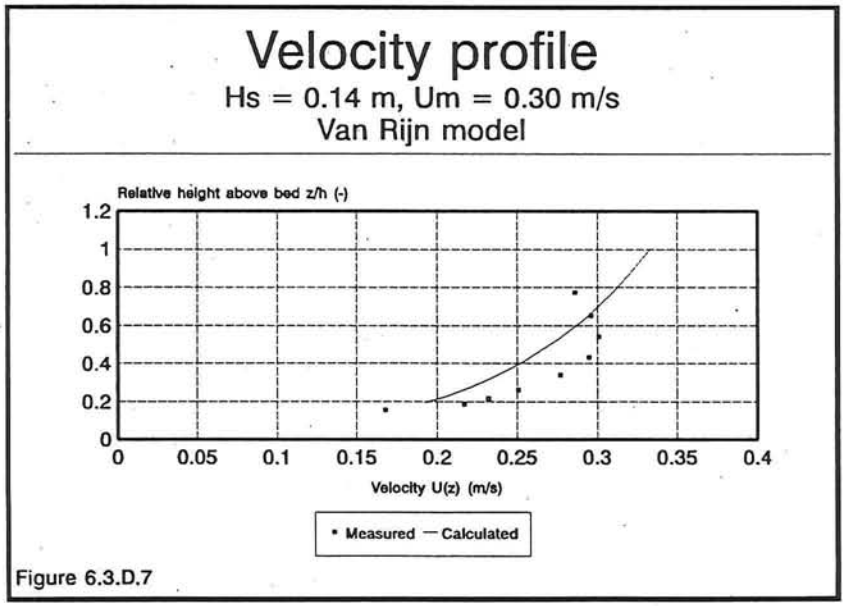

Figure 6.3.D.7